ALTA 2023 27 YEARS

30 April - 6 May | Perth, Australia

27TH Annual Conference Proceedings

Nickel-Cobalt-Copper Conference

Sponsored by

ALTA Metallurgical Services, Melbourne, Australia

www.altamet.com.au

PROCEEDINGS OF

ALTA 2023 NICKEL-COBALT-COPPER SESSIONS

1-3 May 2023

Perth, Australia

978-0-6487739-5-5

ALTA Metallurgical Services Publications

SolvExtract™ | by SOLVAY

1 Data Collection

The platform accesses most recent plant data through secure communication interface, compatible with data capturing software with convenient features such as custom alerts.

2 Analysis

The platform enables live data flows between the operation and Solvay's proprietary SX simulator, which monitors key variables and compares actual values and trends to those predicted by the model. The platform flags any divergence from defined acceptable ranges, and notifies plant operators and Solvay personnel.

3 Recommendations and trends

The platform delivers recommendations for corrective actions and regularly monitors trends for improvement opportunities. Continued improvements are made with tailored recommendations based on previous data and results.

Real time insights for faster decision making and improved profitability

SolvExtract™ is a digital platform that helps copper solvent extraction operations reduce process variability, boost productivity and improve bottom line. This app-based solution provides reagent recommendations to users at an unprecedented easiness and is accessible anytime, anywhere, to any authorized user.

Contact a Solvay representative to learn more about how SolvExtract™ can support your operational goals.

solvay.com

SOLVAY

Progress beyond

Nickel-Cobalt-Copper Contents

Sponsored by

NICKEL-COBALT-COPPER OPENING KEYNOTE

HEAP LEACHING – LOW COST, LOW CO_2 TECHNOLOGY FOR RECOVERING NICKEL AND COBALT PRODUCTS FROM LATERITE ORES

By

Anne Oxley, [1, 2]

[1]Brazilian Nickel, UK
[2]Scientific Associate of the Natural History Museum, UK

Presenter and Corresponding Author

Anne Oxley
aoxley@brnickel.com

ABSTRACT

Heap leaching is a low cost and inherently low carbon footprint process to recover nickel and cobalt from laterite ores. In comparison with other processing methods for laterites, it is a simple delinked process that has a straight forward ramp-up to steady state production, allowing both lower capital and operating costs.

Located in north-eastern Brazil, Brazilian Nickel's (BRN) Piauí Nickel Project (PNP) heap leach operation aims to be the first large scale commercial nickel and cobalt heap leach facility in the world. The first smaller scale commercial plant, the PNP 1000, produced first nickel product in June 2022 and is ramping-up to produce approximately 1,400 tpa Ni and 35 tpa cobalt in intermediate nickel and cobalt hydroxide products. The next scale of operations will be construction of the full scale plant to produce circa 25,000 tpa Ni and 1000 tpa Co contained in separate hydroxide products. The full scale operation is targeted to begin production in 2025.

Intermediate nickel and cobalt products, such as those produced at the PNP, are now the preferred product for the electric vehicle (EV) battery market. They are easily re-dissolved, either to form sulphates or direct to precursor, for the cathode active materials for the EV batteries.

Advantages of heap leaching for EV battery raw materials include lower capital intensity, lower operating costs, smaller environmental footprint and reduced CO_2 emissions. On the latter, the PNP has been independently benchmarked and will potentially produce one of the lowest carbon-intensity products in the nickel industry, and BRN is looking at innovative ways to reduce or eliminate the CO2 emissions with a view to becoming a net carbon zero or even carbon negative producer.

Keywords: Nickel Laterite, Heap Leaching, Low Carbon, Carbon Capture, Nickel, Cobalt, Battery Raw Materials, EVs.

Why Heap Leaching ?

- Lowest capital cost of the hydromet processes
- First quartile operating costs
- Stable known Ramp-up
- Simple flexible process, (but needs know-how)
- Resource utilization maximised
- Low energy intensity
- Low CO_2
- All residues are dry – no tailings dam
- Low construction risk

Nickel Laterite Heap Leaching Development

BRN brings together a team of experts that have been at the forefront of the development of nickel laterite heap leaching, leading projects at…

Project	Country	Dates	Largest Test/Production	Stage
Bitinçka	Albania	1999-2008	Bottle Rolls & Columns	PFS
Çaldağ	Turkey	2003-2010	Pilot Plant	BFS & FEED
Cerro Matoso	Colombia	2005-2010	Pilot Plant	BFS
Acoje	Philippines	2007-2010	Pilot Plant	PFS
Piauí	Brazil	2013 – present	Demo Plant Small Scale Production	Detailed Engineering

Piauí Nickel Full Scale Project Overview

The PNP, located in NE Brazil, is expected to produce an average of 26ktpa nickel and 1.0ktpa cobalt over the first 10 years of mine life from peak production

Located in Piauí State, Brazil	• **Established mining jurisdiction** • 6 key ports, 11 inland routes and 3 international airports
Peak and Average Production	• **Peak production in 2027**: 34ktpa nickel, 1.2ktpa cobalt • **Average production in 2027-2036**: 26ktpa nickel, 1.0ktpa cobalt

First Large Scale Production	• **Current production expectations**:
	  • First nickel in Q2 2026
	  • First cobalt in Q1 2027

Mining and Processing Methods	• **Mining method**: Open pit • **Processing method**: Heap leach
Current Status	• **Early production**: PNP1000 completed • **Feasibility Study**: Completed in July 2022 for Full-Scale PNP • **Licenses**: Awarded the 5 necessary Preliminary Licenses ("LP")

Piauí Nickel Project History

The PNP deposit is a nickel-cobalt laterite deposit that has undergone extensive exploration work and drilling since its discovery in the 1970s

Project Location

PNP Site

Past Drilling Campaigns at the Project

Years			Total Drilling
1973-74	Rio Doce Geologia e Mineracão		1,435m
2003	VALE		2,346m
2004-05	VALE		53,827m
2006	VALE	Vale Test Mine Excavated	-
2008	VALE		19,518m
2016	BRAZILIAN NICKEL PLC	BRN Demo Heap Sampling	737m
2021 & 2023	BRAZILIAN NICKEL PLC	PNP1000 Grade Control Drilling	9,460m
Total Drilling			87,323m

Piauí Nickel Project Timeline

Shovel ready project with first production of products essential to the clean energy transition and EV battery value chain within 3 years

- Feasibility Study, completed in July 2022, confirms the technical and economic viability of the Project
- Installation / construction licence application has been submitted in Q4 2022 with approval expected Q2/Q3 2023
- Project has received a "Laudo de Servidão Mineral" which reinforces the national public interest in the Project
- Front End Engineering Design (FEED) completion expected Q1 2024
- Construction expected to start Q2 2024
- Ongoing discussions with key suppliers suggest that first nickel production is expected Q2 2026

Laudo **de Servidão** Mineral – *issued in August 2022 by the Agência Nacional de Mineração ("ANM"), which is a Brazilian federal agency.*

ANM

LAUDO TÉCNICO PARA INSTITUIÇÃO DE SERVIDÃO

PROCESSO Nº 27221.804290/1970-57
INTERESSADO Nº PIAUÍ NÍQUEL METAIS S.A
ASSUNTO SERVIDÃO MINERÁRIA

Considerando os termos do **PARACER 150/2022/DITIL/SOT-ANM/DIRC** que ora adoto como fundamento;

Considerando que, a atividade de Mineração é de interesse nacional, utilidade pública e com rigidez locacional, conforme disposto no Art. 2º do Decreto 9.406/1918;

Considerando que os fundamentos e justificativa técnica presentes no requerimento de servidão se enquadram nos requisitos do Art. 59, alíneas "a", "b" "c " e "d" do Código de Mineração - Decreto Lei 227/1967;

Considerando que, para o pleno aproveitamento da jazida o estabelecimento das Servidões pretendidas tornam-se imprescindíveis;

Considerando os termos do inciso VIII, do Art. 1º da Portaria ANM 1.056/2022 que subdelegou aos Gerentes da Unidades Regionais da ANM a competência para emissão de Laudo de Servidão Minerária, Julgamos que a instituição de Servidão Minerária é necessária no presente caso, devendo abranger: **3.593,57 hectares para a Servidão de Lavra/Beneficiamento/Concentração; 886,93 hectares para a Servidão da Linha de Transmissão de 69 KV e 1.318,08 hectares para a Servidão da Adutora de Água,** nos terrenos dos superficiários indicados pelo próprio concessionário (fls. 132/133 DOC SEI 0762111).

Teresina PI, 25 de agosto de 2022.

Antônio Sânzio Áuila Cavalcante
Gerente Regional ANM/PI

The document reinforces the national public interest of the Project and mining concession license, and can be used to support any judicial proceedings should a landowner deny land access required for the Project (to be used only when good faith negotiations have not succeeded)

Project Timeline

June 2022	First PNP1000 production
Q1 2024	FEED completed
Q1 2024	Project financing completed
Q1 2024	First stage of detailed engineering completed
Q2 2024	Construction commences
Q1 2026	Mining commences
Q1 2026	Acid plant completion
Q2 2026	First nickel production
Q1 2027	First cobalt production

PNP 1000

De-risking of the heap leach process through the operation of PNP1000 and introduction of products into the battery metal supply chain

Commentary

- PNP1000 construction commenced in January 2021 and the first nickel product was produced in June 2022
  - PNP1000 has a production capacity of 1,400tpa of nickel contained in NHP and 35tpa of cobalt contained in CHP
- Fully Licenced
- While PNP1000 is on a smaller scale, the systems and processes installed are transferable to the Full-Scale operation
  - Heap height is the same at 4.5m
- The people recruited and trained for the PNP1000 will form the core of the expanded workforce for the Full-Scale Project, allowing significant experience to be carried over

PNP1000

PNP1000 Key Milestones

PNP1000 kick off	January 2021
Mining commenced	January 2022
Stacking of first module began	March 2022
Heap irrigation started	May 2022
First nickel produced	June 2022

PNP1000 Full-Scale Project Comparison

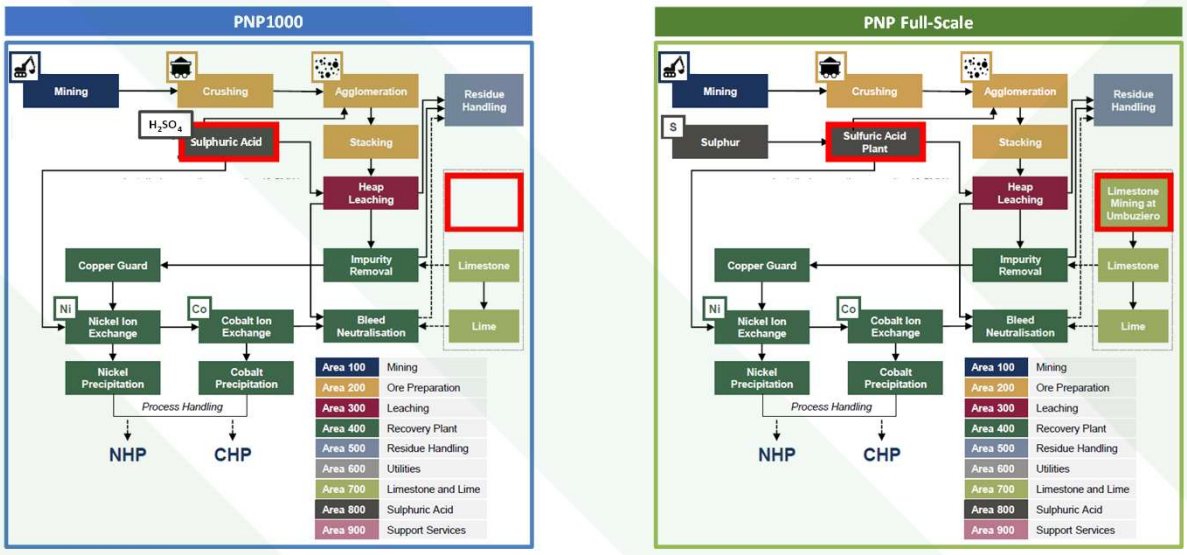

PNP1000 - Mine

PNP1000 – Leach Pad

PNP1000 from the Demo Heaps

PNP1000 – Downstream Plant

PNP1000 – Solid Waste

PNP1000 – Product

PNP1000 Results

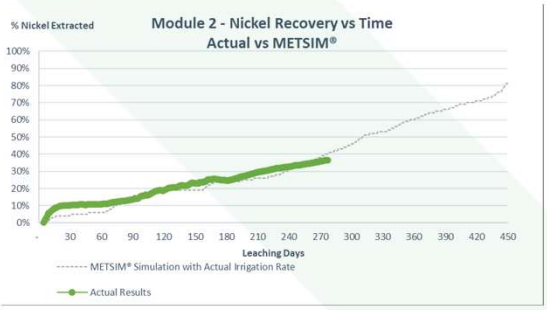

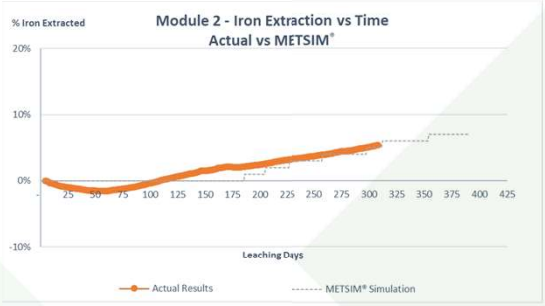

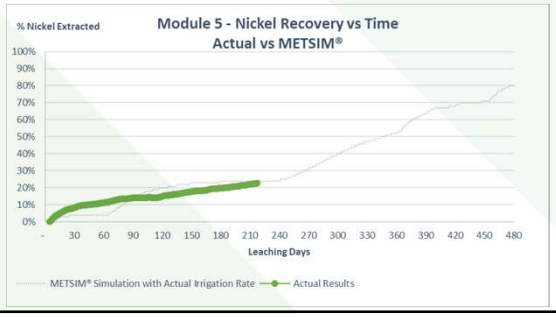

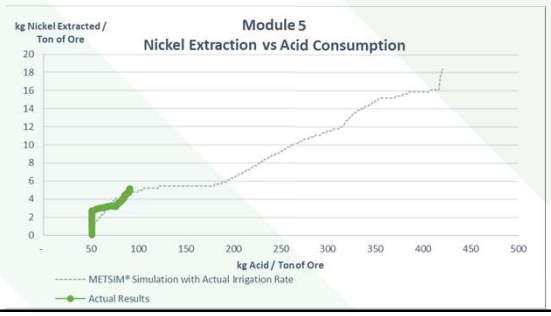

ESG is an Integral Process

Robust framework designed in accordance with the UN sustainable development goals

United Nations Sustainable Development Goals

Forms the basis of BRN's ESG framework

ESG Framework and Nickel Mark Pilot Program

- BRN measures its ESG performance across 9 key areas, designed in accordance with the UN Sustainable Development Goals
- PNP1000 has allowed BRN to implement these frameworks and build expertise in monitoring performance and allowing transfer to the Full-Scale Project
- In conjunction with the UN's Sustainable Development Goals and ESG initiatives, BRN has recently joined the Nickel Mark pilot program
- The Nickel Mark will demonstrate nickel producer's and the industry's responsible production practices in an effort to promote transparency and accountability
- The Nickel Mark demonstrates BRN's commitment to working towards global Net Zero targets and reducing carbon emissions

ESG is an Integral Process

ESG is an integral part of the PNP, with key permitting, social, environmental and governance plans already in place

Permitting

- Mining concession in place
- Main LPs awarded in January 2020 following local community engagement
- ESIA completed with 21 E&S action plans approved by the environmental authority (SEMAR) for the LPs award
- Installation licenses – applied in Q4 2022 and expected in Q2/Q3 2023 to allow construction start
- Water extraction permit and power connection permit obtained

Social

- PNP1000 had high levels of local employment with >75% of current workforce hired locally (c.300 people)
- On average, local employees are paid 76% above Brazilian minimum wage
- Provided free 3 month technical training course to +130 local candidates
- Member of Paradigm for Parity
  - c.33% of current workforce is female
- Major positive social impact in a poorly developed region

Public Hearing for Environmental Licensing

Energy, Water and CO_2

- Carbon free power to be provided from on-site sulphuric acid plant, with excess power to be sold back to the grid
- The PNP's processing technology is a significantly less energy intensive way to produce nickel and cobalt
- High water use efficiency with filtering, recycling, no effluent discharge and no wet tailings dams
- Low scope 1 and 2 CO_2 emissions of 11.95t CO_2 / t NiEq

Governance

- Sustainability management system heading to full compliance with IFC performance standards
- Looking to become ESG accredited in the near term

Daily Safety Meeting

Source: Brazilian Nickel management team

Environmental

The Project's Environmental Management Plans provide a framework to identify, monitor and mitigate environmental impacts across all stages of the Project

Commentary

- Minimised energy intensity
  - PNP produces all power from the acid plant and sells excess power back to the grid (HPAL the same size would require 3x more energy)
- Increased resource utilisation,
  - Less mine waste and longer operational life
  - All ore above cut-off grade is processed and no blending/separation of ore types required
- Minimal water use and acid consumption
- Only solid residues
  - No tailing dams required and no deep sea disposal

Propagation of Native Tree Species Seedlings

Effluent Monitoring

Only Solid Residues

Source: PNP July 2022 Feasibility Study

Social

The local community is actively engaged to ensure a major positive social impact in the surrounding regin

Commentary

- Strong relationships and engagement with local communities
- High levels of local employment
  - >75% of current workforce hired locally
- Member of Paradigm for Parity
  - c.33% of current workforce is female
- Major positive social impact in a poorly developed region

Training Courses for Local Candidates

Building Community Relationships

Daily Water Sprinkling to Suppress Dust on Project Access Roads

Source: PNP July 2022 Feasibility Study

Full-Scale Capital Intensity

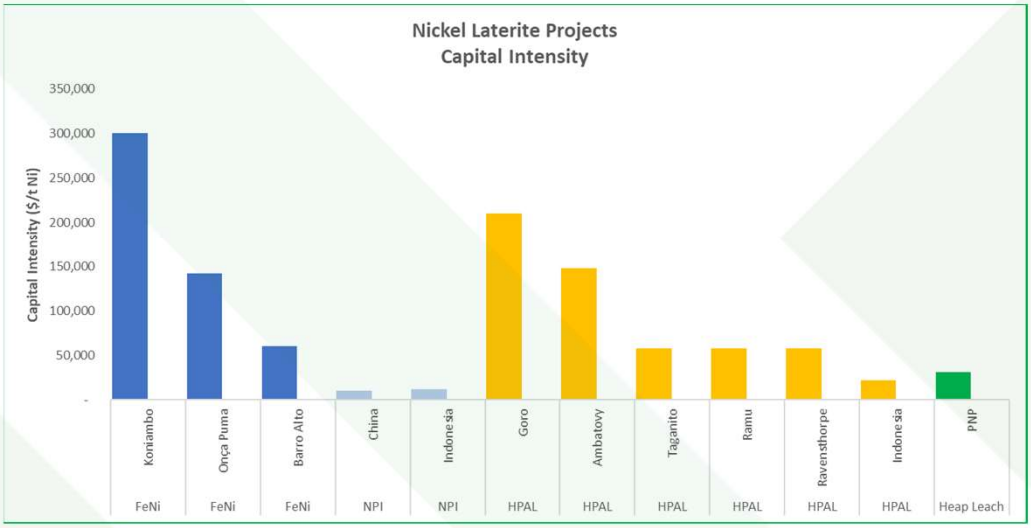

Source: Wood Mackenzie, BRN

Full Scale Operating costs (C1)

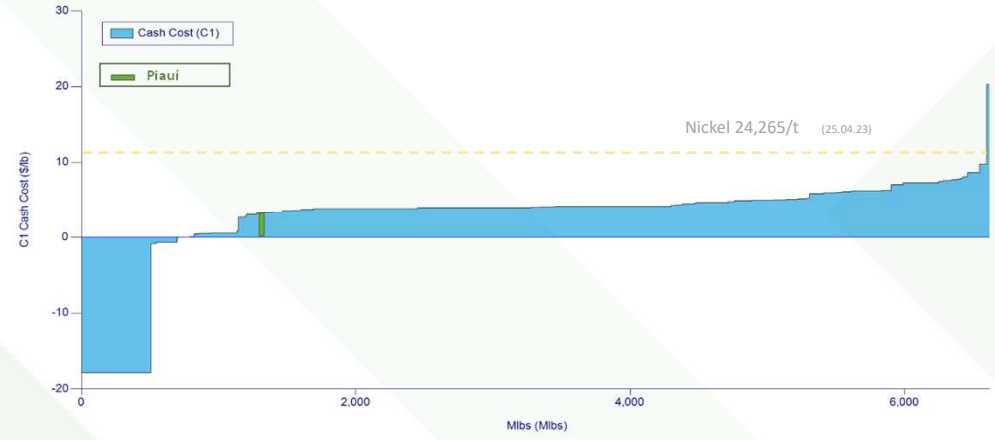

Source: Wood Mackenzie Ltd, Dataset: 2022 Q1

CO2e Intensity Benchmark

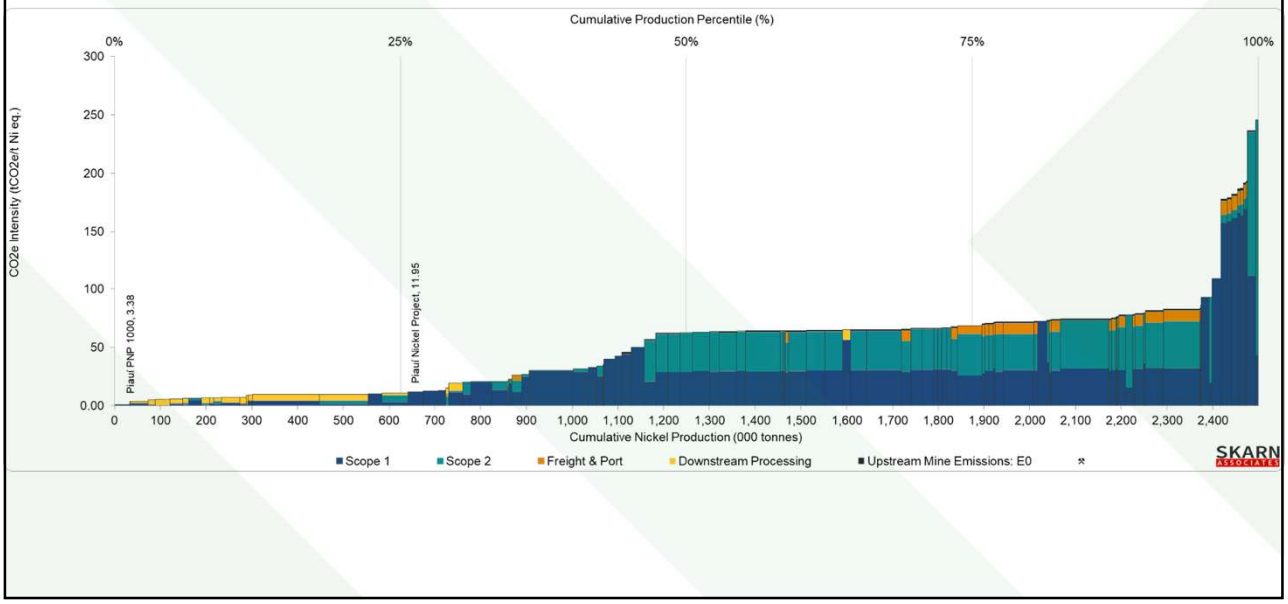

CO2 Reduction Schematic

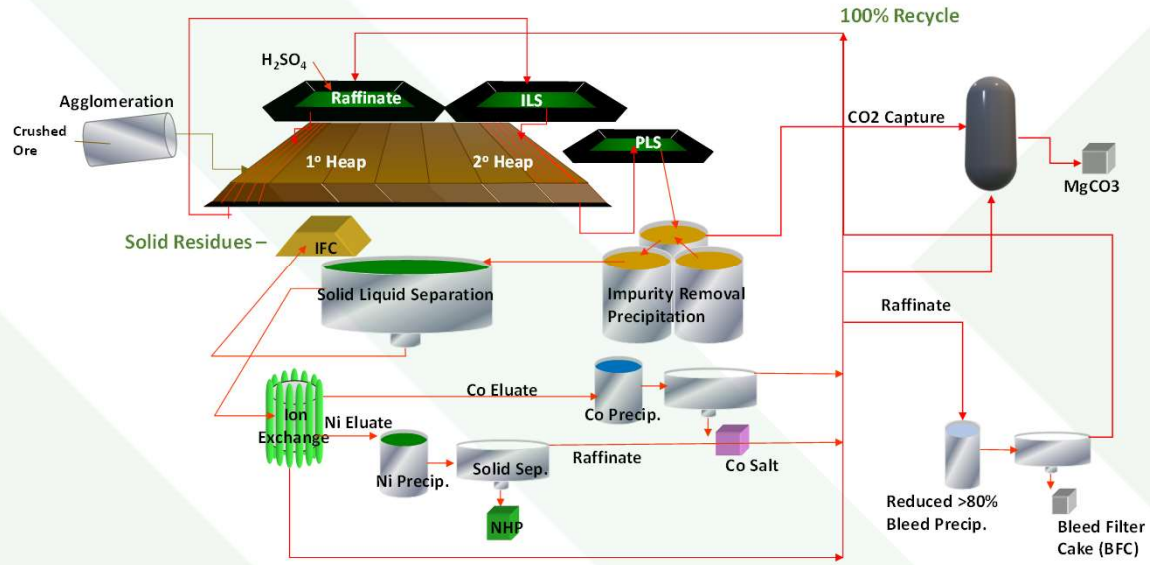

CO2 Reduction Partners PLANETARY

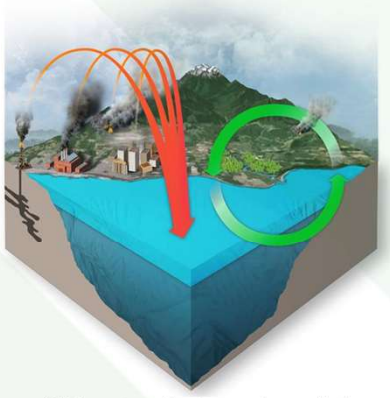

- 1) The oceans are the key regulate the Earths climate
- Absorbing 40% of all human made CO2 emissions
- Causing widespread ocean acidification and devastating marine ecosystems

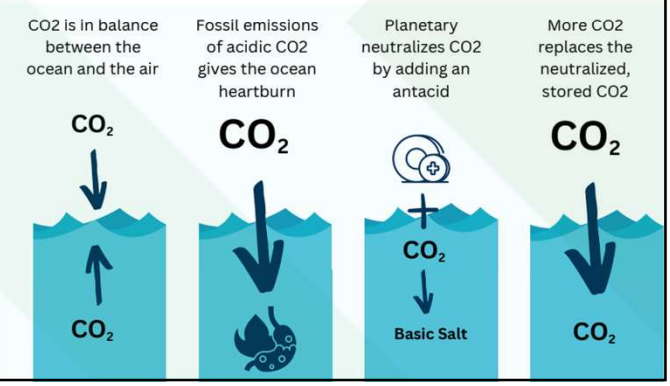

2) Planetary is pioneering solution which involves adding alkaline material to the ocean to:

- Restore ocean chemistry and the marine environment
- Enhance the ocean's natural ability to absorb and permanently store CO2 from the air

How it could work

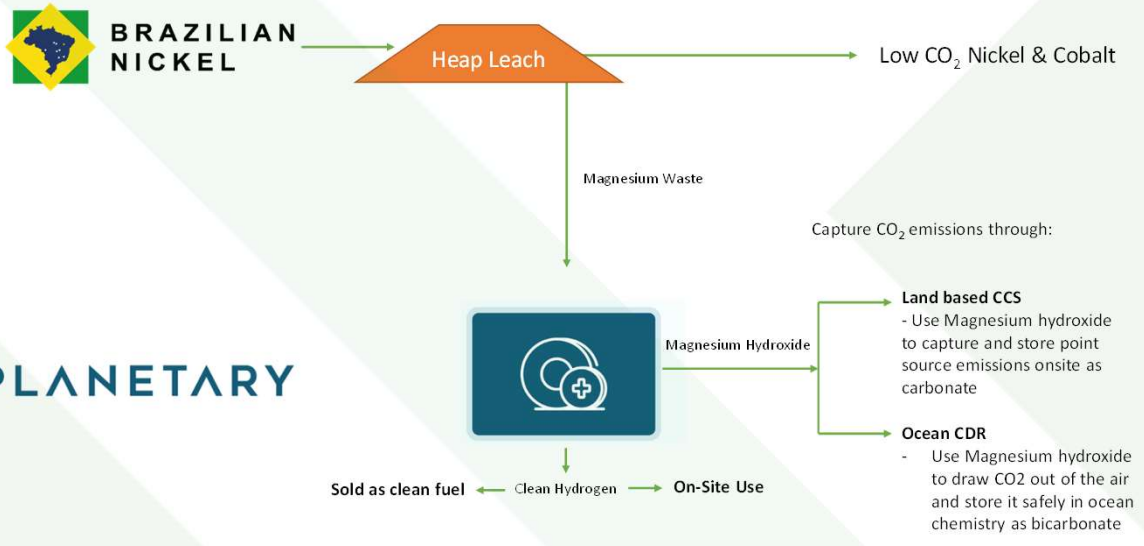

CO2e Intensity Benchmark

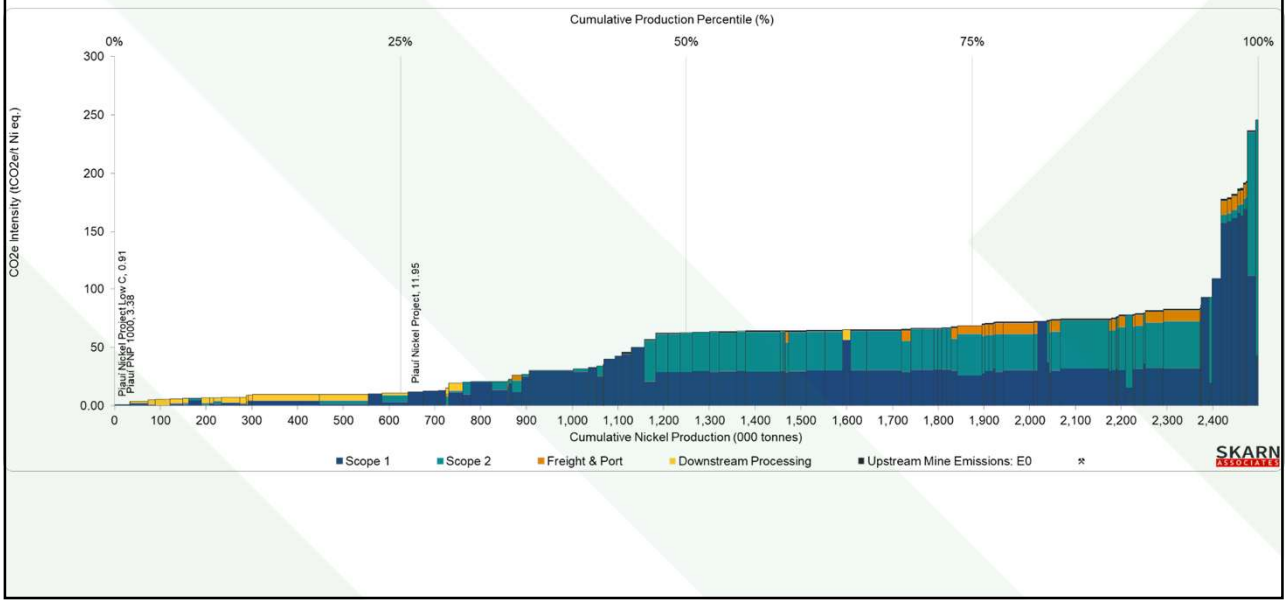

CO2e Intensity Benchmark Laterites

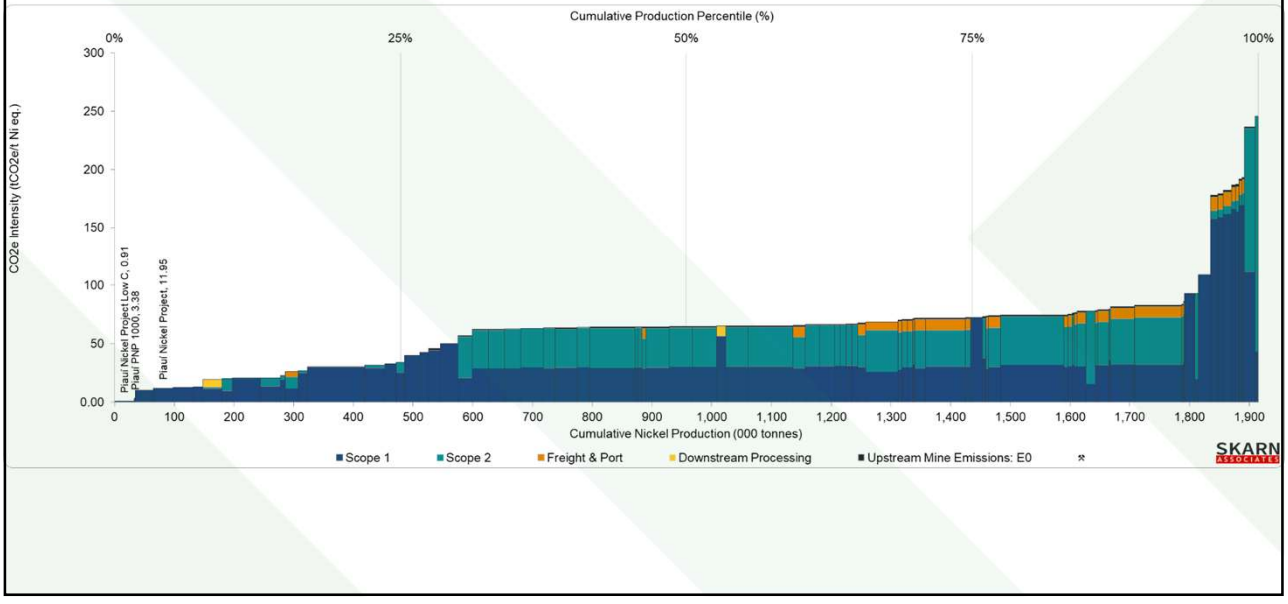

Laterite Deposits

Growth potential through project replication of the transformative heap leach process on a pipeline of other nickel laterite deposits globally

Global Nickel Laterite Deposits

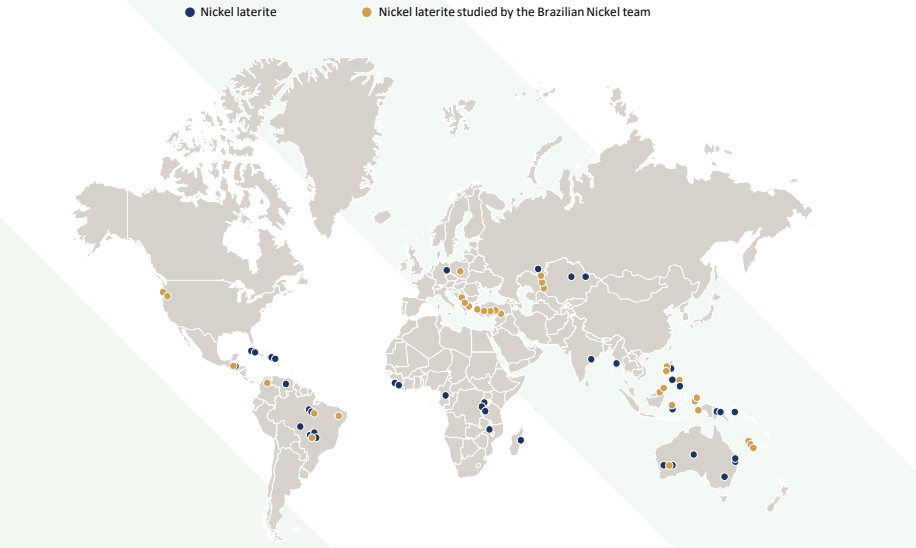

Commentary

- The PNP process was developed from different pilot plant tests all over the world, including projects in Colombia, Turkey and the Philippines
- This process was later replicated in the PNP Demonstration Plant and showed that target nickel extractions could be met, and even exceeded, with low acid consumption and attractive leach kinetics
- The countries currently under active consideration by Brazilian Nickel are Brazil, Australia and the United States

KABANGA NICKEL – THE ROLE OF HYDROMETALLURGY IN UNLOCKING A WORLD-CLASS ASSET FOR LOW-EMISSIONS GREEN METALS PRODUCTION

By

Mike Adams, Keith Liddell, Lisa Smith, Chris Medway

Lifezone Metals, Isle of Man

Presenter and Corresponding Author

Mike Adams
mike@kellprocess.com

ABSTRACT

There is a compelling outlook for nickel demand and responsibly sourced "green metals". Kabanga Nickel is one of the world's largest and highest-grade undeveloped nickel sulphide deposits that for years has remained undeveloped under a conventional concentrate offtake strategy with smelters. Lifezone through its Tanzanian Joint Venture company Tembo Nickel is now developing the Kabanga Nickel project under a new strategy of in-country processing of concentrate to refined Class 1 nickel, cobalt and copper metals using its hydrometallurgy technology suite. Kabanga Nickel also enjoys Government of Tanzania support as 16% shareholder in Tembo Nickel. Vertical integration provides the ability for the country to capture full benefit of its sovereign natural resources. The overall strategy has been further endorsed by leading strategic partner BHP whose investment in Lifezone and Kabanga Nickel validates the economics and enhances project execution.

A substantial body of work was completed previously on the Kabanga Nickel project, with $293 million spent by prior owners on drilling and feasibility studies, including six flotation pilot plant runs and almost 600 km of drilling. Kabanga Nickel has augmented this by undertaking additional drilling and metallurgical testwork, as well as substantive work on the ground in Tanzania.

Kabanga concentrate shall be transported some 320 km by road to the refinery site at Kahama, utilising some of the pre-existing infrastructure and permitting of the Buzwagi gold mine, which ceased operations mid-2021 due to ore depletion and is currently undergoing rehabilitation. The hydrometallurgical flowsheet for Kabanga concentrate includes total pressure oxidation, recovery of copper by solvent extraction and electrowinning, iron removal, and recovery of nickel and cobalt into a mixed hydroxide precipitate for releaching and refining by solvent extraction and electrowinning. All residues are backhauled to the Kabanga minesite for use as underground pastefill. The binding properties of the gypsum allow for part replacement of cement as pastefill binder and the siliceous residue has also been activated by the leaching process. By this means, residue, tailings and slag stockpiles are eliminated at the Kahama refinery site. Moreover, the desulphurised residues allow for a greater proportion of tailings to be stored underground, reducing the size of the surface tailings storage facility.

The role of hydrometallurgy in unlocking this world-class asset spans several key layers within the project. Economics are enhanced, via high metals recoveries, low capital and operating costs, elimination of the carbon footprint of bulk shipping, near elimination of concentrate transportation costs and reduction in pastefill cement consumption. Environmental benefits include the elimination of sulphur dioxide emissions, by conversion of sulphides to gypsum binder for underground pastefill. Carbon emissions are substantially reduced compared to industry baseline as published by the Nickel Institute. Social and community benefits are significant, with the creation of a metals refining hub at Kahama, resulting in job and skills creation, training and education as well as secondary business opportunities.

Kahama refinery has the potential to become a multi-metals processing facility that could expand into refractory gold, nickel, cobalt, copper, platinum group metals and rare earths, from the broader region – effectively becoming a major East African metals refining hub.

Keywords: Nickel, cobalt, copper, hydrometallurgy, pressure oxidation, solvent extraction, electrowinning, Tanzania

Background

Lifezone Metals – The supply chain solution for clean metals

Unlocking a world-class asset for low-emissions green metals production

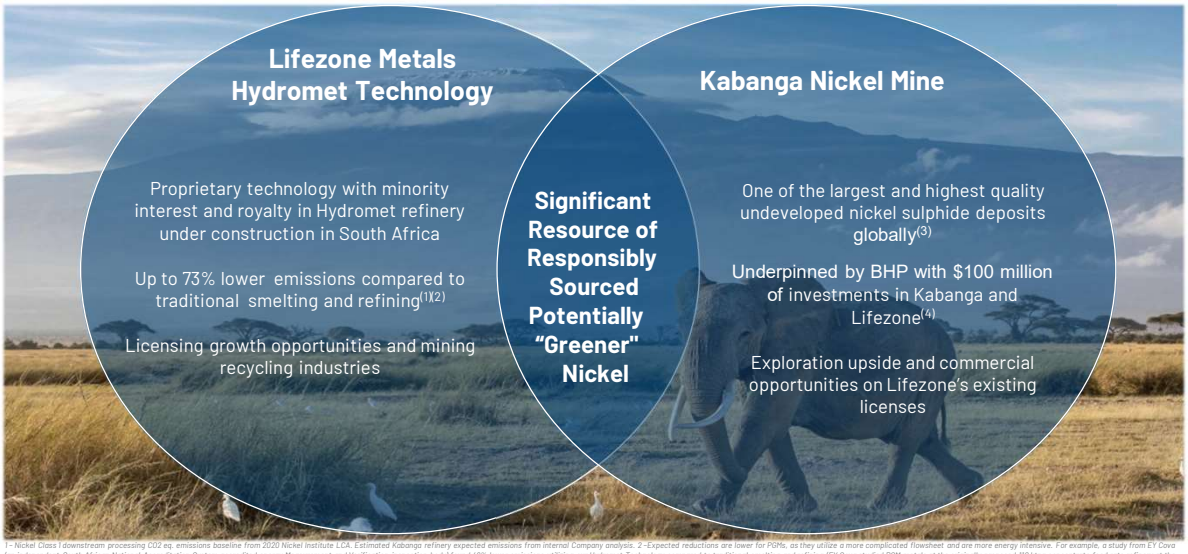

1 – Nickel Class 1 downstream processing CO2 eq. emissions baseline from 2020 Nickel Institute LCA. Estimated Kabanga refinery expected emissions from internal Company analysis. 2 –Expected reductions are lower for PGMs, as they utilize a more complicated flowsheet and are more energy intensive. For example, a study from EY Cova (an independent South African National Accreditation System accredited energy Measurement and Verification inspection body) found 46% lower emissions utilizing our Hydromet Technology compared to traditional smelting and refining (EY Cova studied PGM metals at the originally proposed 110 ktpa concentrate feed rate refinery at the Sedibelo plant site in South Africa under the then-applicable conditions in 2020 and assuming reagents not manufactured on-site; actual results could differ). Results will vary for specific PGM projects. 3–Based on analysis of the largest undeveloped nickel deposits from S&P Capital IQ Pro, as modified per public data on each mining project. The Kabanga Project's resource metrics reflect the measured, indicated and inferred resources referred to in the Kabanga Mineral Resource Estimates as of 15 February 2023 from the TRS, as set out on slide 20. 4 –In December 2021, BHP invested $10 million into Lifezone and $40 million into KabangaNickel Limited, a subsidiary of Lifezone; in February 2023, BHP agreed to invest an additional $60 million in KabangaNickel Limited, a subsidiary of Lifezone.

Nickel sulphide: Supply shortage of greener nickel

Battery Demand for Nickel to Catalyze Nickel Supply Growth [1]

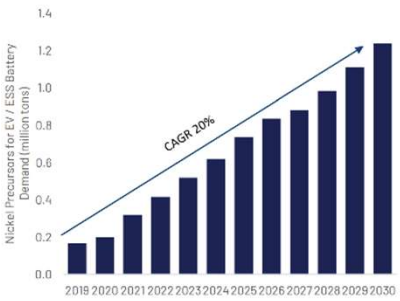

Most Supply Growth Expected From Nickel Laterites [2]

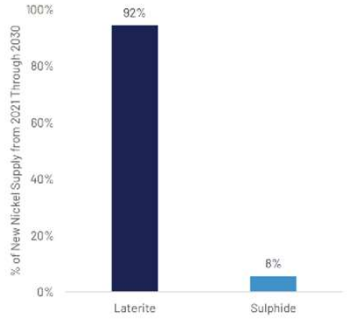

Nickel Sulfides Have Lower GHG Intensity – Further Enhanced by Kabanga's Integrated Refining [3]

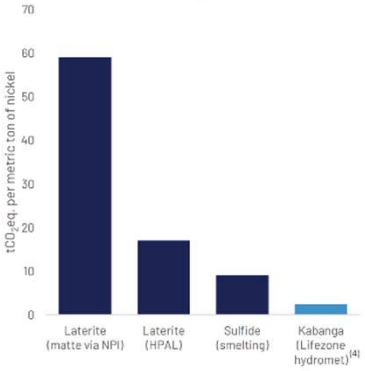

1 – Bespoke Nickel Market Outlook for Lifezone, a product of Wood Mackenzie, September 2022. Based on battery demand from electric vehicles and energy storage applications.

2 – Bespoke Nickel Market Outlook for Lifezone, a product of Wood Mackenzie, September 2022.

3 – IEA The Role of Critical Metals, March 2022.

4 – Kabanga GHG intensity is based upon data provided by Lifezone and Wood Mackenzie analysis, is estimated as of 2030 by Wood Mackenzie and assumes power supply as hydro and solar and may also include scope 3 emissions. The figures for laterite and sulfide only include Scope 1 and Scope 2 emissions.

Kabanga Nickel Project

Overview

Kabanga Project Overview

High Quality Mineral Resource

- Nickel sulphide attributable Mineral Resource to Lifezone of 40 Mt grading 2.61% Ni and containing 2,325 million lbs. of nickel [(1)]
- $293 million spent by prior owners on drilling & feasibility studies
- Globally significant high-purity Ni, Co & Cu end-products

Potentially Significant Reduction in Emissions Relative to Traditional Smelting

- Expecting up to 73% reduction in estimated CO_2 eq. emissions and zero SO_2 emissions [(2)] at Kahama refinery

Eliminates Need to Transport Concentrates Globally

- Eliminates the carbon footprint of international bulk shipping of concentrate with relatively short distance between operating mine and refinery
- Shorter haulage distances significantly reduces carbon emissions

Increased Beneficiation (Ore to Refined Material) Within Tanzania

- Vertical integration provides ability for the country to capture increased value benefits of sovereign natural resources
- Government of Tanzania is a 16% shareholder in the Kabanga Project

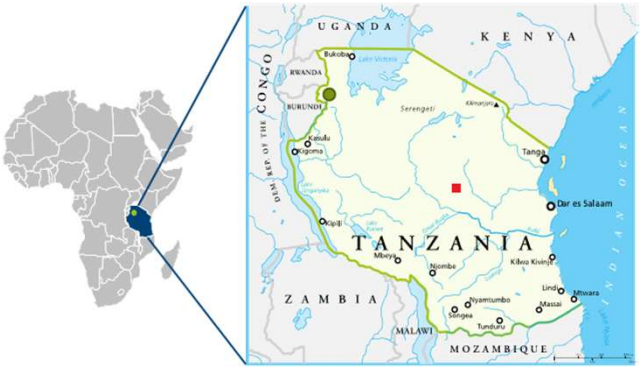

1 –69.713% of the Kabanga Mineral Resource Estimates as of 15 February 2023. The Kabanga Project's resource metrics reflect the measured, indicated and inferred resources referred to in the Kabanga Mineral Resource Estimates as of 15 February 2023 from the TRS, as set out on slide 20. 2 –Nickel Class 1 downstream processing CO2 eq. emissions baseline from 2020 Nickel Institute LCA. Estimated Kabanga refinery expected emissions from internal Company analysis. 3 –Expected reductions are lower for PGMs, as they utilize a more complicated flowsheet and are more energy intensive. For example, a study from EY Cova (an independent South African National Accreditation System accredited energy Measurement and Verification inspection body)found 46% lower emissions utilizing our Hydromet Technology compared to traditional smelting and refining (EY Cova studied PGM metals at the originally proposed 110 ktpa concentrate feed rate refinery at the Sedibelo plant site in South Africa under the then-applicable conditions in 2020 and assuming reagents not manufactured on-site; actual results could differ). Results will vary for specific PGM projects.

Kabanga is one of the world's largest and highest quality nickel deposits

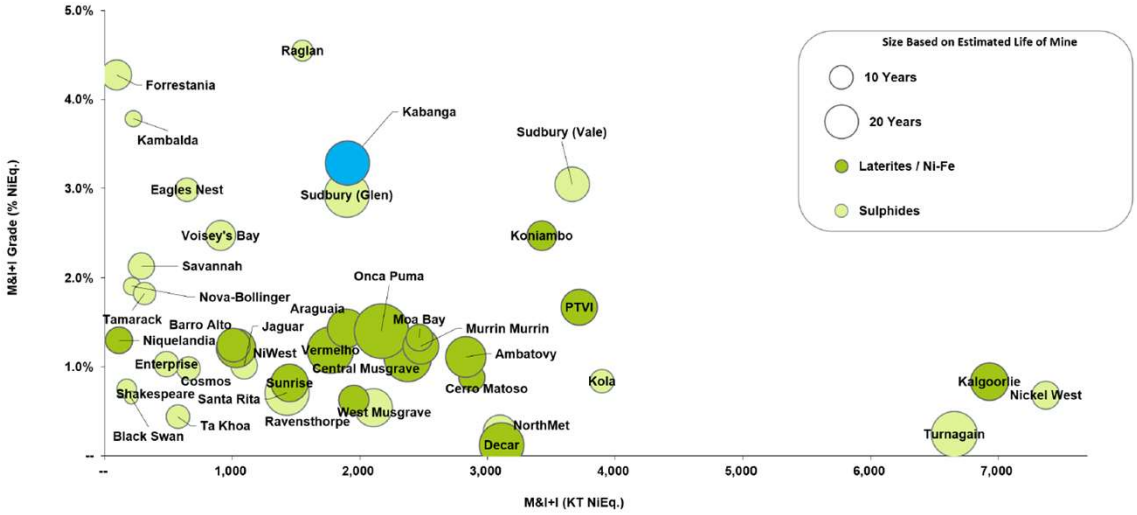

Source: S&P CapitalIQ Pro, as modified per public data on each mining project.
1 –NiEq. Values calculated using input prices of Nickel:$20,944/T, Copper $8,818/T and Cobalt $57,320/T, Chrome $4,409/T, Platinum $1,046/oz, Palladium $1,946/oz, Gold $1,798oz, Zinc $3,247/T, Silver $23.11/oz. No value was assigned for Iron. No additional recoveries or payabilties have been applied to published data.
2 –The Ni/NiEq% is based on nickels value in-situ versus the other elements according to the above pricing mechanisms.

Kabanga Deposit Overview

- More than $293 million spent by prior owners Glencore and Barrick to accurately delineate the ore body
- This enables the updated Feasibility Study to be produced on an accelerated timeframe

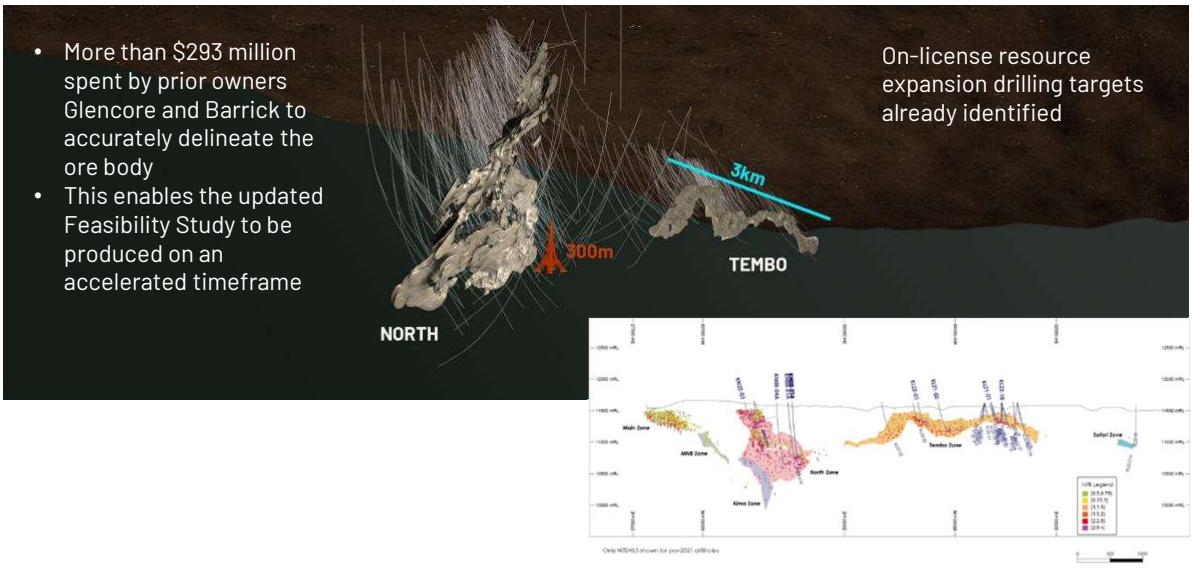

Historic Drilling

Years	Companies	Metres Drilled	Discovery (purpose)
1976 – 1979	UNDP Regional Exploration	20,068	Main zone
1991 – 1992	Sutton Resources	12,974	
1993 – 1995	Sutton – BHP JV	37,947	North zone
1997 – 1999	Sutton – Anglo American JV	56,227	
2000 – 2004	Barrick Gold Corporation	39,931	MNB zone
2005 – 2008	Glencore – Barrick Gold JV	64,957	North Deep zone (scoping study 1)
		81,256	Tembo zone (scoping study 2)
		242,347	Safari/Kima zones (prefeasibility study)
2008 – 2009		21,368	(feasibility study)
2011 – 2012	Glencore – Barrick Gold JV	5,303	
2014		3,320	
2021 – 2022	KNL	8,611	Tembo North (infill) and Safari
		4,163	Tembo and North (metallurgical)
Total		598,472	

Kabanga Nickel Project

Unlocking the Asset with Lifezone Metals Hydrometallurgy

Unlocking and refining Tanzania's nickel to refined products for export

KABANGA SITE
Mine + Concentrator Conceptual Layout

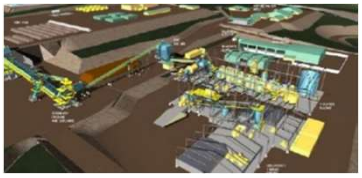

A processing alternative to shipping concentrate to smelters overseas

- In-country beneficiation
- Traceable production
- Equitable share of benefits with stakeholders
- Fewer metallurgical constraints

Concentrate Transport
Road transport of concentrate
From mine site to hydromet refinery
Distance: ~340 km
Avg. steady state vol: ~244,000 t p.a.

Refinery Waste Disposal
Road transport
Gypsum waste transported back to mine site to use as paste for underground backfill
Economic & environmental benefits

KAHAMA
Hydromet Refinery

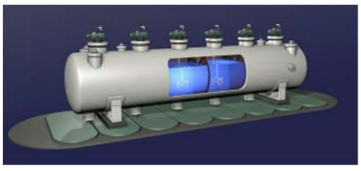

Refined End Product Transport
Containerised rail to export facility
Hydromet refinery to port
Kahama to Dar es Salaam
Distance: 970 km
High-purity Ni, Cu and Co end-products
Avg. steady state vol: ~40,000-60,000 t p.a.

REFINED PRODUCT EXPORT
High-Purity Ni, Cu & Co End-Products

Kabanga DFS and development status

- DRA Global Limited (DRA) has been appointed as the **principal consultant for the Definitive Feasibility Study**, and study work is underway across all technical disciplines
- The initial assessment assumes an **underground mining rate of 2.2 Mtpa**. The mining method is underground stoping with backfill, and the extracted mineralized material will feed into an on-site concentrator. Concentrate is assumed to be transported to an off-site hydrometallurgical processing facility to produce final nickel, copper, and cobalt metal, with transport of the final metal to Dar es Salaam and export to markets for sale
- **Metallurgical testwork** continues for the concentrator confirmation testwork and development of the refinery flowsheet. The scope of this work has been awarded to DRA Global's in-house hydrometallurgical specialist team.
- Results of **recent drilling largely consistent** with location, thickness, and tenor of previous results from historical drilling. Key intersections include KN08-04A; 21.90 m at 3.85% Ni and 4.74% NiEq from 1,075.30 m downhole and KN22-03; 39.83 m at 3.03% Ni and 3.65% NiEq from 244.10 m downhole
- Memorandum of Understanding ("MoU") signed with Tanzania Electric Supply Company Limited ("TANESCO") for **project power supply**
- **Environmental studies** progress for Kabanga mine and Kahama refinery

Hydromet processing for the Kabanga project

The full value of Kabanga as a key source of new high-purity nickel, cobalt and copper end products will be unlocked by low energy-intensity hydromet processing technology:

- Leaching metallic concentrates in aqueous medium
- Significantly reduces Class 2 emissions and transportation costs
- Has the potential to reduce overall electricity consumption
- Eliminates SO_2 emissions
- Reduction in CO_2 equivalent emissions

By adopting hydromet technology for processing nickel concentrate, Kabanga's environmental footprint is expected to outperform industry baselines[1]

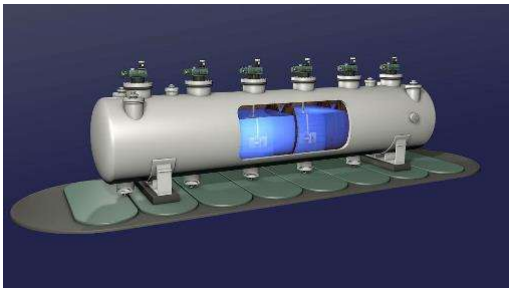

1 – CO_2 eq. emissions baseline from 2020 Nickel Institute LCA. Estimated Kabanga refinery expected emissions from internal Company analysis. conditions in 2020. This assumes reagents not manufactured on-site.

Pressure Oxidation Testwork (POX)

- Two POX leach tests completed February 2023 in the first phase of a currently ongoing testwork programme from comminution to metals separation and purification
- Aimed to provide a preliminary indication of refinery metal recoveries
- POX leach extractions for these non-optimised tests were:
  - **POX Test 1**

    99% nickel, 97% copper and 98% cobalt
  - **POX Test 2**

    99% nickel, 99% copper and 99% cobalt

Lifezone Hydromet Testwork – Metals Extraction Results

PGM-Au-Ni-Cu-Co Concentrate		Overall Recoveries into Solution (%)						
Sample ID	Type	Pt	Pd	Rh	Au	Ni	Cu	Co
	Kabanga Nickel Scoping Test Results - Test 1	-	-	-	-	98.5	96.9	97.5
	Kabanga Nickel Scoping Test Results - Test 2	-	-	-	-	99.7	99.6	99.8
A	UG2	99	97	93	99	97	93	99
B	UG2	99	98	96	97	95	96	83
C	Merensky	99	98	97	99	99	99	98
D	UG2-Merensky	99	98	96	99	98	99	93
E	Platreef	99	98	96	99	99	99	99
F	Platreef	98	99	97	96	99	99	99
G	Polymetallic Great Lakes	97	99	95	96	99	99	99
H	Polymetallic Great Lakes	99	99	-	99	99	99	99
I	UG2-Merensky	99	98	90	99	97	96	95
J	Polymetallic North America	95	99	-	99	99	99	98
K	Great Dyke	99	98	95	98	98	98	96
L	Great Dyke	99	98	89	99	99	99	96
M	Polymetallic Australia	99	99	-	92	99	99	93
N	Platreef	98	99	-	97	99	99	99
O	Platreef	97	93	93	94	99	99	98
P	Platreef	99	98	94	97	99	99	98
Q	Ni-Cu-Co Sulphide	-	-	-	-	98	99	99
	Mean	**98**	**98**	**94**	**97**	**98**	**98**	**96**

Au-Ag-Cu-Co-Zn-Pb-Sb Concentrate		Overall Recoveries into Solution (%)						
Sample ID	Type	Au	Ag	Zn	Pb	Cu	Co	Sb
1	High-grade carbonaceous polymetallic ore	91	95	99	95	98	-	-
2	Refractory gold concentrate	96	-	-	-	98	97	-
3	Refractory gold polymetallic concentrate	98	97	99	97	99	-	95
4	Double refractory Cu-Au concentrate	98	98	-	-	99	-	-
5	Refractory gold concentrate	98	98	-	-	-	-	-
	Mean	**96**	**97**	**100**	**96**	**99**	**97**	**95**

Liddell, K.S., Adams, M.D., Smith, L.A., and Muller, B 2019. Kell hydrometallurgical extraction of precious and base metals from flotation concentrates – Piloting, engineering, and implementation advances. Journal of the Southern African Institute of Mining and Metallurgy.

Kabanga Concentrate Treatment Plant (CTP) & Refinery

- **Kabanga Nickel 2014 feasibility study considered export of sulphide concentrate to commercial smelters, which is no longer allowed by the GoT**
- **CTP to be located at the site of the now depleted Buzwagi Gold Mine near Kahama, 35 km from the proposed rail loadout facility at Isaka.**
- **The CTP is expected to consist of the following process operations:**
  - pressure oxidation leaching through oxygen injection
  - solid-liquid separation followed by pre-neutralization, to remove excess free acid
  - copper separation using Solvent Extraction (SX)
  - metal recovery by Electrowinning (EW)
  - iron removal using limestone under aeration
  - nickel and cobalt separation and metal recovery using SX/EW
- **Final products are planned to be nickel and copper cathode and cobalt rounds**
- **Residues from the CTP at Kahama are planned to be be used as pastefill at Kabanga**

Addendum: Kabanga Mineral Resource Estimates as at 15 February 2023

Kabanga Historical Mineral Resource Estimates as of 15 February 2023
Based on $9.50/lb Nickel Price, $4.00/lb Cu and $26.00/lb Co[1][2][3][4][5][6][7][8]

Mineral Resource Classification	LZM	Grades				Contained Metal			
	Tonnage (Mt)	NiEq2023 (%)	Ni (%)	Cu (%)	Co (%)	NiEq2023 (M lbs.)	Ni (M lbs.)	Cu (M lbs.)	Co (M lbs.)
Measured	4.9	3.03%	2.34%	0.32%	0.20%	325	251	34	22
Indicated	2.2	2.20%	1.69%	0.22%	0.15%	108	83	11	7
Inferred	2.1	3.05%	2.41%	0.31%	0.18%	140	111	14	8
Tembo Total	**9.2**	**2.83%**	**2.20%**	**0.29%**	**0.19%**	**573**	**445**	**60**	**37**
Measured	4.7	3.37%	2.64%	0.35%	0.21%	348	273	37	22
Indicated	11.9	3.80%	3.05%	0.41%	0.21%	998	801	107	55
Inferred	12.0	3.29%	2.64%	0.35%	0.18%	868	698	93	48
North Total	**28.6**	**3.52%**	**2.81%**	**0.37%**	**0.20%**	**2,214**	**1,772**	**236**	**125**
Measured	-	-	-	-	-	-	-	-	-
Indicated	2.14	2.44%	1.92%	0.28%	0.15%	115	91	13	7
Inferred	-	-	-	-	-	-	-	-	-
Main Total	**2.14**	**2.44%**	**1.92%**	**0.28%**	**0.15%**	**115**	**91**	**13**	**7**
Measured	-	-	-	-	-	-	-	-	-
Indicated	-	-	-	-	-	-	-	-	-
Inferred	0.51	1.98%	1.52%	0.20%	0.13%	22	17	2	2
MNB Total	**0.51**	**1.98%**	**1.52%**	**0.20%**	**0.13%**	**22**	**17**	**2**	**2**
Measured	9.6	3.20%	2.49%	0.34%	0.21%	673	525	71	43
Indicated	16.3	3.40%	2.71%	0.36%	0.19%	1,221	974	131	70
Inferred	14.6	3.21%	2.57%	0.34%	0.18%	1,031	826	109	58
Total	**40.4**	**3.28%**	**2.61%**	**0.35%**	**0.19%**	**2,925**	**2,325**	**311**	**171**

Attributable resources presented above exclude effect of BHP's October 2022 investment agreement to increase ownership in Kabanga Nickel from 8.9% to 17.0%

1 – Historical Mineral Resource reported in the TRS with effective date 15 February 2023. 2 – The TRS QPs have not done sufficient work to classify the Historical Mineral Resource estimates as current estimates of mineral resources and LHL is not treating the estimates as current estimates of mineral resources. 3 – Mineral Resources are reported exclusive of Mineral Reserves. There are no Mineral Reserves to report. 4 – Mineral Resources are reported showing only the LHL attributable tonnage portion, which is 69.713% of the total. 5 – Cut-off uses the NiEq22 using a nickel price of ($20,943 per metric ton), copper price of ($8,818 per metric ton), and cobalt price of ($57,320 per metric ton) with allowances for recoveries, payability, deductions, transport, and royalties. NiEq22% = Ni% + Cu% x 0. 411 + Co% x 2.765. 6 – The point of reference for Mineral Resources is the point of feed into a processing facility. 7 – All Mineral Resources in the TRS were assessed for reasonable prospects for eventual economic extraction by reporting only material above a cut-off grade of 0.58% NiEq22. 8 – Totals may vary due to rounding.

Acknowledgements

Lifezone Metals
Government of Tanzania
BHP
Simulus Engineers & Laboratories
DRA Global
Orewin
Various other consultants

Disclaimer

LOW CARBON NICKEL AND COBALT PRODUCTION FROM NICKEL SAPROLITE ORES USING THE ATLAS MATERIALS PROCESS

By

Jeremy Ley, David Dreisinger

Atlas Materials, DE, USA

Presenter and Corresponding Author

David Dreisinger
David.dreisinger@atlasmaterials.com

ABSTRACT

The demand for nickel and cobalt battery materials for transport is poised to increase exponentially. The natural resource to meet this demand is the large global resource base of saprolitic nickel ores.

Atlas Materials have developed an innovative hydrometallurgical extraction process using hydrochloric acid leaching. The application of hot hydrochloric acid produces a residue that can be used as a supplemental cementitious material. The nickel, cobalt and magnesium containing leachate can be processed through a series of precipitation steps including (1) iron and aluminum removal, (2) mixed hydroxide precipitation for recovery of nickel and cobalt, (3) manganese rejection by oxidation/precipitation and finally (4) magnesium hydroxide precipitation. The precipitating agent is sodium hydroxide. At the end of the circuit, the spent electrolyte is essentially concentrated sodium chloride solution. This solution may be used as an input to a chlor-alkali facility to produce chlorine and hydrogen and caustic (NaOH). The chlorine and hydrogen are burned to make hydrochloric acid for recycle to leach. In this way, the chemical consumption of the process is low (mainly makeup NaCl). The process requires supply or renewable electricity for salt splitting. The overall process produces low carbon nickel and cobalt to supply the EV battery sector.

The bench and pilot plant results for this process will be presented.

Keywords: Nickel, cobalt, MHP, saprolite, low carbon, chlor-alkali

INTRODUCTION

The decarbonization of the global energy and transport sectors is accelerating. The decarbonization of the transport sector is in full swing with accelerating uptake of electric and hydrogen powered vehicles. Power generation from wind and solar sources is increasing, and storage of electricity to stabilize grid power dependent on renewables is advancing.

The demand for raw materials to enable many of the emerging transformative technologies is increasing rapidly. Specifically, lithium, nickel, cobalt, and manganese are required for lithium-ion battery manufacture, and rare earth elements are needed for electric vehicle traction motors and wind turbines. Further, when recovering critical raw materials for future use, the extraction industry must focus on zero waste production. All by-products/co-products should be considered for use rather than storing in liquid or solid waste impoundments. Lastly, and perhaps most importantly, recovery of critical materials should be performed to produce a “low carbon” product, i.e. the best outcome would be to provide for future supply while creating pathways to remove carbon from the atmosphere.

Atlas Materials was founded to develop innovative technologies for critical materials supply, with by-products to enable an overall low carbon outcome. Technology development has focused on treatment of nickel saprolite ores. Nickel saprolite ores contain magnesium silicate or magnesium hydroxy silicate minerals in addition to nickel and cobalt, iron. and other minor elements. The vision of Atlas is to process these materials for nickel and cobalt battery material supply, silica products carrying iron and aluminum for material substitution in the cement industry, and magnesium hydroxide. Magnesium hydroxide from the NEM process may be used in the future to sequester atmospheric carbon dioxide using a variety of processes.

The NEM general process flowsheet is shown below (Figure 1). The process involves a series of mineral processing and hydrometallurgical steps.

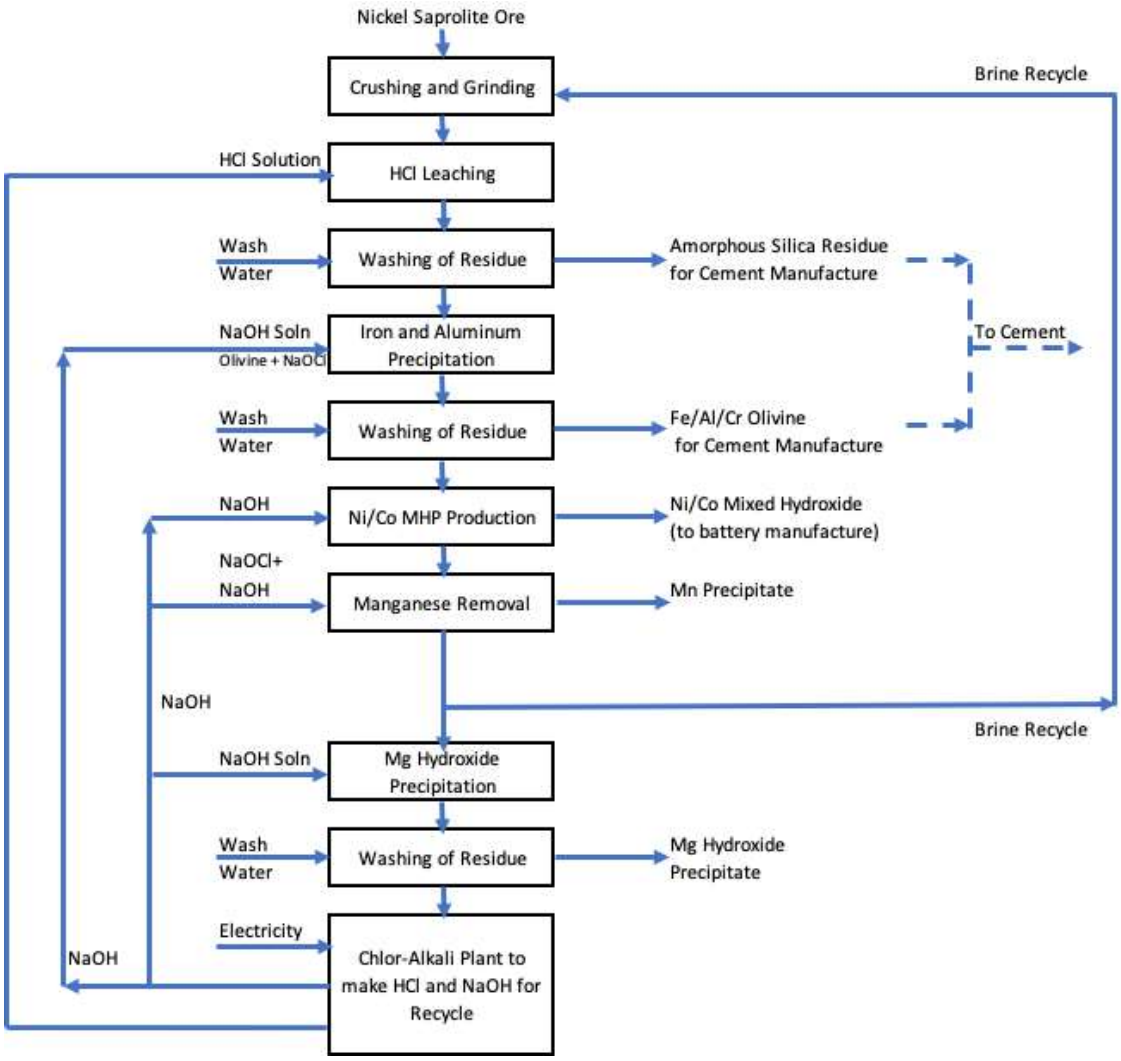

Figure 1: The ATLAS Simplified Process Flowsheet

Crushing and Grinding

Crushing and grinding in recycle brine solution containing a variety of chloride salts including magnesium chloride and sodium chloride. The purpose of recycle of a brine solution is to avoid the addition of water which can only be managed by evaporation which is expensive in terms of energy.

HCl Leaching

This process uses HCl at high strength (typically 36% HCl by weight in water; a typical product from an HCl production facility attached to a chlor-alkali plant). The raw materials contain a variety of silicate minerals including magnesium, iron, nickel, cobalt, and minor impurity elements.

The chemistry is therefore comprised of the following major reactions:
$Mg_2SiO_4 + 4HCl = 2MgCl_2 + SiO_2 + 2H_2O$
$Ni_2SiO_4 + 4HCl = 2NiCl_2 + SiO_2 + 2H_2O$
$Fe_2SiO_4 + 4HCl = 2FeCl_2 + SiO_2 + 2H_2O$

Note other minerals present such as iron oxides or aluminum oxides may also react with HCl to form additional salts in solution.

$FeO(OH) + 3HCl = FeCl_3 + 2H_2O$
$AlO(OH) + 3HCl = AlCl_3 + 2H_2O$

Note that natural minerals are not pure compounds. The minerals may contain a variety of elements (eg. Mg, Ni, Co, Fe in one silicate mineral) and may be hydrated or weathered. Suitable feed materials include;
A. Nickel saprolite ores
B. Olivine ores
C. Asbestos ores and tailings

The leaching temperature is close to the boiling point to ensure rapid extraction. Acid addition ranges from 500 to 1000 kg HCl per dry tonne of solid feed and will vary with the chemical composition of the feed. The brine recycle solution in the flowsheet below ensures that acid leaching is performed with a high total salt content as, for example, NaCl or $MgCl_2$ or both.

The leaching time can vary from 1 hour to 8 hours. The leaching can in principle be arranged as a single stage or two stage process. Single stage means that the acid and ore are added together and allowed to react at temperature to completion, while two stage means that fresh ore is contacted with partly reacted solution to maximize the consumption of acid (low terminal acidity) and in the second stage, the partly leached ore (from the first stage) is contacted with high acid to maximize extraction of Mg/Ni/Co/Fe, etc. The two-stage process requires an additional solid/liquid separation step to ensure countercurrent movement of solids and liquids.

The products of HCl leaching are a weakly acidic solution containing various chloride salts and a silica rich residue recovered as a solid product. This residue is washed to remove salts and excess acid with fresh water and then may be directed to cement manufacture where the silica is used as a replacement for other materials (thus lowering the carbon intensity of cement manufacture) and a strengthener to improve the yield strength of concrete (high performance concrete).

Iron and Aluminum Removal

The iron and aluminum content in the solution may be precipitated in two ways. First, sodium hydroxide may be added to form a mix of oxide and hydroxide solids. Secondly, the pH may be raised by addition of ground olivine mineral to precipitate the metal impurities.

The NaOH solution may be added as a 50% solution and may be diluted with recycle brine solution for process convenience and enhanced pH control (it may be difficult to control pH by adding such a strong base). The NaOH neutralizes the excess acid and precipitates Fe/Al and other trivalent cations if present, according to the following reactions:

$HCl + NaOH = NaCl + H_2O$
$FeCl_3 + 3NaOH = FeO(OH) + 3NaCl + H_2O$
$2FeCl_3 + 6NaOH = Fe_2O_3 + 6NaCl + 3H_2O$

$AlCl_3 + 3NaOH = AlO(OH) + 3NaCl + H_2O$
$2AlCl_3 + 6NaOH = Al_2O_3 + 6NaCl + 3H_2O$
$CrCl_3 + 3NaOH = CrO(OH) + 3NaCl + H_2O$
$2CrCl_3 + 6NaOH = Cr_2O_3 + 6NaCl + 3H_2O$

The pH adjustment is conducted with stoichiometric amounts of NaOH. Over addition will result in precipitation of Ni/Co (undesirable) so careful control of addition must be maintained. The temperature will be 75 °C to the boiling point. Seed (precipitate) may be recycled to ensure growth of suitable sized particles for enhanced solid/liquid separation. Precipitation time can be 1 to 8 hours. NaOH is added progressively through the precipitation tanks (continuous) so as to enhance precipitation of coarser/separable precipitates. The product undergoes S/L separation and washing.

The iron and aluminum removal process with sodium hydroxide addition may be performed in a two stage arrangement to allow recycle of the second stage precipitate to the leaching section to minimize any nickel and cobalt loss and to maximize the removal of iron, aluminum and chromium. Further, if the iron is partly in the ferrous state, a small amount of sodium hypochlorite may be added to oxidize residual ferrous to the ferric state.

The addition of olivine may be used as an alternative to addition of NaOH. Olivine with a high magnesium content is desired.

$4HCl + Mg_2SiO_4 = 2MgCl_2 + 2H_2O$
$4FeCl_3 + 3Mg_2SiO_4 + 2H_2O = 4FeO(OH) + 6MgCl_2 + 3SiO_2$
$4AlCl_3 + 3Mg_2SiO_4 + 2H_2O = 4AlO(OH) + 6MgCl_2 + 3SiO_2$
$4CrCl_3 + 3Mg_2SiO_4 + 2H_2O = 4CrO(OH) + 6MgCl_2 + 3SiO_2$

Olivine often contains nickel, cobalt and iron. These elements will also react with the acidic leachate. Nickel and cobalt extraction from olivine is beneficial to the production of nickel and cobalt as hydroxide. Iron may extract as ferrous iron from olivine and with the addition of sodium hypochlorite may be oxidized to precipitate. Finally, the extraction of magnesium will lead to a higher overall production of magnesium hydroxide.

Nickel and Cobalt Recovery

Nickel and cobalt are present in solution as $NiCl_2$ and $CoCl_2$ salts. The recovery of Ni/Co can be done in many ways including the direct precipitation of mixed hydroxide precipitate. This can be done directly from the solution coming from the iron precipitation.

$NiCl_2 + 2NaOH = Ni(OH)_2 + 2NaCl$
$CoCl_2 + 2NaOH = Co(OH)_2 + 2NaCl$

Other metals will also precipitate with the Ni/Co in minor amounts, such as Mn and Fe (remaining iron in solution). If an excess of sodium hydroxide is added, then magnesium will co-precipitate as magnesium hydroxide. The selectivity of MHP precipitation can be enhanced by using two stage MHP precipitation. The second stage precipitate is recovered and recycled to the first stage MHP precipitation process or to the discharge from the main leaching step (where acid is present to redissolve the Ni/Co and other metals from the second stage leach).

The mixed hydroxide precipitate is recovered by S/L separation and washing. A pressure filter is often used with a “squeeze” cycle to minimize the entrained moisture in the washed MHP cake prior to shipping.

The precipitation is carried out between 25- 90 °C and terminal pH is in the range of 5-8. Note that pH measurement is difficult in a strong salt solution, and sodium hydroxide addition may also be controlled by stoichiometry. The precipitation time is 1-8 hours. Seed recycling is used to maximize particle size and minimize contamination. The process (as in all steps) is conducted continuously.

Manganese Removal

Manganese is an undesirable impurity in magnesium hydroxide, and cannot be selectively precipitated as a hydroxide in the presence of magnesium hydroxide. Accordingly, oxidation and precipitation is used to remove manganese from solution.

$MnCl_2 + NaOCl + 2NaOH = MnO_2 + H_2O + 3NaCl$

The manganese dioxide precipitate is filtered and washed.

Magnesium hydroxide precipitation

The remaining magnesium in solution is precipitated by addition of NaOH to form $Mg(OH)_2$.

$MgCl_2 + 2NaOH = Mg(OH)_2 + 2NaCl$

This can be done by adding NaOH to $MgCl_2$ solution or by reversing the order of addition. The goal is to provide a near complete removal of Mg as $Mg(OH)_2$ from solution, requiring a near stoichiometric addition of NaOH.

Chlor-Alkali plant

The final solution is NaCl and H_2O with some minor contaminants in solution. This solution is directed to a chlor-alkali plant for manufacture of NaOH, Cl_2, and H_2. This involves many steps. The Cl_2 and H_2 can be burned and water-scrubbed to form strong HCl solution for recycle to leaching.

The excess heat from combustion may be recovered as steam and used to evaporate excess water from solution.

EXPERIMENTAL RESULTS

Raw Materials for Leaching

The three types of raw materials used in this study were obtained from various sources. Table 1 shows the elemental composition of the raw materials tested. The asbestos tailing was obtained from a tailing deposit in Quebec. Olivine (used as a foundry sand material) was provided by Essix Resources under the trade name Incast75.

The nickel and cobalt content of the material increases from asbestos tailing to olivine to nickel saprolite samples. Iron levels are variable from ~5% for the olivine sample up to 18% for the saprolite. The magnesium content was highest for olivine at 29.79% and only 12.2% for nickel saprolite. The silicon content varied over a narrow range of 15.6 to 19.49% Si.

Table 1. Composition of Raw Materials for Extraction

Analysis(%)	Asbestos Tailing	Olivine	Nickel Saprolite #1	Nickel Saprolite #2
Ni	0.239	0.34	1.81	1.83
Co	0.011	0.011	0.052	0.02
Cu	0.0019	0.002	0.005	NA
Zn	0.0019	0.004	0.02	NA
Fe	7.51	5.13	18.0	8.39
Mg	22.2	29.79	12.2	17.4
Al	0.5	0.19	2.19	0.50
Cr	0.25	0.28	0.78	0.43
Mn	0.07	0.08	0.65	0.14
Ca	0.26	0.08	0.33	0.22
Si	16.5	19.49	15.6	18.1
Na	0.06	0.04	0.02	0.03
S	NA	NA	0.02	NA

The samples were either used as received or ground to finer size as required.

HCl Leaching Test Results

A series of HCl leaching tests was performed to assess the extraction of the key elements (Ni/Co/Mg/Fe/Al) and the quality of silica residue produced as a product.

The leach extractions were most sensitive to the acid addition reported as kg HCl/tonne of material. The basis is kg HCl on a 100% basis and per tonne of dry ore (Figure 2). The nickel extraction for the saprolite sample (Figure 2) approached 100% at ~750 kg HCl/t of ore. Iron and magnesium

extractions were slightly lower. It was feasible to produce ≥75% SiO_2 content in the residue at the 750 kg HCl/t addition rate.

The olivine extraction results (Figure 3) showed very similar extractions of Ni/Mg/Fe, consistent with the uniform mineralogy of the olivine sample. The acid required to reach maximum extraction was nearly 1200 kg HCl/t ore due to the more basic character of the olivine. The SiO_2 grade of the leach residue exceeded 80%.

The results of the leaching of asbestos tailings (Figure 4) showed very high Ni/Mg/Fe extractions at +800 kg HCl/t. The SiO_2 grade again exceeded 80% in concert with high base metal extractions.

The batch leaching results showed that a variety of raw materials could be treated with suitable levels of HCl to maximal extraction of the key metals and production of a silica rich residue.

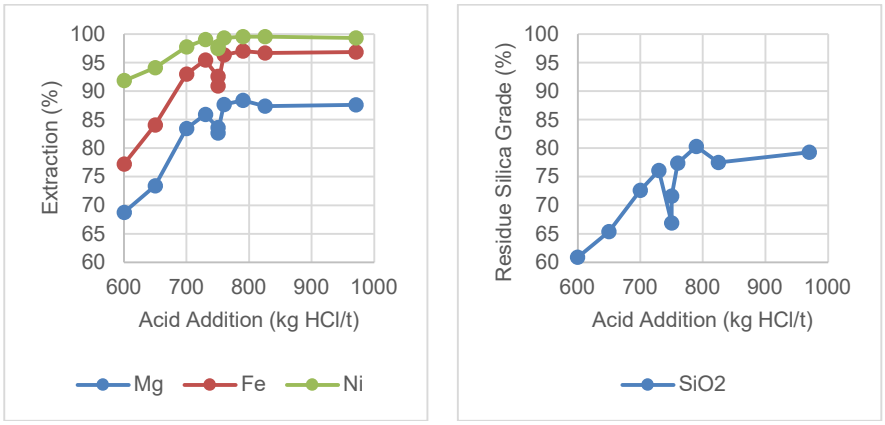

Figure 2. Batch leaching of saprolite #1. Typical conditions: Temperature 100 °C, 4 h, 87 g/L Mg (as $MgCl_2$)

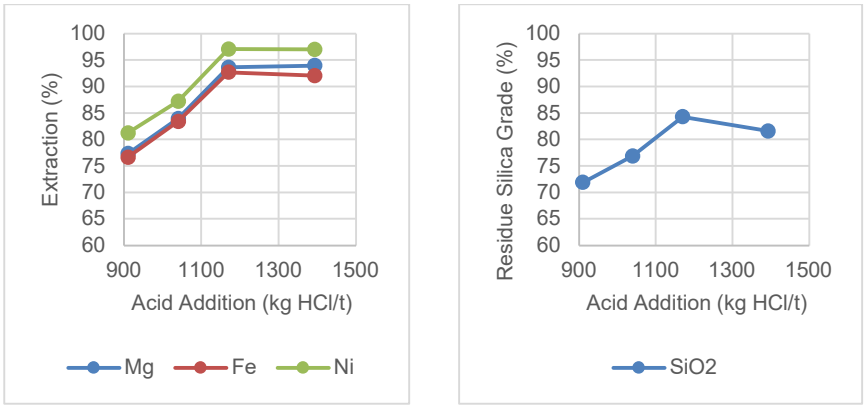

Figure 3. Batch leaching of olivine. Typical conditions: Temperature 100 ºC, 4 h, 87 g/L Mg (as $MgCl_2$)

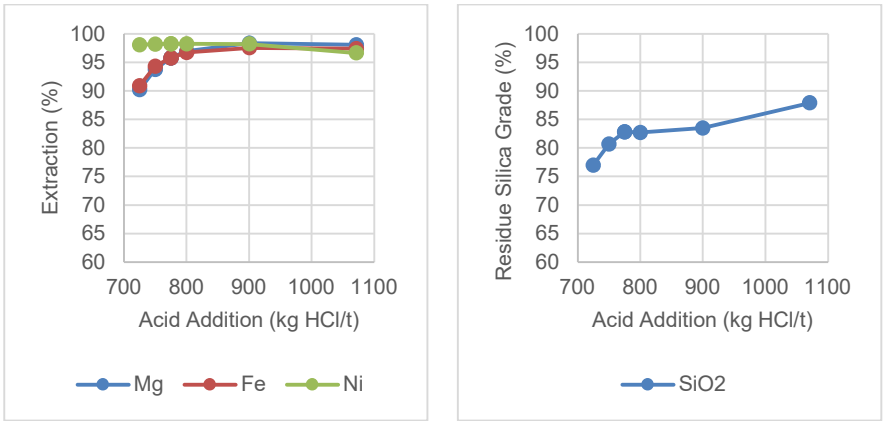

Figure 4. Batch leaching of asbestos tailings. Typical conditions: Temperature 100 ºC, 4 h, 87 g/L Mg (as $MgCl_2$)

Cementitious Properties of the Leach Residues

An extensive study of the cementitious properties of the leach residues is currently being conducted by the LMC laboratory EPFL (Lausanne, Switzerland). The micro-silica leach residue product has a reactivity similar to fly ash. This is important as fly ash availability will decrease over time with reduced use of carbon-based fuels. Micro-silica can be used to replace fly ash. Further testing has shown that with up to 30% substitution for Ordinary Portland Cement (OPC) the compressive strength of mortars is unaffected, the compressive strength of concrete is increased 14-19% and the concrete containing Atlas micro-silica has a 10-fold improvement in chloride penetration resistance compared to reference OPC.

Batch Testing of the Downstream Process Operations

In addition to an extensive series of batch leach tests, the downstream operations were also tested step by step in a series of further experiments. **Error! Reference source not found.** below shows the changing composition of solutions within the sequential unit operations in the NEM flowsheet.

Table 2. Solution Compositions (mg/L) Through Downstream Unit Operations (Leach = HCl Leach, IR = Iron Removal with NaOH addition, MHP = Mixed Hydroxide Precipitation, MnR = Manganese Removal, MP = Magnesium Hydroxide Precipitation)

Operation	Leach	IR	MHP	MnR	MP
Mg	69600	63000	68800	62300	3.1
Ni	3370	2210	300	1.7	0.6
Fe	36900	3.6	0.3	0.2	0.5
Al	3470	10	0.2	0.2	0.2
Mn	750	640	630	0.05	0.05
Na	24	25500	27400	25200	125000

The leach solution contains over 3 g/L of Ni and high levels of Mg, Fe, and Al. The IR solution shows very low terminal Fe and Al concentrations and somewhat reduced Ni concentration, a consequence of some dilution due to base addition and some co-precipitation of Ni. The sodium level is increased due to NaOH addition, while manganese is diluted to 640 mg/L Mn in solution. The MHP (primary) solution shows very low Fe/Al and significant reduction in Ni. This experiment produced a high grade MHP product (+40% Ni on a dry basis). The MnR solution shows an excellent rejection of Mn from solution (to 0.05 mg/L of Mn) by oxidation and pH adjustment. Further, the MP precipitation results show very low residual content of Mg, Ni, Fe, Al, and Mn. The final concentration of Na was 125 g/L Na, corresponding to 318 g/L NaCl. This brine would undergo further treatment in a conventional chlor-alkali circuit to polish minor contamination before electrolysis.

In more recent testing of the iron removal process using olivine addition with hypochlorite addition to oxidize iron, excellent results were obtained with respect to extent of removal of iron, aluminum and chromium. A leach filtrate was mixed with ground olivine mineral slurry (40% solids) at 70 °C for 2 h. A small amount of sodium hypochorite solution (11% NaOCl) was added to maintain +700 mV ORP. The results are summarized in Table 3.

The nickel content of the solids dropped from 0.34% Ni to 0.19% Ni with approximately 17% weight gain due to iron and aluminum precipitation. There was net extraction of nickel from olivine. Iron was reduced from 24.2 g/L to 0.2 mg/L, aluminum dropped from 571 to <0.2 mg/L and chromium dropped from 274 to <0.2 mg/L indicating quantitative removal of the three impurities. Accordingly, the residue composition increased in iron, aluminum, and chromium while the magnesium content dropped from 29.79% to 13.4%.

Continuous Pilot Plant Results

A continuous pilot plant was established at SGS Canada to integrate the key elements of the process, from ground ore feed to the production of silica residue, iron/aluminum precipitate, mixed hydroxide of nickel and cobalt, manganese precipitate, and finally magnesium hydroxide precipitate. The barren solution after magnesium removal is also a product but in this case for recycle through a chlor-alkali facility for manufacture of sodium hydroxide and hydrochloric acid supply.

Table 3. Olivine Precipitation of Iron, Aluminum and Chromium from Laterite Leach Solution

Sample	Leach Soln (mg/L)	INCAST75 (%)	Filtrate (mg/L)	Wash (mg/L)	Residue (%)
	520 mL	60 g	508 mL	1902 mL	70 g
Ni	5670	0.34	4920	358	0.19
Fe	24200	5.13	0.2	0.2	21.8
Mg	64600	29.79	71300	4910	13.4
Al	571	0.19	<0.2	5.2	0.58
Cr	274	0.28	<0.2	<0.2	0.41
Si	40.7	19.49	37.1	7.1	16.08
Na	17300	0.04	15600	1170	0.05

The pilot plant was run on a prepared sample of ground saprolite (Table 1) with grinding performed in recycle brine solution. Leaching was performed with ~750-800 kg HCl/t feed material and 95 °C for 10 days total (two periods of 5 days). The leach slurry was collected and filtered in a pressure filter to recover the silica residue and the leach solution was directed to primary neutralization. A hematite-rich seed slurry was added to the feed solution as it entered four stages of neutralization with NaOH solution. The slurry product was thickened and the thickener UF was divided into seed recycle and final product. The primary neutralization thickener overflow was sent through secondary neutralization (four stages followed by thickening), where additional NaOH solution was added. The secondary neutralization thickener UF was recycled to leaching and the OF was directed to MHP production. MHP production was performed in two stages (primary and secondary), and the second stage MHP thickener UF was recycled to leaching. The MHP thickener OF was sent to manganese removal. This was performed by oxidation with NaOCl and pH adjustment (with caustic addition) to form a manganese oxide product. Finally, the manganese free filtrate advanced to magnesium hydroxide precipitation with sodium hydroxide addition.

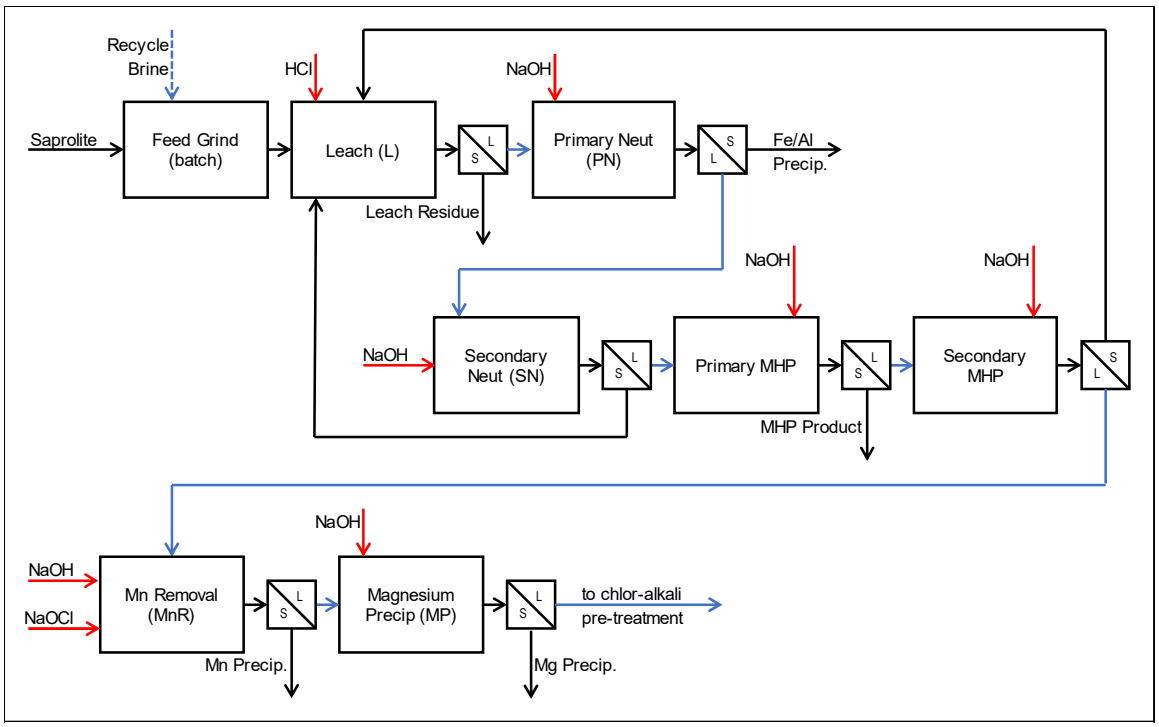

Figure 5. Overall flowsheet of the continuous pilot plant

Saprolite Leaching. The pilot plant operation was divided into 18 periods over which data was collected and mass balances calculated. **Error! Reference source not found.** shows metal extraction version time over these periods. The extraction of Ni in the saprolite leaching process was generally in the range of 96-99%. The Fe extraction was slightly lower and the Mg lower again. The acid addition rate was varied during the run and the changing extraction results are reflected by an

increase or decrease in acid addition. The reported extractions are calculated by the Si-tie method where Si is assumed to be insoluble.

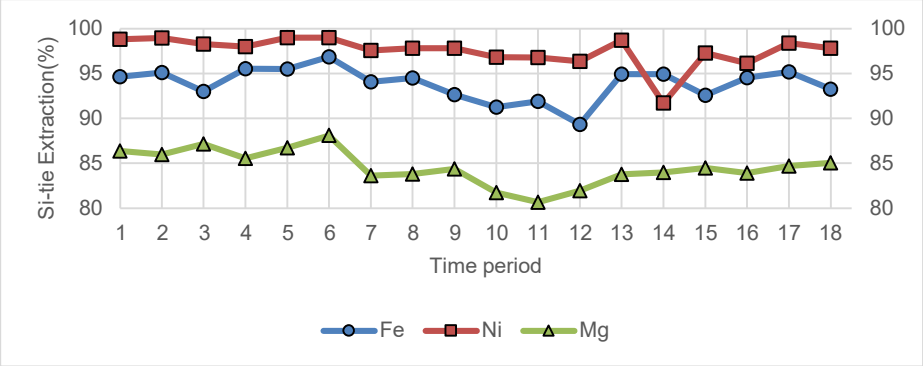

Figure 6. Saprolite leaching results over the 18 time periods of the pilot plant operation

Primary Neutralization. The primary neutralization results are shown in **Error! Reference source not found.** and **Error! Reference source not found.**. The iron removal results are consistent at nearly 100% efficiency. The aluminum removal results showed an increase toward the end of the pilot plant with a commensurate rise in nickel coprecipitation. The nickel in the primary neutralization residue is lost from the circuit so better control is required to avoid a nickel loss while still removing sufficient Al in this step. Aluminum precipitation is an indicator of potential nickel loss. It is important to not over-add NaOH at this stage, otherwise nickel loss will increase. The solid assay from the primary neutralization circuit showed a plateau of approximately 80% Fe_2O_3 with 5.5% Al_2O_3 and 4% Cl. The iron and aluminum precipitates are hydrated and the chloride in the residue is likely due to formation of hydroxy chloride precipitates of iron and aluminum.

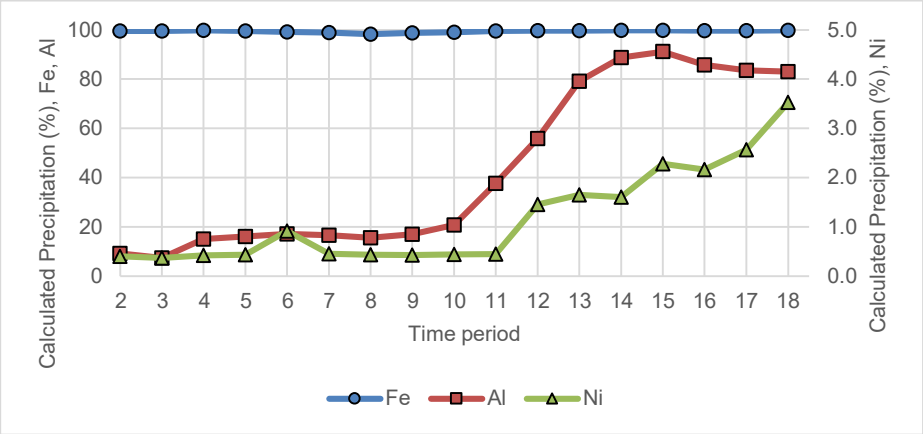

Figure 7. Primary neutralization calculated precipitation

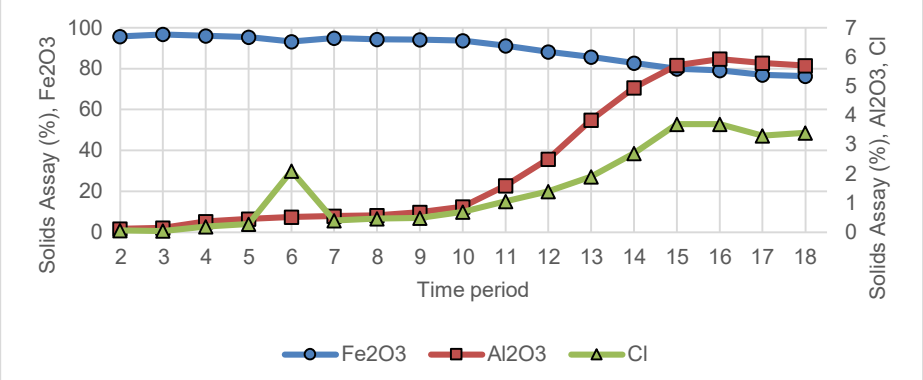

Figure 8. Primary neutralization solids assay

Secondary Neutralization. The secondary neutralization results (**Error! Reference source not found.** and **Error! Reference source not found.**) show excellent removal of iron and aluminum. However, if aluminum removal is too efficient, the precipitation of nickel increases. This is not a

problem in the sense that the secondary neutralization residue is recycled and nickel is releached. However, the nickel needs to move downstream to MHP precipitation, and therefore nickel coprecipitation and aluminum removal have to be kept in balance to avoid excessive nickel buildup in the Leach-Secondary Neutralization part of the circuit. This was an important learning from the pilot plant.

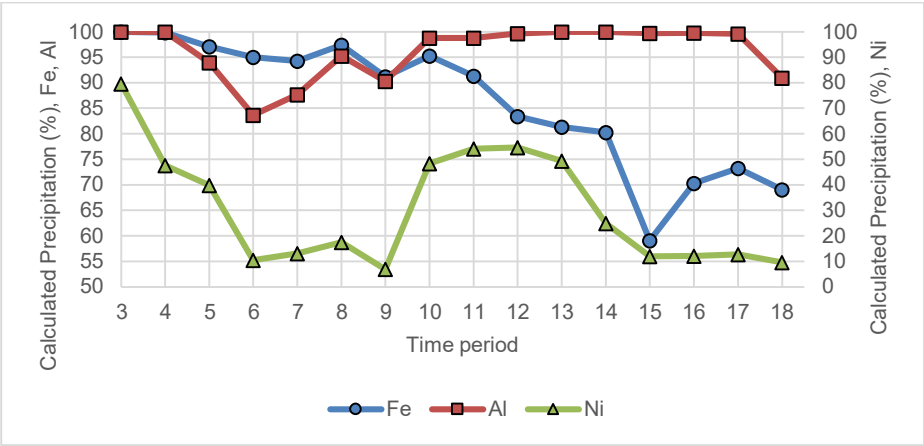

Figure 9. Secondary neutralization precipitation efficiency

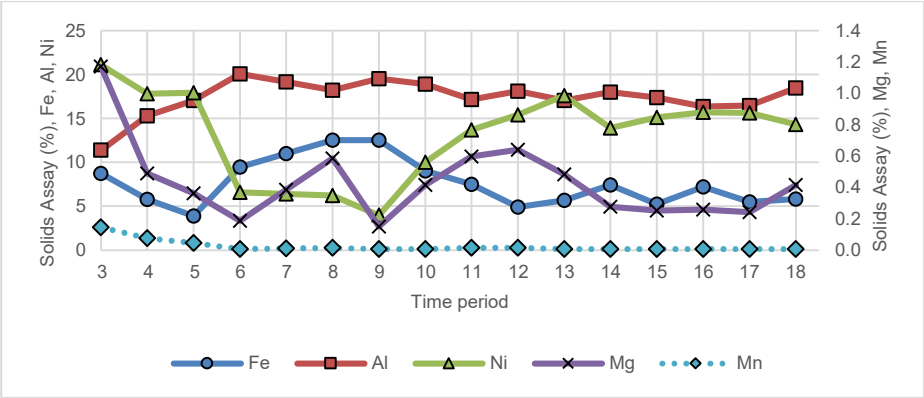

Figure 10. Secondary neutralization solids assay

Primary and Secondary Mixed Hydroxide Precipitation. The primary mixed hydroxide precipitation results (**Error! Reference source not found.** and **Error! Reference source not found.**) showed that nickel could be precipitated to form high grade MHP at as high as ~40% Ni on a dry basis (periods 5-8). The results also show the need for effective control of NaOH addition. During periods 9-18, excess NaOH was added, leading to increased precipitation of Mg and some Mn. The stability of this circuit is impacted by the upstream process steps and especially by the recycles of nickel and cobalt back to leach. Further, the measurement of pH in the strong brine solution as a measure of control is difficult and impacts the control of the MHP circuit. Future pilot plant operations will have improved pH electrode sensors and control.

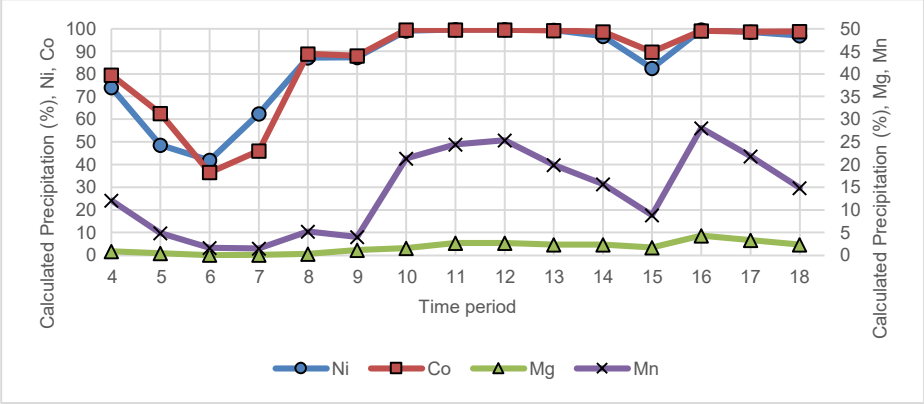

Figure 11. Primary mixed hydroxide precipitation efficiency

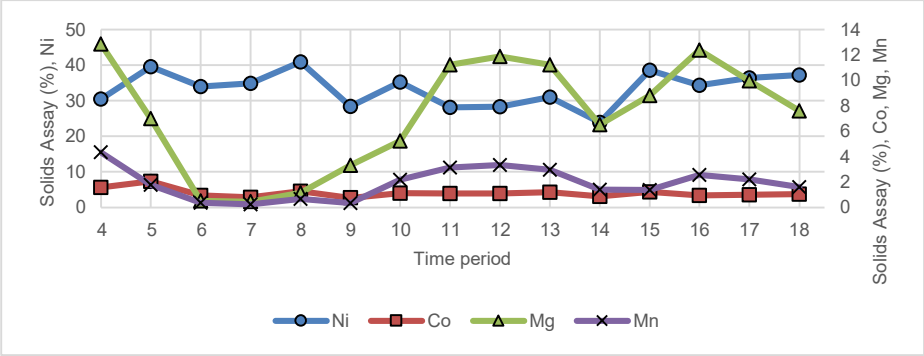

Figure 12. Primary mixed hydroxide precipitation solid assay

The secondary mixed hydroxide precipitation results (**Error! Reference source not found.** and **Error! Reference source not found.**) generally show the effective capture of residual nickel arriving from the primary mixed hydroxide circuit. Again, the correct dosage and control of NaOH addition is a critical issue moving forward with the process scaleup. Under-addition of NaOH will result in loss of soluble Ni and Co to the manganese removal circuit while over-addition will cause the precipitation of Mg and Mn.

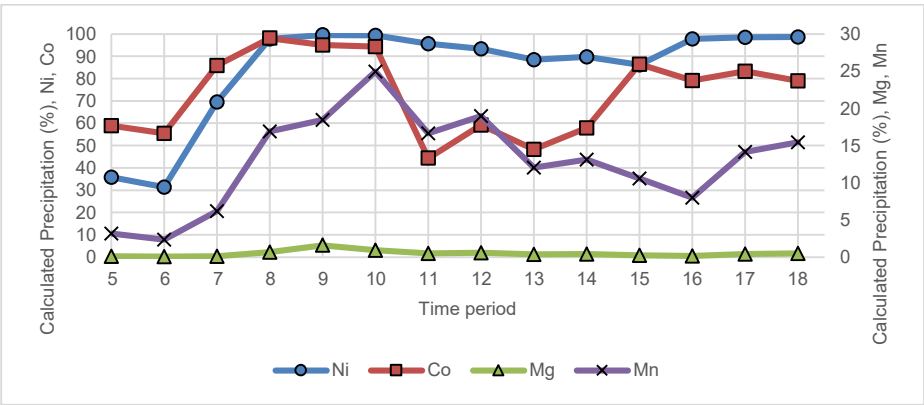

Figure 13. Secondary mixed hydroxide precipitation efficiency

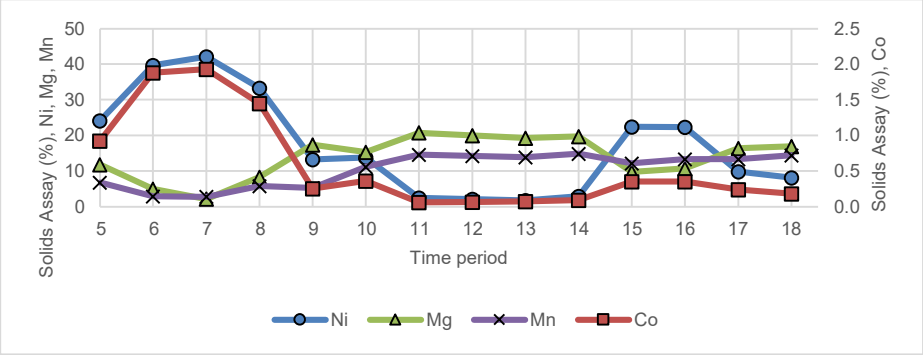

Figure 14. Secondary mixed hydroxide precipitation solids assay

Manganese Precipitation. The manganese removal circuit (**Error! Reference source not found.** and **Error! Reference source not found.**) was stable and yielded very high levels of manganese removal by effective oxidation and pH adjustment. Small levels of magnesium precipitation occurred through the operation, unavoidable due to the elevated pH used for manganese removal. The operation between period 5 and 10 showed some nickel in the manganese precipitate, due to incomplete nickel removal in the secondary mixed hydroxide precipitation circuit. Beyond this point (periods 11 and beyond), the nickel in solution in the feed to manganese precipitation was very low and hence the content of the manganese precipitate was very low.

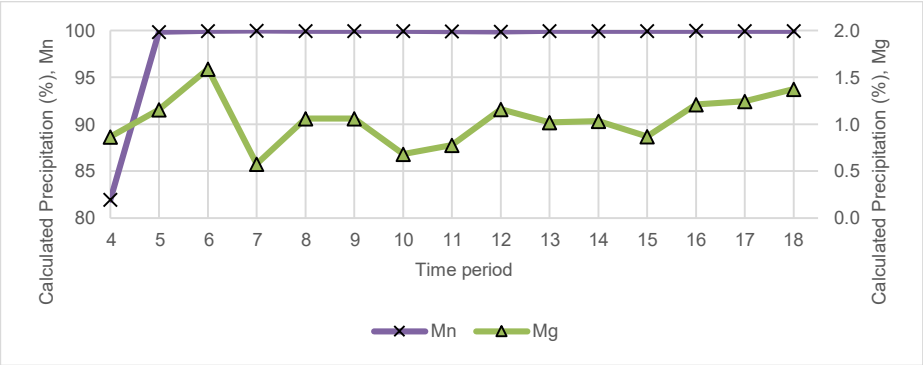

Figure 15. Manganese precipitation efficiency

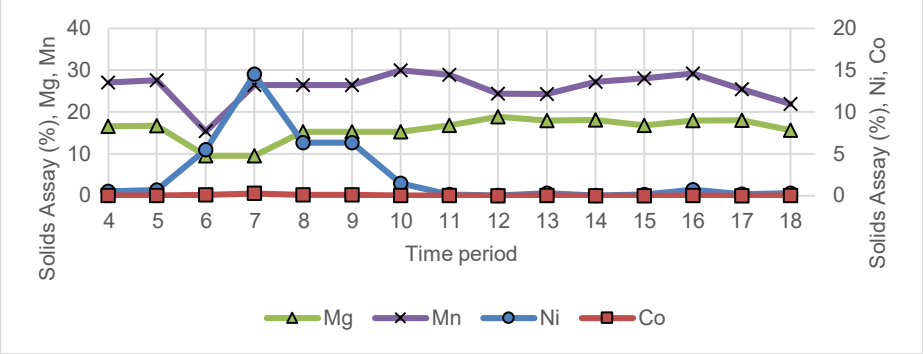

Figure 16. Manganese precipitation solids assay

Magnesium Precipitation. The magnesium precipitation results were excellent (Table 3). The magnesium precipitation circuit operated toward the end of the 10 day pilot plant run. The key impurity elements were generally very low except for chloride, which likely formed magnesium hydroxy chloride precipitates under startup conditions. Any of the other di- or tri-valent metals present in the feed to magnesium precipitation will co-precipitate with the magnesium. Magnesium precipitation efficiency was ~100%. The brine formed as a product from this process step is ideal as a feed to brine softening ahead of the chlor-alkali plant operation.

Table 4. Magnesium precipitate analysis.

Chemical Analysis (%)							
Sample	Fe	Al	Cl	Ni	Co	Mn	MgO

16	<0.01	0.02	4.4	<0.01	<0.01	<0.01	61.3
17	0.01	0.04	0.2	0.11	<0.01	0.01	63.1

CONCLUSIONS

Following an extensive bench test program, the Atlas Materials process was piloted on a sample of nickel saprolite ore for a total of 10 days. All the key metrics were achieved in the pilot plant operation.

- The leach extractions of nickel and cobalt were in the range of 96-99% in the primary HCl leach.
- The primary neutralization circuit removed iron and aluminum effectively with minimal co-precipitation of nickel and cobalt.
- The secondary neutralization circuit was effective at polishing residual iron and aluminum content from the solution prior to mixed hydroxide precipitation.
- The primary mixed hydroxide precipitation produced product grading up to 40% Ni on a dry basis. Under controlled conditions, co-precipitation of magnesium and manganese could be avoided. The testing highlighted the need to develop improved measurement of pH in the strong brine solutions used in this process so as to enhance control and selectivity of the key process steps.
- The secondary mixed hydroxide precipitation was effective at precipitating residual value metals.
- The manganese removal circuit utilizing oxidation and pH adjustment for precipitation was outstanding in performance with virtually 100% removal of manganese from solution.
- The magnesium precipitation process product was high grade and low in metallic impurities. The magnesium precipitation process is dependent on all of the upstream processes to produce a suitable precipitate product. The brine from the magnesium precipitation process was virtually free of any impurities and suitable as a source of NaCl brine to proceed to brine softening and chlor-alkali processing to regenerate HCl and NaOH for the process.

The silica leach residue from batch leaching of saprolite, olivine and asbestos tailing was evaluated as an additive to cement. The results confirmed that the leach residues were reactive and suitable for cement making.

A new unit operation has recently been developed and has been incorporated into the base flowsheet. Olivine may be added to the iron/aluminum removal stage to precipitate these elements. Excellent results have been achieved in batch testing. Residual iron/aluminum and chromium levels are in the range of <5 ppm in solution with negligible nickel co-precipitation.

The overall recovery of nickel and cobalt from the process is expected to be in the range of +95%. The MHP product is suitable for further post processing to produce battery material precursor materials to support the rapidly increasing demand in the electric vehicle space. The magnesium hydroxide product from the process is an ideal material to support decarbonization.

Atlas Materials will operate an extended Demonstration Pilot Plant later in 2023. The Demonstration Pilot Plant will confirm process chemistry, provide engineering data for a feasibility study for a 100,000 tonne per annum ore treatment facility and provide larger samples of products for off-take evaluation.

COPPER AND COBALT RECOVERY FROM OLD FLOTATION TAILINGS

By

[1,2] Pavel Spiridonov,[2] Richmond Asamoah, [2] Larissa Statsenko, [2] William Skinner, [2] Jonas Addai-Mensah, [3] Joe Mifsud, [1] Alexey Latay, and [2] George Abaka-Wood

[1] InnovEco Australia
[2] University of South Australia
[3] COOE

Presenter and Corresponding Author

Pavel Spiridonov
pavel.spiridonov@unisa.edu.au

ABSTRACT

The global mining industry produces millions of tons of mineral waste annually, with tailings being the most common and accumulating to over 280 billion metric tonnes worldwide. Yet, these tailings represent an incredible opportunity as a source of base, precious, and critical metals, with an estimated value of US$3.4 trillion. However, several barriers prevent cost-effective reprocessing of tailings, including the low content of valuable metals and high content of fine fractions, which hinder effective metal recovery and require costly filtration. Additionally, tailings pose significant environmental risks, including seepage and overtopping of harmful compounds into surrounding ecosystems.

InnovEco Australia has developed a novel metal recovery technology, the resin in moist mix (RIMM) method, which uses ion exchange to enable the cost-effective recovery of valuable metals from low-grade ores and fine minerals, including tailings. The RIMM bench top tests and drum model tests have demonstrated that this technology can recover near 100% of the acid-soluble copper and cobalt from South Australian tailings. Mineralogical investigations will confirm the presence of oxide and sulphide minerals in future tests.

Supported by the Australia-India Strategic Research Fund, this project represents a significant step towards overcoming the barriers to tailings reprocessing, unlocking the immense potential of mineral waste for the mining industry and beyond.

Keywords: Copper and cobalt Recovery, Ion Exchange, Resin in Moist Mix, Tailings Reprocessing.

INTRODUCTION

The mining industry plays a critical role in the global economy, but it is not without its drawbacks. Millions of tons of mine waste, particularly tailings, are generated every year, with over 280 billion[1] metric tonnes accumulated worldwide. The geophysical stability of tailings dams[2-4] is a major concern, as dam failure can result in significant destruction and loss of life. Additionally, tailings pose environmental problems such as seepage and overtopping of harmful compounds, potentially contaminating soil, water, and air[5-7].

Despite these issues, accumulated tailings represent a valuable source of base, precious, and critical metals worth an estimated US$3.4 trillion[1]. However, two major barriers hinder cost-effective reprocessing of tailings: the low content of valuable metals and the high content of fine fractions. Conventional technologies such as heap leaching and filtration are not economically viable[8, 9].

This study explores a novel metal recovery technology developed by InnovEco Australia[10 - 12], the Resin In Moist Mix (RIMM) technology[13], which utilises ion exchange for cost-effective recovery of valuable metals from low-grade ores and fine minerals such as tailings. The study uses samples from a historical copper mine located approximately 450km northwest of Adelaide and provides results of sample characterisation and basic copper and cobalt recovery tests.

CHARACTERISATION OF MINERAL SAMPLES

Water Content

The water content of tailings samples M-1, M-2 and T-3, taken at different sampling spots of the tailings dam, was determined by drying them in an oven at 60°C. Table 1 shows the wet and dry weight of each sample and their corresponding water content. The average water content varies from 5.5% to 9.7% for the samples M-2 to T-3.

Table 1: Water content in tailings samples

Parameter	T-3	M - 1	M - 2
Wet mineral, weight, g	341.1	347.3	355.3
Dry mineral, weight, g	307.9	324.5	335.9
Water content, %	9.7	6.6	5.5

Particle Size Distribution

The particle size distribution of the tailings samples was determined by dry sieving. The dried tailings were sieved on 425, 300, and 125 micron screens, and the weight percentage of each particle fraction was calculated. Table 2 and Figure 1 show the weight percentage of each particle fraction in the tailings samples. The largest fraction is >125 <300 µm, which varies from 42.4% in M-1 to 47.8% in M-2. The smallest fraction is >425 µm, which varies in the range of 8.1% (T-3) to 12.5% (M-1). The other two fractions (>300 µm-<425 µm and <125 µm) are in the range of 15.5% to 28.8%.

Table 2. Weight percentage of particle fractions in the tailings (separated by dry sieving)

Fraction µm	T-3		M - 1		M - 2	
	Weight, g	%	Weight, g	%	Weight, g	%
>425	25.6	8.1	39.9	12.5	28.7	8.6
>300<425	63	20.0	84.1	26.3	92.1	27.7
>125 <300	137.2	43.5	135.5	42.4	159.1	47.8
<125	89.9	28.5	60.4	18.9	52.9	15.9

Total	315.7	100.0	319.9	100.0	332.8	100.0

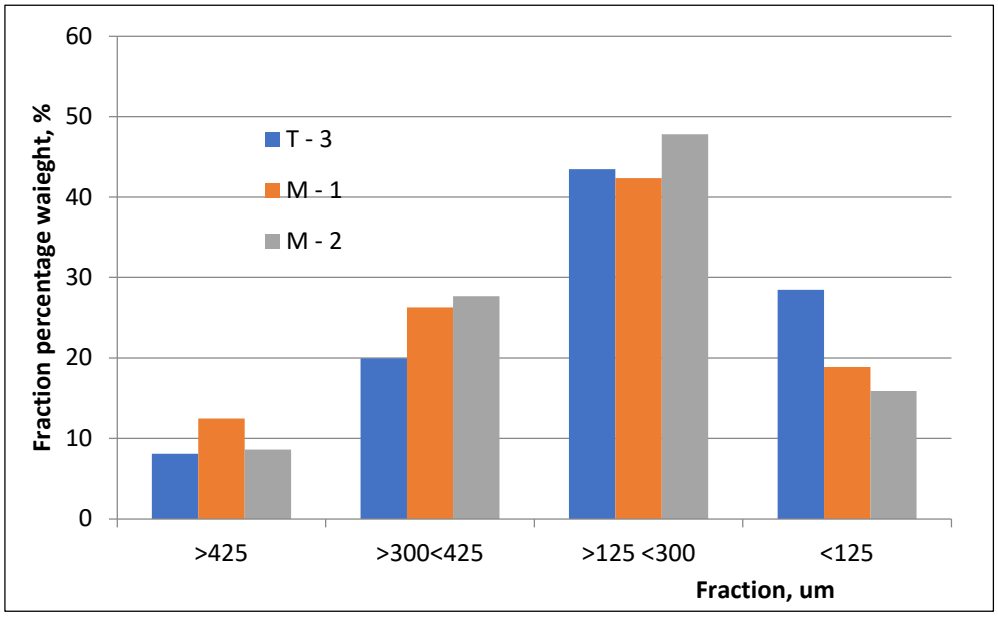

Figure 1: Weight percentage of particle fractions in the tailings samples T-3, M-1 and M-2

Characterisation of ore

The ore sample (~4.6kg) was crushed in a jaw crusher and milled in a roller mill. The crushed and milled minerals were sieved on an 850 micron screen, and a smaller portion of <850 µm fraction was further sieved on a 300 micron screen. Table 3 shows the weight percentage of each particle fraction in the ore sample. The finer fraction <300 µm takes 50.5% of the <850 µm fraction, and the coarser fraction >300 µm takes 49.5%.

Table 3. Weight percentage of particle fractions in the ore after jaw crusher and roller mill (separated by dry sieving)

Fraction, µm	Weight, g	Weight, %
<850	3312	71.3
>850	1335	28.7
Sieving <850µm fraction	348.4	100
<300 µm	175.9	50.5
>300 µm	172.5	49.5

Chemical composition

The University of South Australia employed two methods, XRF and ICP-OES, to determine the chemical composition of the tailings samples. The direct analysis of solids by XRF and digestive solutions by ICP-OES revealed significant differences between the metal content of the ore and tailings. In Table 4, it can be observed that the average cobalt and copper content in the ore sample is 0.01% and 10.32%, respectively. In contrast, the metal content of the tailings samples varied from 0.1% to 0.3% for cobalt and 0.19% to 0.66% for copper.
As expected, the lead and zinc content in the ore samples was higher than that in the tailings. The lead content was 0.39%, and the zinc content was 0.11%, while in the tailings, the range of lead and zinc content was 0.01% to 0.06% and 0.02% to 0.09%, respectively.

Table 4. Metal content in ore samples

Sample ID	Fraction	Co %	Cu %	Fe %	Mn %	Pb %	Zn %
AIS-21	Ore >850μm	0.012	14.377	1.178	0.022	0.820	0.163
AIS-22	Ore <850μm	0.009	8.917	0.863	0.017	0.264	0.091
AIS-23	Ore >300μm	0.006	8.559	0.560	0.014	0.163	0.068
AIS-24	Ore <300μm	0.013	9.409	1.184	0.025	0.296	0.111
	Average	0.01	10.32	0.95	0.02	0.39	0.11

Table 5. Metal content in tailings samples

Sample ID	Fraction	Co %	Cu %	Fe %	Mn %	Pb %	Zn %
	Tails T-3						
AIS-25	>425μm	0.004	0.207	0.224	0.003	0.011	0.015
AIS-26	300-425μm	0.005	0.136	0.290	0.003	0.008	0.017
AIS-27	125-300μm	0.007	0.152	0.357	0.004	0.008	0.021
AIS-28	<125	0.011	0.257	0.506	0.005	0.011	0.034
	Average	**0.01**	**0.19**	**0.34**	**0.00**	**0.01**	**0.02**
	Tails M-1						
AIS-29	>425μm	0.015	0.160	0.155	0.003	0.014	0.048
AIS-30	300-425μm	0.022	0.228	0.209	0.003	0.018	0.069
AIS-31	125-300μm	0.027	0.270	0.273	0.004	0.022	0.087
AIS-32	<125μm	0.037	0.402	0.515	0.004	0.036	0.147
	Average	**0.03**	**0.27**	**0.29**	**0.00**	**0.02**	**0.09**
	Tails M-2						
AIS-33	>425μm	0.009	0.281	0.134	0.002	0.024	0.029
AIS-34	300-425μm	0.014	0.508	0.200	0.002	0.039	0.040
AIS-35	125-300μm	0.016	0.604	0.238	0.002	0.047	0.049
AIS-36	<125μm	0.027	1.256	0.436	0.004	0.120	0.091
	Average	**0.02**	**0.66**	**0.25**	**0.00**	**0.06**	**0.05**

Table 6 compares the cobalt and copper content in the ore and tailings samples analysed using two different methods - XRF and ICP-OES. The results show that both methods provide comparable values. The cobalt content shows a variation between XRF and ICP-OES of 7.97% - 14.95%, and the copper content shows a variation of 11.46% - 19.15%. The variation was measured by the method of relative percent difference (RPD). Taking into account that the variation under 50% RPD may be considered as negligible, we may state that both methods provide statistically the same results.

Table 6. Comparison of the Co and Cu content determined by XRF and ICP-OES methods

Mineral	XRF		ICP		Variation, %	
	Co, %	Cu, %	Co, %	Cu, %	Co, %	Cu, %
Ore <300μm	0.013	9.197	0.014	10.316	7.97	11.46
Tails M-1 <300μm	0.026	0.421	0.030	0.347	14.95	19.15

Table 6 shows that the copper content in the ore samples is relatively high at 10.32%, which is not representative of the entire ore body. To achieve a copper content of around 0.6% - 0.7%, several mixes of ore and tailings were made, and their proportions are listed in Table 7. The results of the experiments conducted using these mixes are described in the following sections.

Table 7. Ore and tailings mixes

Sample ID		Ore, g	Tails T-3, g	Tails M-1, g	Tails M-2, g	Ore to tails ratio
AIS-40	Mix-1	40.0		80.0	80.0	1 : 4
AIS-49	Mix-2	11.2	113.6			1 : 10
AIS-50	Mix-3	18.0	120.1	61.9	60.7	1 : 15
		Ore, g	**Tails Mix T, g**	**Tails Mix M, g**		**Ore to tails ratio**
AIS-56	Mix-4	25.0	237.5	237.5		1 : 19
AIS-57	Mix-5	17.0	246.5	246.5		1 : 29

THE ACID SOLUBILITY TESTS

The acid solubility test was conducted to determine the leachability of copper and cobalt from the solid minerals using a dilute sulphuric acid solution. The test involved mixing and stirring 5 g of solid samples with 100 mL of the acid solution.

Table 8 presents the acid solubility results, indicating that the ore samples have an average acid solubility of 48.8% for copper and 44.8% for cobalt, with the amount of acid soluble copper and cobalt in the ore samples ranging from 41.1% to 52.2% and 40.8% to 49.8%, respectively. These results suggest that copper and cobalt in the ore may exist in both oxide (acid-soluble) and sulphide (acid-insoluble) forms. Further investigation is needed to confirm this theory

Table 8. Total content and acid solubility of copper and cobalt in ore

Ore fraction	Original content, %		Residual content, %		Acid soluble, % of total	
	Co %	Cu %	Co %	Cu %	Co	Cu
>850µm	0.012	14.377	0.007	6.874	41.8	52.2
<850µm	0.009	8.917	0.005	5.256	44.1	41.1
>300µm	0.006	8.559	0.003	4.221	40.8	50.7
<300µm	0.013	9.409	0.006	4.790	49.8	49.1
Weighted average	0.010	10.316	0.005	5.285	44.8	48.8

A second leachability test was carried out on the <300µm fraction of the ore sample. In this test, 10 g of mineral samples were mixed with 100 ml of an acidic solution containing varying amounts of acid, with the neat acid to mineral ratio ranging from 0 to 200 g of sulphuric acid per kg of the mineral sample. The results are illustrated in Figures 2 and 3.

As depicted in Figure 2, the leachability of copper and cobalt increases with the acid to solids ratio up to approximately 100g/kg and attains 47.9% for copper and 54.7% for cobalt. Beyond this point, both parameters remain relatively constant and plateau. A similar trend was observed for copper concentration in leachates, which rises with the acid to solids ratio up to roughly 50g/kg, peaking at 3,128mg/L, and then slightly decreases to 2,555g/L. These findings support the notion that the leachability of copper and cobalt is primarily determined by the mineral chemistry and is not influenced by the quantity and concentration of the leaching agent (sulphuric acid).

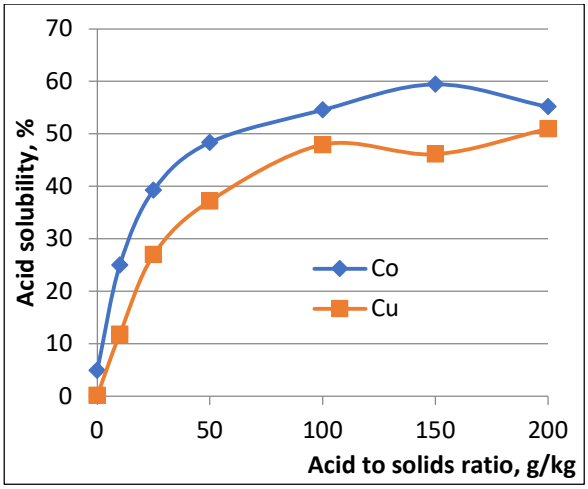

Figure 2. Copper and cobalt leachability from the ore (fraction <850µm)

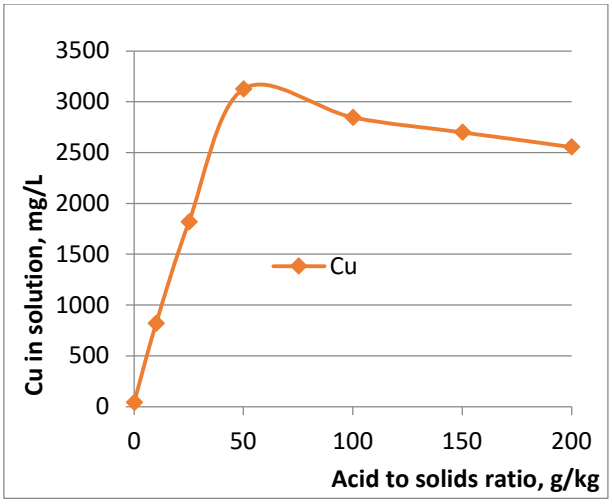

Figure 3. Copper content in the leachate

Table 9 presents the acid solubility test results for the tailings samples. Compared to the ore samples, the tailings have lower copper content, ranging from 0.183% to 0.662% on average, and slightly higher cobalt content, ranging from 0.008% to 0.027% on average. The residual content of copper and cobalt in different fractions of tailings M-1 and M-2 ranges from 0.004% to 0.034% and 0.001% to 0.004%, respectively. The residual copper content in tailings T-3 is slightly higher, ranging from 0.032% to 0.055%. The residual cobalt content in tailings T-3 is 0.001% in all fractions.

The acid solubility of copper and cobalt from different fractions of tailings samples M-1 and M-2 ranges from 94.1% to 98.5% and 86.6% to 96.3%, respectively. For tailings sample T-3, the acid solubility of copper and cobalt from different fractions varies from 70.0% to 87.7% and from 80.6% to 88.2%, respectively. The weighted average values in Table 9 were calculated considering the weight of each fraction. Calculating the weighted average involves multiplying each metal percentage by the weight of the relevant sample, summing those products and then dividing the sum by the total weight of all samples.

Table 9. Total content and acid solubility of copper and cobalt in tailings

Ore fraction	Original content		Residual content		Acid soluble, % of total	
	Co %	Cu %	Co %	Cu %	Co	Cu
Tails T-3						
>425µm	0.004	0.207	0.001	0.055	80.6	73.7
300-425µm	0.005	0.136	0.001	0.041	81.7	70.0
125-300µm	0.007	0.152	0.001	0.033	85.3	78.2
<125	0.011	0.257	0.001	0.032	88.2	87.7
Weighted average	0.008	0.183	0.001	0.036	83.9	77.4
Tails M-1						
>425µm	0.015	0.160	0.001	0.010	95.4	94.1
300-425µm	0.022	0.228	0.001	0.008	96.3	96.7
125-300µm	0.027	0.270	0.001	0.017	95.8	93.8
<125µm	0.037	0.402	0.003	0.016	91.3	96.1
Weighted average	0.027	0.270	0.001	0.013	94.7	95.2

Tails M-2						
>425µm	0.009	0.281	0.001	0.004	93.8	98.5
300-425µm	0.014	0.508	0.001	0.012	92.9	97.6
125-300µm	0.016	0.604	0.001	0.011	93.6	98.2
<125µm	0.027	1.256	0.004	0.034	86.6	97.3
Weighted average	0.017	0.662	0.001	0.015	91.7	97.9

Table 10 displays the results of acid leachability tests conducted on Mix-4 and Mix-5, which are a combination of ore and tailings samples. The acid solubility of copper and cobalt in Mix-4 ranges between 64.3% and 68.3%, while for Mix-5, it ranges between 86.6% and 89.8%

Table 10. Total content and acid solubility of copper and cobalt in ore and tailings mixes

Sample ID		Original metal content, %		Residual metal content, %		Acid soluble, % of total	
		Co %	Cu %	Co %	Cu %	Co %	Cu %
AIS-56/58	Mix-4	0.01	0.66	0.002	0.21	86.6	68.3
AIS-57/59	Mix-5	0.01	0.51	0.001	0.18	89.8	64.3

THE METAL RECOVERY TESTS

Bench Top Tests

The patented resin in moist mix (RIMM) process was used to conduct metal recovery tests in bench top conditions. Fine fractions of minerals (~50g) were blended with a specific amount of acidic solution and ion exchange (IX) resin, which was determined by the total copper and cobalt content in the samples. The tests could be conducted in either one or two stages, with the latter involving the separation of the loaded resin after stage 1 and the addition of a new portion of resin.

Table 11 presents the results of the RIMM tests using the <300µm fraction of the ore samples. Tests 1 and 2 were conducted in one stage, while test 3 was conducted in two stages. The results show that the highest recovery rates of copper and cobalt were achieved after stage 2 in test 3, with values of 55.1% and 74.7%, respectively. These values are higher than the copper and cobalt leachability from this ore fraction alone (49.1% and 49.8%, respectively), as shown in Table 8.

Table 11. Copper and cobalt recovery from the ore sample in the RIMM tests (Ore fraction <300µm)

Sample ID		Original metal content, %		Residual metal content, %		Recovery rate, %	
	Ore <300µm	Co %	Cu %	Co %	Cu %	Co %	Cu %
AIS-41	RIMM test-1	0.012	10.32	0.006	7.03	50.5	31.8
AIS-43	RIMM test-2	0.012	10.32	0.004	5.67	68.1	45.0
AIS-47a	RIMM test-3a	0.012	10.32	0.003	6.45	71.2	37.5
AIS-47b	RIMM test-3b	0.012	10.32	0.003	4.63	74.7	55.1

Table 12 displays the outcomes of the RIMM test carried out on the <300µm tailings samples M-1 and M-2. The tests were conducted in one stage, resulting in recovery rates for copper and cobalt that range from 75.6% to 86.9% and from 90.3% to 91.7%, respectively. It should be noted that these values are inferior to the acid leachable copper and cobalt shown in Table 9, which are 91.7% - 94.7% and 95.2% - 97.9%, respectively.

Table 12. Copper and cobalt recovery from the tailings samples in the RIMM tests

Tails <300µm	Original metal content, %		Residual metal content, %		Recovery rate, %	
	Co %	Cu %	Co %	Cu %	Co %	Cu %
Tails M-1	0.03	0.35	0.003	0.08	90.3	75.6
Tails M-2	0.02	0.75	0.002	0.05	91.7	86.9

Table 13 displays the results of the RIMM tests conducted in two stages on ore and tailings mixes Mix-1 and Mix-2, indicating the recovery rates of copper and cobalt. The cobalt recovery rates ranged from 87.4% to 87.8% and 91.9% to 93.0% in both RIMM stages for Mix-1 and Mix-2, respectively. However, due to the high original copper content in the mixes, the copper recovery rate was initially low at 38.7% in the first stage for Mix-1. After the second RIMM stage, the copper recovery rate increased to 74.1%. In the case of Mix-2, the copper recovery rate remained similar in both stages, measuring at 49.4% and 49.6% for stage 1 and stage 2, respectively.

Table 13. Copper and cobalt recovery from the ore and tailings mixes 1 and 2 (<300µm fraction) in the RIMM tests

	Ore & Tails mixes <300µm	Original metal content, %		Residual metal content, %		Recovery rate, %	
Sample ID	Description	Co %	Cu %	Co %	Cu %	Co %	Cu %
Mix-1							
AIS-46a	RIMM test-1a	0.020	2.605	0.003	1.597	87.4	38.7
AIS-46b	RIMM test-1b	0.020	2.605	0.002	0.675	87.8	74.1
Mix-2							
AIS-48a	RIMM test-1a	0.007	0.983	0.001	0.498	93.0	49.4
AIS-48b	RIMM test-1b	0.007	0.983	0.001	0.496	91.9	49.6

Table 14 presents the results of RIMM tests conducted with Mix-4 and Mix-5 in one stage, with samples taken at 1 hour and 2 hours into the tests. Cobalt recovery was achieved at levels similar to acid leachable cobalt (Table 10) - 86.5% - 87.1% for Mix-1 and 88.1% - 85.6% for Mix-2. There was only a slight increase in the cobalt recovery rate after an additional hour of the RIMM test.

For Mix-4, copper recovery was 64.7% after 1 hour and 76.9% after 2 hours, which is higher than the acid soluble copper content - 68.3% (Table 10). On the other hand, for Mix-5, copper recovery was lower than the acid soluble copper content (64.3%) at 44.3% and 51.7% for 1 hour and 2 hours tests, respectively.

Table 14. Copper and cobalt recovery from the ore and tailings mixes 4 and 5 (<300µm fraction) in the RIMM tests

Sample ID		Original metal content, %		Residual metal content, %		Recovery rate, %	
		Co %	Cu %	Co %	Cu %	Co %	Cu %
Mix-4							
AIS-60	1 hour	0.01	0.66	0.002	0.233	86.5	64.7
AIS-61	2 hours	0.01	0.66	0.002	0.153	87.1	76.9
Mix-5							
AIS-62	1 hour	0.01	0.51	0.001	0.284	88.1	44.3
AIS-63	2 hours	0.01	0.51	0.002	0.247	85.6	51.7

RIMM Drum Model Tests

A different type of RIMM test was conducted using a drum model, illustrated in Figure 4. This involved mixing approximately 300 grams of the mineral sample with acidic solution and resin in H^+ form, stirring the mixture in the drum for about an hour, and then separating the loaded resin from the mineral pulp using a 425 micron screen. The separated pulp was then filtered with a paper filter on a Buchner funnel to separate the solids from the liquid phase. Several fractions of the filtered solids were dried and digested with reverse aqua regia in a specialised microwave oven. The dissolved during digestion metals were analysed using a ICP-OES spectrometry.

Figure 4: RIMM Prototype Model

Table 15 presents the results of the copper and cobalt recovery rates from the ore and tailings Mix-3 in the RIMM tests performed using the drum model. The metal recovery rates varied among different fractions, with the cobalt recovery ranging between 85.2% and 95.0% and the copper recovery rate between 36.3% and 56.4%.

Table 15. Copper and cobalt recovery from the ore and tailings mixes (Mix-3 fraction <300µm) in the RIMM Drum tests

Sample ID	Fractions	Original metal content, %		Residual metal content, %		Recovery rate, %	
		Co %	Cu %	Co %	Cu %	Co %	Cu %
AIS-51coarse	1	0.012	0.906	0.002	0.467	85.2	48.5
AIS-51a	2	0.012	0.906	0.002	0.577	86.3	36.3
AIS-51b	3	0.012	0.906	0.001	0.432	91.7	52.3
AIS-51c	4	0.012	0.906	0.001	0.395	95.0	56.4

Table 16 shows the results of additional drum model tests conducted with Mix-4 and Mix-5. The tests were either run for 2 hours or included a pre-leach stage followed by a 1-hour RIMM test. During the pre-leach stage, the mix was mixed with an acidic solution using an overhead mixer for 1 hour. Then, the pre-leached pulp was transferred to the drum model, and resin in H^+ form was added.

The results, which are the weighted average values, indicate copper and cobalt recovery rates varying from 61.9% to 69.2% and from 83.3% to 85.8%, respectively. These rates are consistent

across all four tests. When compared to the acid solubility of copper and cobalt from the mixes (See Table 10), it can be observed that Mix-4 recovered 90.6% - 97.9% of acid-soluble copper and 96.4% - 97.3% of acid-soluble cobalt, while Mix-5 recovered 104.6% - 107.6% of acid-soluble copper and 92.8% - 95.5% of acid-soluble cobalt.

These tests demonstrate that the RIMM process can achieve near 100% recovery of acid-soluble copper and cobalt from ore and tailings mixes.

Table 16. Copper and cobalt recovery from the ore and tailings mixes 4 and 5 (fraction <300µm) in the RIMM Drum tests

Sample ID	Description	Original metal content, %		Residual metal content, %		Recovery of total metal, %		Recovery of leachable metal, %	
		Co %	Cu %	Co %	Cu %	Co %	Cu %	Co %	Cu %
	Mix-4								
AIS-64	1 RIMM stage 2 hours	0.01	0.66	0.002	0.25	84.3	61.9	97.3	90.6
AIS-67	Pre-leach + 1 RIMM stage, 1 hour	0.01	0.66	0.002	0.22	83.5	66.8	96.4	97.9
	Mix-5								
AIS-65	2 RIMM stage, 1.5 hours	0.01	0.51	0.002	0.16	85.8	69.2	95.5	107.6
AIS-66	Pre-leach + 1 RIMM stage, 1 hours	0.01	0.51	0.002	0.17	83.3	67.0	92.8	104.2

SUMMARY OF TEST RESULTS

Metal Content

Three types of minerals, namely copper ore, old tailings, and mixtures of ore and tailings, were subjected to RIMM tests to determine their metal content.

- The copper ore has an average composition of 0.01% cobalt, 10.32% copper, 0.95% iron, 0.39% lead, and 0.11% zinc.
- The tailings had varying metal content, with cobalt ranging from 0.1% to 0.3%, copper from 0.19% to 0.66%, lead from 0.01% to 0.06%, and zinc from 0.02% to 0.09%.
- The copper and cobalt content of the mixtures of ore and tailings ranged from 0.51% to 2.61% and 0.007% to 0.02%, respectively.

Acid Solubility

- Copper and cobalt in the ore samples are mostly not soluble in acidic solutions, which suggests that they may be present in the form of sulphides. Further investigation is needed to confirm this.
- Copper and cobalt in the tailings samples are mostly soluble in acidic solutions, indicating that they are likely present as oxide minerals.
- The acid solubility of copper and cobalt in the tailings mixtures is in the range of 64.3% - 68.3% and 86.6% - 89.8%, respectively.

RIMM Tests

The RIMM method showed a higher recovery rate of copper and cobalt for the <300µm fraction of the ore compared to the acid leachability - 55.1% and 74.7% respectively versus 49.1% and 49.8% respectively.

- The RIMM tests with the <300µm fraction of tailings samples M-1 and M-2 resulted in copper and cobalt recovery rates ranging from 75.6% to 86.9% and 90.3% to 91.7% respectively,

which were lower than the acid leachable copper and cobalt - 91.7% - 94.7% and 95.2% - 97.9% respectively.

- For Mix-1 and Mix-2, the cobalt recovery rate in the RIMM tests was achieved at the level of 87.4% to 87.8% and 91.9% to 93.0% respectively. However, the copper recovery rate for Mix-1 was low in the first stage at 38.7%, but increased to 74.1% after the second RIMM stage. For Mix-2, the copper recovery rate was similar in both stages - 49.4% and 49.6% in stage 1 and stage 2 respectively.
- The RIMM tests with Mix-4 and Mix-5 showed that the cobalt recovery was similar to the acid leachable cobalt (see Table 10) - 86.5% - 87.1% for Mix-4 and 88.1% - 85.6% for Mix-5. There was only a slight increase in the cobalt recovery rate after an additional hour of the RIMM test.

RIMM Drum Model Tests

- The RIMM tests on Mix-3 showed that the copper and cobalt recovery rates vary across different fractions. The cobalt recovery rates range between 85.2% and 95.0%, while the copper recovery rates range between 36.3% and 56.4%.
- For Mix-4 and Mix-5, the RIMM drum model tests resulted in copper and cobalt recovery rates ranging from 61.9% to 69.2% and from 83.3% to 85.8%, respectively. This means that 90.6% to 97.9% of acid soluble copper and 96.4% to 97.3% of acid soluble cobalt were recovered from Mix-4. Similarly, Mix-5 showed recovery rates of 104.6% to 107.6% for acid soluble copper and 92.8% to 95.5% for acid soluble cobalt.

CONCLUSION

This study investigated the metal content and acid solubility of copper and cobalt in ore, tailings and mixtures of ore and tailings using RIMM tests. The study found that copper ore contained 0.01% of cobalt, 10.32% of copper, 0.95% of iron, 0.39% of lead and 0.11% of zinc in average. In the tailings, the major part of copper and cobalt were oxide minerals.

In conclusion, the RIMM bench top and drum model tests indicate that it is possible to recover almost 100% of the acid soluble copper and cobalt from the ore, tailings, and mixes. However, before further testing, a mineralogical investigation is necessary to identify and quantify the oxide and sulphide minerals present in the ore.

In the future, it would be beneficial to test the minerals in a continuous process using the RIMM mini pilot plant, once it is constructed. This would provide a more accurate representation of the potential recovery rates and efficiency of the process.

ACKNOWLEDGMENTS

This article presents the initial research results of the project “Advanced recovery of the battery materials and REE from ores and wastes” supported by the Australia - India Strategic Research Fund. George Abaka-Wood and William Skinner wish to acknowledge support from the Australian Research Council for the ARC Centre of Excellence for Enabling Eco-Efficient Beneficiation of Minerals, grant number CE200100009.

REFERENCES

1. Leonida, C. 2022. Mine Tailings: Waste Not, Want Not. The Intelligent Miner, 30/03.

2. Psarropoulos, P. N.,. and Tsompanakis, Y. 2008. Stability of tailings dams under static and seismic loading. Canadian Geotechnical Journal, 28 May, https://doi.org/10.1139/T08-014

3. Clarkson, L., & Williams, D., 2020. Critical review of tailings dam monitoring best practice. International Journal of Mining, Reclamation and Environment, 34:2, 119 - 148, DOI: 10.1080/17480930.2019.1625172

4. Martínez. J., Mendoza, R., Rey, J., Sandoval, S., and Hidalgo, M. C. 2021. Characterization of tailings dams by electrical geophysical methods (ERT, IP): Federico Mine (La Carolina, Southeastern Spain). *Minerals, 11*(2), 145; https://doi.org/10.3390/min11020145

5. Kossoff, D., Dubbin, W.E., Alfredsson, M. , Edwards S.J., Macklin M.G., Hudson - Edwards, K.A. 2014. Mine tailings dams: Characteristics, failure, environmental impacts, and remediation. Applied Geochemistry. Volume 51, December 2014, Pages 229-245. https://doi.org/10.1016/j.apgeochem.2014.09.010

6. Cacciuttolo, C., and Cano, D.2022. Environmental impact assessment of mine tailings spill considering metallurgical processes of gold and copper mining: case studies in the Andean countries of Chile and Peru. *Water, 14*(19), 3057; https://doi.org/10.3390/w14193057

7. Zarubin, M.; Statsenko, L.; Spiridonov, P.; Zarubina, V.; Melkoumian, N.; Salykova, O., 2021. A GIS Software Module for Environmental Impact Assessment of the Open Pit Mining Projects for Small Mining Operators in Kazakhstan. Sustainability. 13, 6971. https://doi.org/10.3390/su13126971

8. Case Study: Fines Control to Improve Copper Leaching Recovery, Andacollo Mine, Chile www.oricaminingservices.com | Document reference: 200102

9. Quaicoe, I., Nosrati, A., Addai-Mensah, J., Skinner, W., 2011. Agglomeration behaviour of model clay and oxide. CHEMECA 2011, NSW, Australia.

10. Spiridonov, P.N., Echenique, M.R., 2013. Ion exchange technology: solving existing problems in copper mining. Proceedings of Copper 2013, Santiago, Chile.

11. Spiridonov, P., Skinner, W., Addai-Mensah, J., Hein, H. and Hein R. 2019 Further Development of The Continuous Ion Exchange Process for Copper, From Fines. Proceedings of the ALTA 2019 conference, Perth, Australia.

12. Spiridonov, P., 2014. Metal Recovery from Fines. 2014. Australian patent AU2014225291.

13. Hein, H.C., Spiridonov, P., Hein, R.O., 2015. Process for metal extraction with sorption leaching in wet solids. Australian patent AU201533455

COBALT BLUE'S BROKEN HILL DEMONSTRATION PLANT – SECOND UPDATE ON THE COB PROCESS DEVELOPMENT

By

Andrew Tong

Cobalt Blue Holdings Pty Ltd, Australia

Presenter and Corresponding Author

Andrew Tong
andrew.tong@cobaltblueholdings.com

ABSTRACT

Cobalt Blue is developing the Broken Hill Cobalt Project. As part of feasibility studies, the company constructed and operated a testing facility in Broken Hill. Initially 90 t of ore was processed in batch campaigns in 2021-2022, with scale-up to continuously operating campaigns on up to 5,500 t of ore in 2022-2023. The patented process flowsheet was designed to concentrate cobalt-pyrite from the ore, convert the pyrite into pyrrhotite through pyrolysis, leach the pyrrhotite, and subsequently recover the cobalt as a precipitated hydroxide. The Demonstration Plant comprises all the key circuits. In addition to confirming overall process recoveries of >95% of the cobalt from the pyrite concentrate, the plant workstream has enabled COB to improve engineering designs, equipment selection, operating procedures, and recruit and develop staff.

Keywords: cobalt extraction, pyrite ore, process development, decomposition of pyrite, leaching of pyrrhotite

INTRODUCTION

Development Status of the Broken Hill Cobalt Project

Cobalt Blue has been developing the Broken Hill Cobalt Project since 2017. A status update was presented to Altamet 2020 (Tong, Efficient recovery of cobalt from pyrite - update on COB process development, 2020). This paper provides a follow-on update, and focuses on piloting of the process flowsheet at the Demonstration Plant.

Presently, the project is being evaluated at a Definitive Feasibility Study (DFS) level. Cobalt Blue has engaged Worley to deliver the process plant engineering designs and costings, as part of the owner-led DFS. SRK are delivering the geological models and mining plans, and GHD are delivering the non-process plant infrastructure, mine waste management system, and the applications for project approvals and permits.

A key component of DFS process plant engineering, is collection of sufficiently credible data for process design criteria. Given the innovative nature of the flowsheet, it was imperative to scale up testwork to a complete end-to-end pilot-demonstration facility. Cobalt Blue advanced this in two stages, with a pilot facility built and operated in 2020-2021, and a Demonstration Plant in 2022-2023.

The key outcome of the pilot plant was to confirm process chemistry upon scale-up to continuous processing, compared to static / batch bench tests. Whereas, the Demonstration Plant is aiming to obtain operational data for commercial plant equipment design / selection.

In total, Cobalt Blue is anticipating spending A$10-15m on the pilot-demonstration activities. This represents appropriate expenditure to de-risk the DFS engineering, and thus improve the robustness of the commercial scale plant operations.

Project Overview

Cobalt is commonly associated with copper-cobalt sulphides, nickel-cobalt laterites, and cobalt-arsenic sulphides. There are also known occurrence of cobalt hosted in pyrite, which are sometimes referred to as cobaltiferous pyrite. One such deposit is Cobalt Blue's (COB's) Broken Hill Cobalt Project (BHCP), which has a Mineral Resource of 118 Mt containing 81,100 t of cobalt at 275 ppm CoEq cut-off (compliant with JORC 2012 code). In this deposit, cobalt has substituted for iron atoms into the pyrite mineral crystal lattice. There are very minor amount of other sulphide or oxide minerals hosting copper, zinc, and nickel. The BHCP is located 25 km from Broken Hill in New South Wales Australia. The site is well-serviced (see Figure 1).see with major road and rail connections, and can readily connect to the National Electricity Market (via Broken Hill substation) and reliable water supply (via Broken Hill-Wentworth pipeline). There is good availability of local mining skills and project services.

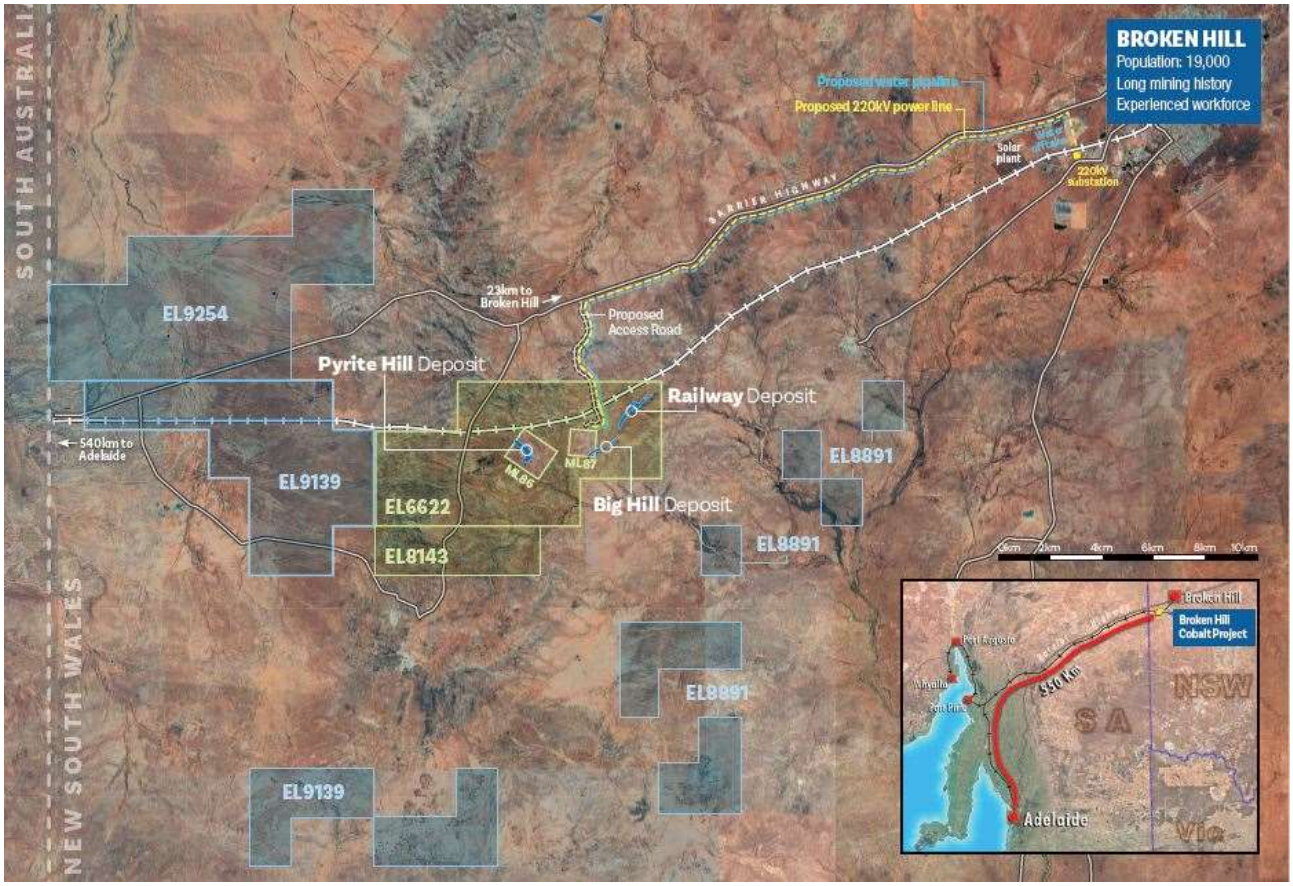

Figure 1: Broken Hill Cobalt Project location

Cobalt Blue Flowsheet

Commercial development of cobaltiferous pyrite deposits must focus on cost-effective treatment of pyrite. Historically processing options for pyrite have included roasting, pressure oxidation, and more recently bioleaching.

Cobalt Blue has developed and patented a flowsheet for treatment of pyrite (Australia Patent No. 2018315046, 2018). Firstly, the pyrite is thermally decomposed into artificial pyrrhotite and elemental sulphur (Reaction 1). Secondly, the artificial pyrrhotite is leached to produce stable hematite and elemental sulphur residue (Reaction 2), while solubilising the target metals. The process chemistry is given in the following 'ideal' reactions:

Reaction 1 $7FeS_{2(s)} + \text{energy} = Fe_7S_{8(s)} + 6S_{2(g)}$

Reaction 2 $Fe_7S_{8(s)} + 11.5O_{2(g)} = 3.5Fe_2O_{3(s)} + 8S_{(s)}$

The DFS is evaluating a ~20 yr project with throughput between 5.5-7.5 MTPA ore to produce 3,500 tpa cobalt (as cobalt sulphate) and 300,000 tpa elemental sulphur. A summary of the BHCP throughputs and grades is shown in Figure 2.

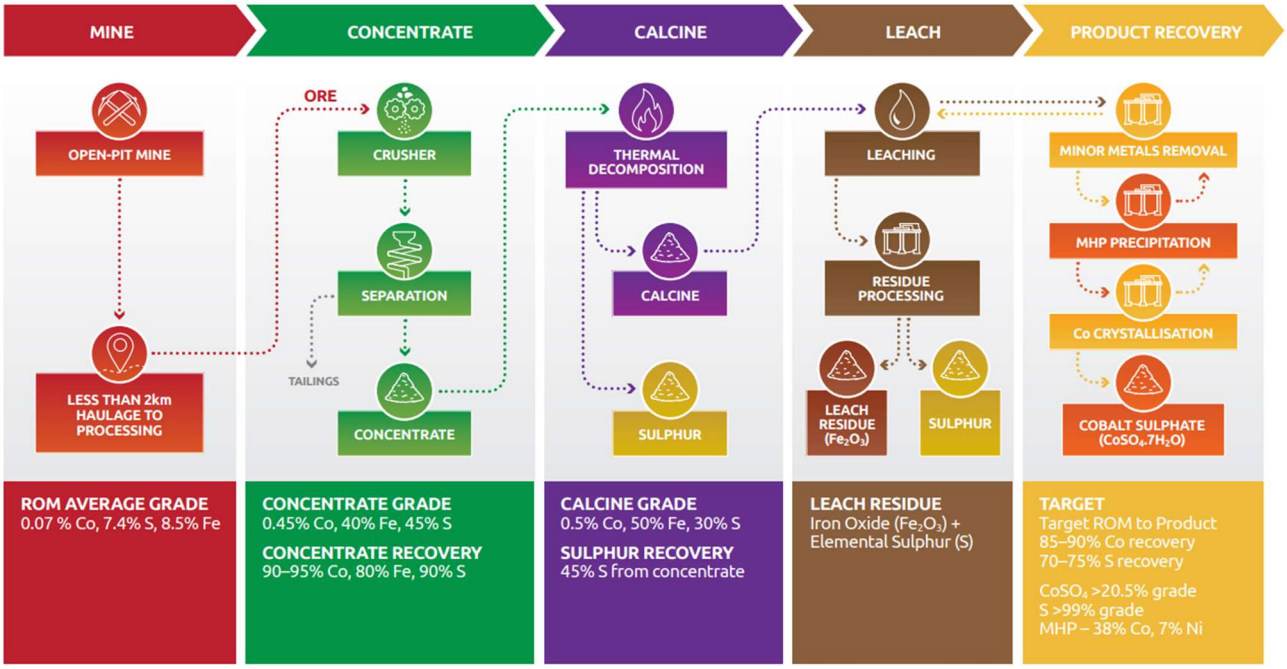

Figure 2: Overview of BHCP mining and processing stages

FLOWSHEET TESTING AT PILOT AND DEMONSTRATION PLANT SCALE

Broken Hill Testing Facility

The testing facility was designed, constructed and operated by Cobalt Blue. It is located in the industrial zone, on the edge of Broken Hill. Approximately 25-30 local staff are employed at the facility, and it provides an excellent opportunity to recruit / train employees, build a community footprint, and showcase the processing technology.

Initially, a concentrator and hydrometallurgical pilot plant were installed in 2020-2021. The concentrator processed 45 t of reverse cycle drill chips to generate cobalt-pyrite concentrate. A second 45 t parcel was also concentrated at ALS. The concentrate was thermally treated offsite (at a specialist furnace facility), with the kiln calcine returned for leaching and cobalt recovery trials.

Following successful piloting, the pilot plant was completely rebuilt and upgraded to the Demonstration Plant scale in 2022-2023. This included development of an underground portal at the mine site to extract >5,000 t of ore, establishment of a mine-site concentrator, installation of a kiln and sulphur recovery circuit, and upgrades to the leach circuit.

A comparison of the pilot and demonstration plants are given in Table 1.

Table 1: Comparison of Pilot and Demonstration Plant

	Pilot Plant	Demonstration Plant
Feed ore	45 t RC chips from drilling + 45 t processed at ALS	5,000 t from underground mine
Operating mode	24-72 hour campaigns	Continuous 24/7 for steady multi-week campaigns
Onsite unit operations	Concentrate, leach, MHP, refinery	Concentrate, kiln, leach, MHP, refinery
Throughput rate concentrator	2 t/hr	10 t/hr
Throughput rate leach	35 kg/hr	100 kg/hr

The plant operations were supported by:

- A Honeywell SCADA control system. Approximately 750 data points monitored at Demonstration Plant.
- Manual sampling of process streams, with onsite laboratory for sample preparation and assays by XRF.
- External laboratories used for verification assays (ICP) and ancillary testwork (e.g. filtration, rheology, materials handling, etc)

Process Scale-up to Demonstration Plant

Each individual circuit, and their collective interaction as a whole flowsheet, was closely investigated in the project planning stage to define KPIs that required validation at 'scale' compared to laboratory testwork. Examples of these are provided in the following descriptions of the concentrator, calcine and leach circuits.

Concentrator Circuit

Cobalt-pyrite is concentrated from the ore using a gravity spiral circuit. The gravity tails are then further processed through a flotation circuit for scavenging remaining pyrite. This two-step approach targets coarser pyrite (generally > 75-100 um) on the spirals, and fine pyrite (generally < 75-100 um) on the float circuit.

An overview of scale-up KPI's are given in Table 2, along with photos of the mine site footprint in Figure 3, construction of the concentrator in Figure 4, separation of pyrite on the gravity spirals in Figure 5, and stored bags of concentrate in Figure 6.

Table 2: Concentrator scale up KPI's

Parameter	Pilot Plant	Demonstration Plant	Comment
Ore variability	Drill samples across the proposed deposits, representing ore across entire project life	6 parcels of ore from single underground portal, representing majority of ore in first 10 years	Pilot focused on flowsheet suitability for entire project life, with Demonstration plant confirming recoveries for initial project start up
Gravity spiral model selection	Various models used	Selected only HG10's for rougher and cleaner duties	Used full commercial scale spirals in testwork
Flotation of gravity tails	Single fines flotation cell for scavenger duty	Single fines flotation cell for scavenger duty, with combination of fine and coarse flotation at vendor laboratories	Optimisation of classification and float cell performance completed by vendors
Particle size and metal deportment	RC chips were fine (p80 150-250 um), and thus >40% of pyrite deported to float concentrate	Ore samples milled to p80 ranging from 350 um up to 2 mm, thus <20% of pyrite deported to float concentrate	Preferred topsize for DFS design criteria selected at 1mm, with p80 850 um.

Figure 3: Underground bulk sample and concentrator footprint

Figure 4: Demonstration Plant concentrator during construction

Figure 5: Separation of pyrite on the gravity spiral (LHS), concentrate bags (RHS)

Figure 6: Concentrate storage in bulk bags ready for transport to the plant in Broken Hill

Calcine circuit

The cobalt-pyrite concentrate is dried to remove moisture, and then thermally decomposed at 650-750 ºC in a rotary kiln under a nitrogen (inert) atmosphere. The calcine (pyrrhotite) is collected from the kiln for downstream leaching, while the elemental sulphur is condensed out of the kiln off-gas.

An overview of scale-up KPI's are given in Table 3, along with photos of the demonstration plant kiln in Figure 7, sulphur condenser in Figure 8, and feed concentrate / calcine / sulphur in Figure 9.

Table 3: Kiln scale up KPI's

Parameter	Pilot Plant – ANERGY/ANSAC Purpose criteria for demo plant kiln	Demonstration Plant	Comment
Wet concentrate handling	Identified handling properties of wet concentrate from 5-20% moisture	Designed continuous feeder system for wet feed	Vendor testing of materials handling properties required
Requirement for drying concentrate ahead of calcining	Combined duties of drying and calcining	Separated drying mode and calcining mode for kiln operation	Pilot identified interaction of water and sulphur vapours were difficult to control, so Demonstration plant separated operational duties
Offgas management – sulphur recovery	Operations limited to 4-5 hours, due to sulphur batch collection	Dedicated sulphur condenser installed to permit continuous operation	Significant design hurdles for offgas management at small scale (scrubber, fan – pressure control loops, sulphur condenser)
Offgas management - scrubbing	Offgas burner used	Lime/limestone scrubber used, as typical for flue gas scrubbing	Scrubber to be vendor package at commercial plant
Conversion of pyrite versus particle size	Development of laboratory analytical techniques – via CRC-P grant with UNSW / ANSTO	In-house techniques utilised to monitor conversion of pyrite to pyrrhotite versus kiln parameters and particle size ranges	Confirmed conversion of pyrite to pyrrhotite follows a shrinking-core model

Figure 7: Demonstration Plant kiln

Figure 8: Sulphur condenser for kiln offgas

Figure 9: Feeding wet concentrate (LHS), concentrate and calcine, elemental sulphur (RHS)

The progress of the pyrite to pyrrhotite conversion was evaluated by x-ray diffraction (mineral identification) and scanning electron microscopy. Example SEM images are shown in Figure 10, with the shrinking core model for the reaction visually confirmed.

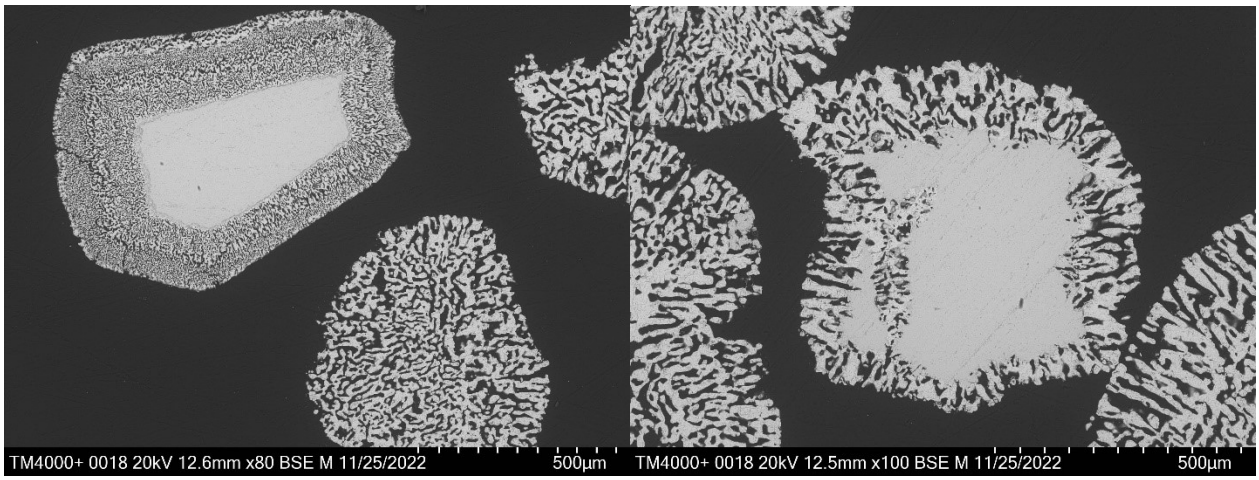

Figure 10: SEM images of pyrite to pyrrhotite conversion confirming shrinking core model

Leach Circuit

The pyrrhotite calcine is leached in an autoclave at 130 °C and < 150 kPa pressure. The cobalt is extracted into solution for downstream recovery. The leach residue predominately contains elemental sulphur (from the oxidation of the sulphide sulphur in the pyrrhotite) and precipitated hematite.

An overview of scale-up KPI's are given in Table 4, and a photo of the leach autoclaves is given in Figure 11,

Table 4: Leach scale up KPI's

Parameter	Pilot	Demonstration	Comment
Leach conditions - pressure	Design up to 225 kPa	Design was specifically limited to 120-140 kPa	Overall pressure reduced to < 150 kPa, to decrease capital costs and increase range of suitable 'off the shelf' equipment
Heat management	Identified heat profile along reactor train	Applied water cooling per vessel based on automated control loops	Design of heat balance (cooling) critical to commercial plant autoclave design
Sulphur management	Confirmed dispersant adequate for minimising sulphur agglomeration	Optimisation of dispersant dose rate versus feed rate	Trial and error testwork
Slurry discharge valve (flash letdown)	Single exit from autoclave through a pressure regulated pinch valve	Separate gas / pressure management valve Metered slurry discharge system	Flash let down system to be vendor designed for commercial plant

Figure 11: Demonstration Plant autoclave train

The entire leach autoclave circuit design was from first principles. The various design selections are summarised in Table 5, and photos of the autoclave feed slurry pump in Figure 12, and the slurry discharge system in Figure 13.

Table 5: Key design aspects of the leach circuit

Design aspect	Selection	Comment
Type of autoclave	4 vessel CSTR arrangement	Provided flexibility to readily modify residence time, individual heat management per reactor, individual oxygen addition (hence extent of reaction) per reactor
Material of construction	Titanium grade 2	No corrosion/erosion observed on reactor bodies to date. Noticeable wear on agitator blades. Oxygen sparge line failure when buried in solids.
Agitator seal	Titanium magdrive unit	Suitable for pressure, temperature and solution
Feed pump	Hose pump	Required pulsation dampeners to overcome backpressure from autoclave
Offgas venting	Pressure release valve	Each vessel tied into a single off-gas vent, which controlled total autoclave circuit pressure via a pre-set pressure release valve
Heat management	Water cooling jackets on each reactor	Linked to temperature indicators and SCADA control loop
Slurry discharge	Actuated pinch valve, linked to slurry weight in discharge chamber	Measured release of slurry, to provide known discharge flowrate. This was important to decouple from overall pressure control (offgas vent valve).

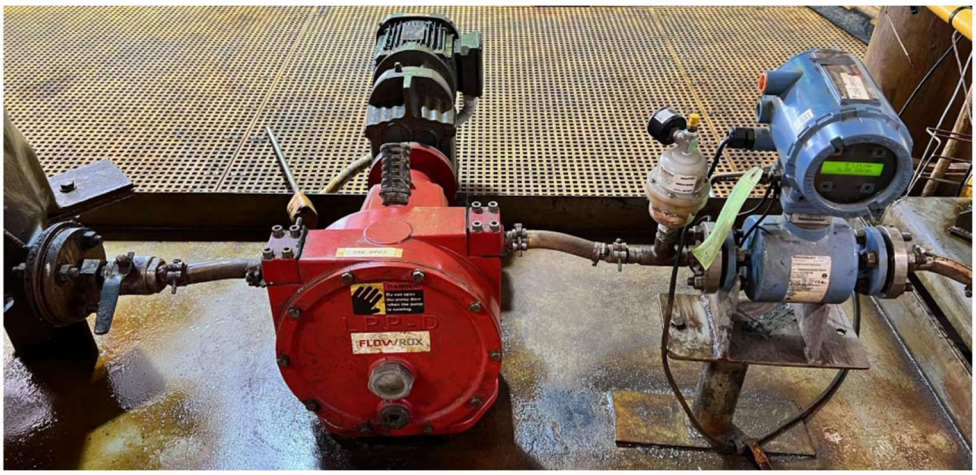

Figure 12: Autoclave slurry feed pump, pulsation dampener and flowmeter

Figure 13: Demonstration autoclave discharge system – actuated pinch valve based on weight of slurry in discharge chamber

Comments

The following comments are provided as reflections for those considering scaling up testwork programs:

- The overall pilot and demonstration plant activities are expected to cost Cobalt Blue ~ A$10m over a 36 month period. This expenditure was split into A$3m for pilot and A$7m for demonstration plant (inclusive of ore extraction).
- Scaling up metallurgical testing to the pilot and demonstration plant scale requires significant cross-discipline expertise across civil, structural, electrical and instrumentation facets of design and implementation.
- The key tangible outcome is definition of credible plant design criteria for use in the engineering studies. This includes process flowsheet recoveries, operating parameters, and guidelines for equipment selection.
- Intangible benefits include project staff recruitment, development of training manuals, local community engagement, and the opportunity to advance contractor / vendor / supplier relationships ahead of the commercial plant.
- Often vendors are unable to supply equipment at the small scale, and innovative thinking is required.
- Operating the plant is challenging due to the small scale, e.g. pipe diameters are small and prone to blockages.
- The activities should not be focused on production or throughput, but rather on the collection of data for engineering design.
- It is much more cost-effective to deal with encountered problems at the pilot-demonstration scale, than at the commercial scale.

CONCLUSIONS

Adequately testing metallurgical flowsheets at pilot and demonstration plant scales is expensive. However, the long-term value is to de-risk the project by improving the knowledge base for engineering design. These steps are often overlooked in systematic project development.

ACKNOWLEDGEMENTS

The author would like to thank all of the staff at Cobalt Blue Holdings who have contributed to the development of the project to-date. It has been a real team effort.

REFERENCES

Tong, A. (2018). *Australia Patent No. 2018315046.*

Tong, A. (2020). Efficient recovery of cobalt from pyrite - update on COB process development. *Altamet*, (pp. 454-464). Perth.

BIOEXTRACTION AS AN ALTERNATIVE FOR TRADITIONAL MINERAL PROCESSING - AN ECONOMIC AND ENVIRONMENTAL GAME CHANGER

By

Renee Grogan,

Impossible Metals, Australia

Presenter and Corresponding Author

Renee Grogan
Renee.grogan@impossiblemetals.com

ABSTRACT

Impossible Mining is developing a novel, energy efficient, microbial bioextraction method for the processing of minerals critical to green energy production, that include nickel (Ni), cobalt (Co), copper (Cu) and rare earth elements (REEs). Bioextraction is different to traditional bio-leaching where the bacteria is used to generate acid to allow leaching of metals. By comparison, bioextraction occurs at neutral pH, in a process that is complete within 1-2 days.

The bioextraction methodology draws on knowledge gained from basic research on a group of bacteria that can rapidly dissolve various metal oxides, including insoluble iron (Fe) and manganese (Mn) oxides, under anaerobic conditions, thereby reducing the metal oxides to soluble metal salts. This technique will enable low-energy processing of minerals without traditional reagents like arsenic and cyanide, without generating toxic waste and without using freshwater. Furthermore, we will aim to achieve carbon neutrality, and eventually carbon negativity, by utilizing fossil fuel independent carbon and energy sources for the microbes.

Bioextraction has been tested at a small-scale laboratory level on polymetallic manganese nodules and shown to be extremely effective, achieving recovery rates of multiple target metals, commensurate with existing mineral processing methodologies, and without the generation of a waste stream. The process is currently also being tested on terrestrial ores, as well as terrestrial waste streams (in relation to recovery of metals such as cobalt and REEs, which may be present in tailings streams but not previously targeted or recovered).

Current work is focused on scaling the process from very small-scale laboratory tests, to a pilot-plant scale, over the next ~18 months – for both polymetallic nodules, and terrestrial targets. It is expected that, if scaling is successful, bioextraction will be extremely cost effective when compared to any other form of mineral processing, for both capex and opex, due to the low energy inputs, lack of reagent inputs and the lack of waste storage infrastructure required.

When proven at scale, we believe this technology will completely disrupt current mineral processing methods, delivering a pathway to carbon-neutral, waste free processing for the minerals industry.

Keywords: mineral processing, green energy, critical metals, bacteria, bioextraction

Bio-Extraction Summary

- Naturally occurring process of bacterial respiration (**not** leaching)
- Discovered by Co-Founder Prof. Ken Nealson, patent pending
- Bacterial respiration liberates metals, yielding slurry of soluble $MnCl_2$, $FeCl_2$, and chloride salts of nickel, copper and manganese
- Operating parameters - room temperature, neutral pH, fresh/saltwater
- Bacterial substrate/food source= organic carbon (e.g. food waste)
- Lab testing indicates high efficacy on polymetallic nodules (unweathered)

24 hour reaction →

← Abiotic control

Bacteria

- Motile – gentle stirring required
- Identified strains capable of operating in low and high temperatures, salt and freshwater
- Identified strains that have a metabolic preference for iron or manganese oxides

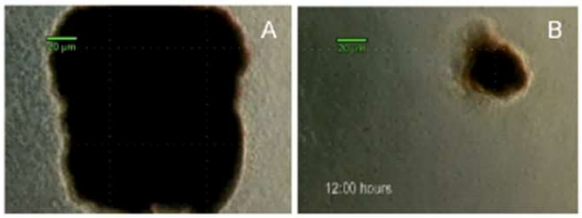

Manganese oxide reduction by *Shewanella oneidensis* MR-1. (A) Image taken at 0 hours. (B) Image taken at 12 hours.

- Adding a single organic substrate (food source), the bacteria are able to dissolve the nodules completely, yielding a solution of soluble chlorides and chloride salts and a very small volume of solids (mostly clay)

Bacteria Respiration

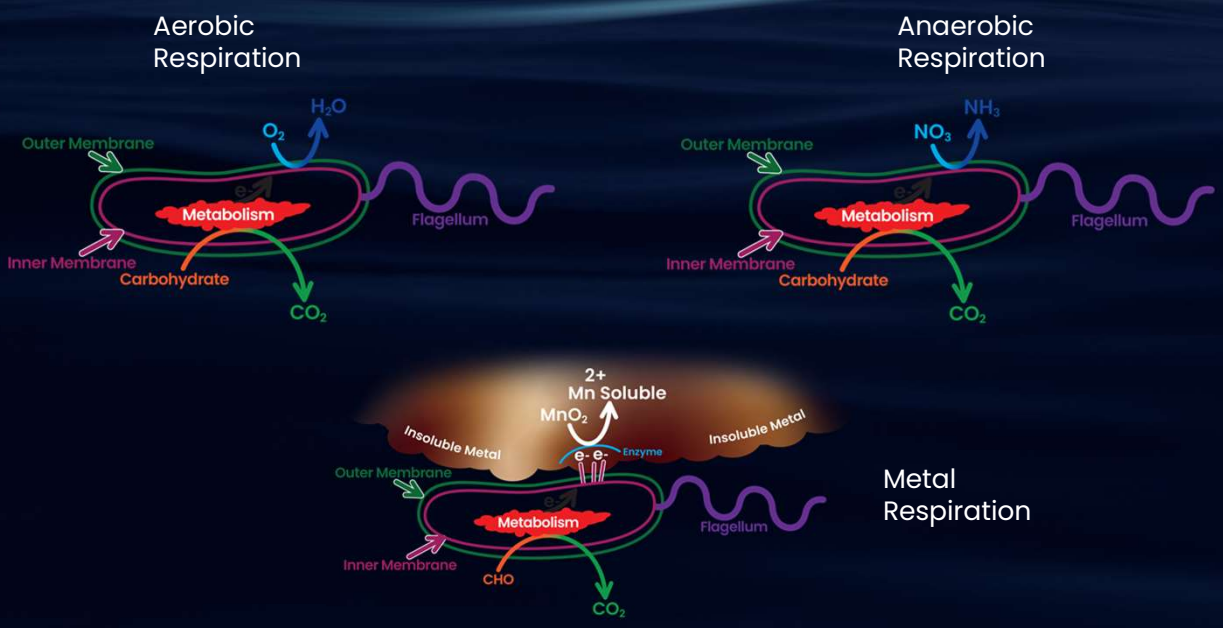

Benefits of Bio-Extraction

- No freshwater use - can use seawater of saline groundwater
- No tailings
  - No use of toxic chemicals or highly concentrated acids
  - Neutral pH wastewater, suspended sediment will depend on clay content etc. - may require flocculation/filtration prior to release (low volume solid waste stream)
  - Significantly reduced rehabiltiation liability
- Expect lower CAPEX and OPEX than traditional processing
- Lower environmental risks and impacts
- Low energy requirements (can achieve carbon neutrality)

Concept Flowsheet - Bioextraction

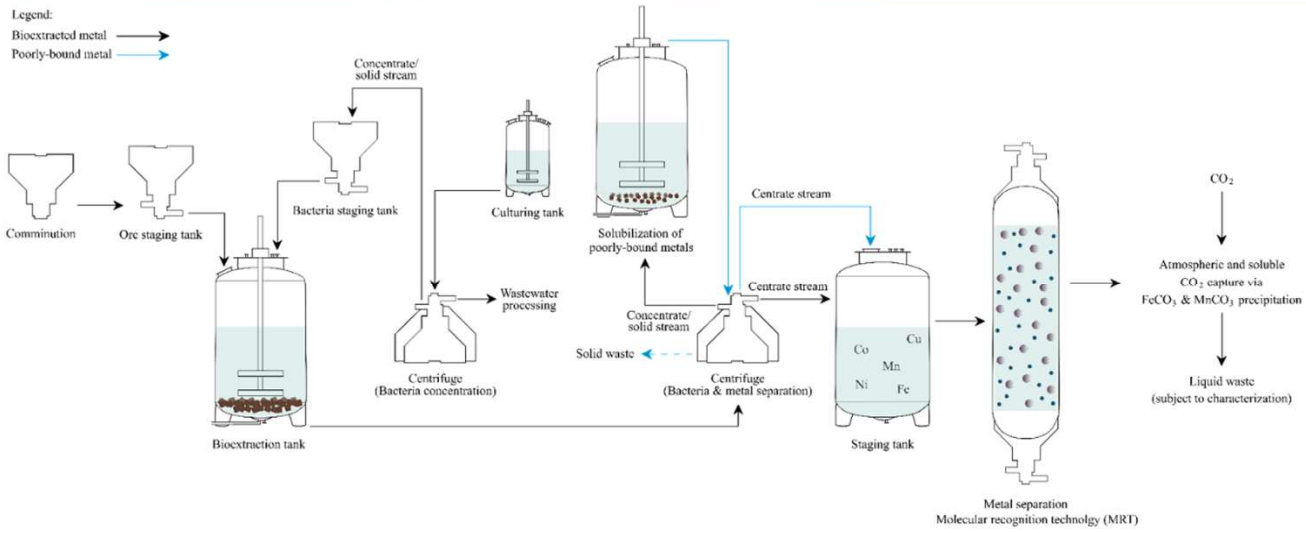

Initial Bench-Top Findings

- Preliminary data on different manganese (Mn) and iron (Fe) oxides show excellent yields in short periods (multiple published studies)[1] in both fresh/sea water
- Early results show recovery approaching that of other options (e.g. Cuprion method), with concurrent solubilization of all metals.
- Findings are driving optimization on:
  - Carbon source
  - Bacterial strains
  - Combination of strains
- Adaptive evolution highly effective, can be undertaken for each ore target

1. e.g. https://pubs.acs.org/doi/pdf/10.1021/es00010a012

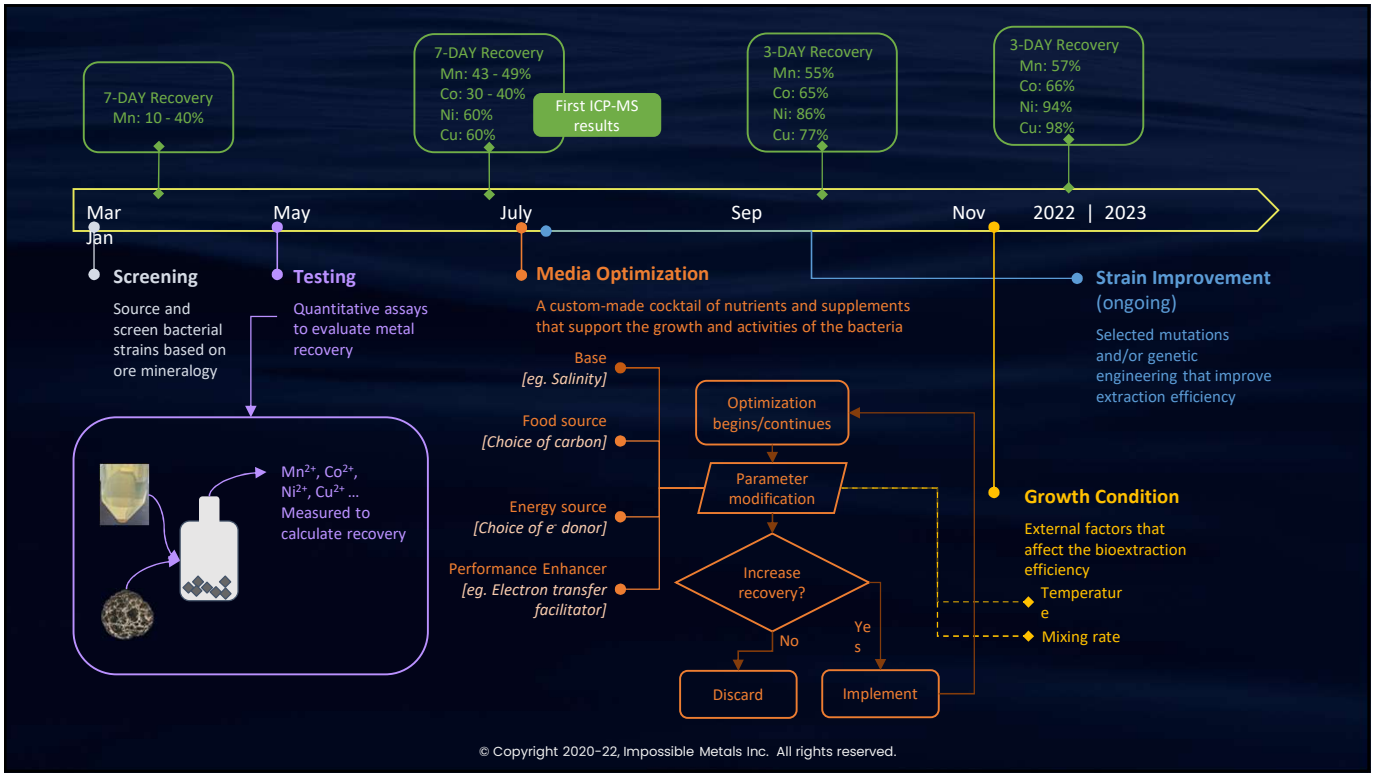

Current PMN Results

Using Base Seawater as Extraction Medium with an addition of electron carrier at different concentrations

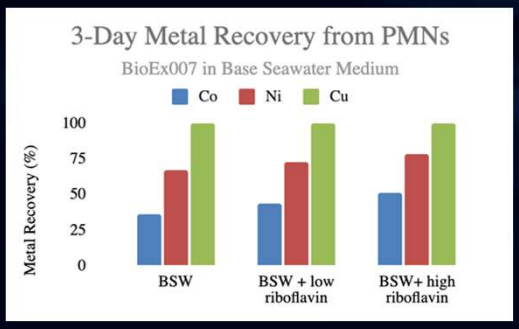

In-house evolved BioEx007 achieved higher recovery rates than BioEx007

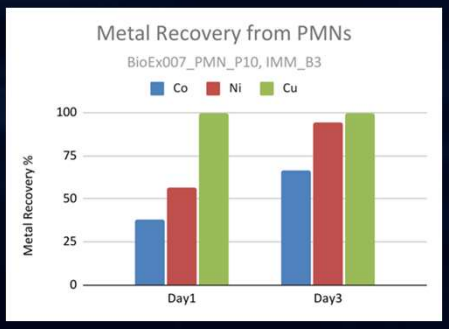

A Path to Extracting REEs

- Our ICP-MS analysis is detecting some REEs in solution, along with Ni, Co, and Cu
- This is encouraging because it means at least some of the REEs are being released from the mineral matrix as a result of bioextraction

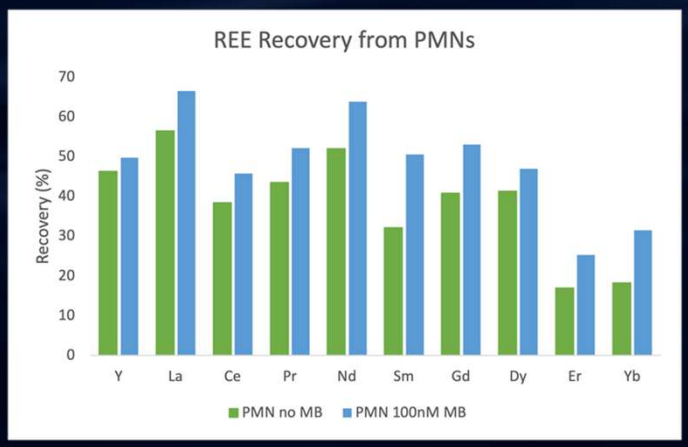

Potential Strategies for REE Separation

- Some bacteria have the ability to adsorb to multiple lanthanides, which can then be differentially desorbed from the bacterial surface by varying pH washes, allowing for feasible REE separation
- A recent study has identified genes involved in REE adsorption - which includes some of our BioEx strains
- A sensitive colorimetric method has been developed for some lanthanides, that can be used as a quick and easy screen for testing various bacteria
- Synthetic biology techniques, and adaptive evolution experiments can be conducted to further enhance the ability of the bacteria to bind different/higher concentrations of REEs

Relevant Learnings from Early Stage Studies

- Adaptive evolution is extremely effective
- Bacteria are more versatile than we realized - Can adapt strains for both target metal recovery and impurity recovery
- Consortia of different species or strains of bacteria greatly improves target metal recovery
- Areas where traditional processing/beneficiation is challenging, or has constraints, are of interest
- Mineralogy is important - understanding how the minerals are hosted tells us whether bacterial processes are feasible

Bringing Bioextraction to Market

Small scale benchtop studies

Focus on optimization of parameters and achieving target recovery rates and recovery durations

Large scale benchtop studies

Focus on achieving 1000x scale in the laboratory, followed by pilot plant construction and feasibility study

Complete FS, pilot plant for PMNs and potentially other ores

Completion of full scale feasibility study for PMN processing, execute partnerships with PMN contractors
Progress to pilot plant for other ores

Production scale plant(s)

Production scale plants for PMNs and/or terrestrial ores (depending on permitting for DSM projects) potentially co-locating with battery manufacturer in the USA

RECOVERY OF COBALT WITH ACIDIC AND AMINE-BASED EXTRACTANTS FROM HYDROMETALLURGICAL PLANT SIDE STREAM

By

Mohammadreza Arefzadeh, Sami Virolainen

LUT University, Finland

Presenter and Corresponding Author

Mohammadreza Arefzadeh
Seyedmohammadreza.arefzadeh@lut.fi

ABSTRACT

During metal extraction processes, a significant amount of acidic waste solutions containing valuable metals and organic acids can be generated as side-streams. It is efficient and beneficial for the environment, resource utilization, and economics to recover metals with high purity and organic/inorganic acids from these side-streams in metallurgical plants. Several methods can be used to recover metals from side-streams, such as chemical precipitation, solvent extraction, ion exchange, electrowinning, and thermal treatment. The most suitable method for recovering a specific metal from a side stream depends on several factors, including the type of side stream, the concentration of the targeted metal, and the desired level of purity. In some cases, a combination of methods may be needed to achieve efficient metal recovery.

This study explores three different approaches for recovering cobalt from a synthetic acidic solution containing 37 and 10 g/l of hydrochloric and oxalic acids, respectively. The first option for cobalt recovery from the feed solution involves chemical precipitation. This process does not require any pre-treatment or purification of the feed solution and involves adjusting the pH with NaOH. The resulting cobalt precipitate is separated from the solution through filtration and/or centrifugation which can be further processed to obtain high-purity metals. Chemical precipitation is a highly effective and easily operable method for recovering metals with high concentration from solutions that have low levels of impurities.

The second option for recovering cobalt involves solvent extraction of cobalt in its anionic form from a solution that has a high concentration of chloride. This is done using amine-based extraction systems such as Aliquat 336 (quaternary amine), trioctylamine, and Alamine 304-1 (tertiary amine). In this method, an anion exchange occurs between the amine extractants and the $CoCl_4^{2-}$ species, which is achieved by adding an HCl+NaCl solution to the feed to increase the chloride concentration. Based on the preliminary results obtained, it appears that this is a promising method for the recovery of cobalt.

The third option for recovering cobalt involves extracting it in its cationic form using commercially available acidic extractants such as D2EHPA and Cyanex272. However, prior to this extraction process, oxalate removal is required as a pre-treatment step. This is because increasing the pH of the acidic feed solution, as is necessary for the cation exchange mechanism, would cause cobalt precipitation in the presence of oxalate in the solution (which is the first approach).

In the batch equilibrium experiments the effect of some operational factors like, initial concentration of chloride in the aqueous phase, Acidity of feed solution (pH), concentration of extractant, the influence of time and temperature on the equilibrium have been studied. The stoichiometric coefficient of extracted cobalt species from aqueous solution has been determined based on the correlation between logarithmic distribution coefficient and concentration of extractant. Extraction isotherm experiments have been conducted, and McCabe-Thiele diagrams are constructed for initial process design (number of counter-current stages, phase ratio) to obtain highest possible yield and purity for cobalt. The results of solvent extraction experiments show that the recovery and separation of cobalt from the hydrochloric-oxalic acid solution using acidic and amine-based extractants as cation and anion exchangers is possible. Additionally, it is possible to recover cobalt with high purity through precipitation without pre-treating the feed solution. However, in this method, co-precipitation of oxalate is a significant issue that can result in the oxalate waste.

Keywords: Plant side-stream, Hydrometallurgy, Solvent extraction, Cobalt, Amine extractants, Acidic extractants, Precipitation

Hydrometallurgical Plant Side Stream

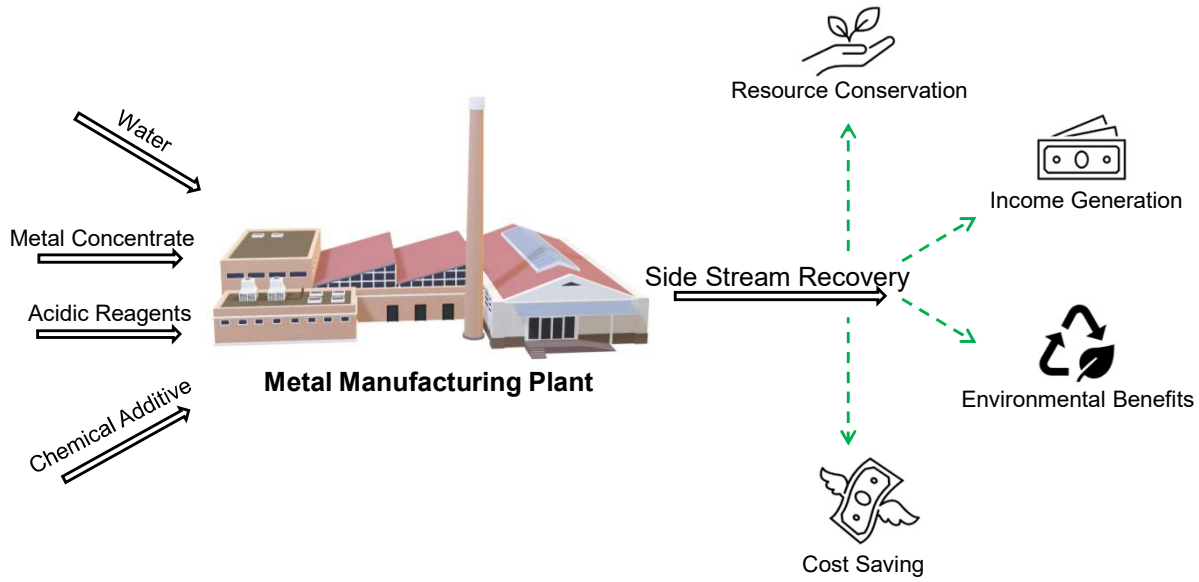

Cobalt . Oxalate Precipitation

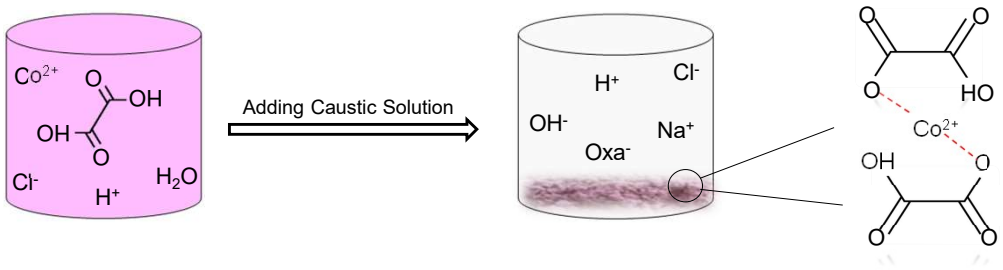

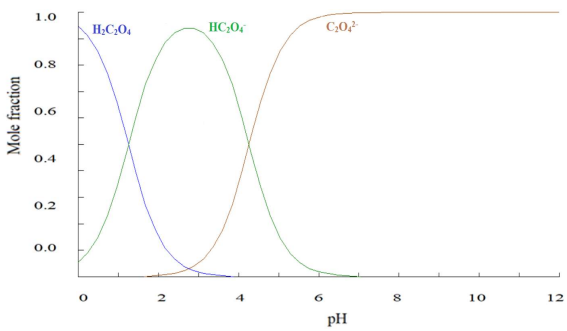

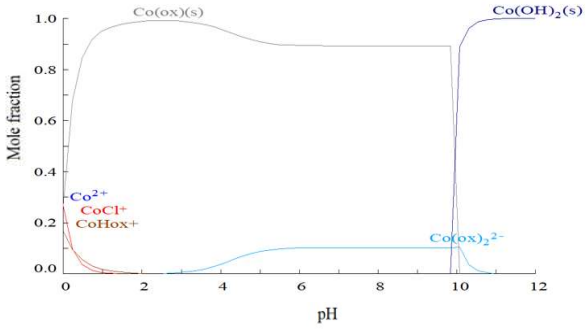

Screening Experiment of Acidic Solvent Extraction

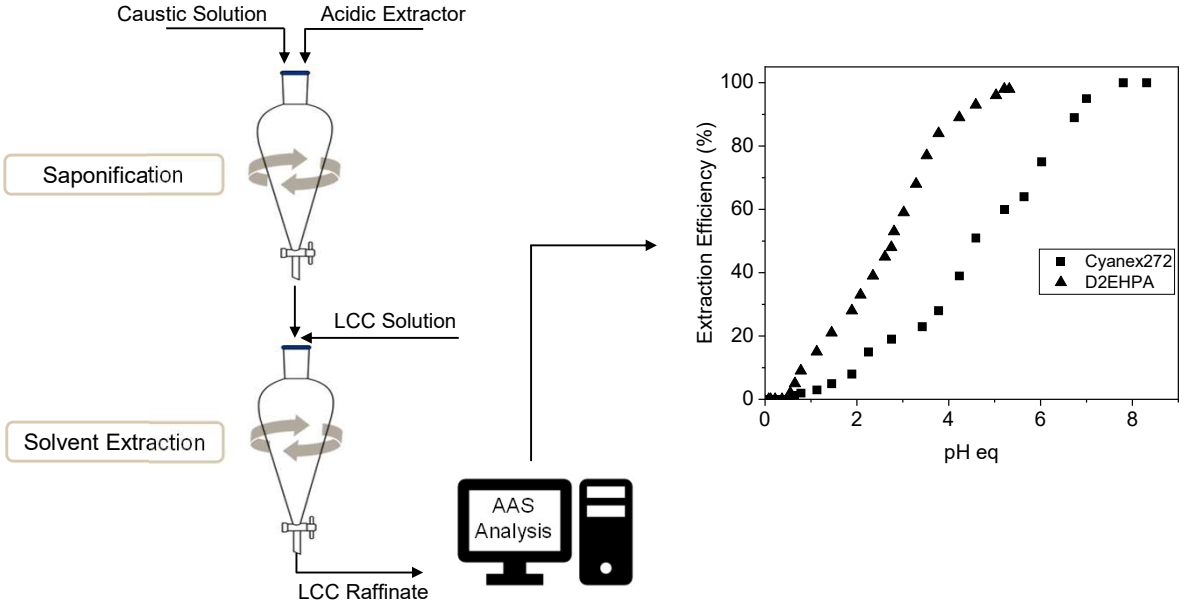

Effect of Solvent Concentration

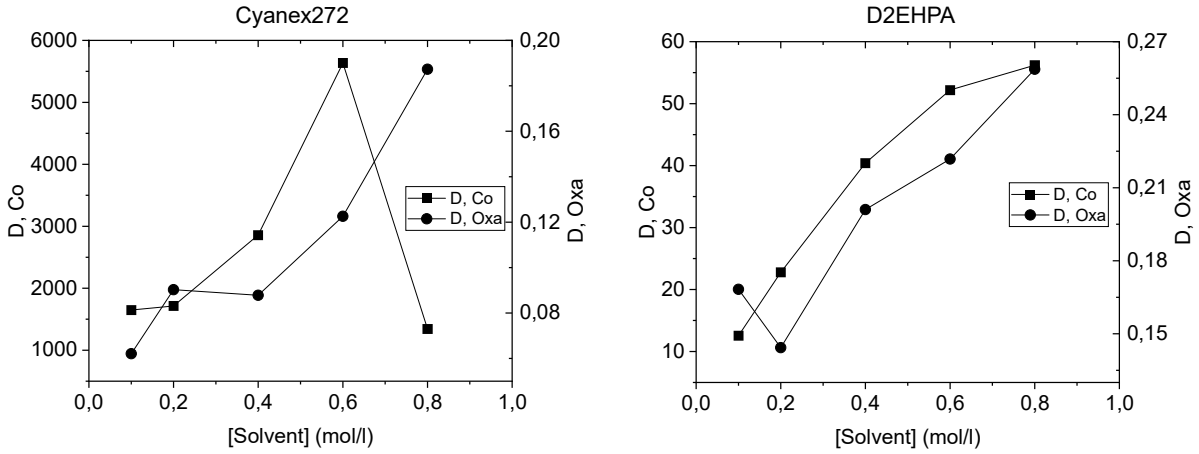

Effect of Time on Cobalt Separation

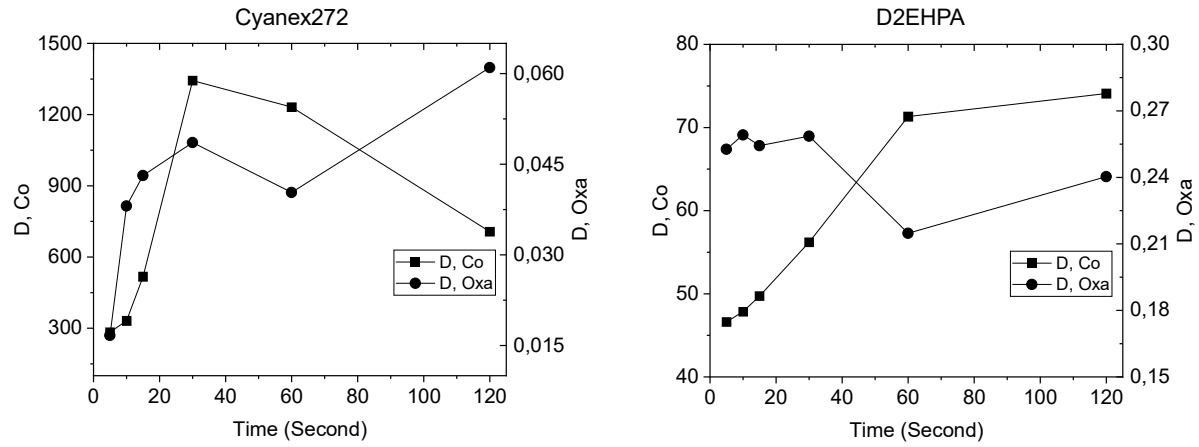

Preliminary Stripping Experiments

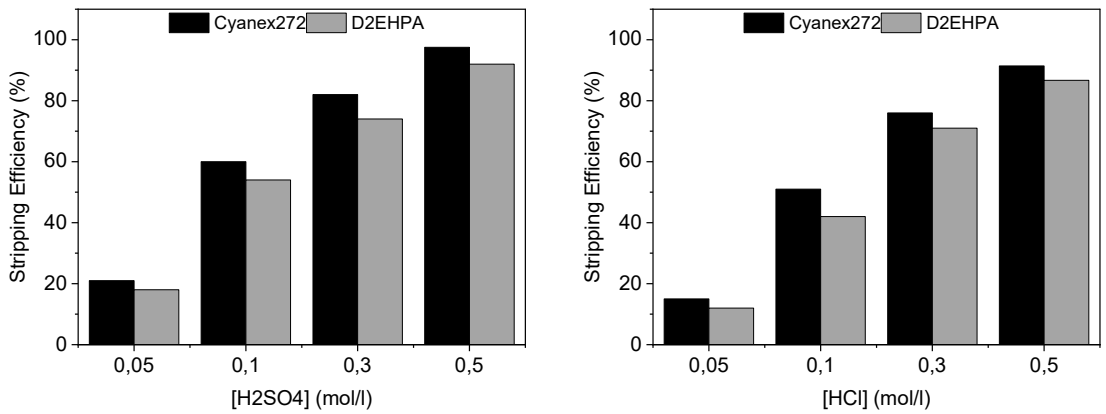

Screening Experiment of Amine-Based Solvent Extraction

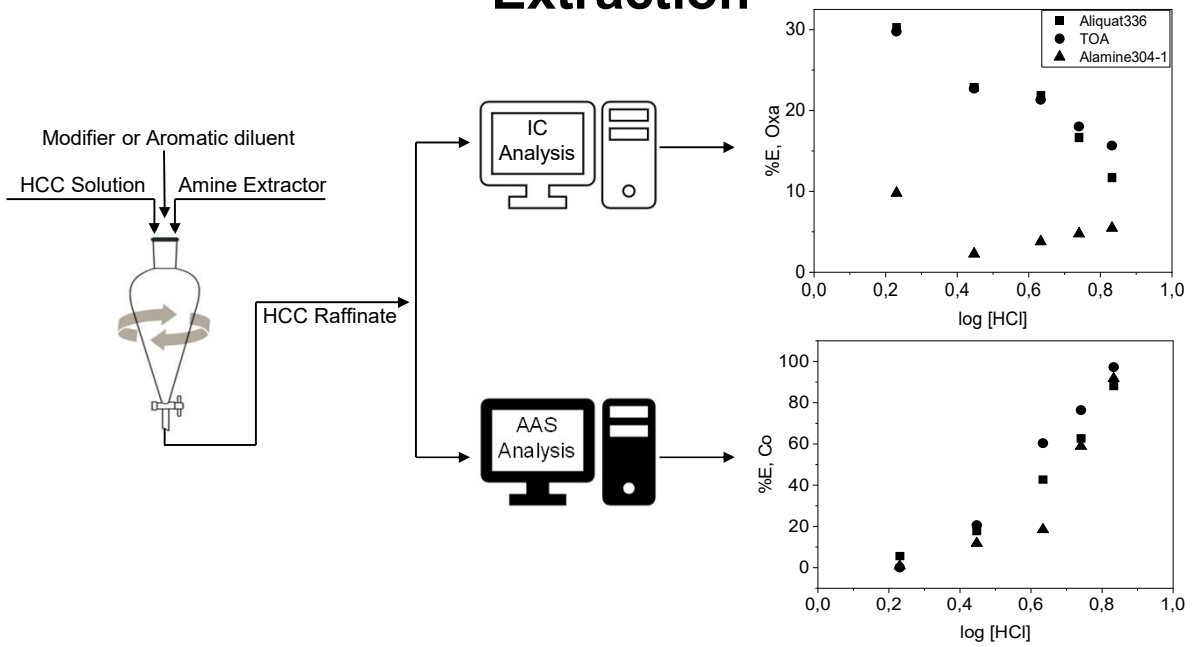

Impact of Solvent Concentration on Cobalt Separation

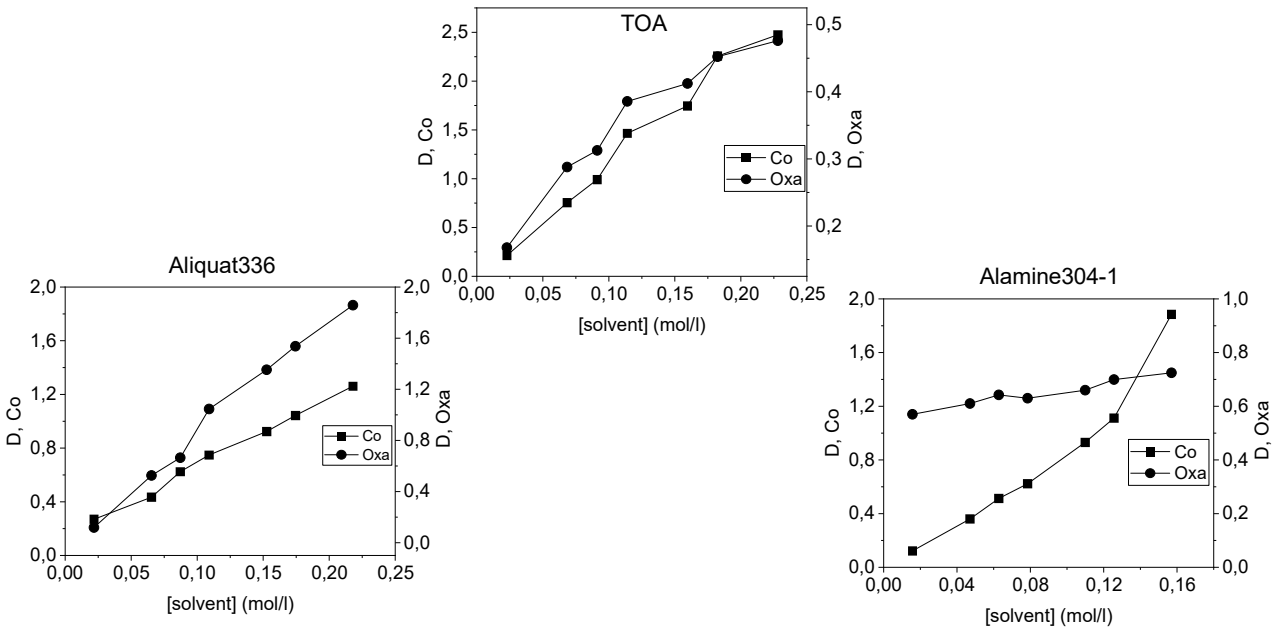

Effect of Time and Temperature on Cobalt Separation

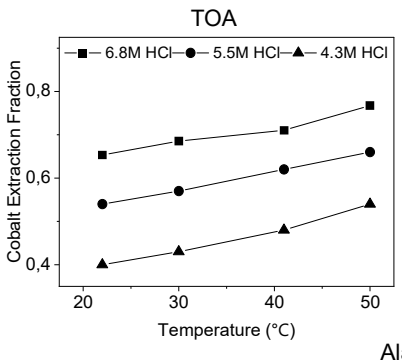

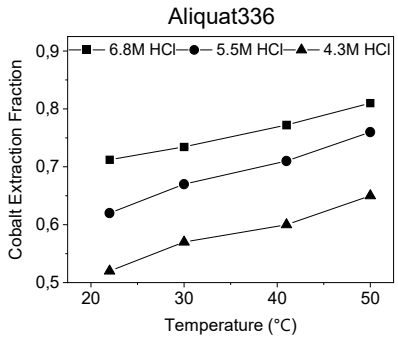

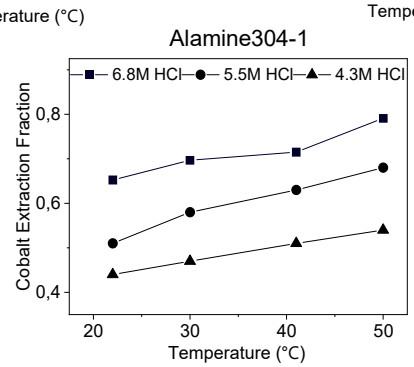

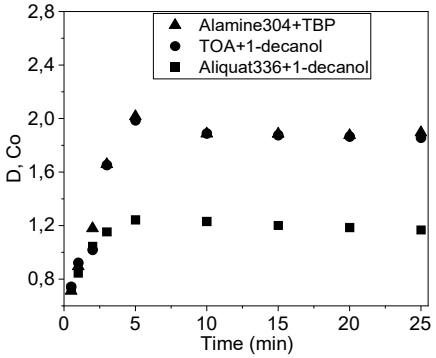

Preliminary Stripping Experiments

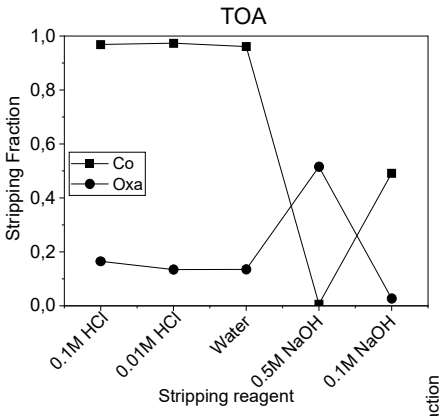

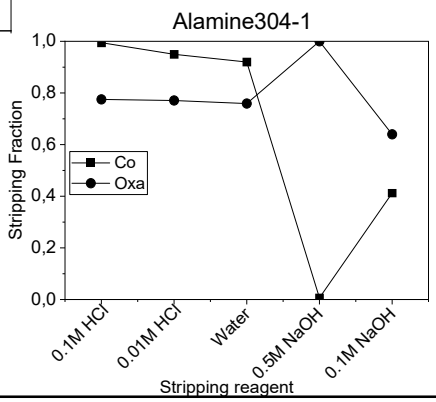

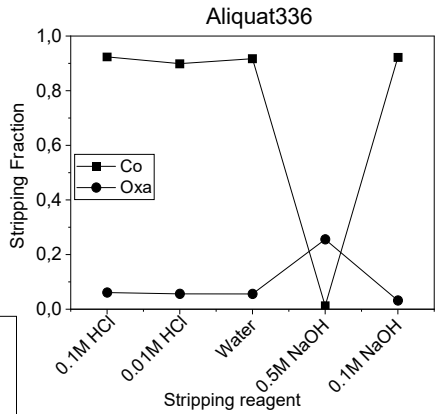

McCabe-Thiele Diagram

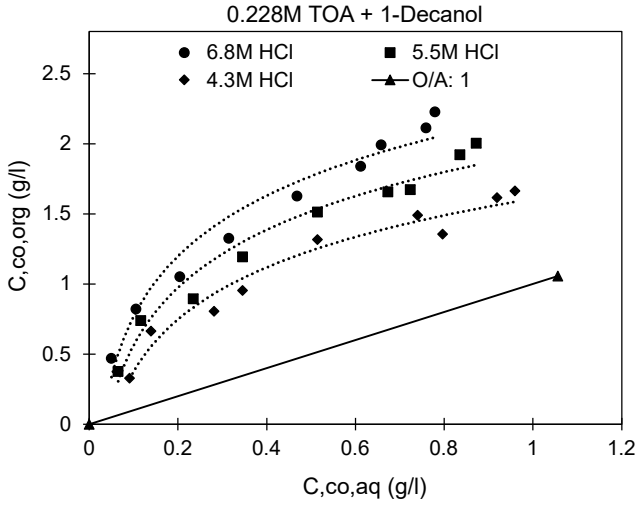

Acidic Solvent Extraction - Conclusion

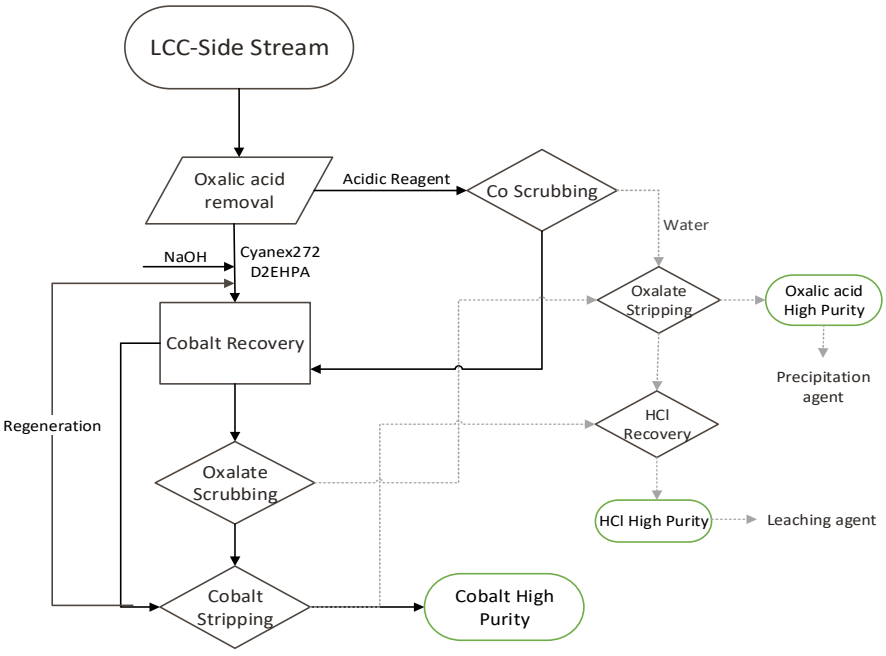

Amine-Based Solvent Extraction - Conclusion

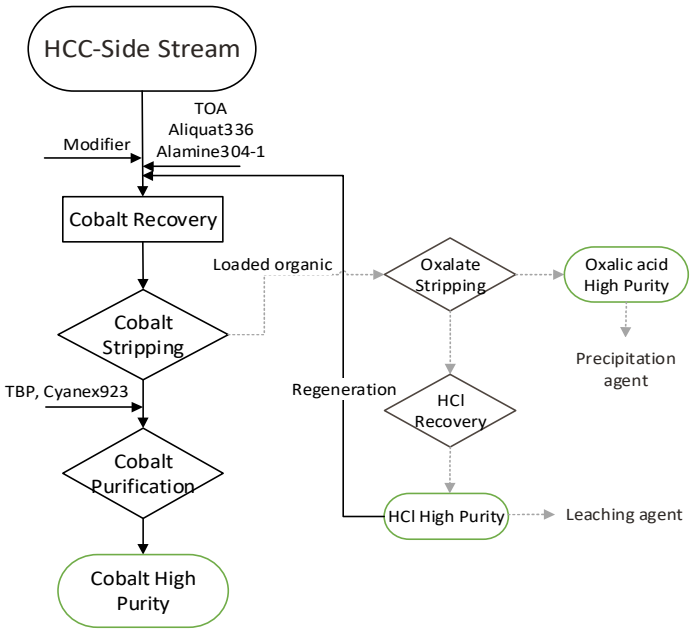

SPECIATION ASSAYS FOR NI AND CO ORES

By

Mining and Process Solutions Pty. Ltd.

Presenter and Corresponding Author

Frank Trask, MSc, MAIG, Technical Director
ftrask@mpsinnovation.com.au

ABSTRACT

Co (Group IX) and Ni (Group X) are metals commonly associated with sulphides that occurs within mafic and ultramafic rocks, and in the non-sulphide portions of these rocks that have been weathered sufficiently to concentrate either of the two above metals enough to form laterite or residual deposits. The further occurrence of cobalt in both copper sedimentary deposits and the IOCG deposits is also described.

A series of speciation assays for each element is defined, and the use of these assays is considered. Tables are presented that make the meaning of the assays clear. The various analytical procedures will be discussed, and the implications for both Ni and Co being included in the water soluble, the dilute acid soluble, the peroxide/ascorbic acid soluble, the SO_2 soluble, and the 4 acid soluble classifications made clear. The purpose of the assays is to guide process selection for these ores.

MPS will also consider the relationship between various speciation assays and the availability of specific metal anions to the various glycinate species. The use of the assays to classify ores into treatment groups is considered, and some examples are given.

MPS now have analytical chemistry capabilities within their Process Development Laboratory, and one of its principal importance for the future is to constantly work on development of speciation assays to help in the understanding of treatment selection for ore bodies.

Keywords: Speciation assays, Nickel Ores, Cobalt ores, Analytical procedures, Glycinate species, Treatment selection

Sequence Assays for Ni and Co

- What is the purpose of these Assays?

- Their purpose is to identify the mineralogy groups that the metals are associated with and thus help in understanding how to isolate/ extract the metals contained in the minerals
- This first requires an understanding of the mineralogy of Ni and Co in the sample from the deposits

Nickel and Cobalt Mineralization

- Ni deposits are broadly divided into two groups
  - Weathered silicate deposits where the Ni is substituted for the Mg position in various silicates, and this includes most of the ultramafic minerals
  - Deposits where the Ni is contained within primary sulphides and arsenide minerals

Weather Deposits or Laterites

- There are 2 types of these laterite or weathered deposits, and they can have the Ni present in two broad categories
  - The common deposits are comprised of Limonite type laterites (or oxide type) are highly enriched in iron due to very strong leaching of magnesium and silica. They consist largely of goethite and contain 1-2% nickel incorporated in goethite
  - The saprolite nickel ore formed beneath the limonite zone. It contains generally 1.5-2.5% nickel and consists largely of Mg-depleted serpentine in which nickel is incorporated. The Ni is bound in newly formed phyllosilicate minerals

Sulphide Nickel Deposits

- Deposits where the Ni is contained within primary sulphides and arsenide minerals. It is important to understand that the origin of these deposits is where the Ni has been mobilized (Covalent silicate bond broken) from the primary silicate rocks by the actions of sulphidation and concentrated as sulphides by the physical response to both settling and flow of the dense molten sulphide melt
- Sulphidation is never complete, and there will always be residual Ni associated with silicates that make the mafic or ultramafic accompanying rock mass

Example of Partial Sequence Analysis

Table 5. Nickel Sequential Analysis

Sample	Sulphide Ni (%)	Non – Sulphide Ni (%)	Total (%)
Minerals	Pentlandite; Heazlewoodite; Millerite; Gersdorffite; Orcelite; Vaesite	Nickeliferous Limonite; Garnierite	
Nickel Ore Sample	0.670	0.246	0.916
	73.14%	26.86%	100.0%

- Sample is from a komatiite (Kambalda Style B) Ni deposit
- The sample has been estimated to have 73% of the its Ni present as sulphides as determined with an Ascorbic acid/hydrogen peroxide assay
- The analyst proposes that the non-sulphide Ni is present as minerals that could have come from weathering of the komatiite, but these minerals are not seen under a microscope
- Microscopic examination shows obvious pentlandite/pyrrhotite blebs

Lessons from a Simple Assay

- Leaching tests using the GlyAmm^{TM} leaching process indicate 77% recovery of the contained Ni. This extraction fell short conventional extraction of 92% Ni so was assumed to be caused by poor leaching
- Microscopic (x 40 Binocular scope) examination of the leach residue failed to observe any sulphide minerals other than a trace of pyrite
- An ALS Global Assay, ME-ICP09, was undertaken
- This is specific assay applicable for assessing the proportion of nickel suitable for sulphide flotation, or in our case, available for Ni sulphides leaching
- It utilizes an ascorbic-hydrogen peroxide solution (L-ascorbic acid) that preferentially dissolve the sulphides minerals
- The determination matched the GlyAmm^{TM} leach extraction

Ni-Co Speciation Assay

- Involves 5 leach assays
  - Acid-soluble determination, Ni and Co + Chalcophile metals
  - Reducible Acid soluble determination
  - Ascorbic Acid soluble Ni
  - Oxidizable metals bound in sulphides and organic bound metals in porphyrins
  - Total 4 acid total metal determination

(Assay 1) Acid Soluble Determination

- Acid-soluble (AS) determination. This determines the easily soluble carbonate and simple oxide metals. This includes Ca, Mg, Sc, V, Cr, Mn, Fe, Co, and Ni. It also includes the Ni in garnierite, and in addition to this it includes several transition metals such as Cu and Zn. These Ni/Co minerals are rare!
- This will include the metals in the Calcium and Magnesium carbonate group, Rhodochrosite, siderite, rare cobalt (II) oxides, and Gaspeite (basic Ni carbonate). There may be traces of other metals, and these should be noted
- Assay: Take 1 gram of –100 micron sample, and boil in 20 mL of 5% sulphuric acid for 5 minutes. Wash through filter funnel with 3 x 20 mL aliquots of hot demineralized water, cool, dilute to 100 mL and determine by AAS or ICP, report PPM

(Assay 2) Reducible Acid soluble (SO_2 Soluble)

- This determines the V^{5+}, $Cr^{5+,6+}$, Fe^{3+}, Mn^{4+}, Co^{3+}, and Ni^{3+} in the goethite group as well as the metals in adsorbed or co-precipitated in the Manganese dioxide. Determined on the residue from the Acid soluble test (1)
- This will include the metals that are bound in goethite, (Fe and Ni), Heterogenite (Co), and trace V and Cr. It will also include the Mn in manganese dioxide and any of the transition metals that are bound in asbolane and other complex Mn^{4+} and Mn^{3+} minerals. Large amounts of Cu, Ni and Co can come out of these under the right circumstances
- Assay: Weigh 1.000 g of sample, disperse in 5 mL of water, add 20 mL of 5% sulphuric acid and 5 mL of 6% sulphurous acid, and boil for 5 minutes. After 5 minutes add 5 mL of the sulphurous acid and boil for a second 5 minutes. Filter and wash with 3 x 20 mL aliquots of demineralized wash water (hot). Dilute the filtrate to 100 mL and estimate metal content via AAS or ICP, report PPM

(Assay 3) Ascorbic Acid Soluble Ni

- Nickel-bearing sulfide deposits consist predominantly of pyrrhotite ($Fe_{(1-x)}S$), with associated pentlandite [$(Fe,Ni)_9S_8$] and chalcopyrite. In lower grade deposits, disseminated Ni sulphides may be mixed with nickel-bearing silicates. This poses a problem in ore grade evaluation because the silicate bound nickel is not recoverable with flotation or GlyLeach™ but is reported in Total Metal assay. It is therefore essential that the concentration of sulfide-bound nickel be accurately determined for ore deposit evaluation and interpretation of metallurgical test results
- Assay: Weigh 1.000 g of sample into a 250 mL beaker. Add 50 mL of 1% (w/v) ascorbic acid, 20 mL of 30% hydrogen peroxide, and shake for 1 hour on shaking table. Transfer to 100 mL volumetric flask, with 3 washes of the flask, and fill to the 100 mL mark with water. Allow to settle and estimate the Ni and Co with either AAS or ICP. Available as commercial assay

(Assay 4) Oxidizable metals not determined in Assay 2 and 3

- Oxidizable metals bound in sulphides and organic bound metals in porphyrins. This determines the copper sulphides in total, the native copper, and the remaining copper in cuprite and dellafossite. Also, the Ni and Co not solubilized in Assay 2. It also includes the whole spectra of the base metal sulphides not determined in procedure 2 and 3
- Assay: Weigh 1.000 grams and place in a 250 mL beaker and disperse in 5 mL of water. Add 20 mL of 5 % sulphuric and heat to boiling. As it boils add 3 mL of concentrated nitric in 1 mL aliquots and allow this to boil off. Allow to boil for 4 minutes for each of the 3 x 1 mL additions. Cool, and filter, washing with 3 aliquots of hot demineralized water. Dilute filtrate to 100 mL and estimate the metal content using either AAS or ICP, report PPM

(Assay 5) Total Metals Assay

- This is the normal 4 acid digestion assay that is offered universally by commercial laboratories
- This assay is normally done using a base of sulphuric acid, to which other acids are added, nitric, hydrochloric, and lastly perchloric acid. This is evaporated to fuming SO_3, diluted, and analyzed by ICP
- This is the total amount of contained Ni against which all the sequential assays are summed and evaluated. Available as commercial assay

Response of Minerals

Formulae	$NiSiO_4$	$NiCO_3$	NiO	$CoCO_3$	$CoAsO_4$	CoOOH	Ni_2O_3	(Ni,Fe)OOH	NiFeS	NiFeS	$CuCo_2S_4$	NiS	NiS	CoAsS	NiAsS
Test	Garnierite	Gaspeite	Bunsenite	Spherocobaltite	Erythrite	Heterogenite	Trevorite	Ni Goethite	Pentlandite	Violarite	Carrolite	Heazelwoodite	Millerite	Cobaltite	Gersdorffite
AS Ni,Co (1)	x	x	x	x	x										
Reducing Acid (2)						x	x	x							
Ascorbic acid (3)									x	x	x	x	x		
Total Ni, Co (4)	x	x	x	x	x				x	x	x	x	x	x	x
Total Metal Assay (5)	x	x	x	x	x	x	x	x	x	x	x	x	x	x	x

A Practical Use of the Ascorbic Acid H_2O_2 Assay

- Eurobattery Minerals announced the start of a new drilling campaign as part of its Spanish Corcel Project
- The results of the mineral test conducted in Perth, Australia, confirmed the economical grade nickel sulphide found in the Corcel Project
- The results from the analytical method utilized by ALS Global (MEICP09) confirmed that 75 to 85% of the nickel in the samples submitted is attributable to nickel sourced from economic sulphide minerals
- The accuracy of the sulphide Ni determinations has been supported by both QEM scans and good old fashioned microscopic point counts
- A good use of assays to craft a nice JORC Resource estimate!

Other Uses for this Assay

- The Ascorbic Acid method is often used as an umpire assay to determine flotation recoverable Ni in Sulphide ores
- It is also used in mills to determine the Ni from sulphides lost in tailings
- It can also used to describe the performance of Leach Available Ni in sulphide ores

Problems with the Ascorbic Acid H_2O_2 Assay

- The Ascorbic acid method is designed to extract nickel sulphides while leaving nickel oxides and any other Ni minerals undigested. This is achieved using a short digestion time at room temperature
- This provide a subjective (empirical) approximation of the proportion of nickel present as sulphides, and as such the test is like many sequence assays, a subjective assay
- Variation of the time and temperature may lead to a different answers or determinations

Minerals that Respond to Glycine

- Minerals that are solubilized by the Ascorbic/H_2O_2 estimate what is soluble by our GlyLeach™ or GlyAmm™ process. This is also regulated by dissolved O_2 and temperature
- Essentially Ni sulphide minerals that are soluble in an Ascorbic assay, can be equally recovered via either flotation or GlyLeach™
- Minerals that are dissolved by the Reducible acid methods can also, after SO_2 or similar treatment, be recovered and separated via the use of GlyLeach™
- Minerals that are solubilized with the normal AS estimation methods are not common, but they can also be recovered via the use of GlyLeach™. Gaspeite as an example is solubilized slowly at room temperatures, but a modest heat will easily release the Ni as glycinate complexes

Draslovka's Innovation Development Laboratory

- Draslovka is now building up their assay capability to meet internal assay requirements
- Improves turn around and delivery of projects
- Our new assay laboratory
  - cold fusion digestor
  - AAS
  - ICP
  - and soon XRF
- Gearing up to be able to perform these sequential analysis to better estimate the leaching performance with ore samples

THE RADFLOW™ THICKENER FEEDWELL: REDEFINING THICKENER SIZING AND FLOCCULANT USAGE

*A. Krassnokutski, [2]M. Gillespie

Krassno Consulting, South Africa.

[2]Roytec Global (Pty) Ltd, South Africa

ABSTRACT

The development of the novel Radflow™ thickener feedwell and its successful application is investigated. Typical thickener feedwell deficiencies were demonstrated and systematically overcome to ultimately culminate in the design of an advanced feedwell. Scale model methodologies, in addition to Computational Fluid Dynamics (CFD), are presented to show the Radflow's superior energy dissipation characteristics in comparison to other standard industrial feedwells.

Three Radflow feedwell case studies are then presented; two retrofits and a new thickener installation by Roytec Global (Pty) Ltd. These case studies demonstrate that the *standard thickener design heuristics* (rules of thumb) of limiting rise rates and flux rates are *excessively conservative* when operating a thickener with a more *efficient feedwell* design. Alternatively, it is shown that if the Radflow is used in a thickener that has been conservatively sized or operated, then it is unnecessary or sometimes even counterproductive to follow the standard practice of enhancing the settling characteristics. Excess flocculant adds to additional operational expenses, but can also limit the achievable underflow density. Additional dilution of the feed can also attribute to design and operational complexities, along with added energy consumption.

Hence, an argument is presented that the thickener design scale-up *safety factors* (limiting rise and flux rates) are *relaxed* to more reasonable values, which approach the free-settling rates achieved in laboratory tests, if a well-designed feedwell is used. This is because the specific volumetric sizing flux ($m^3/m^2.h$) can approach the limit of the free settling rate when a thickener's flow dynamics are tightly controlled. This is particularly important in dealing with slow settling (and notoriously difficult to thicken) materials such as clays and fine precipitates. However, since thickener diameters are often dictated by external parties or other factors, a consolation argument is made (for conventionally sized thickeners) that the flocculant dosing rate should be minimized during thickener commissioning, to a level where the operational liquid rise rate is marginally lower than the floccule free-settling rate achieved in laboratory tests. This argument can be extrapolated to an extreme case in which some conservatively sized or operated "high-rate" thickeners may not require any flocculant at all and hence revert back to a so-called "conventional" thickener. While this may not be a practical or feasible for most thickeners, there are applications in which the use of polymer flocculants is undesirable and hence the Radflow feedwell presents an elegant enabling solution by limiting the thickener size for these cases.

Keywords: Feedwell, flocculant dosing, thickener sizing, thickener rise rate, thickener flux, Radflow™ feedwell

**Corresponding Author: A. Krassnokutski, alex@krassno.co.za, +27(0) 82 751 7077*

INTRODUCTION

The advent of High Rate Thickeners in the 1980's was underpinned by the increased dosage of flocculant, this overcomes the negative effect of the feed kinetic energy in smaller thickener tanks. Therefore, the importance of the feedwell which governs the flow regime inside the thickener body is almost always underestimated. This is not surprising because, from an specific electrical energy consumption viewpoint, a thickener's energy dissipation (typically > 5 W/m^3) is so tiny in comparison to other pieces of mining equipment that it is often, incorrectly, considered inconsequential.

Simplistically put, a thickener turns muddy water into mud and water; hence, a thickener has outputs of (i) underflow density and (ii) the overflow clarity. Therefore, the amount of solids in the overflow and more importantly the amount of liquid in the underflow are inversely indicative of a thickener's performance. These outputs are calculated in relation to a thickener's size or cross-sectional area (fixed parameter). So-called *high-rate thickeners* have an input of *flocculant dosing* (typically measured in grams of flocculant per dry ton of solids).

Thickeners are commonly sized on the material settling and compaction characteristics, which typically use the so-called *static batch* method (settling cylinder tests). This method entails mixing a measured amount of flocculant into a cylinder of slurry and measuring the fall of the clarified supernatant/mud bed interface level at regular time intervals. From this, the resultant so-called "free settling velocity" (m/hr) can be derived to use as the basis for a thickener's volumetric sizing (m^3/m^2/h). The solids residence time in the cylinder is also monitored against the settled mud density, which can be used to determine solids inventory in the commercial thickener required to achieve a certain underflow density, see Figure 1. However, it must be pointed out that more advanced techniques such as *dynamic batch mode*, or better yet, *dynamic continuous modes* (duplicating the same continuous operation as an actual thickener in a laboratory scale model) can yield more representative results, (Vietti & Dunn, 2012).

In order to size a commercial thickener, vendors and external consultants will commonly multiply the laboratory measured, static batch, free settling velocities and volumetric flux rates by a *design fraction* (f < 1), which is the inverse of the *safety factor* ($S.F. = f^{-1}$). This will determine the required thickener size for a given feed flow rate. By way of example, the industry commonly uses a safety factor of 4-6 and hence divides the free settling velocity by this value to determine a thickener's volumetric flux (m^3/m^2.h or maximum rise-rate (m/h). This is then checked against the historic/generic values[1] of:

- Normal Grind Gold Slurries: 4 to 7.5 m/hr.
- Higher Density or Coarser Solids: 5 to 10 m/hr.
- Clays/precipitates: 1 to 3 m/hr.

Similarly, the static batch solid flux rate calculated from cylinder tests will also be multiplied by this design fraction to predict the achievable solids flux rates (t/m^2.h) from full-scale machines. This value is then checked whether it fits within the generic flux range of:

- Normal gold: 12 to 18t/m^2.day (Most high rate thickener applications)
- High Gold / Magnetite, high-density material (SG>4): 18 to 24 t/m^2.day
- Poor settling materials (clay's and precipitates): 4 to 8 t/m^2.day

These generic rule-of-thumb values are de-rated further if necessary. Introducing a safety factor is important because the initial conditions of a cylinder test are not congruent with that of a continuous thickener. In particular the lack of energy in the cylinder test as compared to the considerable kinetic energy introduced with commercial thickener feed operation. Moreover, this safety factor is also

[1] In-house values used for thickener sizing by Roytec Global (Pty) Ltd.

necessary to compensates for dynamic factors attributable to a thickener's operation, including but not limited to:

i. Upset conditions
ii. Changes in thickener operating styles (operator preferences)
iii. Changes in ore type (in particular that of clays and fine precipitates)
iv. Feedwell inefficiencies.

It is believed that pt. (iv): feedwell inefficiencies are largely responsible for both this bloated safety factor, and excess flocculant usage. This is because the feedwell governs the flow regime and therefore the effectiveness of flocc settlement and distribution inside the thickener body. Hence, it is proposed that for a well-designed feedwell, this safety factor can comfortably be reduced to within the range of 2 < S.F. < 3. In **Case Studies**, p.11, three case studies are presented to support this argument.

Conversely, if a thickener has been designed conservatively with a highly efficient feedwell (such as the Radflow), or is being run below its designed flux/rise rate, it is recommended that the flocculant dosing rate should be reduced to where the operational liquid rise rate is marginally lower than the floccule free-settling rate achieved. This not only reduces operational expenses, but introduceds advantages of:

i. increasing underflow density,
ii. increasing the thickener's operational stability
    a. reducing the rake torque
    b. Less chance of "doughnutting[2]" or the formation other over-flocked obstructions.

Figure 1 shows the static batch settling curves for a 5% kaolin slurry dosed with flocculant at 50g/t (purple) and 20g/t (green). The free settling rate at 20g/ton is 4.3 m/h which is half that achieved at 50g/t. However, plotting time on a logarithmic axis shows that the ultimate consolidation of the "under-dosed" sample is greater than that achievable by the "optimal" dosed sample with a cross-over point occurring at about 2700s, or about ¾ of an hour, proving that lower flocculant dosages can achieve better compaction.

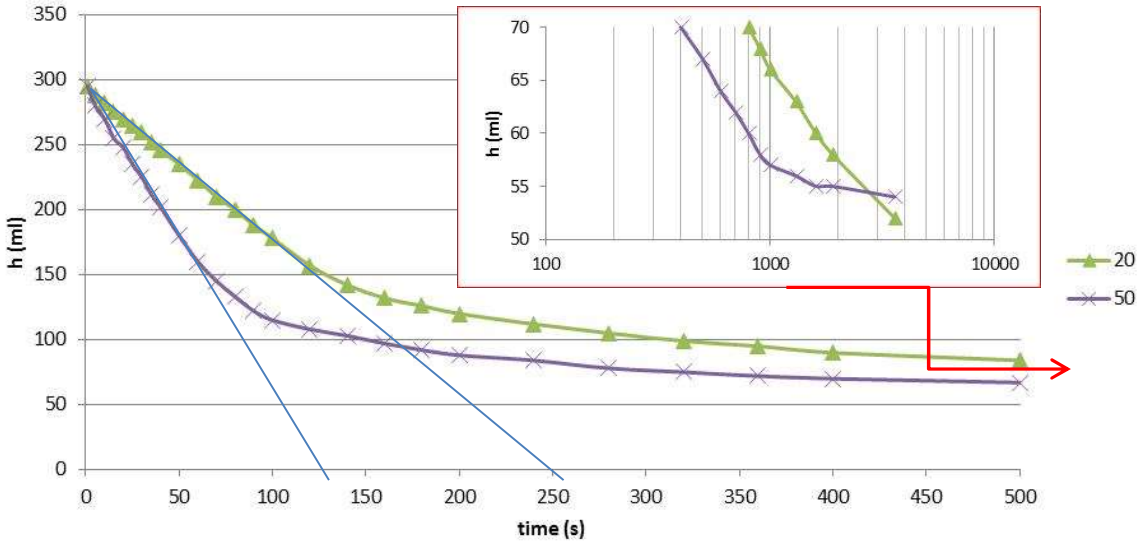

Figure 1: Static batch (jar) test results showing free settling velocity and ultimate consolidation of a kaolin slurry at flocculant dosing of 20 and 50 g/t.

[2] This flow feature occurs when an accumulation of underflow solids accumulate around and rotate along with the raking structure.

BACKGROUND

According to Outotec (Triglavcanin), a feedwell has 6 primary functions, namely:

1. To dissipate the energy of the incoming feed.
2. To introduce dilution water to achieve the optimal density in the feedwell for flocculation to occur.
3. Mix the flocculant into the incoming feed.
4. Retain the feed in the feedwell whilst dilution and flocculation occurs.
5. Distribute the flocculated material evenly over the thickener diameter.
6. De-aerate the incoming feed.

The importance of energy dissipation was only fully appreciated through in-house experimentation and Computational Fluid Dynamics (CFD) as elaborated upon in the following chapters.

Experimental Testing

In 2011, Roytec commissioned the design, building and testing of a Ø1m scale model thickener, Figure 2 (a). This thickener was tested with various standard industrial feedwell designs; see Figure 2 (b).

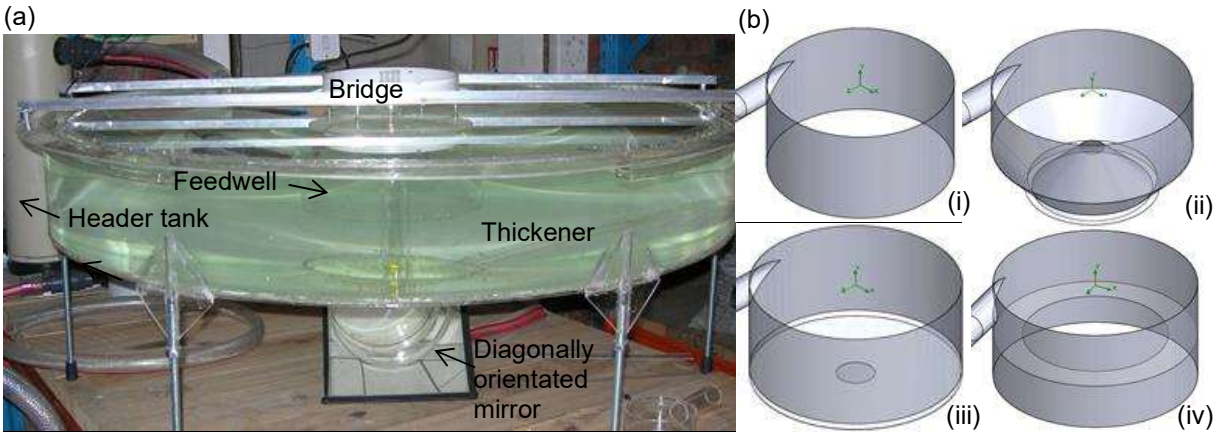

Figure 2: (a) Perspex Ø1m scale model thickener and (b) schematics of the tested standard industrial feedwells, namely open: (i) *open*, (ii) *closed*, (iii) *open with false floor* and (iv) *open with shelf*.

Adverse Flow Effects

Water was used as a working fluid which was recirculated between the header tank and the thickener (rise rate ~ 2m/h) and dye was used for some elementary tracer analysis. In Figure 3 (a) dye is drawn upwards as a vertical trace; however, the resulting image shows a large radial outflowing on the thicker floor and a smaller inwardly flowing component above this region. These flows are depicted in magnitude and direction by the red arrows and illustrate the adverse flow effect of *radial recirculation*. In addition, the dye appears to be drifting off of the diagonally positioned mirror beneath the thickener, indicating another adverse flow effect: *tangential swirl* in the thickener's tank, indicated by the blue arrow. Anyone that has ever stood on a thickener bridge will probably have observed this gentle rotation of the tank's contents.

Ion exchange resin (ρ ≈1200 kg/m^3, Ø ~800µm) was subsequently used as tracer particles which were added to the header tank to observe the distribution pattern on the tank floor. Of the tested feedwell

(a) (b)

designs, the open feedwell performed worst of all with a high-velocity tail which essentially inhibited particle settlement on a third of the thickener's floor. When the amount of traces was increased to mimic the pulp-bed formation, this high-velocity tail scoured a bald patch on the thickener floor as can be seen in Figure 3 (b).

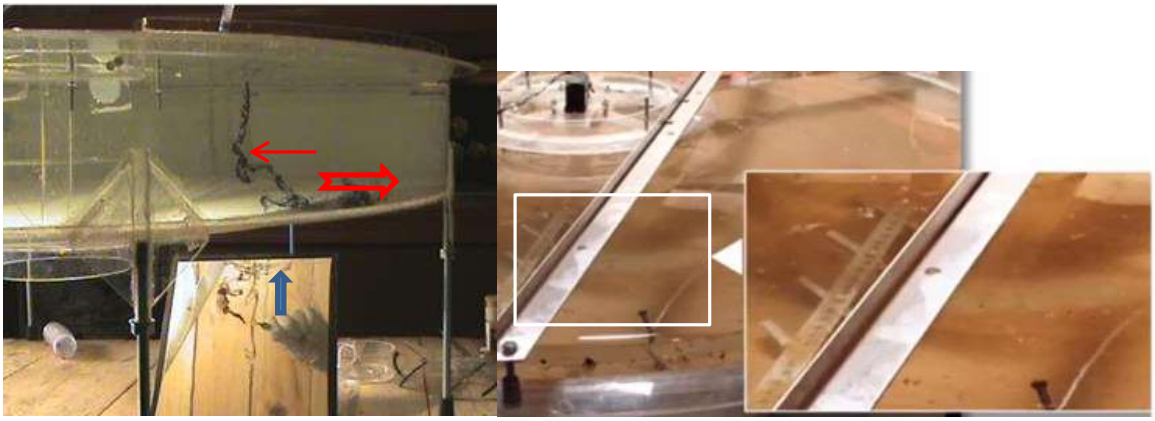

Figure 3: (a) Dye tracer tests showing tangential swirl and radial recirculation and (b) Preliminary sedimentation tests showing mud bed scouring with the open feedwell, i.e. flow asymmetry.

This observation of bed scour is crucial because it shows that the feedwell not only controls the settling characteristics of newly formed floccs, but also has the potential to re-suspend and break up already settled flocc composing the pulp-bed.

Furthermore, if this asymmetrical flow occurs, then floccule deposition is preferential on one side of the thickener and bed scouring is preferential on the other. This has the knock-on effect is that the rakes will experience an asymmetrical and cyclical loading which can cause the rake to rock vertically and cause the raking mechanism to wear prematurely. Again, this is often observed on site by the rocking of the raking mechanism's slab hinge.

In summary, the above three adverse flow conditions limit a thickener's performance and are depicted in Figure 4.

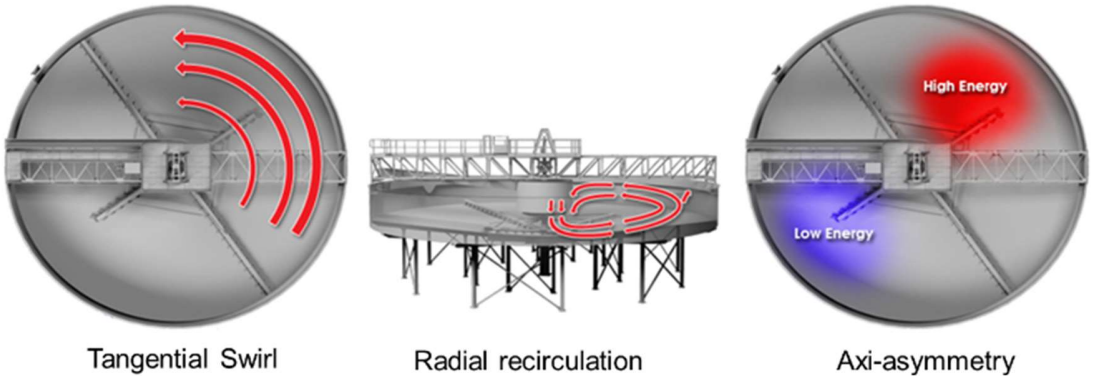

Figure 4: Adverse flow conditions associated with standard industrial feedwells

The Radflow Feedwell

The Radflow feedwell was developed to counter the aforementioned adverse flow conditions shown in Figure 4, with the intentions of achieving an axi-symmetric, quiescent settling zone inside the thickener body in order to promote flocc settling and minimise bed scouring.

The Radflow is typically supplied with a forced dilution pump christened the ETAQ™ pump (Efficient flow:ηQ) as is shown in Figure 5 (b), however, this is process dependent.

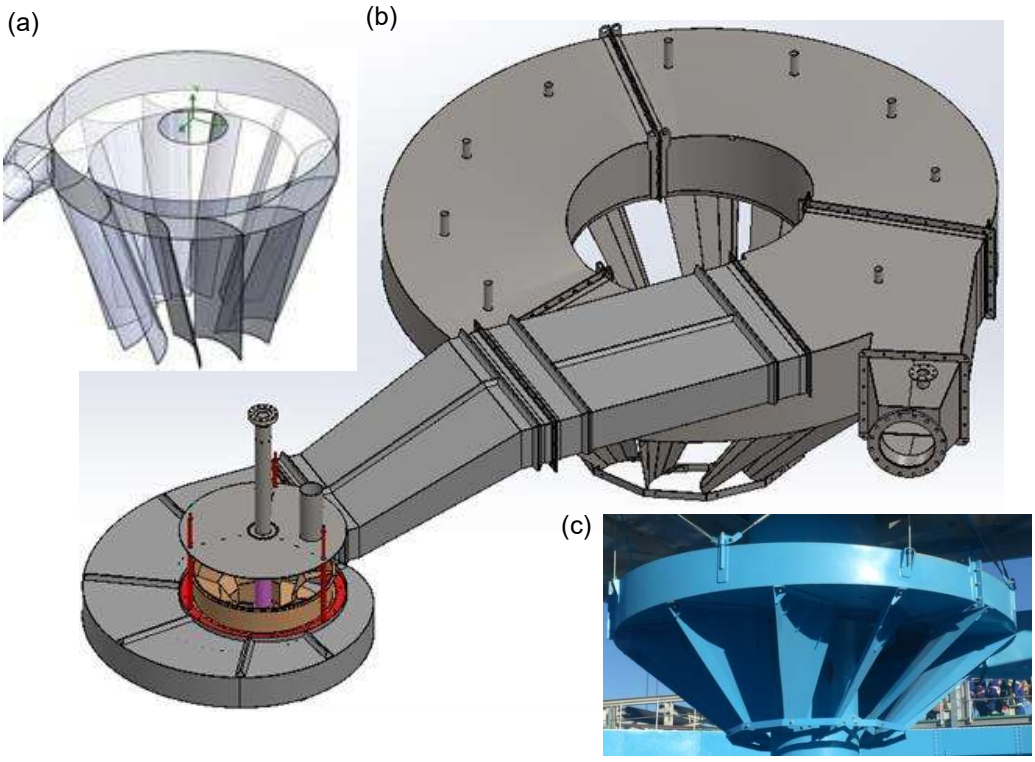

Figure 5: (a) Schematic of an early Radflow concept, (b) CAD model of standard Radflow™ feedwell and ETAQ pump designs and (c) Ø3.6m Radflow™ feedwell installation.

An evolutionary experimental approach was adopted in the Radflow's development. For example, it is apparent that the shelf geometry used in the open feedwell modifications, Figure 2 (b) (iv), has been carried through into the Radflow design, Figure 5. The *vane* or *flow shaper* section concept began as multiple flat plates, hung vertically and radially off the shelf to reduce tangential swirl. These evolved into inclined quarter pipe sections shown in Figure 5 (a) and then finally into the tapering, curved and inclined vane geometry as shown in Figure 5 (b) and (c).

The so-called "raceway" section was initially formed by installing an additional shelf in the feedwell, above the feed pipe, Figure 5 (a). However, both experimental work and CFD indicated a slight flow asymmetry associated with this geometry which was later corrected by spiraling the top shelf so that the raceway acts like a volute of a pump (working in reverse). This geometry had the further advantage of providing a dilution injection port adjacent to the feed pipe entry point, Figure 5 (b)

Comparative Experimental Results

In the experiments that followed, the level of solids (ion exchange resin) was increased to approximately half-fill the tank which is about the level of the (Open/Closed) feedwell discharge levels. The theory is that the exchange resin now behaves more representedly like that of the Hindered Settling Zone (HSZ) of a thickener rather than the compacted bed. This is speculated to be a more appropriate analogue because of the large void fraction is common to both the resin analogue and the HSZ.

The performance improvement of the Radflow is best illustrated by comparing the perturbed regions surrounding the various feedwell designs, shown in Figure 6. The Radflow feedwell shows a remarkable reduction in the HSZ perturbations in comparison to the other feedwells. On the other hand, the open feedwell performs worst of all with the largest perturbed area surrounding the feedwell. Moreover, this perturbed pattern is also the most asymmetrical, as previously defined as axi-asymmetry and shown in Figure 4.

While it is acknowledged that this experimental technique is a simplification of a thickener's true operation and only illustrates the settling aspect of uniformly sized particles, these simplifications allow us to peer beneath the surface of a thickener and develop a image of what occurs inside of a commercial thickener. The behavior of ion exchange resin as a HSZ analogue appears to mimic an actual thickener's behavior accurately as witnessed by the occasional formations of plumes, see Figure 6. Plumes are particles ejected from the HSZ, by short-circuiting, energy flows from the feedwell, which will reach the water surface. Similarly, dark patches are occasionally observed as on the supernatant surfaces of typical operating thickeners.

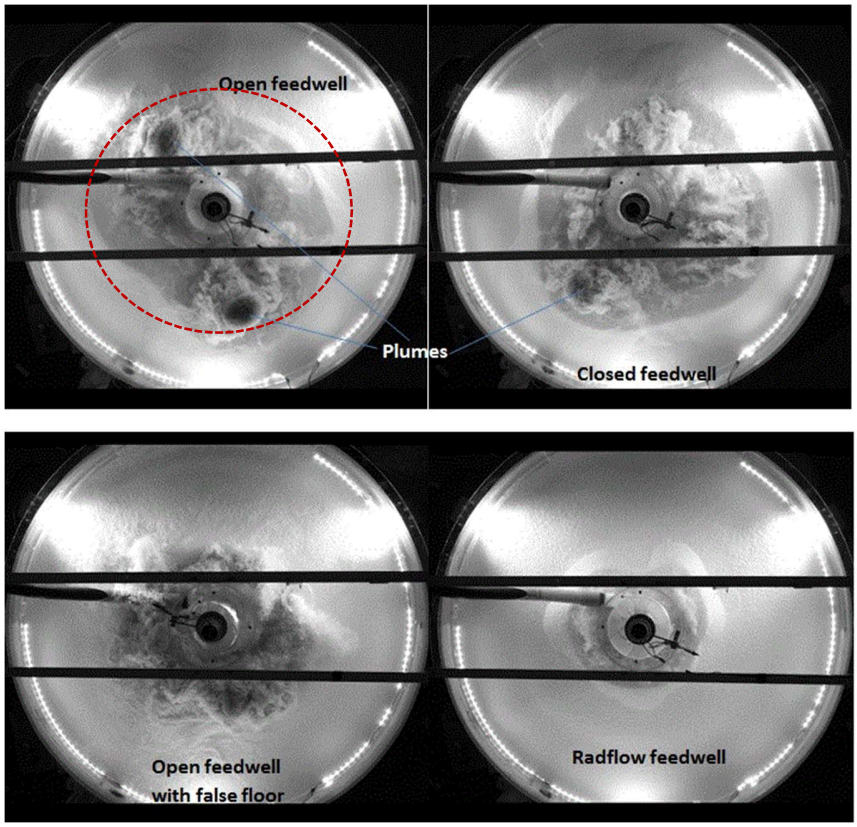

Figure 6: Perturbed regions surrounding different feedwell designs at a rise rate of 3m/h.

Quantifiable results are also determinable from this simplified experimental technique. More specifically, the perturbed region surrounding the feedwell is circumscribed, [red dashed line in Figure 6 (open feedwell)] and measured as a fraction of the thickener diameter. This is done over a range of feed rates, for the different feedwell types. These results are interpolated and/or extrapolated to determine the rise rate at which the perturbed region reaches the circumference of the thickener. The results are given by:

- Open: 3.6 m/h,
- Open with false floor: 5.3 m/h,
- Closed: 4.2 m/h,
- Radflow: 9.9 m/h.

These results suggest that the Radflow can operate at approximately double the rise rate of the closed feedwell (and open with false floor) and almost triple that of the open feedwell. This simplistic analysis only simulates the settling of uniform spheres in a very narrow Particle Size Distribution (PSD) range, nevertheless, these results strongly support the case of reducing the thickener's design safety factors.

CFD Analysis

A complete Computational Fluid Dynamic (CFD) simulation of a thickener, including the flocculation process, is exceedingly complex. In order to achieve realistic results, the CFD code needs to encompass a *population balance* model to model the flocculation process and the solver also needs to be coupled to a Discrete Element Methods (DEM) solver in order account of how the settling solids (floccs) influence the flow through gravitational acceleration. This complex modeling has achieved some degree of success in the AMIRA P266 program (Fawell, 2009).

For the CFD analysis presented, it was elected to perform an elementary, first approximation, analysis on a thickener, using water as the working fluid. Hence, these simulations are more akin to the scale-model results as shown in the previous sections. While limited, this allows these results to be compared directly against the scale model results.

CFD Setup and Assumptions

FloEFD™ is the CFD solver used for this analysis. FloEFD is a RANS (Reynolds Averaged Navier Stokes) solver and uses the $k-\varepsilon$ turbulence model, run as a steady state analysis. Hence, the resultant pressure and velocity fields represent the *averaged* or *most likely* results. In reality, however, the system is extremely turbulent and therefore transient flow features, such as eddy formations will be prevalent in the thickener and feedwell. An example of this is the transient plume formation shown in Figure 6 (open feedwell) and described in the associated text.

CFD simulations of a Ø 21m thickener operating at a rise rate of 4 m/h was modeled for a thickener using an open, a closed and a Radflow™ feedwell (all simulated under identical conditions). Similar to the scale model experimentation, this model uses water as a working fluid with no underflow and in which raking structure was omitted.

The models were set to converge on goals of averaged velocity and pressure. Each model consisted of approximately 500k cells.

CFD Results

When comparing the velocity magnitudes (colour contours) of Figure 7a), b) and c), it can be see that the velocities in thickener body using the open feedwell is greatest, while that of the Radflow™ feedwell is significantly less than both the open and closed feedwells. This indicates that the Radflow™ feedwell dissipates the greatest amount of the feed's incoming kinetic energy and gently introduces the feed into the thickener body. Velocity/energy in the thickener body impedes flocc settling and therefore the quiescent zone surrounding the Radflow™ feedwell allows for floccules to settle out of the solution more quickly, thus enabling a greater flux rate. These results are consistent with scale modeling results for low pulp-bed experiments (Figure 6) which shows that the Radflow™ exhibits a step-change in settling performance.

Figure 6a) and b) show a large velocity flowing from the feedwell radially outward along the thickener floor, identical to Figure 3 (a). It is this velocity that induces the radial recirculation pattern, shown in Figure 4, which can lead to floccs short circuiting.

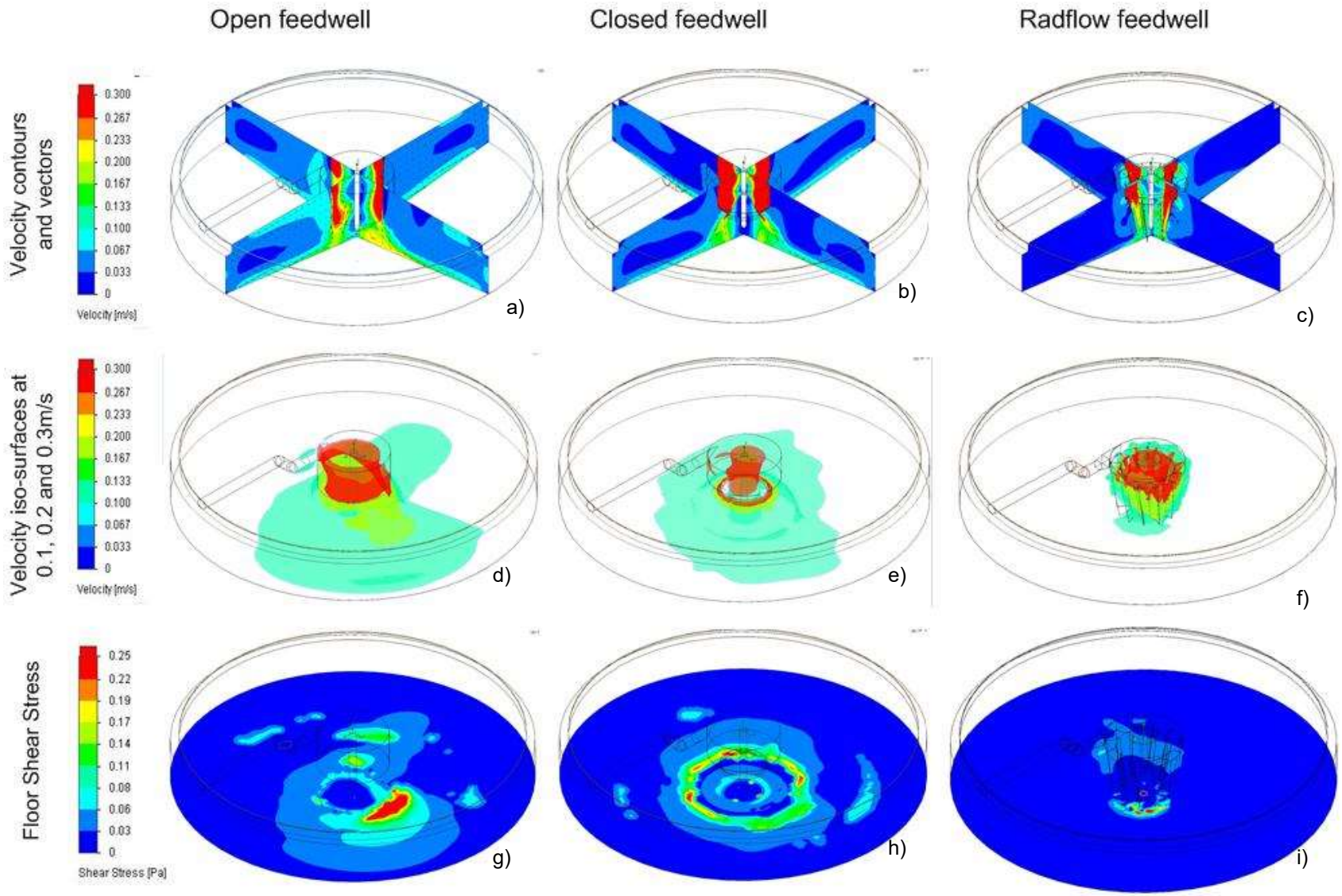

Figure 7: CFD comparisons of various feedwell designs.

An alternative way to view the velocity magnitudes is to view the velocity iso-surfaces in the thickener body as shown in Figure 7d), e) and f). Again, it is apparent the Radflow™ feedwell dissipates almost all the feed's kinetic energy within the feedwell as compared with the other feedwell designs. Figure 7d), shows a large velocity iso-surface "tail" extending along the thickener floor opposite to the feedpipe entry point. This is consistent with the plume observed in Figure 6 (open feedwell).

Lastly, Figure 7g), h) and i) show the shear stress on thickener floor. It is observed that the open feedwell induces a patch of high shear on the floor, induced by the abovementioned high velocity tail and is consistent with the scoured patch illustrated in Figure 3 (b).

Figure 8 shows velocity contours and streamlines through 3 individual sectional planes which help illustrate how the Radflow dissipates the incoming kinetic energy so effectively. The incoming velocity is bound between the upper and lower shelves to maintain a high swirl velocity in this *raceway section* (shown in vertical plane and the upper horizontal plane). The lower horizontal plane shows how this swirl velocity is maintained to a degree inside the core of the Radflow's *flow shaper* section. However, in order for the flow to exit this region, it must first reverse direction to flow out along the positive camber of one of the vanes. Furthermore, by moving radially outwards, a source flow is initiated which, by definition, entails velocity reduction.

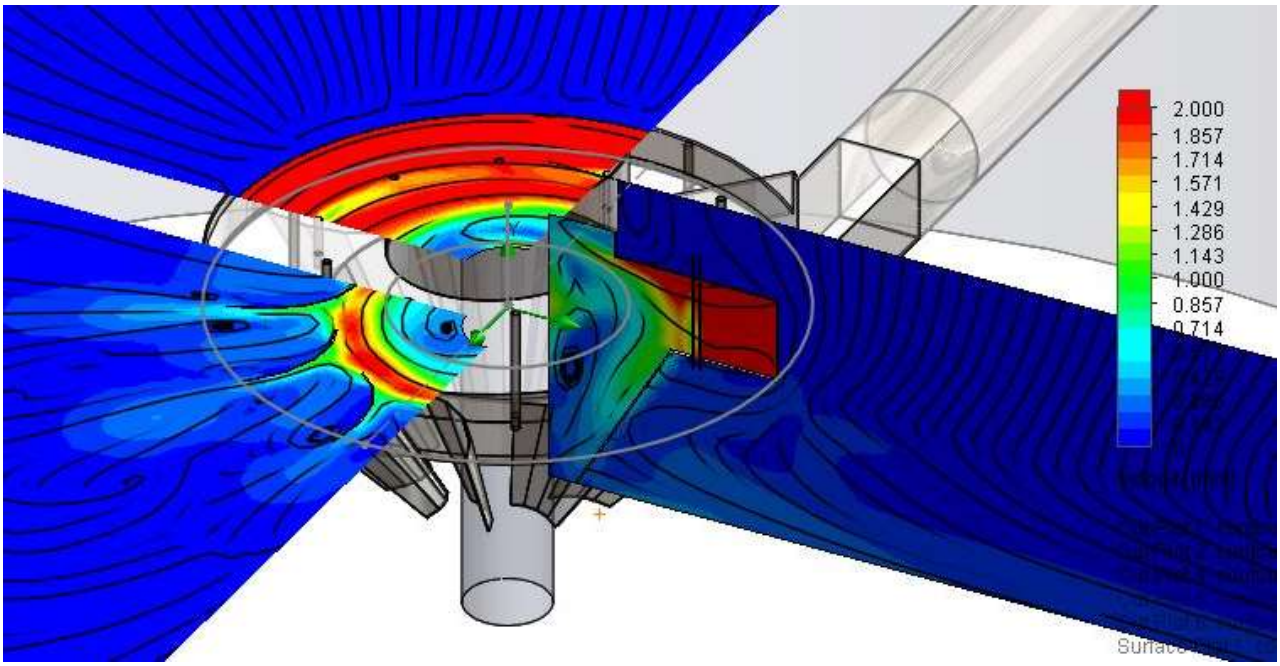

Figure 8: Shows velocity contours and streamlines through the Radflow feedwell on 3 planes.

CASE STUDIES

The above chapters show that the Radflow theoretically outperforms the other tested standard industrial feedwell in terms of kinetic energy dissipation and therefore particle settling characteristics. However, it is acknowledged that other relevant factors, such as the flocculation dynamics are not considered in these analyses.

Hence, the logical question to ask is, “What is the *weighting* of *energy dissipation* in the entire thickening process?” There is no clear-cut answer because each thickener and process requirement combination is unique. Therefore, reviewing some Radflow feedwell case studies is the best way to shed light on this question.

Goro Nickel

Goro Nickel is a Vale owned, large Nickel mine in the south of New Caledonia. In 2016, Goro retrofitted two hydroxide precipitate thickeners (Ø16 m and Ø14.3 m) with Radflow feedwells (Ø5.4 m and Ø4.4 m respectively), see Figure 9.

Figure 9: (a) Ø16 m thickener retrofitted with a Radflow feedwell and (b) underwater picture of the Ø5.4 m Radflow feedwell operating at 2000 m^3/h.

The feed solid concentration to the thickeners is 2.5% (m/m) with an underflow density requirement of 14% (m/m) yielding a low solids flux requirement of under 4 $t/m^2.day$. However, the volumetric flux/rise rate of the units is set at ~9m/h (2000 m^3/h for the Ø16 m unit) while the flocculated solids have a free settling rate of only 12m/h (as measured in laboratory cylinder tests). Therefore, the rise rates of these clarifiers far exceeded the recommended limit of 2-4 m/h (for precipitates) and therefore violate the recommended *safety factor* of 4 and instead operate with a safety factor of only 1.3.

Figure 9 (b) shows an underwater still from GoPro footage in which overflow clarity of less than 30 ppm was comfortably achieved (whereas the process guarantee stipulated >100 ppm)

Phola Coal

Phola Coal is a coal feedstock processing facility jointly owned by Anglo-American and South32, located in Ogies, Mpumalanga, South Africa. The Phola processing plant includes two Delkor Ø35 m thickeners originally outfitted with open feedwells, both fed by a common feed-box arrangement.

Roytec initially performed laboratory and pilot plant test campaigns to address the thickeners' inadequate settling performance, underflow density and overflow clarity. This included determining the optimal feed concentration and flocculant screening. In addition to process optimisations, it was agreed to retrofit a single thickener with a Ø5.4 m Radflow feedwell and depending on the performance improvement, the second thickener could be retrofitted at a later stage.

This presented a unique opportunity for Roytec to perform side-by-side test on full-scale thickeners using the Radflow and the other using a standard open feedwell, similar to the tests performed in scale model experiments shown in Figure 6. The common feedbox arrangement could also be configured to change the weighting of the flow from a 50/50 split to 100% for either thickener.

The tonnage throughput requirement of the thickeners varies dramatically depending on the quality of the coal feedstock. Initially, during the test campaign, the process stream (for both thickeners) was approximately 200 t/h and the Radflow performed commendably. More specifically, the retrofitted thickener's could increase its throughput from ~1400 m^3/hr to ~2000 m^3/hr at 8.7% (m/m) solids, with 25% less flocculant consumption yielding superior underflow, with a underflow density increase from 27% to 38% while maintaining similar overflow clarities (30 < ppm < 70), (Whitford, Gillespie, & Kruger, 2021). While impressive, the resultant flux and rise-rates still fell within the typical design limits of 5 t/m^2.day and 2 m/h respectively.

However, it was subsequent to Roytec's test campaign that the plant's throughput, through a mass balance conducted by the mine, was approximately doubled from 200 t/h to 400 t/h (to process a more weathered coal feedstock) and it is this that shows the Radflow's merit in that the entire throughput could still be processed by the single Radflow retrofitted thickener. To achieve this, the dilution stream (externally added) was increased to lower the feed solids concentration to 5.2% (m/m) resulting in a maximum volumetric flow rate of 7542 m^3/hr. This translates to a solids flux rate 10 t/m^2.day and a volumetric flux/rise rate peaking at 7.8 m/h and averaging at 6 m/h. While the solids flux rate is still within the range of 6 -12 t/m^2.day (for poor settling materials), a lower flux would certainly have been selected for design purposes due the slurries poor settling characteristics. On the other hand, the maximum volumetric flux / rise rate almost doubles that of the recommended upper limit of 4 m/h and approaches settling rate of the material which is approximately at 12 m/h yielding a resultant factor of safety of only 1.5.

Figure 10 (a) shows the Phola's Radflow retrofit in progress and (b) shows the two Ø35 m thickeners during the test campaign (taken from the Radflow retrofitted thickener's bridge). During the test campaign it was observed that the supernatant surfaces "textures" of the thickeners were very different, despite being fed at a 50/50 feed split. The open feedwell showed a rippled or choppy surface while that of the Radflow retrofitted thickener is glassy smooth.

The Radflow's impressive performance negated the need to retrofit the second thickener which is currently being used as a cyclone overflow tank.

(a) (b)

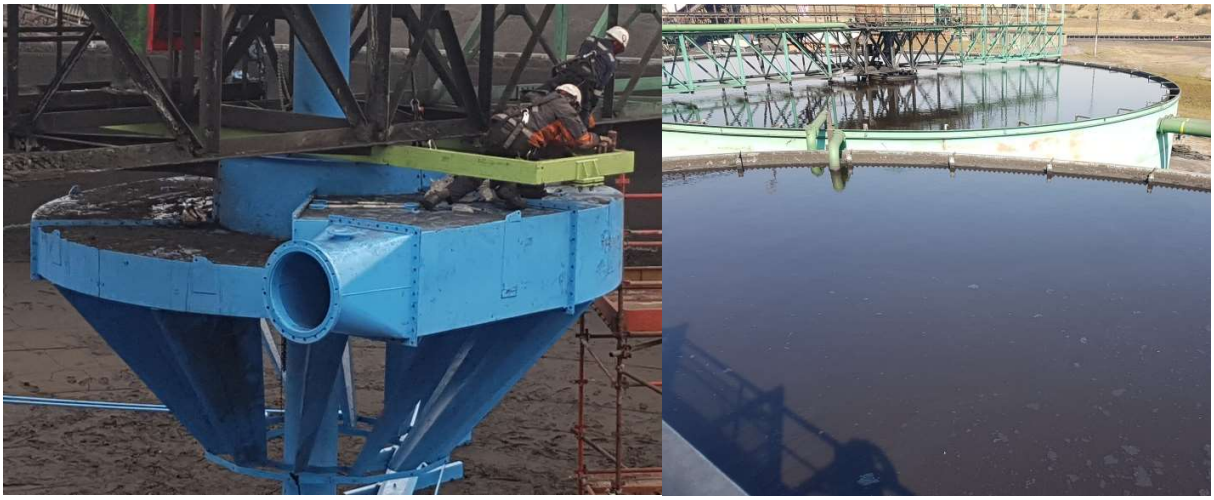

Figure 10: (a) Phola's thickener being retrofitted and (b) Bridge-view of the Phola's two Ø35 m thickeners

DRD Gold

Roytec installed and successfully commissioned a Ø45m mill thickener at DRD Far West Recoveries in Driefontein, Carltonvile, South Africa. This thickener features a Ø7.5m Radflow feedwell with a Ø1.4m ETAQ pump.

This gold tailing reprocessing plant was initially designed to process 921 t/hr, so Roytec initially offered a Ø40m thickener (with a design flux of 17.6 t/m^2/.day), which was increased to a Ø45 m thickener based on the client's conservatism (with a flux of 13.9.day). This is because the thickener feed commonly fluctuates between 900 and 1500 t/h, with peak throughputs being measured at 1900t/h. This translates to a flux rate of 29 t/m^2/day with the thickener still maintaining good operational stability, and is over 160% of the upper design flux limit of 18 t/m^2/day [for normal gold ore (SG of 2.7)]. The laboratory calculated free settling solids flux of the flocculated slurry was 48 t/m^2/day, yielding a safety factor of 1.65; substantially less than recommended value of 4.

In addition to this already impressive performance, the flocculant dosing for DRD typically ranges between 14-20 g/t, even though it was designed to operate with a flocculant dosing of 25 g/t (free settling rate of 37 m/h at 10% (m/m)). This decreased flocc dosing reduces the free settling rate by approximately 30%, to 26 m/h. This is because the flocculant pump was set up for the original solids loading of only 921 t/hr and was programmed to step up between half and full dosing flows, triggered by an ultrasonic bed level detector.

Unlike the previous 2 case studies, DRD uses the ETAQ forced dilution pump, shown in Figure 5 (b), to dilute the incoming feed from 30% (m/m) down to 12.5%. In turn, this increases the flow rate through the Radflow from 2520 m^3/h (feed flow) to 6788 m^3/h (diluted flow), a flow increase of over 2.5 times. However, dynamic pressure is proportional to the square of flow rate (Q^2), according to Bernoulli's equation: $p = ½ \rho v^2$ (for a constant cross-sectional area), and can be thought of a *blowing force*. Hence, while the flow rate may increase by 2.5, the dynamic pressure will increase by over 6 times. Therefore, it is crucial for the feedwell to effectively dissipate this incoming kinetic energy to take full advantage of the benefits offered by feed dilution.

Figure 11: DRD Gold's Ø45 m thickener.

CONCLUSION

The Phola Coal case study showcases the dramatic improvement in thickener performance after retrofitting a conventional open feedwell with a Radflow feedwell. The volumetric flux (rise rate) was increased by over 5 times and the solids loading (solids flux) increased by a factor of 4, while the thickener still maintained good operational stability and superior results. This presents a strong parallel to the dramatic experimental and CFD results presented on Figure 6, p. 7 and Figure 7, p.10 respectively and supports the philosophy that *kinetic energy dissipation* is the *paramount function* of a *feedwell*. Hence, in response to the posed question in the introductory paragraphs of **Case studies** (p.on page 12); kinetic energy dissipation, and consequently flocc settling, appears to be deserving of a high, if not the highest weighting of in the entire thickening process.

Moreover, the greater the kinetic energy dissipation, the more intense the mixing of the flocculant, feed (and diluent) inside the feedwell and therefore the better the solid/flocculant contacting‡.The considerable reduction in flocculant dosing at DRD Gold supports this statement. Hence, the Radflow feedwell truly enables a win-win scenario in terms of kinetic energy dissipation and flocculant reduction.

Both Phola Coal and Goro Nickel show that the rise rate can approach the laboratory cylinder settling rate with a greatly reduced safety factor of approximately S.F. ≈ 1.5 and still exhibit good operational stability. This challenges the overly conservative safety factors of 4-6 which are still predominantly used in the industry today.

It follows that if a thickener, incorporating an efficient feedwell (Such as that of Roytec's Feedwell), it has been conservatively designed or operated (regarding rise-rate, say S.F. > 3), then the flocc dosing rate should be dialed back to a level slightly above that where laboratory free settling rates exceed that of the operational rise rate. This is equivalent to reducing the safety factor (in determining the rise rate) and can be done during commissioning, as was inadvertently done at DRD Gold.

Naturally, reducing the flocculant dosing rate will also have an effect on the achievable solids flux rate. If there is a very short solids residence time, then reducing the flocc dosing rate will reduce the achievable underflow density; see Figure 1 for $t < 2700$ s. However, since residence times are typically much greater than 1 hour§, lowering the flocculant dosing rate should result in a higher underflow density. This conjecture is strongly supported by DRD Gold which not only operates at a far lower safety factor of S.F. = 1.65 (flux rate), but also does so with 20-50% less flocculant.

In the extreme, it may be found that certain high-rate thickeners do not require any flocculant at all. However, it is noted that typically the overflow (clarified zone) will only clarify to an acceptable clarity with the use of flocculants. On the other hand, there are some instances in which use of flocculants may become contaminants for the subsequent processes (i.e. Lithium Conversion) and are thus eliminated from the process stream (i.e. Lithium Conversion).

The philosophy outlined above fundamentally opposes the common practice to "optimize the flocc dosing", which is typically recommended after a thickener audit. Here "optimizing" means maximizing the free settling rate before an excessive flocculant dosing requirement (diminishing margins of return). In the context of standard industrial feedwell, this practice makes sense as it will dampen the spurious flows such as plumes shown in Figure 6, so the suspended particles are less likely to reach the overflow launder. However, for the Radflow feedwell, with negligible associated bed perturbations, this practice becomes unnecessary and often counter-productive.

This philosophy also suggests changing the aspect ratio of standard high-rate thickeners. More specifically, since rise rates can be calculated with a far lower safety factor, this suggests that thickeners could be built with a smaller diameter but with a deeper tank. This geometry allows for the increased volumetric flux (reduced area) while providing sufficient thickener volume to allow a the solids residence time needed to achieve the desired underflow density. Hence, an increase in bed depth will compensate for the diametrically lost volume. Again, this proposed evolutionary path is only enabled through the use of a more effective feedwell design.

Krassno Consulting and it's licensee (Roytec) have gained sufficient confidence, over the past 8 years of supplying Radflow feedwells, to de-rate the scale-up or safety factor from 4 to 2 < S.F.<3 under normal design considerations**. However, it is new thickener projects, like DRD Gold, where the throughput and

‡ The degree of mixing/shear can be moderated by splitting the flocculant feed to different sparging points located around the feedwell to minimize flocc degradation, should that become an issue.

§ Figure 1 shows the settling curves for kaolin (very slow settling) which would almost certainly have residence time longer than 1 hour.

** Naturally, this includes providing full process guarantees.

solids loading can be pushed well beyond the established design parameters. Similarly, Radflow retrofits are becoming appealing option to de-bottleneck plants with modest budgets.

ACKNOWLEDGMENTS

The authors would like to thank the staff and management of Roytec for their collaboration and provision of data to prepare this paper. The views of the authors do not necessarily present those of the Companies.

REFERENCES

Fawell, P. D. (2009). 20 years of AMIRA P266 Improving Thickener Technology-how has it changed the understanding of thickener performance?.". *Proceedings of the 12th International Seminar on Paste and Thickened Tailings.*

Krassnokutksi, A. (2015). Improving Thickener Performance using the Radflow™ Feedwell: From CFD Modelling to Commercial Implementation. *Copper Cobalt Africa.* Livingston: SAIMM.

Nguyen, T. V., Farrow, J. B., Smith, J., & . Fawell, P. D. (2012). Design and development of a novel thickener feedwell using computational fluid dynamics. *African Institute of Mining and Metallergy*, vol.112, n.11.

Triglavcanin, R. (n.d.). *Outotec introduces the "next-generation" feedwells.* Retrieved 2023, from Mining.com: https://www.mining.com/outotec-introduces-%E2%80%98next-generation%E2%80%99-feedwells/

Vietti, A., & Dunn, F. (2012). A description of the Sedimentation Process During Dynamic Thickener Operation. *Paste2014* (pp. 1-10). Vancover: Australian centre for Geomechanics.

Whitford, G., Gillespie, M., & Kruger, N. (2021). Thickener Basics and the Development of the Nover Radflow Feedwell in a Coal Processing Case Study. Secunda: SACPS.

REDUCTIVE PERCOLATION LEACHING OF A COPPER-COBALT ORE PART I: SODIUM SULPHITE AS REDUCING AGENT

By

Mpumelelo Ndhlalose, Petrus Basson, Stefan Robertson, Nontobeko Nxumalo

Mintek, South Africa

Presenter and Corresponding Author

Mpumelelo Ndhlalose
mpumelelon@mintek.co.za

ABSTRACT

The Democratic Republic of the Congo (DRC) contains approximately half of the world's cobalt reserves, with an estimated production of 130 000 tonnes, accounting for nearly 70% of primary global cobalt production in 2022. Although mineralogical composition varies with depth and location, cobalt occurs typically in trivalent form as heterogenite (CoOOH) in the oxidised zone of deposits. It therefore needs to be reduced to the divalent state (Co(II)) before it can be leached in acidic sulphate solutions. In this study, the effect of sodium sulphite (Na_2SO_3) as a reducing agent in the ore agglomeration step was investigated on the rate of leaching of cobalt from heterogenite in 1 m (tall) leach columns.

An ore sample that originated from the DRC was used for the testwork. The sample contained 0.29% cobalt, 3.6% copper, 3.53% iron and 6.81% carbonate. The sample was crushed to 100% passing 25 mm with 80% passing 20 mm, 30% passing 5 mm and 13% passing 150 µm. Percolation leach tests were performed in Φ 160 mm (inside diameter), 1 m (tall), water-jacketed, polypropylene columns.

The leach results showed that cobalt dissolutions were sensitive to the Na_2SO_3 dosage used in agglomeration, increasing from 43% (0 kg SO_3 / t) to 62% (5 kg SO_3 / t) with open circuit irrigation of the orebed. Cobalt dissolution was further enhanced to 79% by operating in closed circuit with recycled Cu-SX raffinate, at the same reductant dosage (5 kg SO_3 / t) in agglomeration. Increasing the curing time from 3 days to 7 days had no effect on cobalt dissolution. Specific reagent consumptions were between 0 and 2.74 kg SO_3 / kg Co leached. The addition of sodium sulphite in agglomeration at dosages of up to 5 kg SO_3 / t ore had little effect on copper dissolution, with overall dissolutions of 90% to 95% achieved.

Keywords: Cobalt, Copper, Percolation, Reductive leach, Heap leaching

INTRODUCTION

Cobalt (Co) is a transition metal with unique physical properties, which makes it essential for high-technology applications such as high-strength materials, magnets and rechargeable batteries[2]. Due to its relatively low concentration in ores, cobalt is usually produced as a by-product of other metals, such as copper (Cu) and nickel (Ni). It occurs in a wide variety of deposit types, mostly Cu-Co sediment-hosted deposits[1][6]. Since cobalt is often not the primary focus of the mining operation, recoveries tend to be low, with cobalt regularly reporting to tailings or smelter slags[5]. Mount Cobalt mine in Queensland, Australia, and Bou Azzer mine in Morrocco are examples where cobalt is the primary target metal[2].

The Democratic Republic of the Congo (DRC) contains approximately half of the world's cobalt reserves, with an estimated production of 130 000 metric tonnes, accounting for nearly 70% of primary global cobalt production in 2022[7]. Although mineralogical composition varies with depth and location, cobalt occurs typically in trivalent form as heterogenite (CoOOH) in the oxidised zone of deposits[4]. It therefore needs to be reduced to the divalent state (Co(II)) before it can be leached in acidic sulphate solutions.

From the standard potentials of the redox reactions below, it can be seen that sulphite ions (SO_3^{2-}), meta-bisulphite ions ($S_2O_5^{2-}$), aqueous sulphur dioxide ($SO_{2\,(aq)}$), metallic copper (Cu) and ferrous ions (Fe^{2+}) can all reduce heterogenite to soluble cobaltous ions (Co^{2+}) since these are all lower than that for the CoOOH / Co^{2+} redox couple[7].

$$CoOOH + 3H^+ + e^- \leftrightarrow Co^{2+} + 2H_2O \qquad E° = 1.76\ V\ (vs.\ SHE) \qquad (1)$$

$$SO_4^{2-} + 2H^+ + 2e^- \leftrightarrow SO_3^{2-} + H_2O \qquad E° = -0.107\ V\ (vs.\ SHE) \qquad (2)$$

$$2SO_4^{2-} + 6H^+ + 4e^- \leftrightarrow S_2O_5^{2-} + 3H_2O \qquad E° = 0.035\ V\ (vs.\ SHE) \qquad (3)$$

$$SO_4^{2-} + 4H^+ + 2e^- \leftrightarrow SO_{2\,(aq)} + 2H_2O \qquad E° = 0.158\ V\ (vs.\ SHE) \qquad (4)$$

$$Cu^{2+} + 2e^- \leftrightarrow Cu \qquad E° = 0.337\ V\ (vs.\ SHE) \qquad (5)$$

$$Fe^{3+} + e^- \leftrightarrow Fe^{2+} \qquad E° = 0.771\ V\ (vs.\ SHE) \qquad (6)$$

Iron(III) oxides such as goethite (FeOOH) and limonite may also be present in copper-cobalt oxide ore deposits. On reaction with acid, these oxides release ferric ions into solution resulting in increased ferric-to-ferrous ratios and, as a result thereof, solution potentials as high as 650 mV (vs. Ag/AgCl; 3 M KCl). Such oxidative conditions may be kinetically unfavourable for the leaching of heterogenite by reductive dissolution in acidic sulphate soluitons.

In this study, the effect of sodium sulphite (Na_2SO_3) as a reducing agent in the agglomeration step was investigated on the rate of leaching of cobalt from heterogenite in 1 m (tall) leach columns. The effect of Na_2SO_3 dosage, curing time and mode of operation (open or closed cycle) were investigated.

EXPERIMENTAL

Materials

The sample used in this study was a Cu-Co oxide ore from the DRC. The ore sample was jaw / cone crushed to 100% passing 25 mm. The crushed ore was blended and split into 30 kg batches. Three batches were randomly selected and screened using the following sieve sizes: 25 mm, 16 mm, 13.2 mm, 12.5 mm, 9.5 mm, 6.7 mm, 4.75 mm, 3.35 mm, 2.36 mm, 1.7 mm, 1.18 mm, 0.850 mm, 0.600 mm, 0.425 mm, 0.300 mm, 0.212 mm, 0.150 mm, 0.106 mm, 0.075 mm, 0.053 mm and 0.038 mm. After screening, the sizes were combined into 4 size classes (-25+6.7 mm, -6.7+3.35 mm, -3.35+1.18 mm and -1.18 mm) for head assay.

Chemical Assays

Solids

Solid head and leach residue samples were analysed by Inductively Coupled Plasma-Optical Emission Spectroscopy (ICP-OES) for: aluminium (Al), calcium (Ca), copper (Cu), cobalt (Co), chromium (Cr), iron (Fe), lead (Pb), magnesium (Mg), manganese (Mn), nickel (Ni), silicon (Si), titanium (Ti), vanadium (V) and zinc (Zn). Carbonate (CO_3^{2-}) was determined by combustion technique (LECO). Potassium (K) and sodium (Na) were assayed by Atomic Absorption Spectroscopy (AAS). Total sulphur (S(T)) and sulphide sulphur (S^{2-}) were analysed by combustion technique (LECO).

Solutions

Daily pregnant leach solution (PLS) samples were analysed for copper and iron by AAS. Monthly accumulated PLS samples were analysed by ICP-OES for: Al, arsenic (As), Ca, Cu, Cr, Fe, lithium (Li), Mg, molybdenum (Mo), Ni, Pb, Si, Ti, V and Zn as part of the ICP base metal suite. Ferrous ion (Fe(II)) and sulphuric acid (H_2SO_4) concentrations were determined by titration methods.

All reported redox potentials were recorded against a 3 M KCl, Ag/AgCl reference electrode.

Mineralogy

The solid head sample was submitted for mineralogical investigation. The mineralogical information was obtained by Quantitative Evaluation of Minerals by Scanning Electron Microscopy (QEMSCAN) on a 100% -0.3 mm sample for individual size classes.

Column Leach Tests

Leach tests were performed in 1 m (tall) columns (Figure 1). All tests were conducted in Φ 160 mm (inside diameter), single sectioned, water-jacketed, polypropylene columns. The experimental matrix is summarised in Table 1.

During agglomeration, sodium sulphite (Na_2SO_3) was dissolved in 7 g/L H_2SO_4 solution and sprayed onto the ore while rolling on a plastic sheet to a total moisture content of 8%. All the columns were operated at 25 °C. Dosages of 0, 0.5, 1 and 5 kg SO_3 / t were added as Na_2SO_3.

Tests were performed in open circuit (C1, C2, C3, C4 and C6) with 7 g/L H_2SO_4 in water (Rand Water Board) at 6 L/m^2/h or in closed circuit (C5) with return raffinate. Test C5 was irrigated with 7 g/L H_2SO_4 in water, and the PLS was accumulated in batches. Copper removal by batch solvent extraction (SX) was then performed on the PLS. The acid concentration of the raffinate was adjusted to 7 g/L and the solution recycled back to the column.

The effect of curing time was evaluated by increasing the curing period from 3 days (C1, C2, C3, C4 and C5) to 7 days (C6).

Figure 1: 1 m Column Set-up

Table 1: Experimental Test Matrix

Condition	Units	Test					
		C1	C2	C3	C4	C5	C6
Temperature	°C	25	25	25	25	25	25
Moisture content in agglomeration	% w/w	8	8	8	8	8	8
Acid in agglomeration	kg H_2SO_4 / t	24	24	24	24	24	24
Reductant in agglomeration	kg SO_3 / t	0	0.5	1	5	5	5
Curing time	days	3	3	3	3	3	7
Acid in irrigation	g/L	7	7	7	7	7	7
Irrigation rate	L/m^2/h	6	6	6	6	6	6
Mode (of irrigation)		Open	Open	Open	Open	Closed	Open

All reagents were supplied by Associated Chemical Enterprises (ACE) as follows:

- H_2SO_4: sulphuric acid (98%)
- SO_3: as sodium sulphite (Na_2SO_3) (min. 97%)

RESULTS AND DISCUSSION

Particle Size Distribution (PSD)

Figure 2 shows the PSD's of three randomly selected 30 kg batches of the head sample, and the average PSD by mass. The narrow grouping between the profiles indicate that the blending and splitting of the head sample were performed satisfactorily. On average, the head sample had a

P_{80} (80% passing) of 20 mm with 30% passing 5 mm, 20% passing 1 mm, 13% passing 150 µm and 11% passing 75 µm.

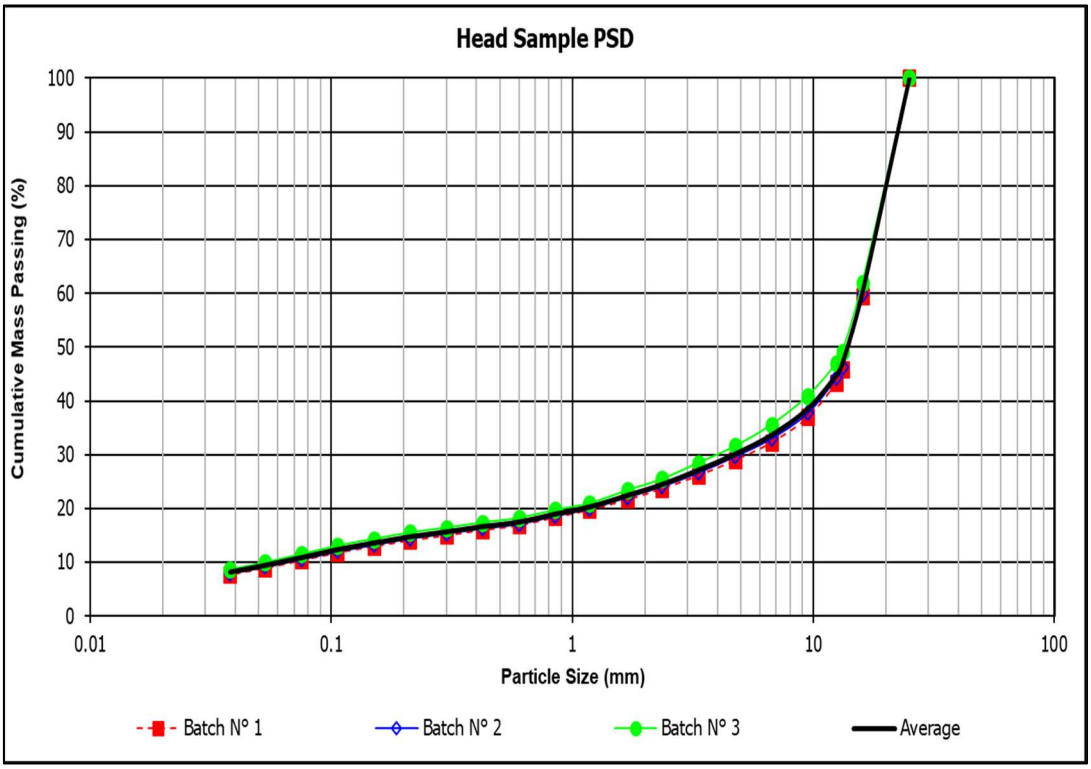

Figure 2: Head Sample PSD

Chemical Head Assays and Mineralogical Analysis

Table 2 shows the constituted chemical analysis of the head sample. The sample contained 3.6% copper, 0.29% cobalt, 3.53% iron and 6.81% carbonate (CO_3^{2-}).

Table 3 shows size-class chemical analysis and the constituent distributions in the different size classes of the head sample. Copper (67%), cobalt (55%), iron (61%) and carbonate (82%) occurred primarily in the coarsest size fraction (-25+6.7 mm).

QEMSCAN analysis showed that copper deported as malachite (71.7%), chrysocolla (19.9%), pseudo-malachite (4%), chalcocite (4%) and very little chalcopyrite (< 1%). Cobalt occurred as heterogenite.

Table 2: Chemical Analysis of the Head Sample (Major Constituents)

Cu (%)	Co (%)	Fe (%)	CO_3^{2-} (%)
3.60	0.29	3.53	6.81

Table 3: Size Class Chemical Analysis and Distributions of Major Constituents

Size Class	Cu		Co		Fe		CO_3^{2-}	
(mm)	(%)[1]	(%)[2]	(%)[1]	(%)[2]	(%)[1]	(%)[2]	(%)[1]	(%)[2]
-25+6.7	3.64	67.0	0.24	54.7	3.26	61.3	8.43	82.2
-6.7+3.35	3.90	7.02	0.29	6.40	3.81	7.01	5.60	5.34
-3.35+1.18	4.67	8.89	0.37	8.68	4.57	8.89	5.01	5.05
-1.18	3.05	17.1	0.44	30.3	3.97	22.8	2.50	7.43
Total	3.60	100	0.29	100	3.53	100	6.81	100

1) Constituent content for the ore size class.
2) Constituent content for the ore size class as a percentage of the total constituent content.

1 m Column Leach Tests

PLS pH and Potential Profiles

The PLS pH profiles are presented in Figure 3. The pH of the breakthrough solutions ranged from 1.5 to 2.7, after which levels increased to between pH 4 and pH 4.5. Thereafter the levels decreased, and remained within the range pH 1.4 to pH 2 from Day 95 up to the end of the leaching period. The high PLS pH that was experienced for a significant period of the leach was in all likelihood due to the high carbonate content (6.81%) of the ore sample. A water wash was implemented on Day 181 for all the tests except test C6 (Day 177), corresponding to the immediate pH rise at that point.

The PLS potential profiles are shown in Figure 4. The profiles for tests C1, C2 and C3 were similar over the first 20 days of leaching. However, a small decrease in corresponding potential with increased reductant dosage in agglomeration over the range 0 to 1 kg SO_3 / t is noticeable. It can also be seen that tests C2 (0.5 kg SO_3 / t) and C3 (1 kg SO_3 / t) remained at lower corresponding potentials for some time when the potential of test C1 (0 kg SO_3 / t) increased to about 550 mV. This may be explained by longer duration wash out of residual reductant in the orebed. Increasing the reductant dosage further from 1 to 5 kg SO_3 / t ore (C4, C5 and C6) resulted in a more pronounced decrease in corresponding potential, e.g. by at least 100 mV, as can be seen during the first 30 days of leaching. Over time the potential profiles of tests C1, C2, C3, C4 and C6 reached levels of up to about 650 mV.

The PLS potential for test C5 (5 kg SO_3 / t), which was operated in closed circuit with recycled raffinate solution, remained low in comparison with the other columns.

Cobalt and Copper Dissolution Profiles

Cobalt and copper dissolution profiles are presented in Figures 5 and 6, respectively. These were plotted from the recalculated metal head grade and metal in solution assays. The recalculated head grade entails a 100% element mass balance (i.e. element out / element in) with respect to both solid and solution phases over the leach, water wash and drain-down stages.

The use of a reductant in agglomeration at dosages of 0.5 kg SO_3 / t (C2) to 1 kg SO_3 / t (C3) achieved noticeable improvement of initial and overall cobalt dissolution, with significant further enhancement at a dosage of 5 kg SO_3 / t (C4 and C6). Moreover, raffinate recycling in conjunction with 5 kg SO_3 / t in agglomeration rendered the highest overall cobalt dissolution of 79% (C5) compared with the other tests (43% to 61%; Table 4). From Figure 5 it can be seen that test C5's rate of cobalt dissolution became 'negative' directly after introduction of the recycled raffinate solution. This is due to the fact that the raffinate entering the orebed contained a higher cobalt concentration than the solution in the bed at that time. Once this volume was 'pushed' out of the bed, daily cobalt dissolution calculated as $\Sigma(\text{mass of cobalt})_{PLS} - \Sigma(\text{mass of cobalt})_{irrigation}$ became positive again. Hereafter, the rate of cobalt dissolution showed a marked increase as is evident from the steeper dissolution profile. Closed circuit operation with Cu-SX raffinate solution could return unreacted sulphite ions beneficially for the leach, and / or even other reductants that have accumulated in solution such as ferrous ions (Equation 6). This presents a plausible explanation for test C5's lower PLS potentials (from Day 35 onwards) compared with those for tests C4 and C6, which were operated in open circuit with acidified water only.

Similar dissolution profiles for tests C4 (5 kg SO_3 / t, 3 days curing) and C6 (5 kg SO_3 / t, 7 days curing) indicated that curing for longer than 3 days had no effect on initial and overall cobalt dissolutions.

The addition of reductant in agglomeration up to 5 kg SO_3 / t had little effect on copper dissolution during the initial stages of leaching. Overall copper dissolutions were similar and ranged between 90% and 95% (Table 4), with a slightly higher dissolution achieved for the test operated in closed circuit (C5).

Reductant and Acid Consumptions

Specific reductant consumptions, in kg SO_3 / kg Co (leached), were calculated from the reductant dosage used in agglomeration, the recalculated cobalt head grade and overall cobalt dissolution. The values are listed in Table 4.

Table 4 also includes acid consumptions that were calculated as follows:

Total Acid Consumption (TAC):

$$mTAC = mFEED - mPLS \quad (7)$$

Net Acid Consumption (NAC):

$$mNAC = mFEED - mPLS - mSX \quad (8)$$

mTAC: total acid consumption, in kg H_2SO_4 / t (dry) ore
mFEED: acid in the irrigation solution and agglomeration, in kg H_2SO_4 / t (dry) ore
mPLS: acid in the PLS, in kg H_2SO_4 / t (dry) ore
mSX: acid in the raffinate solution after copper solvent extraction (SX), in kg H_2SO_4 / t (dry) ore (1.54 kg H_2SO_4 / 1 kg Cu extracted)

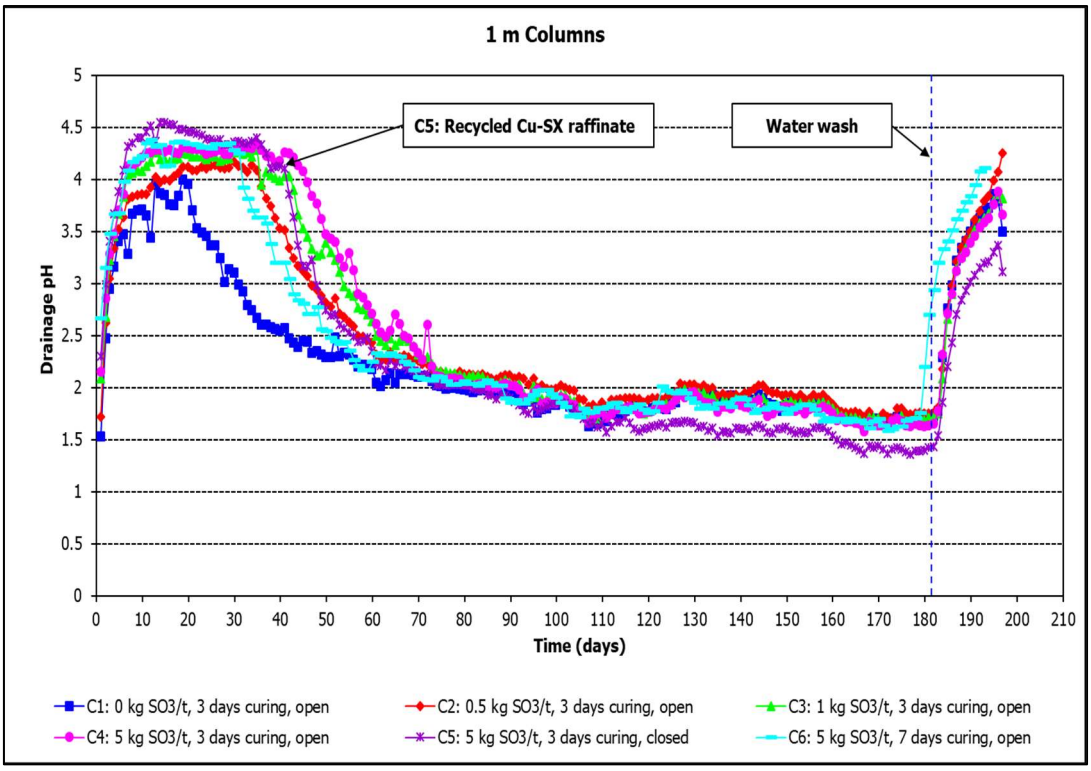

Figure 3: PLS pH

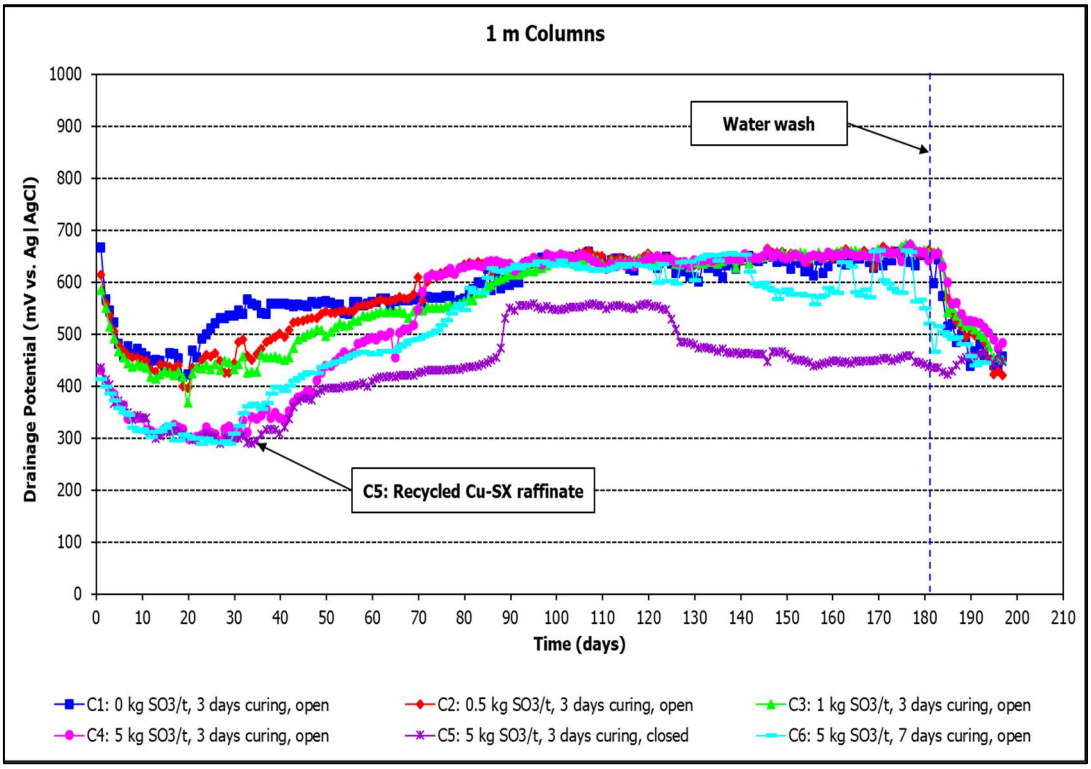

Figure 4: PLS Potential

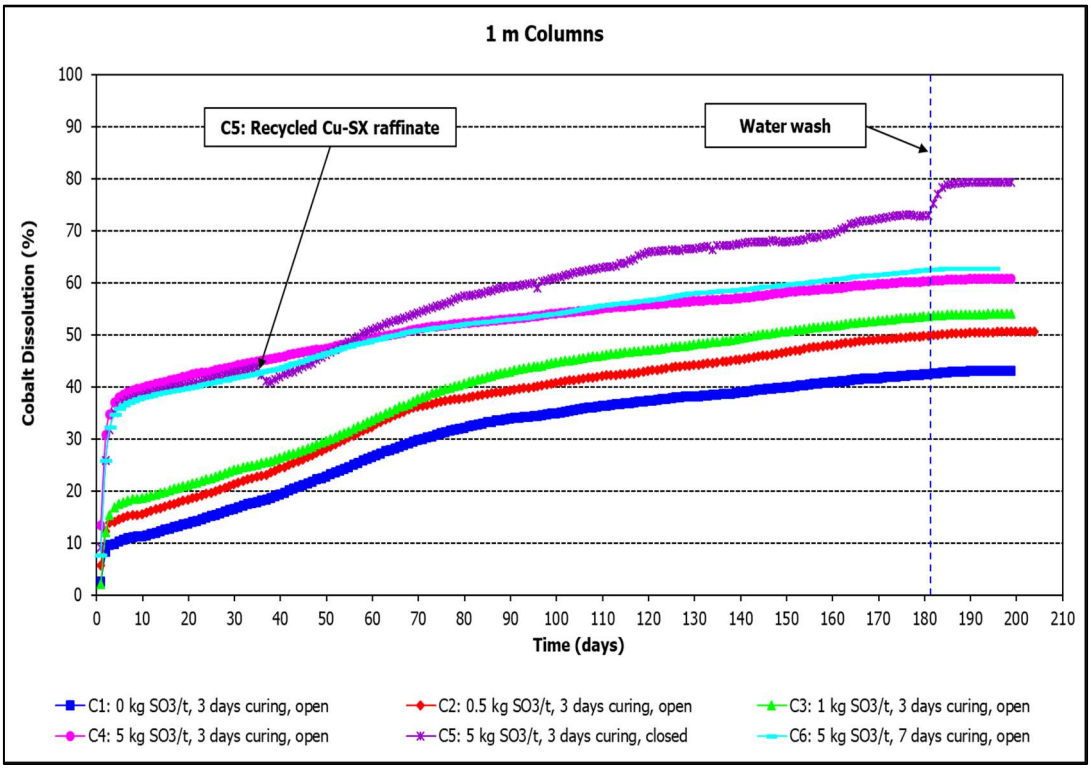

Figure 5: Cobalt Dissolution vs. Time

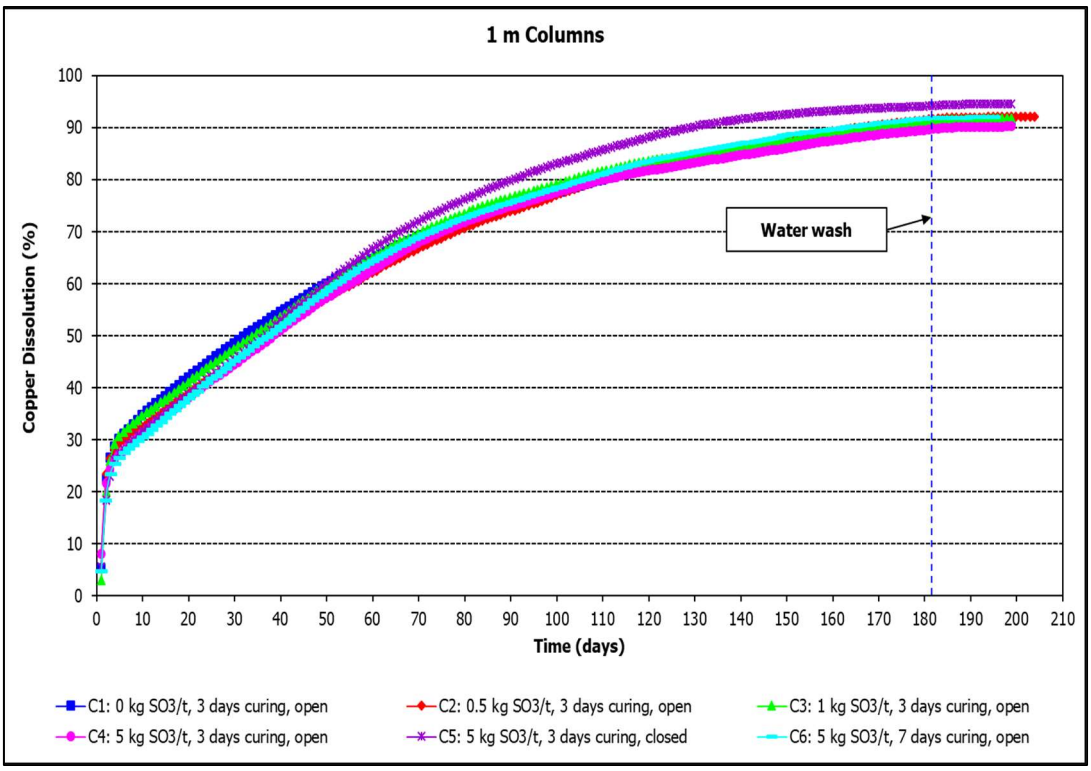

Figure 6: Copper Dissolution vs. Time

Table 4: Cobalt Dissolutions, Copper Dissolutions, Acid and Reductant Consumptions

Test	Conditions (dosage; curing; mode)	Metal Dissolution		Reagent Consumption		
		Co (%)	Cu (%)	TAC (kg H_2SO_4 / t)	NAC (kg H_2SO_4 / t)	Reductant (kg SO_3 / kg Co)
C1	0 kg SO_3 / t; 3 days; open	43.1	91.0	162	111	0
C2	0.5 kg SO_3 / t; 3 days; open	50.6	92.1	161	109	0.37
C3	1 kg SO_3 / t; 3 days; open	54.0	91.8	163	113	0.65
C4	5 kg SO_3 / t; 3 days; open	60.8	90.3	157	109	2.74
C5	5 kg SO_3 / t; 3 days; closed	79.4	94.6	128	76	2.00
C6	5 kg SO_3 / t; 7 days; open	62.8	92.1	147	99	2.66

CONCLUSIONS

Enhanced cobalt recoveries were achieved in 1 m column leach tests by the addition of a reductant (Na_2SO_3) in the ore agglomeration step prior to leaching. This potentially provides a simple and practical way of improving cobalt recoveries during heap leaching of Cu-Co ores, where cobalt is in the form of heterogenite.

Cobalt dissolutions were sensitive to the reductant dosage, increasing from 43% (0 kg SO_3 / t) to 62% (5 kg SO_3 / t) in open circuit. Cobalt dissolution was further enhanced to 79% by operating in closed circuit with recycled Cu-SX raffinate, at the same reductant dosage (5 kg SO_3 / t) in agglomeration. Increasing the curing time from 3 days to 7 days had no effect on cobalt dissolution. Specific reagent consumptions were between 0 and 2.74 kg SO_3 / kg Co leached.

The addition of sodium sulphite in agglomeration at dosages of up to 5 kg SO_3 / t ore had little effect on copper dissolution, with overall dissolutions of 90% to 95% achieved.

ACKNOWLEDGMENTS

The authors would like to thank the staff and management at Mintek for funding the work presented.

REFERENCES

1. Dehaine, Q., Filippov, L.O., Filippova, I.V., Tijsseling, L.T. and Glass, H.J., 2019a. Processing of a complex carbonate-rich Cu-Co mixed ore via reverse flotation, in: Flotation'19. MEI, Cape Town.

2. Fisher, K.G., Cobalt processing developments. Bateman Engineering Projects. The Southern African Institute of Mining and Metallurgy, 6th Southern African Base Metals Conference 2011: 237-258.

3. Outotec HSC Chemistry 6.1 software.

4. Schmidt, T., Buchert, M. and Schebek, L., 2016. Investigation of the primary production routes of nickel and cobalt products used for Li-ion batteries. Resour. Conserv. Recycl. 112, 107-122.

5. Slack, J.F., Kimball, B.E. and Shedd, K.B., 2017. Cobalt. In: Schulz, K.J., DeYoung, J.H., Seal, R.R. and Bradley, D.C., (Eds.), Critical Mineral Resources of the United States.

6. Smith, C.G., 2001. Always the bridesmaid, never the bride: cobalt geology and resources. Transactions of the Institution of Mining and Metallurgy Section B-Applied Earth Science 110, B75-B80.

7. U.S. Geological Survey, Mineral Commodity Summaries, January 2023.

REDUCTIVE PERCOLATION LEACHING OF A COPPER-COBALT ORE PART II: FERROUS ION AS REDUCING AGENT

By

Nontobeko Nxumalo, Petrus Basson, Mpumelelo Ndhlalose

Mintek, South Africa

Presenter and Corresponding Author

Nontobeko Nxumalo
nontobekon@mintek.co.za

ABSTRACT

Oxidised copper-cobalt ore deposits from the Central African Copperbelt contain cobalt(III) oxide minerals, such as heterogenite (CoOOH), which require reduction of Co(III) to soluble Co(II) for dissolution in acidic sulphate solutions. Reducing agents used in hydrometallurgical plants include sodium metabisulphite ($Na_2S_2O_5$; SMBS), sulphur dioxide (SO_2), ferrous ion (Fe(II)) and scrap copper metal (Cu°). Several studies have been conducted on the subject matter showing that these reductants can improve cobalt recovery up to 90% when applied in tank leaching. There are limited studies focusing on reductive cobalt recovery from economically marginal ores, which are only treatable by low-cost processes such as heap leaching. This study investigated the effect of ferrous ion as a reducing agent in the percolation leach of a copper-cobalt oxide ore.

A copper-cobalt ore sample from the Katanga Province of the Democratic Republic of the Congo (DRC) was used for the testwork. The ore sample contained 952 ppm cobalt, 2.33% copper, 4.05% iron and 1.27% carbonate, with 92% acid-soluble copper. The ore sample was crushed to 100% passing 25 mm with 80% passing (P_{80}) 18 mm. The percolation leach tests were conducted in Φ 160 mm (inside diameter), 6 m (height), water-jacketed, polypropylene columns.

The addition of ferrous ion in the irrigant improved the extent of overall cobalt dissolution by up to 41 percentage points. About 50% of the cobalt could be leached within 9 days with the addition of 3.7 kg ferrous / t ore in agglomeration. The extents of overall cobalt dissolution achieved were 40% in the absence of ferrous ion and up to 81% with ferrous in agglomeration and in the irrigant. The reductive conditions did not have an adverse effect on the copper dissolution, with the average extent of overall copper dissolution reaching 95%.

Keywords: Cobalt, Copper, Percolation leaching, Reductive leach, Heap leaching

INTRODUCTION

Cobalt is generally recovered in low quantities as a by-product during other major metal extraction processes such as copper and nickel[1]. The increase in cobalt demand in recent years, mainly driven by the demand in lithium-ion batteries, has compelled operations to seek effective methods of recovering this valuable metal[6].

The Central African Copperbelt boasts approximately half of the world's cobalt reserves[1]. The Democratic Republic of the Congo (DRC) is by far the world's largest producer of cobalt, accounting for roughly 70 percent of global production. The country has been the top producer of cobalt for some time, with a reported output of 130 000 metric tonnes in 2022, and is likely to remain a crucial cobalt producer for the near future[2][4].

Oxidised copper-cobalt ore deposits from the Central African Copperbelt contain cobalt(III) oxide minerals, such as heterogenite (CoOOH), which require reduction of Co(III) to soluble Co(II) for dissolution in acidic sulphate solutions. Reducing agents used in hydrometallurgical plants include sodium metabisulphite ($Na_2S_2O_5$; SMBS), sulphur dioxide (SO_2), ferrous ion (Fe(II)) and scrap copper metal (Cu^o). Several studies have been conducted on the subject matter showing that these reductants can improve cobalt recovery up to 90% when applied in tank leaching[3][5]. There are limited studies focusing on reductive cobalt recovery from economically marginal ores, which are only treatable by low-cost processes such as heap leaching.

In this study, the effect of ferrous ion in agglomeration and in the irrigation solution on the rate and extent of cobalt dissolution from an oxidised copper-cobalt ore was investigated in 6 m (height) percolation leach columns. The achievement of satisfactory cobalt dissolution at mildly reductive conditions (solution potentials > 350 mV vs. Ag/AgCl; 3 M KCl) will be a reagent cost saving for cobalt producing heap leach operations. Ferrous ions are significantly less expensive than reductants such as sulphite and can be produced on site from scrap iron and sulphuric acid whilst other reductants / reagents are typically transported to site from a remote location[7].

EXPERIMENTAL

Ore Sample

The sample used in this study was a Cu-Co oxide ore from the Katanga Province in the DRC. The ore was jaw / cone crushed to 100% passing 25 mm. The crushed ore was blended and submitted for particle size distribution (PSD) analysis on the following sieve sizes: 25 mm, 16 mm, 13.2 mm, 12.5 mm, 9.5 mm, 6.7 mm, 4.75 mm, 3.35 mm, 2.36 mm, 1.7 mm, 1.18 mm, 850 µm, 600 µm, 425 µm, 300 µm, 212 µm, 150 µm, 106 µm, 75 µm, 53 µm and 38 µm. Thereafter the material was combined into four size classes: -25+16 mm, -16+6.7 mm, -6.7+1.18 mm and -1.18 mm for head analysis by size class.

Chemical Analysis

Solids

Solid head and column leach residue samples were analysed by inductively coupled plasma-optical emission spectroscopy (ICP-OES) for: aluminium (Al), calcium (Ca), copper (Cu), cobalt (Co), chromium (Cr), iron (Fe), lead (Pb), magnesium (Mg), manganese (Mn), nickel (Ni), silicon (Si), titanium (Ti), vanadium (V) and zinc (Zn), as well as sequential / diagnostic copper leaching (acid and cyanide digestion method). Carbonate (CO_3^{2-}) was determined by combustion technique (LECO). Potassium (K) and sodium (Na) were assayed by atomic absorption spectroscopy (AAS). Total sulphur (S(T)) and sulphide sulphur (S^{2-}) were analysed by combustion technique (LECO).

Solutions

Daily pregnant leach solution (PLS) samples were analysed for copper and iron by AAS. Monthly accumulated PLS samples were analysed by ICP-OES for: Al, arsenic (As), Ca, Cu, Cr, Fe, lithium (Li),

Mg, molybdenum (Mo), Ni, Pb, Si, Ti, V and Zn as part of the ICP base metal suite. Ferrous ion (Fe (II)) and sulphuric acid (H_2SO_4) concentrations were determined by titration methods.

All reported redox potentials were recorded against a 3 M KCl, Ag/AgCl reference electrode.

Mineralogical Analysis

The solid head sample was submitted for mineralogical investigation. Automated image analysis, utilising Backscattered Electron (BSE) and Energy Dispersive X-ray (EDX) signals from a Scanning Electron Microscope (SEM), was used to create digital images in which each pixel corresponds to mineral species in the corresponding region under the electron beam. A QEMSCAN Particle Mineral Analysis (PMA) protocol was used for the analysis. This method was selected so as to attain the overall mineral assemblage of the sample, as well as the copper and cobalt deportments.

QEMSCAN: quantitative evaluation of minerals by scanning electron microscopy

Column Leach Tests

Five 6 m (height) column leach tests were conducted in 160 mm (inside diameter), water-jacketed, polypropylene columns. The experimental matrix is summarised in Table 1.

The columns were operated in open circuit, at 25 °C. Irrigation was carried out with synthetic raffinate at 10 L/m^2/h. The ore was agglomerated with synthetic raffinate and 98% H_2SO_4 to a total moisture content of 8% and a total amount of 10.8 kg/t H_2SO_4 in agglomeration. The effect of adding ferrous ion in the ore agglomeration step on the rate of cobalt dissolution was evaluated by using a 3.7 kg/t dosage (C5). The rest of the tests were conducted at varying ferrous concentrations in the irrigation solution. The ferrous concentrations tested were: 0 g/L (C1; base case), 0 mg/L to 400 mg/L (C2), 300 mg/L (C3 and C5) and 1.5 g/L (C4). The ferrous ion was added as 99% ferrous sulphate ($FeSO_4 \cdot 7H_2O$) (supplied by Associated Chemical Enterprises (ACE)).

Figure 1: 6 m Column Set-up

Table 1: 6 m Column Leach Test Matrix

Conditions	Units	C1	C2	C3	C4	C5
Crush size (100% passing)	mm	25	25	25	25	25
Column inside diameter (ID)	mm	160	160	160	160	160
Temperature	°C	25	25	25	25	25
Cure / rest duration	days	3	3	3	3	3
Leach duration	days	248	248	248	248	248
Agglomeration / Loading						
Loading bulk density (dry)	t/m^3	1.4	1.4	1.4	1.4	1.4
Moisture content	% w/w	8	8	8	8	8
Concentrated acid (98% H_2SO_4)	kg/t	10	10	10	10	10
Total acid (conc. + raffinate)	kg/t	10.8	10.8	10.8	10.8	10.8
Total iron (Fe(T))	kg/t	0.105	0.105	0.105	0.105	3.7
Ferrous (Fe(II))	kg/t	-	-	0.021	0.105	3.7
Ferric (Fe(III))	kg/t	0.105	0.105	0.083	-	-
Aluminium (Al)	kg/t	0.110	0.110	0.110	0.110	0.110
Magnesium (Mg)	kg/t	0.105	0.105	0.105	0.105	0.105
Irrigation Solution						
Irrigation flowrate	$L/m^2/h$	10	10	10	10	10
[H_2SO_4]	g/L	10	10	10	10	10
[Fe(T)]	g/L	1.5	1.5	1.5	1.5	1.5
[Fe(II)]	g/L	-	0 - 0.4(1)	0.3	1.5	0.3
[Fe(III)]	g/L	1.5	1.5 - 1.1(1)	1.2	0	1.2
[Al]	g/L	1.6	1.6	1.6	1.6	1.6
[Mg]	g/L	1.5	1.5	1.5	1.5	1.5

1) The ferrous concentration of the irrigation solution was increased from 0 to 400 mg/L after 97 days of leaching.

All reagents were supplied by ACE as follows:

- Al : aluminium sulphate ($Al_2(SO_4)_3 \cdot 18H_2O$) (100-110%)
- Fe(II) : ferrous sulphate ($FeSO_4 \cdot 7H_2O$) (99%)
- Fe(III) : ferric sulphate anhydrous ($Fe_2(SO_4)_3 \cdot xH_2O$) (20-23% Fe)
- Mg : magnesium sulphate ($MgSO_4 \cdot 7H_2O$) (99-100.5%)
- H_2SO_4 : sulphuric acid (98%)

RESULTS AND DISCUSSION

Head Sample Characterisation

Particle Size Distribution

Figure 2 shows the particle size distributions of three, randomly-selected batches of the crushed head sample together with the average (by mass). The blending and splitting of the sample were satisfactory as confirmed by the narrow grouping of the PSD profiles. On average, the head sample had a P_{80} (80% passing) of 18 mm with 26% passing 1.18 mm and 13% passing 150 µm.

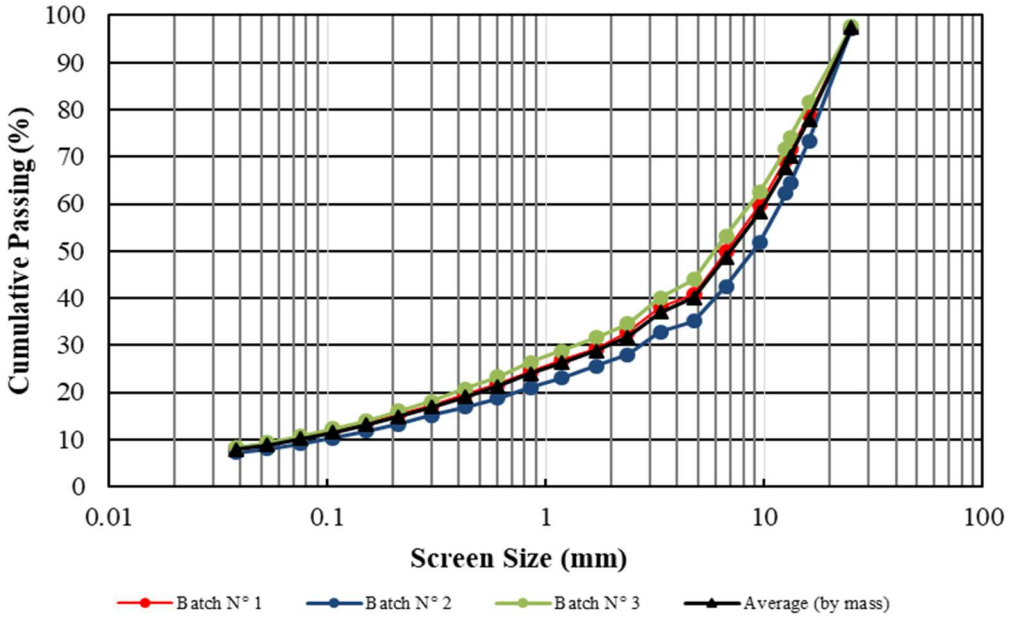

Figure 2: Particle Size Distribution of the Head Sample

Chemical and Mineralogical Analysis

Table 2 shows the chemical analysis and distribution of the major constituents of the head sample. The average assays were calculated from the composite head sample and constituted head sample from particle size classes -25+16 mm, -16+6.7 mm, -6.7+1.18 mm and -1.18 mm.

Table 2: Major Constituent Mass Distribution of the Head Sample

Size Class	Mass	Co		Cu		Fe		CO_3^{2-}
(mm)	(%)	(ppm)(1)	(%)(2)	(%)(1)	(%)(2)	(%)(1)	(%)(2)	(%)
-25+16	22.0	530	11.3	1.21	12.0	3.30	18.0	
-16+6.7	29.3	724	20.5	2.14	28.4	3.41	24.8	
-6.7+1.18	22.4	862	18.6	2.60	26.3	3.99	22.1	
-1.18	26.2	1956	49.6	2.81	33.3	5.40	35.1	
Overall	100	1035	100	2.22	100	4.04	100	
Composite		868		2.45		4.07		1.27
Average		952		2.33		4.05		1.27

1) Constituent content for size class or composite.
2) Constituent content for size class as a percentage of the total constituent content.

The ore sample contained 2.33% copper, 952 ppm cobalt, 4.05% iron and 1.27% carbonate. The element distributions show that 50% of the cobalt and 33% of the copper were contained in the -1.18 mm size class.

The sequential copper leach analysis indicated that the sample contained 92% acid-soluble copper, a marginal amount of cyanide-soluble copper (less than 1% of the total copper) and 7% non-soluble copper, which is in good agreement with the low sulphide sulphur concentrations assayed.

Copper occurred as malachite (53%), pseudo-malachite (20%), goethite Cu (9%), MnFeCuCoSilicate wad (8%), chrysocolla (6%), cuprite (1%) and very little (< 1%) of chalcocite, CuCoMn wad, Cu-bearing chlorite, bornite and chalcopyrite. Cobalt was present as MnFeCuCoSilicate wad (67%), heterogenite (28%) and Cu-Co wad (5%).

The chemical analyses of the other constituents of the head sample are presented in Table 3.

Table 3: Chemical Analysis of the Head Sample (other constituents)

Element	Unit	Size (mm)				Overall	Composite	Average
		-25+16	-16+6.7	-6.7+1.18	-1.18			
Mass	%	22.0	29.3	22.4	26.2	100		
Al	%	6.69	6.29	5.75	5.42	6.03	6.05	6.04
As	ppm	155	276	347	409	300	228	264
Ca	%	0.36	0.20	0.19	0.20	0.23	0.23	0.23
Cr	ppm	23	29	25	36	29	32	30
K	%	-	-	-	-	-	2.78	2.78
Mg	%	4.36	3.25	2.75	3.05	3.33	3.38	3.35
Mn	%	0.06	0.06	0.06	0.22	0.1	0.09	0.10
Na	ppm	-	-	-	-	-	218	218
Ni	ppm	120	115	118	162	129	141	135
Pb	ppm	108	231	306	431	273	335	304
Si	%	31.0	32.2	32.8	31.8	32.0	31.3	31.6
S(T)	%	-	-	-	-	-	0.03	0.03
S^{2-}	%	-	-	-	-	-	< 0.01	< 0.01
Ti	%	0.80	0.74	0.65	0.66	0.71	0.70	0.70
V	ppm	249	369	417	440	372	360	366
Zn	ppm	243	368	418	686	435	418	427

Column Leach Tests

The testwork comprised five column leach tests: C1, C2, C3, C4 and C5. The vertical broken line in the subsequent graphs denotes the end of the leaching stage; thereafter follows the water wash / rinsing stage.

Redox Potential and pH Profiles

Figures 3 and 4 display the redox potential and pH profiles of the irrigation solutions, respectively. The potential was between 600 mV and 650 mV for columns C1 and C2, which were conducted in the absence of ferrous iron (all the iron in the irrigation solution was ferric). However, 400 mg/L of ferrous was introduced into the irrigation solution for column C2 after 97 days; thus reducing the potential to about 480 mV. The average potential was 480 mV for columns C3 and C5, which were irrigated with 300 mg/L ferrous. Column C5 was irrigated with all iron as ferrous; thus at the lowest potential of 370 mV.

The H_2SO_4 concentration in the irrigant was kept constant at 10 g/L, which kept the pH relatively constant between 1 and 1.2. The initial pH of the PLS ranged from 2.5 to 3.2, with the lowest being that of column C5 which was agglomerated with 3.7 kg/t ferrous. The PLS pH profiles peaked between 3.8 and 4.0, and thereafter decreased steadily to between 1.4 and 1.6 after 248 days of leaching. The decrease in pH is likely due to the slower leaching of acid-consuming gangue minerals over time.

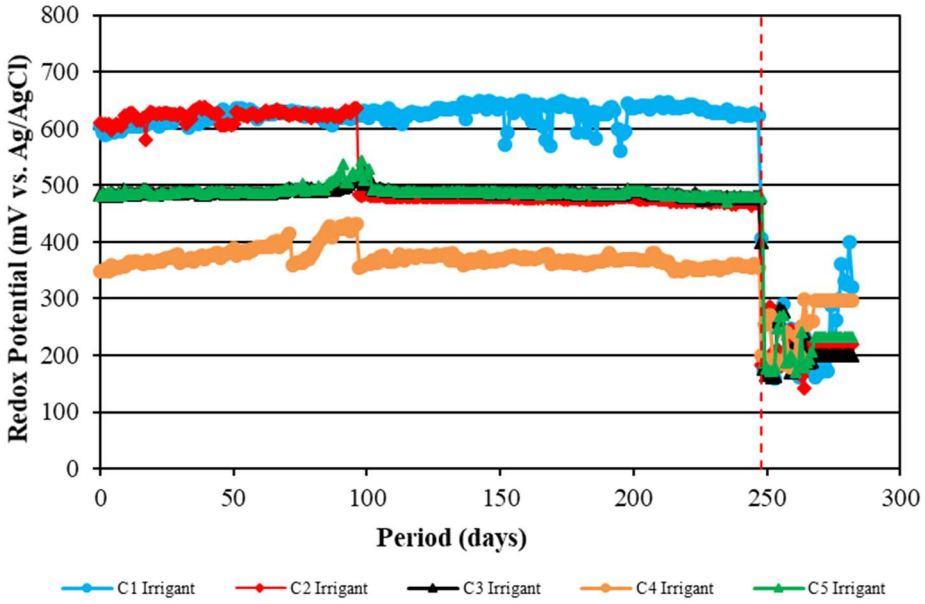

Figure 3: Redox Potential Profiles (Irrigant)

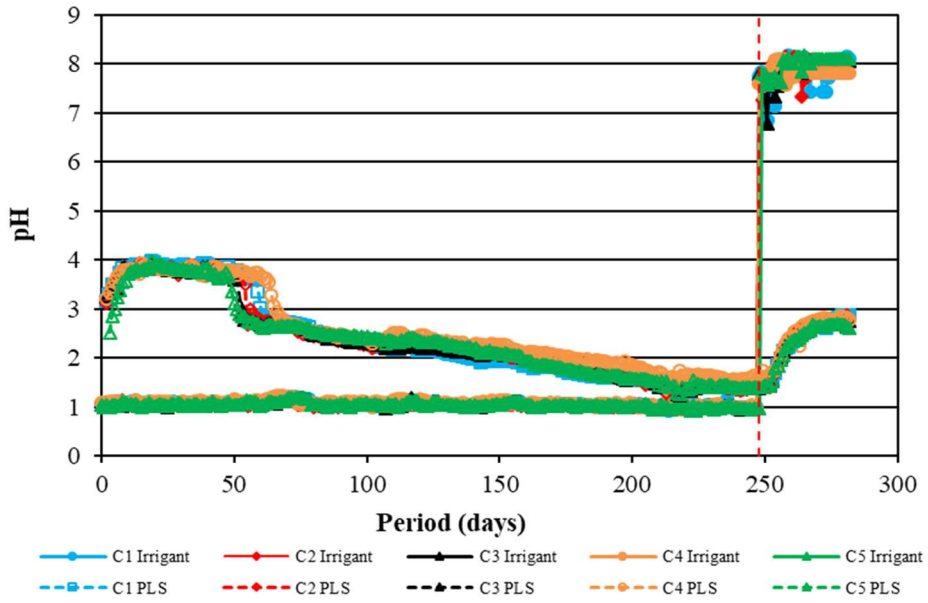

Figure 4: pH Profiles

Copper, Cobalt and Iron Dissolutions

Copper, cobalt and iron dissolution profiles are presented in Figures 5 to 7, respectively. These were plotted from the recalculated metal head grade and metal in solution analyses. The recalculated head grade entails a 100% element mass balance (i.e. element out / element in) with respect to both solid and solution phases over the leach, water wash / rinsing and drain-down stages.

Similar copper dissolution profiles were observed for all the tests. The overall copper dissolutions were between 94% and 96% after 248 days of leaching.

Column C1, which did not have any ferrous in the irrigant, showed the lowest cobalt dissolution of 40%, the solution potentials were high (> 600 mV) and not conducive for cobalt dissolution. A notable improvement in the rate of cobalt leaching was observed for column C2 after 97 days, which corresponded with the addition of 400 mg/L ferrous in the irrigant. The addition of ferrous in the irrigant (300 mg/L to 1.5 g/L) improved the extent of overall cobalt dissolution by between 38 and 41 percentage points. The effect of adding ferrous in agglomeration on the initial rate of cobalt dissolution was more pronounced than that of adding ferrous in the irrigation solution. This is supported by the

rapid initial cobalt dissolution for column C5 (at 3.7 kg ferrous / t ore in agglomeration), reaching 50% after 9 days. This is much higher than that of column C3 (300 mg/L ferrous in the irrigant) and column C4 (1.5 g/L ferrous in the irrigant) which were only at 11% and 16% dissolution respectively, after 9 days. The overall cobalt dissolutions after 282 days were: 40% for C1, 78% for C2, 80% for C3, 81% for C4 and C5.

The negative iron dissolutions depicted (up to 132 days) were because of iron precipitation (i.e. ferric) during the high pH period experienced in the ore beds. The profiles show a gradual increase in the iron in solution after 60 days, which corresponds to a rapid drop in pH to between 1.8 and 2.3. The overall iron dissolutions were between 11% and 14% after 282 days.

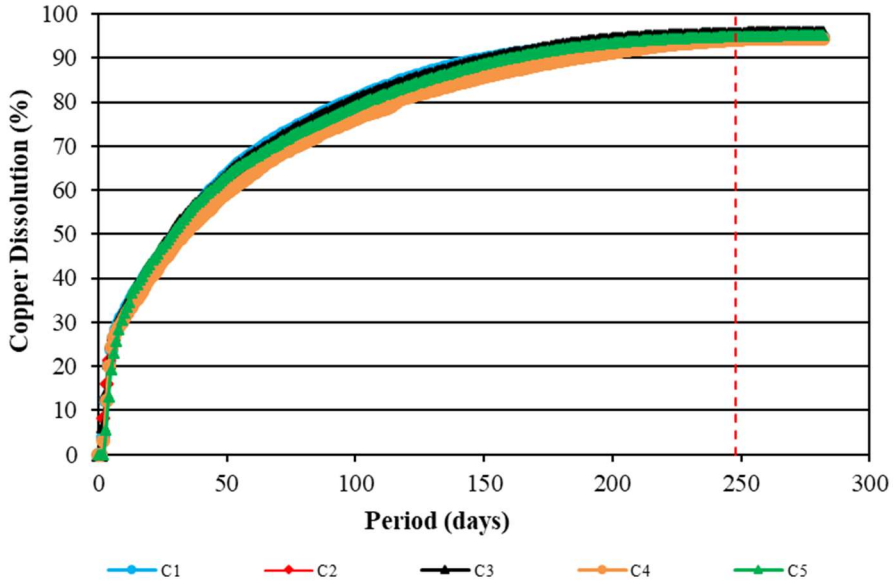

Figure 5: Copper Dissolution Profiles

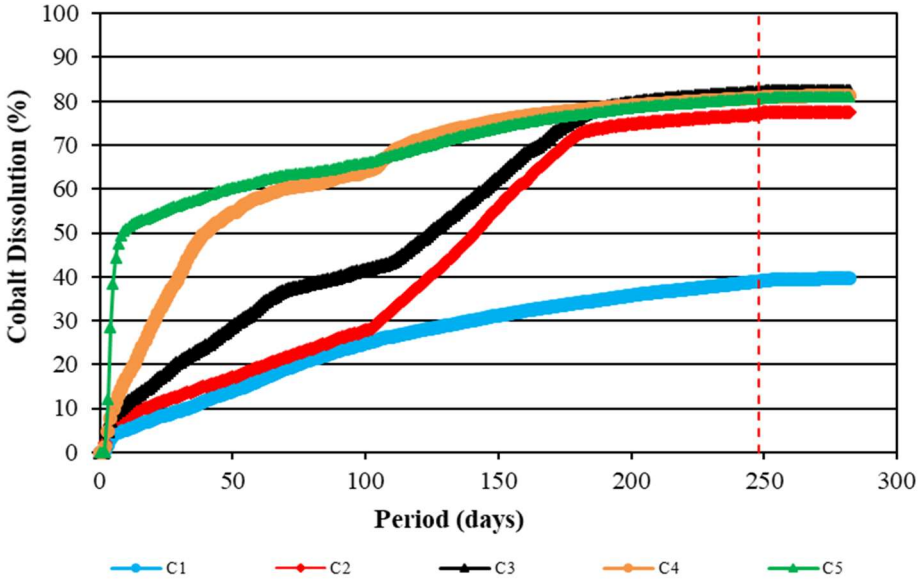

Figure 6: Cobalt Dissolution Profiles

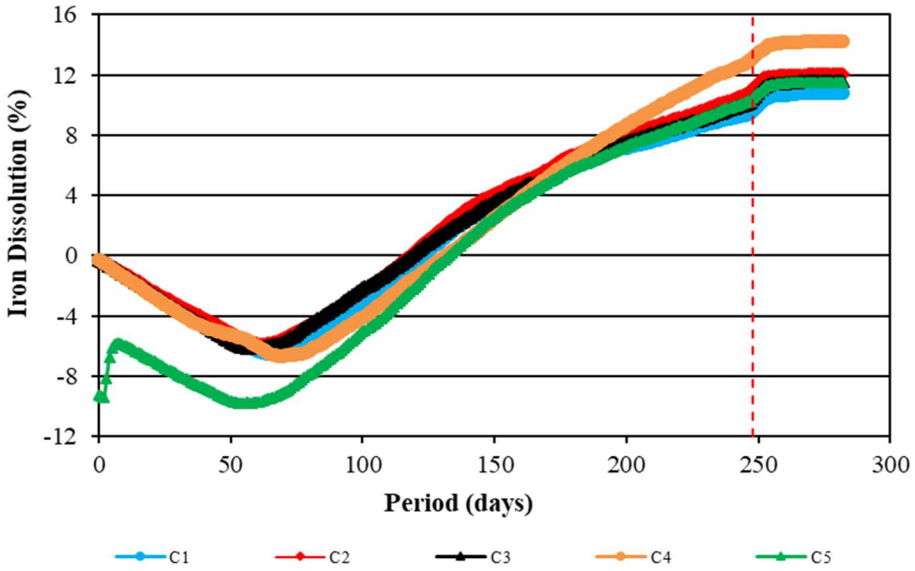

Figure 7: Iron Dissolution Profiles

Acid Consumption Profiles

The net acid consumption (NAC) profiles corresponding to the aforementioned metal dissolutions are depicted in Figure 8. These are defined as follows:

$$mNAC = mFEED - mPLS - mSX \quad (1)$$

With:

mNAC : net acid consumption, in kg H_2SO_4 / t (dry) ore
mFEED : acid in the irrigation solution, in kg H_2SO_4 / t (dry) ore
mPLS : acid in the PLS, in kg H_2SO_4 / t (dry) ore
mSX : acid in the raffinate solution after copper solvent extraction (SX), in kg H_2SO_4 / t (dry) ore (1.54 kg H_2SO_4 / 1 kg Cu extracted)

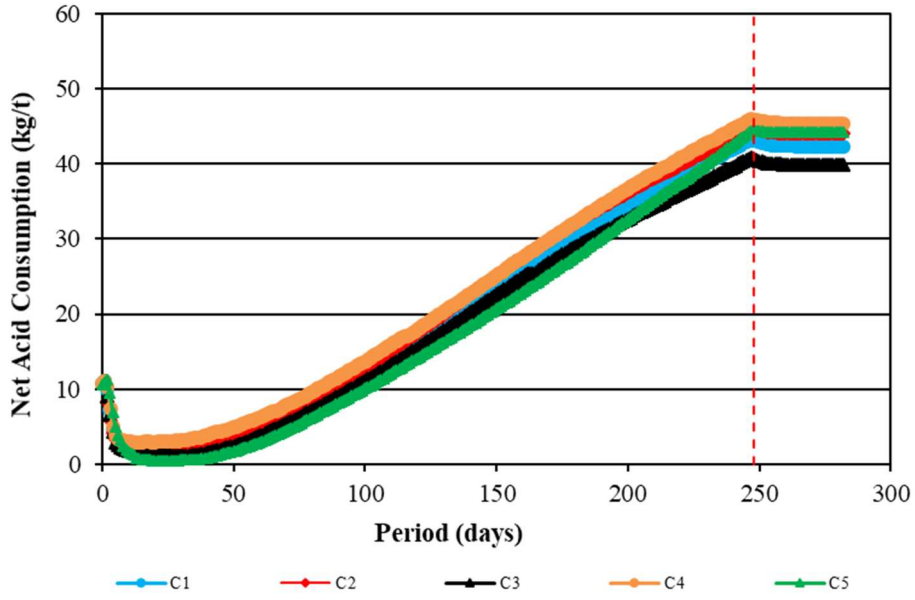

Figure 8: Net Acid Consumption Profiles

The acid consumption profiles were very similar, this was expected since the tests were conducted on the same ore sample and the same amount of acid was added in agglomeration and in the irrigation solutions. The average net acid consumption was 43 kg H_2SO_4 / t ore after 282 days.

CONCLUSIONS

The results presented in this paper demonstrate the ability of ferrous ion to enhance the dissolution of Co(III) minerals at solution potentials above 350 mV, by the addition of as little as 300 mg/L Fe(II) in the irrigation solution. A significant improvement in the initial rate of cobalt dissolution was achieved with the addition of Fe(II) in the agglomeration step. The addition of Fe(II) had no adverse effect on the copper dissolution, with the average extent of overall copper dissolution reaching 95% over a period of 282 days.

ACKNOWLEDGMENTS

The authors would like to thank Mintek for financial and technical support.

REFERENCES

1. Fisher, K.G., Cobalt processing developments. Bateman Engineering Projects. The Southern African Institute of Mining and Metallurgy, 6th Southern African Base Metals Conference 2011: 237-258.

2. Kelly, L., Top 10 cobalt producers by country (Updated 2023). https://investingnews.com/where-is-cobalt-mined/ (accessed 20 March 2023).

3. Mwema, M.D., Mpoyo, M. and Kafumbila, K., Use of sulphur dioxide as reducing agent in cobalt leaching at Shituru hydrometallurgical plant. Journal of the South African Institute of Mining and Metallurgy, 2002.

4. National Minerals Information Centre, United States Geological Survey. Cobalt statistics and information, Annual Publication 2023. https://pubs.usgs.gov/periodicals/mcs2023/mcs2023-cobalt.pdf (accessed 05 April 2023).

5. Seo, S.Y., Choi, W.S., Kim, M.J. and Tran, T., Leaching of Cu-Co ore from Congo using sulphuric acid-hydrogen peroxide leachants. Department of Energy & Resources Engineering, Chonnam National University, Gwangju, Korea. Journal of Mining and Metallurgy, 2013, Section B: Metallurgy 49:1-7.

6. Sole, K.C., Parker, J., Cole, P.M. and Mooiman, M.B., Flowsheet options for cobalt recovery in African copper-cobalt hydrometallurgical circuits. ALTA 2018, Nickel-Cobalt-Copper Proceedings.

7. Welham, N. J., Johnston G.M. and Sutcliffe M.L., AmmLeach® A new paradigm in copper-cobalt processing. Copper Cobalt Africa, incorporating the 8th Southern African Base Metals Conference, Livingstone, Zambia, 6-8 July 2015, Southern African Institute of Mining and Metallurgy.

TECHNICAL CHALLENGES OF MIXERS AND SETTLERS OPERATING IN COPPER SOLVENT EXTRACTION PLANTS OF THE DEMOCRATIC REPUBLIC OF CONGO

By

[1]Godfrey Mitshabu, [1]Patty Bwando, [1]Hugues Ngwanza and [2]Yi Zhou

[1]BASF South Africa, D.R. Congo
[2]BASF Canada, Canada

Presenter and Corresponding Author

Godfrey Mitshabu
godfrey.mitshabu@basf.com

ABSTRACT

The first commercial copper solvent extraction plant of the Democratic Republic of Congo was successfully commissioned in 2008. Over the last 14 years more than 40 small, medium, and relatively large size copper solvent extraction sites have joined this challenged contest of “fast-track” projects implementation. In 2021, electrowon copper cathodes have contributed by 81% to over 1,6 million tons copper exported by the country, making it rank among the 3 top world copper producing countries. Over this period, opportunity was given for learning from various technical challenges faced by most of these operations at various stages of their still ongoing journey. This paper aims to offer a non-exhaustive review of some of these many learnings. This could serve as a background for possible upcoming upgrades of running operations and for the design of better documented greenfield projects still to come. Mixers and settlers design and operation have an impact on the stability of emulsion phase continuity and on the control of impurity transfer from the leach solution to the electrolyte. Mixer O/A ratio can be increased without affecting copper production either by recycling organic or by increasing the organic flow. Solvent extraction plants of the Democratic Republic of Congo that were designed with the possibility of increasing organic recycle and/or organic flow without reducing mixer residence time below 2 minutes and/or increasing settler specific flow above say 3.5 $m^3/h/m^2$ were better prepared for the control of mixer continuity in the presence of aqueous contaminants like colloidal silica even without the need of using a coagulant to reduce the content of colloidal silica in the leach solution. On the other hand, they achieve the least transfer of impurities from the leach solution to the electrolyte even without the need of a washing stage in the solvent extraction configuration.

Keywords: challenges, copper, solvent extraction, democratic republic of Congo

INTRODUCTION

Copper mining in the Democratic Republic of the Congo (DRC) mainly takes place in the Copper Belt of the southern Haut-Katanga and Lualaba provinces of the country. In the DRC the Copperbelt is about 70 kilometres wide and 250 kilometres long between Lubumbashi and Kolwezi towns. It includes some of the highest-grade copper deposits in the world. In some reserves the grades are above 5% copper. Many orebodies also contain relatively high grades of cobalt. There are large deposits that have yet to be explored using modern technology, so the size of the reserves may be understated. Copper demand is growing, currently led by China. Between 1970 and 1988 DRC copper metal production was roughly constant at between 400,000 and 500,000 tonnes, the DRC Government owned Gécamines being the main contributor. Production then dropped steeply to under 50,000 tonnes annually between 1992 and 2001. Attracted by the new incentive mining code released in 2002, some audacious investors gained interest for the mining sector of the DRC. Since then, production has steadily grown, reaching about 300,000 tonnes in 2008. According to DRC provisional statistics published in Jan 2023, the country exported about 2.4 million tons copper in 2022(1).

Up to the early 1990s, the hydrometallurgy route for copper production included typically flotation concentration, sulphatising roasting of sulphides concentrates, leaching of copper oxide concentrate and sulphatised concentrates, followed by direct electrowinning. Relatively high-grade leach solutions (55 to 60 g/L copper) were submitted to electrowinning (EW) without inclusion of solvent extraction (SX) as a purification route.In an SX plant copper is selectively extracted from a pregnant leach liquor solution (PLS) and transferred into the EW electrolyte. A direct current is then used to plate copper mostly onto stainless steel cathode plates.

The DRC site where copper cathodes were first produced via a process including copper solvent extraction was Ruashi Mining in August 2008. It was followed two months later by Chemaf with their Usoke plant. From that time up to 2022, not less than two mining sites including copper SX were commissioned on average every year in the region. Some of the more recent projects used lessons learned from drawbacks of earlier DRC SX plants to design SX plants better adapted to process DRC type of leach solutions. Unfortunately, many are still being designed with “weaknesses” such as the absence of organic recycles at mixers, too low throughput O/A ratio…

This paper reviews some of the main technical challenges faced by DRC SX plants involving, directly or indirectly, solvent extraction mixers and settlers from 2008 to 2022. Among others these include the management of silica, organic in aqueous and/or aqueous in organic entrainment, depending on SX plant design and operation.

SPECIFICITY OF SOME DRC SX MIXERS AND SETTLERS DESIGN

Specificity of some of SX Plant Design parameters

It is assumed that most of earlier engineering of DRC SX plants was mostly inspired by experience from existing American and/or Australian plants, although most were designed for different operating conditions (heap versus agitation leach, low versus high content of suspended solids, moderate versus high silica content, low to moderate versus high copper grade…).

Table 1. A few design data of a few DRC SX plants

		Chemaf Usoke	**MMG Kinsevere**	**Ruashi**	**Chemaf Etoile**
	Start-up & Expansion	10/2008 & 09/2013	05/2011	08/2008	11/2016
SX layout	Number of trains	1	2	2	1
	Configuration	2E, 2E, 2S, 1W	2E, 2S	2E, 1S, 1W	2E, 2E, 2S, 1W
Mixers	Organic recycle	Yes	No	No	Yes
	Achievable O/A	**HG: 3**	**1.4**	**HG: 2.4**	**HG: 2.4**
	Tip speed [m/s]	4.9 – 5.9	5.0	4.7 – 5.4	4.0 – 5.0
Settlers	**Specific flow [$m^3/m^2/h$]**	**HG: 2.7 – 3**	**4.6**	**3.9 – 5.1**	**4 – 4.5**

Many factors may have significant impact on SX plant performance. In the current evaluation we have mostly taken in consideration two of them. The first is the “achievable” mixer O/A ratio (adjustable preferably by increasing the numerator to avoid affecting copper production if PLS flow is reduced). The second is the settler specific flow. Our understanding is that they have been very determinant in DRC SX plant behaviour over the period under review. Both affect capital cost. We have summarized them for a few typical DRC SX plants in Table 1. The impact of variations of mixers tip speed was difficult to evaluate as in both SX plants where our investigations were carried out interstage phase transfer was seriously affected below 90% of maximum tip speed.

Recommended settler specific flow varies with sources from a relatively small range of 3.6 to 4.8 $m^3/m^2/h$ (2), through a medium range of 3 to 5.5 $m^3/m^2/h$ (3), to a relatively wide range of 2 to 6 $m^3/m^2/h$ (4). To mitigate crud related issues with relatively high concentrations of fine solids encountered with DRC agitation leach PLS, mixers of all SX stages are commonly set to run organic continuous (OC). This makes the settler crud compact at the organic/aqueous interface rather than being dispersed into or on top of the organic phase when mixers are running aqueous continuous (AC). In “normal” conditions (moderately contaminated aqueous and/or organic), an O/A ratio of at least 1.1/1 is enough to set a mixer to run organic continuous. The reverse applies when aqueous continuity is desired. Not much information was found in the literature regarding highest achievable mixer O/A ratio required to sustain organic continuity when aqueous and/or organic phases are contaminated significantly. In this regard colloidal silica is a common DRC aqueous contaminant. Its presence has required setting up uncommonly high mixers O/A ratio to sustain organic continuity or using a coagulant to reduce its concentration in the leach solution. O/A ratio cannot not be increased above say 1.5 in many earlier DRC SX plants without reducing PLS flow.

DRC “extreme” examples, as far as achievable mixer O/A ratio and settler specific flow are concerned, include Chemaf Usoke and MMG Kinsevere. The first could achieve O/A ratios as high as 3 when needed to sustain organic continuity. For extended periods, Usoke SX plant was mostly running at relatively low throughput compared to design. Settlers’ specific flows were mostly below 3 $m^3/m^2/h$. On the other hand, Kinsevere settlers operate mostly above 4.5 $m^3/m^2/h$ of settlers’ specific flow. In this plant organic recycles were not installed during construction. The O/A ratio that can be achieved without reducing aqueous flow below design is 1.4 only.

The common objective of aqueous recycles is to adjust mixer O/A ratio close to 1.1/1 even when PLS and advance organic flow are quite different, to ensure good mixing efficiency. In the presence of aqueous contaminants like colloidal silica, to sustain organic continuity in a mixer it is required in many DRC SX plants to increase the O/A ratio well above 2. Where possible this may include opening organic recycles valves and/or splitting the aqueous feed, especially in the stripping section of the SX plant.

COLLOIDAL SILICA

Introduction

One of the major challenges faced by many DRC copper solvent extraction plants is the disturbance of mixer stability associated with the presence of colloidal silica in aqueous phases (leach solution and/or electrolyte). The magnitude of the impact which the silica has upon the solvent extraction process is dependant upon several factors including the physical form or forms in which the silica is present, the particle size distribution of the silica particles, the chemistry of the pregnant leach solution and the magnitude of the pH shift in the mixer as protons are exchanged for copper. Changes in the physical form of the silica can result in increased process disruption without a large change in total silica concentration of the PLS. This can make management of the situation problematic as crud runs are not easily predicted. In most plants where silica is present in the PLS, there are issues with increased crud formation and slower phase disengagement resulting in increased transfer of undesirable impurities to the electrowinning circuit, significant increases in reagent losses to raffinate and, in some cases, transfer of electrolyte to extraction further reducing extraction efficiency due to reduced pH in the PLS. Phase disengagement in aqueous continuity tends to be most severely impacted and crud formation in aqueous continuity can occur in very large volumes. Unfortunately, it can also be very difficult to maintain organic continuity in the mixers when silica is present in high concentrations. As a consequence of the surface-active nature of the silica colloids mixer stability is not maintained, the emulsion flips to aqueous continuity and massive crud runs through the plant can occur very quickly. Production losses in both quantity and quality are almost unavoidable in this case. Depending on the design of the SX plant, silica related issues could be mitigated so far in two ways in the DRC:

- The addition of a coagulant to reduce silica content in the leach solution. This has the advantage of being virtually applicable to all plants. A key point is to dose the coagulant well ahead of the solid liquid separation, like in the last leach tank. It has an impact mostly on the operating cost.

- The increase of organic to aqueous (O/A) ratio above standards values. This requires having enough organic inventory in the SX circuit. This solution is applicable only in plants designed to run either with high advance O/A ratios or where organic recycles are provided.

If capital is available for a DRC Cu project expected to last at least 10 years, calculations have shown that it makes sense to invest in a relatively big and operationally flexible SX plant (settler specific flow 3 ≤ $m^3/h/m^2$, mandatory organic recycles and high organic inventory) [5].

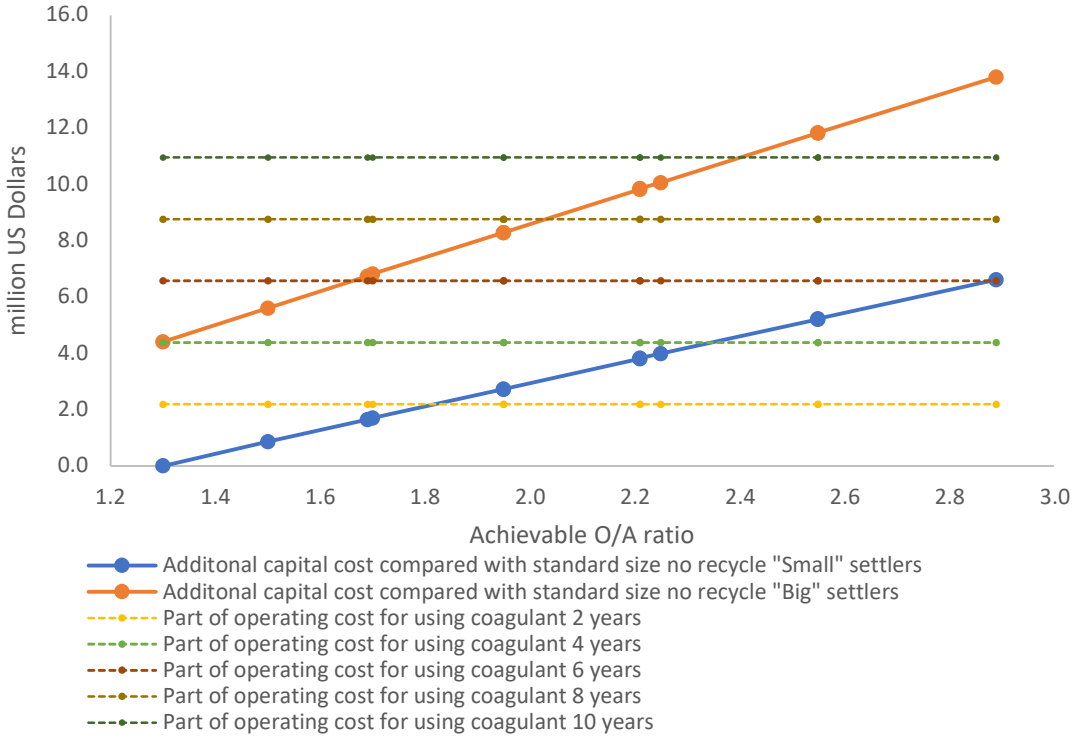

Figure 1: Capital and Operating Costs versus achievable O/A ratio

DRC Colloidal Silica related examples [5], [6]

During the construction of Kinsevere and Ruashi SX plants, sections of pipes giving the option for recycling internally part of the organic of a mixer–settler stage were not installed. Both SX plants experienced colloidal silica related issues, one in 2017 and the other in 2018. On the other hand, Chemaf Usoke and Chemaf Etoile were commissioned with organic recycles and could achieve relatively high mixers O/A ratios when needed, without reducing the flow of PLS. The mitigation of colloidal silica related issues in these 4 SX plants was experienced in the two ways described above.

From December 2018 to May 2019, a Cu production loss caused by crud runs associated with high colloidal silica in the leach solution at MMG Kinsevere was evaluated at 850 tons. To control the stability of mixers in organic continuity in absence of internal recycles of organic it was not possible to increase mixers O/A ratios above the designed value of 1.4 without reducing PLS flow. This was affecting copper production targets. The straightforward solution to the problem was to add a coagulant to reduce silica content in the leach solution. The operation was successful mainly because the coagulant was added to the last leach tank rather than directly into the leach solution. Earlier attempts to use a coagulant in the DRC were disastrous towards the SX plant.

Owing to problems caused by silica leaching, silica polymerization in the SX circuit and high crud levels, in March 2017, the operability of Ruashi SX plant was dramatically affected for two weeks or so. Over 470 tons of Cu production (and 45 tons of Co) were lost. Mixers could not stay consistently

in organic continuity while the SX plant was running within designed parameters. To stabilize mixers operation, it was required to increase the organic flow by 10 to 17% above design values to keep overall production unchanged. This necessitated the addition of diluent to top up the organic inventory. Unfortunately, the higher settlers' specific flows incurred resulted in relatively high organic in aqueous and aqueous in organic entrainment values, making it difficult to reduce contamination of the electrolyte.

Chemaf Usoke experienced colloidal silica related issues as early as July 2013 with stripping mixers often flipping from OC to AC, accompanied by "crud runs" where the crud floating within the organic phase of the first stripping settler would start overflowing to the next stripping settler. This would progressively transfer crud and acid to extraction stages, increasing thus the free acid in the extraction aqueous. Extraction mixers would then also flip from OC to AC, generalizing the crud run all over the SX train. But here the problem could be quickly mitigated. To do that, the spent electrolyte had to be turned off completely for 20 minutes or so and restarted with a stepwise flow increase. Since that period, Chemaf Usoke has been typically running with higher than "standard" values of mixers O/A ratios, still achieving production targets quite easily. This can be explained by the relatively long mixing time, and the relatively low settler specific flow. Chemaf Usoke experience was considered in the design of Chemaf Etoile SX plant which was commissioned in 2016. Colloidal silica related issues were also experienced at Chemaf Etoile in 2018 and 2019, but they were easily mitigated by running higher than standard mixers O/A ratios when required.

ORGANIC IN AQUEOUS AND AQUEOUS IN ORGANIC ENTRAINMENT

Introduction

A typical stage of a DRC copper SX train mostly includes one or two mixing boxes where the organic and the aqueous phases exchange copper and protons. An emulsion is generated, made of droplets of one phase (mostly the aqueous phase) dispersed within a continuous second phase (mostly the organic phase containing a copper extractant). This type of emulsion is called an "organic continuous" emulsion where the organic is the continuous phase. The reverse applies for an "aqueous continuous" emulsion. The second major equipment of an SX stage is a settler where phase separation takes place. Stages of concern regarding organic in aqueous entrainment include the raffinate stage in extraction and the advance electrolyte stage in stripping. Aqueous in organic entrainment is dreaded in stages producing respectively stripped organic and loaded organic. In theory, relatively higher organic in aqueous entrainment is expected in the aqueous phase when a raffinate stage or a stage providing advance electrolyte are running aqueous continuous. Conversely, higher aqueous in organic entrainment may be expected in loaded or stripped organics running organic continuous. Nevertheless, to control crud at organic/aqueous interface virtually all DRC SX plants run organic continuous in all stages.

Causes of high entrainment depend on SX plant design and operating conditions. These include settler size and internal arrangement, setup of transition of emulsion from mixer to settler, mixer tip speed, O/A ratio, settlers' depth profiles, viscosities of phases involved, presence of surface-active phases contaminants which affect their disengagement rate etc.
Organic in aqueous entrainment may lead mainly to loss of plant organic, and/or poor copper cathodes quality. Aqueous in organic entrainment may affect copper recovery and/or electrolyte contamination by manganese and/or silica.

DRC entrainment related examples [7]

Most of the equipment of Chemaf Usoke SX plant (currently shut down) was acquired second hand from an Australian plant. Compared with the rest of the plant equipment upstream and downstream of the SX, mixers and settlers were mostly running "oversized". This offered a major advantage to the operability of the SX plant, especially in conditions of low copper input. Entrainments were relatively low within the range of usual operating parameters. On the other hand, to control capital cost, the size of Ruashi SX plant was optimised to match the rest of the upstream and downstream equipment. Organic entrainment in raffinates, aqueous entrainment in loaded organics were compared in these two plants over a period of more than one month in 2018.

Comparison of organic entrainment in Chemaf Usoke and Ruashi raffinates in 2018

Averages of organic entrainments in Ruashi and Chemaf Usoke SX raffinates of over one month were plotted in a simplified way versus advance O/A ratios in 2018 (figure 2). It was found that Ruashi had much higher organic entrainment numbers with a somehow upward trend relative to the increase of

O/A. On the other hand, Chemaf numbers were much lower and much stable despite the relatively higher range of advance O/A ratio the plant was running.

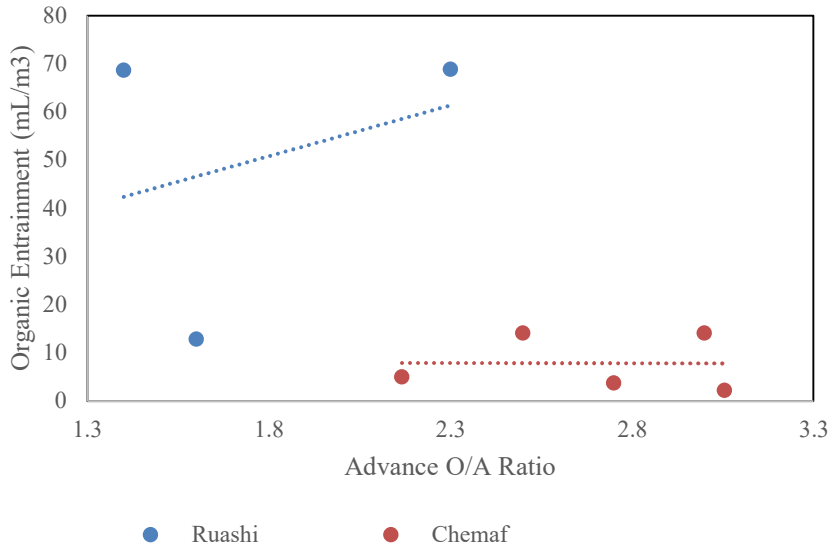

Figure 2: Comparison of organic entrainment between Ruashi and Chemaf

Comparison of aqueous entrainment in Chemaf Usoke and Ruashi loaded organics

Aqueous entrainments were also measured in loaded organics of those two plants during the same period and plotted in a simplified way (Figure 3). No measurable quantity of aqueous was ever detected in samples of loaded organic collected at Chemaf Usoke. Conversely, aqueous entrainment in Ruashi loaded organic was relatively high and in an increasing trend relative to the advance O/A ratio. On the other hand, at Chemaf Usoke O/A ratios as high as 3 could be run with a total mixer residence time well above 3 minutes.

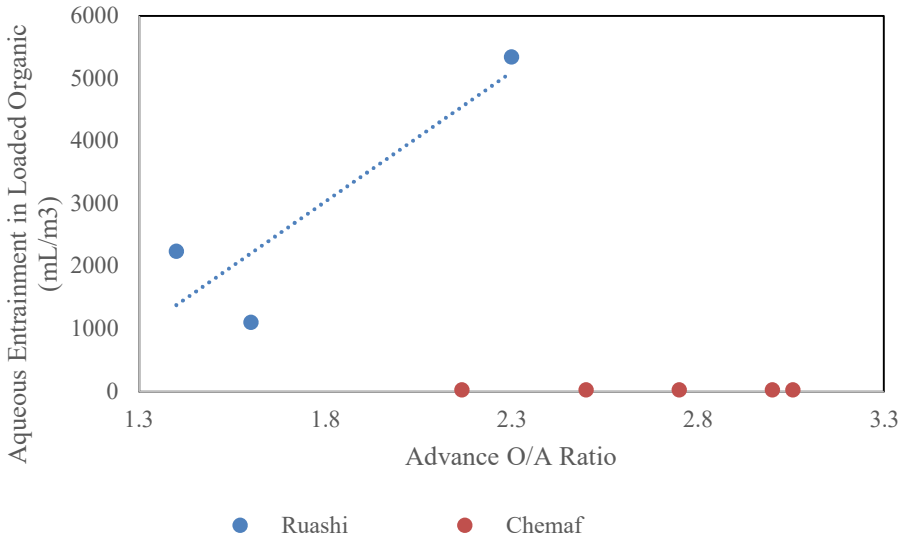

Figure 3: Comparison of aqueous entrainment between Ruashi and Chemaf

Impurities transfer

As far as DRC SX current experience is concerned impurities entrained from the PLS and likely to badly affect the electrowinning process downstream of the SX include manganese and iron ions, and silica. Most of DRC electrolytes contain cobalt ions although it is not deliberately added to the electrolyte. Virtually all this cobalt in the electrolyte is a balance of the quantity physically entrained from the PLS and the one lost in the electrolyte bleed.
Compared with other DRC SX-EW plants, Ruashi electrolyte inventory is quite high. This has advantages in terms of buffering due to higher copper storage offered, especially owing to power

restrictions experienced in the area. On the other hand, contamination of the electrolyte takes long to show up, but the disadvantage is the relatively long time and effort it takes to “decontaminate” the electrolyte inventory once contaminated. In 2017 crud runs resulted in high transfer of manganese and suspended solids into the electrolyte, with an impact on copper cathode quality, illustrated by nodular copper deposition.
Usually, during the commissioning stage of SX and EW plants, $FeSO_4$ is added to the electrolyte up to 1000 ppm at least to control the electrolyte redox. Afterwards, concentrations of Mn and Fe in the electrolyte are adjusted mostly by bleeding.
Below say 3 g/L total iron in the PLS, even without a washing stage many DRC SX plants have well managed iron transfer to the electrolyte without the need of bleeding more than 3% of total spent electrolyte flow.

OTHER DRC CHALLENGES

Other design related challenges

To “have a hand” on capital expenditure some DRC SX projects were mastered “in house” from the engineering to the construction phases. Earlier SX plants constructed that way had quite a lot of operational issues. In some cases, little consideration was given to safety standards, especially for quite small plants constructed with very limited budget. Over the last 14 years 4 SX plants were designed and constructed at 3 production sites belonging to one DRC group company. It is fortunate that learnings from errors of earlier SX plants were included in the design and construction of more recent ones. Despite such learnings, many SX plants, including many designed in China more recently do not include organic recycles at mixers, and other features that add to the flexibility of the circuit.

Operational challenges

The presence of relatively high level of suspended solids in DRC leach solutions from agitation leaching is often associated with high interface crud depths and bottom mud in settlers reducing thus their working volumes. In many SX plants crud handling is quite challenging even where crud removal features were considered in the design. Periodic cleaning of bottom mud from settlers is required. This involves putting the stage involved or all the SX plant offline before emptying the settler. Earlier SX designs had no provision for isolating one stage without the need of completely shutting down the SX train. One DRC SX plant running both 1m depth and “open” settlers in a high roof shelter and a more recent design deeper than 1m and covered settlers have noticed substantial savings in the consumption of organic diluent. Settler bottom mud removal with quasi no plant shutdown and manual involvement would be a good future target for SX equipment designers.

To minimize copper losses associated with unexpected spikes in the PLS, most of DRC plants often run with unnecessarily high extractant concentration in their plant organic. It is assumed that incurred organic entrainment losses due to relatively high organic viscosity would not outweigh potential copper losses and/or penalties related to copper entrainment in the cobalt containing by-product of many DRC copper operations.
To increase O/A ratios or/and to mitigate entrainment at critical stages, in some SX plants the flow of spent electrolyte is split between 2 stages, with less aqueous flow sent to each stage.

High spent electrolyte temperature related issues

A couple of DRC SX plants are confronted with temperatures well above 40 °C, especially in stripping stages. For some reasons, spent electrolyte leaving the EW at more than 45 °C is not cooled enough before returning to the SX. The plant organic is thus exposed to accelerated acid catalyzed hydrolysis of contained oximes. The higher the temperature, the higher the evaporation rate of the diluent, especially in settlers. Safety related risks are also increased.

CONCLUSION

Although SX plant performance depends on many factors, our discussion was mostly based on achievable O/A ratio and settler specific flow. A too high increase of internal recycle of organic will affect mixer efficiency by reducing mixing time. Settlers specific flow will also increase, inducing higher entrainment values.

High colloidal silica and aqueous entrainment related issues were best managed in DRC SX plants designed to handle relatively high throughput O/A without compromising mixer efficiency by a too

high reduction of the mixing time. When this was not possible it was required to add a coagulant well ahead of the SX plant to reduce the concentration of colloidal silica in the leach solution.
Capital cost for building “oversized” SX plants is admittedly high but later saving on operating costs would assuredly make it worth, if for example the amount of achievable copper transfer with DRC leach solutions per total settler area was compared with this same ratio in other parts of the world.

If many DRC SX plants could be redesigned, one would recommend:

- Possibility of running with relatively high advance O/A ratio (≥ 2) when needed, without reducing the designed PLS flow.
- Compulsory organic recycles.
- Settler’s specific flow ≤ 3.5 m3/m2/h.
- The possibility of splitting electrolyte or/and PLS flow between two stages when needed.

ACKNOWLEDGMENTS

The authors would like to thank their BASF colleague Gift Chisakuta for reviewing this paper internally.

REFERENCES

1. Ministry of Mines, Democratic Republic of Congo, 2023. Statistiques Minières Provisoires et Partielles Exercice 2022, 21 - 22.

2. Merigold C. R. (1996). LIX® Reagent solvent extraction plant operating manual, Henkel Corporation, Minerals industry division (now part of BASF), Tucson, Arizona, USA.

3. Cognis – now BASF (2007). Operation of copper solvent extraction plants, a Cognis review. (Unpublished copper solvent extraction training manual).

4. Taylor, A. and Jansen M.L. (1998) Solvent extraction mixer-settler design, Proceedings of Mineral Processing and Hydrometallurgical Design – World’s Best Practice. Perth, WA. (Published by Australian Mineral Foundation in Book form in 1999).

5. Mitshabu G *et al* (2020). Silica issues versus copper solvent extraction plant design, proceedings of ALTA conference online. Perth, Australia.

6. Kashala, A. et al (2018). Management of Mixing Continuity in a Solvent-Extraction Plant with a Leach Solution of High Silica at Ruashi Mining, Copper cobalt Africa, The 9th Southern African base metals conference, Livingstone, Zambia.

7. Mitshabu, G et al (2019). Management of copper solvent extraction plants running at reduced throughput, proceedings COM conference. Vancouver, Canada.

SX CIRCUIT, CRUD TREATMENT USING GEA DECANTER CENTRIFUGES, DCONTROL®

By

Tore Hartmann

GEA Westfalia Separator Group, Germany

Presenter and Corresponding Author

Tore Hartmann
tore.hartmann@gea.com

ABSTRACT.

For the economic extraction of important precious metals - nickel, zinc, platinum, gold, cobalt, uranium and rare earths, there are various process engineering routes to extract these important metals from the ore. One established and economical process is the hydrometallic process route with integrated solvent extraction (SX), which separates these metals after leaching in a solution.

All pilot and commercial SX systems experience the formation of crud - a solid- stabilized emulsion that accumulates at the aqueous/organic interface in the settlers of the solvent extraction stages. It is caused by a variety of substances entering the SX circuit, such as windblown dust, entrained solids from leaching, impurities in the plant solutions. While a thin layer of at the aqueous/organic interface can promote coalescence of fine droplets, excess crud interferes with phase separation resulting in greatly reduced extraction efficiency of the settling tanks. Crud prevents mass transfer from proceeding efficiently at the phase interface.

This crud can be solved by our technology of 3-phase decanter centrifuges. By centrifugal force we are able to separate this crud layer continuously into its individual components.

How the 3-phase decanter centrifuge technology works;

The design and operation of the three-phase centrifuge is similar to that of a decanter (two-phase separation). The solids settle on the inner wall of the bowl under the action of centrifugal force. The screw takes care of the solids transport for centrifuged solids with a differential speed to the decanter bowl.

The decisive difference to the decanter lies in the separate expulsion of the two liquid phases. In the 3-phase decanter centrifuge, the light liquid is discharged under pressure with subsequent DControl monitoring. The heavy liquid flows out without pressure. The DControl allows stepless adjustment of the pond depth during operation and leads to fast and precise adaptation to changing feed conditions without interrupting operation. This DControl system is presented in detail in this paper and presentation.

Keywords: SX circuit, crud treatment, decanter centrifuges

INTRODUCTION

The extraction of copper from ore involves various process engineering routes, including the hydrometal process route with integrated solvent extraction (SX). However, all commercial SX plants experience the formation of crud, a solid-stabilized emulsion that accumulates at the aqueous/organic interface in the settlers of the solvent extraction stages. This can lead to loss of copper and organic components in the raffinate, which can cost the plants hundreds of thousands to millions of dollars per year. Therefore, there is a need for effective technologies to separate the crud layer and recover the organic solution, while maintaining the efficiency of the loading and stripping process, control over the pH value, and extending the life of the cathode during electrolytic recovery.

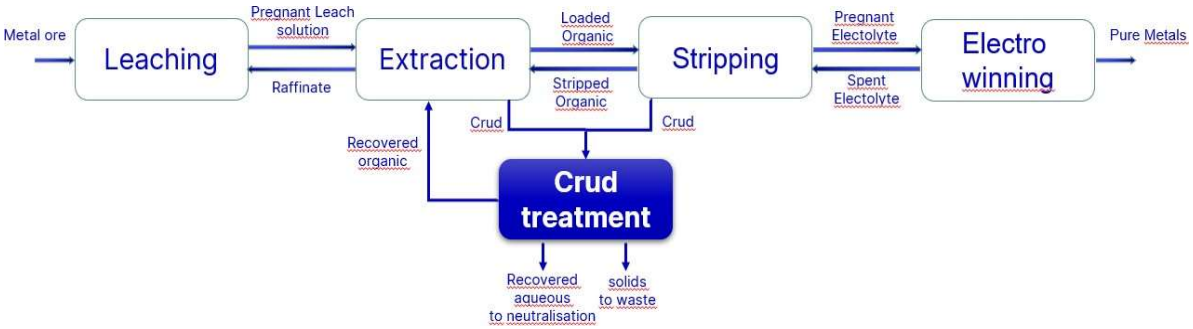

Fig. 1. Hydrometallurgy process including crud treatment

METHODOLOGY

In this paper, we present a three-phase decanter centrifuge technology that effectively separates the crud layer into its individual components in a targeted manner, namely the organic phase, aqueous phase, solid phase, and fourth phase that accumulates at the organic-aqueous interface.

The design and operation of the three-phase centrifuge is similar to that of a decanter(two-phase separation). The solids settle on the inner wall of the bowl under the action of centrifugal force. The scroll takes care of the solids transport for centrifuged solids with a differential speed to the decanter bowl.

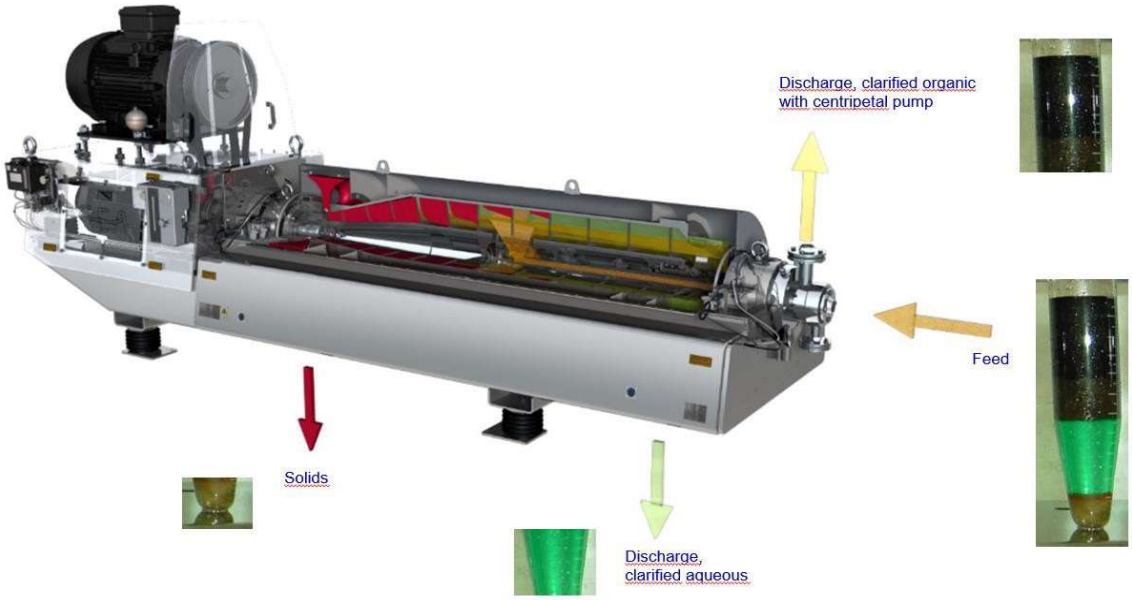

Fig. 2. Design of 3 phase decanter centrifuge for crud treatment

The decisive difference to the decanter lies in the separate expulsion of the two liquid phases. In the 3-phase decanter centrifuge, the light liquid is discharged under pressure with subsequent DControl monitoring. The heavy liquid flows out without pressure. The DControl allows stepless adjustment of the pond depth during operation and leads to fast and precise adaptation to changing feed conditions without interrupting operation.

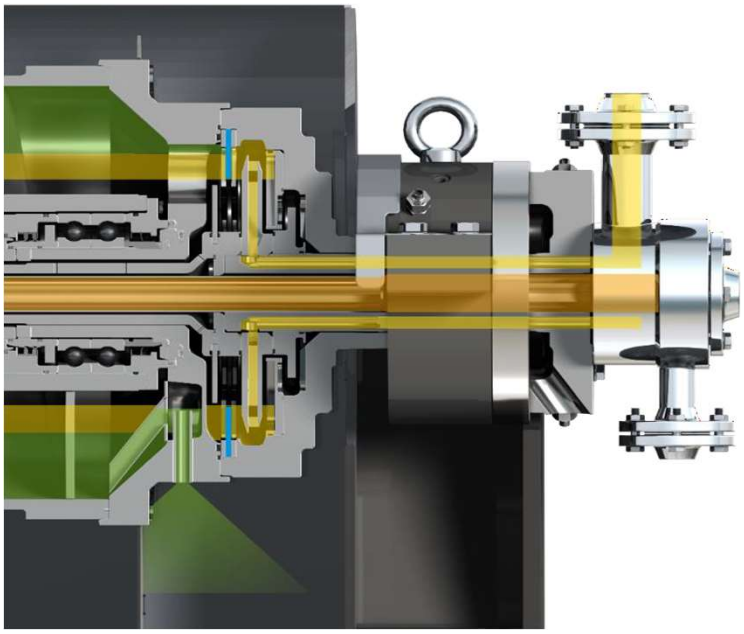

Fig.3. Detailed Liquid discharge organic and aqueous discharge of a decanter centrifuge

RESULT AND DISCUSSION

The three-phase decanter centrifuge technology offers many advantages, including higher purity of recovered organic solution even under fluctuating process conditions, maximum solvent recovery, and avoidance of plant downtime due to settler cleaning. The technology enables precise adjustment during operation and maintains the efficiency of the loading and stripping process, as well as control over the pH value. The extended life of the cathode during electrolytic recovery is also ensured by this technology.

The DControl system is an integral part of the 3-phase decanter centrifuge technology and is designed to allow online displacement of the separation zone based on a suitable control parameter. The goal is to achieve the most effective separation process possible by adapting the separation zone to the given phase distribution in the feed suspension, which can fluctuate over time depending on the raw materials and process control.

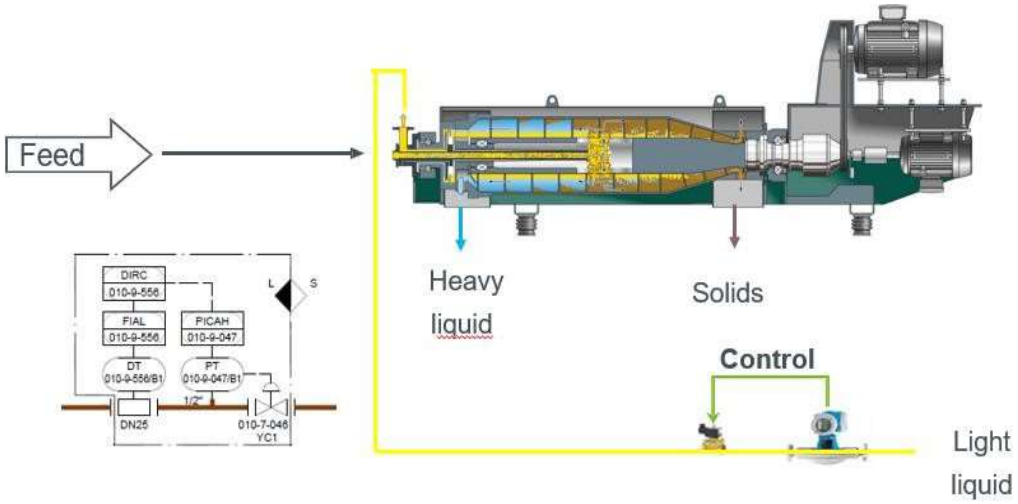

Fig.4. Principle Dcontrol

The DControl system integrates a density measuring device in the organic phase, in addition to the usual pressure gauge. The density measuring device provides a signal that is evaluated in the control unit to determine the contamination by the organic phase. The measured signal is then compared with a limit value, and if the permissible limit value is exceeded, the valve is actuated accordingly, resulting in a higher discharge pressure.

The increase in discharge pressure leads to an increase in the pond depth, which shifts the separation zone outward. By shifting the separation zone outward, the annular volume of the organic phase in the bowl increases, and the residence time in the centrifugal field becomes longer. The result is an improvement in the degree of purity of the organic phase due to the externally induced increase in discharge pressure.

Overall, the DControl system ensures the highest possible yield of the organic phase by allowing for precise online control of the separation zone based on the density of the organic phase. This leads to improved efficiency and purity of the separation process.

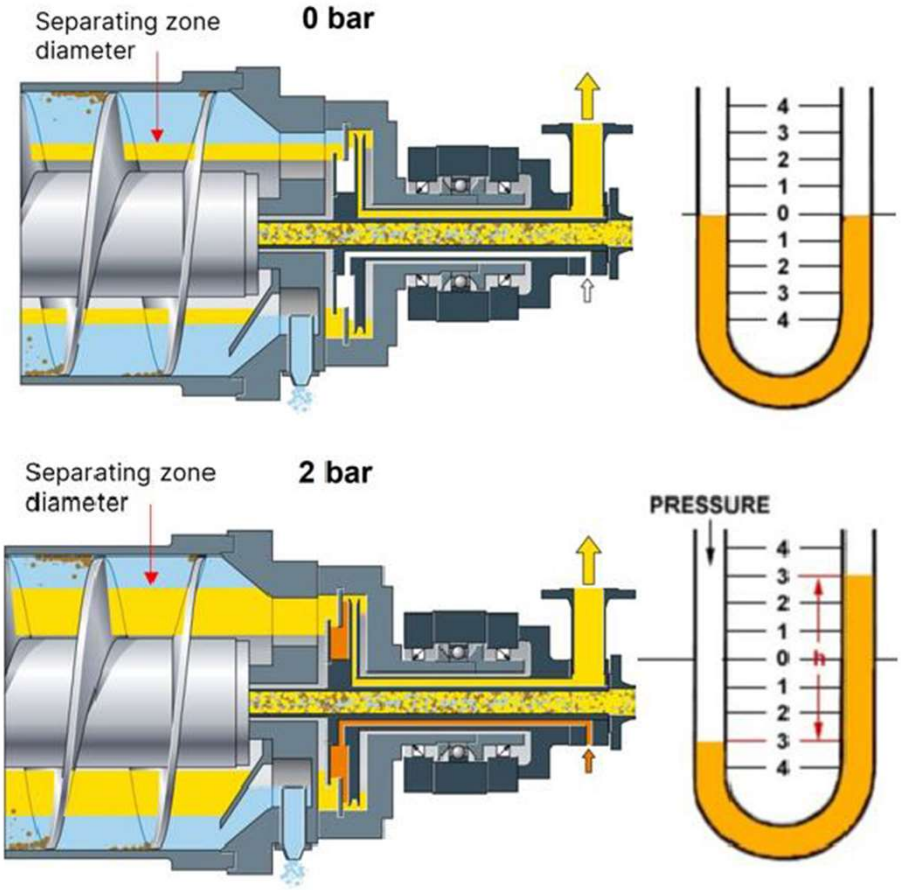

Fig.5. description Dcontrol and inline changing of the separating zone diameter in the decanter centrifuge

CUSTOMER BENEFITS OF DCONTROL

The customer benefits of using the DControl system in a 3-phase decanter centrifuge are:

Increased efficiency: The DControl system allows for online displacement of the separation zone, which ensures the most effective separation process possible. This increases the efficiency of the separation process and leads to a higher yield of the clear phase.

Improved purity: The integration of a density measuring device in the clear phase and the online control of the separation zone based on this parameter leads to an improvement in the degree of purity of the clear phase. This ensures that the customer obtains a high-quality product.

Cost savings: By optimizing the separation process and improving the purity of the clear phase, the DControl system can help the customer save costs in terms of raw materials and downstream processing. Additionally, the precise online control of the separation zone reduces the need for manual intervention, which can lead to cost savings in labor and maintenance.

SUMMARY

The three-phase decanter centrifuge technology effectively separates the crud layer and provides many advantages for the economic extraction of pure copper, cobalt, nickel, uranium and rare earth.

The technology offers higher purity of recovered organic solution, maximum solvent recovery, and avoidance of plant downtime due to settler cleaning.

The decanter centrifuge warranties a high degree of economic efficiency by eliminating the need for further preparation steps and separation stages.

The technology enables precise adjustment using Dcontol during operation and maintains the efficiency of the loading and stripping process, as well as control over the pH value.

FILTER CAKE DESATURATION: A LABORATORY-SCALE STUDY OF TWO COPPER SULPHIDE FLOTATION TAILINGS SLURRIES DEWATERED IN A FILTER PRESS

By

Francesco Kaswalder[1], Nicola Finocchiaro[1], Andrew Hawkey[2],

[1]Diemme Filtration Srl, Italy
[2]Diemme Filtration Srl, Australia

Presenter and Corresponding Author

Andrew Hawkey
Andrew.hawkey@diemmefiltration.com

ABSTRACT

Cake desaturation (often referred to as 'cake blowing') is a critical step in the dewatering of the majority of mineral tailings slurries. It is achieved by introducing compressed air on one side of the filter cake. The air displaces the interstitial liquid which is pushed to the opposite side of the filter cake and exits from the chamber through one (or both) of the filtrate discharge manifolds. Further cake moisture reduction can be achieved by extending the cake blowing time for several minutes after the displacement has been completed. The aim of filter cake desaturation is to reduce the cake moisture content to the point where it is no longer thixotropic. This is to avoid liquefaction in filter cake transport (by trucks or conveyor) and at the stacking location. Usually, the final cake moisture target is determined by the geotechnical engineer designing the dry stack. The moisture target varies widely, depending on the mineralogy of the solid particles and the particle size distribution.

Optimising the desaturation process during the filtration tests is very important in minimising the capital cost of the air compressors and the energy consumption of their operation. Considering the massive throughputs of tailings dewatering facilities, particularly in the copper sector, the amount of money to be saved by appropriate focus on the filtration test work, with particular attention to the cake blowing stage, is significant. Predicting the CAPEX and OPEX accurately can influence the viability of the project.

In this paper, two copper sulphide flotation tailings slurries with differing mineralogy and particle size are dewatered in a laboratory-scale filter press and the resulting filter cakes are blown with compressed air at different compressed air flow rates and for a range of times. The mineralogy of the two slurries are examined to help explain the differing desaturation performance and resulting final cake moisture content.

Keywords: filtration; filter press; tailings; dewatering; desaturation; mineralogy

INTRODUCTION

Cake desaturation in a filter press is essentially achieved by displacing the interstitial liquor in the filter cake with compressed air. This step is often referred to as “cake blowing” and usually follows the feeding and compaction steps. It is often applied together with membrane squeezing, depending on the plate pack configuration.

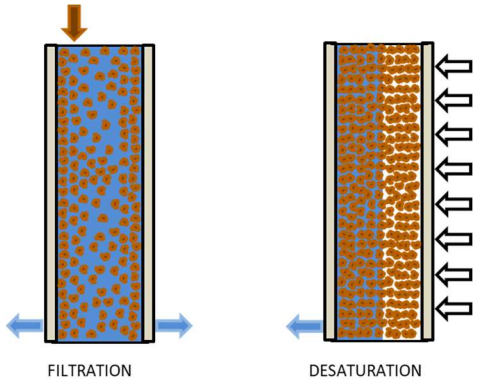

Figure 1: simplified illustration of the filtration and cake desaturation process

Cake blowing is used to reduce the moisture content of the filter cake. It can be applied for a number of different reasons:

- To avoid cake liquefaction where saturated cakes are thixotropic. These cakes typically have a high void ratio.

- To reach the cake moisture target set by geotechnical engineers so that it can be stacked safely to the desired height, particularly when the target cannot be reached without desaturation of the filter cake.

Cake blowing includes two stages. The first is the displacement of the interstitial liquor by compressed air, where the air ultimately replaces the liquor. The second stage is sometimes referred to as ‘drying’ but it also involves an entrainment process where the compressed air is forced through the cake for several minutes (typically less than five minutes) picking up some of the remaining liquor that coats the solid particles. Drying continues after the entrainment ceases but the moisture reduction is relatively slow.

The cake moisture content reduction that can be economically achieved is related closely to the filter cake permeability. Cakes with low permeability are more difficult to desaturate than cakes with high permeability. At the extreme end of this permeability range are filter cakes that are effectively impermeable. Permeability typically decreases as the solid particle size distribution becomes finer (we are particularly interested in the finest particles of the distribution). However, mineralogy can have an even stronger influence and the presence of clays can severely decrease the permeability of a filter cake. The influence of particle size on cake permeability is illustrated in the graph below (figure 2).

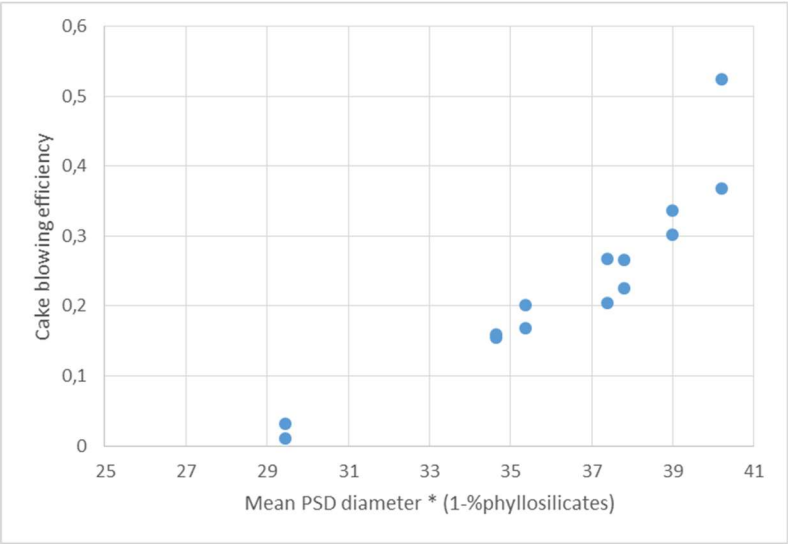

Figure 2: correlation between cake blowing efficiency, particle size and clay content

There are many minerals that are classified as clay. They are found in ore bodies associated with sedimentary rocks. Some clays affect tailings filterability more than others. The permeability of tailings filter cake is always reduced with the presence of clays. Serpentine and kaolin (for instance), reduce permeability and hence filtration rate and may increase the cake moisture content but usually do not threaten the economics of the project . However, the presence of clays such as montmorillonite and saponite (often referred to as smectites) means that close attention is needed for sample collection to make sure that the worst case is tested. Smectites are 'swelling' clays and can severely reduce permeability and filtration rate even in small concentrations. The presence of these clays also has a significantly negative effect on thickening, resulting in a lower underflow density. This in turn further increases the filter cycle time resulting in more or larger filters.

Mineral tailings is dewatered in filter presses to produce a dry filter cake that is safe to stack to heights of up to 100 m or higher. To do this safely, there will be a cake mosture target that is set by the geotechnical engineers who have designed the stack. To achieve this target, it may be necessary for the filter cake to be desaturated using compressed air. In order to size the filter presses and the cake blowing compressors it's critical that the filtration test work includes a comprehensive study of the desaturation process. It is essential to know exactly how much air is required and how long the cake blowing stage should be to reach the cake moisture target.

Particularly with copper mining, tailings filtration and stacking plants must process very high throughputs (70,000 – 150,000 tonnes per day are typical and can even be significantly higher). To optimize the cost per tonne of this dewatering process, it's important to first set the correct cake moisture target and then to size the filters and the cake blowing compressors so they can reach that target without being overly conservative. This requires precise test work, which, if not performed properly, can result in very expensive CAPEX and OPEX errors in the full-scale plant.

Particle size distribution and mineralogy of mineral tailings (including copper tailings) can vary widely. A study of two different copper tailings samples with respect to their cake desaturation performance is reported below.

TEST PROCEDURE AND RESULTS

Two samples of copper mine tailings slurry were received from separate copper mines. Each sample was received in thickened slurry form (underflow from thickener). To compare the effects of particle size distribution, both samples have been tested as received and subsequently tested after milling using a laboratory-scale rod mill. The two samples have significantly different mineralogy.

The table below lists the main physical characteristics of the slurries.

Sample	Sample A		Sample B	
Slurry form	As received	Milled	As received	Milled
Origin	Copper tailings 1		Copper tailings 2	
Density (kg/l)	1.40	1.41	1.41	1.40
Solid content (% w/w)	43.5	44.9	45.4	44.7

The particle size distribution was analyzed using a laser sizer. The particle size distribution of the samples as received is shown below in figure 3.

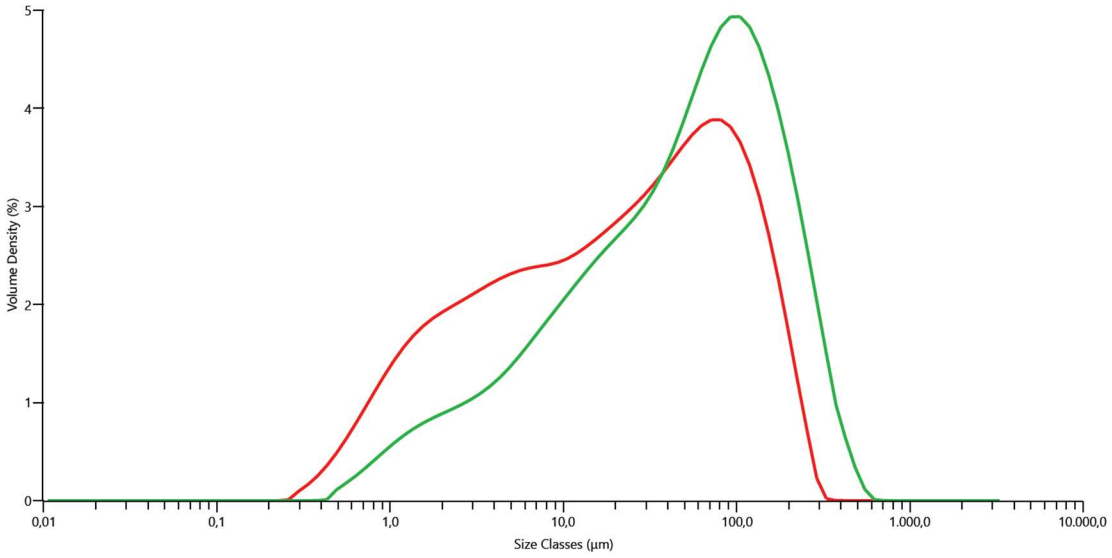

Figure 3: particle size distribution profile of tailings A (green) and B (red), original samples

Effects on the particle size after milling are shown below in figure 4.

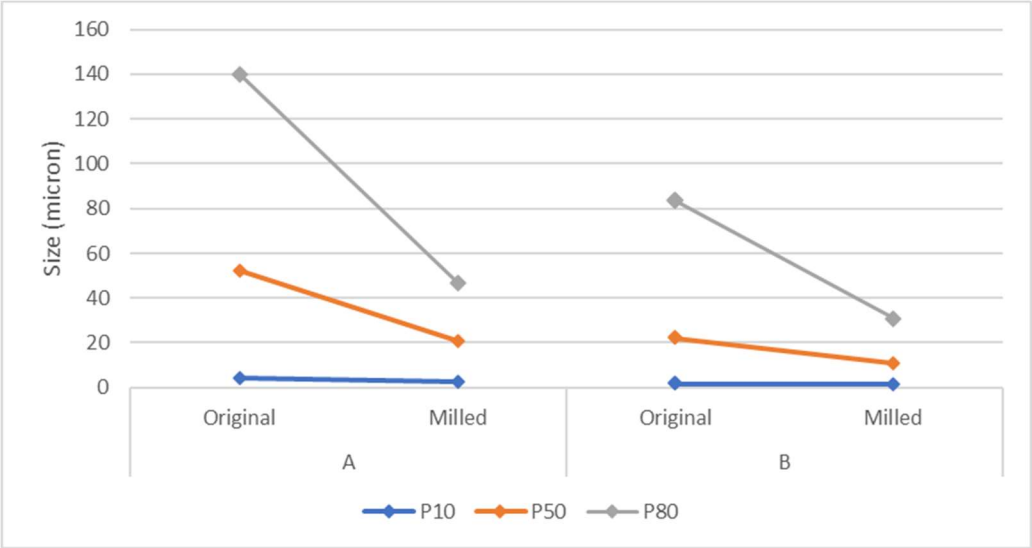

Figure 4: particle size distribution (P10; P50; P80)

The mineralogical composition of each sample, as received, has been analysed using XRD spectroscopy. The results are reported in the table below:

Sample A	
Phase	Content (% w/w)
Quartz	23.0%
Albite	51.3%
Orthoclase	12.4%
Clays	13.3%

Sample B	
Phase	Content (% w/w)
Quartz	27.6%
Andradite	35.7%
Sanidine	12.2%
Clays	24.5%

The samples were tested on a bench-scale test filter press with the following chamber configuration, feed pressure and cake blowing details:

- Filtration chamber type: recessed (fixed volume cavity);
- Filtration area: 0.0079 m^2;
- Filtration chamber thickness: 40 mm;
- Feed pressure: 10 bar;
- Total blowing air volume: 0.45 m^3/m^2 (N);
- Blowing time: 100 seconds, 150 seconds, and 300 seconds.

The simplified process flow diagram of the test filter is illustrated below in figure 5:

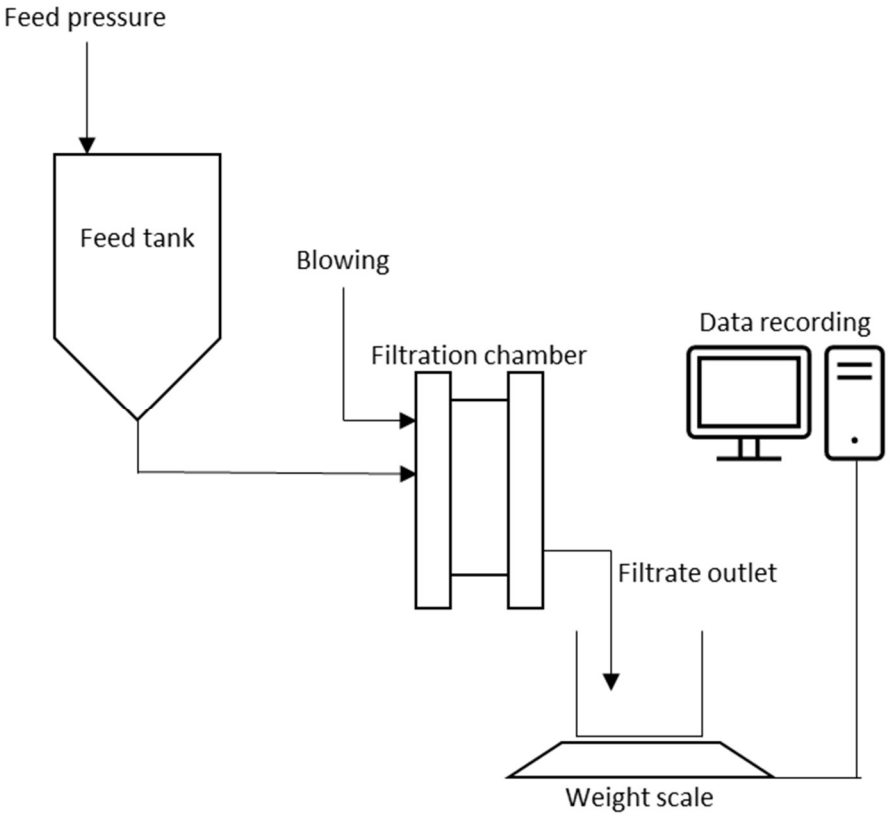

Figure 5: Simplified flow diagram of the test filter

The specific cake resistances of the two samples (as received and milled) are shown in the table below:

Sample		Specific cake resistance, α, (m.kg^{-1})
Sample A	As received	1.159 x 10^{11}
	Milled	1.052 x 10^{12}
Sample B	As received	4.878 x 10^{12}
	Milled	6.855 x 10^{12}

After cake formation (feeding and compaction), each sample was blown with the same total air volume but at different air flowrates. The cake moistures of the samples vs cake resistance for each blowing time (100 seconds, 150 seconds and 300 seconds) are shown in figure 6 below:

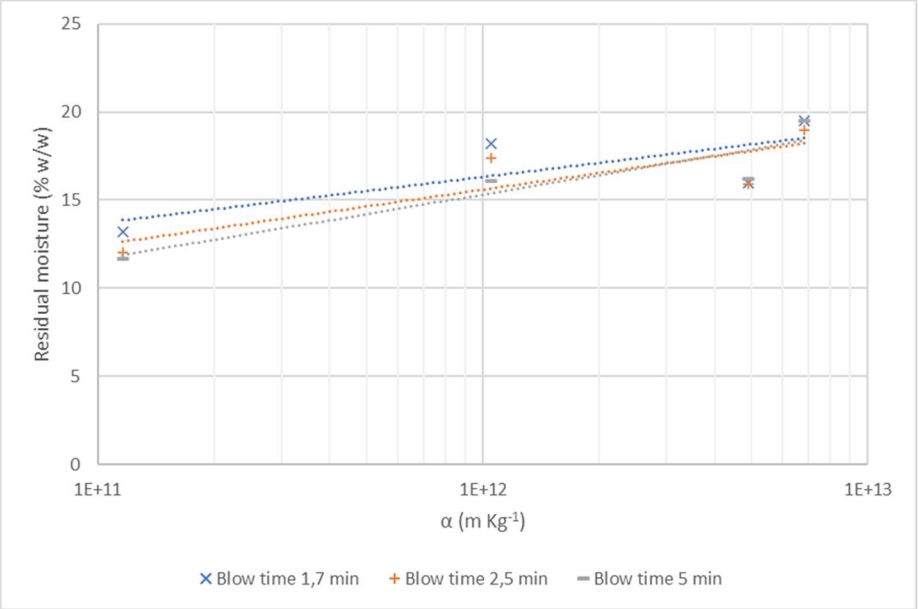

Figure 6: Cake moisture vs specific cake resistance (100 s, 150 s, 300 s blowing time)

The blowing curves for samples A and B, showing the trend of the cake residual moisture reduction over time during cake blowing can be seen below in figures 7 and 8 respectively. The curves have been created using mass balance by measuring cumulative filtrate volume vs time.

There are three curves corresponding to the three air flowrates for the as-received sample (‘as it is’) and three curves corresponding to the three air flowrates for the milled sample.

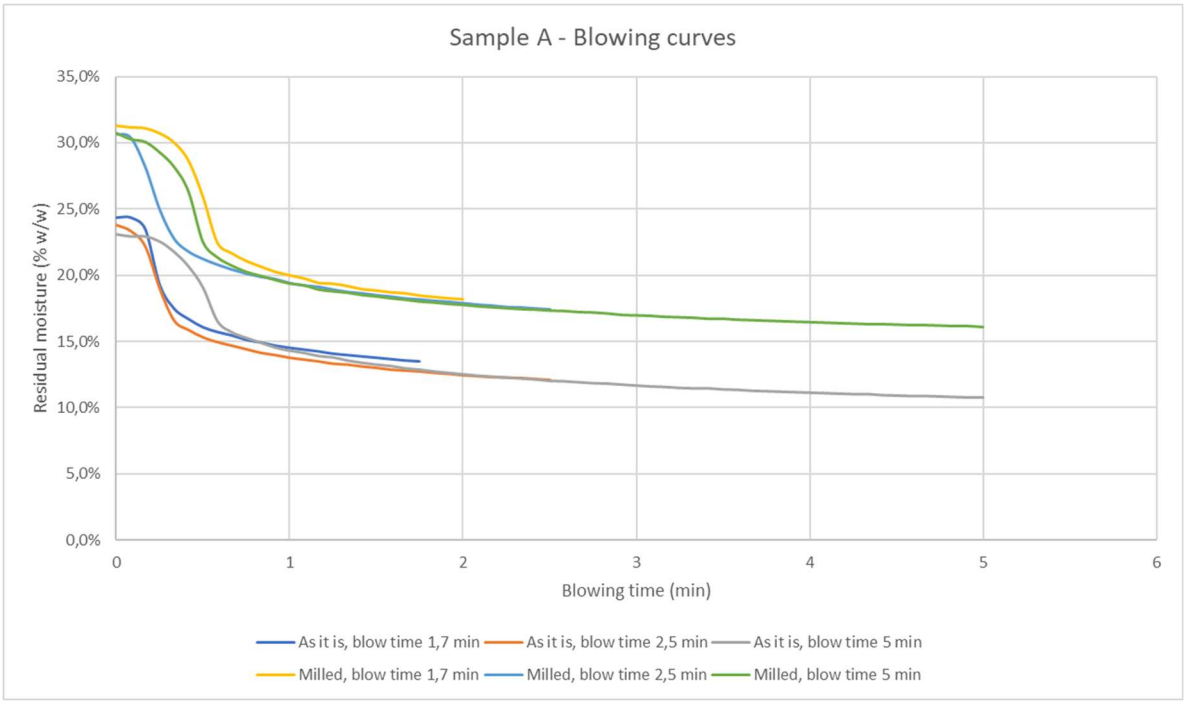

Figure 7: Cake blowing curves, sample A

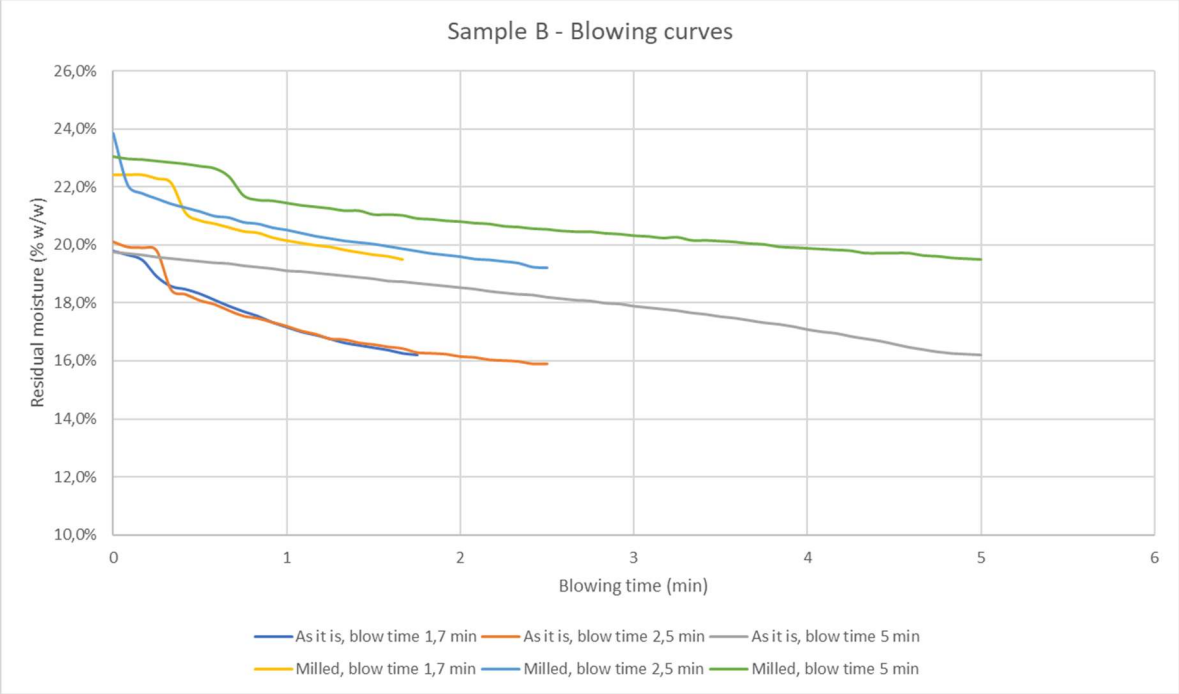

Figure 8: Cake blowing curves, sample B

DISCUSSION

For both tailings samples, the blowing curves of the cake formed by filtration of the slurry after milling show a similar moisture content reduction trend to that of the cakes formed by the filtration of the slurry as received. The difference is that the cake moisture of the milled slurries is higher at both the beginning of cake blowing and at the end. Effectively, the curves are similarly sloped but the milled sample curves are 2 – 3 percentage points higher in moisture for a given blowing time.

An interesting observation is that the tailings B cake has a very steep moisture content reduction curve for the first few seconds. It then shows a more gradual moisture reduction. However, sample A shows a flatter curve during the first few seconds but then a much steeper curve for the next 25 seconds than the sample B curve during this period. The moisture reduction for the sample A cake is greater and quicker overall than for the sample B cake.

Sample A cake has a higher void ratio and hence contains more moisture before the cake blowing begins. There seems to be an initial resistance to the displacement of the liquor but after a few seconds there is a steady transition from saturated to desaturated. There is significant further moisture reduction due to entrainment of some of the liquor coating the surface of the particles and drying (evaporation).

For tailings B, the transition from displacement to the entrainment/drying step is less obvious. The explanation for this may be that the entrainment/drying step has a much lower contribution to the overall desaturation. The displacement step may be sufficient to reach the target. Continuing the blowing far beyond that point may be uneconomic.

CONCLUSIONS

The results of the cake blowing stage of filtration tests need to be interpreted carefully to avoid oversizing (or undersizing) the CAPEX and OPEX estimates for very large tailings dewatering facilities. As can be seen in this study, particle size distribution is important but mineralogy can have

a much stronger influence on the filterability and, more importantly, the cake desaturation performance. In summary:

- For a mineral tailings such as sample A that filters quickly and forms a highly-permeable cake, a longer blowing time significantly reduces the final cake moisture content. The study indicates that blowing the same compressed air volume through the cake for a longer time results in a cake with a lower moisture content than that achieved with a faster flow for a shorter time. This means that smaller (or fewer) compressors are needed (lower CAPEX). The blowing should be stopped after the moisture target is reached to avoid an unnecessarily high OPEX.

- For a mineral tailings with lower filterability and low cake permeability (such as sample B), the study indicated that blowing time is relatively independent of final cake moisture content, using a fixed compressed air volume. For a tailings slurry such as this, a larger compressed air flowrate is preferred so that displacement is achieved quickly but there is little incentive to extend the blowing time past the displacement step. This requires larger or more compressors but the operating time is shorter (a higher CAPEX but OPEX is limited).

For both cases above, to optimize CAPEX and OPEX of cake blowing compressors, it's important to correctly sequence the filter presses so that the cake blowing stage occurs concurrently on as few filters as possible.

Figure 9: The scale of copper tailings dewatering today requires very large filters such as Diemme Filtration's GHT5000.

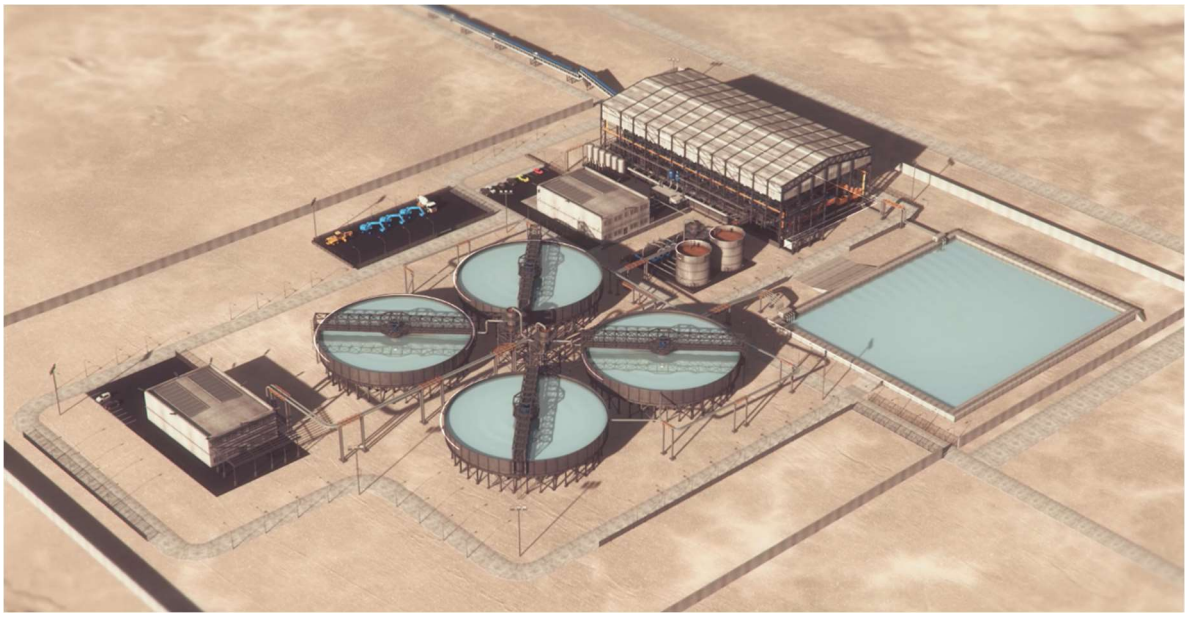

Figure 9: Copper tailings dewatering plant capable of processing 80,000 t/d of dry solids.

Figure 10: Air compressor room in a tailings dewatering plant with multiple 500 kW compressors

BIBLIOGRAPHY

1. Grosso A, Kaswalder F, Hawkey A, 2001. Clay-bearing mine tailings analysis and implications in large filter press design, Paste and Filtered Tailings Conference, 2021.

2. Finocchiaro N M, Kaswalder F, Grosso A, 2021, Filter press solid-liquid separation: comparative study on cake drying and washing performance with different plate designs, Filtech Conference, 2021.

3. Wilson M J, 2013, Rock-forming minerals, volume 3C: sheet silicates, Geological Society

4. Huggett J, 2013, Clay minerals, reference module in earth systems and environmental sciences, Elsevier 2015.

5. Wilson M J, 1999, Formation of clay – clay minerals, The mineralogical society, 1999.

INTERDISCIPLINARY PROBLEM SOLVING FOR HYDROMETALLURGY

By

M. Robert Mock, Brant Mock

NOVA Hydromet Ltd., Canada

Presenter and Corresponding Author

M. Robert Mock
robm@novahydromet.ca

ABSTRACT

Hydrometallurgy encompasses a unique set of engineering and scientific disciplines, the understanding of each of which is crucial to plant design and operation. Universities currently support the specialization of students by grouping disciplines under individual courses of study (chemical, mechanical, electrical engineering, etc.). However, the persistent problems faced by the hydrometallurgy industry are not neatly discretised into just one discipline or another. In particular, multiple disciplines will need to be understood and applied together to solve complex autoclave problems.

Organizational silos further complicate interdisciplinary problem-solving by placing barriers between personnel from different internal departments, decision makers, and external subject matter experts. Effective solutions will often require going over silo walls to incentivise problem solving, obtain and analyse operating data, model the interaction of physical systems, change operating parameters, and make equipment changes. Personnel from different on-site departments are often so busy addressing emergency issues, that they do not have time to step back and consider problems from an interdisciplinary perspective. The inter-organizational impetus for this type of high-level problem solving will often require a champion or change agent within the organization.

Third parties can also be prone to one-dimensional problem solving. Equipment suppliers will tend to suggest equipment changes or upgrades as solutions, software suppliers will tend to suggest software solutions, etc. Engineers tend to rely on their intuition and solve problems inside their technical comfort zone. The industry needs impartial third parties with the ability to apply multiple scientific disciplines (e.g., control theory, mathematical modelling, and materials science).

Herein, the authors introduce examples of selected widespread autoclave issues along with corresponding interdisciplinary solutions. Further, suggestions are included about how to facilitate crossing organizational silo boundaries to achieve lasting solutions for costly recurring autoclave issues.

Keywords:

Autoclave Letdown, Interdisciplinary Problem Solving, Organizational Silos, Recurring Issues

en·gi·neer

Solving problems you didn't know you had

In ways you can't understand

Specialization

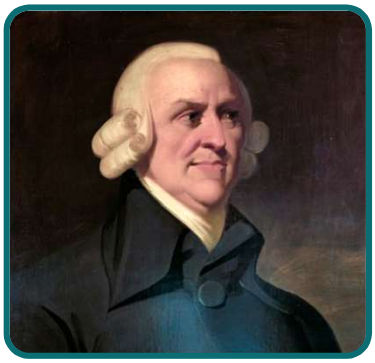

Adam Smith
Father of Economics

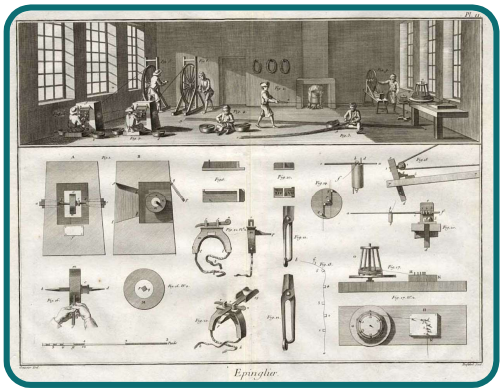

Pin Manufacturing Example

Integrated Circuit Example (Alternate)

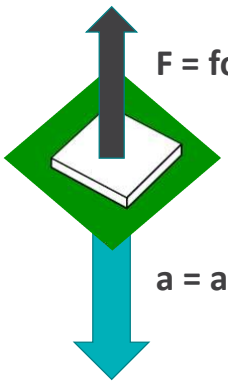

$$F = m \cdot a \qquad \sigma = \frac{F}{A}$$

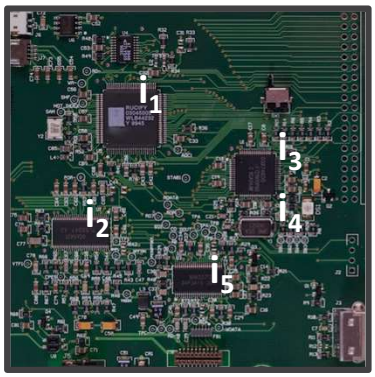

$$Power = V \cdot (i_1 + i_2 + i_3 + i_4 + i_5)$$

Complex Hydrometallurgy Problems

Costly

Complicated

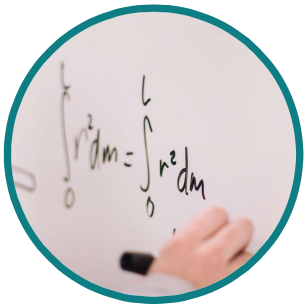

Mathematical
Crossing Disciplines

Natural Phenomena Cross Discipline Boundaries

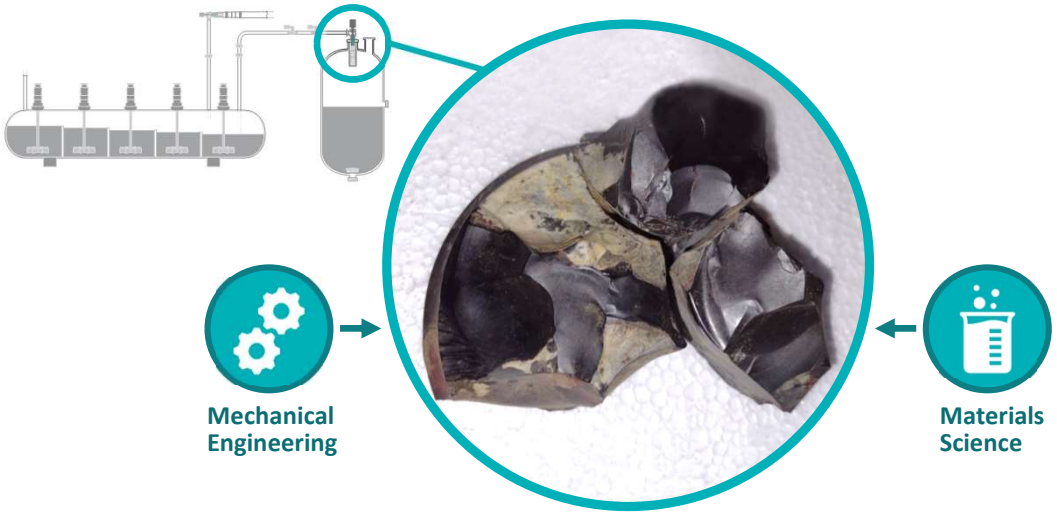

Example: Ceramic Fracture Probability

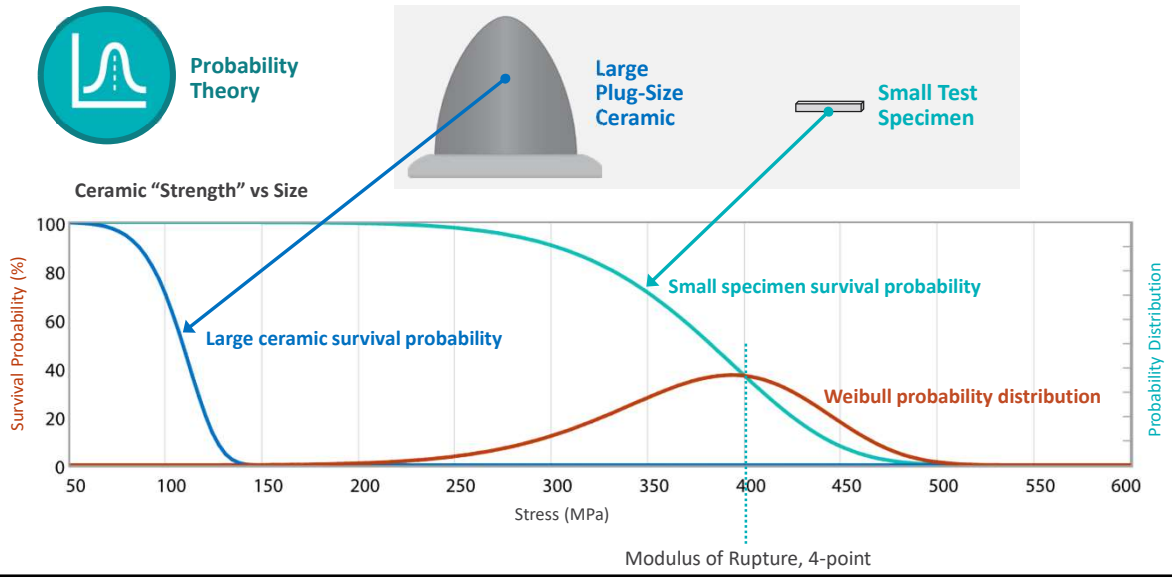

Example: Thermal Shock

Thermo-elasticity

Fluid Dynamics

Materials Science

Heat Transfer

Fracture Mechanics

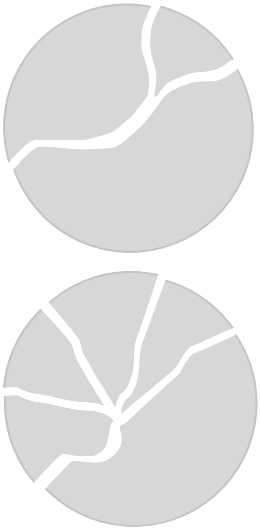

TRIAL & ERROR TRAP

System Dynamics and Control Theory

Control Theory

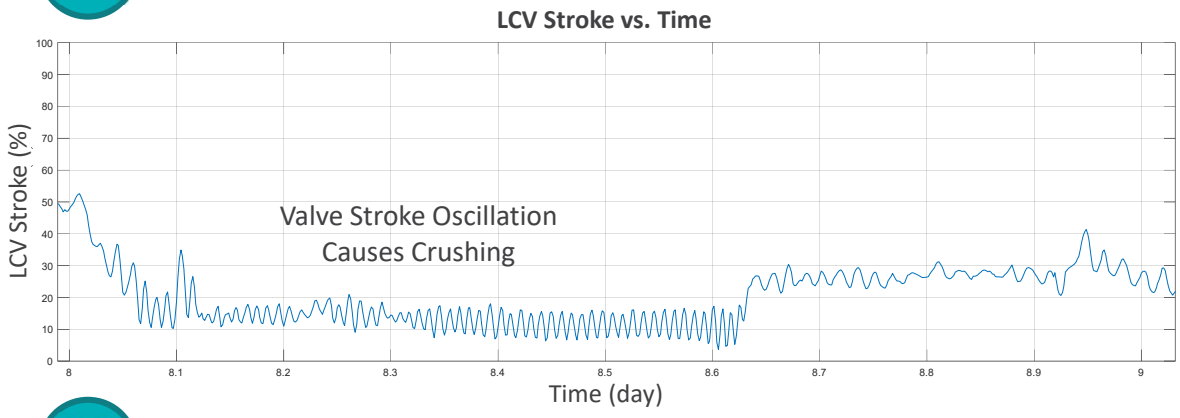

Data Science

Add Control Block Diagram, Transfer Function and Bode Plots

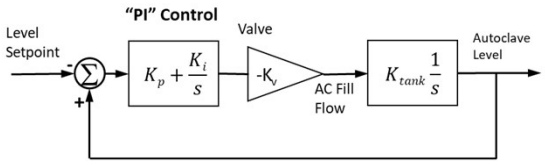

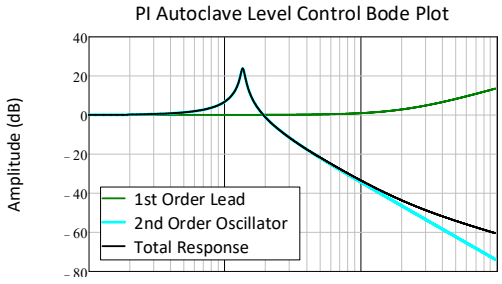

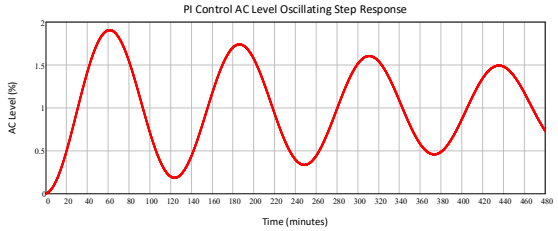

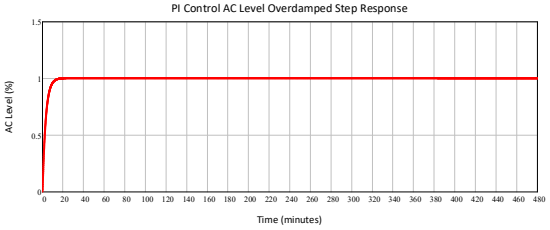

Control Loop Perspective

Statistical Process Control

Control Theory

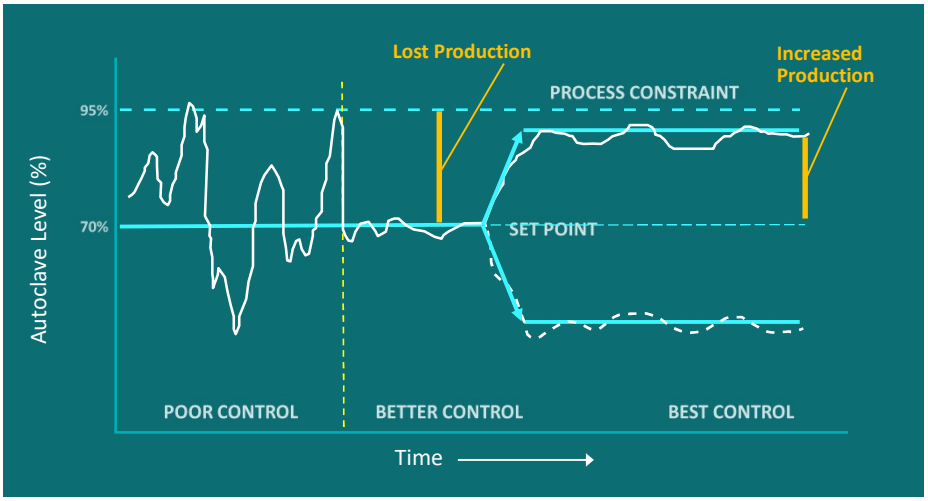

Opens the Hidden to View

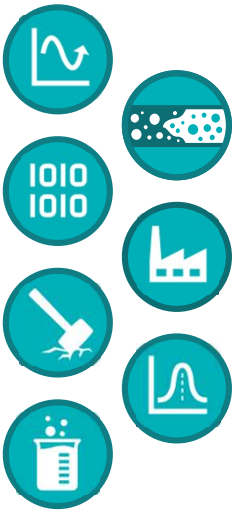

HIDDEN CONSEQUENCES

VIRTUAL
AUTOCLAVE BOTTLENECKS

Multiphase Compressible Flow

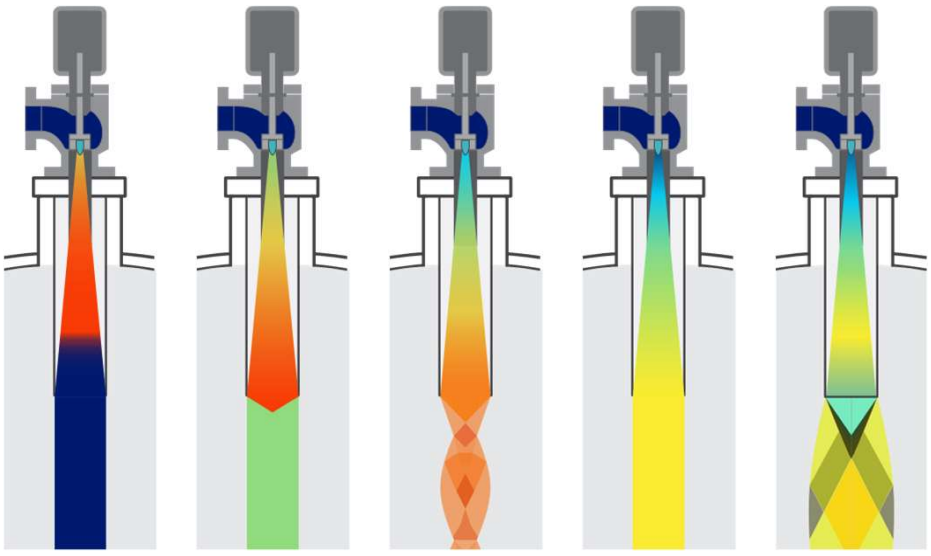

Benefits from Combining Disciplines

Reduce LDV trim fracture and erosion problems

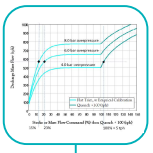

Elimination of impingement block, blast tube and flash tank damage by supersonic plume

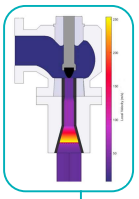

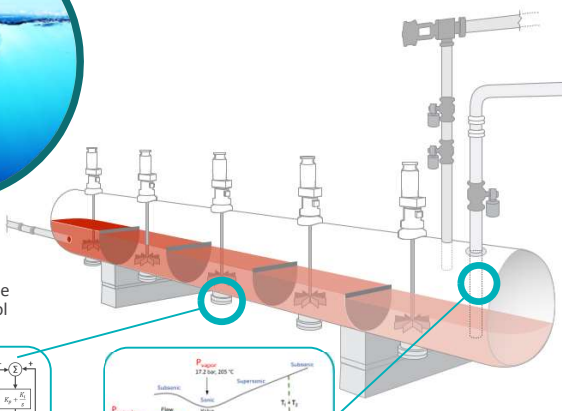

Reduce control response trips and Tighter Control for Better Yields

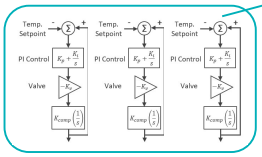

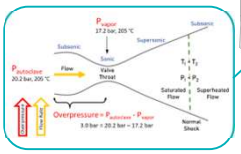

Get rid of LDV throughput limitation

Requires the Right Team

NOVA Technical Group

On-Site Champion

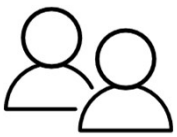

Subject Matter Experts

You

Role of the Interdisciplinarian

Sir Isaac Newton

"If I have seen a little further it is by standing on the shoulder of Giants"

Adam Smith

"Many improvements have been made by [those who]… are often capable of combining together the powers of the most distant and dissimilar objects."

Final Thoughts

Overcome Silos

Be The Catalyst

Think Differently

Getting Out of The Ruts

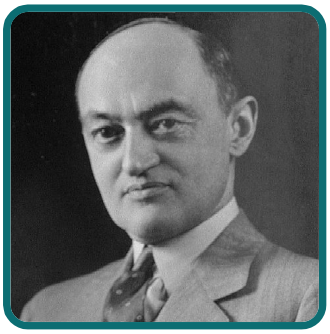

Joseph Schumpeter
Father of Economics of Innovation

Be someone who overcomes "the **ruts of established practice**."

THE WEAKEST LINK IS OFTEN OF THE LEAST CONCERN

By

Corin Holmes

Jenike & Johanson Pty Ltd Australia

Presenter

Corin Holmes
cholmes@jenike.com

ABSTRACT

Bulk-solids handling systems dictate the overall operational performance of the entire processing plant but are often the most undervalued components. They are typically the weakest link in a processing plant's value chain.

Liquid handling plant designers consider density and viscosity which are well known and commonly used design parameters. Bulk solids system design is similar however, the relevant parameters in handling bulk solids are instead compressibility, friction (i.e. cohesive strength and wall friction), and permeability. These frequently vary depending on the ore's mineralogy, shape and size distribution, moisture content, storage time-at-rest, temperature, and consolidation pressure.

Measuring flow properties and applying them correctly to design bulk-solids handling systems will reduce project risk, save capital, and increase throughput. This is especially true when handling sticky laterite materials.

Keywords: Bulk Solids, Material characterisation, system design, flow properties, laterites

The Weakest Link… The Back Story

The Weakest Link… The Back Story

Process steps:

- Designed
- Fabricated
- Installed
- Re-designed
- Fabricated
- Installed

$

The Weakest Link… The Result

Installed and removed from operation during first shift

Why?

Don't Be A Statistic

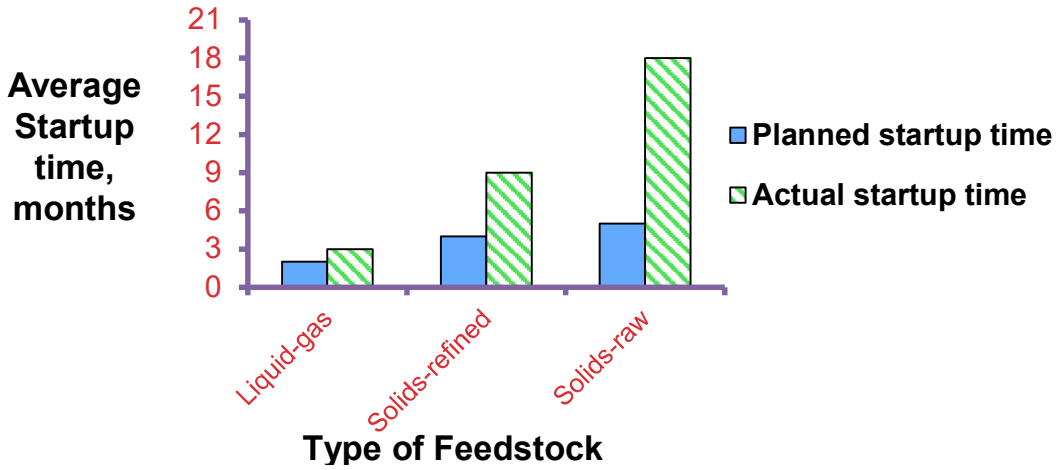

[1] RAND Study: Sample of 40 plants in US and Canada over a 6 year duration. Merrow, E., "*Problems and progress in particle processing*", Chemical Innovation, Jan. 2000 & Chemical Engineering; Oct. 1988, Vol. 95, Issue 15

Don't Be A Statistic

- Materials handling is an interdependent system.
- Appreciating the compounded effect is the dominant root cause responsible for reduced FLOW and highest value destruction over the life of assets.

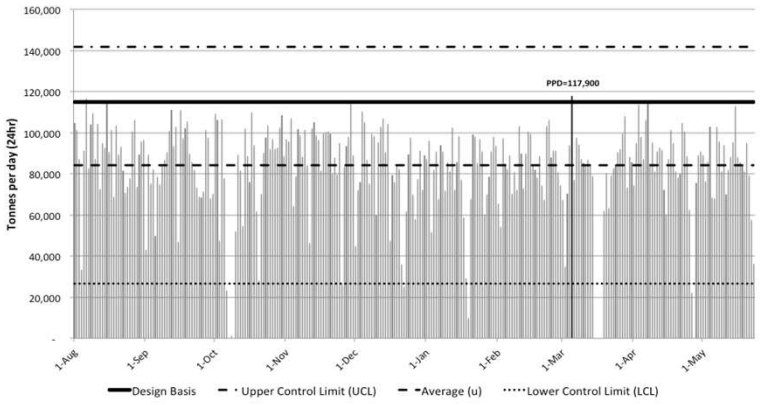

Perfect production day run chart for a direct ship ore operation*

*Wellwood, G.A., 2017. One perfect (production) day – a bulk solids handling perspective. In Iron Ore 2017. Perth, Western Australia, Jul 24, 2017. Perth, Western Australia: Australian Institute of Mining and Metallurgy (AusIMM).

Liquids vs. Solids

Bulk solids

- Internal friction
- Can form piles
- Sensitive to pressure
- Compressible

Liquids

- No internal friction
- Cannot form piles
- Not sensitive to pressure
- Incompressible

It's All About Flowability

Simplified way to compare the strength of two or more materials at a specific consolidation pressures.

- The ratio of the major consolidating stress ($\sigma 1$) to the unconfined yield strength (Fc) i.e. $FF=\sigma 1/Fc$.

Materials can generally be classified into 4 groups:

- FF < 2 very cohesive, non-flowing
- 2 < FF < 4 cohesive
- 4 < FF < 10 easy flowing
- 10 < FF free flowing

Note: Classifications DO NOT consider equipment (size or shape) or the flow pattern and serve only as a relative measure.

It's All About Flowability

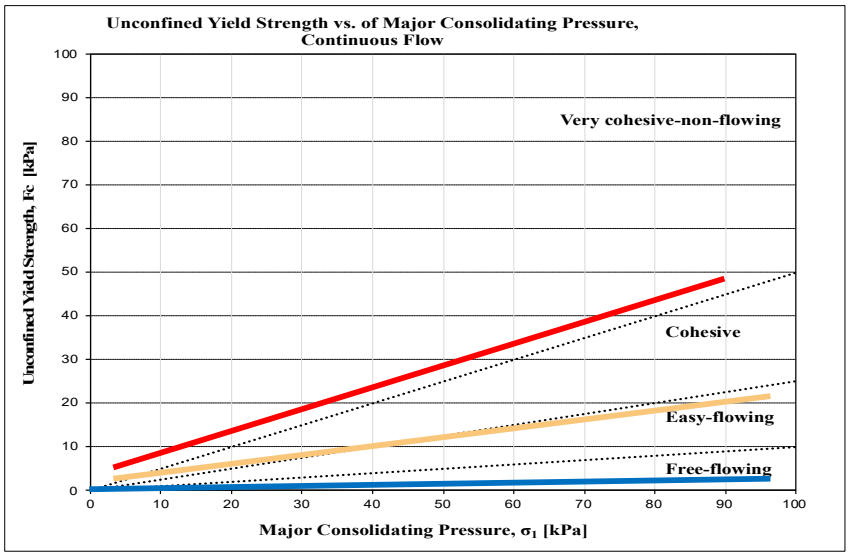

It's All About Flowability

- A function of… flow properties
  - Particle to particle friction,
  - Particle to wall surface friction
  - Compressibility (density) etc.
- Particle
  - shape
  - size & distribution
- Moisture
- Storage time (continuous or time at rest)
- Environment (Temperature, Relative humidity)

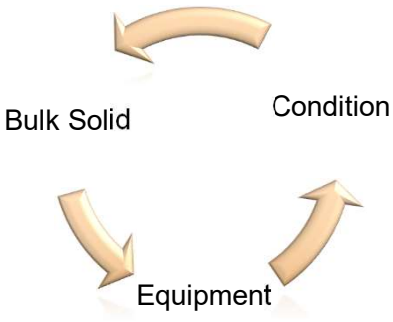

How to Achieve Reliable Flow?

Tests used to determine:

- Critical outlet size required to prevent bridging and ratholing
- Effective angle of internal friction (δ)
- Internal angle of friction (ϕ)
- Wall friction (ϕ') to ensure material will flow along the walls

How to Achieve Reliable Flow?

DIRECT SHEAR TESTER

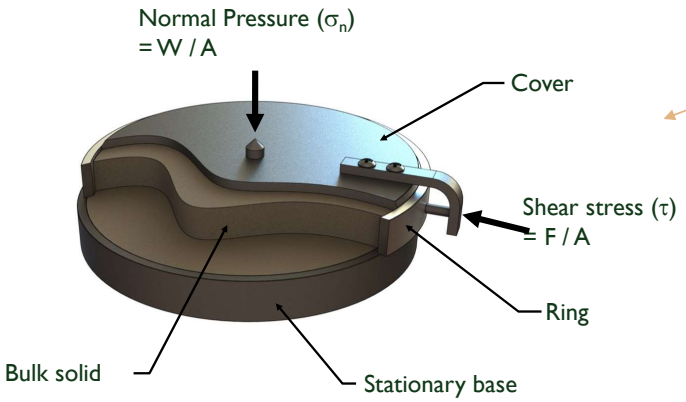

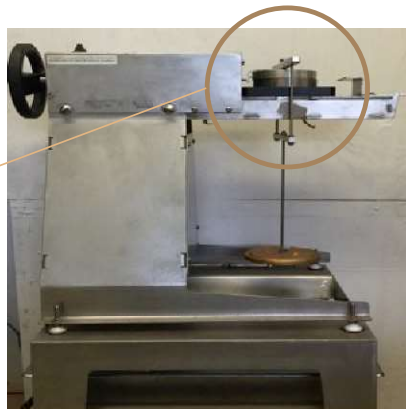

How to Achieve Reliable Flow?

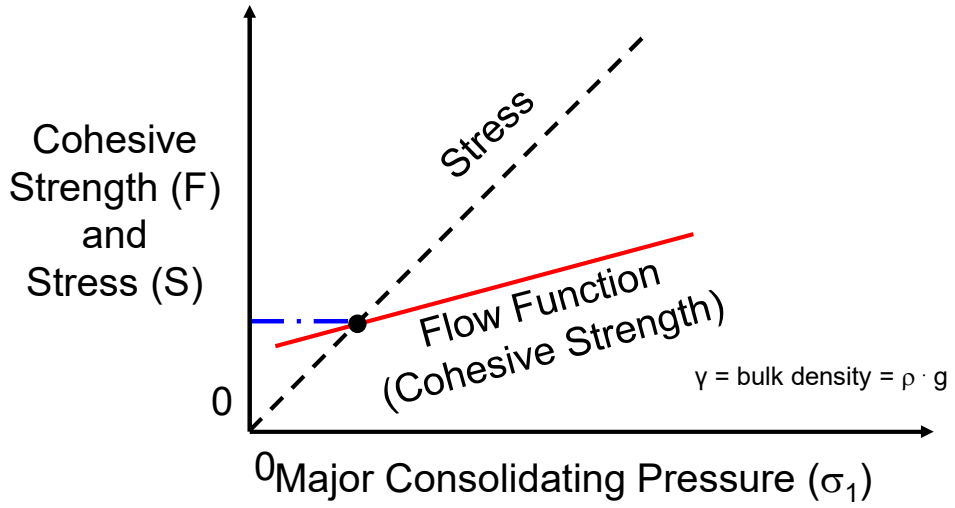

How to Achieve Reliable Flow?

Surfaces matter

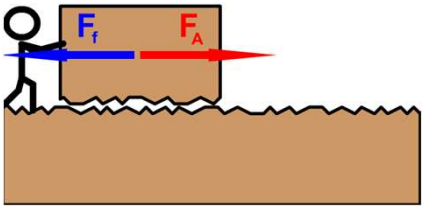

How to Achieve Reliable Flow?

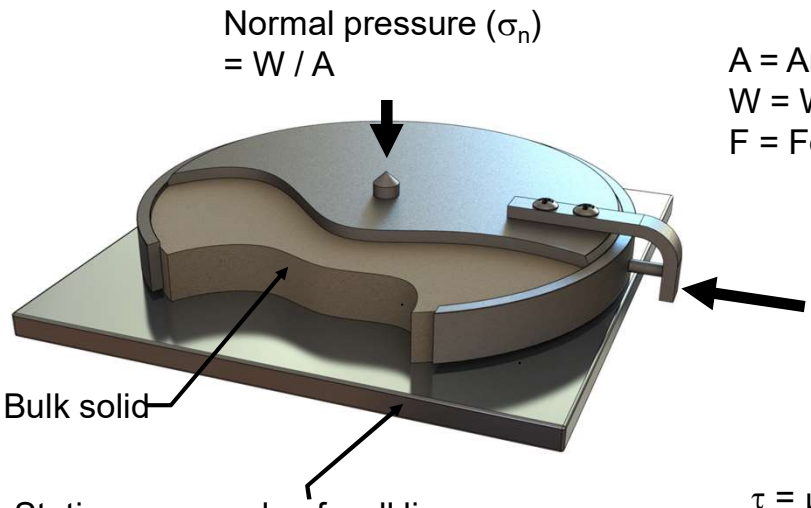

$\tau = \mu \bullet \sigma_n$

How to Achieve Reliable Flow?

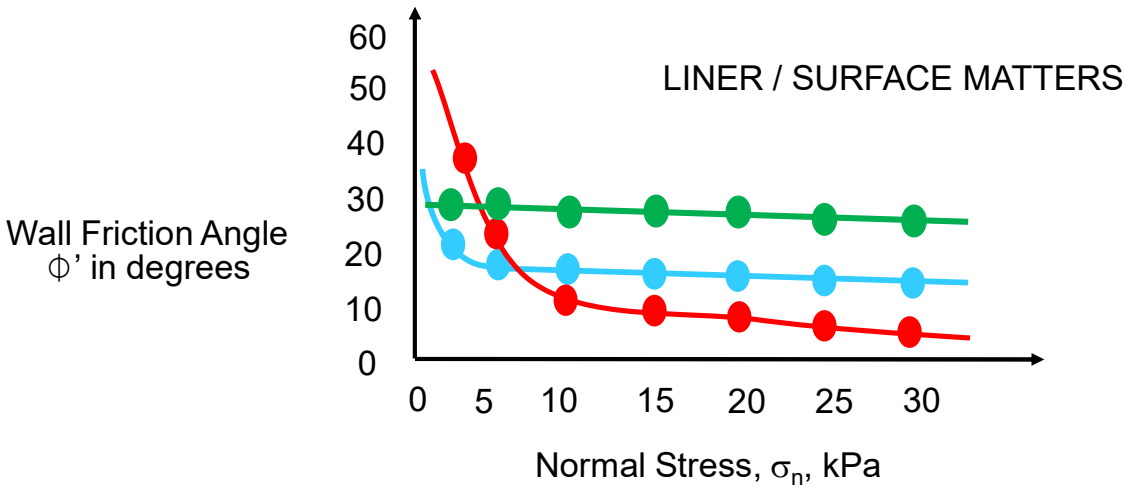

How to Achieve Reliable Flow?

- Test to measure relevant flow properties
- Determine appropriate flow pattern
- Use proven design methodology
- Leverage the science!

How to Achieve Reliable Flow?

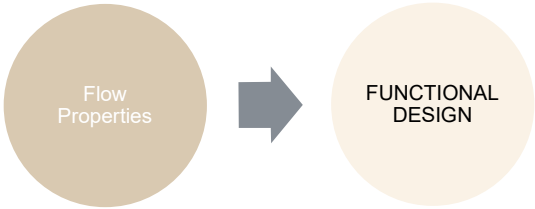

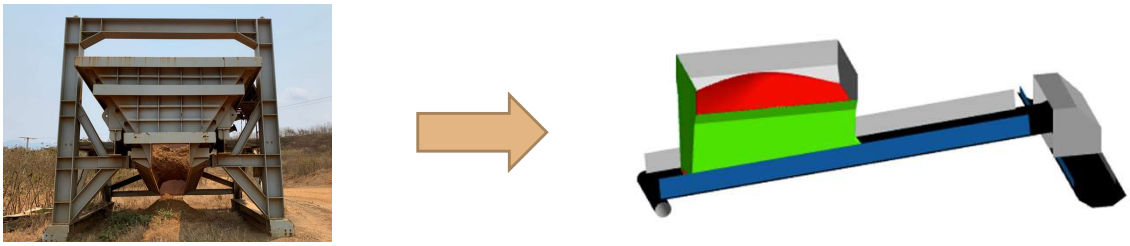

ICSG AND COPPER MARKET TRANSPARENCY: LESSONS LEARNED IN 2007-2022 AND CHALLENGES FOR 2023-2030

By

Carlos Risopatron

International Copper Study Group, Portugal

Presenter and Corresponding Author

Carlos Risopatron
risopatron@icsg.org

ABSTRACT

A review of selected ICSG activities focused on the improvement of global copper market transparency in 2007-2022 and challenges for the future is the main objective of this presentation. A review of commissioned ICSG research projects related to copper mine supply, demand and to use of recycled copper are compared with research of special interest for ICSG member countries in the period of analysis. We summarize key findings of selected ICSG research projects every year for the period of analysis and then we identify the main challenges to improve transparency in the global value chain in the future.

A review of global copper demand and copper end use trends in recent years is followed by a review of the reasons why capex in the copper mining industry has stagnated and it is not expected to grow in line with the optimistic long-term copper demand and copper end use perspectives of the green energy transition. Then we discuss the need to invest in a more accurate and updated assessment of the location of the global copper resources and by-products and in increasing the public information about the mineral composition of copper deposits including ore grades for copper and its main by-products. We assess the urgency to reallocate copper processing plants and develop new technologies to process base metals with increasing contents of hazardous wastes such as arsenic, mercury and cadmium to reduce pollution risks in the industrializing economies of Asia and in the value and transport chain from mining economies. Needs to develop alternative technologies to process more complex copper sulphide concentrates closer to copper mine sites are discussed versus the need to sustain increases in copper smelting capacity in Asia, using blending between complex and increasingly scarce clean concentrates.

Reallocation trends of the global value chains of many copper end use products closer to where the most affluent consumers live are also discussed. Then we discuss how the war in Ukraine sparked a global scramble for minerals resource security in 2022 emerging copper demand based on governments guaranteeing loans to traders and miners to develop new mine supply of strategic minerals and copper industry by-products. Then we discuss concerns in the copper industry that monetary policies such as higher interest rates might decrease capital expenditure to develop new copper mines and expansions of operational copper mines over 2023-2024, increasing the risk of potential shortages of global copper mine supply and global deficits of refined copper.

We assess the claims that the copper industry must be prepared for the future end use of copper in decarbonization, on expected higher standards of living of the most affluent population, and on more electrification of the population in developing economies and lower income countries in the next three decades. Then we discuss mineral industry consulting firms' forecasts about a potential need for around 10 million tonnes of new copper mine supply over the next decade, from projects that have yet to be approved by governments and financed. Finally, we review forecasts on mineral output capacity likely to come on stream in 2023 and 2024 and the potential of a copper mine capacity growth deceleration driven on by ESG-related and cost constraints.

Keywords: copper supply, demand, fabrication, mineral resource security, capex, mine capacity

Presentation Contents:
Copper Market Transparency: Lessons and Challenges

1. Copper Demand Trends and Global Scramble for Minerals Resource Security
2. Global Copper Mine Supply and Capacity Expansion: Complexities to 2028
3. Copper Smelters Capacity Trends and Complexity Challenges to 2028
4. Global Recycled Copper Raw Materials Trends: Potential Growth to 2028
5. Global Balances, Metal Exchange Pricing and Inventory Transparency
6. ICSG Data and Research Available in 2023

International Copper Study Group: Intergovernmental Organization

- Membership open to any country involved in copper production, use or trade.
- Headquarters in Lisbon, Portugal with Lead, Zinc and Nickel Study Groups: 3 Copper Analysts.
- Countries joining recently: Mongolia, DR Congo after Brazil and Iran joined the ICSG.
- 24 ICSG member governments plus the European Union in 2023: 39 countries in the 3 Groups.
- Australia is an active member country participating regularly in the ICSG meetings remotely or in person.

Australia
Belgium
Chile
China
Finland
European Union

France
Germany
India
Italy
Japan
Iran

Luxembourg
Mexico
Peru
Poland
Portugal
Russian Fed.
Serbia

Spain
Sweden
United States
Brazil
Mongolia
DR Congo

ICSG Share in the World Copper Market in 2023

Aggregated production and usage from ICSG member countries.

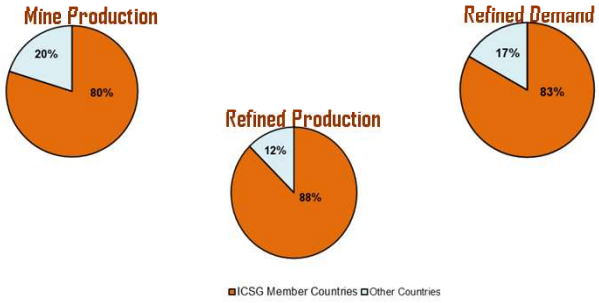

ICSG membership is open to any country producing or using copper

ICSG - MAIN OBJECTIVES AND FUNCTIONS

- To increase copper market transparency.
- To improve statistics on copper.

- To conduct consultations and exchanges of information
- on the international copper economy.

- To undertake studies on issues of interest to the Group.

- To consider special problems or difficulties that exist
- or may arise in the international copper economy.

ICSG provide its membership with information on capacities, production, usage, trade, stocks, prices, technologies, research and development, and other areas that may influence global supply, trade and demand for copper.

ICSG Secretariat Professional Staff: 2 Statisticians + 1 Economist

Slow start of the green energy transition in the use of refined or scrap copper in European Union +UK fabrication.

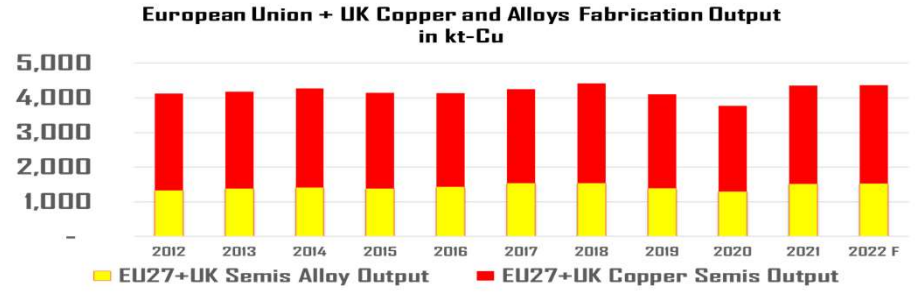

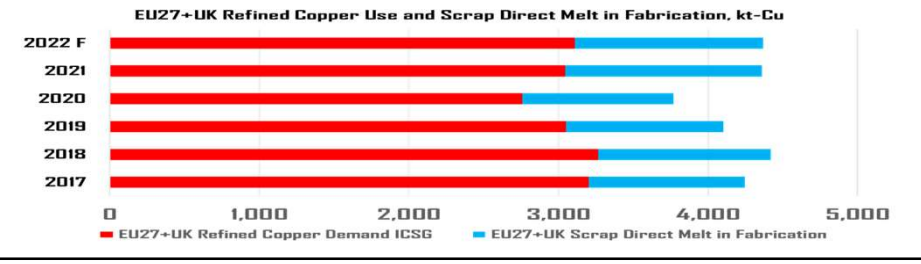

Japan, South Korea and Taiwan´s use of refined copper and copper scrap in fabrication: downtrend in the last 6 years.

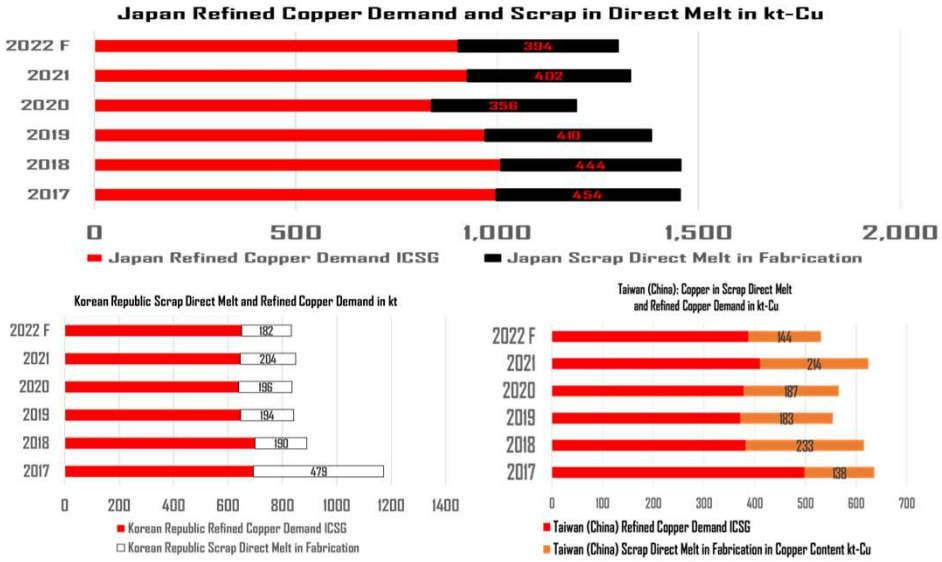

North American refined copper demand and scrap direct melt use stagnated <3.5 Mt-Cu for many years and down in 2019-2022.

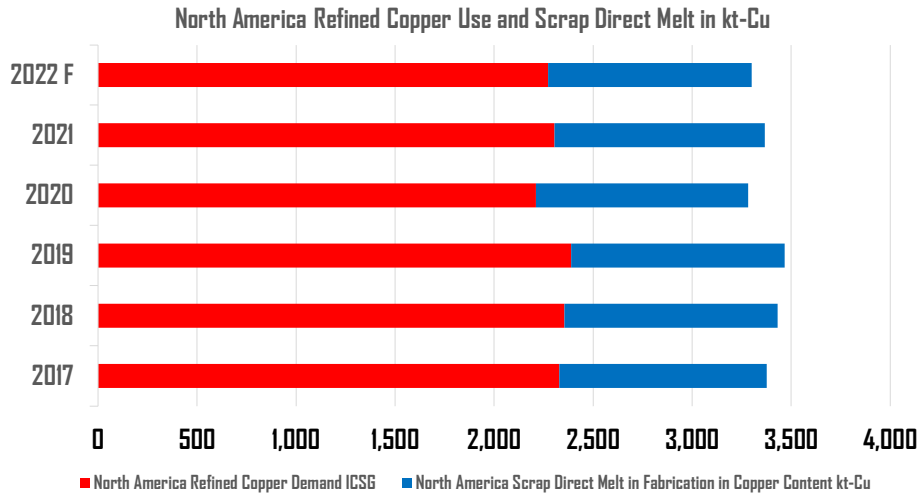

Strong growth in the industrial copper use in ASEAN, India, the Middle East and Africa.

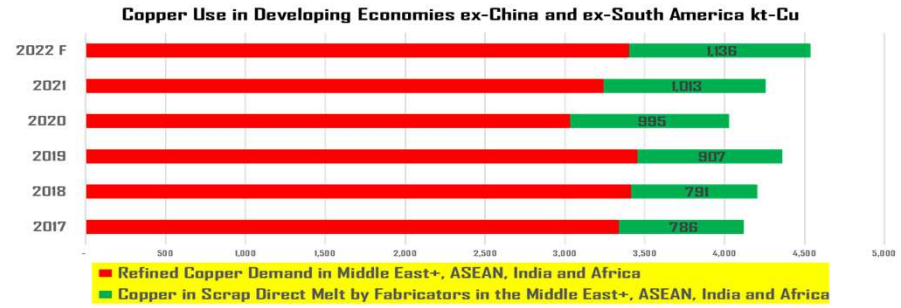

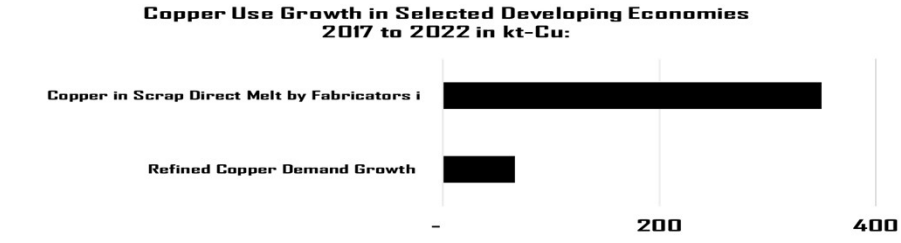

Increasing copper use in China in 2019-2021 and more expected in 2023 and 2024.

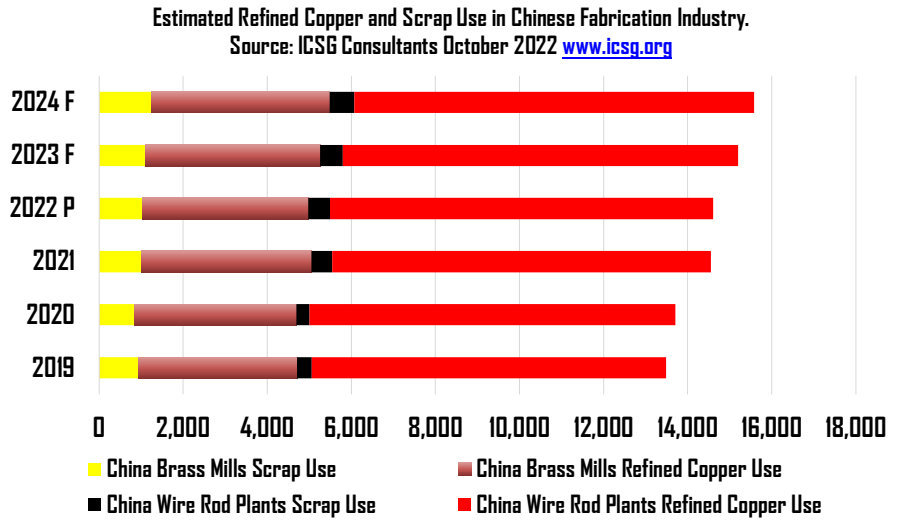

For a decade, China´s financial sector invested 40% to 50% of its annual GDP every year...

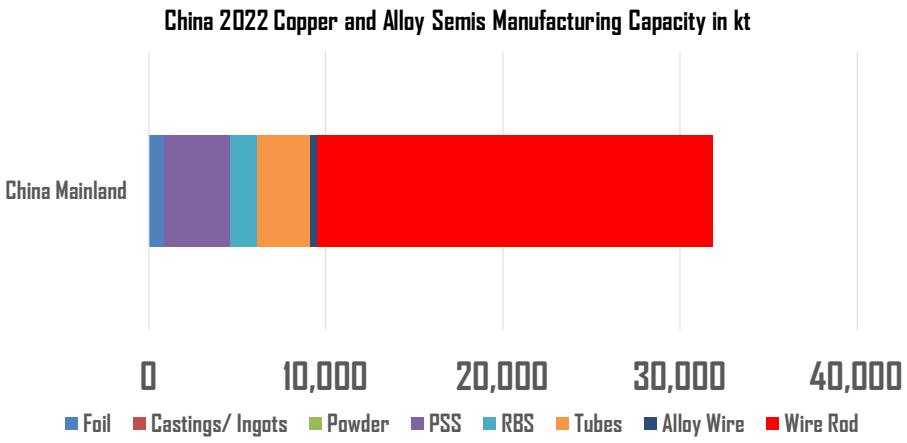

...as a consequence, China´s capacity to use refined copper and scrap became higher than the global use of copper in 2022.

The Chinese capacity to manufacture copper is highly concentrated in copper wire, foil and tube plants.

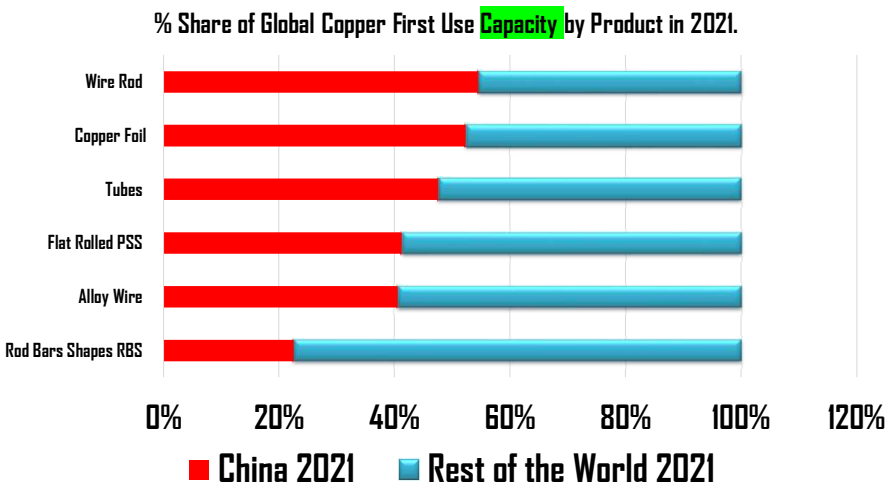

New fabrication capacity in the world ex-China: also growing and might add +2.7 Mt more in 2019-2024.

World ex China Fabrication Capacity 2019-2024 in kt, preliminary.
More projects identified in 2023 to be reported in 2024.

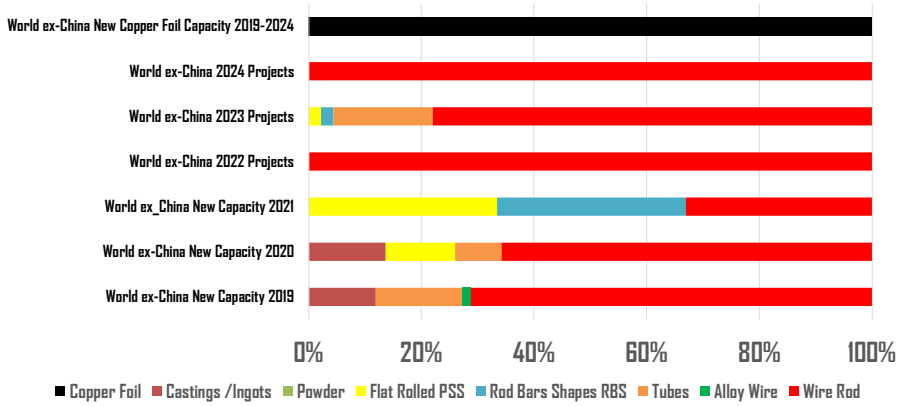

Discounting new copper foil plants using copper wire as an input.

The global capacity to use scrap and refined copper is growing faster than refineries, smelters and copper mine capacities.

2019-2021 Global Copper Value Chain Capacity Growth (in kt)

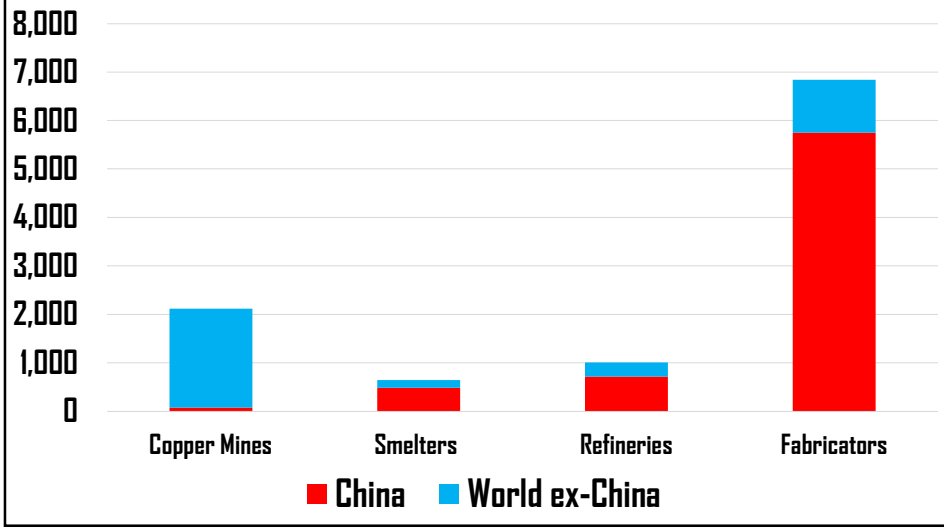

2022 New Global Copper Supply: 31.1 Mt-Cu

SX-EW Copper Mine Refined + Concentrate Refined = ~21.5 Mt-Cu

Scrap Refined + Scrap Direct Melt by Fabricators* = ~9.6 Mt-Cu in 2022

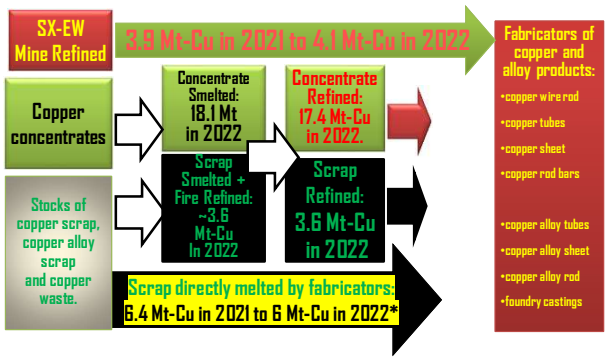

Lower global trade of scrap in 2022 and lower refined copper prices versus 2021.
Less copper in the scrap directly melted by fabricators in 2022*versus 2021.

Global industrial use of copper growing +500 kt-Cu every year.

Global copper fabrication output reported:~30.4 Mt-Cu in 2022.

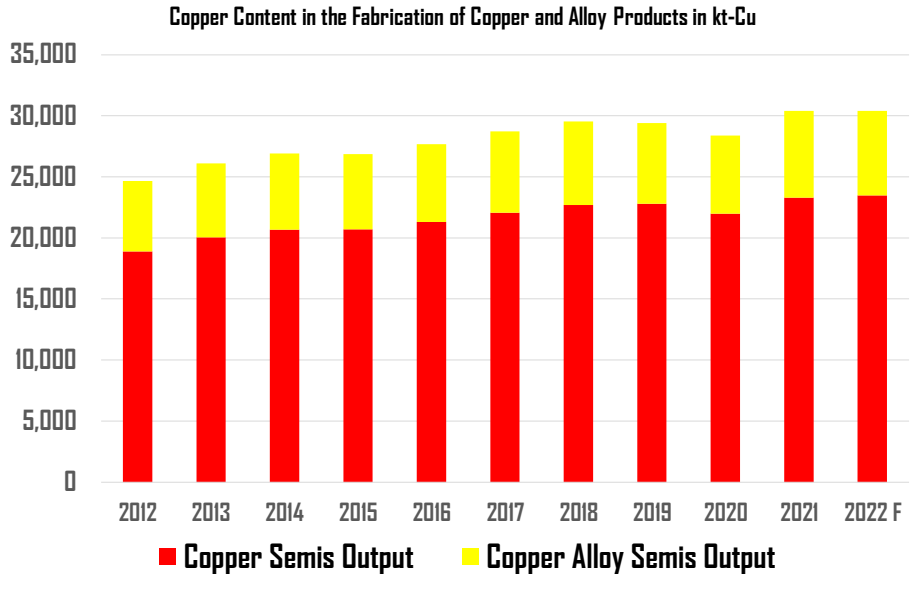

Record ICSG global demand for copper in 2022: 32.1 Mt-Cu

ICSG demand for copper grows more than the reported industrial uses:
difference explained by +refined copper stocks and under estimated uses.

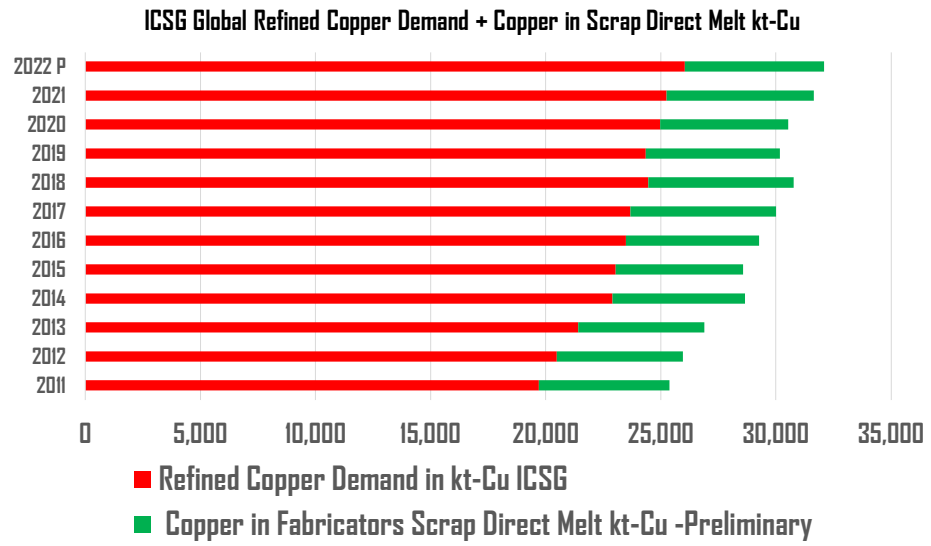

World copper end uses below ICSG reported copper demand too.

Industry underestimation of fabrication + increase of under-reported stocks.

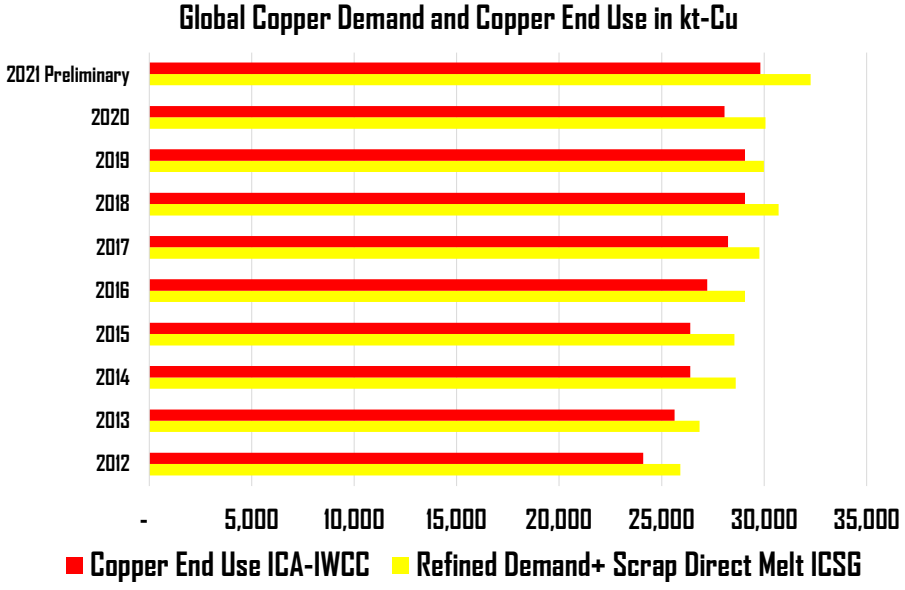

End uses of copper growing faster in power grids, consumer products, ammunition, electronics, air conditioners, building and automovile cables, versus other uses.

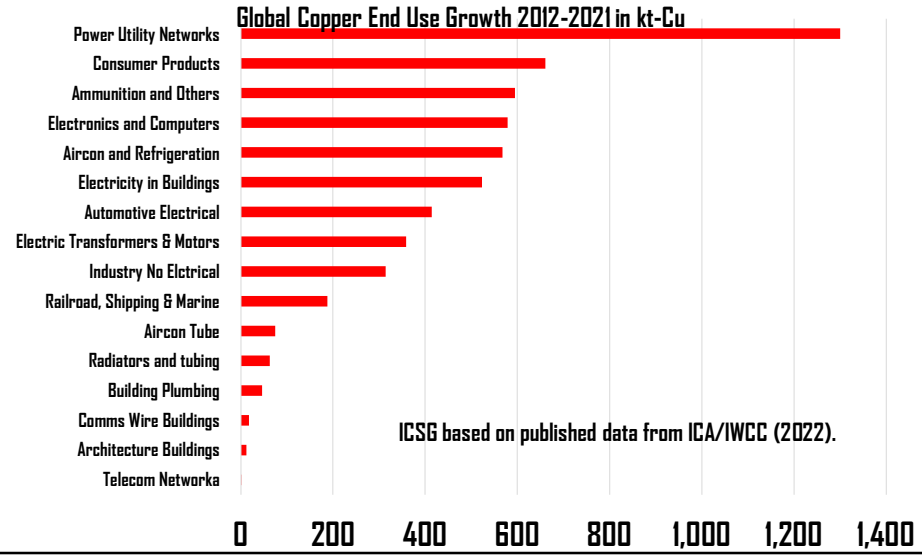

Three European companies, Nexans, NKT and Prysmian, control most of the European wire and cable market in 2023

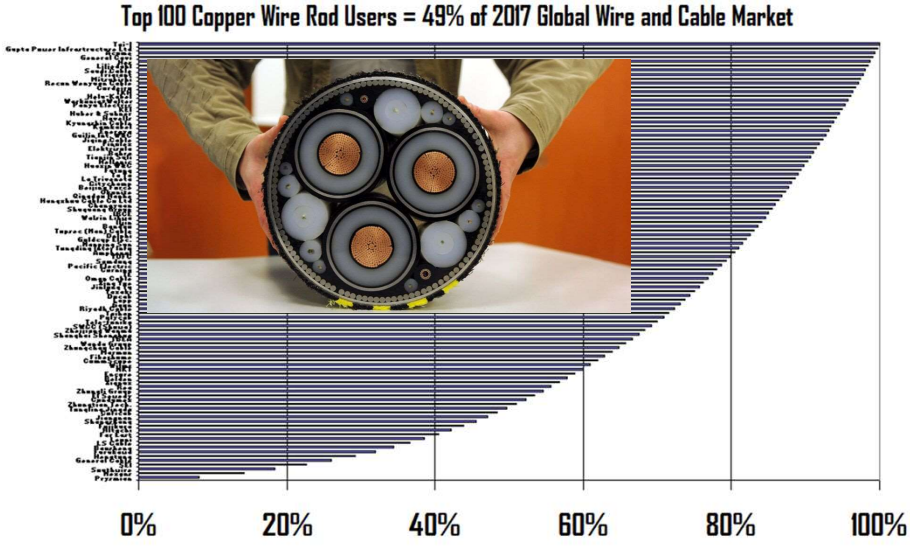

More refined copper exported from the Russian Federation to the European Union and to Turkiye in 2022.

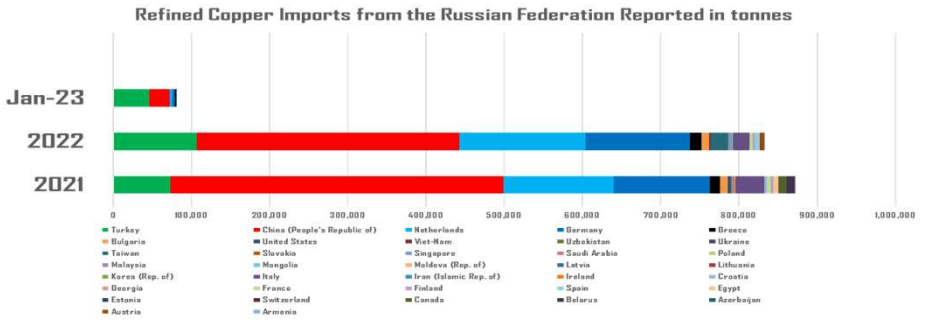

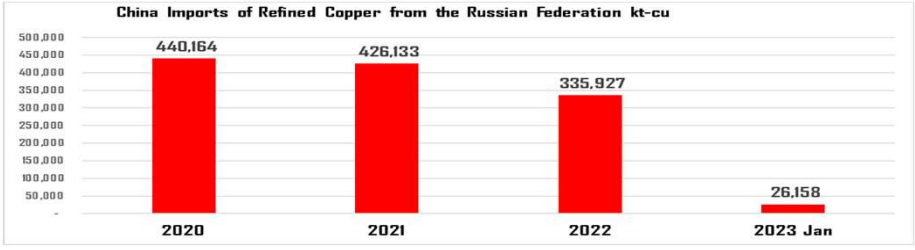

Demand for refined copper in the Russian Federation returned to historic levels in 2022.

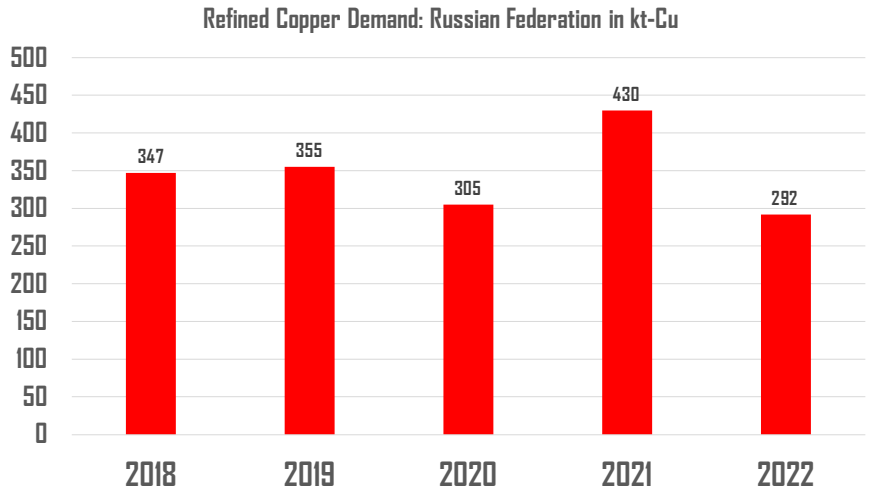

Increased global military spending in 2023 supporting physical copper demand against developed economies use slowdown.

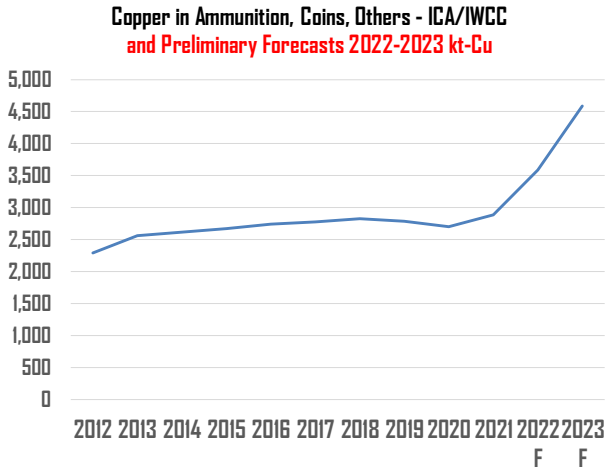

Industry associations report copper end use use in ammunition, coins and other copper end uses in 2012-2021

EU's Critical Raw Materials Act 2023: copper included as "strategic"

= more demand for strategic sectors and +hidden stocks.

Figure 2. Semi-quantitative representation of flows of raw materials to the fifteen technologies and five sectors

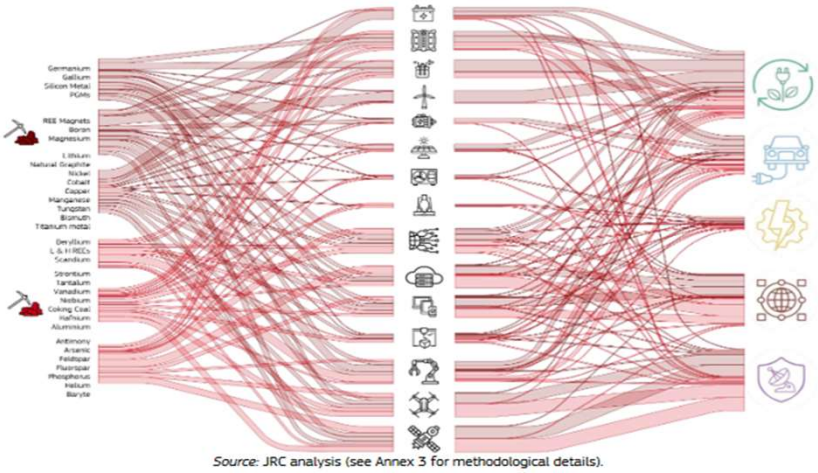

Source: JRC analysis (see Annex 3 for methodological details).

https://rmis.jrc.ec.europa.eu/uploads/CRMs_for_Strategic_Technologies_and_Sectors_in_the_EU_2023.pdf

New copper demand in 2023+ based on governments guaranteeing loans to buy copper "for resource security"

funding commodity trading companies on the way.

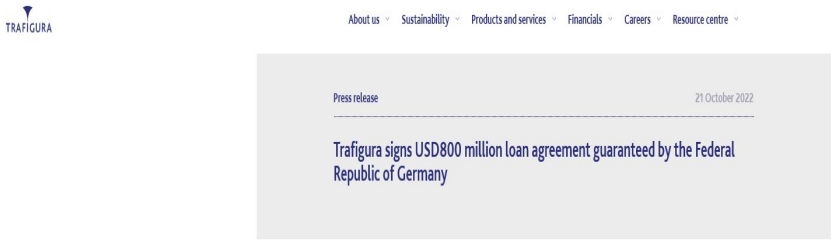

- *EU's Critical Raw Materials Act 2023: copper included as "strategic"*
- ***= more strategic demand from governments and +EU-27 stocks.***
- *In Germany 40% of new loans are guaranteed by the government ,*
- ***including a guarantee to buy 500 kt of refined copper.***
- *Commodity traders rely on bank credit to finance deals.*
- ***Companies are passing on costs or exiting from some trades.***

Climate ambitions: much more copper mine and scrap capacity needed. In the short term: inflation control, financial instability and more coal use.

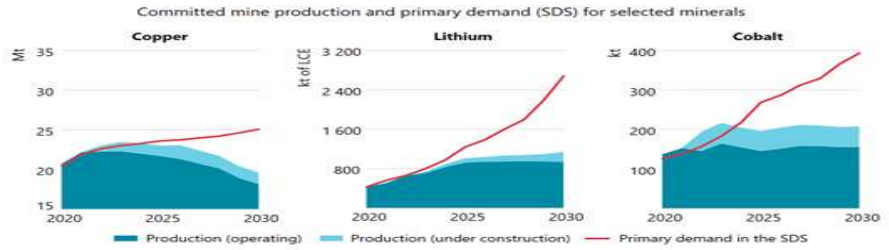

Natural decline is faster than energy transition

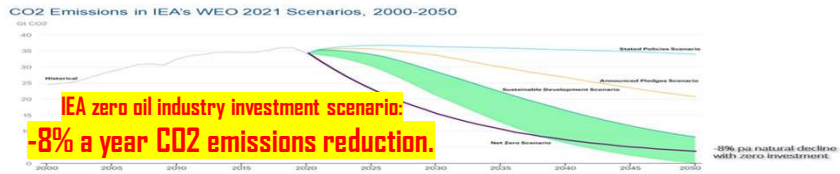

IEA zero oil industry investment scenario:
-8% a year CO2 emissions reduction.

Under no realistic scenario will copper supply capacity be added fast enough to offset the decline of oil production with zero investment.

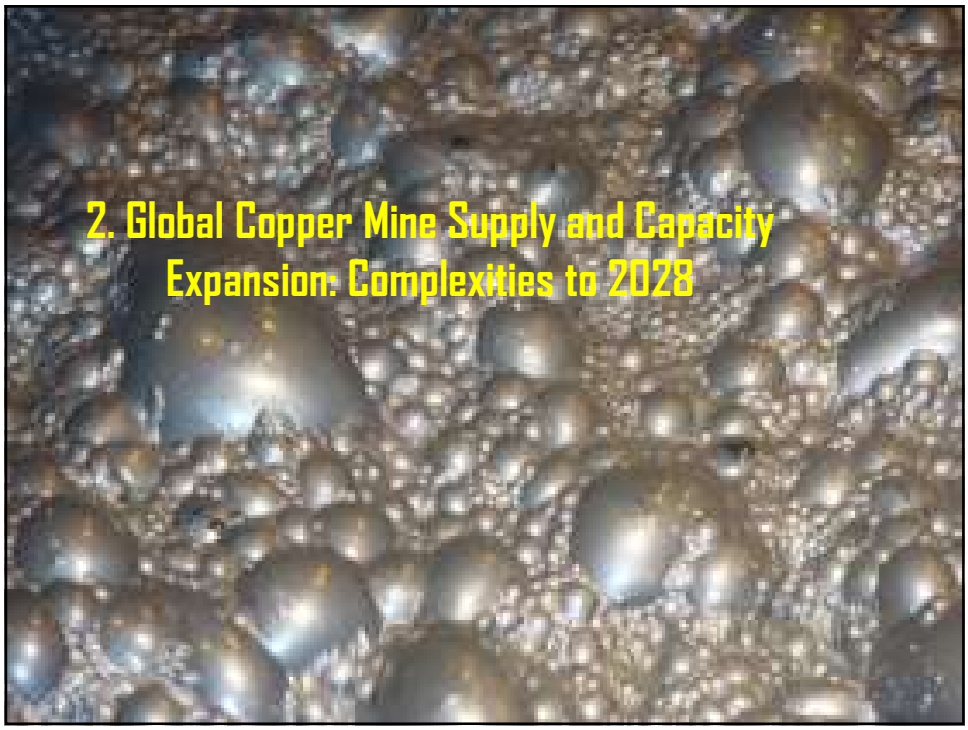

2. Global Copper Mine Supply and Capacity Expansion: Complexities to 2028

Copper miners: always optimistic about future concentrate and SX-EW capacity.

But the average global output growth trend is more conservative.

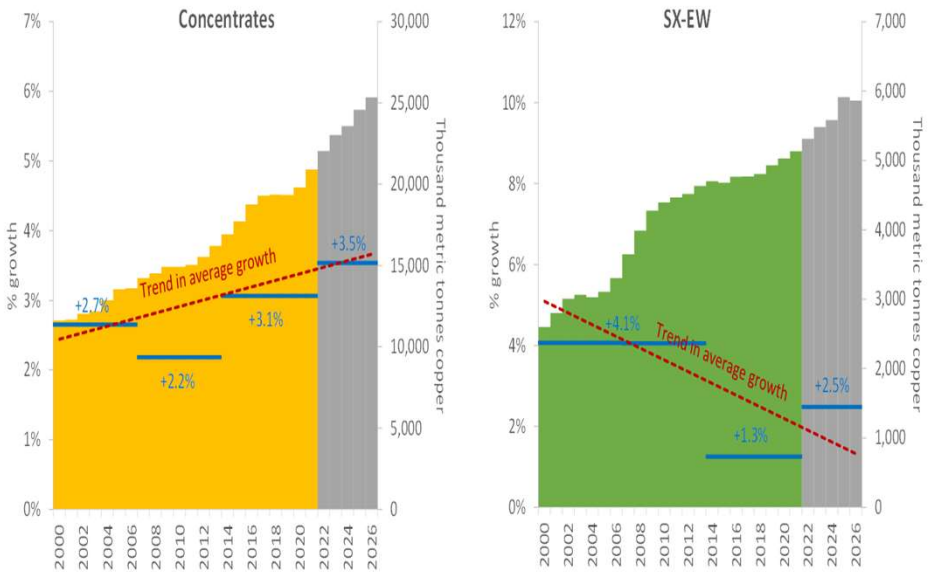

Global output of copper concentrates up +5 Mt-Cu in 2010-2017,

but in 2018-2020 no much global copper concentrate output growth

Global copper mine production up in 2022 to record 21.8 Mt-Cu: +700 kt-Cu.

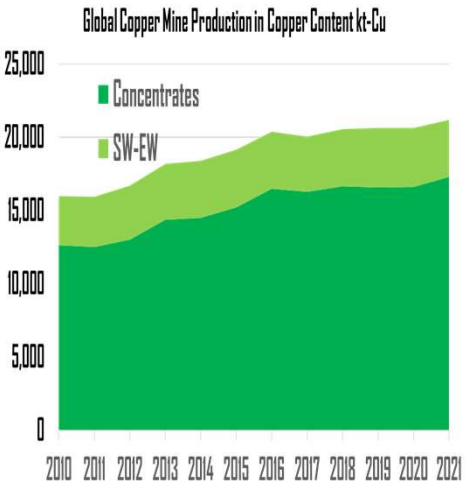

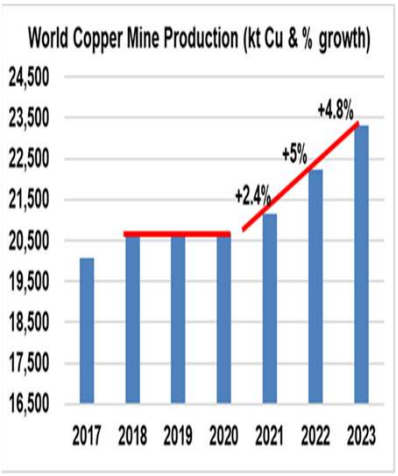

Record 2022 global output of copper concentrates: >17.7 Mt-Cu per year.

SX-EW global copper mine refined output 4.1 Mt-Cu

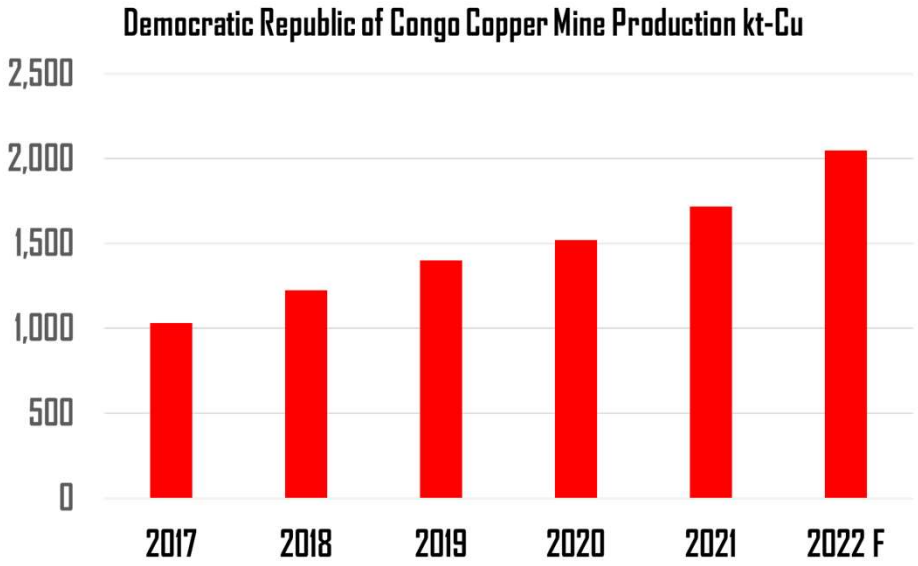

If global concentrate and scrap supply and quality stop growing,
the copper smelter capacity boom would have been unsustainable.

New copper mine capacity became operational in 2021-2023.

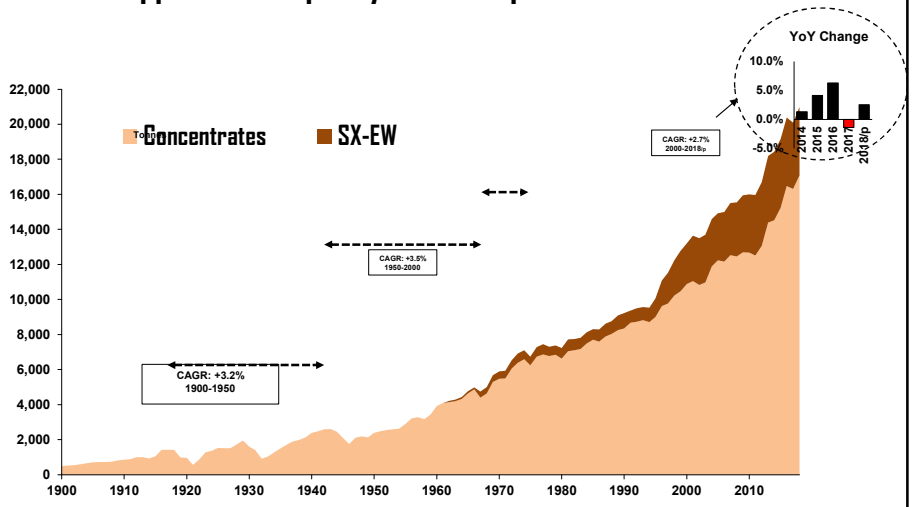

Strong interest from India and ASEAN countries
to secure copper concentrates from South America in 2023-2025

After no commissioning of major new copper mines in 2017-2020
major new copper mine projects and expansions started in 2021-2023.
Only six new projects in 2023-2025. The rest for 2027 and beyond.

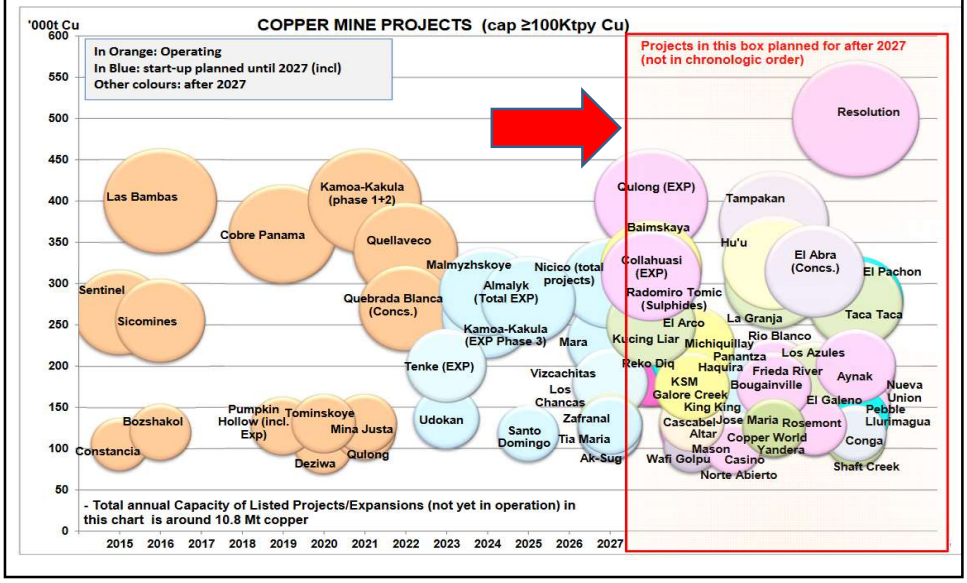

Strong global miners CAPEX recovery: +12% in 2023.
Will future new mine capacity be affected by higher capital costs and less commercial banks credit?

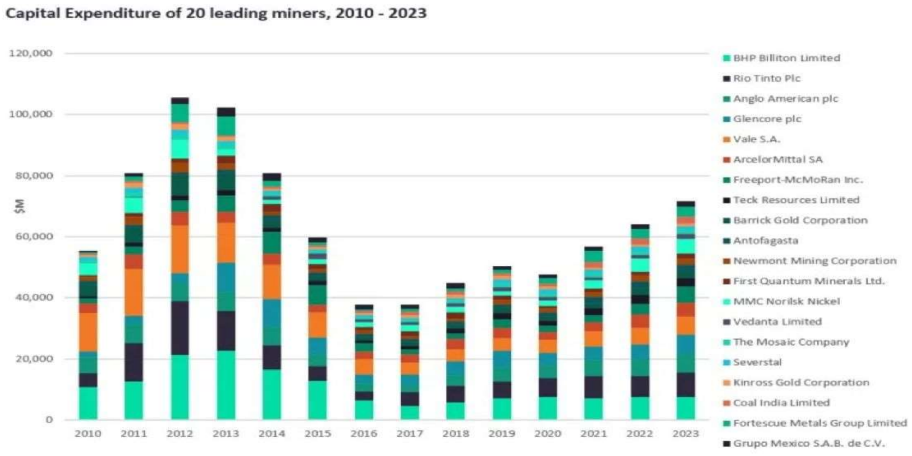

Source: GlobalData, company reports & announcements.
Note: Figures for BHP and Fortescue are for FY end 30 June, and Vedanta and Coal India for FY end 31 March

Mineral resources are not a restriction to produce more copper for the new copper smelters, refineries and fabricators.

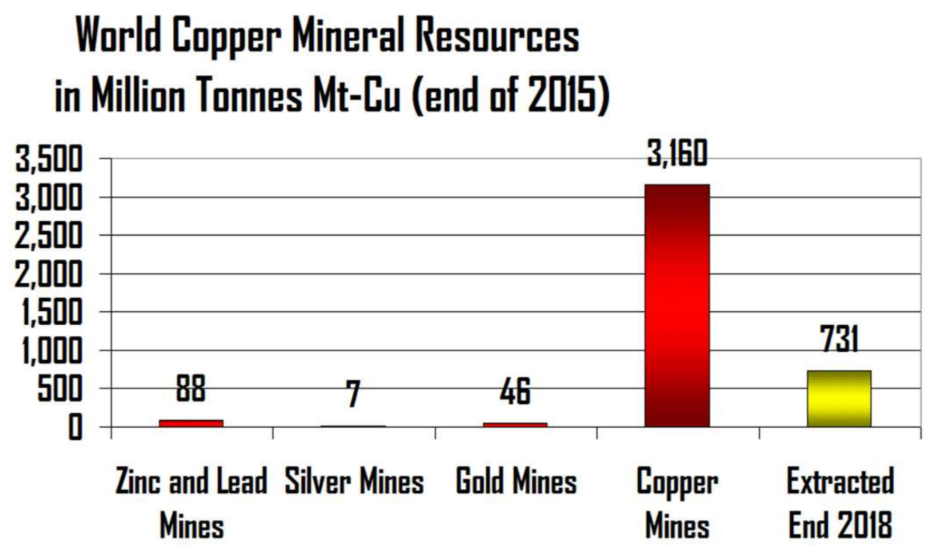

However, copper resources in mineral deposits with high copper content are very limited.

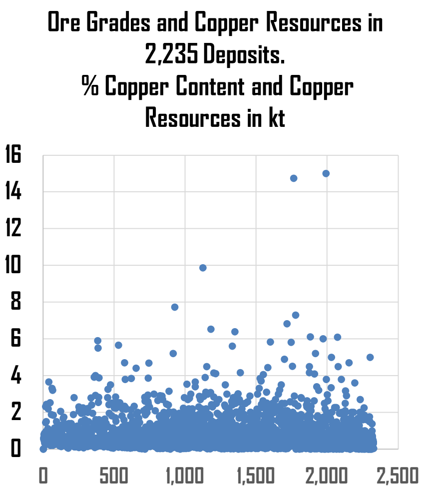

Copper Deposits With Reported Copper Content Over 3% Copper

Mine	Country	Copper Resources Mt-Cu	Copper Content %
Phu Taxan (Phuda)	Laos	0.0	15
Home of Bullion	Australia	0.0	14.7
Valentorskoe	Russia	0.1	9.87
Solwara 1	Papua New Guinea	0.2	7.7
Solwara 12	Papua New Guinea	0.0	7.3
Al Hajar	Saudi Arabia	0.0	6.8
Dikulushi	Congo-DRC	0.1	6.5
Ishkinino	Russia	0.1	6.4
Kiivenjoki	Finland	0.0	6.11
Caledonia (Cascade)	Canada	0.0	6.1
Flamingo Group	Australia	0.0	6.0
Hofrat-en-Nasah	South Sudan	1.2	5.9
Caribou Dome (Denali)	USA	0.0	5.84
North Kaluga	Russia	0.0	5.81
Cobar-CSA	Australia	0.7	5.65
Alaverdi (Alaverdi)	Armenia	0.1	5.6
Miniere de Musoshi et Kinsenda SARL	Congo-DRC	1.2	5.5
Explorer 142	Australia	0.0	5.21
Cerattepe (Kafkasor)	Turkey	0.2	5.2
Sabababianca	Colombia	0.0	5
Peak	Canada	0.0	5
Avaroa	Bolivia	0.0	4.9
Doolgunna-DeGrussa-Conductor	Australia	0.6	4.7
Fault Creek	Canada	0.0	4.7
Osennee	Russia	0.3	4.69
Madan Bvira	Peru	0.0	4.51
Rubtzovskoe	Russia	0.1	4.5
Khusib Springs	Namibia	0.0	4.5
Toad River	Canada	0.0	4.5
Yulalinskoe	Russia	0.0	4.44
Alexandrinka	Russia	0.4	4.4
Hudson Bay-Reed	Canada	0.1	4.17
Mount Pleasant	Australia	0.0	4.16
Bytom Odrzański	Poland	0.1	4.14
Chibuluma South	Zambia	0.1	4.1
Buttle Lake-Trumpeter	Canada	0.0	4.1
La Plata	Ecuador	0.0	4.06
Omar	USA	1.3	4
Redstone-Coates Lake (Yukon)	Canada	1.3	3.92
Talganskoe	Russia	0.1	3.9
Ambler	USA	1.1	3.88
Artana	Georgia	0.4	3.87
Kaluginskoe	Russia	0.0	3.86
Bushman Group	Botswana	0.5	3.85
Mavrovouni	Cyprus	0.6	3.8
Magail South	Oman	0.0	3.8
Kundalyan	Afghanistan	0.0	3.8
Karma	Albania	0.0	3.71
Kamoto Group	Congo-DRC	14.9	3.67
Honggou	China	0.1	3.66
Red Bore	Australia	0.0	3.6
Shamlugh	Armenia	0.2	3.54
El Roble	Colombia	0.1	3.51
Zeskho	Georgia	0.8	3.5
Poderosa	Spain	0.0	3.5
Turner-Albright	USA	0.1	3.4
June Creek	Canada	0.0	3.4
Copper Road (East/West)	Canada	0.0	3.35
Lubambe-Lubambe Extension	Zambia	9.6	3.32
West Ansil	Canada	0.0	3.31
Upper Kobuk-Arctic	USA	0.9	3.26
Kastere	Turkey	0.0	3.23
Kakula	Congo-DRC	9.4	3.21
Snow Lake-Lon	Canada	0.0	3.2
Başköy	Turkey	0.0	3.18
Dzhusinskoe	Russia	0.2	3.16
Kavundi Central	Congo-DRC	0.1	3.1
Chillagoe-Griffiths Hill	Australia	0.0	3.1
Boise	Australia	0.1	3.09
Corner Bay	Canada	0.1	3.01
Salgadinho	Portugal	0.3	3
Xiaorequanzi	China	0.2	3
Balta Tau	Russia	0.1	3
Ortaklar	Turkey	0.1	3
San Miguel	Spain	0.0	3
Bunmahon	Ireland	0.0	3.0

Most of the copper resources available worldwide are in deposits not fully operational or with no significant CAPEX growth expected in 2023-2025.

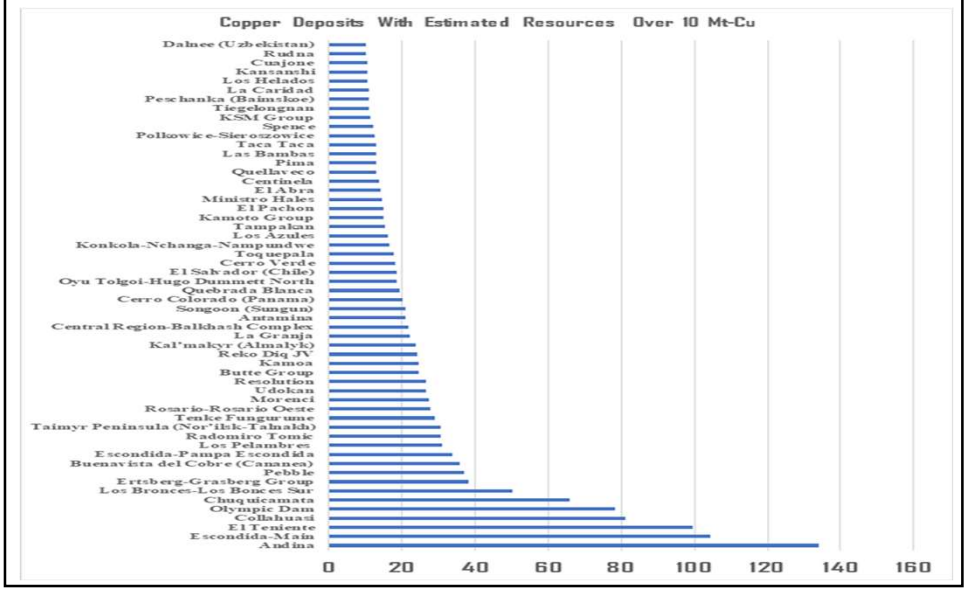

Copper miners are using more electricity and fossil fuels and money, to produce similar volumes of copper.

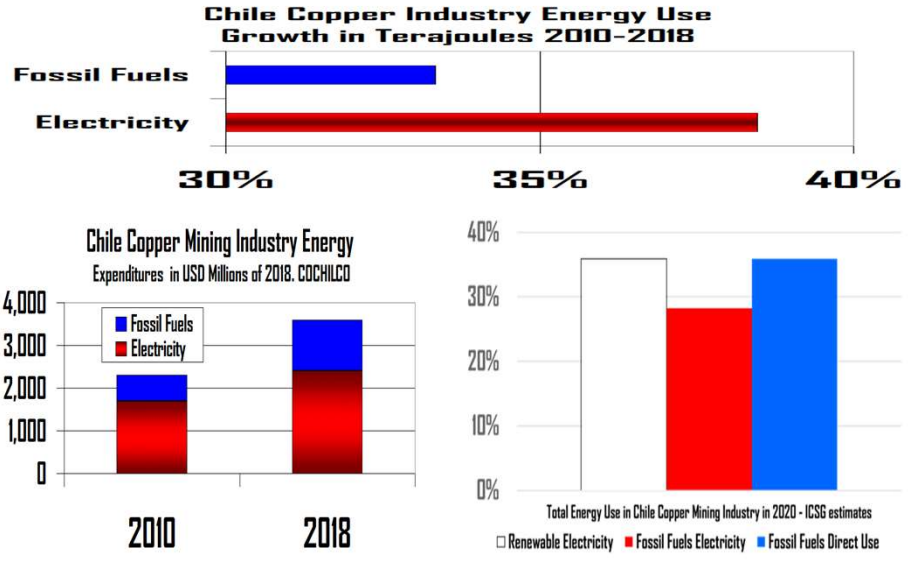

Reduction in copper ore grades challenge present and future mine supply due to cost inflation +energy costs to extract low-grade and complex ores.

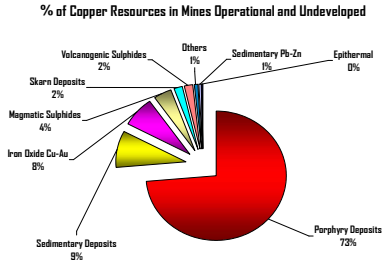

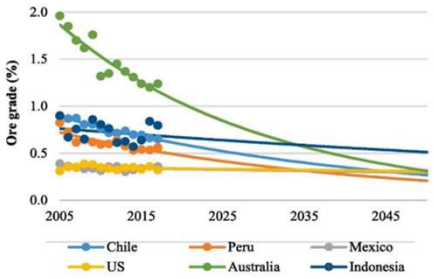

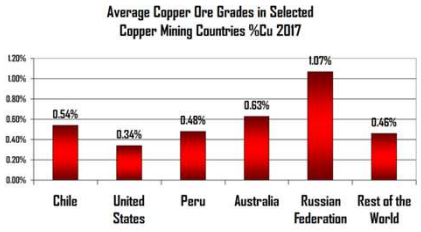

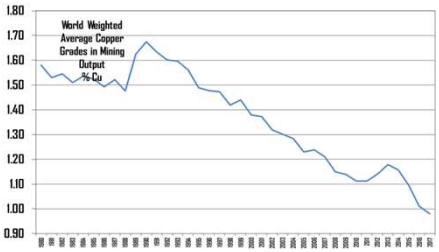

Mines developing and in study are more complex, deeper and lower grades. Upward pressure on energy and water costs observed in 2015-2022.

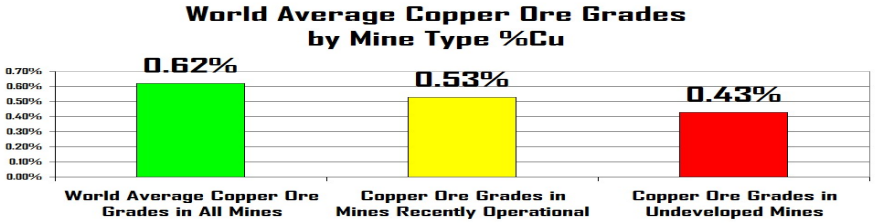

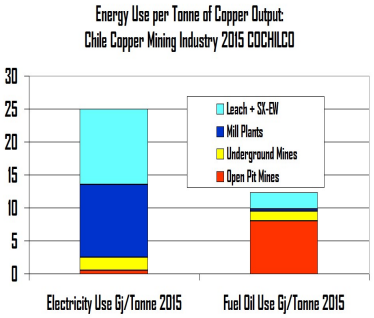

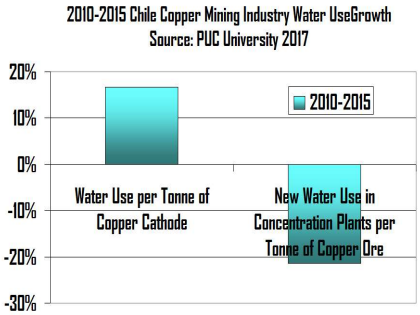

"Green energy" driven supply of refined copper is a difficult challenge for the industry due to high fossil fuels in power generation.

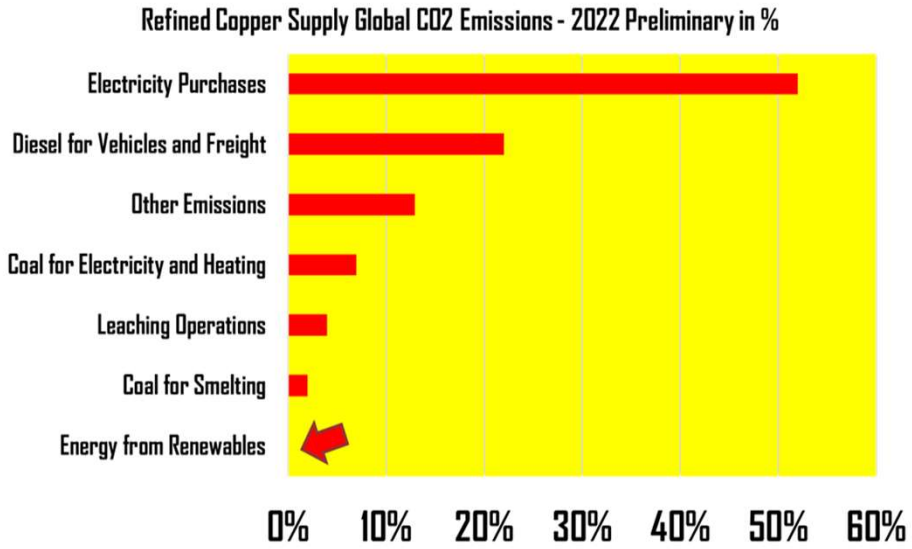

In some large copper mines, more copper output expected in coming years.

However in older copper deposits, depletion observed with output falling below historic averages.

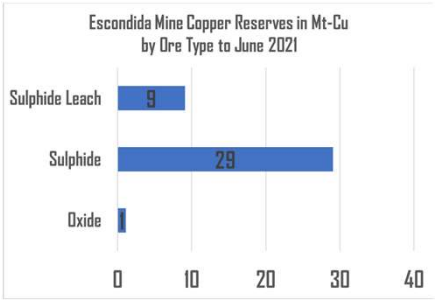

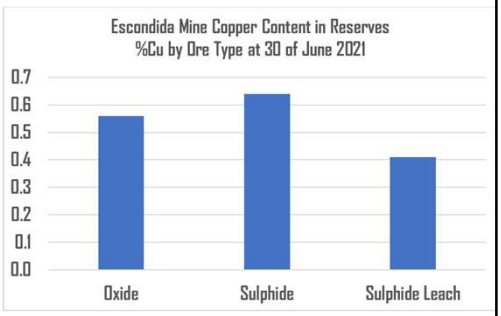

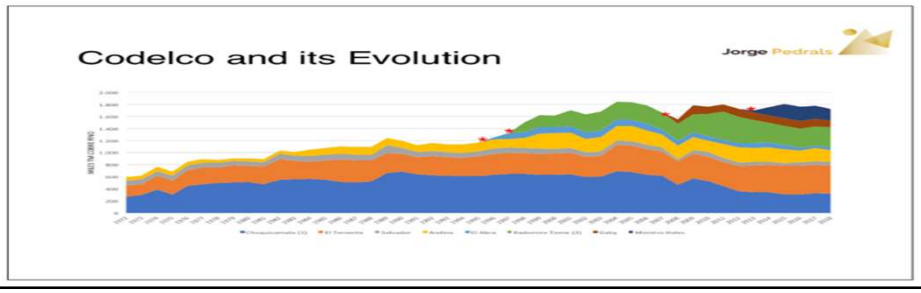

Most of copper reserves are in deposits with relatively low copper ore grades.

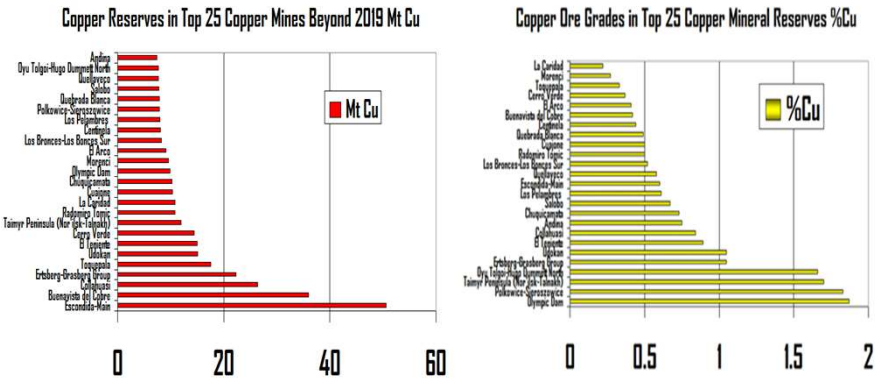

Mineral reserves in deposits with higher copper ore grades might be less expensive to develop.

In gross weight, most of the global trade of copper concentrates is between 2 main exporters and a small group a big importers.

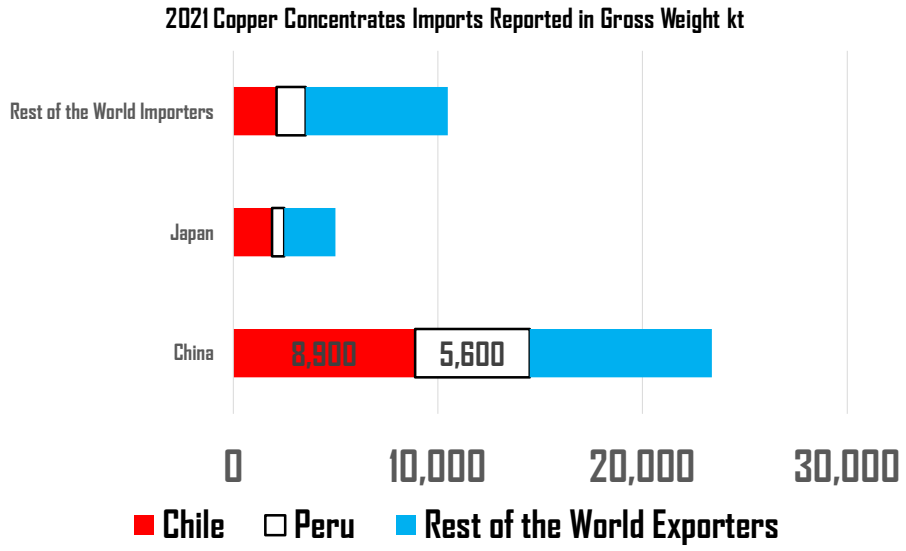

In 2015 the global weighted average of copper concentrate output, based on ICSG reported data fell to 25.6 % Cu

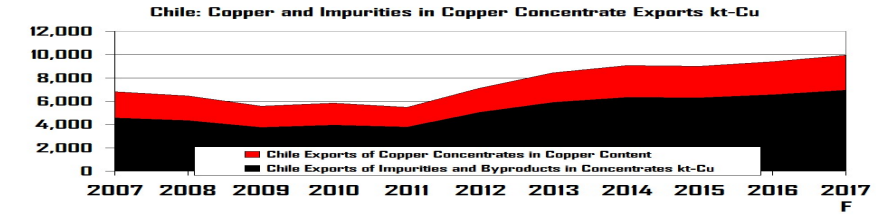

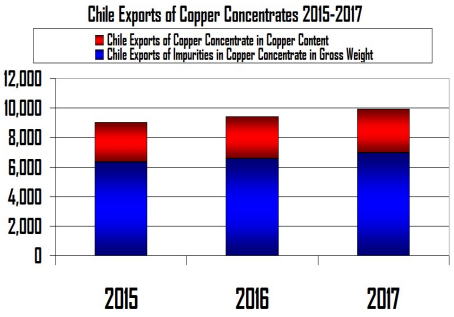

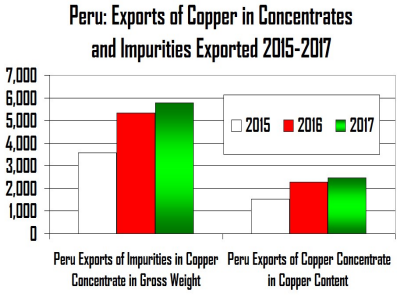

In 2016-2021 the copper content in reported global exports of copper concentrates remained stagnated around 10 Mt-Cu

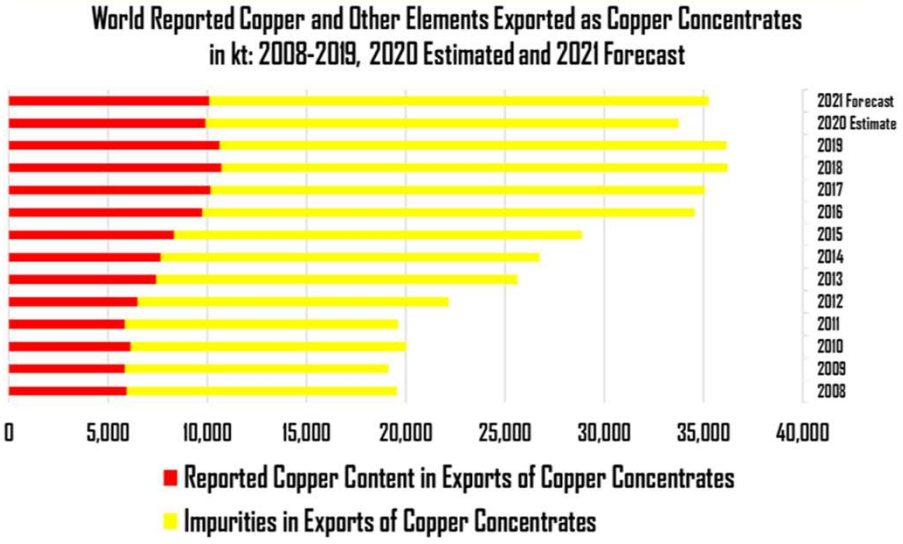

Increasing volumes of imported copper concentrates into China, but imports of copper in concentrates stagnated along 2019-2021

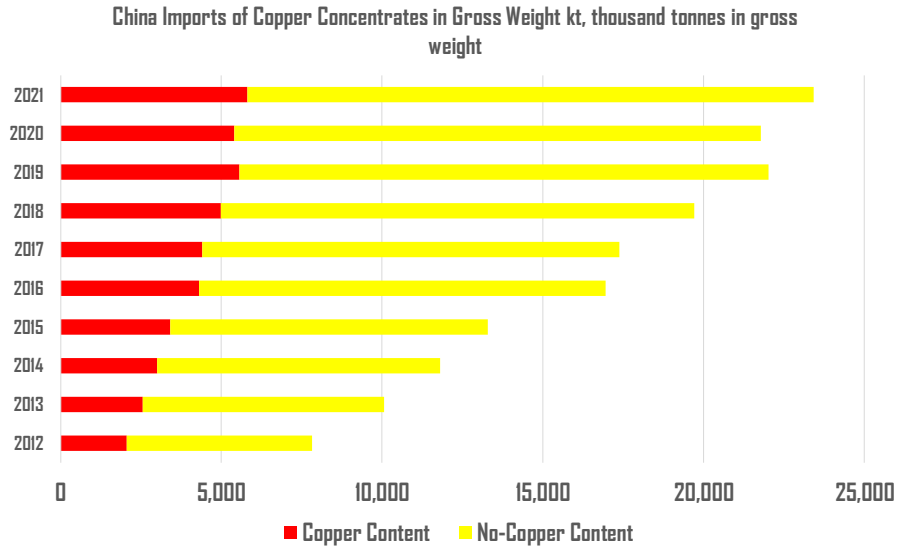

In recent years, falling ore grades reduced copper contents of the top importer of copper concentrates below 25% Cu.

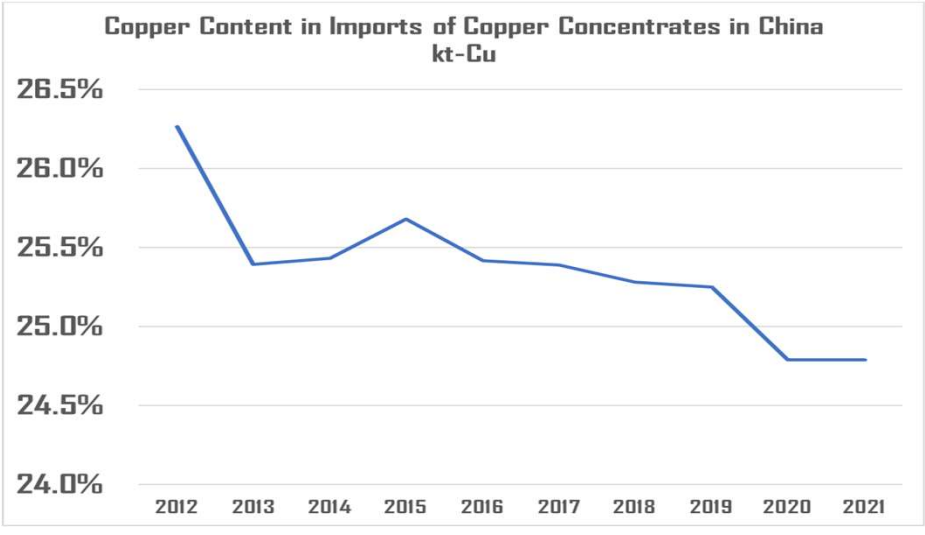

Global average arsenic content in concentrate reported ~50% of the limit accepted to import copper concentrates to China.

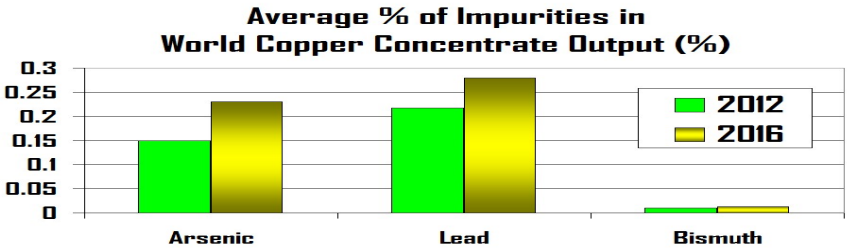

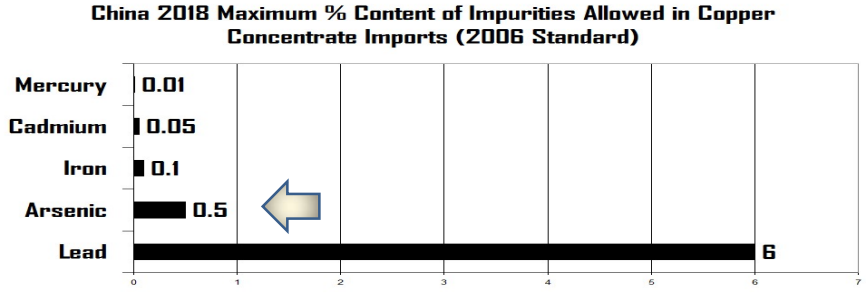

Most of the copper concentrates available in the global market containing <0.3% Arsenic, are still called "clean concentrates".

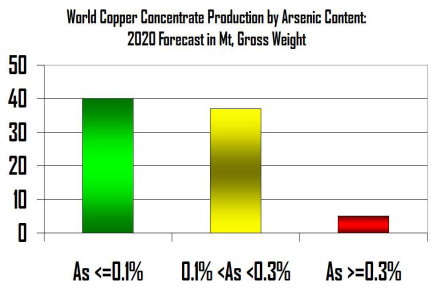

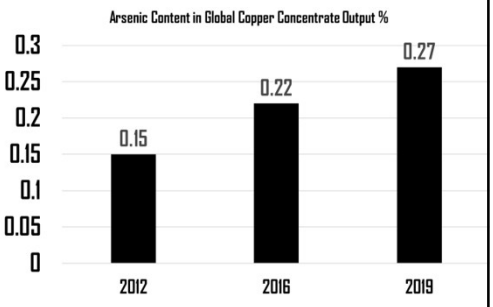

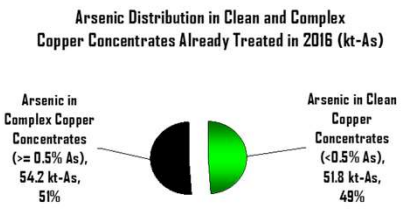

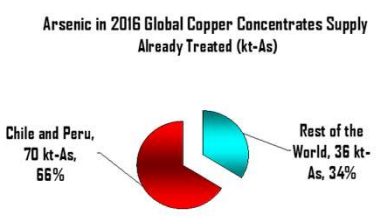

Important volumes of valuable and hazardous metals reported in global exports of copper concentrates traded internationally in recent years.

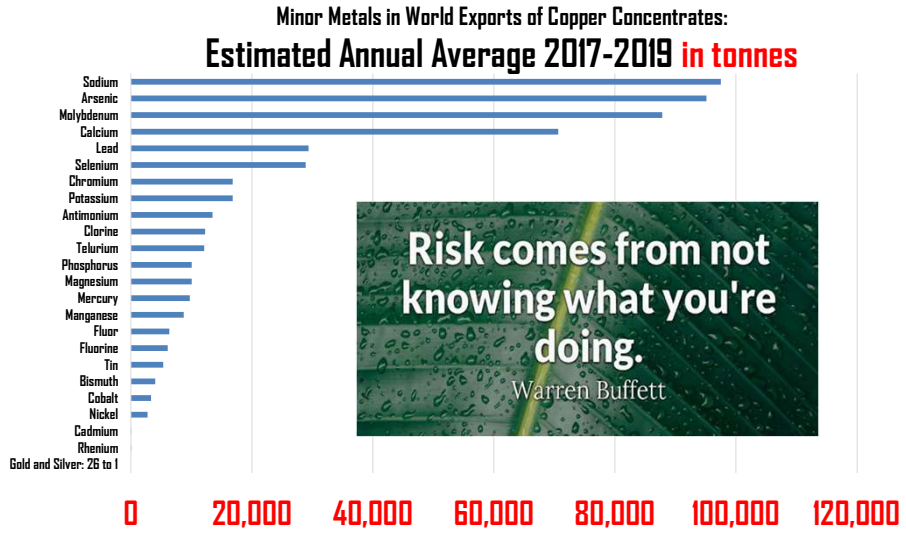

Mineral composition of Chile exports of copper concentrates changing fast.

But no one knows in detail how the composition is changing.

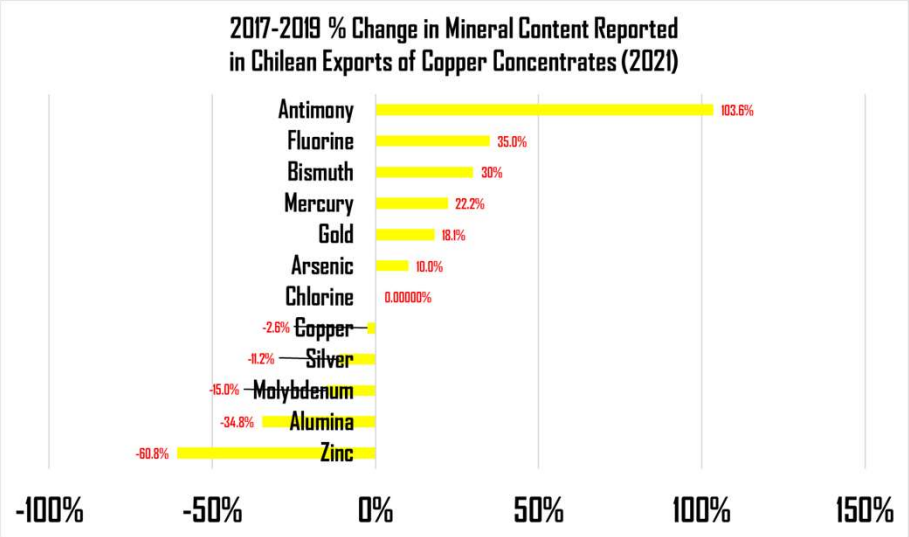

Chile publish only 39% of the mineral composition and is the country with more public information of changes in the mineral composition in exports.

Mineral composition changes in the rest of the world remain publicly unknown.

Chile: Mineral Content Reported in Copper Concentrates Exports Reported to Customs. % Weighted Average 2017-2019.

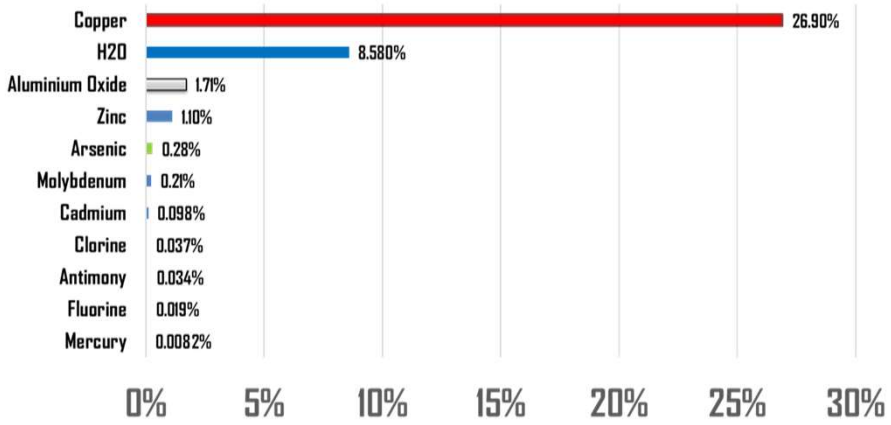

Permits to process complex concentrates and new blending plants in China keep arsenic flowing to Chinese smelters and hazardous waste disposal places in China.

New Limits Proposed in 2019 to Imports of Copper Concentrates to China (% Versus Existing Limits)

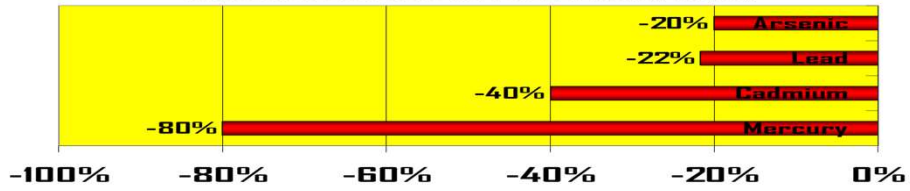

Arsenic Volumes in Global Copper Concentrates Output (kt) by Arsenic Content (% As) Source: ICSG on Aurubis estimates (2018)

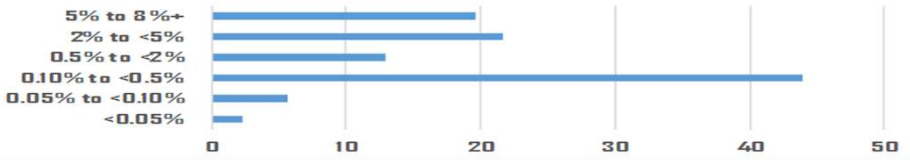

Half of copper concentrate output complies with China´s Arsenic limits.

If the limit was tightened, blenders might not source enough "clean" concentrate.

Instead of reallocating copper smelters closer to copper mines, more blending plants in and ex China are increasing shipments of complex concentrates.

Global Copper Concentrates Blending Facilities Before 2021

thousand tonnes per kea t kt

Country	Port/City	Blending Capacity	Copper Content
Peru	Callao	1150	299
Mexico	Manzanillo	600	156
Chile	Antofagasta+Copiapo	600	156
Spain	Huelva	550	143
Taiw an China	Qw angyang	500	130
Malay sia	Port Klang	400	104
Georgia	Poti	400	104
Bulgaria	Varna	120	31
Emirates	Sahar	100	26
Netherlands	Moerdiskj	50	13
China	Daye+Sangmengxia+FanCHenDang	2500	650
China	Ningde	1000	260
China	Taichung	500	130
China	Shandong	300	78
China Before 2021		4,300	1,118
Rest of the World 2021		4,470	1,162

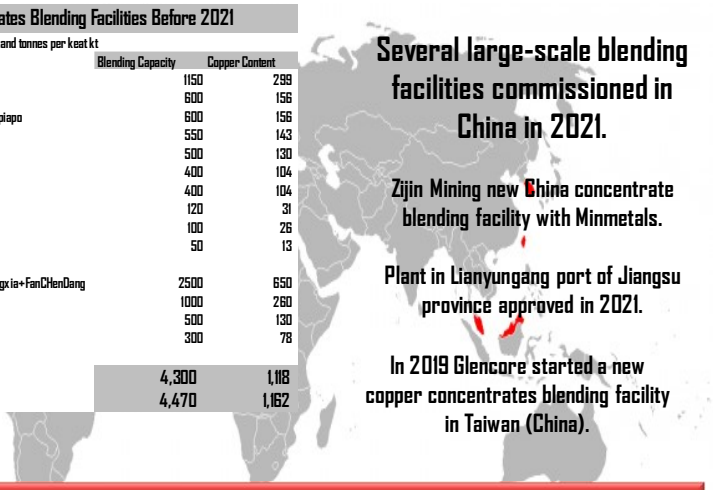

Several large-scale blending facilities commissioned in China in 2021.

Zijin Mining new China concentrate blending facility with Minmetals.

Plant in Lianyungang port of Jiangsu province approved in 2021.

In 2019 Glencore started a new copper concentrates blending facility in Taiwan (China).

No new limits to minor metals in concentrates imports in China in 2022.
Permits to process complex concentrates and new blending plants in China:
+ hazardous waste flows to Chinese smelters and +hazardous waste disposal places in China.

Chinese copper smelters processed ~50 ktY of Arsenic before 2017.
In 2021 arsenic inflows to copper smelters ~100 kt, small outflows.

China Copper Smelters Output and Impurities Flow in 2017
in tonne. Estimate based on ICSG and BGRIMM data.

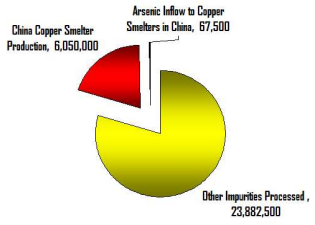

Average Cu and As in concentrates treated in Chinese smelters:
18% to 20% copper
0.20% to 0.25% arsenic.

Source: BGRIMM- Procedings of EMC Conference 2017

A long process with high costs and ~45% of the arsenic to be re-melted.
In 2008-2023 China started using arsenic sulphide pressure leaching plants.

Arsenic Trioxide Production from Japan Copper Sulphate Process Results in China Guixi Smelter (BGRIMM 2017)

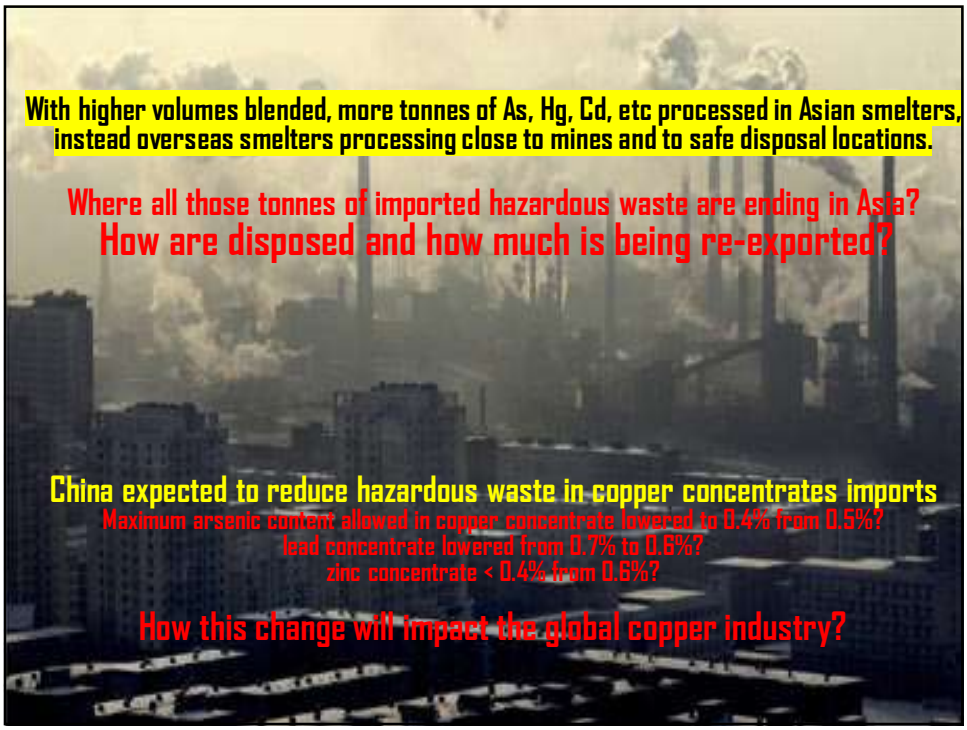
With higher volumes blended, more tonnes of As, Hg, Cd, etc processed in Asian smelters, instead overseas smelters processing close to mines and to safe disposal locations.
Where all those tonnes of imported hazardous waste are ending in Asia?
How are disposed and how much is being re-exported?
China expected to reduce hazardous waste in copper concentrates imports
Maximum arsenic content allowed in copper concentrate lowered to 0.4% from 0.5%?
lead concentrate lowered from 0.7% to 0.6%?
zinc concentrate < 0.4% from 0.6%?
How this change will impact the global copper industry?


3. Copper Smelters Capacity Trends
and Complexity Challenges to 2028

ICSG reported copper smelter capacity expansion plans growing

well over 5 Mt-Cu of new concentrates smelting capacity expected for 2030

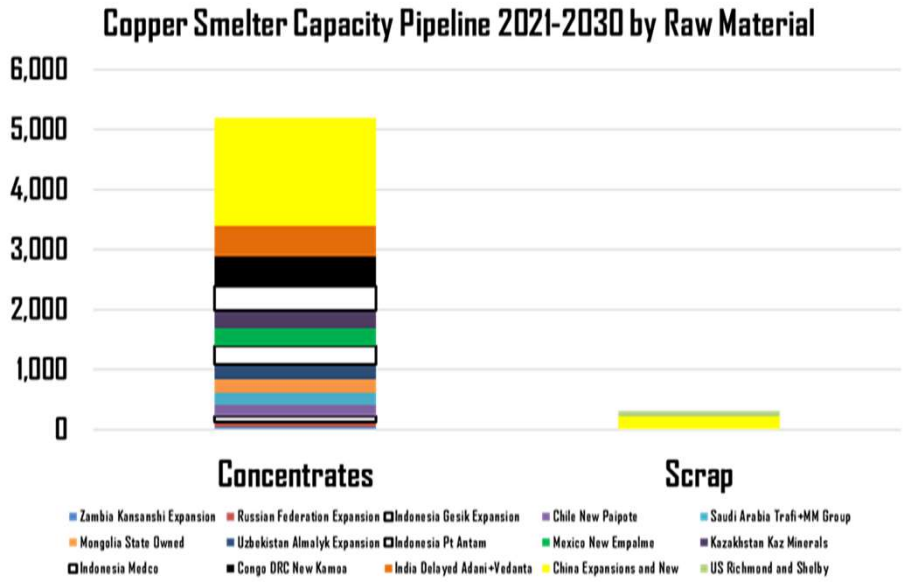

Copper smelter capacity commissioned sooner that expected in India and Indonesia.

New demand for copper concentrates +3 Mt-Cu to 4 Mt-Cu in 2024-2026

= up to +16 Mt per year in gross weight.

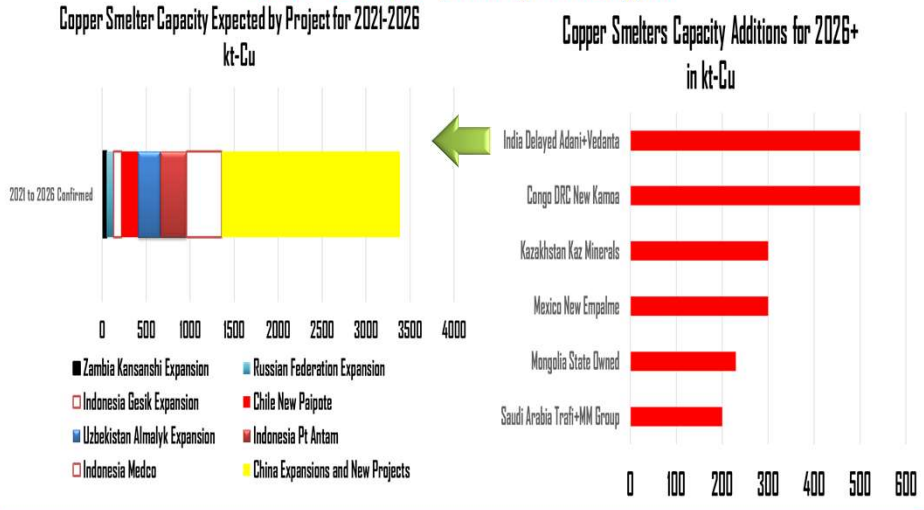

New copper smelters and expansions in China, Indonesia, Uzbekistan, Iran, Russian Federation, South Africa, Zambia, Serbia and United States (scrap) and maybe in Chile.

Increasing arsenic and other minor metals in copper anodes.

Most of the Arsenic is already captured in smelters dust.

Safe disposal of the smelter solid waste a challenge in some plants.

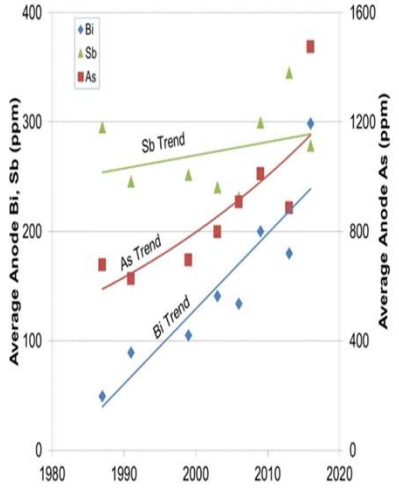

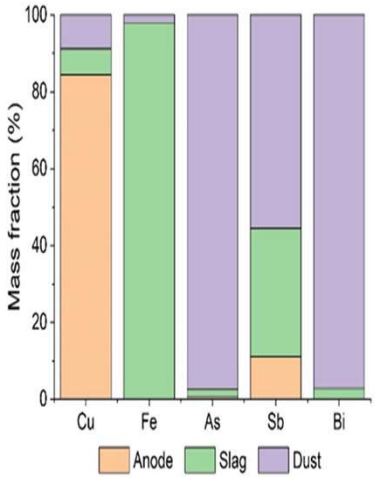

Copper anodes arsenic concentrations ex-China increasing

but appear to have plateaued for Bi, Pb and Te in 2022.

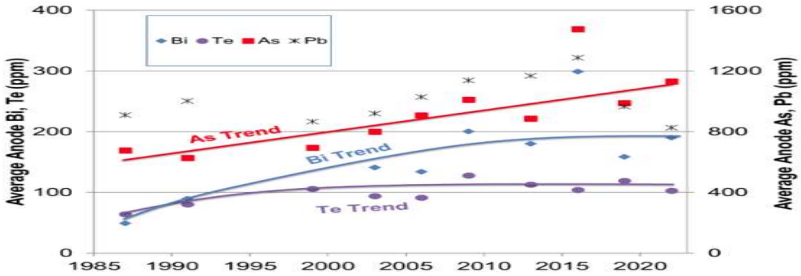

Global survey of average composition of copper anodes.

Source: COPPER 2022 conference in Chile

Element (Unit)	2007	2010	2013	2016	2019	2022
Cu %	99.3	99.3	99.3	99.3	99.2	99.3
Ag ppm	850	840	750	710	680	600
Au ppm	40	60	30	30	30	30
S ppm	30	30	30	20	20	20
Se ppm	340	390	400	410	460	360
Te ppm	100	130	110	100	120	100
As ppm	930	1010	890	1480	990	1130
Sb ppm	240	300	350	280	450	320
Bi ppm	130	200	180	300	160	190
Pb ppm	1060	1140	1170	1290	970	830
Ni ppm	1410	1480	2040	1520	2590	2170
O ppm	1630	1630	1460	1490	1450	1570

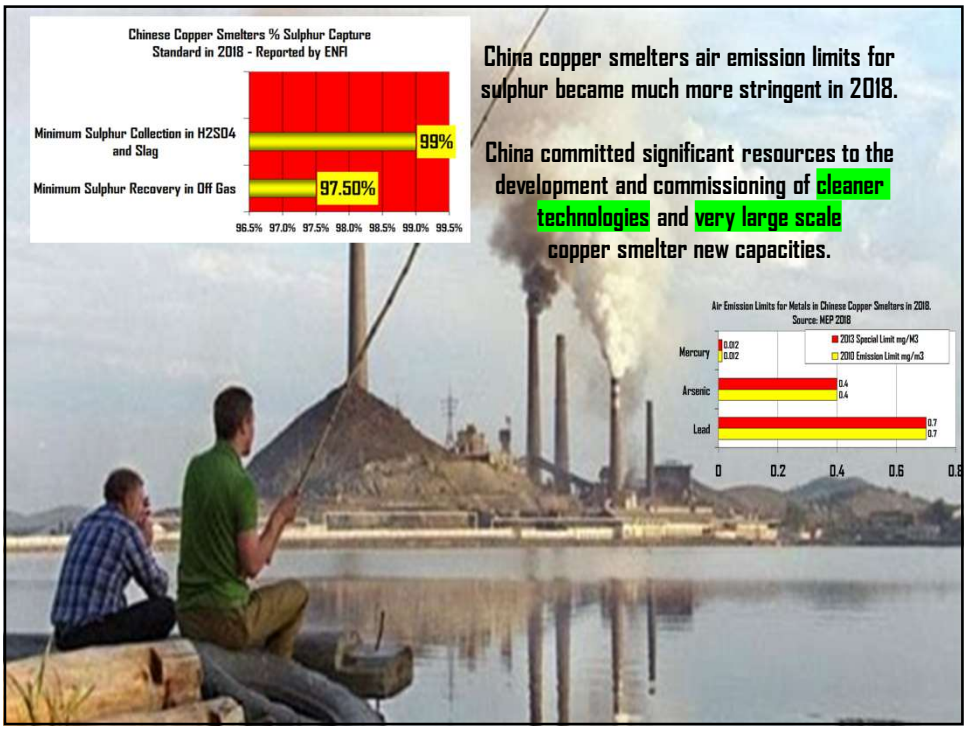

Chinese bottom and side blowing smelting technologies adding new capacity in 2023-2025 to feed new refineries to allow fabrication plants to operate.

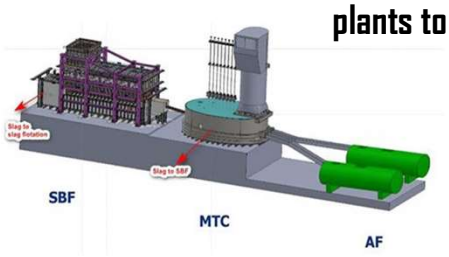

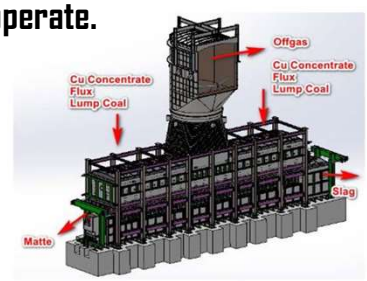

Table 5: List of completed and operating copper smelters using SKS smelting technology.

Smelters	Process	Cu concentrate Capacity	Startup
Smelter No.1	SKS+PS.C	60kt/a	2008
Smelter No.2	SKS+PS.C	800kt/a	2010
Smelter No.3	SKS+PS.C	400kt/a	2011
Smelter No.4	SKS+BBC	700kt/a	2014
Smelter No.5	SKS+PS.C	600kt/a	2014
Smelter No.6	SKS+FCF	1500kt/a	2015
Smelter No.7	SKS+BBC	500kt/a	2015
Smelter No.8	SKS+PS.C	500kt/a	2016
Smelter No.9	SKS+BBC	500kt/a	2017
Smelter No.10	SKS+BBC	500kt/a	2017

copper smelters under construction and in operation using SBF smelting technology.

melters	Process	Cu concentrate Capacity	Startup
melter No.1	SBF+PS.C	220kt/a	2011
melter No.2	SBF+PS.C	480kt/a	2011
melter No.3	SBF+PS.C	400kt/a	2016
melter No.4	SBF+PS.C	500kt/a	2016
melter No.5	SBF+PS.C	700kt/a	2017
melter No.6	SBF+PS.C	500kt/a	2017
melter No.7	SBF+PS.C	500kt/a	2017
melter No.8	SBF+PS.C	240kt/a	2018
melter No.9	SBF+PS.C	700kt/a	2018
melter No.10	SBF+PS.C	500kt/a	2018
melter No.11	SBF+PS.C	1100kt/a	2018
melter No.12	SBF+MTC	600kt/a	2019
melter No.13	SBF+MTC	1700kt/a	2019
melter No.14	SBF+MTC	1400kt/a	2019
melter No.15	SBF+MTC	650kt/a	2019
melter No.16	SBF+PS.C	1000kt/a	2020
melter No.17	SBF+MTC	1700kt/a	2023
melter No.18	SBF+MTC	1100kt/a	2023
melter No.19	SBF+MTC	1000kt/a	2023
melter No.20	SBF+MTC	1400kt/a	2024
melter No.21	SBF+MTC	1400kt/a	2024
melter No.22	SBF+MTC	2500kt/a	2025

https://www.researchgate.net/publication/357997090_Development_of_Bottom-Blowing_Copper_Smelting_Technology_A_Review

New Chinese copper clean smelting technologies will provide much more than 18% of the world´s smelting capacity in 2026.

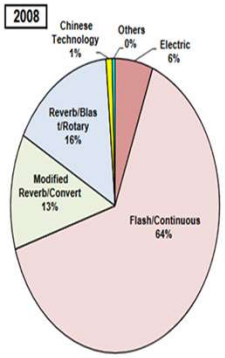

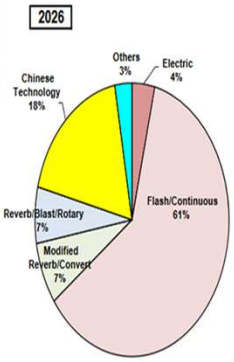

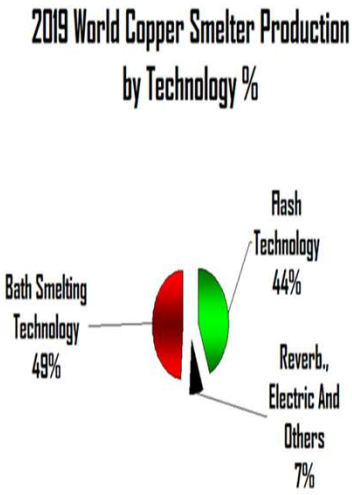

In 2022 copper smelters in Japan faced technological constraints to reduce high arsenic smelter slag to be used in artificial islands and sea bed pillars.

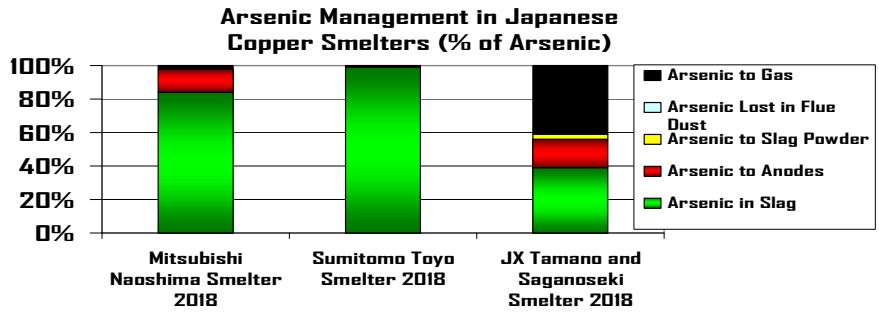

Japan standard for arsenic in slag to be sold for general uses:
150 mg/ As per Kg of slag

Japan standard for disolution of arsenic in slag to be sold for general uses:
0.01 mg/lt As per Kg of slag

Japan standard for arsenic disolution in slag to be used in seashore applications:
0.03 mg/lt As per Kg of slag

In 2023 Japan keep working for hazardous wastes to be removed
before concentrates be exported to Japanese copper smelters.

http://www.jogmec.go.jp/english/news/release/news_10_000062.html

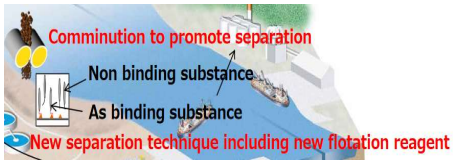

Magnetic Arsenic Ore Separation

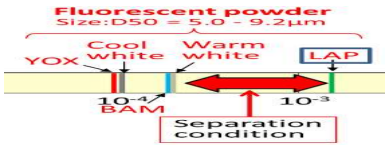

If they succeed , more hazardous waste disposal close to copper mines.

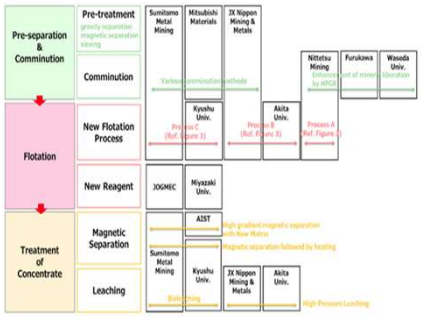

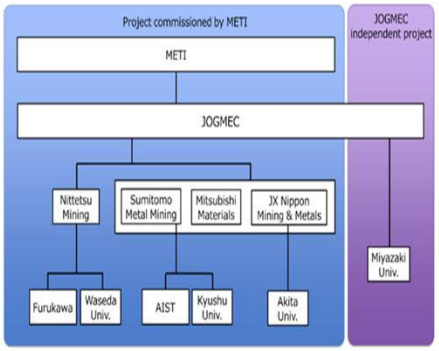

Chile has most of the copper reserves and mine production,
but most of copper smelters technologies are obsolete.

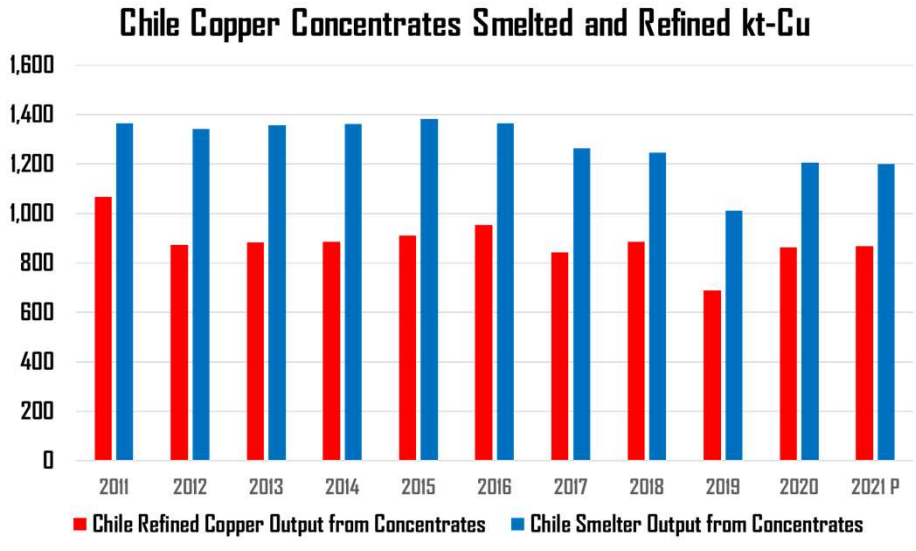


Caletones
Potrerillos
Chuquicamata
Chagres
Alto Norte:
1992-1994
using furnaces recycled from a
from a US smelter,
Japanese arsenic tech
and Chilean engineering.
Paipote 2.0
opportunity
to develop
China – Chile
Copper smelter
Joint Venture
Ventanas:
to be closed
opportunity
to develop
China – Chile
smelter
Joint Venture

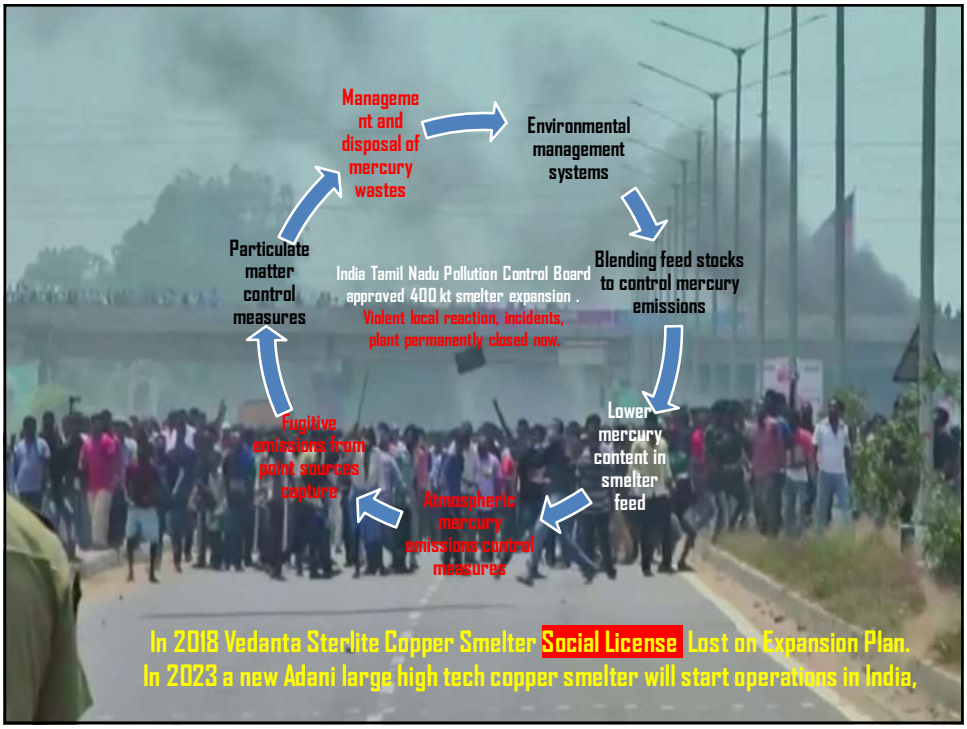
Manageme nt and disposal of mercury wastes
Environmental management systems
Blending feed stocks to control mercury emissions
Lower mercury content in smelter feed
Atmospheric mercury emissions control measures
Fugitive emissions from point sources capture
Particulate matter control measures
India Tamil Nadu Pollution Control Board approved 400 kt smelter expansion .
Violent local reaction, incidents,
plant permanently closed now.
In 2018 Vedanta Sterlite Copper Smelter Social License Lost on Expansion Plan.
In 2023 a new Adani large high tech copper smelter will start operations in India,

In the European Union, stricter emissions controls in 2017-2020
cancelled copper concentrate smelters investment plans,
but copper scrap copper smelter and semis capacity are growing.

European Union BAT 2016 Regulation:
New Emission Limits to Water for Metal Industries (mg/lt)

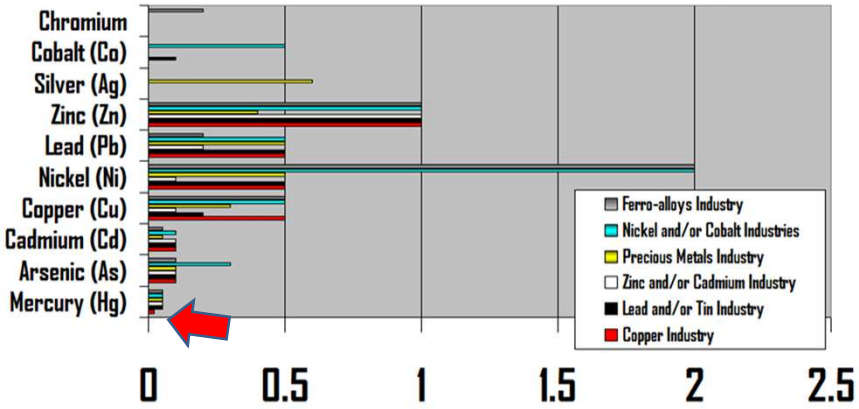

European copper smelters in 2021 and 2022 refocused mainly on copper recycling investments in Europe and in North America.

Anode Slimes Metal Composition (%)
New Aurubis Plant in Hamburg - Copper 2016 Kobe (2016)

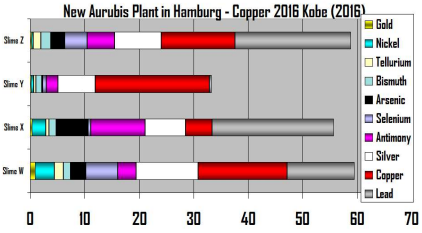

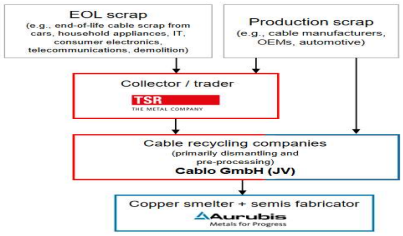

Press Release

Aurubis builds recycling plant in the US and sets its sights on sustainable growth

Hamburg | Wednesday, November 10, 2021

Aurubis
Metals for Progress

METALLO
THE FURNACE OF INNOVATION

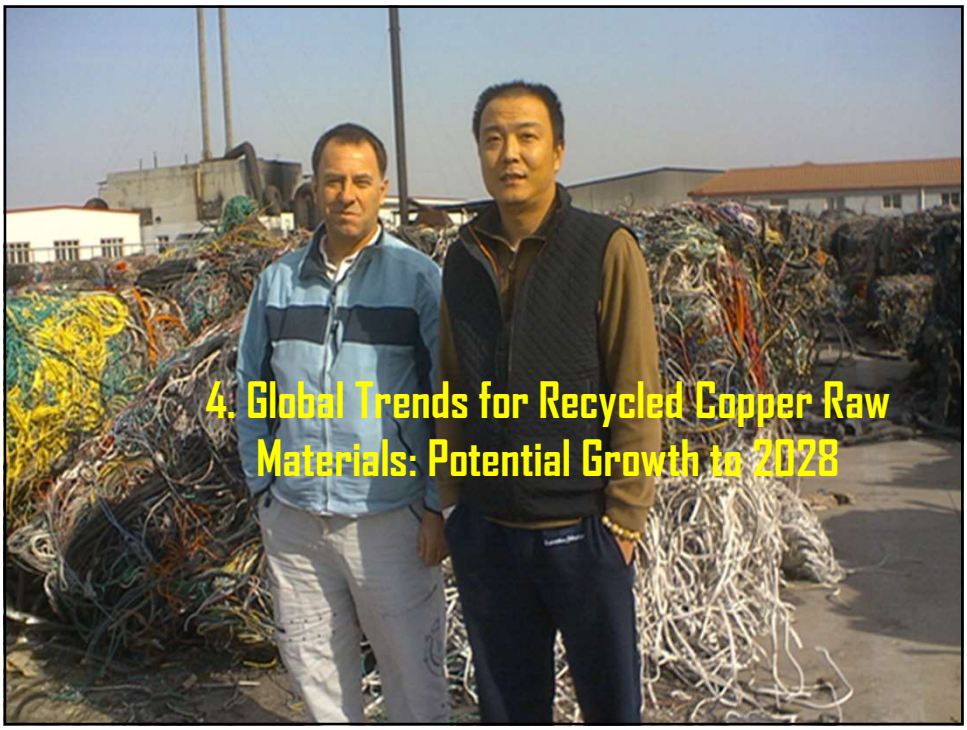

Global trade of recycled raw materials stagnated below 6 Mt per year in gross weight 2019-2022.

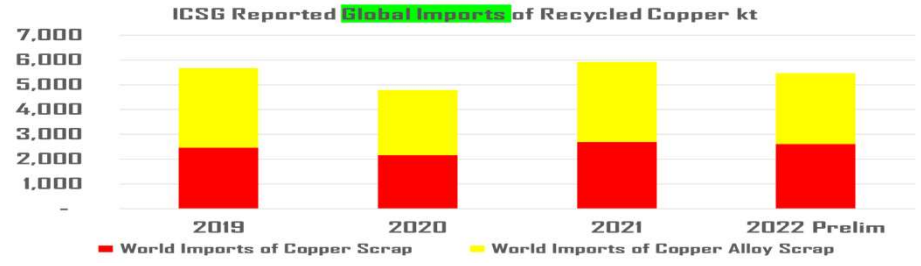

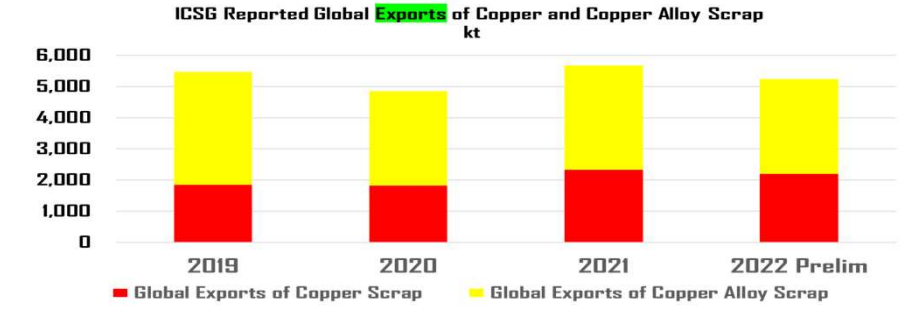

Contraction in copper scrap and copper alloy scrap exports in 2022. Only higher copper prices will increase copper scrap available for trade.

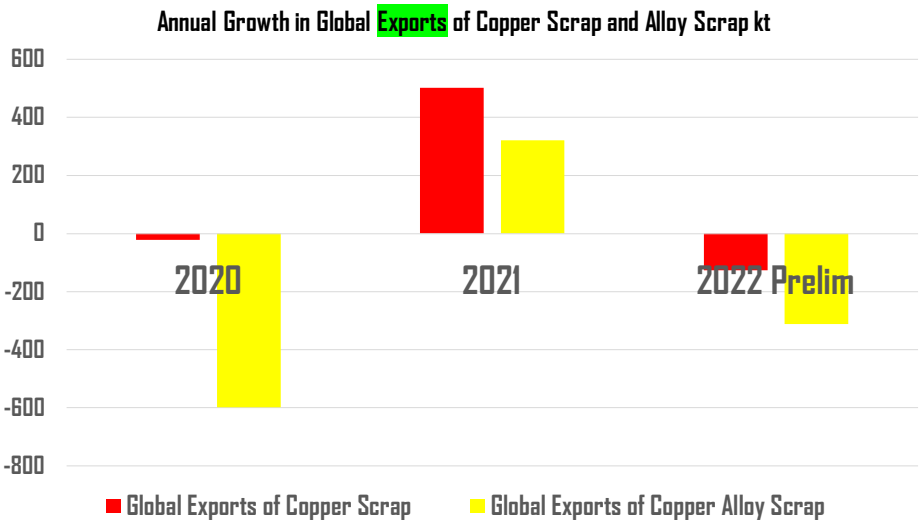

Net recycling copper inflows to China, India and Korea. EU27+UK region net importer in 2022 for the first time.

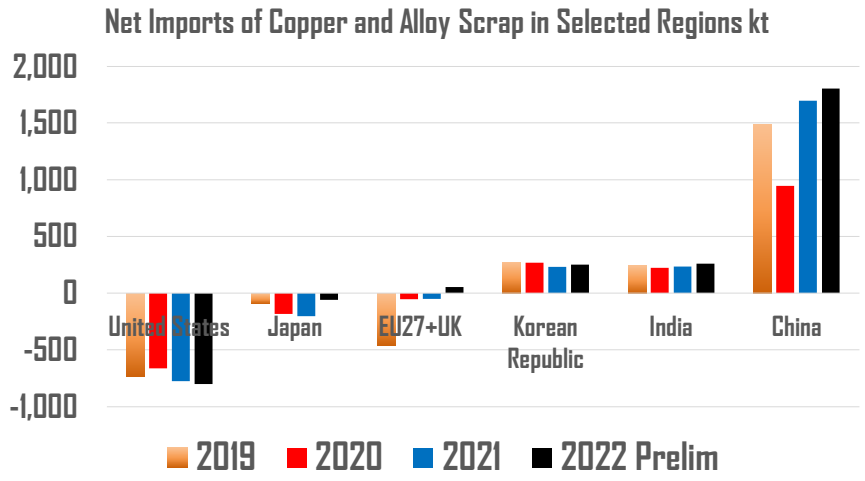

Sources of global trade of recycled copper remain highly diversified: scrap exports from more than 70 countries in 2022.

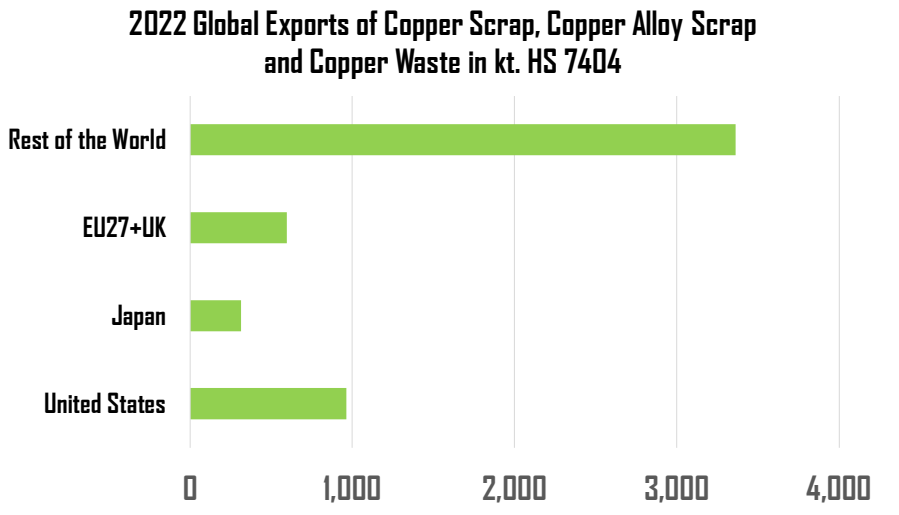

United States top scrap exporter in the world in 2022, with dynamic changes in US export destinations.

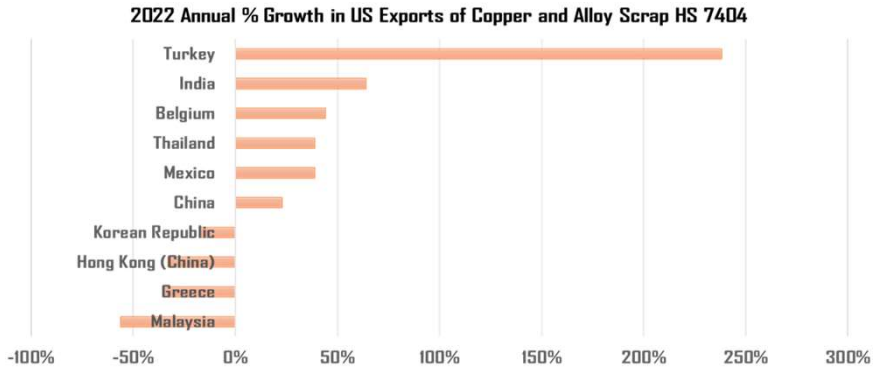

More recycled raw material from the US to China, India, and less to Malaysia and ROW following import bans changes.

New copper scrap smelting capacity in China: +992 kt/year. Where the recycled raw materials will come from in 2024?

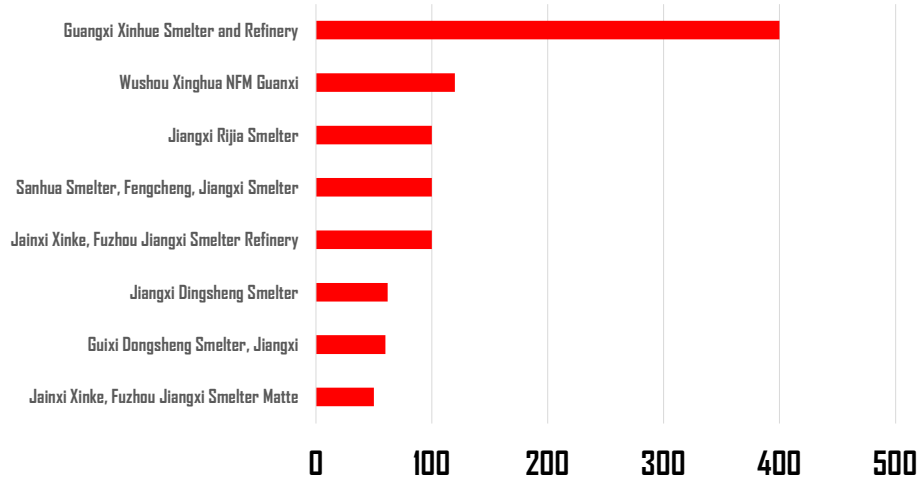

Projects for plants processing scrap raw materials outside China: +680 kt expected operational in 2025.

We discounted plants using process smelter/refinery waste.

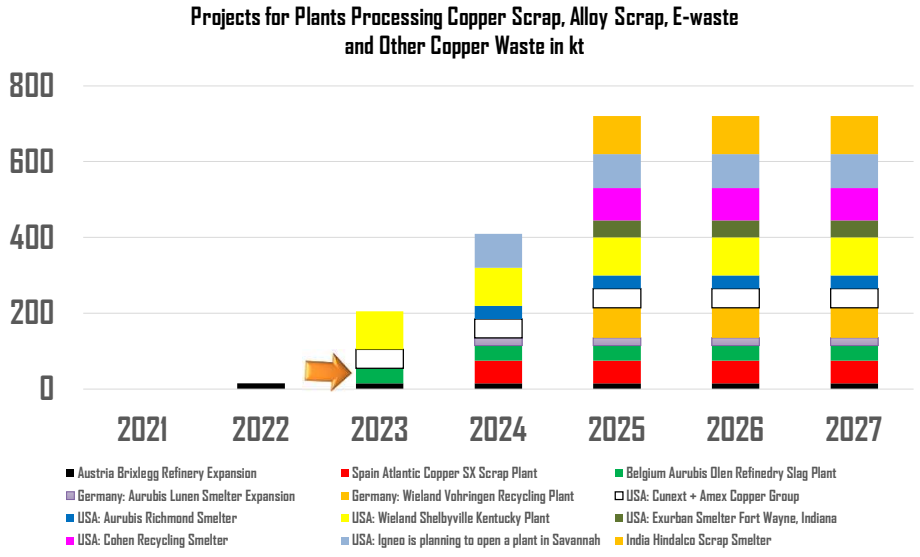

If the capacity to process copper scrap is commissioned as expected, global shortage in exports of recycled copper in 2025-2027.

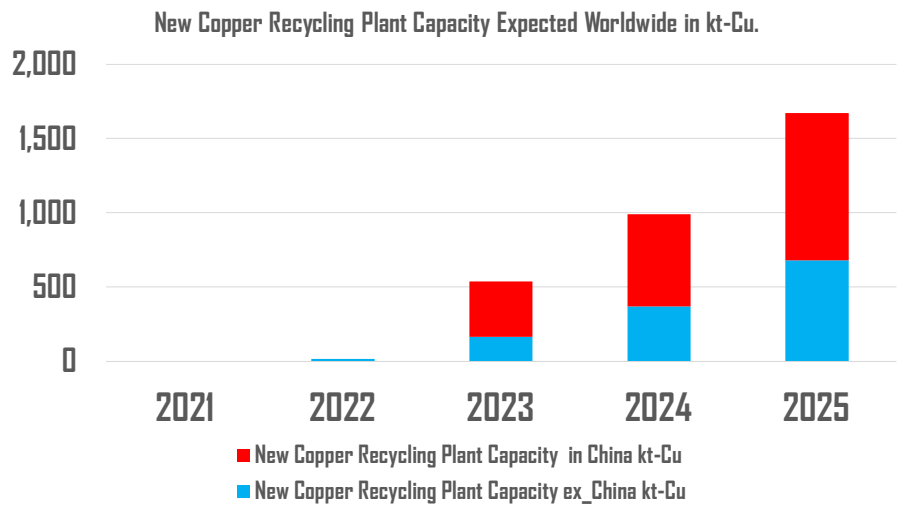

If we add copper in scrap melted by fabricators and scrap refined, recycled copper use remains flat: <10 Mt-Cu per year in 2018-2022

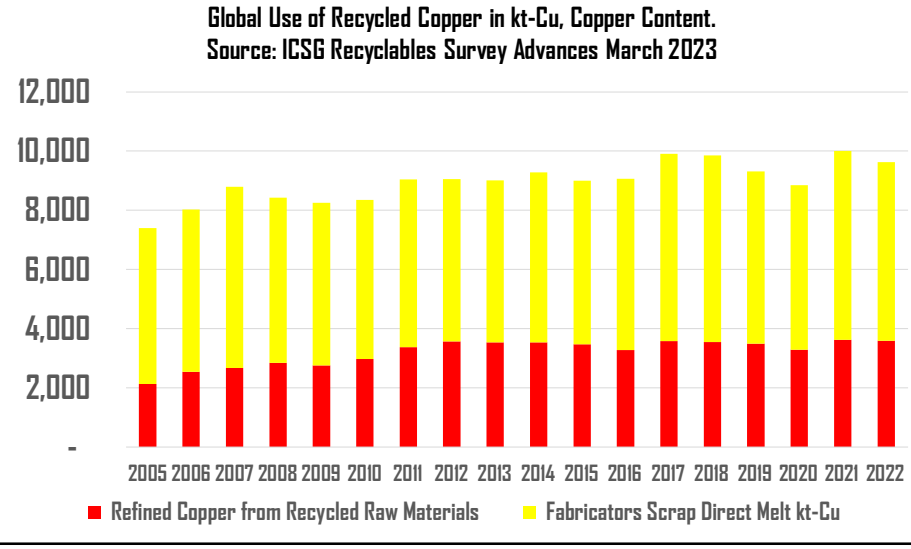

Refined copper output from recycled raw materials stagnated worldwide <3.7 Mt per year in 2012-2022.

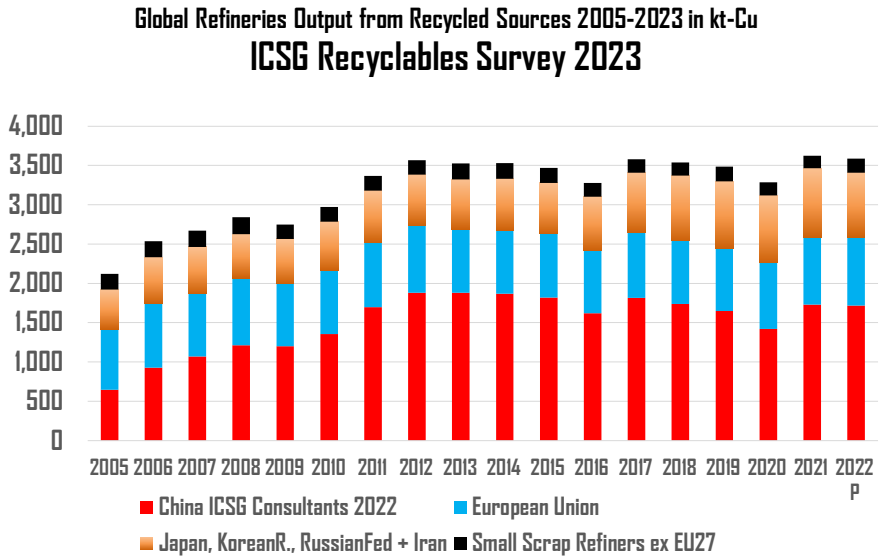

How much refined copper came from recycled sources in 2019-2022 in China? It depends to who you ask.

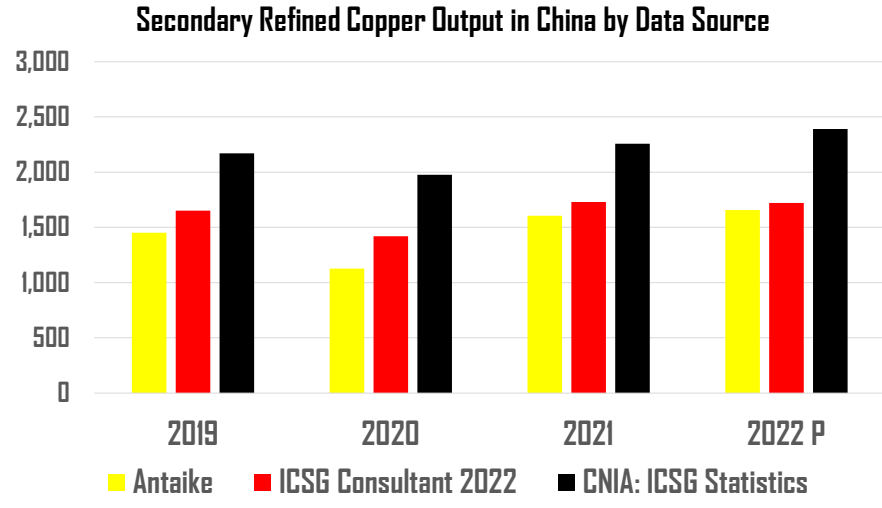

Refined copper from recycled sources in the European Union recovering...but still well below 900 kt per year.

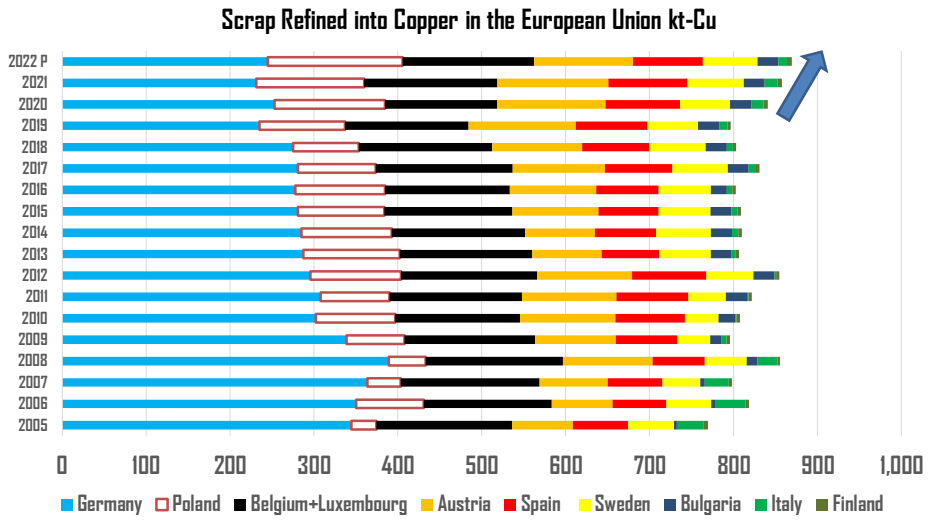

Top 5 most important scrap refiners ex-China and ex-EU-27 refining more scrap than all the European Union.

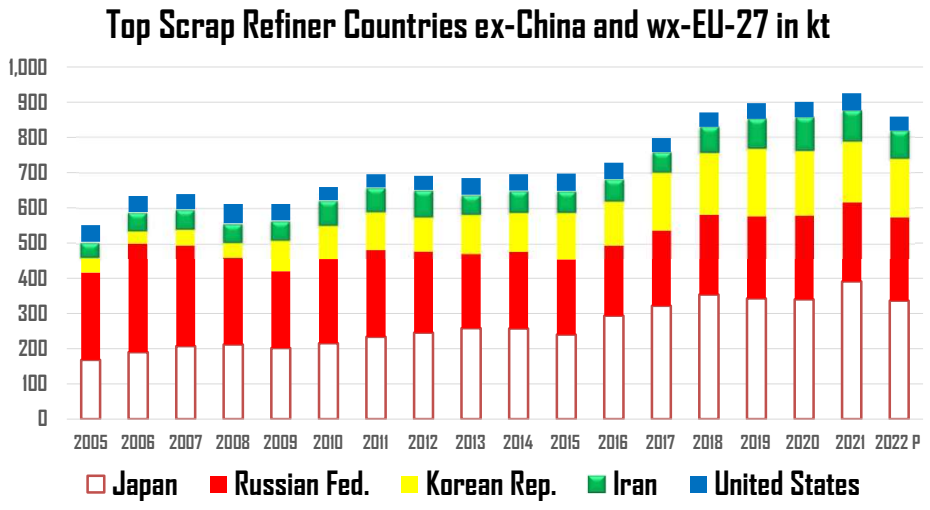

Japan and the Korean Republic dynamic growth of refined copper from scrap.

However the uptrend stopped in 2019-2022 in both countries.

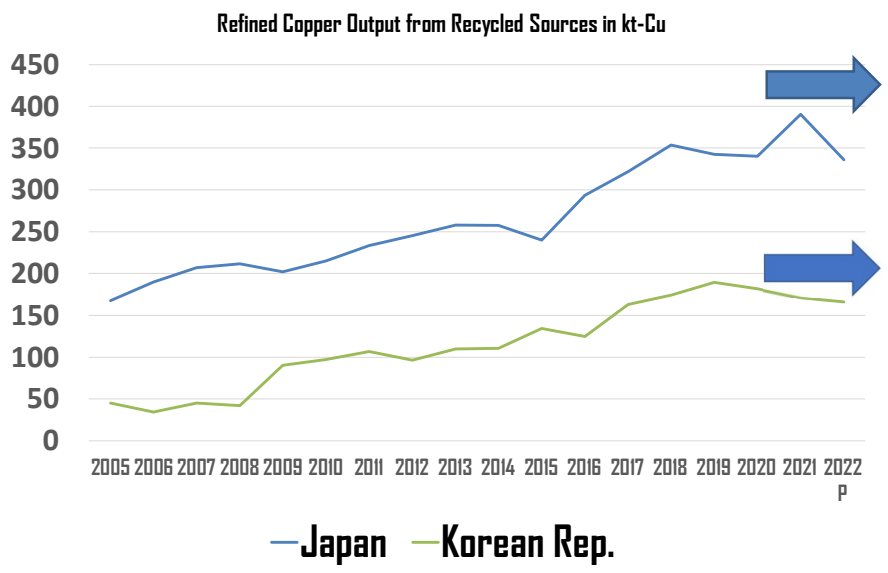

Stable production of scrap refined in the Russian Federation.
Iran refined copper output from scrap remains below 100 kt per year.

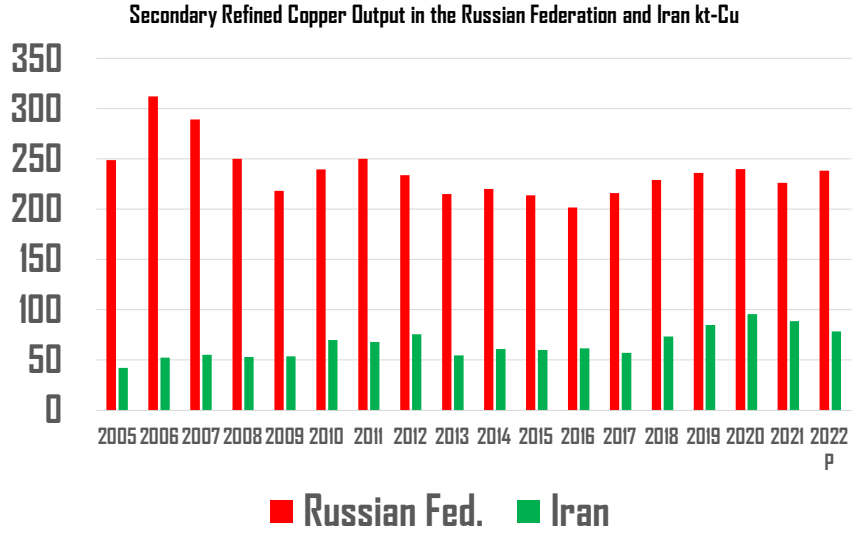

Group of small copper scrap refiners ex-EU27 ex-China :
in 2023 output continue in a downtrend since 2013-2014.

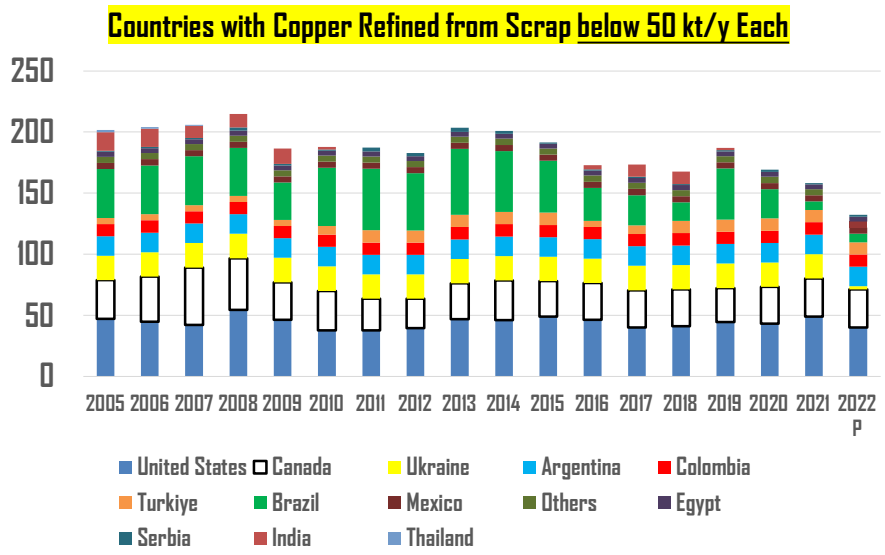

After a record recovery in the global use of recycled copper in 2021
a much modest growth in use of recycled copper in 2022.

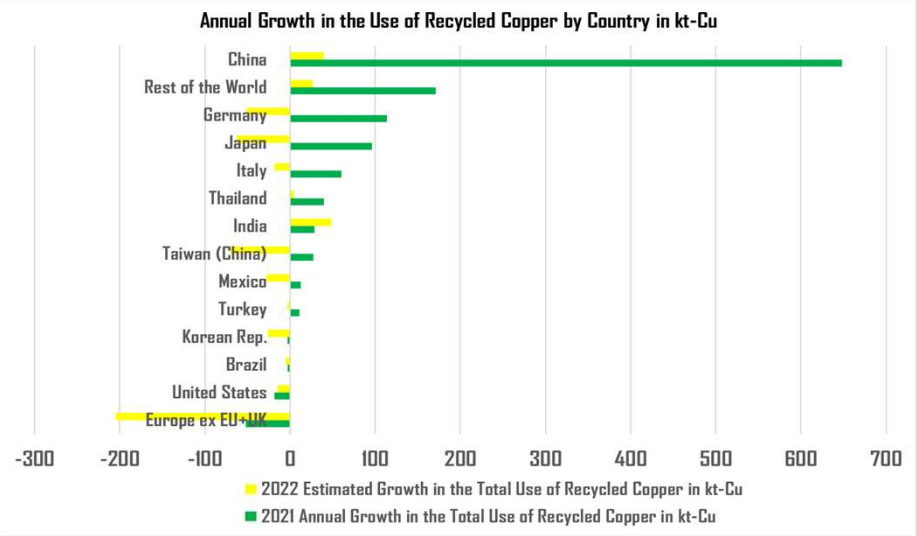

5. Global Balances, Metal Exchange Pricing and Refined Copper Inventory Transparency

In constant US Dollars, the last price super-cycle lasted 90 years: 1934-2004. The new super cycle, less than 20 years, sustained mainly by Chinese demand growth.

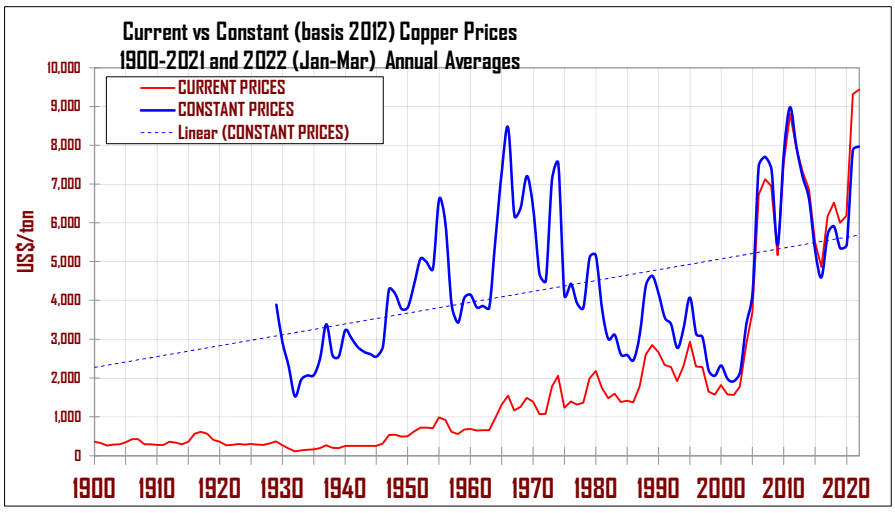

A stable link between copper and gold prices endured through 1974-2022.

But in war times trade of refined copper is restricted:
one tonne of refined copper can cost ~1 kg of gold.

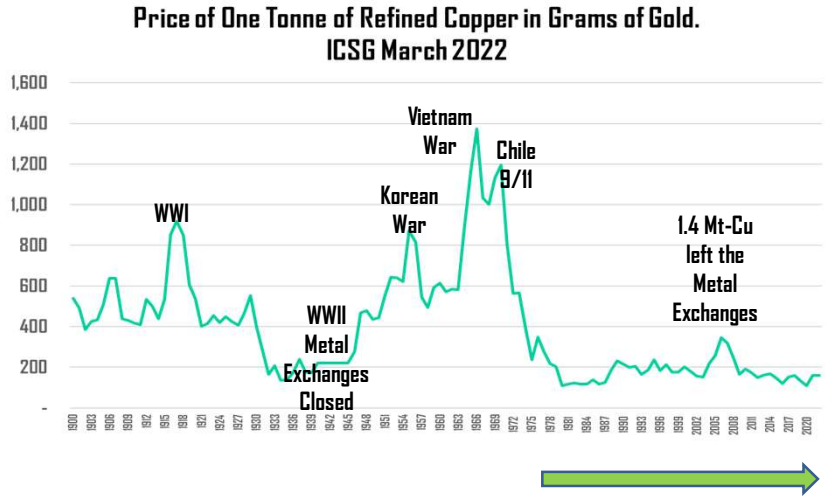

ICSG statistics: global deficits of refined copper every year along 2011-2022

Most of the difference between refined copper demand and industrial use growth
ended as unreported inventories out of the exchanges.

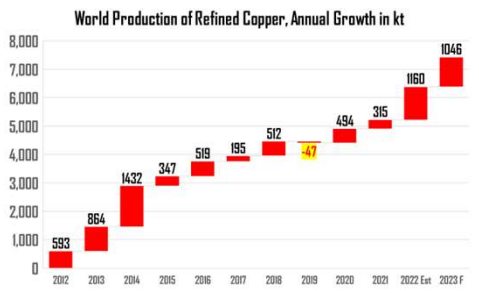

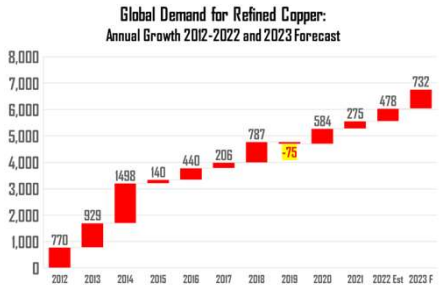

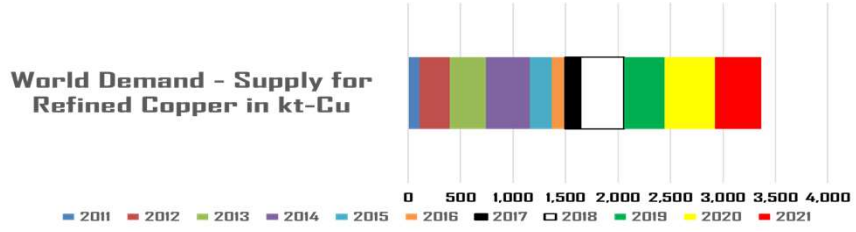

Most of refined copper and scrap is melted by fabricators worldwide:
Fabricators stocks, refined and scrap stocks ex-exchanges:
no public information available.

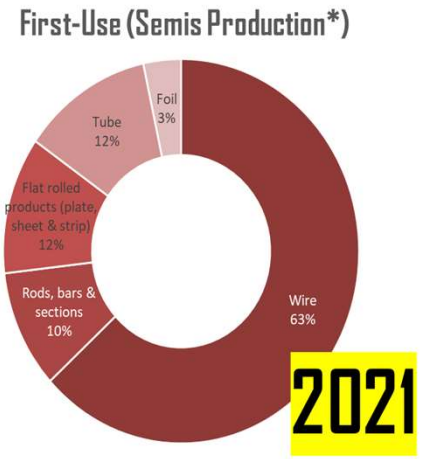

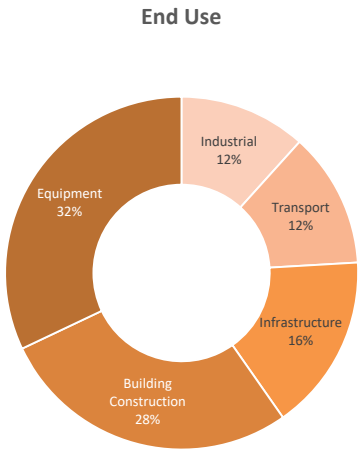

If refined copper inventories at metal exchanges fell in 2018-2022
and the global refined copper market was in deficit from 2011 to 2022
why the copper price was not much higher?

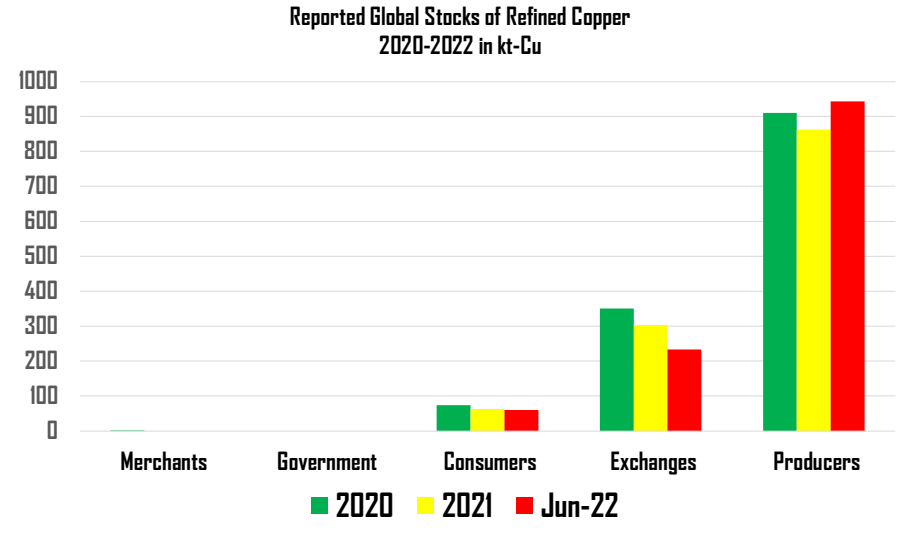

Movements between reported and unreported refined copper inventories remain the driver of refined copper prices volatility in metal exchanges.

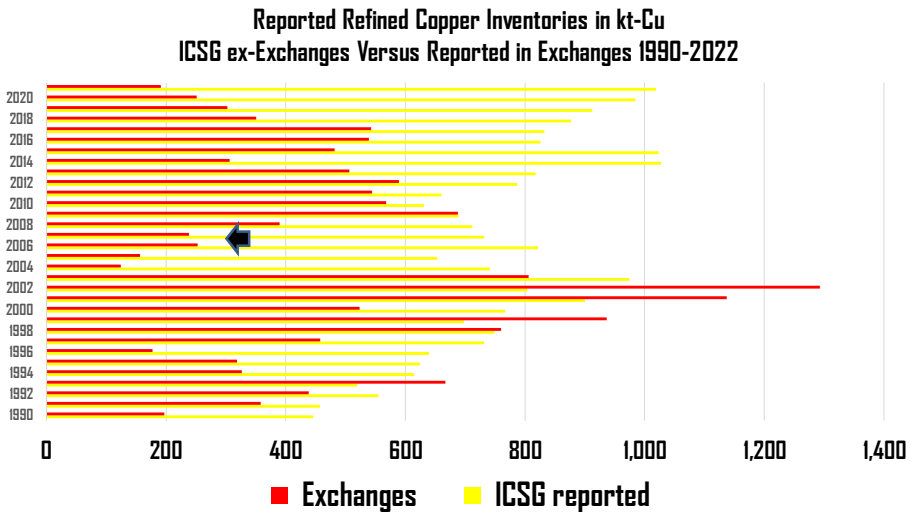

2004 - 2022 trend: more refined copper inventories out of metal exchanges.

December 2010: unreported refined copper stocks suddenly reported in China.

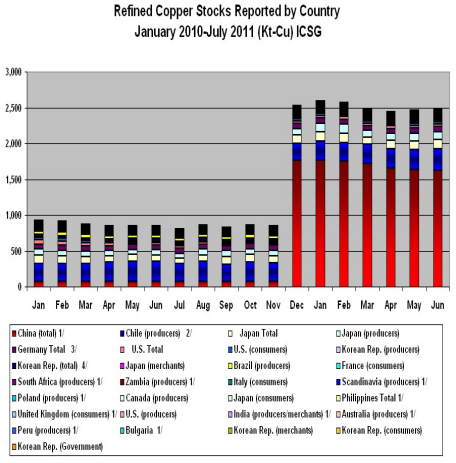

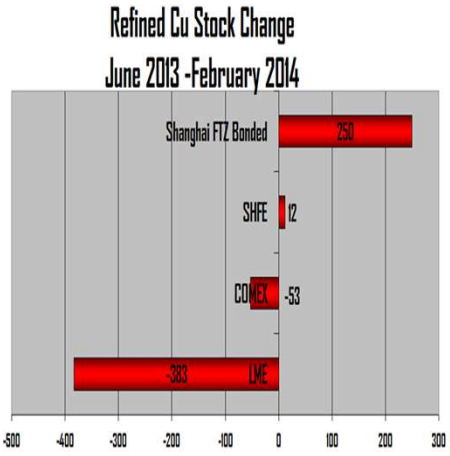

Stocks left the LME in 2013: excess refined in China "exported" to Shanghai funds.
In 2014 SHFE stocks sold at lower prices: short positions closed and fabricators re-stocked.

Only when CODELCO contracts started to use the LME price in 1978,
LME prices of refined copper and other metals correlated strongly.
The financialization of the copper markets separated prices from fundamentals.

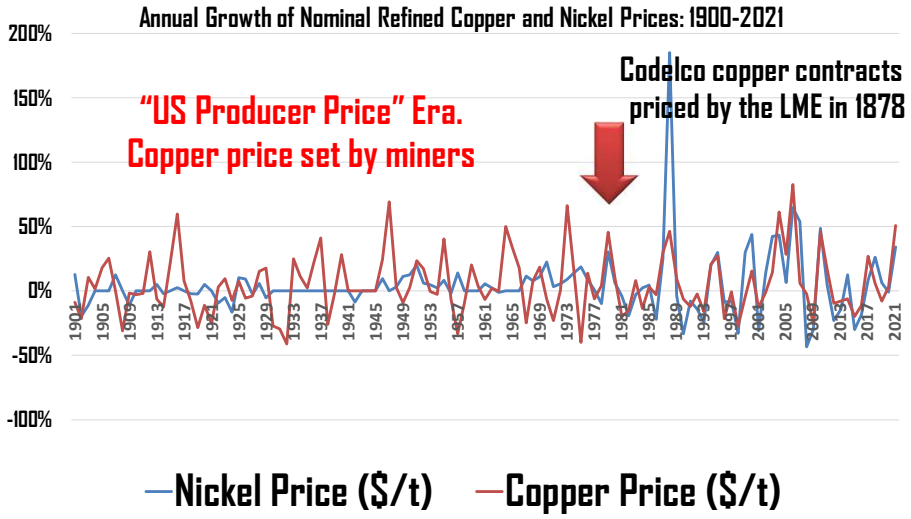

Limited market power of major copper miners ex-China now:
~20% of current copper mine production comes from Chinese miners
and over 30% from medium and small scale copper mining companies.

World Copper Mine Production 2020-2021 and 2022 Forecast

	2020 Production	2021 Production Preliminary	2022 Output Forecast	Output Share 2021 in %
Chinese Miners Overseas and Partners	1,860	2,035	2,350	9.6%
Chinese Miners in China	1,723	1,910	2,003	9.1%
CODELCO and Partners	1,727	1,728	1,730	8.2%
Freeport Mc Moran and Partners	1,178	1,407	1,480	6.7%
Glencore and Partners	1,258	1,196	1,240	5.7%
BHP Billiton and Partners	1,107	1,022	980	4.8%
Southern Copper and Partners	1,001	958	895	4.5%
Nornickel+RCC+Uralelectromed	881	873	800	4.1%
First Quantum and Partners	779	816	910	3.9%
KGHM* and Partners	709	754	790	3.6%
Rio Tinto (Oyu Tolgoy only)	528	494	520	2.3%
Antofagasta Minerals and Partners	492	464	470	2.2%
Angloamerican and Partners	463	463	463	2.2%
Vale and Partners	355	293	300	1.4%
Teck and Partners	276	287	282	1.4%
Medium/Small Scale Miners	6,296	6,397	6,679	30.3%
	Reported	Reported	Fcast Oct 2021	
ICSG Mine Output + Adjusted Forecast	20,633	21,097	21,892	100.0%
* ICSG Preliminary 2021 Forecast 2022		2.2%	3.8%	
Reported by Company	14,337	14,700	15,213	69.7%
		2.5%	3.5%	

6. ICSG Data and Research Available in 2023

- ICSG research on copper **mine supply, demand, trade and recycled** copper in 2007-2023
- Research of **special interest** for ICSG member countries in the period of analysis.
- **Key findings** of selected ICSG research projects for the period of analysis 2007-2023
- Main challenges to improve data transparency in the global copper value chain **beyond 2023**

ICSG Member Countries meetings are twice a year in Portugal:
Environmental and Economics Committee EEC
Statistical Committee STATS
Industry Advisory Pannel IAP
Standing Committee (ICSG member countries only)

Visit: www.icsg.org
Last ICSG Member Countries Meetings: 27-28 April 2023

- Global Copper Mine Supply Forecast 2023-2025
- Survey of Recycled Copper Use in Refineries and Fabricators
- Global Refined Copper Market Balance and Forecast
- Speakers: Governments, Industry Associations, Copper Miners, Users, Funds and Banks.

- Next ICSG Member Countries Meetings:
October 2023 in Lisbon, Portugal
the week before the LME Week in London

Regular Annual Work Program 2007-2022
ICSG Environmental and Economic Committee

- Annual Copper Recyclables Surveys 2007- 2022
- Annual Surveys of Regulatory Developments 2007- 2022
- Annual Directories of Fabricators Capacity 2007- 2022
- Reporting on International Issues: Annual Copper Use Trends
- Reporting on International Issues: Annual Raw Materials Trade
- March 2023: advancing on the 2023 edition of the
- ICSG Annual Survey of Regulatory Developments Affecting Copper to be available for ICSG member countries by October 2023

Regular Annual Work Program 2007-2022
ICSG Statistical Committee

- Monthly Copper Bulletin: Statistics of Output, Trade and Use
- Annual Statistical Yearbook: Past 10 Years Industry Data
- Annual Directory of Copper Mines, Smelters and Refineries
- Online Statistical Database 1995-2022: Output, Trade, Use
- World Copper Factbook and Economic Background

2007-2022 Insights: ICSG Secretariat Papers of Copper-Relevant Subjects for Member Countries

- Copper, Carbon Trading and Climate Change – 2008
- The Financial Crisis and the Copper Industry – 2009
- Impact of Copper Prices on Copper Supply and Demand- 2009
- Democratic Republic of Congo: Country Profile – 2010
- Physical Copper Exchange Traded Funds – 2010
- Alternative Ways of Calculating Refined Copper Use- 2011
- International Maritime Organization IMO Regulations – 2012
- China Copper Industry and New Copper Alloys-2017
- Impurities in Copper Raw Materials: Concentrates - 2018
- Global Copper Scrap Trade and Impact on Copper Markets-2020
- COVID-19 and Copper Supply, Fabrication and Recycling-2021
- Copper Market Transparency 2007-2022: COPPER 2022 Conference in Chile.

ICSG Research Projects 2012-2022 on Industrial Use of Refined Copper and Scrap in Fabrication

- Survey of Scrap and Refined Copper Use in China Copper Manufacturing Plants -2012
- Survey of Copper Use in Brass Mills and Copper Semis ex-Wire Rod in China -2014
- Survey of Copper Use in the Middle East and North Africa Fabricators – 2014
- Survey of Copper Use in India, ASEAN and Oceania Semi Fabricators – 2015
- Survey of Copper Use in Latin America and Canada Copper Fabricators – 2017
- Industrial Use of Refined Copper and Scrap in Fabrication in China – 2017
- Copper Use in Japan, Korea, Taiwan (China) and Vietnam Fabricators – 2018
- Copper Use Survey in the European Union Fabrication Industry -2019
- Survey of Copper Use in the United States, Mexico and Canada – 2020
    - Copper Fabrication Capacity and Use in China – published at the end of 2022
        - as part of an update of China Copper Smelter and Refining Industry

Available for sale: mail@icsg.org

ICSG Research Projects on

Recycling of Copper Raw Materials in 2007-2022

- The Chinese Copper Scrap Market -2009
- The Copper Scrap Market in India -2009
- Copper Scrap Market and Scrap International Trade in Japan -2009
- China Scrap Usage Survey to Smelters and Semis -2009
- Domestic Copper Scrap Generation in China -2009
- ICSG Global Copper Scrap Research Project Final Report - 2010

- Copper Scrap Recovery in North America: Industry and Yard Practices -2012
- Survey of Copper and Alloy Scrap Supply in the European Union – 2013
- Survey of Scrap Use in Smelters and Wire Rod Plants in China – 2013
- ICSG Annual Global Surveys of Recycled Copper Use: 2007-2022
- March 2023 working on the 2023 edition of the Global Survey of Recycled Copper Use.

- More details: mail@icsg.org

ICSG Research Projects on Subjects of

Special Governments Interest

- Taxation, Royalties and Fiscal Policy on Base Metals – 2013

- Cobalt as a By-product of Copper and Nickel Mining- 2014
- Study of By-products of Copper, Lead, Zinc and Nickel – 2012
- Update of By-products of Copper, Lead, Zinc and Nickel -2015

- Social Acceptance for Mineral and Metal Projects – 2015

- China Domestic and Overseas Copper Mining Industry- 2016

- China Copper Mines, Smelters, Refineries and Semis Update – Completed in 2022

- **More details: mail@icsg.org**

Completed ICSG Research Projects to March 2023

Completed Research Projects 2018- 2021

P37 Industrial Use of Copper in Fabrication in China
P38 Smelting/ Hydrometallurgy for Copper Sulphide Ores and Concentrates
P39 Copper Use and Fabrication in Japan, Korean Rep, Taiwan (China) and Vietnam
P40 Waste Flows in Non Ferrous Metal Mines, Smelters and Refineries (Joint Study)
P41 European Copper Use and Fabrication Capacity Report and Database (Delivered)
P43 North America Copper Use and Fabrication Capacity Update (Delivered)

Completed Research Projects in March 2023

P42 Mineral Composition in Copper Concentrates, Regulations and Impacts
P44 China Copper Industry and Fabrication Capacity Update: 2016-2022 and Pipeline

•The Mineral Composition and Regulation of Copper Concentrates, Smelters and Refineries"

• Research project developed in house by ICSG Secretariat over 2018-2023.

•Objective of this project was to provide ICSG members with new information and data on mineral composition in copper supply.

Final Report Published in March 2024 available for sale:
mail@icsg.org

Due to the importance of this subject :
the update of the mineral composition of copper concentrates will be included in the regular work program of the ICSG starting in 2024.

EEC Monitoring and Reporting on International Issues:
2022- 2023 Copper Conferences

"Copper Value Chain: Clean Energy Transition Challenges" CRU Wire and Cable 2022 United Kingdom
"Copper Outputs, Trade, Capacity and Challenges" SMM Copper Summit 2022, China
"Changes in Mineral Composition of Copper Concentrates" ALTA 2022, Perth, Western Australia
"Global Copper Value Chain: The Demand Side in 2022" Canada MET SOC Copper Conference
"The Physical Copper Market: Global Trends in 2022" London Stock Exchange Copper Conference
"Arsenic in the Global Copper Value Chain: Trends 2022" CODELCO/JOGMEC/FF Seminar in Chile
"Relationships Between Primary and Secondary Copper" Fastmarkets Copper Conference, Spain

February 2023: "Global Copper Market Scenario 2023 and Role of India" ICDC, Mumbai, India

May 2023: "Copper Market Transparency: Lessons Learned and Challenges"
ALTA 2023 Metallurgical Conference, Perth, Western Australia

A NOVEL TREATMENT APPROACH FOR COPPER ORES BASED ON GLUTAMATE LEACHING

By

[1, 2]Carlos Perea, [1, 2]Christian Ihle, [2]Humberto Estay, [3]Laurence Dyer.

[1]Department of Mining Engineering, Universidad de Chile, Chile
[2] Advanced Mining Technology Center, Universidad de Chile, Chile
[3] Department of Mining Engineering and Metallurgical Engineering, Curtin University, Australia.

Presenter and Corresponding Author

Carlos G. Perea S.
cperea@ug.uchile.cl

ABSTRACT

Currently, copper mining faces challenges, such as depleting high-grade ore deposits that contain easily extractable copper. Therefore, mining occurs in transitional and secondary sulfide enrichment zones, where oxide and sulfide minerals are mixed, causing difficulties in conventional processing. This paper presents a new alkaline process for extracting copper from copper oxide and sulfide minerals using monosodium glutamate coupled with copper sulfide precipitation. The leaching of tenorite in solutions containing 0.5 M glutamate was conducted at different temperatures (30, 45, and 60°C) in a 250 mL leach reactor with an agitated slurry and pH 9.4, achieving 97.7% copper dissolution within 2 hours at 60°C. Glutamate can also dissolve copper from sulfide mineral concentrated (composed mainly of covellite, lyonsite, bonattite, brochantite, and antlerite) with controlled dissolved oxygen (DO) levels at different temperatures. The copper extraction from sulfide concentrates in 0.5 M glutamate at 0.5 M, a temperature of 60°C and DO range of 10-15 ppm, was almost 100% after 2 h. The recovery of copper as pure copper sulfide was 99.2% at a Cu:NaHS molar ratio of 1:1.2 by sulfide precipitation. This work proposes a sustainable hydrometallurgy process to recover copper from a mixture of oxides and sulfides minerals using a non-toxic amino acid. The procedure involves two main stages: (i) leaching with aqueous alkaline monosodium glutamate solutions at pH 9.4 with varied temperature, glutamate concentration, and dissolved oxygen concentration, and (ii) PLS treatment by sulfide precipitation of copper, using NaHS addition. As a result, overall copper extraction of over 90% in the integrated process has been obtained.

Keywords: mineral processing, copper dissolution, metal sulfide precipitation, amino acids, and monosodium glutamate.

INTRODUCTION

In the Earth's crust layer, copper is present at a low level of 0.0027 wt.% (27 mg/kg), but it is found in considerable quantity in ore deposits formed by hydrothermal processes. Copper deposits are classified into ten categories: porphyry, sediment-hosted, volcanic massive sulfide (VMS), red-bed copper, magmatic sulfide, epithermal, sedimentary exhalative (SEDEX), skarn, veins, and supergenes. Porphyry copper deposits are among the most economically important due to their large ore volumes and broad distributions (often >1000 Mt of ore at a copper content >0.5%). According to estimates, 60 % of all copper globally is produced from these deposits[1]. In addition, as this kind of deposit grows deeper, the weathering and supergene enrichment, on many occasions, can lead to the formation of an oxidized zone, a transitional supergene zone, and a hypogene sulfide zone[2].

Currently, copper ore mining faces several challenges, such as the depletion of high-grade ore deposits containing easily extractable copper, as with ores in the oxide zone[2][3]. In many mining operations, copper mining occurs progressively more in the transition zone and the secondary sulfide enrichment zone. In the transition zone, it is possible to find a mixture of oxide and sulfide minerals, which generates difficulties using conventional treatment. Although flotation is the preferred process route for copper sulfide (such as chalcocite and covellite), recovery is not equally effective in oxidized overburden and transition zones due to poor floatability[2]. There are two types of flotation treatments for oxides and mixed ores: direct flotation and sulfating flotation. Direct flotation for the oxide ores is impractical because collectors are typically expensive, have low selectivity, and have low efficiency. On the other hand, sulfidation flotation requires reagents such as Na_2S, H_2S, and NaHS, which can modify the surface chemistry of copper oxides by forming a kind of "synthetic covellite." This is the most effective flotation method for copper oxides. Nevertheless, it presents the condition that must be strictly controlled for pulp potential and reagent concentration because sub-optimal amounts lead to low copper recovery. At the same time, overdoses result in over-sulfuration, which causes a depression of the valuable mineral[4].

Due to the above, the recovery of copper from low-grade ores through hydrometallurgical routes has gained importance. In addition, it also presents some advantages such as short construction time, low cost, operational simplicity, good performance, and it is friendly to the environment[5][6]. These ores are generally leached with acid media such as sulphuric acid, nitric acid, and hydrochloric acid. However, it is possible to find these copper minerals associated with other oxide minerals and carbonates with high calcium and magnesium content as gangue materials, which, when interacting with acid, can solubilize a variety of metallic cations, resulting in an excessive increase in acid consumption and potentially cause severe operational problems in the solvent extraction stage[2][7][8]. Additionally, in the case of some sulfides, low-leaching kinetics are observed[9]. For these reasons, multiple investigations have been carried out on the leaching of copper from low-grade ores using alternative reagents such as organic acids[10][11][12][13] or reagents in an alkaline medium such as cyanide[14][15], ammonia[3][7][16][17], and organic reagents. In particular, the latter presents some advantages over the acid medium, such as high selectivity in many cases, low corrosivity, and low reagent consumption[8][9]. However, challenges implementing conventional alkaline leaching agents, such as cyanide and ammonia, on an industrial scale are significant due to problems of toxicity, volatility, recovery difficulties, and environmental impact[2][4][9][18][19]. Alkaline glycine has also been reported to selectively leach copper from different sources, such as oxides[2][20], sulfides[8][9][19][21], and metals[18][22].

Recent studies by the authors of the present paper have reported the leaching of Au from pure foils and e-waste[23][24], as well as preliminary results of Cu leaching[25][26], using monosodium glutamate and an oxidant (such as H_2O_2 or $KMnO_4$). Monosodium glutamate, an environmentally benign salt derived from glutamic acid, can bind in a tridentate fashion with metal ions and leaches copper by forming a stable copper (II) glutamate complex[26]. According to Perea et al. (2022), alkaline glycine solution leaches copper from tenorite efficiently, obtaining 90% recovery at 30°C for 24 hours and nearly 100% at 60°C in 2 hours[27]. The authors have also observed that copper can be recovered from alkaline glutamate solutions through metal sulfide precipitation. It is a method of metal removal used in industry with some advantages, such as a lower solubility of metal sulfide precipitates, the ability to remove metal selectively, the ability to react rapidly, better-settling properties, and the ability to re-use sulfide precipitates by smelting[28]. This study proposes two stages of a conceptual process: (i) leaching copper from tenorite and copper sulfide concentrate in alkaline glutamate solutions at room or elevated temperatures using oxygen as an oxidant for sulfide ores, and (ii) PLS treatment by sulfide precipitation of copper by addition of NaHS.

EXPERIMENTAL

Samples preparation and characterization

The experiments were carried out using samples of synthetic tenorite (CuO) and copper sulfide concentrate obtained from Merck and a Chinese supplier. These synthetic ores were characterized with a Malvern Mastersizer instrument to determine the particle size distribution. The results showed that these samples comprised a fine powder with 90 % particle sizes below 39 µm for the tenorite and 38 µm for copper sulfide concentrate composed mainly of covellite (CuS), lyonsite ($Cu_3Fe_4(VO_4)_6$), bonattite ($CuSO_4•3H_2O$), brochantite ($Cu_4SO_4(OH)_6$), and antlerite ($Cu_3(SO_4)(OH)_4$). X-ray diffraction (XRD) analysis to determine the mineralogy of the samples indicated that copper oxide is almost 100% composed of tenorite, for the case of copper sulfide concentrates, in addition to the mentioned copper sulfide, contain hendersonite ($Ca_2V_9O_{24}•8H_2O$) and ferroactinolite ($(Ca, Na, K)_2Fe_5Si_8O_{22}(OH)_2$). Also, the chemical compositions of the samples were determined by X-ray fluorescence spectrometry, as shown in Table 1.

Table 1: Percentage of the elemental composition of the synthetic copper samples determined by XRF.

Sample	Al	Si	P	S	Cl	Ca	Cu	Zn	As	Th	LE
Tenorite	0.59	0.7	0.27	0.0	1.93	0.17	73.88	<LOD	<LOD	0.76	21.52
Sulfide concentrate	0.33	0.41	0.18	7.4	1.6	0.33	42.9	0.05	0.04	0.36	46.4

LE: Light elements, which cannot be detected, include O, Na, C, and N.
LOD: Limit of detection

Copper oxide leaching

All experiments were conducted using solutions prepared from analytical grade reagents and deionized water in a 250 mL glass reactor. The leaching tests were carried out using 1 gram of tenorite (0.5% w/v) in 200 mL of 0.5 M glutamate solutions at 30, 45, and 60°C through water-bath heating at atmospheric pressure and employing magnetic stirring at 300 rpm. At different times, ten samples of 3mL leach solution were collected using a syringe-membrane filter with a pore size of 0.45 um. The copper concentrations in the filtrates were determined using atomic absorption spectrophotometry (AAS).

Copper sulfide leaching

For the leach test with dissolved oxygen (DO) control, the DO level in the leach pulp remained between a range of 10 to 15 ppm. Leaching tests were carried out at 30, 45, and 60°C in a 2 L glass reactor with slurry agitated at 300 rpm with an overhead stirrer. The tests were done using 10 grams of copper sulfide concentrate, added in 2 L alkaline monosodium glutamate solutions. Sodium hydroxide was used to adjust the solution's initial pH to 9.4. The DO level of the leach solution was measured and controlled over the whole leaching time using a RH-8301 DO controller and solenoid valve, as shown in Figure 1.

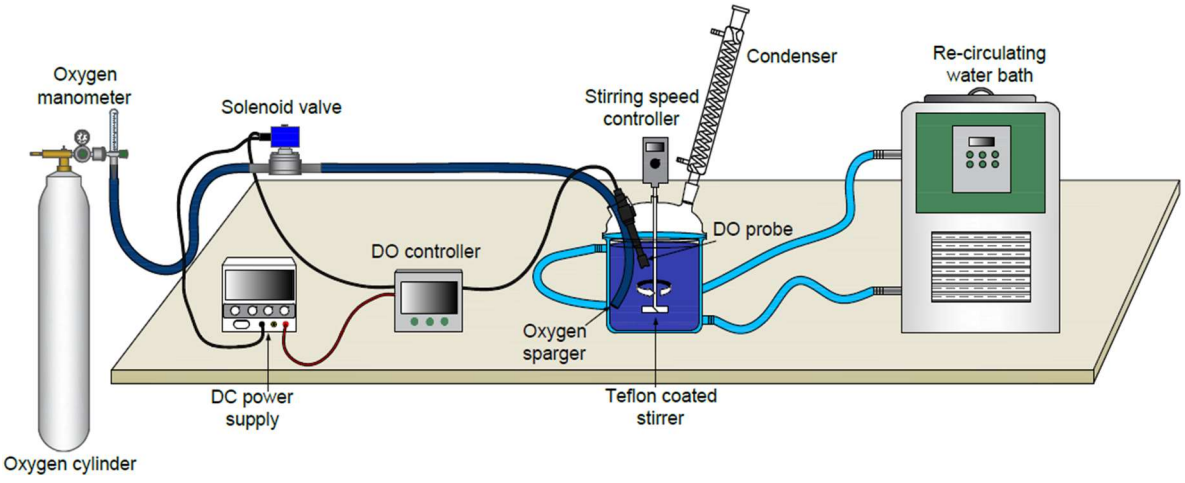

Figure 1. Diagram of copper sulfide leaching apparatus setup.

Copper recovery

Precipitation tests were carried out using synthetic pregnant solutions (PLS) prepared with a concentration of 2.5 g Cu/L and 0.5 M glutamate using pentahydrate copper sulfate ($CuSO_4 \cdot 5H_2O$) and sodium L-glutamate hydrate ($C_5H_{10}NNaO_5$). Sodium hydrosulfide hydrate ($NaHS \cdot 1.5H_2O$) was added in different [Cu]:[NaHS] molar ratios in a 200 mL copper glutamate solution agitated at 300 rpm, pH 9.4, and room temperature. Samples of 10 mL copper glutamate solution were obtained using a syringe-membrane filter after 10 minutes. These samples were analyzed through AAS to determine copper recovery from the glutamate solution. An optical microscope (Leica DM 750 microscope connected to a digital camera HD 5 MGPXL WI-FI, Leica ICC50W) was used to analyze the copper sulfide precipitates after NaHS precipitation to obtain images that can then be analyzed and processed digitally to determine particle size and shape semi-quantitatively[29].

RESULTS AND DISCUSSION

Tenorite leaching

Figure 2 shows that the glutamate solution is effective in leaching copper oxides. It can be seen that copper extraction increases as temperature increases. In 2 hours at 30°C, 52,5% of the copper dissolves, while at 60°C, around 97.7% of the copper dissolves over the same time. After 10 hours, the complete copper dissolution was obtained at 60°C, while at 30 and 45°C, 89% and 92% were obtained, respectively. Similar copper concentrations were obtained after 24 hours at these temperatures, which indicates copper dissolution stopped after 10 hours of leaching. That can be attributed to surface passivation generated by the chemical interaction of the surface with intermediate products generated at these temperatures, such as copper hydroxide[27].

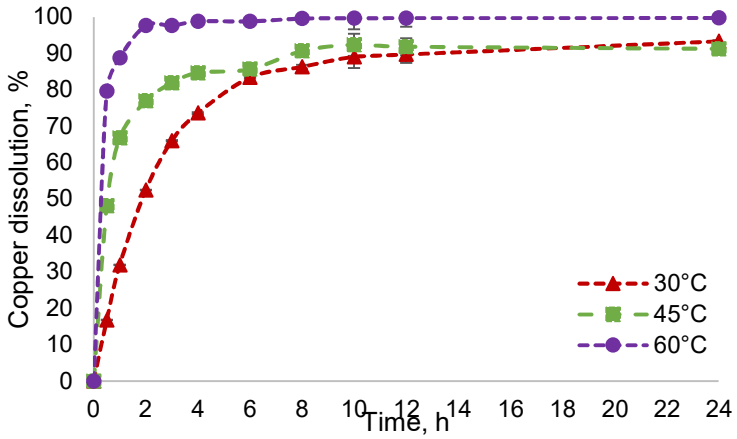

Figure 2. Tenorite leaching at different temperatures. Working conditions: pH = 9.4, glutamate concentration = 0.5 M, and solids content = 5% w/v[27].

Glutamate-controlled oxygen system

The relationship between temperature and copper dissolution rate from copper sulfide concentrate is shown in Figure 3. Like tenorite, the results indicate that temperature affects the copper dissolution rate. Although in the first 30 minutes, the three temperatures had a similar extraction, after 2 hours at 30, 45, and 60°C, the copper dissolution was 83.6%, 89%, and 97.4%, respectively. Achieving the complete dissolution of copper at 45 and 60°C in 6 hours and at 30°C after 12 hours.

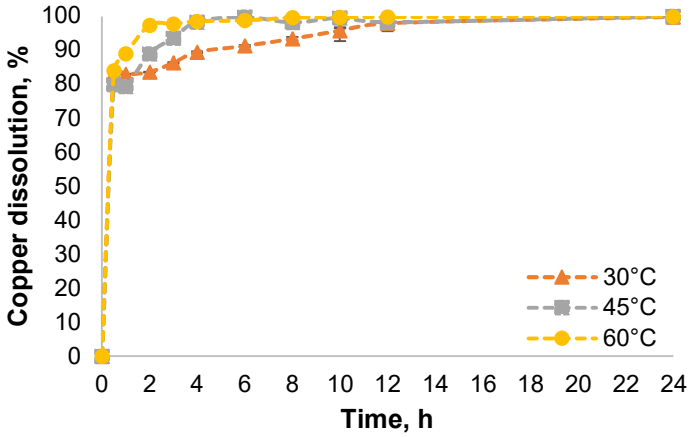

Figure 3. Copper sulfides concentrate leaching at different temperatures. Working conditions: pH = 9.4, glutamate concentration = 0.5 M, solids content = 5% w/v, and DO = 10 – 15 ppm.

Copper sulfide (NaHS) precipitation

In a typical SART process to achieve copper recovery levels greater than 85%, stoichiometric sulfide dosage values vary between 95 and 120%[30][31]. Therefore, for recovery by precipitation, NaHS was added to the synthetic pregnant liquor at [Cu_T]:[NaHS] molar ratios of 1:0.8, 1:1, and 1:1.2 to study the effect that this variable has on the copper recovery from the glutamate solution and the results are shown in Table 2. In this table, it can be seen that the copper removals increase with the increasing [Cu_T]:[NaHS] molar ratio. Obtaining a 99.2% of the copper was recovered from the solution at a [Cu_T]:[NaHS] molar ratio of 1:1.2 in 10 minutes of residence time.

Table 2: Copper extraction from copper glutamate aqueous solution using NaSH at room temperature and pH 9.4.

Sample	Cu Extraction, (%)
Cu:NaHS 1:0.8	71.26
Cu:NaHS 1:1	90.6
Cu:NaHS 1:1.2	99.2

The particle size of the sulfide precipitate was observed for each molar ratio by optical microscopy and image analysis. Figure 4 shows micrographs of suspension samples obtained for each test. As shown by these photos, copper sulfide precipitates formed with [Cu_T]:[NaHS] molar ratios of 1:0.8 and 1:1 have a high aggregation capacity, reaching a size of over 100 µm. While the particle size and aggregation capacity decrease with the increasing of [Cu_T]:[NaHS] molar ratio to 1:1.2. The optical micrographs in Figure 4 are supplemented with semi-quantitative cumulative aggregate size distribution curves derived from image analysis and processing (Figure 5). Ratifying that 90% of particles reached aggregation sizes over 100 µm with [CuT]:[NaHS] molar ratios of 1:0.8 and 1:1. On the other hand, the [CuT]:[NaHS] molar ratio of 1:1.2 showed a maximum aggregation size of 9.1 µm. According to this study, the higher the concentration of NaHS, the faster nucleation occurs, forming very fine particles, which can aggregate before Ostwald ripening dissolves fine particles and redeposits them on larger ones. While at lower concentrations, this happens much slower and more systematically, forming larger primary particles and often subsequently aggregates, which is in accordance with previous research[32].

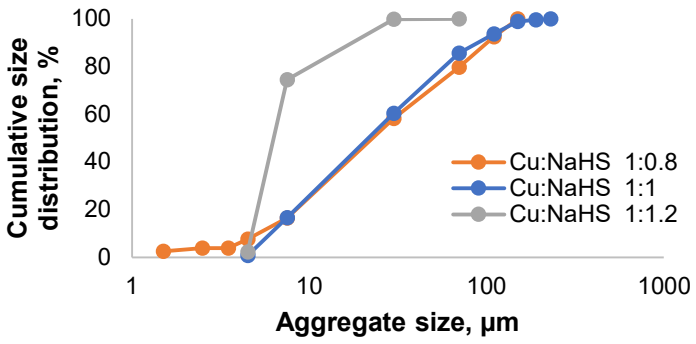

Figure 4. Semi-quantitative cumulative aggregate size distribution curves.

a)

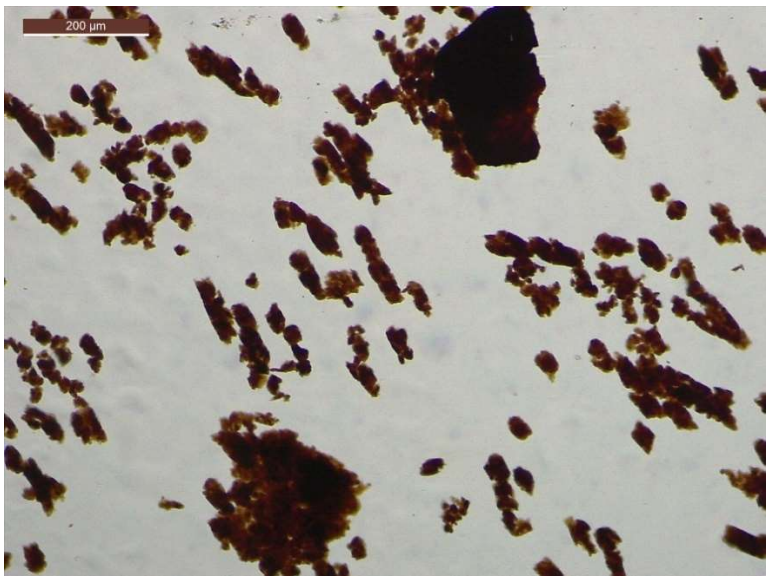

b)

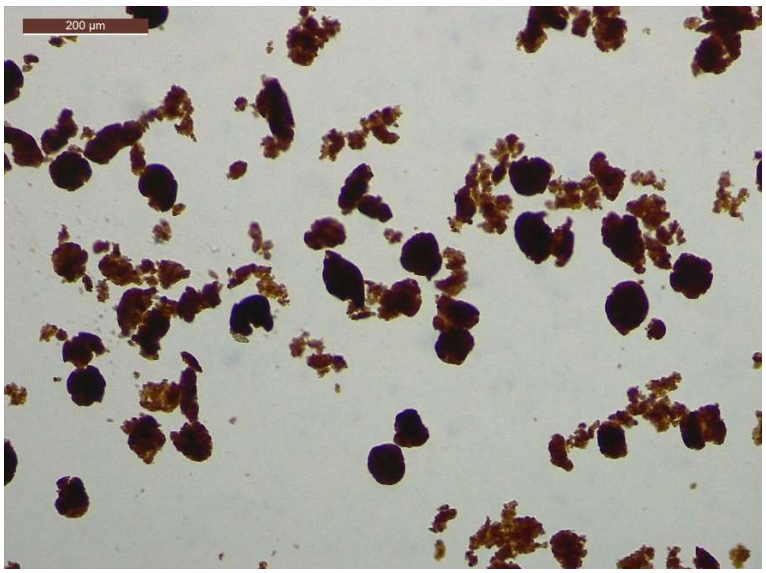

c)

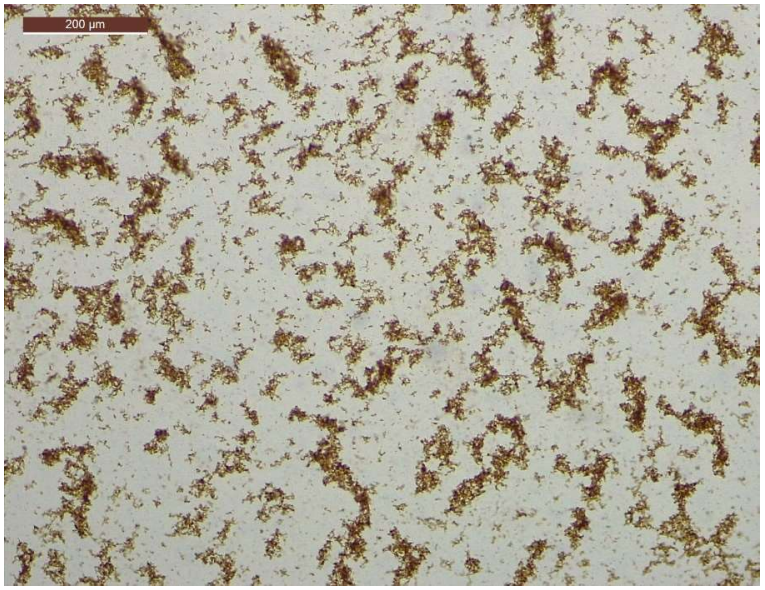

Figure 5. Optical micrographs of copper sulfide precipitates. a) Cu:NaHS 1:0.8, b) Cu:NaHS 1:1, c) Cu:NaHS 1:1.2

Process flowsheet for alkaline glutamate leaching

An integrated copper leaching process can therefore be formed in alkaline glutamate systems by combining copper oxide and sulfide minerals, followed by a stage of copper precipitation and solid-liquid separation to recover copper from the solution and restore glutamate pH 9.4. Figure 6 shows the schematic diagram of the copper recovery. The first stage is the copper leaching in glutamate solutions at pH 9.4, followed by counter-current decantation (CCD) to recover pregnant leach solution (PLS) and eliminate tailings of the leaching process. Copper is recovered from the solution as copper sulfide precipitate using NaHS addition and is separated from the solution by solid-liquid separation using flocculants in a thickening stage and filtration. The allow recovery of the glutamate solution to be used again in the leaching process. However, it is necessary first to adjust the pH and add glutamate makeup, which is proportional to the loss of solution in the filtrate (% moisture in the filter cake) and the leach residue.

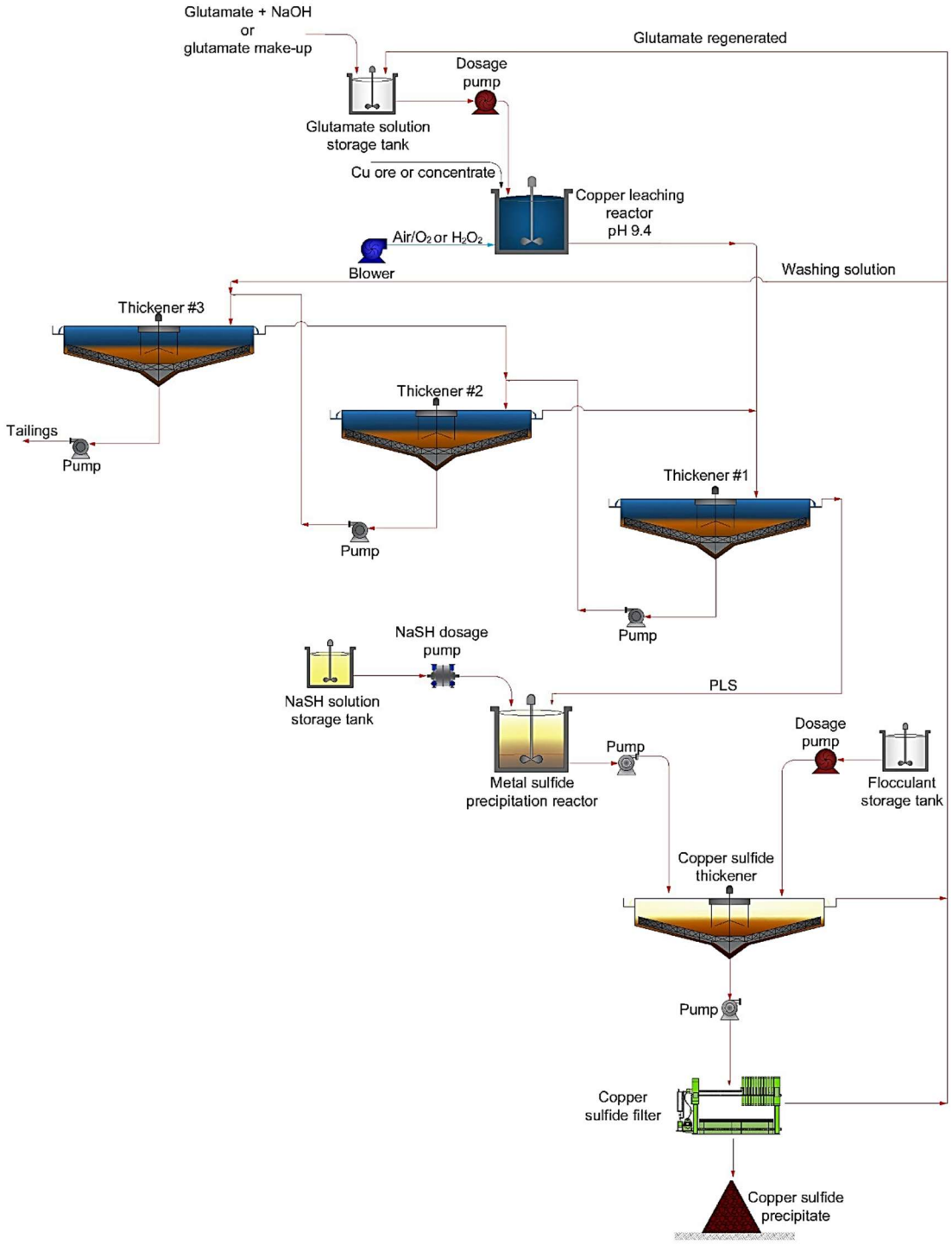

Figure 6. Flowsheet for alkaline glutamate copper leaching and recovery by sulfide precipitation.

CONCLUSIONS

An alkaline process for extracting copper from copper oxides and sulfides has been proposed, as well as the chemistry involved in the main steps of the process, including reagent recirculation. Achieving copper recoveries over 90% at 30°C converts this process into a potential option for the heap leaching of copper oxide and sulfide. However, the temperature significantly influences the kinetics leaching noted, obtaining an almost complete dissolution of copper from tenorite and sulfide concentrate in just 2 hours at 60°C, suggesting mild heating of the leach pulp could improve process efficiency. In addition, the results show that copper can be selectively recovered from glutamate solutions by sulfide precipitation, obtaining a higher grade and smeltable concentrate. Finally, to extract copper from oxides and sulfides, a conceptual flowsheet has been devised, which is technically feasible and can be an alternative for complex copper mineralization treatment that cannot be leached by acid media due to the content of gangue and oxidized minerals that consume acid.

ACKNOWLEDGEMENT

C. Perea gratefully acknowledges the financial support of ANID Chile through the ANID-PFCHA/National doctorate/2020- 21200126 and ANID Project AFB220002, and CODELCO through the “Piensa Minería” contest.

REFERENCES

1. Tabelin, C.B., Park, I., Phengsaart, T., Jeon, S., Villacorte-Tabelin, M., Alonzo, D., et al, 2021. Copper and critical metals production from porphyry ores and E-wastes: A review of resource availability, processing/recycling challenges, socio-environmental aspects, and sustainability issues. Resources, Conservation and Recycling 170(April):105610.

2. Tanda, B.C., Eksteen, J.J., Oraby, E.A., 2017. An investigation into the leaching behaviour of copper oxide minerals in aqueous alkaline glycine solutions. Hydrometallurgy 167:153–62.

3. Liu, Z.X., Yin, Z.L., Xiong, S.F., Chen, Y.G., Chen, Q.Y., 2014. Leaching and kinetic modeling of calcareous bornite in ammonia ammonium sulfate solution with sodium persulfate. Hydrometallurgy 144–145:86–90.

4. Conejeros, V., Pérez, K., Jeldres, R.I., Castillo, J., Hernández, P., Toro, N., 2020. Novel treatment for mixed copper ores: Leaching ammonia – Precipitation – Flotation (L.A.P.F.). Minerals Engineering 149(January):106242.

5. Mohanraj, G.T., Rahman, M.R., Arya, S.B., Barman, R., Krishnendu, P., Singh Meena, S., 2022. Characterization study and recovery of copper from low grade copper ore through hydrometallurgical route. Advanced Powder Technology 33(1):103382.

6. WANG, G. rong, LIU, Y. yuan, TONG, L. lin, JIN, Z. nan, CHEN, G. bao, YANG, H. ying, 2019. Effect of temperature on leaching behavior of copper minerals with different occurrence states in complex copper oxide ores. Transactions of Nonferrous Metals Society of China (English Edition) 29(10):2192–201.

7. LIU, W., TANG, M. tang, TANG, C. bo, HE, J., YANG, S. hai, YANG, J. guang, 2010. Dissolution kinetics of low grade complex copper ore in ammonia-ammonium chloride solution. Transactions of Nonferrous Metals Society of China (English Edition) 20(5):910–7.

8. Tanda, B.C., Eksteen, J.J., Oraby, E.A., 2018. Kinetics of chalcocite leaching in oxygenated alkaline glycine solutions. Hydrometallurgy 178(May):264–73.

9. Eksteen, J.J., Oraby, E.A., Tanda, B.C., 2017. A conceptual process for copper extraction from chalcopyrite in alkaline glycinate solutions. Minerals Engineering 108:53–66.

10. Deng, J., Wen, S., Deng, J., Wu, D., Yang, J., 2015. Extracting copper by lactic acid from copper oxide ore and dissolution kinetics. Journal of Chemical Engineering of Japan 48(7):538–44.

11. Biswas, S., Mulaba-bafubiandi, A.F., 2016. Extraction of Copper and Cobalt from Oxidized Ore using Organic Acids. Hydrometallurgy Conference 2016: Sustainable Hydrometallurgical Extraction of Metals (August).

12. Habbache, N., Alane, N., Djerad, S., Tifouti, L., 2009. Leaching of copper oxide with different acid solutions. Chemical Engineering Journal 152(2–3):503–8.

13. Shabani, M.A., Irannajad, M., Azadmehr, A.R., 2012. Investigation on leaching of malachite by citric acid. International Journal of Minerals, Metallurgy and Materials 19(9):782–6.

14. Rojas, N., Bustamante, O., 2007. Disolución de cobre en cianuración convencional proveniente de ferrita cúprica. Dyna 74:151–7.

15. Medina Ferrer, F., Dold, B., Jerez, O., 2021. Dissolution kinetics and solubilities of copper sulfides in cyanide and hydrogen peroxide leaching: Applications to increase selective extractions. Journal of Geochemical Exploration 230(July):106848.

16. Aracena, A., Vivar, Y., Jerez, O., Vásquez, D., 2015. Kinetics of dissolution of tenorite in ammonium media. Mineral Processing and Extractive Metallurgy Review 36(5):317–23.

17. Oudenne, P.D., Olson, F.A., 1983. Leaching kinetics of malachite in ammonium carbonate solutions. Metallurgical Transactions B 14(1):33–40.

18. Li, H., Oraby, E., Eksteen, J., 2020. Extraction of copper and the co-leaching behaviour of other metals from waste printed circuit boards using alkaline glycine solutions. Resources, Conservation and Recycling 154:1–12.

19. Tanda, B.C., Eksteen, J.J., Oraby, E.A., O'Connor, G.M., 2019. The kinetics of chalcopyrite leaching in alkaline glycine/glycinate solutions. Minerals Engineering 135(October 2018):118–28.

20. Tanda, B.C., Oraby, E.A., Eksteen, J.J., 2018. Kinetics of malachite leaching in alkaline glycine solutions. Mineral Processing and Extractive Metallurgy: Transactions of the Institute of Mining and Metallurgy 0(0):1–9.

21. Oraby, E.A., Eksteen, J.J., 2014. The selective leaching of copper from a gold-copper concentrate in glycine solutions. Hydrometallurgy 150:14–9.

22. Oraby, E.A., Li, H., Eksteen, J.J., 2019. An Alkaline Glycine-Based Leach Process of Base and Precious Metals from Powdered Waste Printed Circuit Boards. Waste and Biomass Valorization 11(8):3897–909.

23. Perea, C., 2018. Procesos alternativos al cianuro para la disolución de oro. Mauritius: Editorial Académica Española.

24. Perea, C.G., Restrepo, O.J., 2018. Use of amino acids for gold dissolution. Hydrometallurgy 177(March):79–85.

25. Perea, C., Restrepo Baena, O.J., 2016. Alternatives process to cyanide for gold dissolution. In: Universidad Nacional de Cuyo. Secretaría de Ciencia T y P-EBDUnc, editor. XIII Jornadas Argentinas Trat. Miner. Mendoza, Argentina: Universidad Nacional de Cuyo. Secretaría de Ciencia, Técnica y Posgrado - Ediciones Biblioteca Digital UNCuyo. p. 2–7.

26. Perea, C.G., Restrepo Baena, O.J., Ihle, C.F., Estay, H., 2021. Copper leaching from wastes electrical and electronic equipment (WEEE) using alkaline monosodium glutamate: Thermodynamics and dissolution tests. Cleaner Engineering and Technology 5:1–7.

27. Perea, C.G., Ihle, C., Estay, H., Dyer, L., 2022. An investigation into the leaching behavior of tenorite in aqueous alkaline monosodium glutamate solutions. In: The Chilean Institute of Mining Engineers (IIMCh), editor. Copp. 2022 Int. Conf., vol. 4. Santiago, Chile: The Chilean Institute of Mining Engineers. p. 254–62.

28. Lewis, A.E., 2010. Review of metal sulphide precipitation. Hydrometallurgy 104(2):222–34.

29. Gim-Krumm, M., Quilaqueo, M., Rojas, V., Seriche, G., Ruby-Figueroa, R., Cortés-Arriagada, D., et al, 2019. Impact of precipitate characteristics and precipitation conditions on the settling performance of a sulfide precipitation process: An exhaustive characterization of the aggregation behavior. Hydrometallurgy 189(August):105150.

30. Deng, Z., Oraby, E.A., Eksteen, J.J., 2019. The sulfide precipitation behaviour of Cu and Au from their aqueous alkaline glycinate and cyanide complexes. Separation and Purification Technology 218(March):181–90.

31. Estay, H., 2018. Designing the SART process – A review. Hydrometallurgy 176(January):147–65.

32. Sampaio, R.M.M., Timmers, R.A., Xu, Y., Keesman, K.J., Lens, P.N.L., 2009. Selective precipitation of Cu from Zn in a pS controlled continuously stirred tank reactor. Journal of Hazardous Materials 165(1–3):256–65.

COPPER LEACHING USING GLYCINE LEACHING TECHNOLOGY

By

Mining and Process Solutions Pty. Ltd, Australia

Presenter and Corresponding Authors

Associate Professor Elsayed Oraby
elsayed.oraby@curtin.edu.au

Dr Glen O'Malley, R & D Manager
gomalley@mpsinnovation.com.au

ABSTRACT

Mining and Process Solutions (MPS) Glycine Leaching Technology (GLT) is also being developed to leach base metals such as copper. We found the GlyLeach™ process can unlock oxide copper deposits that are hosted in carbonates. Such deposits cannot be process through traditional acid leaching due to very high acid usage. But more recently we have also had success in leaching remnant copper from spent heaps in the pursuit of gold through our acidic process (GT™) and copper concentrate leaching with the use our GlyLeach™ and GlyAmm™ processes. The copper leached are sulphides which shows GLT can leach oxide and sulphide copper minerals from ores, concentrate and tails.

Both GlyLeach™ and GlyAmm™ are alkaline leaching processes that can complex copper to form copper glycinate complexes. The real advantages of GlyLeach™ are its ESG benefit of being non dangerous good and harmless to humans and environment, but it also leaves unwanted metals intact such as iron, aluminium silicon and manganese in the residue. Downstream metals recovery for glycine leaching technologies uses existing known processes such as solvent extraction, precipitation, or ion exchange resins to recover the copper from solution. GT™ is our acidic process which can not only leach remnant copper but also the gold from spent heaps. Downstream recovery of the copper from GT™ can be by solvent extraction, precipitation, or ion exchange resins with the gold being recovered onto activated carbon.

This paper updated on the progress of GlyLeach™, GlyAmm™ and GT™ processes for the recovery of copper from oxide and sulphide copper minerals contained in ores, concentrate and tailings where it's our hope to do a site demonstration within 2023 to demonstrate viable process solutions to recover copper from spent heaps, hosted in carbonaceous matrix and from concentrates.

Keywords: Glycine Leaching, GlyLeach™ Process, remnant copper, gold, oxide minerals, sulphide minerals, heap leaching

Content

- Background on GLT
- Chemistry
- Leaching Testwork
- Copper Recovery
- Questions

Introduction

- ❑ Copper deposits are often complex (e.g. porphyries) with significant mineralogical variation in depth.
- ❑ Grades are declining - milling & flotation becoming less economic
- ❑ Acid consuming gangue in oxide zone
- ❑ Altered silicates often lead to silica gel formation during acid leach processes.
- ❑ Native copper often problematic.
- ❑ Gold often associated with copper and copper significant problem during cyanidation.
- ❑ Elemental sulfur problematic during acid leaching of Cu-sulfides.
- ❑ pH (acid-base swing for Cu-Au ore leaching)

Alkaline Vs Acidic leaching

- Alkaline leaching of copper is:
  - ✓ More selective.
  - ✓ Less corrosive.
  - ✓ Lowering reagent consumption.
  - ✓ No special materials of construction are required.
  - ✓ No sulfur, gels and jarosite precipitation.
  - ✓ Particularly useful when followed by alkaline gold or silver leaching (cyanide or glycine based).
  - ✓ Does not passivate gold in a subsequent leach.
  - ✓ Convenience of using NaSH in alkaline domain and high SX extraction selectivity.

Advantages of Glycine Leaching at Alkaline pH

- Low cost, mass produced, available in bulk.
- Not toxic & environmentally benign.
- Simple chemistry and ease of control.
- Selectivity of Cu, Au and Ag over most typical gangue and iron minerals.
- Ease of recovery and reuse.
- Process simplicity and ease of Cu recovery.
- No transport and trade restriction.
- Stability over wide acid-base and redox range.
- Thermally stable and non-volatile.

Options of Glycine Leaching Technology

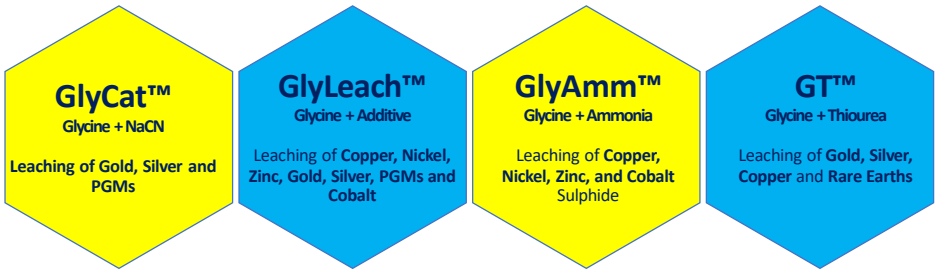

GLT- Copper Minerals Amenability

Mineral	Formulae	Extent of Extraction
Malachite	$CuCO_3.Cu(OH)_2$	>90%
Azurite	$2CuCO_3.Cu(OH)_2$	>90%
Cuprite	Cu_2O	>90%
Covellite	CuS	>90%
Chalcocite	Cu_2S	>90%
Digenite	Cu_9S_5	>90%
Bornite	$2Cu_2S.CuS.FeS$	85-95%
Chalcopyrite	$CuFeS_2$	70-95%
Enargite	Cu_3AsS_4	40-70%
Tetrahedrite	Cu_3SbS_3 & $x(Fe,Zn)_6Sb_2S_9$	40-70%
Dioptase	$CuSiO_2(OH)_2$	>90%
Chrysocolla	$(Cu,Al)_2H_2Si_2O_5(OH)_4.n(H_2O)$	20-90%

Cu-NH_3 vs Cu-Glycine

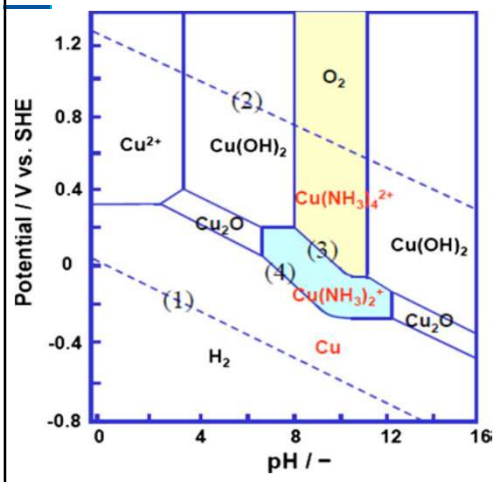

Cu-NH_3

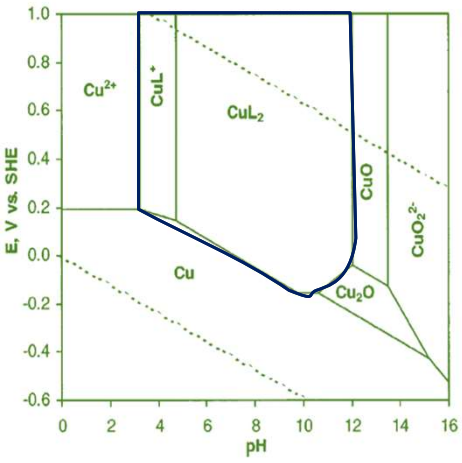

Cu- Glycine

GlyLeach™ Chemistry

- **Leaching of copper and copper minerals**

$Cu + 2\,NH_2CH_2COO^- + 0.5\,O_2 + H_2O \rightarrow Cu(NH_2CH_2COO)_2 + 2\,OH^-$ (Cupric- Main Species)

$Cu + 2\,NH_2CH_2COO^- + 0.25\,O_2 + 0.5\,H_2O \rightarrow Cu(NH_2CH_2COO)_2^- + OH^-$ (Cuprous- Possible)

$2\,CuCO_3Cu(OH)_2 + 8\,NH_2CH_2COO^- + O_2 + 2\,H_2O \rightarrow 4\,Cu(NH_2CH_2COO)_2 + 4\,OH^- + 2\,CO_3^{2-}$

$Cu_2O + 4\,NH_2CH_2COO^- + 0.5\,O_2 + 2\,H_2O \rightarrow 2\,Cu(NH_2CH_2COO)_2 + 4\,OH^-$

$Cu_2S + 4\,NH_2CH_2COO^- + 2.5\,O_2 + H_2O \rightarrow 2\,Cu(NH_2CH_2COO)_2 + SO_4^{2-} + 2\,OH^-$

$CuFeS_2 + 2\,NH_2CH_2COO^- + 4\,O_2 + 2\,OH^- \rightarrow Cu(NH_2CH_2COO)_2 + Fe(OH)_2 + 2\,SO_4^{2-}$

- **Glycine can also leach other base metals like nickel, cobalt and zinc**

GlyAmm™ Chemistry

- **Leaching of copper and copper minerals**

$$Cu + 2\,NH_2CH_2COO^- + NH_4^+ + 0.25\,O_2 + 0.5\,H_2O \rightarrow CuNH_4(NH_2CH_2COO)_2 + OH^-$$

$$2\,CuCO_3Cu(OH)_2 + 8\,NH_2CH_2COO^- + NH_4^+ + O_2 + 2\,H_2O \rightarrow 4\,CuNH_4(NH_2CH_2COO)_2 + 4\,OH^- + 2\,CO_3^{2-}$$

$$Cu_2O + 4\,NH_2CH_2COO^- + NH_4^+ + 0.5\,O_2 + 2\,H_2O \rightarrow 2\,CuNH_4(NH_2CH_2COO)_2 + 4\,OH^-$$

$$Cu_2S + 4\,NH_2CH_2COO^- + NH_4^+ + 2.5\,O_2 + H_2O \rightarrow 2\,CuNH_4(NH_2CH_2COO)_2 + SO_4^{2-} + 2\,OH^-$$

$$CuFeS_2 + 2\,NH_2CH_2COO^- + NH_4^+ + 4\,O_2 + 2\,OH^- \rightarrow CuNH_4(NH_2CH_2COO)_2 + Fe(OH)_2 + 2\,SO_4^{2-}$$

- **Benefit able to hold more copper in solution so applicable for treating concentrates**

Examples of leaching copper resources

Leaching Copper Concentrate- Sample 1

XRF analysis

Elemental analyses of the copper concentr

Element	Content
Cu, %	47.65
Ni, %	0.0115
Fe, %	19.65
Si, %	1.755
K, %	0.141
Mg, %	0.04
S, %	24.15
Mn, %	BDL
Co, %	0.1615
Zn, %	0.036
Au, g/t	20
Ag, g/t	259

PSD analysis

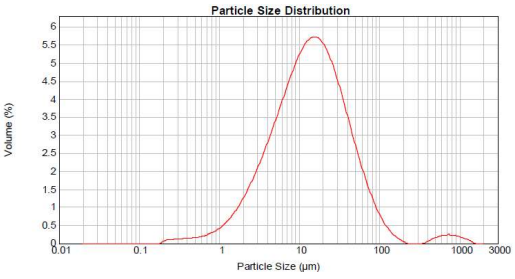

Particle size analysis of the copper concentrate

Parameters	Unit	Value
Surface area	m^2/g	0.352
P80	µm	33.204
Passing 75 µm	%	94.85

Pre-oxidisation of copper concentrate

Effects of grinding

Test ID	Test 1	Test 2	Test 3
Solid, %	20%	20%	20%
K:S	2.1:1	2.1:1	2.1:1
Temperature, °C	75	75	75
Pre-OX time, h	24	24	24
Grinding time, min	0	30	5
P80, µm	33.2	15.7	20.3

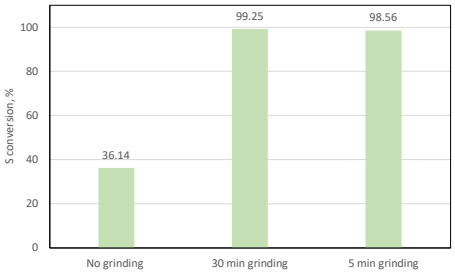

- High S conversions were achieved at 30 and 5 min of grinding, at 99.25% and 98.56%, respectively .
- Longer pre-OX time and higher temperature are required.

Pre-oxidisation of copper concentrate

Effects of pre-oxidation time

Test ID	Test 4	Test 5	Test 6	Test 7
Solid, %	20%	20%	20%	20%
K:S	2.1:1	2.1:1	2.1:1	2.1:1
Temperature, ° C	75	75	75	75
Pre-OX time, h	24	8	4	16
Grinding time, min	30	30	30	30

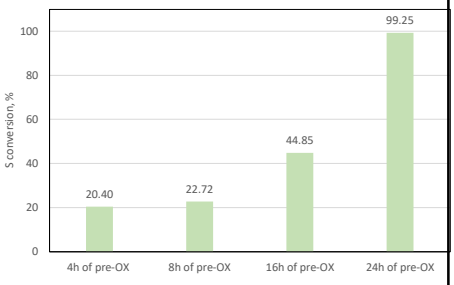

- The sulphide oxidisation increased with the pre-oxidation time.
- The sulfide oxidisation is only 45% at 16 hours, but it increased to 99% at 24 hours.

Leaching of the oxidised copper concentrate

Leach after pre-oxidation

Conditions,	10% solid	5% solid	pH 9.5	pH 11.5	Gly:Cu=2:1	Gly:Cu=4:1	Gly:Cu=6:1
Cu extraction, %	98.50	99.01	98.08	95.15	96.02	98.71	75.15
Accountability, %	100.87	103.96	104.06	100.84	99.83	102.93	92.86

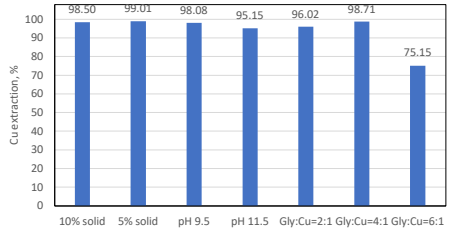

Leach conditions

Test ID	Test 8	Test 9	Test 10	Test 11	Test 12	Test 13	Tet 14
Solid, %	10%	5%	10%	10%	10%	10%	10%
Target pH	10.5	10.5	9.5	11.5	10.5	10.5	10.5
pH modifier	NH3+ KOH	NH3+ KOH	NH3+ KOH	NH3+ KOH	NH3+ KOH	NH3+ KOH	NH3+ KOH
Gly:Cu mole ratio	3:1	3:1	3:1	3:1	2:1	4:1	6:1
Ammonia dosage, M	0.71	0.53	0.45	1.31	0.64	1.18	1.04
KOH, kg/t	499	723	0	1087	394	874	1474
Temperature, °C	35	35	35	35	35	35	35
Leach time, h	30	30	30	30	30	30	30

Different stages for Copper concentrate Leaching

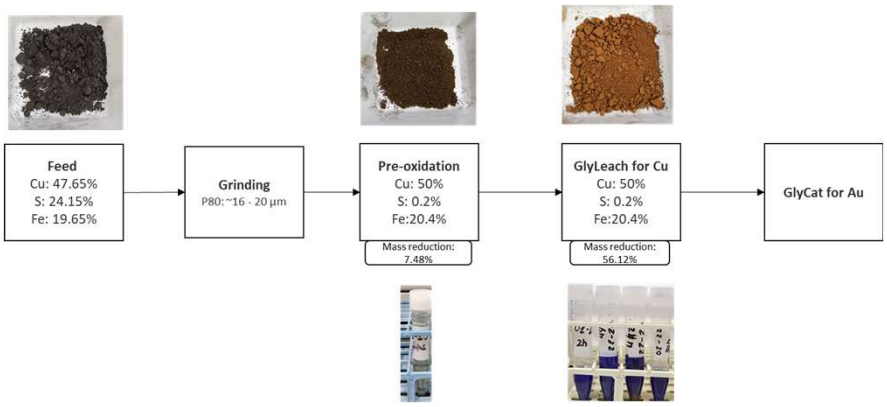

Concentrate Leaching: Optimum Conditions

Example 1 – 46.0% Cu, 0.165% Co

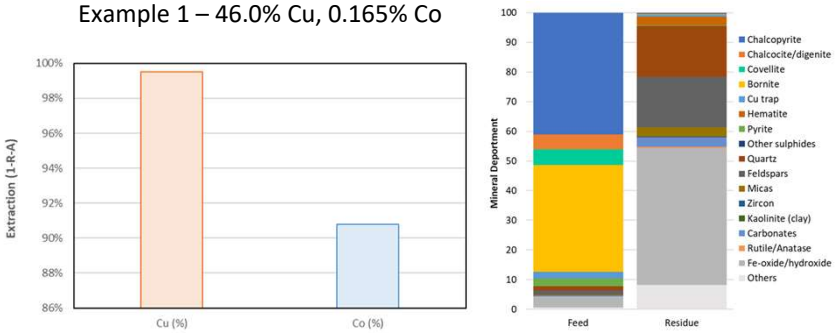

Grinding, pre-oxidisation, P_{80} 15 µm, Gly:Cu molar ratio 3:1, pH 10 and 60°C

Leaching of copper concentrate- Sample 2

Head Assay

Assay ID	Sample	Au (ppm)	Ag (ppm)	Cu (%)	Co (ppm)	S (%)
COPE-01-001	Feed	0.20	334	31.1	242	15.95

Sizing

- Malvern laser analysis at ALS Metallurgy.
- As received sample: P_{80} of 56.6µm - 88% passing 75 microns
- Gruond to ~ P_{80} of 8-15 microns

Fine Grinding

Pre-oxidisation of copper concentrate- Sample 2

- As received sample oxidised **69.5%** of the sulphide
- Ground Sample oxidised **86%** of the sulphide

Test no:		1	2
Method:		Oxidation	Oxidation
Material		Concentrate	Concentrate
Duration	h	30	30
Solids Density	%	20.0%	20.0%
Sizing		Ground	As Is
pH		12.00	12.00
Average pH		14.32	14.44
Average ORP	mV	-411	-429
Head	g/t	0.19	0.19
Residue	g/t	0.20	0.20
Extraction (1-R/AH)	%	-1.1%	-1.8%
Accountability Au	%	101.1%	101.8%
Head	g/t	334	334
Residue	g/t	328	286
Extraction (1-R/AH)	%	5.7%	17.2%
Accountability Ag	%	112.5%	97.1%
Head	%	311,000	311,000
Residue	%	322,500	310,000
Extraction (1-R/AH)	%	0.4%	3.6%
Accountability Cu	%	99.6%	96.4%
Head	%	15.95	15.95
Residue	%	2.33	5.03
Extraction (1-R/AH)	%	86.0%	69.5%
Accountability S	%	109.8%	108.7%
Reagent additions			
Caustic	kg/t	586.0	585.3

Leaching of copper (As Received)- Sample 2

- *GlyAmm™ shown to be best option for copper leaching*

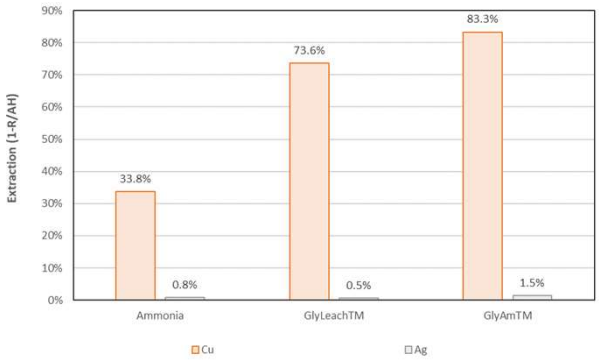

Leaching of copper concentrate- Oxidised

- *GlyAm*^{TM} is still the best process to recover the most copper
- Ammonia leached more silver, followed by *GlyLeach*^{TM}
- High copper recovery
- Milling improve both the copper and silver dissolutions

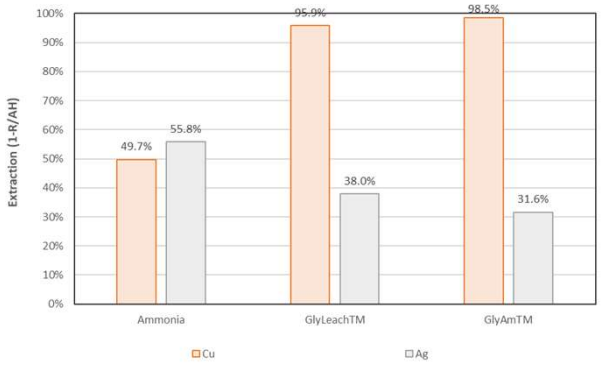

Concentrate Leaching- Optimum Conditions

Example 2 – 31.1% Cu, 0.024% Co

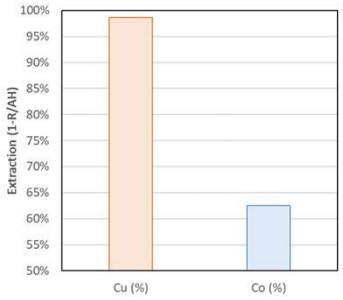

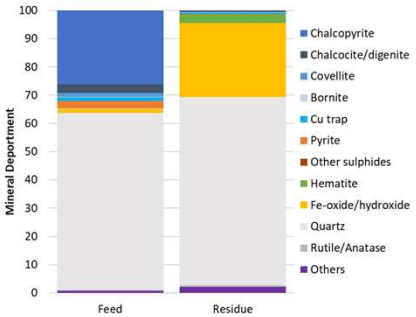

Grinding, oxidisation, GyI:Cu molar ratio 3:1, pH 10 and 60^{o}C

Results Summary Overall

Sample	Au (%)	Ag (%)	Cu (%)	Co (%)
Ground	74.9%	97.2%	98.7%	62.5%
As Received	62.3%	93.6%	89.8%	62.9%

Examples of Ore Leaching

Example 3 – 0.48% Cu

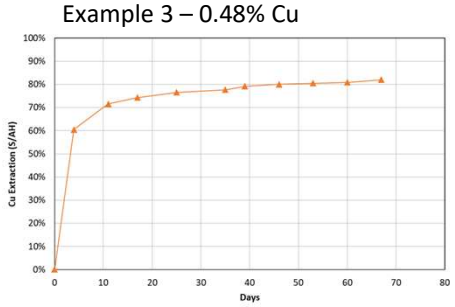

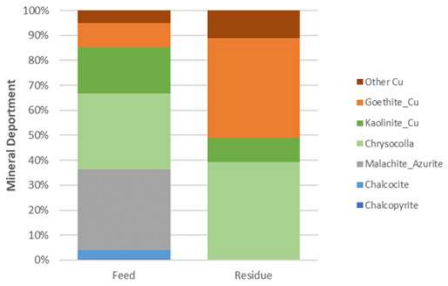

Column Leach, -10 mm, pH 10 and room temperature

Copper recovery from glycinate solution: NaSH precipitation

Sulfide ions were added to the pregnant liquor at different Cu:S^{2-} molar ratios in order to recover copper from the glycine solution.

The copper recovery was up to 99.1% as copper sulfide, Covelite (CuS) at Cu:S^{2-} molar ratio of 1:1 in 10 minutes contact time.

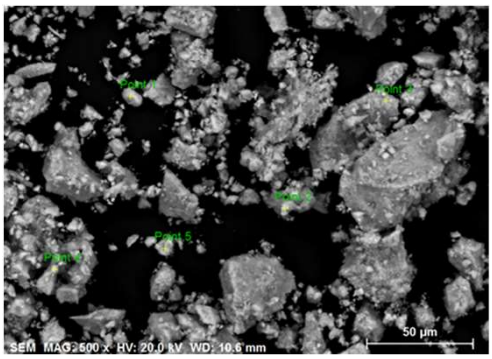

Copper recovery from glycinate solution: Solvent Extraction

Solvent extraction (SX) experiments show that copper glycinate can be easily extracted from the alkaline aqueous medium. Extractant: LIX 84

Concentration in Aqueous Phase, (mg/L)			Extraction, (%)	Stripping, (%)
Sample ID	Equip. pH	Cu	Cu	Cu
Feed	11.5	3596		
Test 1	9.4	65.6	98.2	100
Test 2	10	22.3	99.4	100

Conclusion

- ❑ GlyLeach™, GlyAmm™ and GT™ can extract copper from different copper minerals
- ❑ Glycine leaches copper oxides faster than copper sulfides
- ❑ Pre-oxidisation step is required to extract copper from chalcopyrite concentrates
- ❑GLT works great for high acid consumable copper deposits
- ❑ All processes can recover the copper from solution using existing processes like sulfide precipitation, ion-exchange or solvent extraction
- ❑ Glycine main losses (<5%) occur through adsorption and water loss in the residue
- ❑ Glycine oxidation (<1%) can occur, but determined to be minimal
- ❑ Glycine-ammonia mixture is suitable for high grade copper concentrates.
- ❑ Sulfate removal step is required before glycine recycling.

THE HALION LOOP: COPPER MADE GREEN

By

Dave Sammut

Loop Hydrometallurgy, Australia

Presenter and Corresponding Author

Dave Sammut
dave@loophydromet.com.au

ABSTRACT

Halide hydrometallurgy is widely recognised as offering superior economic and environmental outcomes for the leaching of a wide range of mineral concentrates: copper, nickel, rare earths, lead, zinc, silver, gold, PGMs and more.

Halide leaching is significantly faster than sulphate. Extremely high extraction can be achieved without the need for high pressures, high temperatures, or complicated bacterial processes. The smaller, faster, more efficient leach processes therefore offer capital and operating costs that are only a fraction of conventional sulphate leaching or smelting.

With significantly stronger chelating power, halides can effectively leach a broader range of (more refractory) minerals. Halides can be used for direct extraction of gold, PGMs and other valuable by-products. They are also ideally suited to polymetallic or low-grade concentrates, as well as those that are contaminated with elements such as arsenic.

Metso-Outotec, JX Nippon Mining & Metals and Intec have collectively spent over $100 million demonstrating fast and effective halide leaching processes for copper and other minerals. It can be fairly described as established technology.

However, halide leaching has until now been limited to very niche commercial applications because of difficulties in the direct recovery of the target metals via electrowinning. Unlike sulphate systems, halide electrolytes produce dendritic copper crystals rather than flat plates, and this has hampered E/W cell designs. Accordingly, most proponents of halide leaching have sought to use solvent extraction to allow conventional sulphate electrowinning, but the significant compromises required to make that possible have impeded commercialisation.

Loop Hydrometallurgy has developed a revolutionary new electrowinning cell design that makes practical the direct production of high purity copper from purified halide leachate. Starting from the Cu(I) state and operating at over 1,000A/m^2, this cell uses less than half the power required for conventional E/W. The anolyte is then fully recycled to the leach, which aids in the direct extraction of gold and PGMs.

Leveraging the extensive prior demonstration of halide leaching and more than 50 years of combined experience in the field, Loop Hydrometallurgy's E/W cell is now poised to bring to market the first commercially viable complete cyclic process for the production of high-grade copper from concentrates: at the bottom decile of the industry cost curve; at site; at atmospheric pressure, <100°C; with no noxious gas emissions or liquid effluents, and producing an environmentally stable hematite residue for on-site disposal.

This paper will discuss breakthrough technology for copper processing, and the opportunities to unlock value from Australian and international resources.

Keywords: Copper electrowinning, halide leaching, copper process, hydrometallurgy

INTRODUCTION

For much of the 20th century, a significant portion of copper demand was based on its use in infrastructure, particularly electricity and telecommunications. It is natural, then, that usage in these applications was proportionately greater in developing nations over the last decades, particularly in the rapid urbanisation and industrialisation of China and other Asian nations.

The last decade has seen a major swing in developed nations for the development and uptake of energy-efficient and renewable energy technologies, both in generation and usage. These newer technologies tend to be much more dependent on copper.

Speaking at 'Copper to the World 2022', Bloomberg Senior Metals Analyst Yi Zhu said that "copper demand arising from clean energy technologies may double by 2030 vs 2020 levels."(1)

As example, electric cars typically contain more than four times as much copper as the previous generation of vehicles. Each vehicle now contains approximately 90kg of copper. Copper is used extensively in the transformers, connectors and switches for the underlying electricity infrastructure. The International Copper Study Group notes that EV usage had tripled in 2021 to 16.5 million vehicles, since just 2018(2).

The massive growth in electric vehicle sales, both in China and in western nations; together with the associated copper-based upgrades in the infrastructure required to supply electricity to these vehicles, are both forecast to significantly enhance growth in demand. Goldman Sachs forecasts(3) that green demand will rise four-fold over the decade from 2020, representing over 16% of the total copper demand by 2030. Of the forecast annual growth of 500kT in growth of the global copper market, 300kT is directly attributable to growth in demand for green applications.

With 80% of the world's copper supply still coming from bronze age technology, the positive environmental credentials of these green applications is seriously compromised. The world needs greener sources of copper. But the fundamental divalent chemistry of copper in the sulphate processes that dominate both electrorefining (post-smelting) and electrowinning (inherent to virtually all leaching operations) puts a severe limitation on any attempts to save power – and therefore carbon footprint – from all current metal production.

It has long been understood that chloride hydrometallurgy offers a major breakthrough for that limitation. Copper forms a monovalent ion in chloride, the immediate effect of which is to halve the number of electrons required for reduction to metal, and therefore to halve the power required.

Until recently, no practical electrowinning cell had been designed that could efficiently produce high grade copper metal directly from cuprous chloride solution.

CHLORIDE HYDROMETALLURGY

Advantages

High Metal Solubility / Strong Chelation

The advantages of chloride hydrometallurgy have been well established(4)(5)(6)(7). Chlorides and/or mixed-halides can effectively and thoroughly leach a broad range of minerals, including many that are considered too refractory for other processes.

Metal chlorides are typically highly soluble, particularly with enhanced solubility via the formation of soluble chelates / complexes. This makes chloride processes significantly more efficient, with much smaller process liquor volumes compared to sulphate.

The strong chelating effect of chloride, together with its effect on ion activity(4), means that chloride leaching does not require high pressure and temperature. All of the 'typical' copper minerals: chalcocite, covellite, bornite and chalcopyrite can be leached to 99.5%+ extraction at atmospheric pressure and less than 100°C, in most cases without the need for ultra-fine grinding. Quoted timing varies, but residence times of <6 hours are typical for published chloride processes.

Feedstock Flexibility

This leaching power extends to more refractory copper minerals such as enargite. It also allows the direct leaching of gold and PGMs from mineral feedstocks, without the need for separate processing operations.

Unlike most sulphate leaching technologies, chloride leaching does not require the addition of pure or upgraded oxygen supply. Untreated air is sufficient, representing a significant reduction in capital cost compared to other hydrometallurgical technologies.

Polymetallic Extraction

Major companies including JX Nippon Mining & Metals and Metso-Outotec have developed processes (the Nikko-Chloride[8] and HydroCopper[9] processes, respectively) based upon chloride leaching. Australian variations including the Intec Copper Process[7][10] have also been developed, including multiple years of pilot plant and demonstration plant operations that have scaled up the technologies, and have successfully demonstrated the principles of chloride leaching of copper, as well as lead, zinc, nickel, silver, gold and PGMs. In doing so, these operations have thoroughly established the engineering and materials of construction suitable for chloride systems.

These companies have also demonstrated a range of other key 'upstream' advantages. Chloride hydrometallurgy can effectively and economically process much lower grade concentrates. The Intec Copper Process[7] could process concentrates at 15% Cu grade, and lower grades are likely also possible. This could be a major benefit at mines with poor grade recovery curves.

The same benefit can be leveraged at mines with polymetallic ore bodies. Significant extra metal can be captured between ore and concentrate if there is no need to compromise multiple competing grade-recovery curves to achieve smelter-grade products. Significant capital and operating cost could be saved if, as example, a given mine no longer required a cleaner circuit during flotation. Significant cost, power, and carbon footprint could also be saved where the need for fine- or ultra-fine grinding could be eliminated before leaching.

Furthermore, chloride processes can leach co-product and by-product metals directly, including non-cyanide extraction of gold and PGMs. This can have major advantages in environmentally sensitive areas and in well-regulated jurisdictions.

Monovalent Copper

Of all the advantages of chloride hydrometallurgy, perhaps the most clear and prominent is the massive power saving that could be leveraged from direct electrowinning of the monovalent copper ion. Additional power savings are then possible from the power savings of lower voltages (power = voltage x current).

Operating at very high comparative current density: 1,000+ A/m^2 vs <400 A/m^2 – will yield both energy and operating cost advantages, reducing the cathode area per tonne of copper production by more than 50%.

Table 1: Advantages of Chloride/Mixed-Halide Hydrometallurgy

Parameter	Primary Advantages	Secondary Advantages
High metal solubility	High extraction	No oxygen plant Reduced energy consumption Smaller physical plant Reduced OPEX Reduced CAPEX
Stronger chelation	Rapid leach kinetics	Atmospheric leaching Low temperature Reduced OPEX Reduced CAPEX

Feedstock flexibility	Lower grade concentrates Less grinding Refractory minerals	Improved grade/recovery Energy savings Higher recoveries
Polymetallic extraction	Direct gold & PGM recovery Pb, Zn, Ni, Co, Ag, REEs	Improved grade/recovery
Monovalent copper	50%+ electrowinning power reduction	Reduced carbon footprint

Disadvantages

Materials of Construction

Among the disadvantages of chloride systems is that the materials of construction are more problematic than conventional sulphate. The chloride-enhanced galvanic couple between copper ions and iron means that chloride systems will rapidly corrode virtually any ferrous metal, including most ferrous alloys that would otherwise be considered 'chloride resistant'. This disadvantage has been largely overcome with the advent of modern materials, most particularly the diverse range of polymers that have become ubiquitous in industrial application over the last 30 years.

Metal Separation

A greater challenge lies in the chelating strength of chloride. While this is immensely useful for achieving rapid and thorough leaching, the fact that most metal chloride salts are soluble - particularly in high chloride systems where there is an excess of chloride supporting the formation of soluble metal chloride complexes - results in complex polymetallic process liquors.

In turn, this makes the purification of the liquors more complicated from chloride. Sulphate systems generally rely on a combination of the low solubility of most metal sulphates and the rejection of non-target metals during solvent extraction to achieve copper sulphate solutions of sufficient purity for electrowinning or electrorefining. This inherent solubility differential between copper and other metals is the basis of the formation of 'anode slime' waste.

Over the last fifty years, techniques have been developed and proven to selectively recover other metals from chloride systems. These use a combination of pH, temperature, redox chemistry, solvent extraction, ion exchange and more. On one hand, these add complication to chloride processing; but on the other hand, they unlock the possibility for the direct production of a broad range of co-products and by-products from a single process.

Copper Recovery via Electrowinning

While both the materials of construction and metal separation issues have now been effectively dealt with in chloride systems, the actual recovery of copper from chloride has remained as the persistent problem that has challenged chloride technologies for several decades.

Copper produced electrolytically from divalent copper sulphate naturally forms a flat plate on a cathode. Conventional operations add various smoothing agents to enhance this natural propensity, with the current density at the cathode limited to less than 400A/m^2 to further maintain this property.

By contrast, copper electrowon from chloride forms dendrites – crystalline 'tree-like' structures that grow chaotically from the cathode at uneven and difficult-to-control sites. These dendrites have high surface area, making them subject to oxidation. Their complex structures make physical handling difficult.

Chloride electrowinning is further complicated by the fact that the anode reaction during electrowinning produces high volumes of hot, wet, highly corrosive chlorine gas. The Intec Copper Process[7] overcame this by using two halides – chloride and bromide – which alters the anodic reaction to produce a soluble chloride-bromide complex that can be leveraged on its return to the leach circuit to maximise metal leaching, particularly Au and PGMs. The bromide also enhanced the leaching of by-product metals, such as Ag.

Until recently, no practical electrowinning cell had been developed that could reliably produce dendritic copper directly from the chloride liquor. In the absence of a viable direct route to copper recovery, most developing processes have sought to approach the problem indirectly.

Taking the Nikko-Chloride and HydroCopper Processes as example, both attempted to use solvent extraction to transfer the copper from the chloride system to sulphate. Massive amounts of research capital was expended on these attempts, with neither sufficiently successful to produce a viable commercial process. The problem is that even trace amounts of chloride contaminate sulphate electrowinning (interrupting the production of smooth copper plate), and solvent extraction is not sufficiently selective to achieve the multiple orders of magnitude change in chloride concentration required. Accordingly, both processes were required to make changes to the leach process that ultimately compromised the advantages inherent to chloride leaching.

Loop Hydrometallurgy is the first company to develop an efficient, practical electrowinning cell design for the direct electrowinning and recovery of copper from a halide electrolyte.

THE HALION™ LOOP

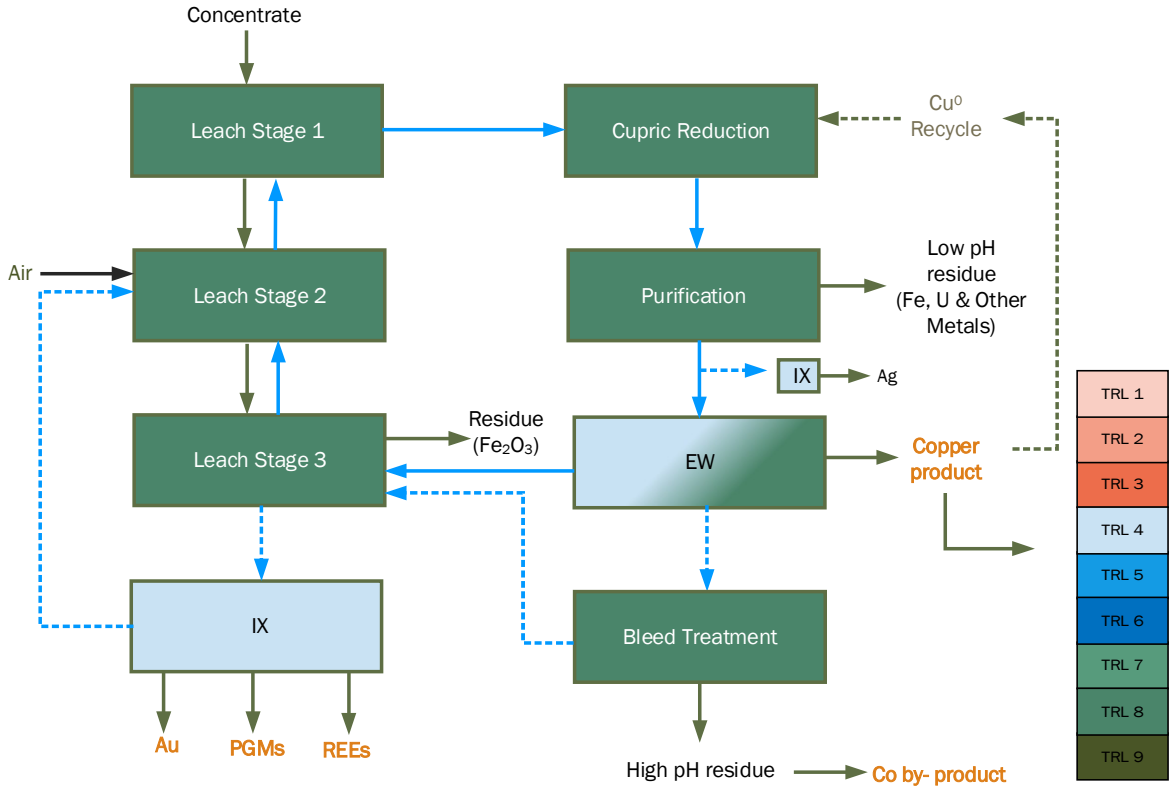

Figure 1: The Halion™ Loop Flowsheet

The Halion™ Loop is a mixed-halide closed-loop hydrometallurgical process for the extraction and recovery of copper, silver, gold, PGMs and REEs from mineral concentrates.

It leverages the broad and thoroughly established global knowledge of chloride leaching and purification, then brings to application new developments for the recovery of key co-products and by-products.

Most particularly, it leverages Loop Hydrometallurgy's breakthrough electrowinning cell design to close the process loop, so that a single process can extract and recover all of the key value metals contained in the concentrate feedstock.

Table 2: Halion™ Process Parameters

Parameter	Primary Advantages
Feedstock	15-65% Cu 25-75 µm Pb, Zn, Ni, Co ✓ Ag, Au, PGMs ✓ High As ✓ REEs ✓
Minerals	Chalcopyrite Bornite Chalcocite Covellite Bastnasite (more)
Operating conditions	Atmospheric pressure <100 °C >5M Cl / Br pH~2
Primary reagents	Air Sulphuric acid Limestone
Residues	Hematite Elemental sulphur Alkaline precipitate

Leaching

Various copper leaching processes claim to be either a copper chloride or a ferric chloride leach. In reality, these are both the same, because copper and iron both extract each other into solution. Once there is any level of copper in solution, then the chemistry is dominated by the redox chemistry of the cupric-cuprous ferric-ferrous 'couple':

$$4Cu^{2+} + CuFeS_2 \rightarrow 5Cu^{+} + Fe^{3+} + 2S \quad (1)$$

$$2Cu^{+} + O_2 + 4H^{+} \rightarrow 2Cu^{2+} + 2H_2O \quad (2)$$

$$2Fe^{3+} + 3H_2O \rightarrow Fe_2O_3 + 6H^{+} \quad (3)$$

Effectively, the net reaction is the cupric-catalysed partial oxidation of the mineral (with ~95% of the sulphide oxidised only to elemental sulphur, rather than to sulphate).

$$2CuFeS_2 + 5O_2 + 14H^{+} \rightarrow 2Cu^{+} + Fe_2O_3 + 4S + 7H_2O \quad (4)$$

This chemistry has been thoroughly demonstrated. It is highly flexible for application to a very broad range of copper and other mineral concentrates, including bastnasite (for REE leaching). Loop Hydrometallurgy is currently developing a variation for monazite resources as well.

The reaction products are simple and stable: primarily hematite and elemental sulphur. A detailed environmental study of operating residues was published in 2002[10].

Notably, the leach can also handle very high levels of arsenic in the concentrate feedstock. If the conditions are controlled correctly, the arsenic is leached and immediately reprecipitated as stable

scorodite ($FeAsO_4$). This can be managed such that no arsenic is detectable in solution, so that the risk of any arsenic escaping the process as liquid effluent or gaseous emission is eliminated altogether.

In the Halion™ Loop, leaching is separated into three counter-current stages. In Stage 1, fresh, incoming concentrate is contacted with process liquor under relatively reducing conditions. By leveraging the redox effect of the mineral leaching, no reagents are required in this stage to achieve the desired reduction of cupric ions to cuprous.

The mineral then progresses to Stage 2, where the bulk of the mineral leaching occurs with air as the primary reagent. By the end of Stage 2, the oxygen has converted at least 99% of the copper in solution to the cupric state.

In Stage 3, the depleted mineral is contacted with recycled high-oxidation potential liquor that has been recycled back from the anode chamber of the electrowinning cell. Gold and PGMs are leached under these conditions, and can be recovered directly from the oxidised liquor using ion exchange. Where REEs are present in the copper concentrate, these will be recovered from the same process stream.

Purification and By-Product Recovery

Process liquor moves in a closed cycle around the Halion™ Loop, proceeding 'backwards' through the leach and becoming increasingly reduced. By the end of Leach Stage 1, 85-90% of the copper in solution will be in the cuprous state, maintained in solution by the significant excess of chloride ions. The remaining cupric is then eliminated using recycled copper metal product.

$$Cu^{2+} + Cu \rightarrow 2Cu^{+} \quad (5)$$

The cuprous chloride then has quite different chemical properties to the other divalent and trivalent metal ions that have been leached from the concentrate. Lead, zinc, uranium and other metals can be recovered, while other non-value or contaminant metals (including excess iron) can be rejected as an alkaline precipitate.

Electrowinning

As with any conventional electrowinning, the cell has a catholyte and anolyte separated by a permeable membrane. Purified cuprous chloride process liquor is fed continuously to the catholyte at high concentration, where copper is reduced at the cathode from the monovalent cuprous state.

$$Cu^{+} + e^{-} \rightarrow Cu \quad (6)$$

The depleted catholyte passes through the membrane to the anode chamber, where the remaining copper is oxidised to cupric, and an oxidised halide complex is formed[10].

$$Cu^{+} \rightarrow Cu^{2+} + e^{-} \quad (7)$$

$$2Cl^{-} + Br^{-} \rightarrow Cl_2Br^{-} + e^{-} \quad (8)$$

This anolyte is recycled to Leach Stage 3, closing the loop for the process cycle.

Process Summary and Economics

Overall, the Halion™ Loop has no gaseous emissions or liquid effluents. The residues are primarily hematite and elemental sulphur, which have been demonstrated[10] to be stable and suitable for on-site disposal.

Independent modelling indicates that the cost of production will be just 17.6 US c/lb. This represents the processing of concentrate to metal. By comparison, the cost of transport, treatment and refining charges, and discounts on payable metal is currently 50 US c/lb for the site used in the modelling exercise.

BREAKTHROUGH ELECTROWINNING CELL

Loop Hydrometallurgy's key breakthrough is its revolutionary electrowinning cell design. Using this new cell, it now becomes practical to close the loop for a continuous process cycle for the direct leaching and recovery of copper and by-products, without having to extract any of the metals away from the chloride system.

For the first time, the Halion™ cell is able to utilise a flat plate cathode to produce dendritic copper. The key to making this possible is by creating controlled growth sites, without the use of secondary materials or complicated manufacturing techniques.

In previous chloride electrowinning process attempts, both of these issues made the resulting cells impractical for use.

The most advanced cell previously developed was that used by the Intec Copper Process (7). It used a 'sawtooth' cathode, which needed to be precisely matched to a set of sawtooth wiper blades, which were in turn mounted to an articulated vertical wiping mechanism that periodically wiped the cathodes clean. The approach had multiple challenges:

- the wiping mechanism required a high-precision match in the sawtooth formations of the wiper and cathode, significantly increasing the cost of manufacture and compromising performance wherever that match was imperfect;
- the combination of high surface area and periodic wiping meant that the effective current density at the cathode could change by several orders of magnitude at each wiping cycle, affecting product quality, morphology and cell voltage;
- the periodic wiping also 'dumped' a large load of copper dendrite to the bottom of the cell in bulk, creating mechanical handling problems for product removal;
- the vertical movement of the wiping mechanism carried cuprous catholyte upwards on every wetted surface during wiping, allowing for oxidation in the air. Carrying this oxidised liquor back into the cell on the downward movement compromised the cell efficiency by several percent;
- this vertical arrangement also required significant space above the cell for the movement of the mechanism; and
- the cell used a conveyor system. This did not handle the smaller copper particles in the particle size range, resulting in accumulation of the cell. The recovered copper was exposed to air and oxidation during the removal process.

All of these issues have been overcome in the Halion™ cell. A key aspect is that the copper is removed from the cathode continuously, but slowly, yielding a product that can best be described as 'coarse copper sand'.

The continuous movement ensures that the electrical conditions within the cell stay stable (and at the lowest possible voltage); and it maintains a permanent quantity of copper on the cell, ensuring that the effective current density is at least 1-2 orders of magnitude lower than the nominal current density (1,000+ A/m^2). Further testing is required to determine how high the nominal current density can be raised.

The simple removal mechanism does not require any complicated articulated mechanism, as a result of which the anode-cathode distance can be narrowed by more than 50%. This reduces the cell voltage.

Moving horizontally, the removal mechanism never 'breaks surface', minimising the air ingress into the cell. It may be practical to cover the cell to prevent air ingress altogether, maximising the cell efficiency. It is expected that the cathodes will be capable of operating and producing copper product continuously for long periods of time (up to 6-12 months), without needing removal from the cell other than for scheduled preventative maintenance.

The copper can then be removed continuously from the bottom of the cell using conventional methods, avoiding exposure of the high surface area product to air before it is washed and dried.

This design represents the first practical method of directly electrowinning copper from the chloride system, that can be applied effectively at the commercial scale.

COPPER MADE GREEN

Electrowinning: Halide vs Sulphate

Taking into account the effects of electrowinning from the cuprous state, current density and other advantageous operating factors, it is estimated that the Halion™ cell will reduce the electrowinning power consumption by as much as 70% compared to conventional copper sulphate electrowinning.

Table 3: Comparison of Electrowinning Technologies

	Halion™ Cell E/W	**Sulphate E/W**
Copper valence state	Cu(I)	Cu(II)
Notional current density	>1,000 A/m^2	<400 A/m^2

Process Environmental Comparison

The CSIRO[11] has modelled the whole-of-process life cycle impact of the dominant copper production technologies. Of the technologies modelled, the Halion™ Loop has the strongest commonality with the Intec Copper Process – both atmospheric, low-temperature, cyclic, mixed-halide processes.

The environmental impacts of smelting (as the current dominant copper production technology) are harder to assess for comparative purposes because much of the energy used in smelter copper production comes from the oxidation of sulphide to sulphur dioxide, rather than from electricity and carbon sources. Effectively, smelting gets a very large 'cheat' on its carbon footprint, at the expense of either producing acid rain (unregulated jurisdictions) or large volumes of sulphuric acid (typically requiring neutralisation).

The life cycle assessment showed that the carbon emissions of the mixed-halide hydrometallurgy were the lowest of the hydrometallurgical techniques for a 'standard' 25% copper concentrate using power supplied from black coal, slightly higher than smelting.

This ratio versus smelting changes in favour of hydrometallurgy for lower-grade concentrates, or when using hydro power. The ratio was also affected by transport distance. Where the hydrometallurgical processes are based at the mine site, the conventional long transport distances associated with transport to smelter and refining added over 2.6MJ/kg to the total energy consumption.

In all scenarios, the acidification potential of smelting was vastly higher (up to 290%) than mixed halide hydrometallurgy.

Table 4: Global Warming Potential (kg CO_2-e/kg-Cu)

	Mixed Halide + Direct E/W	**Pressure Oxidation (average)**	**Bacterial Oxidation (average)**	**Flash Smelting**
25% con. Black coal	4.9	7.3	8.2	4.3
15% con. Black coal	5.0	8.8	10.4	5.2
25% con. Natural gas	3.4	5.3	6.1	3.2
25% con. Hydroelectric power	1.5	2.9	3.6	1.8
25% con. 5,500km transport	4.9	7.3	8.2	4.5

Table 5: Acidification Potential (kg SO_2-e/kg-Cu)

	Mixed Halide + Direct E/W	Pressure Oxidation (average)	Bacterial Oxidation (average)	Flash Smelting
25% con. Black coal	0.033	0.044	0.047	0.057
15% con. Black coal	0.034	0.048	0.051	0.089
25% con. Natural gas	0.010	0.013	0.014	0.039

The improved performance of the Halion™ cell will improve the total energy consumption from the mixed-halide process considered in the CSIRO study.

Depending on concentrate grade, electricity generation source and comparative transportation distance, it is estimated that the Halion™ Loop would be almost equal to or lower than smelting in both total energy consumption and carbon footprint, and significantly lower than all other competing hydrometallurgical process options.

COMMERCIALISATION OF THE TECHNOLOGY

Loop Hydrometallurgy is currently undertaking a commercialisation program to bring this technology to market. The preferred first project for this project may include the following characteristics, which best leverage the advantages of the technology:

- 20-40 kTpa Cu production
- 15-25% Cu grade and/or poor grade recovery curve
- REE, Au, PGM and/or Co co-product credits
- Polymetallic: Pb, Zn, Ni and/or Co
- Arsenic contamination
- Hydroelectric or gas power supply

ACKNOWLEDGMENTS

The authors would like to thank the staff and management of OZ Minerals for supporting its research that led to this breakthrough, as well as the Macquarie University Incubator for supporting Loop Hydrometallurgy in its technology commercialisation programme.

REFERENCES

1. www.energymining.sa.gov.au/industry/geological-survey/mesa-journal/previous_news/news-articles-2022/copper-to-the-world-2022
2. "The World Copper Factbook 2022", International Copper Study Group, https://icsg.org/copper-factbook/#:~:text=World%20Copper%20Factbook%202022,environmental%2C%20and%20sustainable%20development%20issues.
3. Snowdon, N, Sharp, D., Currie, J., 2021, Green Metals: Copper is the New Oil, Goldman Sachs Commodities Research, www.goldmansachs.com/insights/pages/copper-is-the-new-oil.html
4. Harris, G.B., 2014, Making Use of Chloride Chemistry for Improved Metals Extraction Processes, Proceedings of the 7th International Symposium on Hydrometallurgy (Hydro 2014), v1. pp.171-184.
5. Watling, H.R., 2014, Chalcopyrite Hydrometallurgy at Atmospheric Pressure: 2. Review of Acidic Chloride Process Options, Hydrometallurgy 146, 96-110.
6. Lu, J. and Dreisinger, D., 2013, Copper Leaching from Chalcopyrite Concentrate in Cu(II)/Fe(III) Chloride System, Minerals Engineering 45, 185-190.
7. Intec Ltd., 2008. The Intec Copper Process.

8. Ahtiainen, R., Lundstrom, M., 2019, Cyanide-Free Gold Leaching in Exceptionally Mild Chloride Conditions, J. Cleaner Production 234, 9-17.
9. Hyvarinen, O., Hamalainen, M., 2005, HydroCopper™ – A New Technology Producing Copper Directly From Concentrate, Hyrometallurgy 77, 61-65.
10. Sammut, D., Welham, N., 2002, The Intec Copper Process: A Detailed Environmental Analysis, Green Processing Conference, Cairns, 115-124.
11. Norgate, T.E., 2001, A Comparative Life Cycle Assessment of Copper Production Processes, CSIRO report DMR-1768.

THE POTENTIAL OF PYRRHOTITE IN ADDRESSING SUSTAINABILITY: REPLACING OIL INDUSTRY SULPHUR AND CARBON

By

Mike Dry

Arithmetek, Canada

Bryn Harris

NMR360 Canada

Presenter and Corresponding Author

Mike Dry

mike.dry@arithmetek.com

ABSTRACT

There are side-effects to mitigating Climate Change and the drive towards Net-Zero carbon emissions. One is the impact upon the sulphur market. Of the 82 million tonnes of sulphur produced globally in 2021, 51 million tonnes (62%) came from natural gas and petroleum. If humanity is serious about moving away from burning fossil fuels for energy, then the global supply of sulphur will shrink by more than half, with significant unanticipated impacts. This paper examines the potential for extracting sulphur as a primary product from sulphide deposits that would not be considered economic for only the extraction of metals such as nickel, copper, cobalt, zinc. Previous papers have looked at the relevance of pyrrhotite in mitigating the shortfall of critical metals, and the primary focus here is on sulphides, of which there appears to be enough to replace the sulphur presently recovered from hydrocarbons. In addition to the sulphur potential, the reductions in CO_2 emissions by recovering the intrinsic energy in pyrrhotite are also estimated.

Keywords: sulphur, sulphides, pyrrhotite, pyrite, CO_2, energy

INTRODUCTION AND BACKGROUND

There are side-effects which are not readily apparent to mitigating Climate Change and the drive towards Net-Zero by reducing the production and consumption of hydrocarbon-based fuels. One of these is the impact upon the sulphur market. Figure 1 shows the global production of sulphur in all forms for 2022. Over 60 percent of the total was derived as by-product from the extraction and processing of hydrocarbons (oil and gas). Figure 2 is a snapshot of the sulphur market by application, for 2020, showing that over 50 percent of the sulphur consumed globally is used in the production of fertilizers.

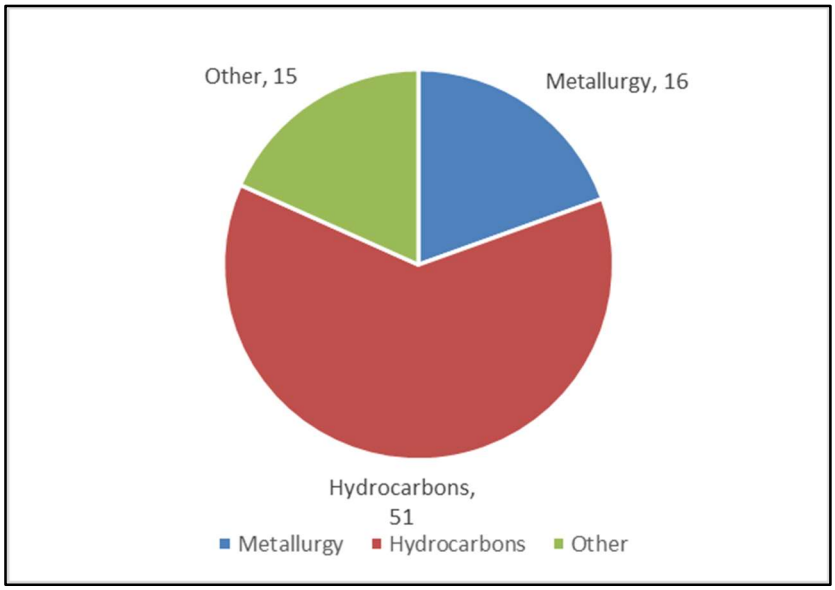

Figure 1 – Global S production for 2021, million tonnes[1]

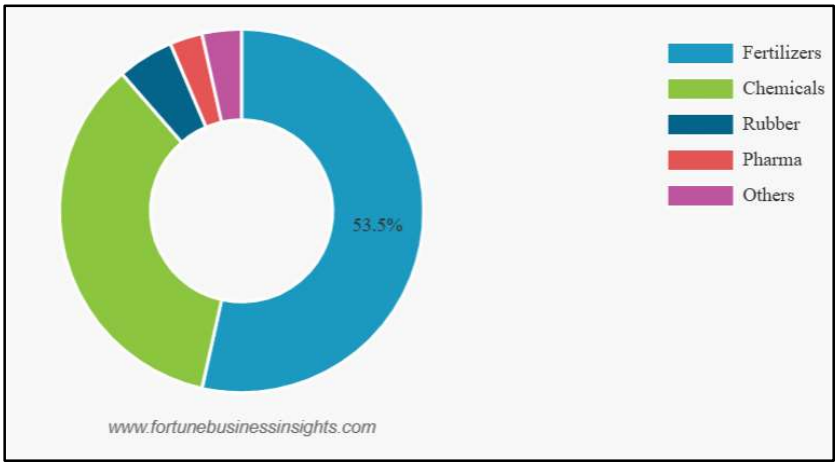

Figure 2 – Global sulphur market by application, 2020[2]

Sulphur is essential for the growth of all crops[3] and from this perspective, a 60 percent drop in its global supply would be disastrous to humanity. The drive to reduce carbon dioxide emissions and use alternative sources of energy requires that the burning of fossil fuels be drastically reduced, meaning that the production of oil, gas and coal for the production of energy must cease or at least diminish greatly. Complete elimination of oil and gas means that the current global supply of sulphur will be reduced by some 60 percent. Such targets are nominally in place for 2050. As the supply of sulphur from oil and gas diminishes, it will have to be replaced from other sources.

That being the case, there are just over two decades left in which to identify and bring into production new sources of sulphur. A previous paper[4] examined re-treating waste nickeliferous tailings dumps, such as those in Sudbury, Ontario, Canada as an obvious resource of nickel and cobalt, but one which the industry seems reluctant to embrace. Table 1, taken from that paper and updated for metal prices as of March 2023, assuming 95% to allow for further refining, shows that such an approach not only remediates old tailings dumps, but is also attractive economically. Assumptions on unit costs were made to give some very preliminary, order of magnitude (high level), indicative costs. An input of 3000 tonnes/day, with a feed analysis of 0.8% Ni was used.

Table 1 - Production and assumed selling price for treating pyrrhotite tailings[4]

Item	Annual Production	Price US$/unit	Revenue, M$/year
Nickel as Ni, in mixed sulphide	8,400 t	12.13/lb	213
Copper as Cu, in mixed sulfide	3,150 t	4.08/lb	26.9
Cobalt as Co, in mixed sulfide	315 t	22.18/lb	14.6
PGMs as metal	64,000 oz	1200/oz	72.9
Hematite (100% Fe_2O_3)	788,000 t	300/t	236
Claus plant sulfur (95% capture)*	348,000 t	70/t	24.3

* - includes 57,000 t S recovered from leach residue

Since the primary emphasis of the previous paper was on the recovery of nickel and cobalt, no particular attention was paid to the recovery of sulphur, which was noted only as a minor addition to the overall revenues.

IRON AND SULPHUR ARISINGS

Table 2 presents the production and reserves of principal metals containing iron and/or sulphur available from base and precious metal ores.

Table 2 - Iron and Sulphur Production[5]

Metal	Production 2022 tonnes	Reserves 2022 tonnes
Aluminium	69 million	High
Chromium	41 million	560 million
Copper	22 million	890 million
Gold	3,100	52,000
Lead	4.5 million	85 million
Manganese	20 million	1.7 billion
Nickel	3.3 million	>100 million
Tin	310,000	4.6 million
Titanium	9.4 million	High
Zinc	13 million	210 million
Iron	1.3 billion	85 billion (ore)
Sulphur	82 million	High*
* - Sulphur reserves include those currently derived from oil and gas.		

The above table details only primary deposits. Importantly, especially in the context of this paper, there are also numerous tailings dumps around the world which are not well-documented, are not included in calculations of reserves, and are not in production. Since the early 1990s alone, Glencore has disposed of 8 million tonnes (dry basis) in the Sudbury area of Canada, with an average grade of ~0.8% Ni[6]. A conservative estimate would be that there are over 100 million dry tonnes of these tailings impounded with an average grade of 50% Fe and 35% S, representing 50 million tonnes of iron and 35 million tonnes of sulphur, as well as the nickel, cobalt, copper and precious metals. These Sudbury tailings are not the only such dump.

Global copper reserves have been estimated at 870 million tonnes, and global copper resources at five billion tonnes[7]. Globally, nickel sulphide deposits are reported to contain 118 million tonnes of nickel[8]. Taking Voisey's Bay as an example, that ore contains very roughly 32 percent sulphur and 2.1 percent nickel, 0.85 percent copper and 0.1 percent cobalt, thus its sulphur content is very roughly ten times its content of base metals. Another example is the Ferguson Lake massive sulphide deposit in Nunavut, Canada; the sulphur content of that deposit is roughly twenty times its base metal content. As a very rough approximation, then, the reported global reserves of nickel in sulphide deposits should imply global reserves of sulphur of between very roughly one and two billion tonnes, or 10 to 20 years of global sulphur production at the 2021 levels. Taking the numbers for copper and assuming it all to be chalcopyrite, gives a further reserve of some 2.5 billion tonnes of sulphur, or some 30 years at current global consumption, not allowing for any other iron sulphides in the copper reserves.

If the ratio of resources to reserves of global sulphide deposits is anything like the numbers reported for copper, there would be enough sulphide sulphur to meet global needs for many decades.

PROCESSING

The drive to Net Zero has been set in stone, and the production of oil and gas must diminish greatly to achieve this overall goal. Humanity cannot logically permit the associated loss of some 60 percent of the global supply of sulphur. Alternative sources will have to be found and brought into production. Crucial questions would be how and at what at what cost could all that sulphide sulphur be recovered.

Peek et al[6] present a summary of several pyrometallurgical options previously developed for processing pyrrhotite tailings, none of which are presently in production. Reasons given include operational complexity and that the silicate gangue in the feed made the iron-bearing calcine unsuitable as a feed to ironmaking (thus making it a residue requiring disposal, not a by-product). Additionally, the base metals (copper, particularly) are not desirable in iron ores, which makes for complex further processing, both to recover the base metals and to make the remaining iron suitable for iron smelting.

This paper extends earlier work[4,9] that examined the recovery of base metals from sulphide tailings containing pyrrhotite. One of the circuits examined is a chloride route in which the hydrochloric acid is fully recycled and hematite (that is very suitable for iron making) is produced in addition to the base metals being recovered as oxides. The first step is leaching with hydrochloric acid, giving gaseous hydrogen sulphide and aqueous ferrous chloride. Table 3 lists the mineral composition used to represent that feed. Figure 3 illustrates the overall circuit. The black lines denote streams containing solids and the blue lines denote liquid streams. The pink lines denote gaseous streams, the red lines are steam, and the green lines are boiler feed water or steam condensate. The dashed black line denotes optionally sending the sulphur formed in the secondary leach to the Claus or WSA plant.

Table 3 – Nickeliferous pyrrhotite feed, mass %

Ni_3S_2	0.16	Fe_7S_8	86.02
Ni_7S_6	1.00	Fe_3O_4	6.06
CoS	0.05	$MgSiO_3$	5.19
FeS	0.65	PtS	0.0002
$CuFeS_2$	0.87	PdS	0.0000

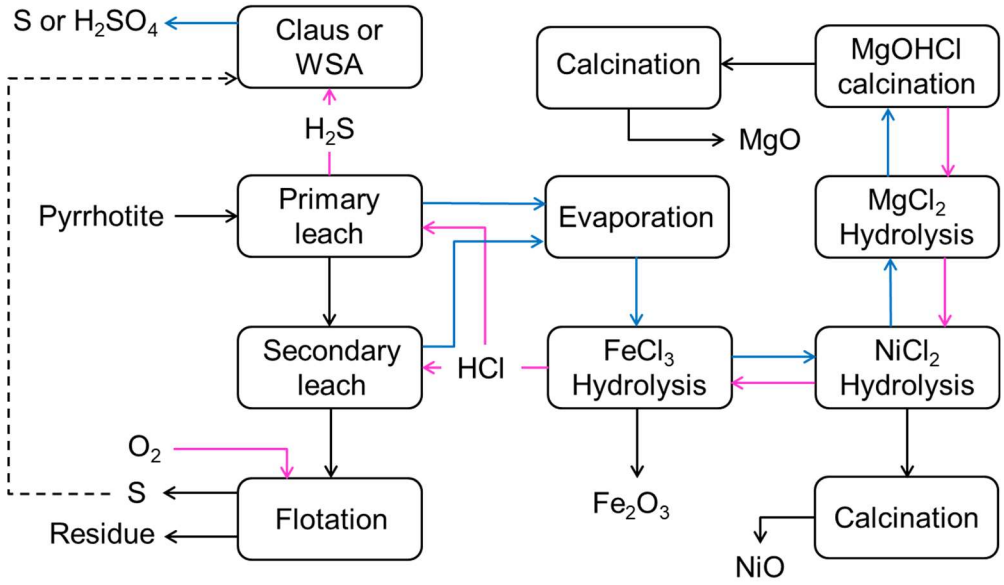

Figure 3 – Overall chloride circuit

The incoming pyrrhotite is leached with hydrochloric acid, producing hydrogen sulphide gas and ferrous chloride. The residue is leached with hydrochloric acid and oxygen (that leach could also use ferric chloride), producing elemental sulphur and dissolved base metal chlorides. The sulphur is recovered by flotation (in this example; there are other ways of recovering sulphur from leach residues) and optionally sent to the sulphur processing section. Solutions from the primary and secondary leaches go to the evaporation section and thence to the oxidation and iron hydrolysis section, where the ferrous chloride is oxidised to ferric chloride that is thermally decomposed to solid hematite and gaseous hydrogen chloride. The hematite is recovered by filtration and washing. The hydrogen chloride exits this step ($FeCl_3$ hydrolysis) as gaseous HCl in steam (about 35-40 percent HCl by mass). The remaining solution (more accurately molten salt containing some water, molten salt-hydrate), containing the base metals and magnesium as chlorides, is hydrolysed in two more steps in which steam is added to sequentially precipitate base metal hydroxy chlorides and magnesium hydroxy

chloride that are removed by filtration and then calcined to oxides. The gaseous HCl released from the three hydrolysis steps is recycled to the two leach steps.

The hydrogen sulphide from the primary leach is converted to elemental sulphur in a conventional Claus plant, or (along with, optionally, the sulphur from the secondary leach) to sulphuric acid in a WSA (Wet gas Sulphuric Acid) plant. The energy released is captured in high pressure steam that is condensed to drive the endothermic evaporation and hydrolysis sections of the circuit. This is not shown in **Error! Reference source not found.** to avoid over-complicating the diagram, but it is covered in the following more detailed description of that part of the process.

The hydrometallurgical part of this process has been described in detail elsewhere[7]. A description of that part of the circuit is appended for convenience. The focus in this study is on the overall energy balance and the recovery of energy and elemental sulphur or sulphuric acid from the hydrogen sulphide produced in the primary leach. The hydrogen sulphide from the primary leach, which is the principal mode of recovering both the sulphur and the energy from the sulphide feed, and (optionally) the elemental sulphur from the secondary leach is handled in two ways, either making elemental sulphur from the hydrogen sulphide in a Claus plant or making sulphuric acid from the hydrogen sulphide and (optionally) also the elemental sulphur in a WSA (Wet gas Sulphuric Acid) plant.

Claus

The option making elemental sulphur from the hydrogen sulphide is illustrated in Figure 4. The hydrogen sulphide from the primary leach is first cooled to 30°C to condense out most of the water vapor and dissolved hydrogen sulphide is stripped from the condensate by contact with incoming air. The remaining condensate leaves as water. The cooled hydrogen sulphide and the air from the stripping step, plus (optionally) the elemental sulphur from the secondary leach, is partially burned in air, with the amount of air being manipulated to give a molar ratio of 2:1 H_2S:SO_2 in the exit gas. That gas then passes through a series of catalyst beds in which the H_2S and SO_2 react to give gaseous elemental sulphur and steam. The elemental sulphur is condensed and leaves the circuit.

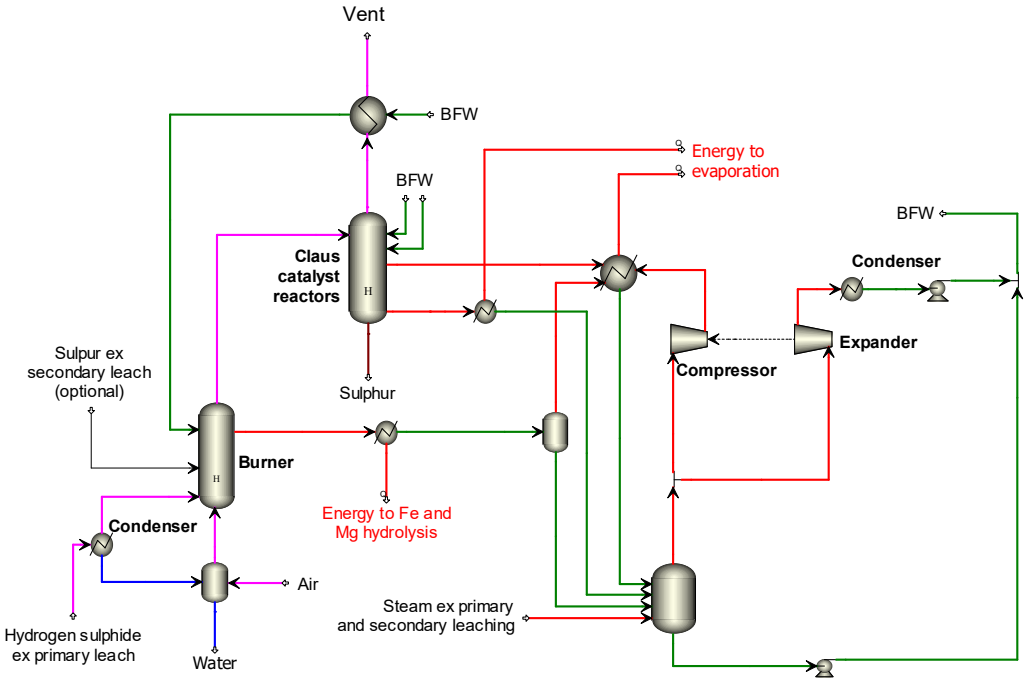

Figure 4 - Claus plant and energy recovery

Heat from the combustion step is captured into high pressure steam (56.5 bar absolute) by heat exchange with high-pressure boiler feed water. Heat from the exothermic formation of elemental sulphur is captured as medium-pressure saturated steam (12 bar absolute) by heat exchange with medium-pressure boiler feed water. Heat from the condensation of the sulphur is captured as low-pressure steam (4.6 bar absolute) by heat exchange with low-pressure boiler feed water.

The high-pressure steam is condensed, its latent heat driving the Fe oxidation and hydrolysis reactions in the preceding part of the circuit. The condensate is flashed to 12 bar absolute, releasing more 12 bar steam that is added to the medium-pressure steam from the Claus reactors. The combined medium pressure steam is condensed, its latent heat being used to drive the evaporation reactions in the circuit. The low-pressure steam is condensed, its latent heat driving the initial part of the evaporation step in the circuit. The resulting medium-

pressure and low-pressure condensates are flashed to 1 bar absolute, releasing atmospheric-pressure steam to which atmospheric-pressure steam from the secondary leach section is added. The combined atmospheric-pressure steam is split, part being expanded to 0.05 bar absolute through a condensing turbine and condenser, the condensate being pumped back up to atmospheric or higher pressure for recycle as boiler feed water. The other part of the atmospheric-pressure steam is compressed back up to 12 bar absolute and recycled to the condensing step supplying energy to the evaporation stage of the circuit. Some, but not all, of the mechanical power required for this recompression step comes from the condensing turbine. The balance has to come from imported electricity via a motor.

WSA

The WSA option making sulphuric acid is illustrated in Figure 5. The hydrogen sulphide from the primary leach is first cooled to 30°C to condense out most of the water vapor and dissolved hydrogen sulphide is stripped from the condensate by contact with incoming air. The remaining condensate leaves as water. The cooled hydrogen sulphide, plus (optionally) the elemental sulphur from the secondary leach, is burned with the air from the stripping step in the burner, with the amount of incoming air being manipulated to make it carry 2.4 moles of oxygen per mole of H_2S in the feed gas, plus 1.2 moles of oxygen per mole of elemental sulphur (when elemental sulphur is also converted to sulphuric acid). The hot gas from that combustion step passes through a series of catalyst beds in which the SO_2 reacts with oxygen to give SO_3 that is then condensed with the water as concentrated sulphuric acid in the wet acid condenser.

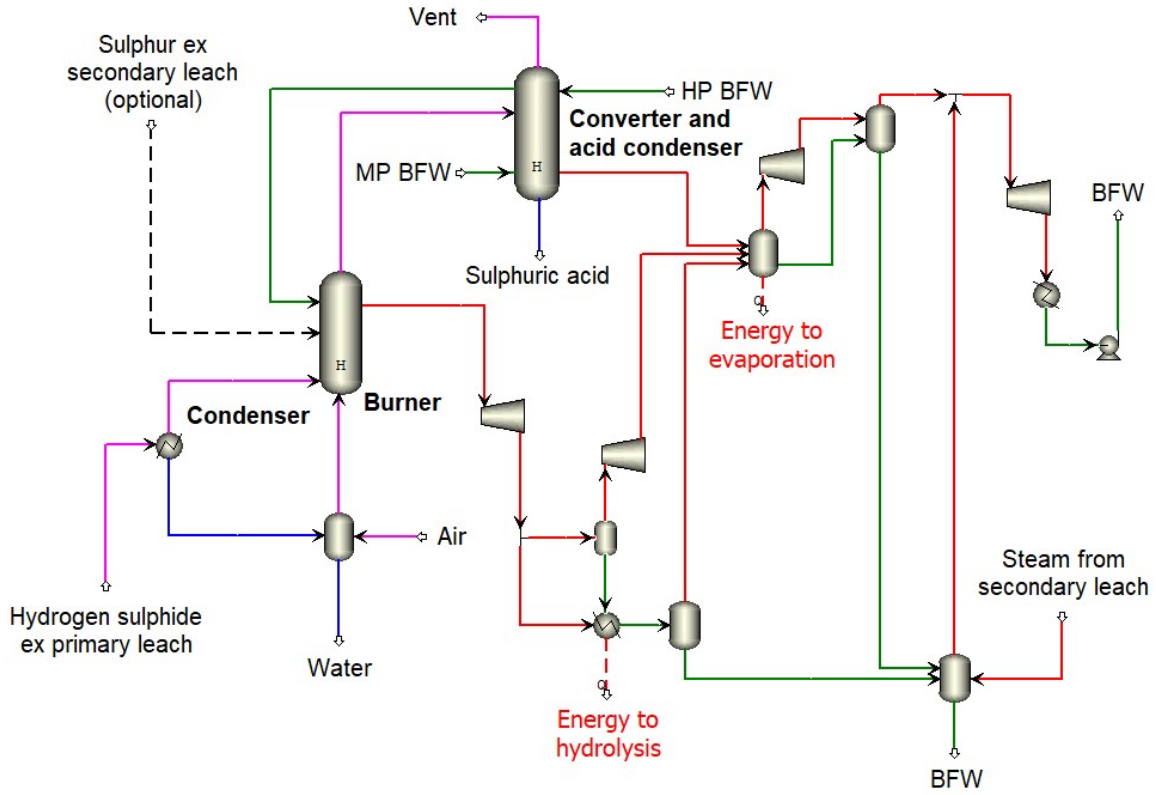

Figure 5 – Wet acid plant

The heat released in the combustion step is captured into high pressure steam (56.5 bar absolute). The heat from the exothermic formation of SO_3 is captured into medium pressure steam (31 bar absolute). The high-pressure steam from the burner is expanded to 31 bar absolute in a turbine, recovering mechanical energy. The 31-bar steam ex the turbine is split, part being condensed to provide the energy required by the hydrolysis steps of the circuit, and the balance being expanded to 12 bar absolute in a second turbine, recovering more mechanical energy. The condensate from the 31-bar condensing step is flashed to 12 bar absolute, releasing more 12 bar steam that joins the 12-bar steam from the second turbine and is partially condensed to provide the energy required by the evaporation section. The remaining 12-bar steam is expanded to 0.6 bar absolute in a third turbine, recovering more mechanical energy. The condensate from the 12-bar flash is mixed with the 0.6-bar steam from the third turbine, flashing off more 0.6-bar steam. Condensate from the 0.6-bar condensation step and atmospheric-pressure steam from the secondary leach are combined and flashed to 0.6 bar absolute, releasing more 0.6-bar steam is expanded to 0.05 bar absolute through a condensing turbine and condenser, capturing more mechanical energy. The final 0.05-bar steam is condensed and pumped back to the various pressures required of the different inputs of boiler feed water. In this model, the mechanical energy recovered in the various turbines is assumed to leave the circuit as electricity, as there is more than enough steam produced at the various pressures to supply the energy needs of the rest of the circuit without needing any recompression of steam.

RESULTS

The purpose of the exercise reported here is to evaluate the recovery of sulphur and non-fossil energy from pyrrhotite-bearing sulphide ores. Table 4 lists the production quantities calculated for each processing option, per tonne of elemental sulphur produced either as elemental sulphur or as sulphuric acid. Table 5 lists the amounts of feed, reagents and utilities consumed, again per tonne of sulphur in the product(s). The power generated or consumed is summarised in Table 6. Table 7 lists the reagent and utility costs calculated for the three options and Table 8 lists the revenues calculated. Residue disposal has been assumed to be a cost, but the residue might also be suitable for road fill.

Table 4 – Production numbers, per tonne sulphur

Item	Sº (Claus)	H_2SO_4	Sº & H_2SO_4
Nickel as Ni, in mixed oxide	23 kg	23 kg	24 kg
Copper as Cu, in mixed oxide	8.7 kg	8.6 kg	8.6 kg
Cobalt as Co, in mixed oxide	0.9 kg	0.9 kg	0.9 kg
Leach residue	265 kg	263 kg	262 kg
PGM in leach residue	0.2 Oz	0.2 Oz	0.2 Oz
Hematite	2172 kg	2151 kg	2151 kg
Magnesia	60 kg	60 kg	60 kg
Elemental sulphur	1000 kg	-	141 kg
Sulphuric acid		3059 kg	2627 kg

Table 5 – Consumption numbers, per tonne sulphur

Item	Sº (Claus)	H_2SO_4	Sº & H_2SO_4
Dry nickelliferous pyrrhotite	2890 kg	2859 kg	2889 kg
Hydrochloric acid (as 100% HCl)	0 kg	0 kg	23 kg
Make-up Matrix for hydrolysis	10 kg	10 kg	10 kg
Oxygen (as 100% O_2)	227 kg	237 kg	245 kg
Water	5849 kg	14806 kg	17676 kg
Electricity (external)	1017 MWh	-	-

Table 6 – Power summary, MW

Item	Sº (Claus)	H_2SO_4	Sº & H_2SO_4
Power from steam expansion	9.4	45.4	38.3
Total power to steam compression	35.4	-	-
Power to calcination	4.6	4.6	4.6
Power for feed preparation	5.0	5.0	5.0
Power for the oxygen plant	6.4	6.4	6.4
Power for pumping, agitation etc.	5.0	5.0	5.0
Total power consumption	**48.6**	**21.0**	**21.0**
External power required	**27.6**	**-23.9**	**-16.8**

Table 7 – Reagent & Utility costs, $ per tonne S

Item	Sº (Claus)	H_2SO_4	Sº & H_2SO_4
Feed ($5/t dry pyrrhotite)	14.45	14.29	14.29
Acid ($2000/t 100% HCl)	0.00	0.45	0.52
Oxygen ($125/ t 100% O_2)	28.43	29.64	29.64
Matrix ($1000/t)	10.07	10.00	10.00
Residue disposal ($5/t)	1.33	0.86	1.31
Fresh water ($2/t)	10.98	29.61	15.77
Electricity ($0.05/kWh)	50.86	-	-
Sub-total, reagent and utility cost	116.12	84.85	71.52

The modelling calculations predict that if the hydrogen sulphide from the primary leach is converted into sulphuric acid, the energy released in the WSA process is more than is needed to run the overall circuit, supplying the required latent heat of condensation from high-pressure steam to drive the evaporation and hydrolysis operations with enough steam remaining for the generation of an appreciable amount of electricity. If the hydrogen sulphide is converted to elemental sulphur through a Claus process, the circuit needs external power.

These numbers and the assumptions listed in Table 9 were used to calculate the simple cash flow graphs shown in Figure 8. Note that these graphs are intended only for comparison of the options studied and are by no means definitive. In particular, use of the same capital cost for all three cases is a simplifying assumption that will require refinement should these processes be evaluated further.

Table 8 – Revenue, $ per tonne S

Product(s)	S⁰ (Claus)	H_2SO_4	S⁰ & H_2SO_4
Nickel ($11000/t)	295	253	252
Copper ($8900/t)	90	77	76
Cobalt ($44000/t)	45	38	39
Hematite ($300/t Fe_2O_3)	760	645	645
Magnesia ($200/t MgO)	14	12	12
Elemental sulphur ($60/t S)	60	-	8
Sulphuric acid ($200/t S)	-	612	525
Surplus power ($50/MWh)	-	28	19
Total revenue per tonne S	1265	1664	1577

Table 9 – Cash flow assumptions

Corporate tax rate	20%
Estimated capital cost	$600 M
Capital expenditure in year -1	50%
Capital expenditure in year 0	50%
Production in year 1	25%
Production in year 2	50%
Production in year 3	75%
Production after year 3	100%

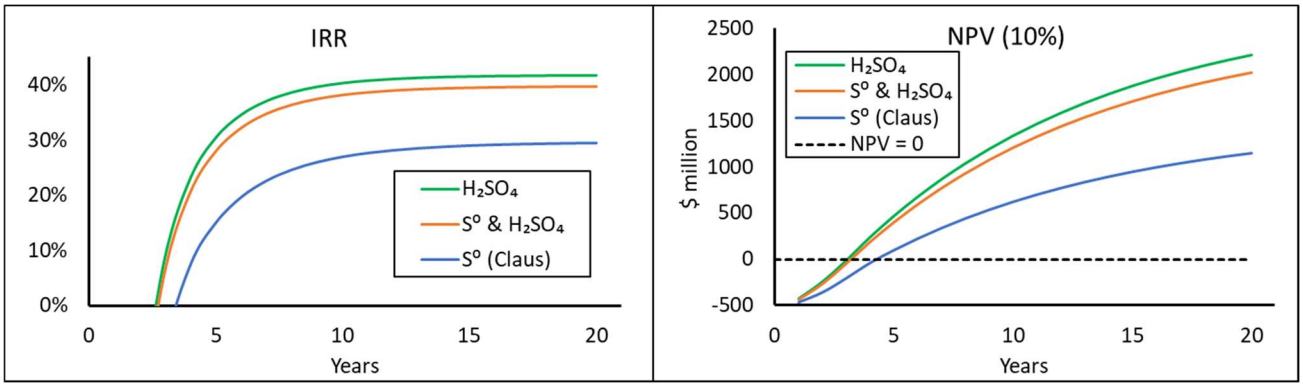

Figure 8 – Indicative cash flow calculations

From these curves, it would appear that making acid would be appreciably more attractive economically than making elemental sulphur, if differences between cost of the shipping of sulphur and that of acid are ignored. It is worth noting that, because the sulphur is not liberated from the feed sulphide by roasting, the sulphur-bearing gas would not carry the volatile metal impurities such as arsenic and mercury that would be in the gas ex roasting if present in the feed, and therefore in the product acid. That means that the acid produced via the route examined here would be of very high purity, thus commanding a premium price. Such acid will be in increasingly high demand, since it is an essential component in the production of the electrolyte for VRFBs (vanadium redox flow batteries), which are presently regarded as being the long-term solution to bulk energy storage[10].

CONCLUSION

One obvious prediction arising from this exercise is that the more profitable way of extracting sulphur from low grade sulphide sources like the nickeliferous pyrrhotite used in this exercise is to make sulphuric acid. Doing so would appear to have the added benefit that the feed sulphide can supply more than the entire energy load of the circuit, with a small but still appreciable surplus that can be exported as fossil-free power.

The approach presented here is just one way of revisiting old tailings stockpiles and other sulphide ores. It might be argued that a simpler approach would be to roast the pyrrhotite and recover the SO_2 in a conventional acid plant. Roasting of high-pyrrhotite materials is technically challenging[6], and where silicate gangue is present (as would be the case for many pyrrhotite-bearing sources, be they stored tailings or sulphide ores) the calcine containing the iron is not suitable for ironmaking and becomes a waste requiring disposal. As noted above, the off-gas would contain undesirable volatile impurities such As, Sb, Bi, Pb, Zn, Hg leading to relatively impure sulphuric acid. Also, the further processing needed to recover the base metals from such a calcine is not trivial. This could be a worthy topic for further study, but the roasting option is intuitively not as attractive as the leaching option.

In addition to sulphuric acid, energy is recovered from the pyrrhotite in this process. Making sulphuric acid from the hydrogen sulphide and the elemental sulphur from the leaching sections of the circuit gives 23.9 MW or surplus power for 3000 tonnes/day of the feed used in this study, or 191 kWh per tonne of dry feed pyrrhotite. That translates to 181 kWh per tonne of sulphuric acid produced. The manufacture of phosphoric acid, by contrast, consumes 120 to 180 kWh of power per tonne of P_2O_5 produced[11]. Producing a tonne of P_2O_5 from tricalcium phosphate consumes 3 moles of H_2SO_4 per mole of $Ca_3(PO_4)_2$, or 2.1 tonnes of H_2SO_4 per tonne of P_2O_5. The energy surplus from making 2.1 tonnes of sulphuric acid from the pyrrhotite used in this exercise is thus about 370 kWh per tonne of P_2O_5 produced, which is well above the power needed by the phosphoric acid plant. Therefore, sourcing the required sulphuric acid from sulphide ore or tailings similar to the material studied in this exercise could make the production of phosphoric acid, and hence phosphate fertilisers, completely carbon neutral, especially if the ammonia required therein is derived from green hydrogen. This combination may well be worth further study.

Generating electricity from natural gas emits about 441 grams of CO_2 per kWh of electricity produced. From coal, the number is 1027 grams of CO_2 per kWh of electricity. The current annual production of phosphoric acid is about 60 million tonnes of P_2O_5[13]. At 120-180 kWh per tonne of P_2O_5 that translates to emissions of about 3.2-4.8 Mt of CO_2 per year from the electricity consumed in manufacturing phosphoric acid, if the fuel is natural gas, or about 7.4-11.1 Mt of CO_2 if the fuel is coal. Global CO_2 emissions were a little below 40 Gt in 2022[14], so the potential impact of making the global production of phosphoric acid zero-carbon, while not huge in the overall context, would also not be trivial and could appreciably assist the fertiliser industry in its overall decarbonation efforts.

It is concluded, therefore, that there are many compelling reasons for processing of pyrrhotite-bearing sulphide ores and especially for the re-processing of old tailings dumps, in particular nickeliferous pyrrhotites, in terms of mitigating against the shortfalls of battery metals and sulphur, as well as contributing to the global reduction of CO_2 emissions.

REFERENCES

1. USGS 2021 Annual Tables
2. https://www.fortunebusinessinsights.com/sulfur-market-102143 (accessed 2023-04-07)
3. https://www.sulphurinstitute.org/about-sulphur/sulphur-the-fourth-major-plant-nutrient/ (accessed 2023-04-07)
4. Bryn Harris and Mike Dry, Re-Treatment of Tailings Using Chloride-Based Processing, Presented at ALTA 2020 On-Line Conference, November, 2020, 440-453.
5. United States Geologic Survey, Mineral Commodity Summaries, 2023.
6. E. Peek, A. Barnes and A. Tuzun, Nickeliferous pyrrhotite – Waste or Resource?, *Minerals Engineering* 24, 625-637.
7. https://copperalliance.org/sustainable-copper/about-copper/cu-demand-long-term-availability/ (sourced on 2023-04-17)
8. Mudd, G. and Jowitt, S. M. A Detailed Assessment of Global Nickel Resource Trends and Endowments. Economic Geology (2014) 109(7):1813-1841. https://pubs.geoscienceworld.org/segweb/economicgeology/article-abstract/109/7/1813/128637/A-Detailed-Assessment-of-Global-Nickel-Resource?redirectedFrom=fulltext
9. Bryn Harris and Mike Dry, Nickelliferous Pyrrhotite – Another Source of Nickel if it can be Extracted Economically. Alta 2010 NCC conference.

10. Lourenssen, K., Williams, J., Ahmadpour, F., Clemmer, R. and Tasnim, S. Vanadium redox flow batteries: A comprehensive review. Journal of Energy Storage 25 (2019) 100844.
11. European Fertilizer Manufacturer's Association. Booklet 4 of 8, Production of Phoshoric Acid. file:///C:/Users/miked/OneDrive/Documents/Alta%202023/NCC/Literature/Booklet_nr_4_Production_of_Phosphoric_Acid.pdf (sourced 2023-04-19).
12. https://www.eia.gov/tools/faqs/faq.php?id=74&t=11#:~:text=In%202019%2C%20total%20U.S.%20electricity%20generation%20by%20the,by%20type%20and%20efficiency%20of%20electric%20power%20plants. (accessed 2023-04-21)
13. https://www.statista.com/statistics/1289304/global-phosphoric-acid-production-capacity/ (sourced 2023-04-19)
14. https://www.iea.org/reports/co2-emissions-in-2022 (sourced 2023-04-19)

APPENDIX

The hydrometallurgical part of the process described in this aper was described previously[4]. The following description is provided here for the reader's convenience.

Primary leach

Figure A1 illustrates the primary leach in more detail. The line colours mean solid/slurry, liquid or gaseous flows, as above. The incoming pyrrhotite is slurried with recycled supernatant from the thickener after the leach and the resulting slurry is used to scrub HCl from the gaseous H_2S leaving the leach. The scrubbed H_2S goes to further processing (to elemental sulphur or sulphuric acid) and the slurry then enters the primary leach train. Recycled HCl/steam from the hydrolysis and calcination sections of the circuit is partially condensed to recapture the hydrochloric acid and return it to the primary leach, and also to condense enough of the steam to manage the energy balance over the primary leach such that it runs at about 90°C and the solution leaving the primary leach train is almost (but not quite) saturated in ferrous chloride.

The slurry leaving the primary leach train is thickened. Part of the supernatant is recycled to slurry the incoming pyrrhotite and the balance proceeds to the evaporation and hydrolysis sections of the circuit. The underflow goes to the secondary leach.

Table A1 shows the stoichiometry used to represent the primary leach. These reactions were assumed to proceed to completion.

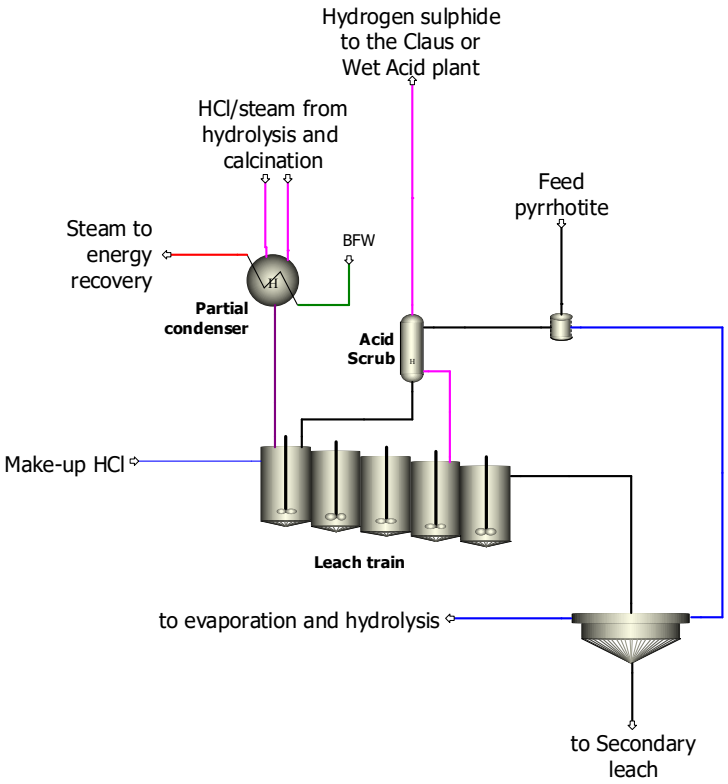

Figure A1 – Primary leach

Table A1 – Primary leach stoichiometry

$FeS + 2H^+ \rightarrow Fe^{2+} + H_2S$
$Fe_7S_8 + 14H^+ \rightarrow 7Fe^{2+} + 7H_2S + S$
$MgSiO_3 + 2H^+ \rightarrow Mg^{2+} + H_2O + SiO_2$

Secondary leach

Figure A2 illustrates the secondary leach in more detail. Thickener underflow from the primary leach is mixed with filtrate from the downstream filtration of hematite and also with gaseous steam/HCl from the iron hydrolysis step, cooled by heat exchange with water (making steam) and then pumped into the secondary leach autoclave, where it is leached with acid and oxygen (5 bar, 120°C), converting the nickel and cobalt sulphides to elemental sulphur and the corresponding aqueous chlorides. These reactions being exothermic, the autoclave is cooled by heat exchange with water, making steam that joins the steam from the heat exchanger before the secondary leach and goes to the energy recovery section. Table A2 shows the stoichiometry used to represent the secondary leach. As for the primary leach, all the reactions were assumed to go to completion.

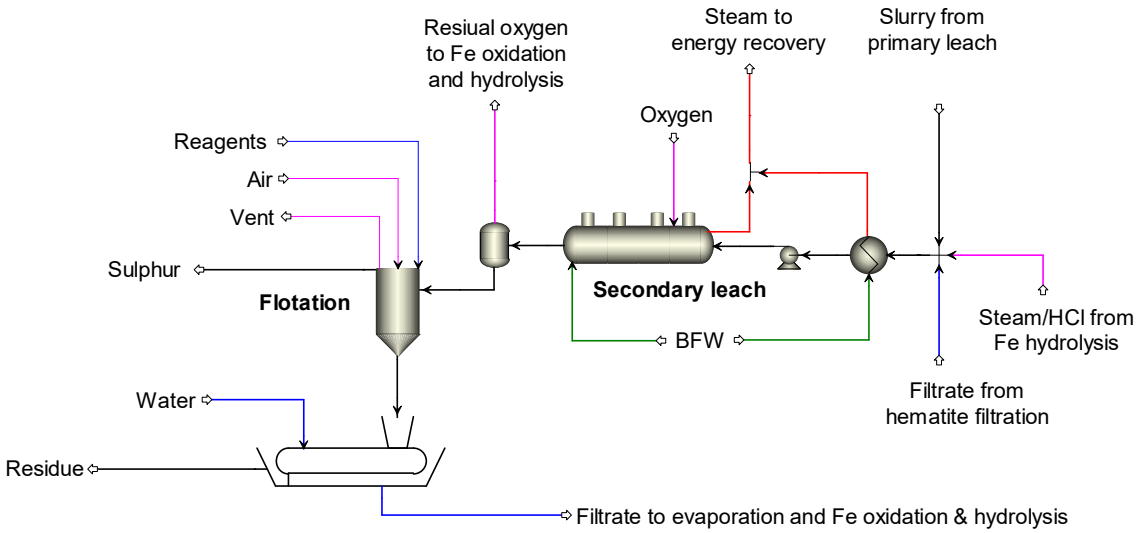

Figure A2 – Secondary leach

Table A2 – Secondary leach stoichiometry

$Ni_3S_2 + 6H^+ + 1½O_2 \rightarrow 3Ni^{2+} + 2S + 3H_2O$
$Ni_7S_6 + 14H^+ + 3½O_2 \rightarrow 7Ni^{2+} + 7H_2O + 6S$
$CoS + 2H^+ + ½O_2 \rightarrow Co^{2+} + H_2O + S$

Evaporation

Figure A3 illustrates the evaporation section. The purpose is to adjust the amount of water in the feed to the Fe oxidation and hydrolysis stage such that the HCl/steam leaving that hydrolysis step contains about 35 to 38 percent HCl by mass.

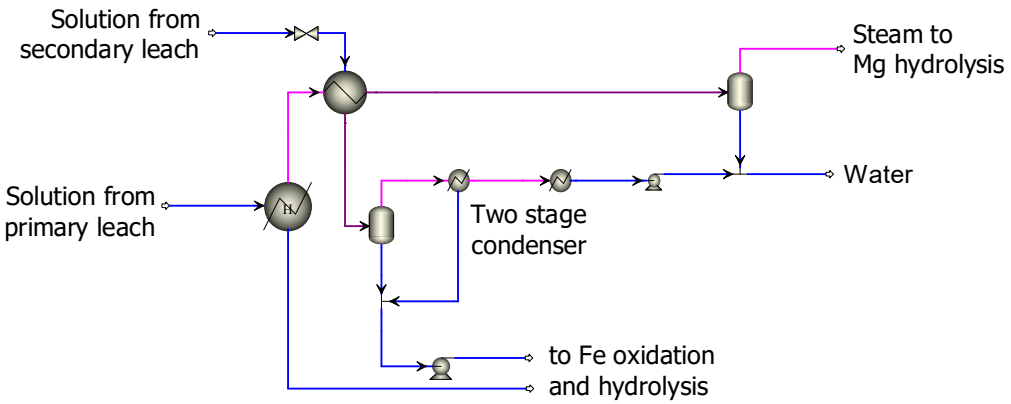

Figure A3 - Evaporation

Solution from the primary leach is boiled at atmospheric pressure, producing steam with a little HCl vapor. The remaining solution goes to the Fe oxidation and hydrolysis step. The solution from the secondary leach is depressurised to 0.1 bar absolute and heat exchanged with the steam from the first boiling step, condensing some water and all of the HCl from the atmospheric pressure steam. The resulting mixture of steam and condensate is separated, and the remaining steam goes to the Mg hydrolysis step. The sub-atmospheric steam and condensate from the heat exchange step is separated and the sub-atmospheric steam is partially condensed to capture any HCl. The resulting condensate joins the other sub-atmospheric condensate and is pumped to the Fe oxidation and hydrolysis step. The remaining sub-atmospheric steam is fully condensed and pumped back to atmospheric pressure and mixed with condensate from the atmospheric pressure steam. In the model the combined condensate leaves the circuit but in reality it would be recycled as process water.

Oxidation and hydrolysis

The stoichiometry used to represent the oxidation and hydrolysis steps is given in Table A3 and Table A4. In the Fe hydrolysis step, the concentrated oxidised slurry is heated further and contacted with steam/HCl recycled from the other hydrolysis steps, causing the ferric chloride to decompose to hematite and HCl, according to the stoichiometry shown for $FeCl_3$ in Table A4.

Table A3 – Oxidation stoichiometry

$6FeCl_2 + 1½O_2 + 3H_2O \rightarrow Fe_2O_3 + 4FeCl_3$

Table A4 – Hydrolysis stoichiometry

$2FeCl_3 + 3H_2O \rightarrow Fe_2O_3 + 6HCl$
$2NiCl_2 + 3H_2O \rightarrow Ni_2(OH)_3Cl + 3HCl$
$2CoCl_2 + 3H_2O \rightarrow Co_2(OH)_3Cl + 3HCl$
$MgCl_2 + H_2O \rightarrow Mg(OH)Cl + HCl$

Figure A4 illustrates the oxidation and hydrolysis section. Concentrated solution from the evaporation section is mixed with recycled hydrolysis mother liquor and oxidised with oxygen, converting almost all of the ferrous chloride to ferric chloride and ferric oxide. (A small amount of ferrous chloride is left to preclude the formation of chlorates and chlorine.)

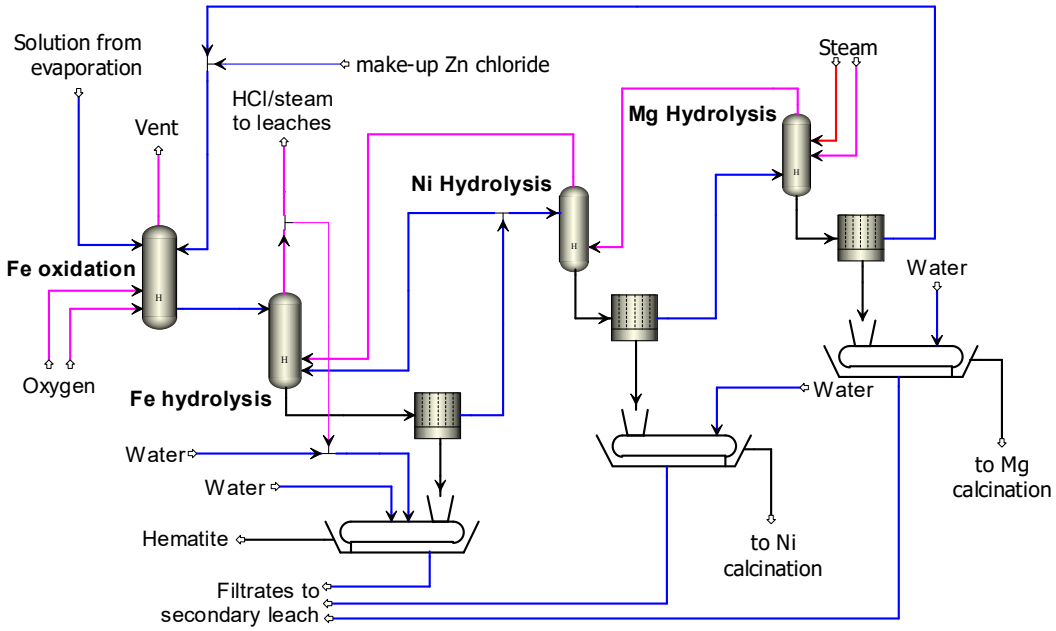

Figure A4 – Oxidation and hydrolysis

The hematite slurry is filtered hot and the filtrate proceeds to the Ni hydrolysis step. The hematite filter cake is washed with dilute acid (water plus a little of the acid/steam ex the Fe hydrolysis step)and again with water. The combined filtrate is returned to the secondary leach and the washed hematite leaves the circuit.

The hot filtrate from the Fe hydrolysis step is contacted with steam/HCl from the Mg hydrolysis step, causing the base metals to hydrolyse to the corresponding hydroxy chlorides according to the stoichiometry shown for nickel and cobalt in **Error! Reference source not found.**. He resulting slurry is filtered hot, the filtrate proceeding to the Mg hydrolysis step. The filter cake is washed with water and the filtrate is recycled to the secondary leach.

The hot filtrate from the Ni hydrolysis step is heated further and steam is added, causing the magnesium chloride to hydrolyse to magnesium hydroxy chloride as per the stoichiometry shown in **Error! Reference source not found.** for magnesium.

Calcination

The washed hydroxy chloride filter cakes from the Ni and Mg hydrolysis steps are converted to the corresponding oxides by calcination in hot air, as illustrated in Figure A5. The stoichiometry used to represent this is listed in Table A5. The resulting oxides leave the circuit and the hot acid-bearing gasses from the calcination kilns are recycled to the partial condenser in the primary leach section.

Table A5 – Calcination stoichiometry

$Ni_2(OH)_3Cl \rightarrow 2NiO + HCl + H_2O$
$Co_2(OH)_3Cl \rightarrow 2CoO + HCl + H_2O$
$Mg(OH)Cl \rightarrow MgO + HCl$

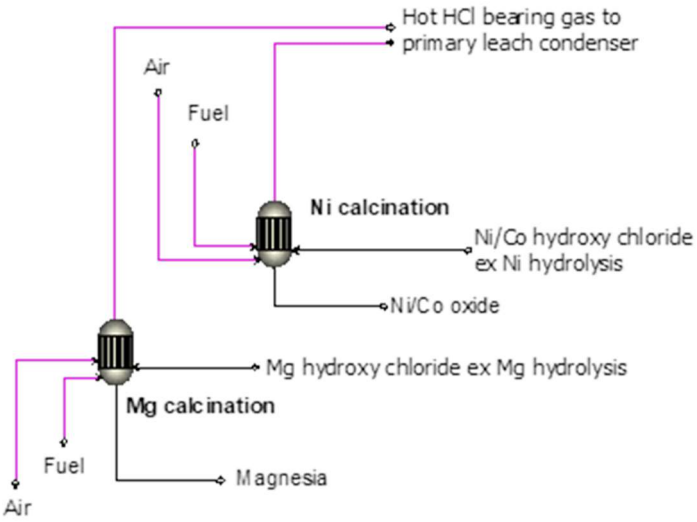

Figure A5 - Calcination

PRODUCTION OF NICKEL–COBALT–MANGANESE MIXTURES WITH TAILORED COMPOSITIONS FROM COBALT-RICH LITHIUM-ION BATTERY LEACHATES BY SOLVENT EXTRACTION

By

Niklas Jantunen, [2]Sami Virolainen, [3]Tuomo Sainio

LUT University, Finland
[2]LUT University, Finland
[3]LUT University, Finland

Presenter and Corresponding Author

Niklas Jantunen
niklas.jantunen@lut.fi

ABSTRACT

Recovery of metals from end-of-life lithium-ion batteries (LIBs) promotes sustainability and resource efficiency. The metals in spent LIB cathodes are typically liberated by reductive acid leaching, which produces heterogeneous multi-metal solutions (LIB leachates). The LIB leachates contain mainly lithium, nickel, cobalt, and manganese, together with significantly lower amounts of aluminium, iron, and copper.

Solvent extraction (SX) is an established technique for separating the metals from the LIB leachates. In conventional SX processes the metals are separated into their own purified solution fractions, from where they can be precipitated or crystallized as pure metal salts, or electrowon. Because of the increasing demand of new batteries and shift towards nickel-rich LIB cathode chemistries, an alternative process concept in which a mixture with a specific stoichiometric ratio of nickel, cobalt, and manganese (*e.g.*, 8:1:1) (NCM mixture), is obtained directly from the SX process. The NCM mixture can then be used as such, or after polishing treatment, in the co-precipitation synthesis of new precursor cathode active materials (PCAM) without additional input of nickel, cobalt, or manganese to the synthesis solution. Furthermore, purified lithium sulphate, manganese sulphate, and cobalt sulphate solutions are obtained simultaneously from the SX process.

The excess manganese and cobalt were extracted from a synthetic cobalt-rich LIB leachate by 0.8 M bis(2-ethylhexyl) hydrogen phosphate (D2EHPA) and 0.8 M bis(2,4,4-trimethylpentyl)phosphinic acid (Cyanex 272), respectively. The remaining cobalt and nickel were extracted together from the leachate by 0.8 M D2EHPA. Mixing of the cobalt- and nickel-bearing D2EHPA with manganese-loaded D2EHPA yields NCM-D2EHPA, from which the NCM sulphate mixture is produced by stripping.

A non-optimized flowsheet was designed based on the measured liquid-liquid equilibrium data, and the extraction characteristics of D2EHPA and Cyanex 272. The key separations of the flowsheet were demonstrated and studied further in continuous counter-current mode in industrial-type laboratory mixer-settlers (MEAB MSU0,5; MEAB Metallextraktion AB, Sweden).

An NCM mixture with n(Ni):n(Co) = 14.16 and n(Ni):n(Mn) = 8.06 was produced by continuous stripping of NCM-D2EHPA. The stoichiometric ratio of nickel, cobalt, and manganese can be adjusted to, for example, 8:1:1 using the cobalt-rich raffinate obtained from the same process. The raffinate from stripping of cobalt-loaded Cyanex 272 contained 102.7 g dm^{-3} cobalt at 99.8 % relative purity without intermediate scrubbing.

Keywords: solvent extraction, lithium, nickel, cobalt, manganese, co-extraction, recycling, lithium-ion batteries

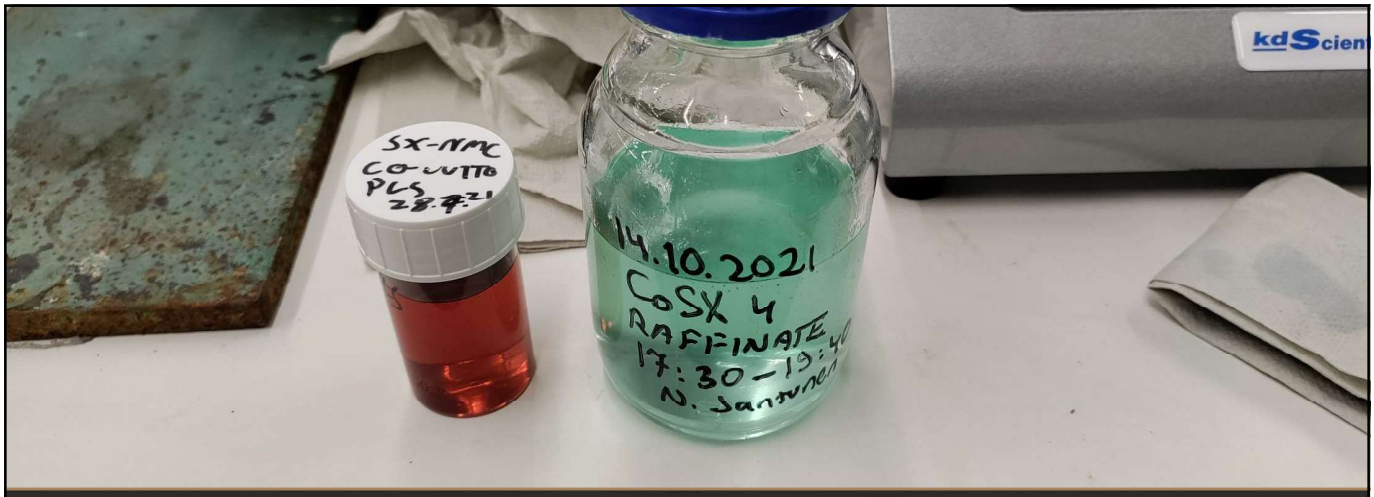

Background

From waste NMC cathodes to new NMC cathodes

Processing of waste LIB cathodes

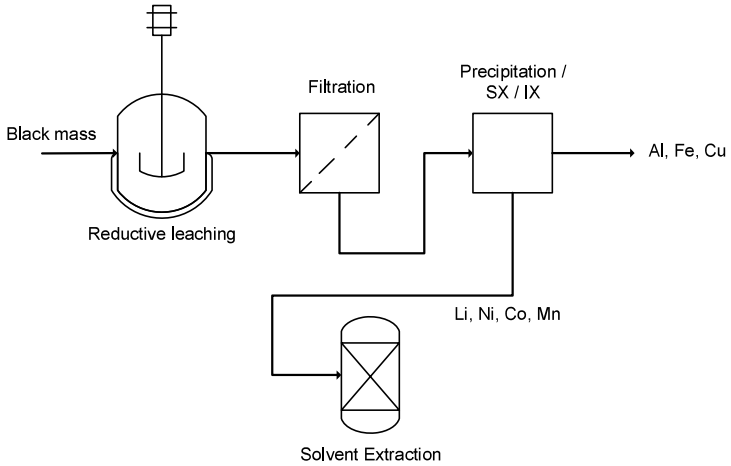

- After mechanical processing, recycled NMC cathode powder (black mass) is leached under reducing conditions to liberate the valuable cathode metals. Leaching by H_2SO_4 and H_2O_2 is an efficient and economical method.
- Aluminium, iron, and copper can be removed from the leachate by precipitation, solvent extraction, and/or ion exchange
- Separation of lithium, nickel, cobalt, and manganese can be done using commercial SX reagents

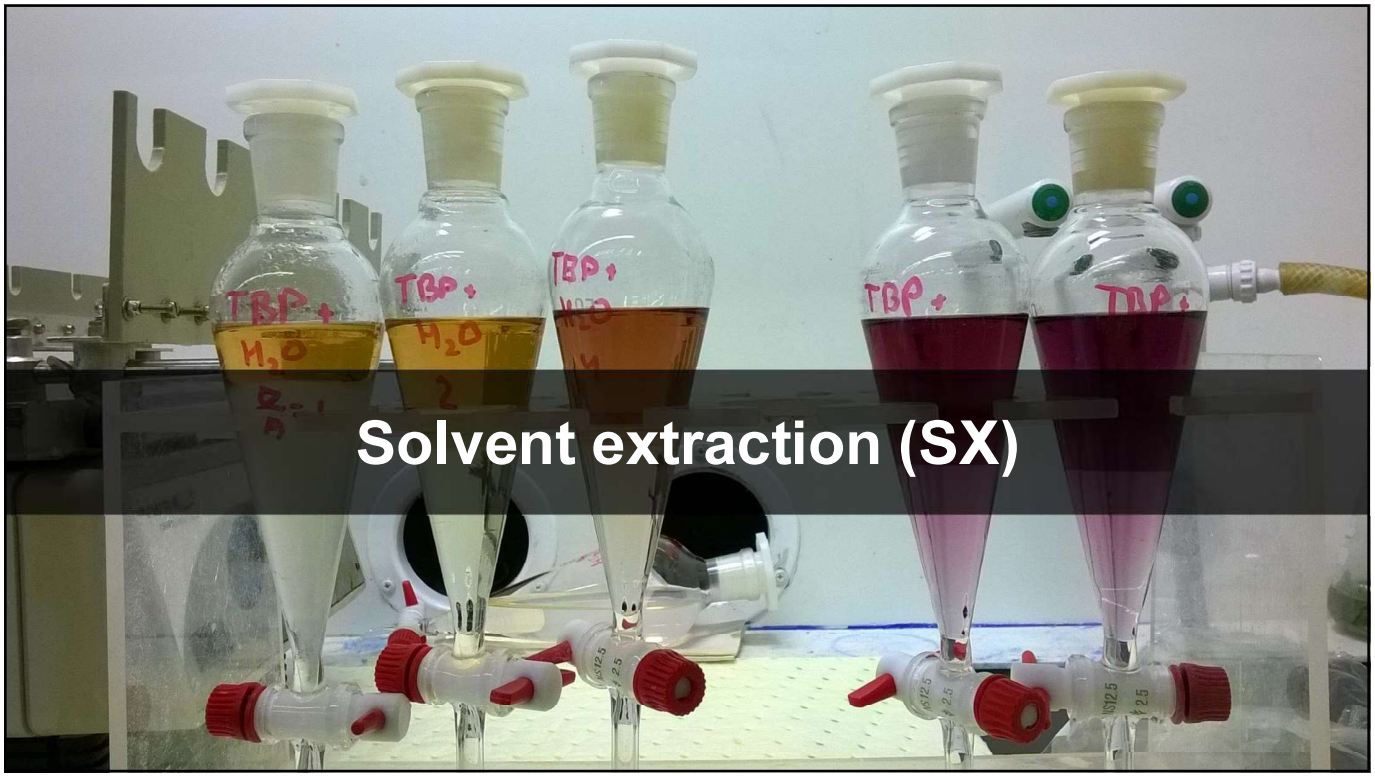

Separation of Li, Ni, Co, Mn – main SX strategies

- Fractionation

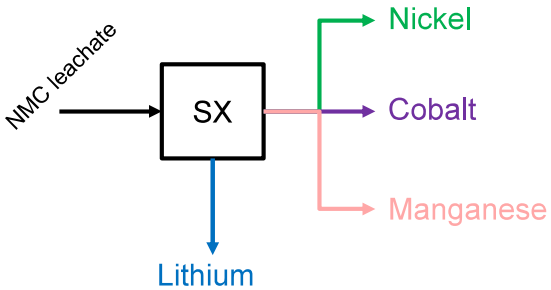

- Co-extraction

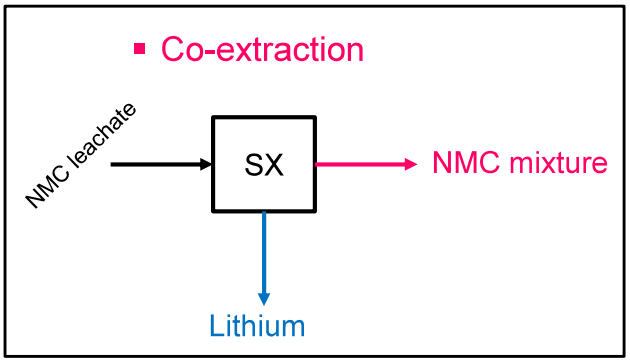

It is possible to separate the metals into their own fractions by SX. However, mixtures of $NiSO_4$, $CoSO_4$, and $MnSO_4$ are used in co-precipitation synthesis of new precursor cathode active materials (PCAM). Discussion here is focused on such SX processes, in which at least one of the products is a mixture containing nickel, cobalt, and manganese. Stoichiometric ratios of nickel, cobalt, and manganese are very specific in PCAM production. When the stoichiometric ratios in the feed are not equal to the target stoichiometry, compositional tuning is required.

Tuning the stoichiometry

- NMC811 precursor
  - n(Ni)/n(Mn) = 8
  - n(Ni)/n(Co) = 8
- Cobalt-rich sulfate feed solution:
  - $[Li]_0$ = 2.5 g/L
  - **$[Ni]_0$ = 2 g/L**
  - **$[Co]_0$ = 16.5 g/L**
  - **$[Mn]_0$ = 2.1 g/L**
  - The stoichiometric constraint is not satisfied

Alternative approaches

1. **Extract all Ni, Co, and Mn to the organic solvent phase**
   - Li remains in the raffinate
   - Strip the loaded organic
   - Composition tuning by addition of pure Ni and Mn sulfates to the stripping raffinate
2. **Separate EXCESS Co and Mn so that the stoichiometric target is met**
   - This is the only way without using additional pure Ni and Mn sulfates (mass balance)

Approach 1 – addition of pure metal salts

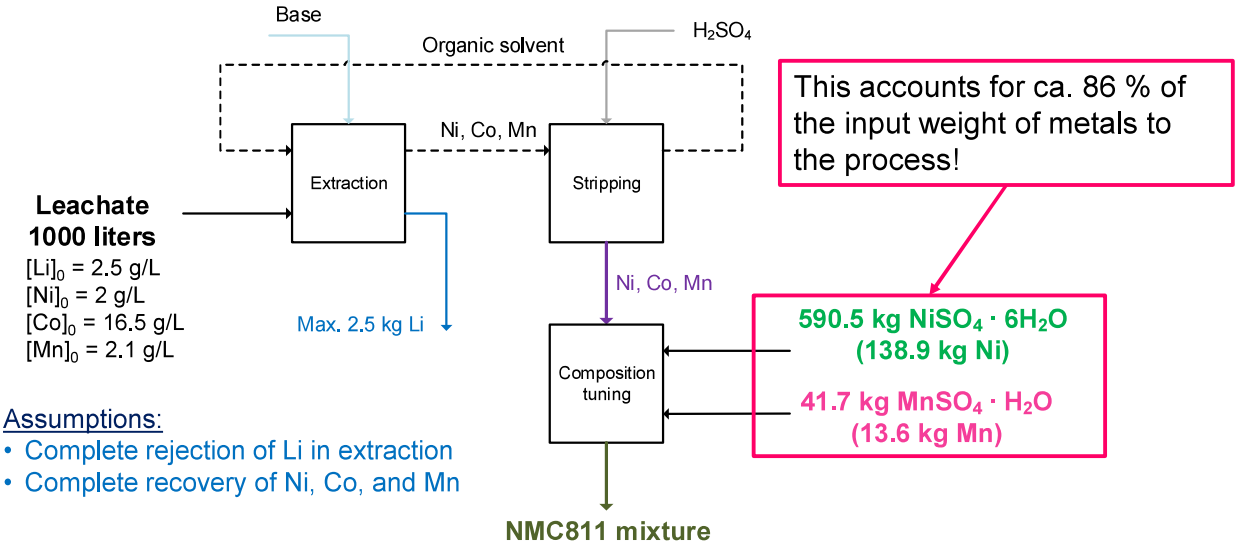

This accounts for ca. 86 % of the input weight of metals to the process!

Assumptions:
- Complete rejection of Li in extraction
- Complete recovery of Ni, Co, and Mn

Approach 2 – partial separation

- *How* the metals are extracted by common acidic SX reagents
- Discussion on flowsheeting

SX of Li, Ni, Co, and Mn by D2EHPA and CYANEX 272

- **D2EHPA**
- bis(2-ethylhexyl) hydrogen phosphate
  - *aka.* di-2-ethylhexyl phosphoric acid

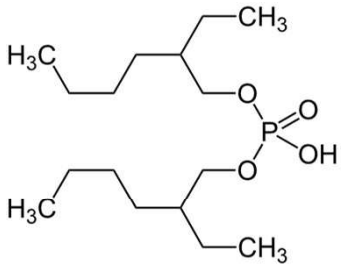

These reagents exchange protons for metal cations
- reversible reactions

- **CYANEX 272**
- 85–90 % bis(2,4,4-trimethylpentyl)-phosphinic acid (BTMPPA)
- 10–15 % tris(2,4,4-trimethylpentyl)-phosphine oxide

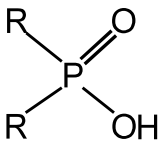

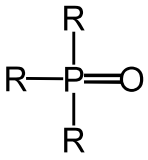

R = 2,4,4-trimethylpentyl-

SX of Li, Ni, Co, and Mn by D2EHPA and CYANEX 272

A cobalt-rich synthetic leachate

$[Li]_0$ = 2.5 g/L

$[Ni]_0$ = 2 g/L

$[Co]_0$ = 16.5 g/L

$[Mn]_0$ = 2.1 g/L

SULFATE MEDIA

Metal stoichiometry of the leachate was taken from literature:
Porvali, A.; Aaltonen, M.; Ojanen, S.; Velazquez-Martinez, O.; Eronen, E.; Liu, F.; Wilson, B.P.; Serna-Guerrero, R.; Lundström, M., Mechanical and Hydrometallurgical Processes in HCl Media for the Recycling of Valuable Metals from Li-Ion Battery, *Waste.Resour. Conserv. Recycl.* **2019**, 142, 257–266. https://doi.org/10.1016/j.resconrec.2018.11.023.

SX of Li, Ni, Co, and Mn by D2EHPA and CYANEX 272

$[Li]_0$ = 2.5 g/L; $[Ni]_0$ = 2 g/L; $[Co]_0$ = 16.5 g/L; $[Mn]_0$ = 2.1 g/L SULFATE MEDIA

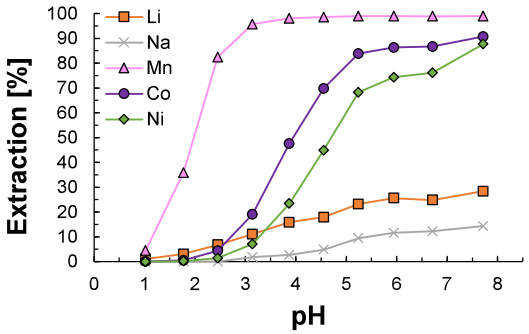

- 0.8 M D2EHPA (5 vol% TBP)
  - O/A = 1; *T* = 25 °C

Diluent: Exxsol D80 (< 0.5 % aromatics)

SX of Li, Ni, Co, and Mn by D2EHPA and CYANEX 272

$[Li]_0$ = 2.5 g/L; $[Ni]_0$ = 2 g/L; $[Co]_0$ = 16.5 g/L; $[Mn]_0$ = 2.1 g/L SULFATE MEDIA

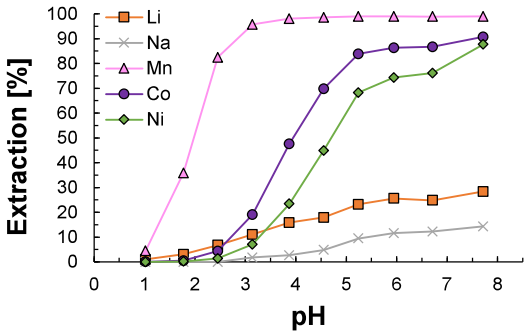

- 0.8 M D2EHPA (5 vol% TBP)
  - O/A = 1; *T* = 25 °C

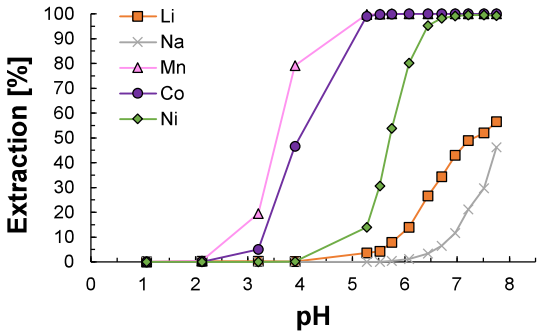

- 0.8 M CYANEX 272
  - **O/A = 2.5**; *T* = 25 °C

Diluent: Exxsol D80 (< 0.5 % aromatics)

SX of Li, Ni, Co, and Mn by D2EHPA and CYANEX 272

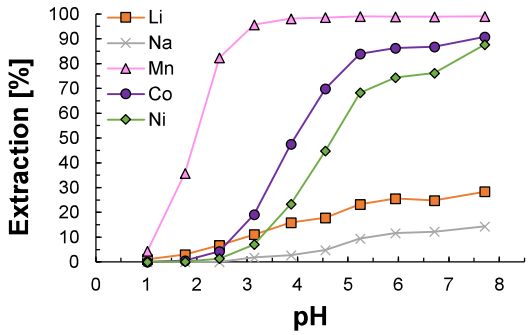

0.8 M D2EHPA (5 vol% TBP) in Exxsol D80

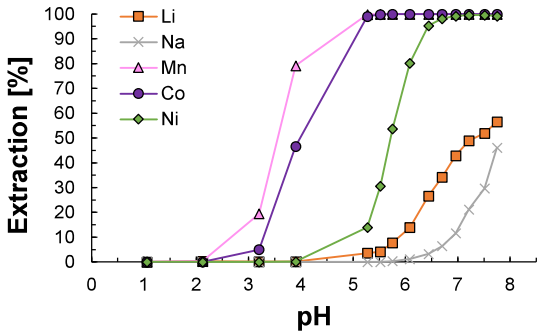

0.8 M CYANEX 272 in Exxsol D80

- D2EHPA: Separation of cobalt and nickel is difficult
- CYANEX 272: Separation of cobalt and manganese is difficult

→ Two different SX circuits

Flowsheeting

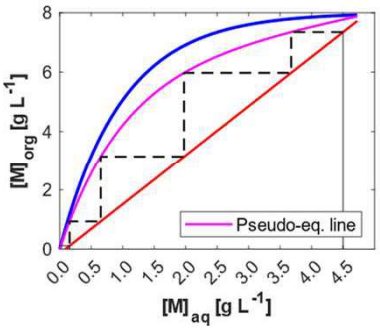

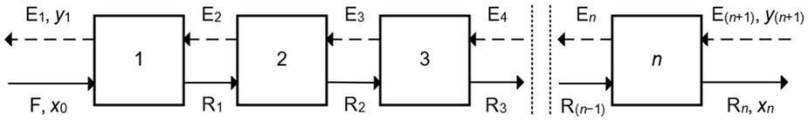

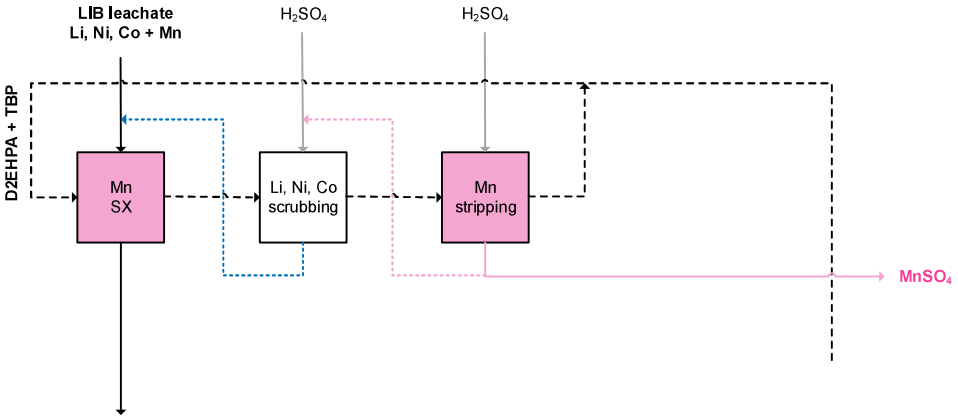

The feed is nickel-deficient with respect to nickel-rich NMC stoichiometries. Therefore, the process must separate excess manganese…

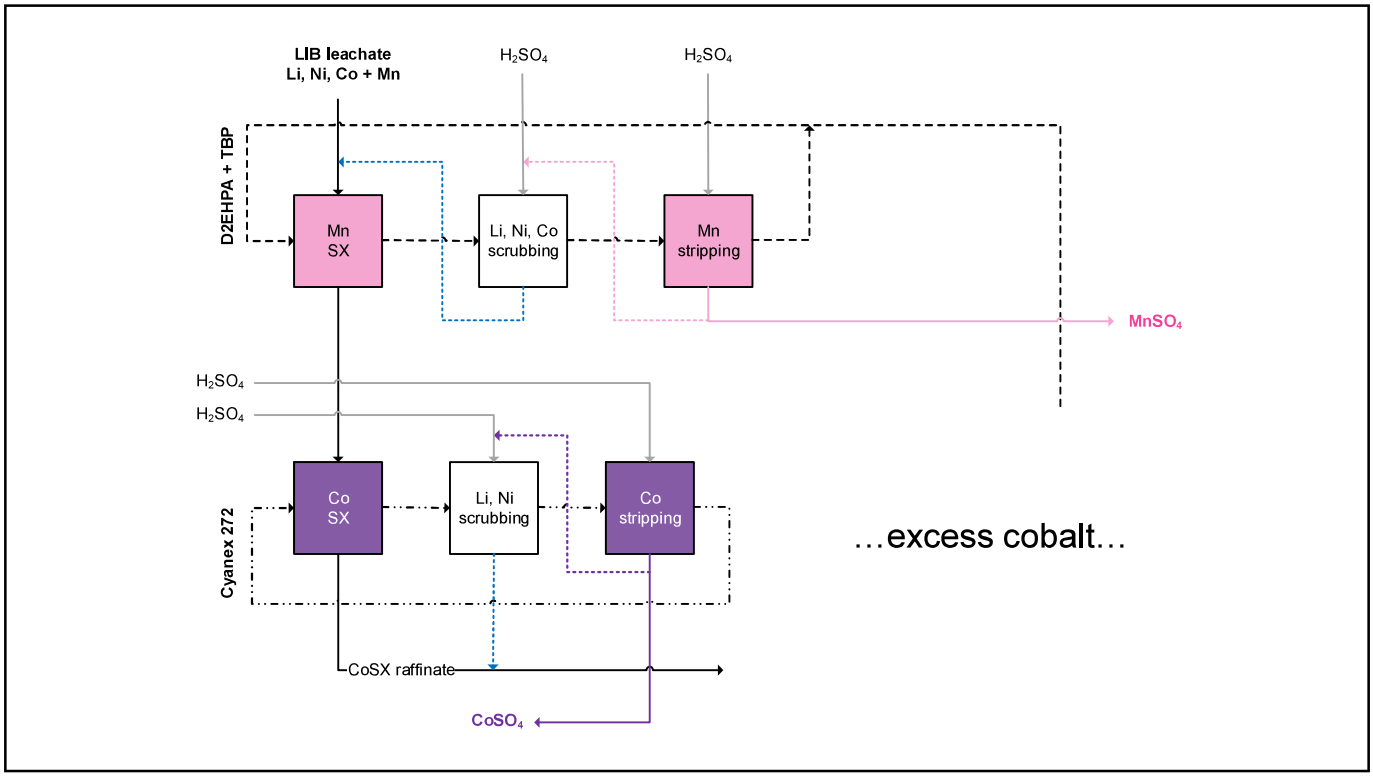
LIB leachate
Li, Ni, Co + Mn
H_2SO_4
H_2SO_4
D2EHPA + TBP
Mn SX
Li, Ni, Co scrubbing
Mn stripping
$MnSO_4$
H_2SO_4
H_2SO_4
Co SX
Li, Ni scrubbing
Co stripping
Cyanex 272
CoSX raffinate
$CoSO_4$
…excess cobalt…

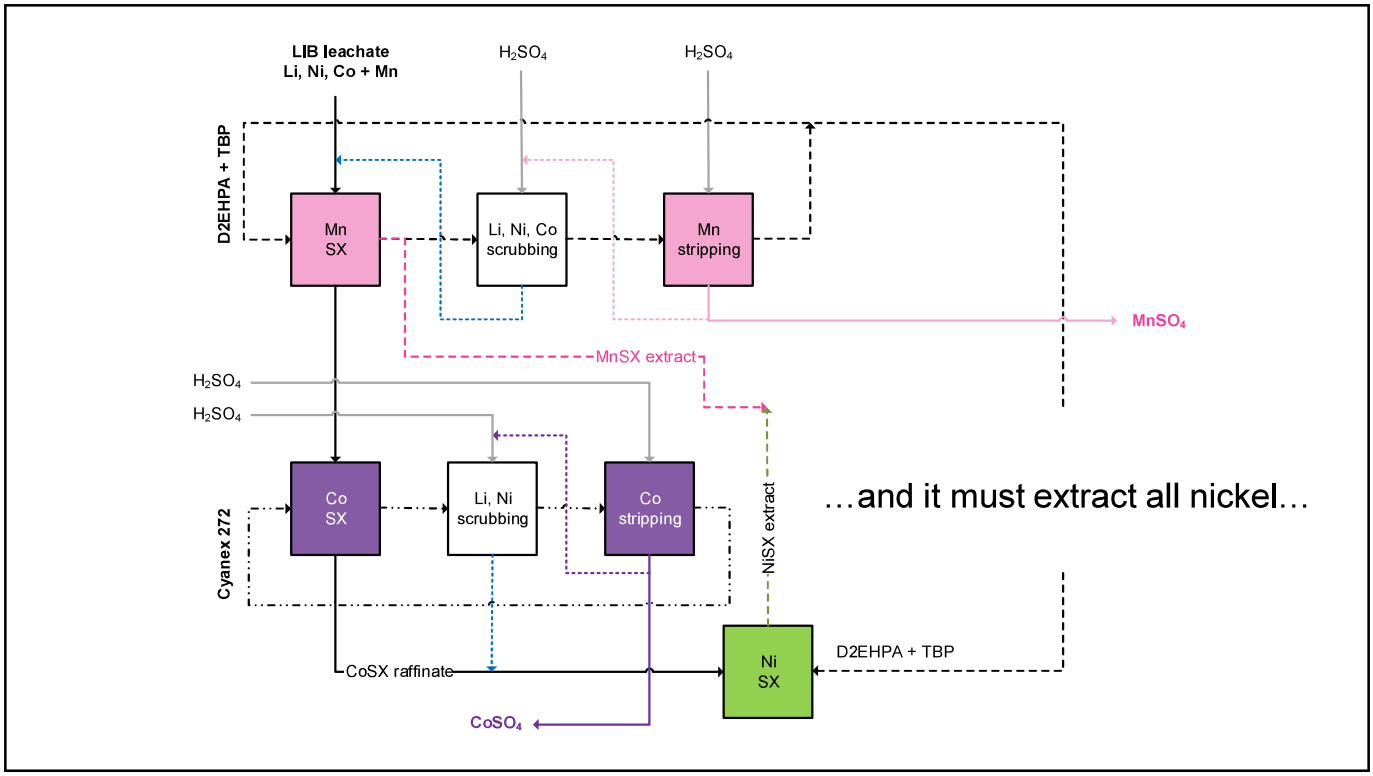
LIB leachate
Li, Ni, Co + Mn
H_2SO_4
H_2SO_4
D2EHPA + TBP
Mn SX
Li, Ni, Co scrubbing
Mn stripping
$MnSO_4$
MnSX extract
H_2SO_4
H_2SO_4
Co SX
Li, Ni scrubbing
Co stripping
NiSX extract
Cyanex 272
CoSX raffinate
Ni SX
D2EHPA + TBP
$CoSO_4$
…and it must extract all nickel…

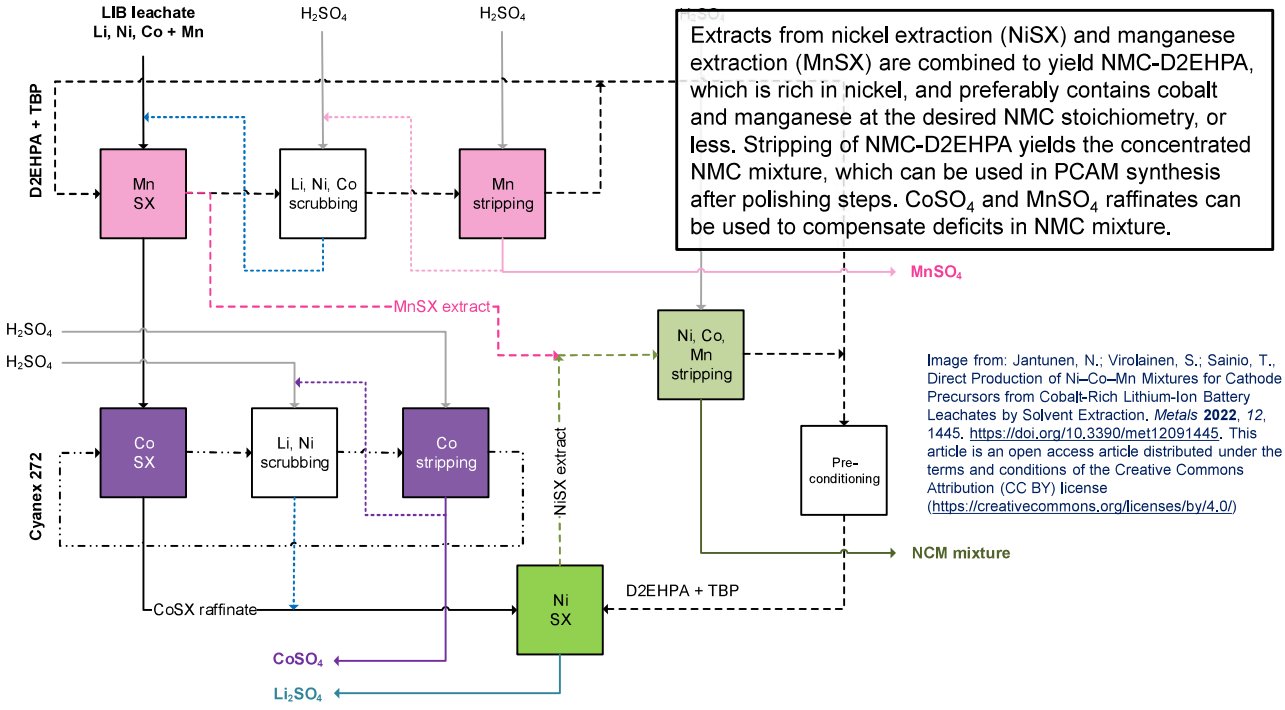

Extracts from nickel extraction (NiSX) and manganese extraction (MnSX) are combined to yield NMC-D2EHPA, which is rich in nickel, and preferably contains cobalt and manganese at the desired NMC stoichiometry, or less. Stripping of NMC-D2EHPA yields the concentrated NMC mixture, which can be used in PCAM synthesis after polishing steps. $CoSO_4$ and $MnSO_4$ raffinates can be used to compensate deficits in NMC mixture.

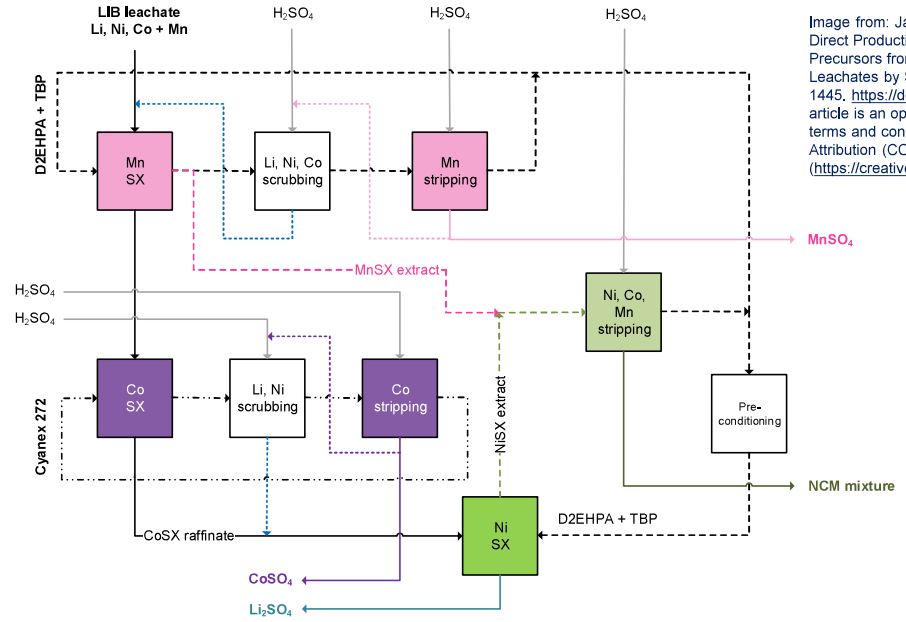

Image from: Jantunen, N.; Virolainen, S.; Sainio, T., Direct Production of Ni–Co–Mn Mixtures for Cathode Precursors from Cobalt-Rich Lithium-Ion Battery Leachates by Solvent Extraction. *Metals* **2022**, *12*, 1445. https://doi.org/10.3390/met12091445. This article is an open access article distributed under the terms and conditions of the Creative Commons Attribution (CC BY) license (https://creativecommons.org/licenses/by/4.0/)

Fill colours indicate experimentally studied parts of the flowsheet

Few more things to consider…

- Management of impurities?
  - Al, Fe, Cu, **Cd, Mg etc.**
- Entrainment and extractant solubility in the aqueous phase
  - Raffinate polishing steps are likely required
- **Scrubbing of the loaded solvents**
  - Can **significantly** improve purities in the stripping raffinates
- Feed composition and process control
  - Online concentration measurements and automation are required

Summary

- Experimental results
  1. Higher than 99 wt% relative purity of cobalt, without scrubbing
     - Over 100 g/L Co
  2. NMC-D2EHPA (0.8 M D2EHPA, mod. 5 vol% TBP in Exxsol D80)
     - n(Ni)/n(Co) = 14.16 ← Cobalt deficit can be compensated using the $CoSO_4$ raffinate
     - n(Ni)/n(Mn) = 8.06
  - Lithium sulfate raffinate
     - **1.68 g/L Li, 26.7 g/L Na**, 1 mg/L Co, 39 mg/L Ni

The presentation is based on Jantunen, N.; Virolainen, S.; Sainio, T., Direct Production of Ni–Co–Mn Mixtures for Cathode Precursors from Cobalt-Rich Lithium-Ion Battery Leachates by Solvent Extraction. *Metals* **2022**, *12*, 1445. https://doi.org/10.3390/met12091445.

THE PRODUCTION OF BATTERY GRADE NICKEL SULPHATE FROM VARYING FEED SOURCES

By

Nipen M. Shah[1], Katherine Lombard [2] and Dave Rogans[2]

[1]JordProxa Pty Ltd, Australia
[2]JordProxa Pty Ltd, South Africa

Presenter and Corresponding Author

Nipen Shah
nshah@jordproxa.com

ABSTRACT

The increasingly rapid growth of the electric vehicle market has led to an exponential increase in the demand for battery materials such as nickel, cobalt, manganese, and lithium. The safety and performance of lithium-ion batteries is greatly affected by impurities in the precursors and hence it is imperative that these chemicals are produced to the highest purity. The specifications for the impurities are becoming more stringent which has driven innovation in the refining and purification processes.

The impurity profile of the feed to the nickel sulphate crystallisation plant is dependent on the ore type and the purification steps (solvent extraction & ion exchange) involved upstream of the process. Crystallisation is an important final step in producing battery grade products. The crystallisation process flow sheet and the equipment design are dependent on the impurities in the feed to the crystalliser and the operating conditions that can produce the desired form of the product.

This paper discusses typical feed chemistries from varying sources, factors affecting the product purity, and the fundamental balance between purity and operating conditions versus capex and opex during flowsheet development.

Keywords: Nickel sulphate, crystallisation, product purity, battery

PURITY - Free from impurities

SUSTAINABILITY - Low carbon footprint

VALUE - High ratio of performance / cost

NiSO4 Crystallisation and Product Forms

1

Simplified crystallisation process

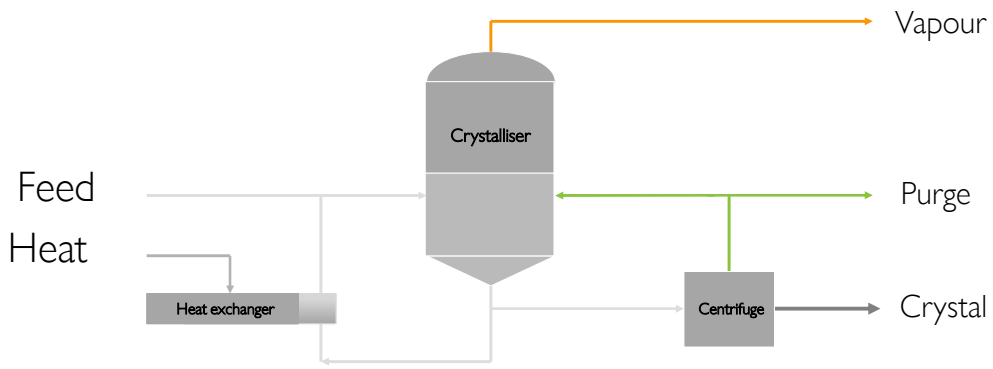

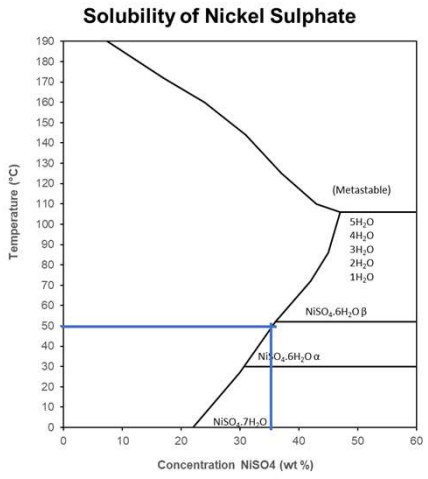

NiSul Crystals – before drying

α - Alpha

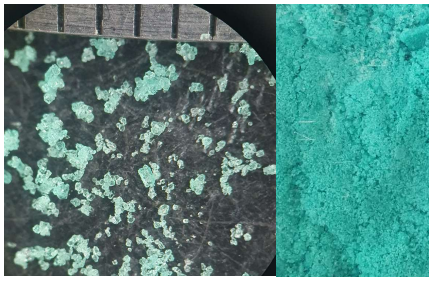

LT at 50 °C
Clarity: Slightly opaque
Colour: Turquoise

β - Beta

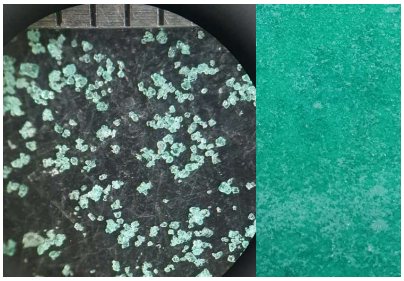

LT at 75 °C
Clarity: Translucent
Colour: Green

NiSul Crystals – after drying

α - Alpha

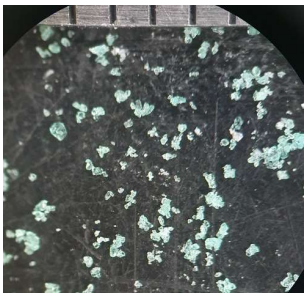

β - Beta

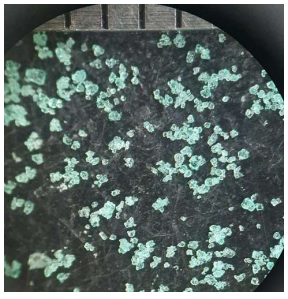

No major changes observed in crystal PSD after drying
(1 hr at 50 °C) for both a and β crystals.

NiSul β Crystals – after 24 hr

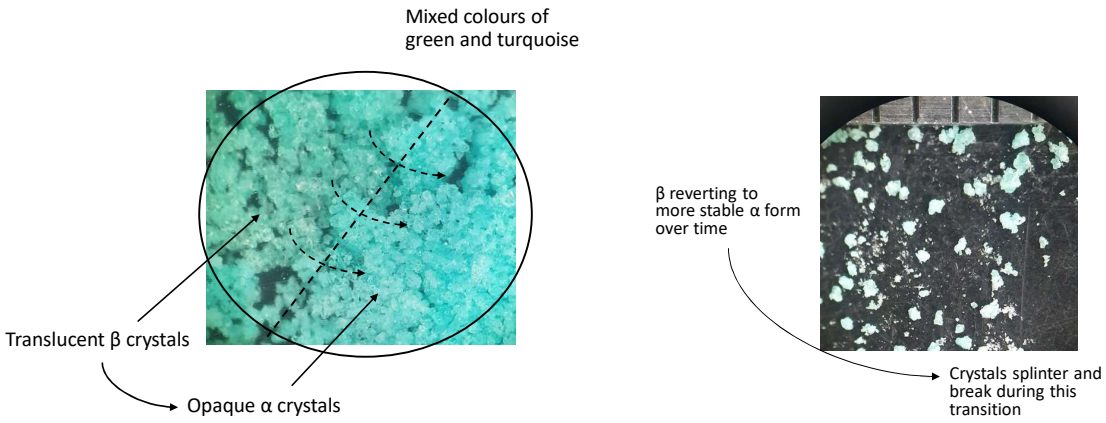

Comparing α and β crystals.

- Distinct differences observed between α and β crystals.
- No changes observed in α and β crystal PSD's after 1hr of drying at 50 °C.
- After 24 hours we observed β reverts to the more stable a form over time (slow kinetics) causing crystals to splinter, and break creating fines.
- Observation on dried crystal clumps (~10 mm): β clumps are substantially harder to break than α clumps.

2

Design Considerations

Design Approach

- Maximise purity
- Maximise yield
- Minimise CAPEX and OPEX costs
- Ease of operation with robust design

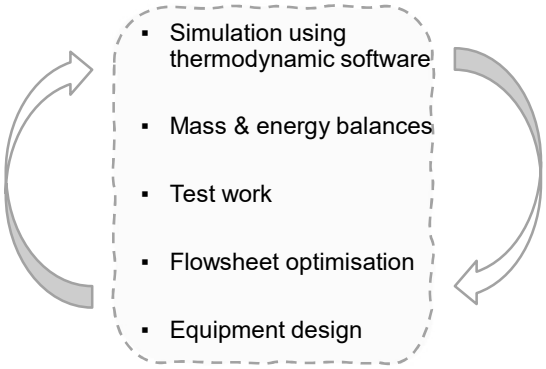

- Sufficient residence time to allow large crystals to grow
- Sufficient mixing to expose large crystals to the zone with highest level of supersaturation
- Control of slurry density
- Control of temperature, pressure and level

FEED QUALITY FROM VARIOUS SOURCES

Element	Unit	Excellent Feed	Good Feed	Typical Feed
Ni	g/L	162	162	162
$NiSO_4$	wt%	30	30	30
$NiSO_4$	g/L	426	426	426
Total impurities	mg/L	72	720	1450
Impurities / NSH	mg/kg	100	1000	2000

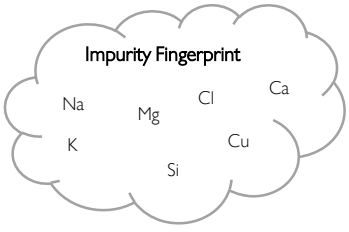

TYPICAL PRODUCT SPECIFICATIONS

Element	Unit	Typical 1	Typical 2
Ni	% min	22.3%	22%
$NiSO_4.6H_2O$	% min	99.9% ("3 nines")	98.5%
Co	ppm max	10	10
Na	ppm max	1	5-20
Mg	ppm max	1	5-20
Cl	ppm max	5	10
Cu	ppm max	1	1-5
Si	ppm max	1	5
K	ppm max	1	5

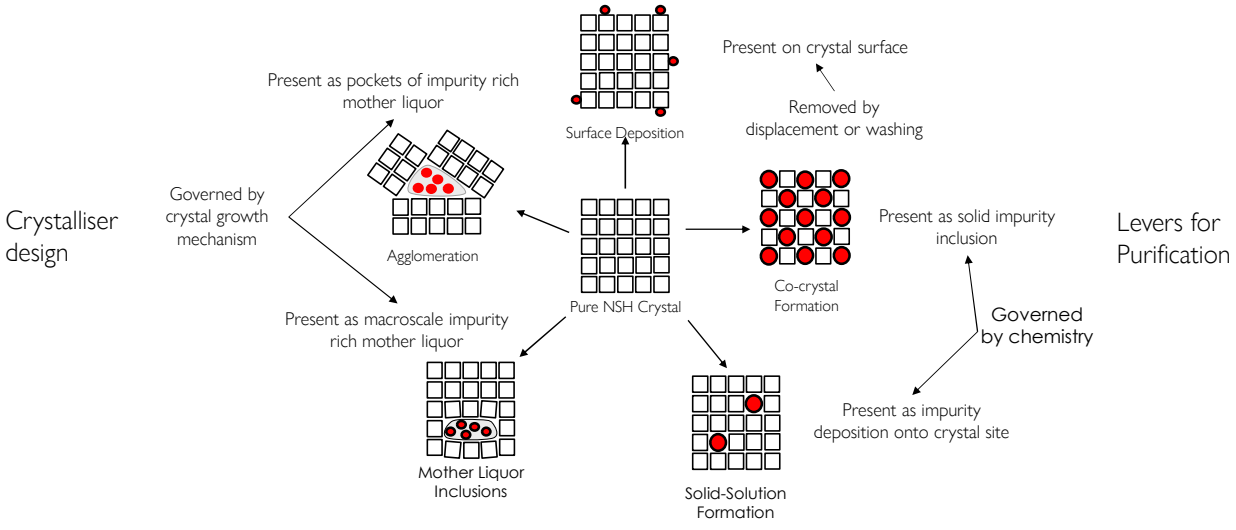

Ref: Urwin, S.J., et al. (2020)

Levers for Purification

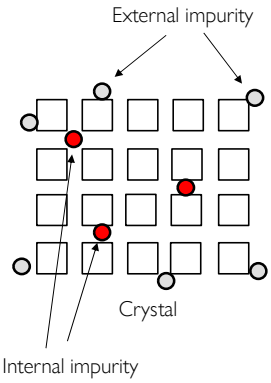

- Centrifugation displaces surface depositions by washing and ML removal.
- Wash legs reduce surface depositions by partly displacing high impurity ML with feed.

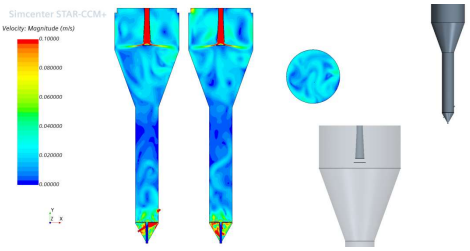

Levers for Purification

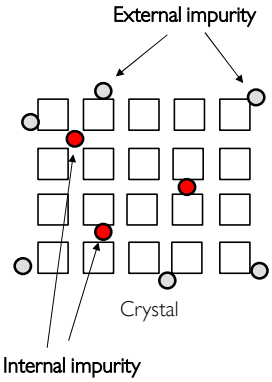

- Staged crystallisation reduces ML impurity fingerprint profile.
- Purge/Recycle rates reduce ML impurity fingerprint profile.

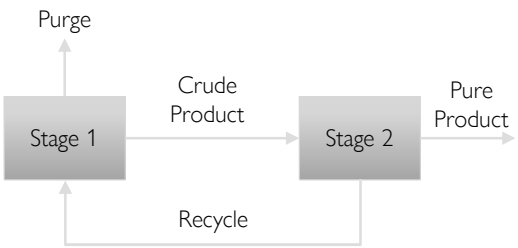

3

Crystalliser Performance

Purity Enhancement Factor (PEF) $= \dfrac{(\text{Impurity / desired species})_{\text{feed}}}{(\text{Impurity / desired species})_{\text{product}}}$

REQUIRED PERFORMANCE TO MAKE BATTERY GRADE

		4 nines product		5 nines product	
	mg impurity / kg NSH	mg impurity / kg NSH	Required PEF	mg impurity / kg NSH	Required PEF
TYPICAL	2,000	100	20	10	200
GOOD	1,000	100	10	10	100
EXCELLENT	100	100	n/a	10	10

CRYSTALLISER PERFORMANCE

	purge fraction	entrainment	wash efficiency	Fraction of impurity		PEF
				purged	on crystals	
conventional single stage	5%	5%	80%	91.3	8.7	10.8
optimised single stage	10%	3%	85%	98.02	1.98	44.6
two stage	5%	5%	80%	99.24	0.76	113

4

Conclusions

CONCLUSIONS

- Crystallisation is a key step in the processing of battery materials such as nickel sulphate to achieve the desired product purity.
- Alpha and beta form of Nickel sulphate hexahydrate products were evaluated. Although the costs associated with producing a beta product is less, it introduces challenges associated with product quality and product handling.
- A carefully designed crystalliser can produce crystals large enough for effective dewatering and washing.

CONCLUSIONS

- A carefully designed crystalliser can produce crystals large enough for effective dewatering and washing.

- We need to control liquor chemistry & kinetics to prevent lattice substitution; formation of double salts; inclusions and agglomerates.

- As the demand for the product purity increases, the requirement for optimisation and further enhances in the technology become critical.

IONQUEST® RANGE PRODUCTS FOR METAL RECYCLING

By

Chiara Francesca Carrozza, Filip Dutoy, Daniele Ciferri

Italmatch Chemicals Spa, Italy

Presenter and Corresponding Author

Chiara Francesca Carrozza
c.carrozza@italmatch.com

ABSTRACT

As of today, metal recycling is a vital process to reduce environmental impact, use fewer resources, and lower the production costs of new materials. In particular, with new challenging ores as raw materials and the increasing interest in metal recycling from secondary sources (e.g. recycled Li batteries), there is an unmet need for developing new solutions capable to selectively extract specific elements such as Mn, Co, Ni and Li and to fit the complexity of different metals matrices.

In this work, a solvent extraction study will be investigated starting from either a sulphate and chloride leach solution of spent cathode material. The data will highlight the improved selectivity and recovery of metals using organic phosphoric acidic extraction here named IONQUEST® products.

The influence of several experimental parameters was examined including aqueous phase pH, extractant concentration, aqueous/organic ratio and pre-neutralization of the extractant. An evaluation of the optimal pH gap between Ni vs Co and Co vs Mn was determined. Results demonstrate the improved selectivity performances for manganese using the strong acidic IONQUEST® 220 and cobalt using IONQUEST® 290 in several conditions. Based on the data collected, two sequential solvent extraction circuits to separate firstly manganese and eventually cobalt and nickel will be shown. The number of stages required for both extraction and stripping processes of cobalt, manganese and nickel was also evaluated.

Finally, the combination of two different extractants and/or the addition of a neutral one in different ratio will be presented aiming to improve the selectivity towards specific metal.

Key words: IONQUEST® products, spent Li-batteries, solvent extraction, selectivity

AGENDA

INTRODUCTION	IONQUEST® RANGE PRODUCTS AND BATTERY RECYCLING
SULFURIC ACID PLS	BATCH EXTRACTION TEST MAXIMUM LOADING SCHEMATIC FLOWSHEET
CITRIC ACID PLS	WHY CITRIC ACID BATCH EXTRACTION TEST AND MAXIMUM LOADING IMPROVED LITHIUM EXTRACTION SCHEMATIC FLOWSHEET
CONCLUSION AND FURTHER IMPROVEMENTS	

IONQUEST® RANGE PRODUCTS AND BATTERY RECYCLING

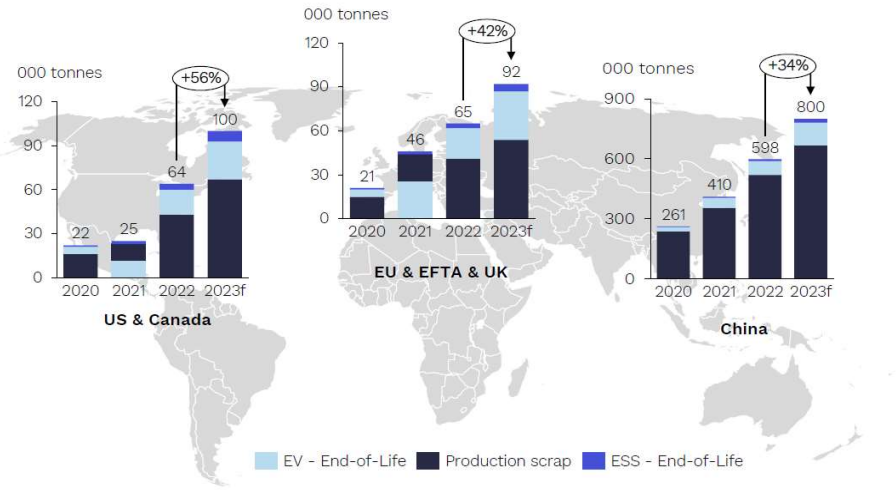

*Rho Motion

IONQUEST® RANGE PRODUCTS AND BATTERY RECYCLING

Global annual scrap material composition

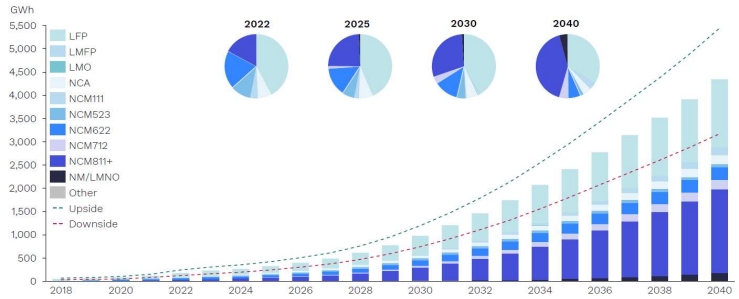

*Rho Motion

Ideal Hydrometallurgy process

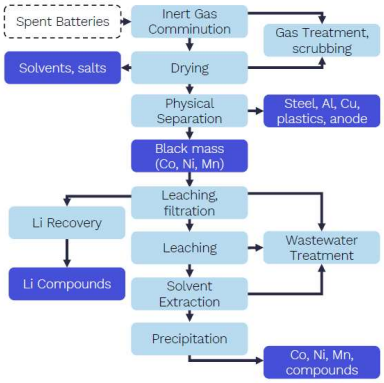

IONQUEST® RANGE PRODUCTS AND BATTERY RECYCLING

Ideal Hydrometallurgy process
Solvent Extraction

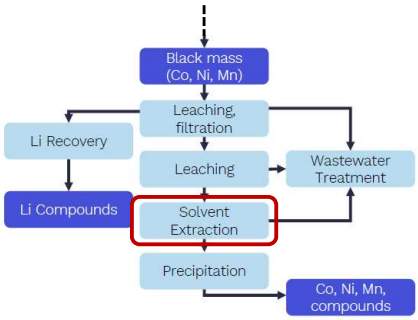

IONQUEST® Solvent Extractants

IONQUEST® 290

- **Extractant of choice for nickel-cobalt separation**
- High purity process
- Already commercialized

IONQUEST® 220

- **Extractant of choice for the removal of impurities (Ca, Zn, Cu, Mn,…) from a Ni/Co feed**
- Novel manufacturing process
- Industrialization on going

IONQUEST® 801

- **Extractant of choice for REE's**
- Novel manufacturing process
- Scale-up under development

IONQUEST® RANGE PRODUCTS AND BATTERY RECYCLING

SULFURIC ACID PLS

NMC is the started leached material

CITRIC ACID PLS

Ca	300 ppm
Co	**25000 ppm**
Cu	795 ppm
Li	3500 ppm
Mg	150 ppm
Mn	**10000 ppm**
Ni	**4000 ppm**
Zn	2000 ppm

pH PLS 3.9
H_2SO_4 1.5 M

Ca	70 ppm
Co	**1540 ppm**
Cu	3000 ppm
Li	600 ppm
Mg	50 ppm
Mn	**1200 ppm**
Ni	**1600 ppm**
Zn	20 ppm

pH PLS 2.9
Citric acid 0.5 M

SIMPLIFIED EXTRACTION FLOWSHEET WITH IONQUEST®

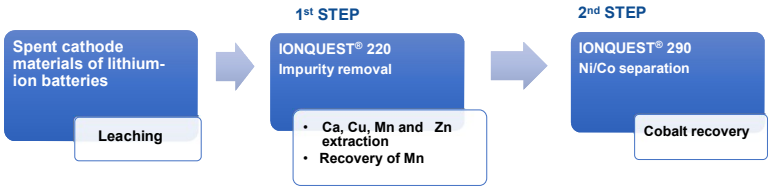

SULFURIC ACID PLS
IONQUEST® 220 - PERFOMANCES

Metals to extract → Ca, Cu, Zn and Mn
Final raffinate composition → Co, Li, Ni

Ca	300 ppm
Co	25000 ppm
Cu	795 ppm
Li	3500 ppm
Mg	150 ppm
Mn	10000 ppm
Ni	4000 ppm
Zn	2000 ppm

pH PLS 3.9
H_2SO_4 1.5 M

SX concentration 16 %
Diluent Escaid 110
Ratio O/A 1
Temperature 40 °C
Mixing time 5 min

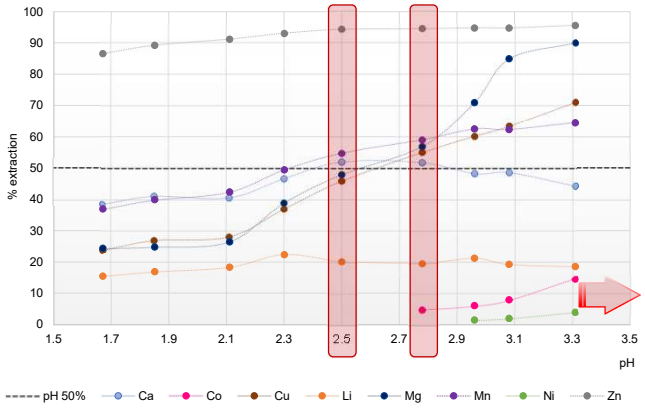

- ✓ Zn full extraction in all pH range
- ✓ At pH 2.5 Mn, Ca, Mg and Cu reach 50% extraction
- ✓ Co and Ni extraction starts after pH 2.75
- ✓ Li extraction remains around 15 – 25% in all pH range

SULFURIC ACID LEACHING
IONQUEST® 220 CIRCUIT – LOADING

Metals to extract → Ca, Cu, Zn and Mn

Final raffinate composition → Co, Li, Ni

pH 2.5
SX concentration 16 %
Diluent Escaid 110
Ratio O/A 1
Temperature 40 °C
Mixing time 5 min

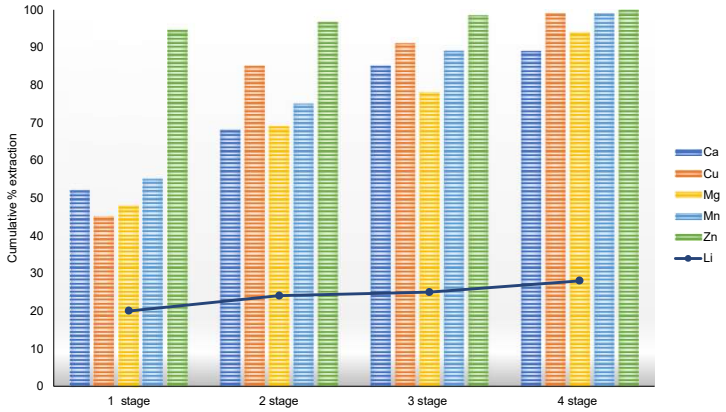

		Ca	Cu	Mg	Mn	Zn
4 stage	ppm in the loaded organic phase	267	787	141	9960	1980
pH 2.5	Total % extraction	89	99	94	99	99

SULFURIC ACID PLS
SCHEMATIC FLOWSHEET

Sulfuric acid feed

Ca	300 ppm
Co	25000 ppm
Cu	795 ppm
Li	3500 ppm
Mg	150 ppm
Mn	10000 ppm
Ni	4000 ppm
Zn	2000 ppm

→ IONQUEST® 220

pH 2.5 and 4 stages

↓

IONQUEST® 220 raffinate

Ca, Zn	< 30 ppm
Cu, Mg	< 10 ppm
Mn	< 40 ppm
Co	**25000 ppm**
Ni	**4000 ppm**
Li	**2520 ppm**

↓

IONQUEST® 290

»» **IONQUEST® 220 loaded**

Ca	267 ppm
Cu	787 ppm
Li	980 ppm
Mg	141 ppm
Mn	9960 ppm
Zn	1980 ppm

Further work
Selective stripping to take out Mn

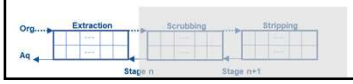

SULFURIC ACID LEACHING
IONQUEST® 290 CIRCUIT – PERFOMANCES

Metals to selectively extract → Co

Final raffinate composition → Li, Ni

Ca, Zn	< 30 ppm
Cu, Mg	< 10 ppm
Mn	< 40 ppm
Co	**25000 ppm**
Ni	**4000 ppm**
Li	**2520 ppm**

SX concentration 10 %
Diluent Escaid 110
Ratio O/A 1
Temperature 40 °C
Mixing time 5 min

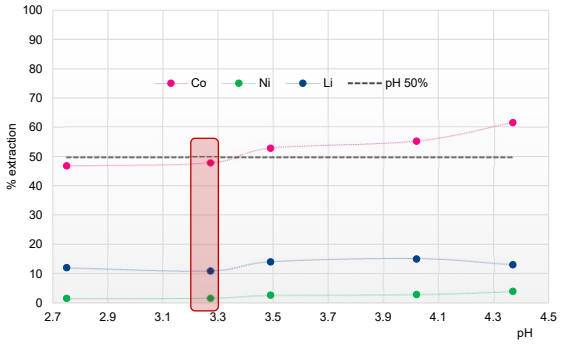

- ✓ Co reach 50 % extraction at pH 3.3
- ✓ Ni co - extraction is below 4% in all pH range
- ✓ Li extraction remains stable in all pH range, below 15%

SULFURIC ACID LEACHING
IONQUEST® 290 CIRCUIT – LOADING

Metals to selectively extract → Co

Final raffinate composition → Li, Ni

pH 3.3
SX concentration 10 %
Diluent Escaid 110
Ratio O/A 1
Temperature 40 °C
Mixing time 5 min

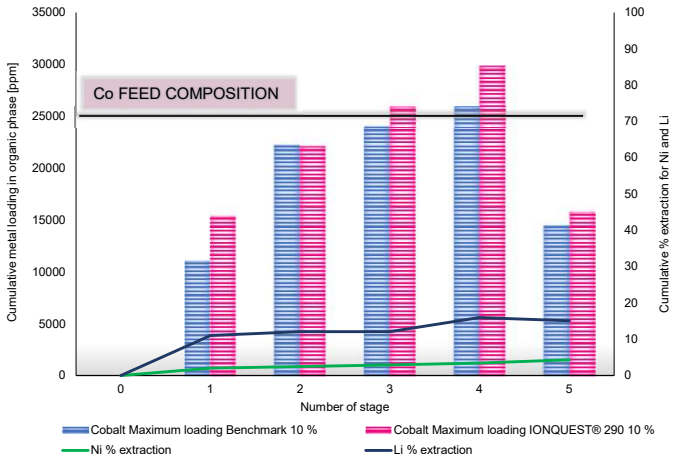

- ✓ IONQUEST® 290 reaches saturation after 4 stages
  - Total cobalt loaded about 25.8 g/L after 3 stages
- ✓ Ni cumulative loading below 4%
- ✓ Benchmark reaches saturation after 4 stages, overall lower Co is loaded in all stages

SULFURIC ACID PLS
SCHEMATIC FLOWSHEET

Sulfuric acid feed

Ca	300 ppm
Co	25000 ppm
Cu	795 ppm
Li	3500 ppm
Mg	150 ppm
Mn	10000 ppm
Ni	4000 ppm
Zn	2000 ppm

→ IONQUEST® 220 →→→ **IONQUEST® 220 loaded**

Ca	**267 ppm**
Cu	**787 ppm**
Li	980 ppm
Mg	**141 ppm**
Mn	**9960 ppm**
Zn	**1980 ppm**

pH 2.5 and 4 stages

↓

IONQUEST® 220 raffinate

Ca, Zn	< 30 ppm
Cu, Mg	< 10 ppm
Mn	< 40 ppm
Co	**25000 ppm**
Ni	**4000 ppm**
Li	**2520 ppm**

Further work
Selective stripping to take out Mn

↓

IONQUEST® 290 →→→ **IONQUEST® 290 loaded**

Co	**25000 ppm**
Ni	**136 ppm**
Li	378 ppm
Impurities from IONQUEST® 220 circuit	**< 40 ppm**

pH 3.3 and 3 stages

↓

IONQUEST® 290 raffinate

Ni	**3864 ppm**
Li	**2140 ppm**

Further work
Scrubbing and stripping to take out only Co

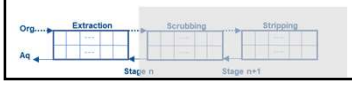

CITRIC ACID PLS

CITRIC ACID is a promising lixiviant*
- Low cost
- Low toxicity
- Good ESG profile
- **Strong chelating abilities: different metal complex in citrate media**

pH PLS 2.9
Citric acid 0.5 M

Ca	70 ppm
Co	1540 ppm
Cu	3000 ppm
Li	600 ppm
Mg	50 ppm
Mn	1200 ppm
Ni	1600 ppm
Zn	20 ppm

IONQUEST® 290
- **Extractant of choice for nickel-cobalt separation**
- High purity process
- Already commercialized

IONQUEST® 220
- **Extractant of choice for the removal of impurities (Ca, Zn, Cu, Mn,…) from a Ni/Co feed**
- Novel manufacturing process
- Industrialization on going

× **High Cu concentration in the PLS**
Reducing the loading and selectivity
Flowsheet modification needed

✓ **With the proper flowsheet modification**
Improved chelating abilities for Li

**Metals 2022, 12, 1400*

CITRIC ACID PLS
IONQUEST® 220 - PERFOMANCES

Metals to extract → Ca, Cu, Zn and Mn

Final raffinate composition → Co, Li, Ni

Ca	70 ppm
Co	1540 ppm
Cu	3000 ppm
Li	600 ppm
Mg	50 ppm
Mn	1200 ppm
Ni	1600 ppm
Zn	20 ppm

pH PLS 2.9

Citric acid 0.5 M

SX concentration 16 %
Diluent Escaid 110
Ratio O/A 1
Temperature 40 °C
Mixing time 5 min

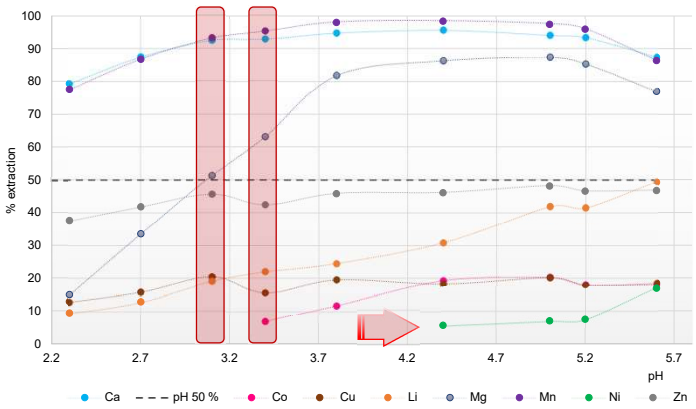

- ✓ Zn extraction below 50% in all pH range
- ✓ Full extraction of Mn and Ca after pH 3, Mg reaches 80% at pH 3.7
- ✓ Co and Ni extraction starts respectively after pH 3.5 and 4.3

Li extraction remains around 15 – 25% until pH 3 then start to increase up to 50% at pH 5.5

CITRIC ACID PLS
IONQUEST® 220 - LOADING

Metals to extract → Ca, Cu, Zn and Mn

Final raffinate composition → Co, Li, Ni

pH 3.0

SX concentration 16 %
Diluent Escaid 110
Ratio O/A 1
Temperature 40 °C
Mixing time 5 min

× **High Cu concentration in the PLS**
Reducing the loading and selectivity
Flowsheet modification needed

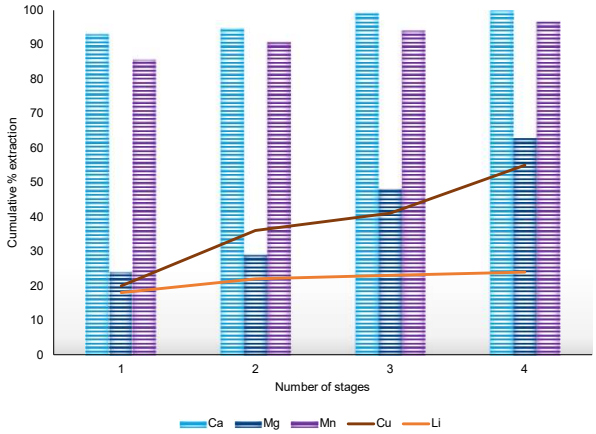

CITRIC ACID PLS
SCHEMATIC FLOWSHEET

Removal of Cu content in the initial PLS

Citric feed

Ca	70 ppm
Co	1540 ppm
Cu	3000 ppm
Li	600 ppm
Mg	50 ppm
Mn	1200 ppm
Ni	1600 ppm
Zn	20 ppm

Cu removal with resin

Leaching pre-treatment with IONQUEST® MPX 317 about 80 % capture

IONQUEST® 220

IONQUEST® 220 raffinate

pH 3.0 and 4 stages

Mn, Mg, Zn	< 30 ppm
Co	**1540 ppm**
Ni	**1600 ppm**
Li	**480 ppm**

IONQUEST® 290

IONQUEST® 220 loaded

Ca	70 ppm
Mg	40 ppm
Zn	< 10 ppm
Mn	1180 ppm
Li	**120 ppm**
Cu	**330 ppm**

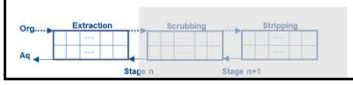

CITRIC ACID PLS
IONQUEST® 290 - PERFOMANCES

Metals to selectively extract → Co

Final raffinate composition → Li, Ni

Mn, Mg, Zn	< 30 ppm
Co	**1540 ppm**
Ni	**1600 ppm**
Li	**480 ppm**

SX concentration 16 %
Diluent Escaid 110
Ratio O/A 1
Temperature 40 °C
Mixing time 5 min

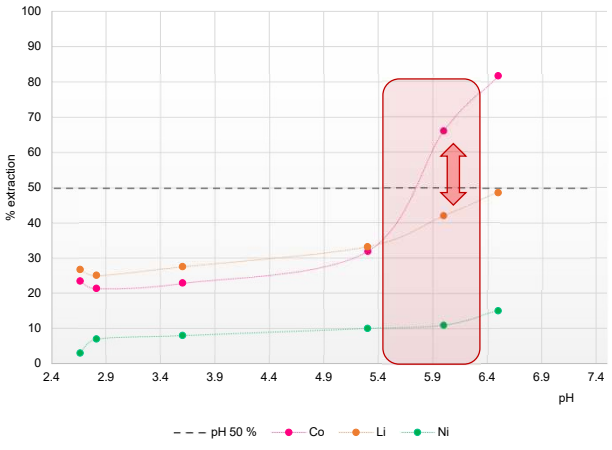

High Co-Li co-extraction with **IONQUEST® 290**

pH 6.0 → 70% Co and 45% Li

CITRIC ACID PLS
IONQUEST® 290 - PERFOMANCES

Metals to selectively extract → Co
Final raffinate composition → Li, Ni

IONQUEST® 220 raffinate

Mn, Mg, Zn	< 30 ppm
Co	**1540 ppm**
Ni	**1600 ppm**
Li	**480 ppm**

pH 6.0
SX concentration 16 %
Diluent Escaid 110
Ratio O/A 1
Temperature 40 °C
Mixing time 5 min

Addition of SX promoter to improve Li-Co selectivity

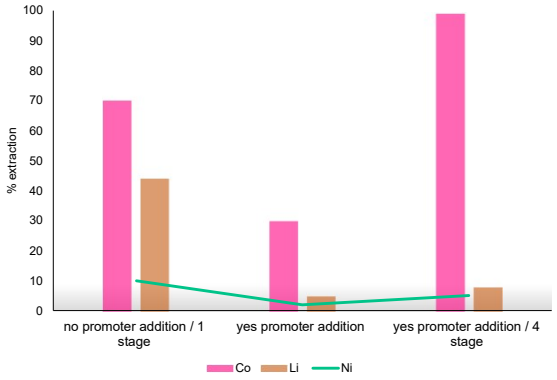

✓ Improved Co selectivity during the extraction when promoter is added
✓ In 4 stages, full Co extraction with Li and Ni carryover below 8%

CITRIC ACID PLS
SCHEMATIC FLOWSHEET

Citric feed

Ca	70 ppm
Co	1540 ppm
Cu	3000 ppm
Li	600 ppm
Mg	50 ppm
Mn	1200 ppm
Ni	1600 ppm
Zn	20 ppm

Cu removal with resin

Leaching pre-treatment with IONQUEST® MPX 317 about 80 % capture

IONQUEST® 220

IONQUEST® 220 raffinate

pH 3.0 and 4 stages

Mn, Mg, Zn	< 30 ppm
Co	**1540 ppm**
Ni	**1600 ppm**
Li	**480 ppm**

IONQUEST® 220 loaded

Ca	70 ppm
Mg	40 ppm
Zn	< 10 ppm
Mn	1180 ppm
Li	**120 ppm**
Cu	**330 ppm**

IONQUEST® 290

Addition of SX promoter

pH 6.0 and 4 stages

IONQUEST® 290 raffinate

Ni	**1520 ppm**
Co	**< 20 ppm**
Li	**440 ppm**

IONQUEST® 290 loaded

Ni	**80 ppm**
Co	**1520 ppm**
Li	**40 ppm**

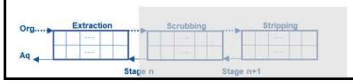

FUTURE IMPROVEMENTS

- Further works on novel selctive extractant and/or SX solutions
- Solvent extraction working in a continuous flow
  - Maximum loading tests
  - Scrubbing and stripping

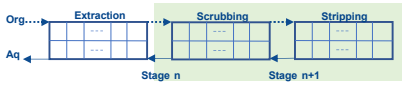

- Simplified modelling approach

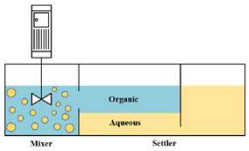

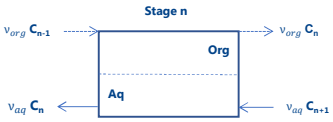

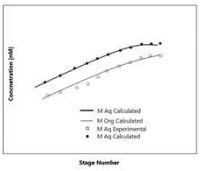

Experiments → Single stage - multi stages modelling process → Optimization

2023 UPDATE ON THE TERRAFAME NICKEL OPERATION

By

Antti Arpalahti

Terrafame, Finland

Presenter and Corresponding Author

D.Sc. Antti Arpalahti
antti.arpalahti@terrafame.fi

ABSTRACT

The Terrafame operation started from the bankrupt Talvivaara deposit in August of 2015, continuing mining directly from September of the same year. Since then, Terrafame has been ramping up the production, increasing nickel production year-by-year and with that, is currently the largest nickel mine in Europe. The deposit is also one of the most significant in Europe, with current life-of-mine extending 30 years with plenty of area worthy of further drilling studies, possibly prolonging the life-of-mine by further decades.

The operation is unique being the only heap leach operation for nickel and zinc and the long ramp up a natural result from a several year lasting retention in the heap leaching stage. The process involves open pit mining, crushing to p80 of 8mm, agglomeration of fines to surfaces of larger particles, dynamic primary heap leaching, multi-lift secondary heap leaching, metals recovery with hydrogen sulphide and naturally, a mine area water management. The historical products of the operation are copper sulphide, unparalleled clean zinc sulphide and MSP, mixed sulphide precipitate of nickel and cobalt.

In 2017, Terrafame started to investigate further refining its products. In 2018, a feasibility study of battery chemicals production was completed and then continued by a declaration by the company to invest into the plant. Construction followed 2019 and 2020 and as of fall 2021, the plant moved from commissioning to ramp-up stage which is continuing in 2023. The new refining process turns the nickel-cobalt sulphide into battery grade nickel sulphate and battery grade cobalt sulphate, feeding the hungry and growing electric vehicle industry.

Nickel, Heap leaching, Cobalt, Zinc, Copper, Battery Chemicals

Terrafame location

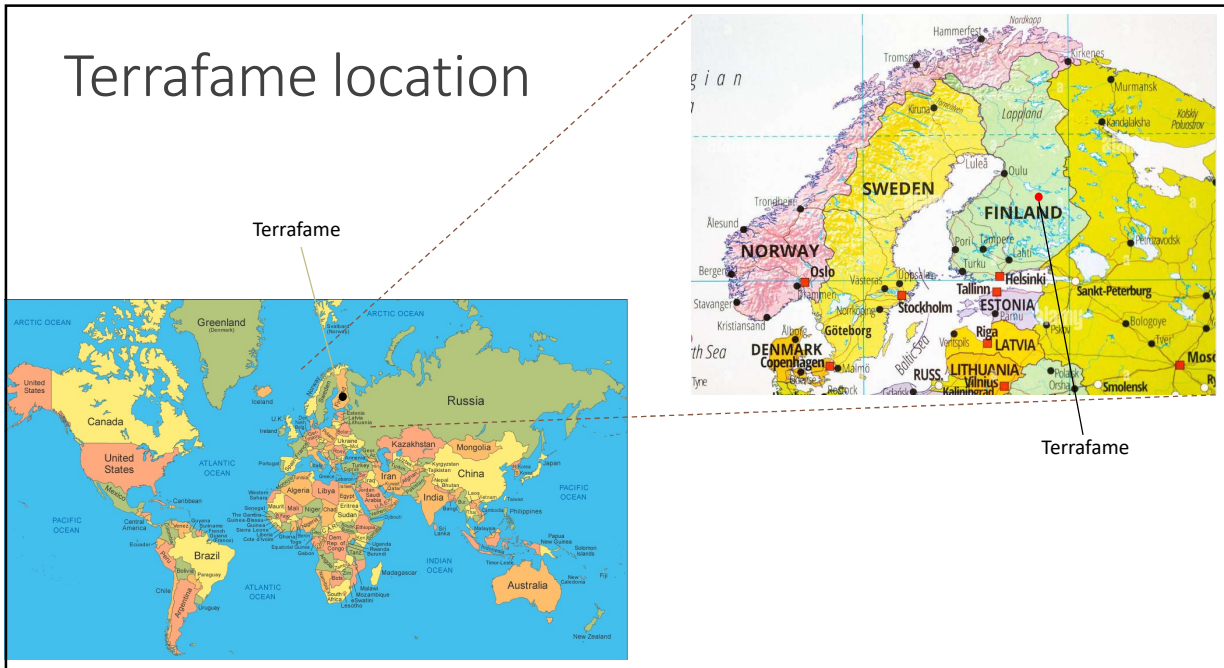

- Terrafame is the largest nickel producer in Europe.
- Europe's largest nickel ore reserves are located in Sotkamo, Finland.
- Terrafame is one of the ten largest zinc producers in Europe.
- Terrafame's battery chemicals production line is one of the largest in the world.
- Terrafame's carbon footprint is clearly smaller than traditional production methods.

Terrafame in numbers

Net sales 2022	Net sales of battery chemicals business 2022	Operating result 2022	Terrafame employees 31.12.2022
584.4 MEUR	207.1 MEUR	93.9 MEUR	763
Partner companies' personnel, average 2022	**Nickel production 2022**	**Nickel sulphate production capacity***	**Cobalt sulphate production capacity***
783	31,550 t	170,000 t/a	7,400 t/a

The new battery chemicals plant's ramp-up is ongoing.

Historical production at Terrafame mine

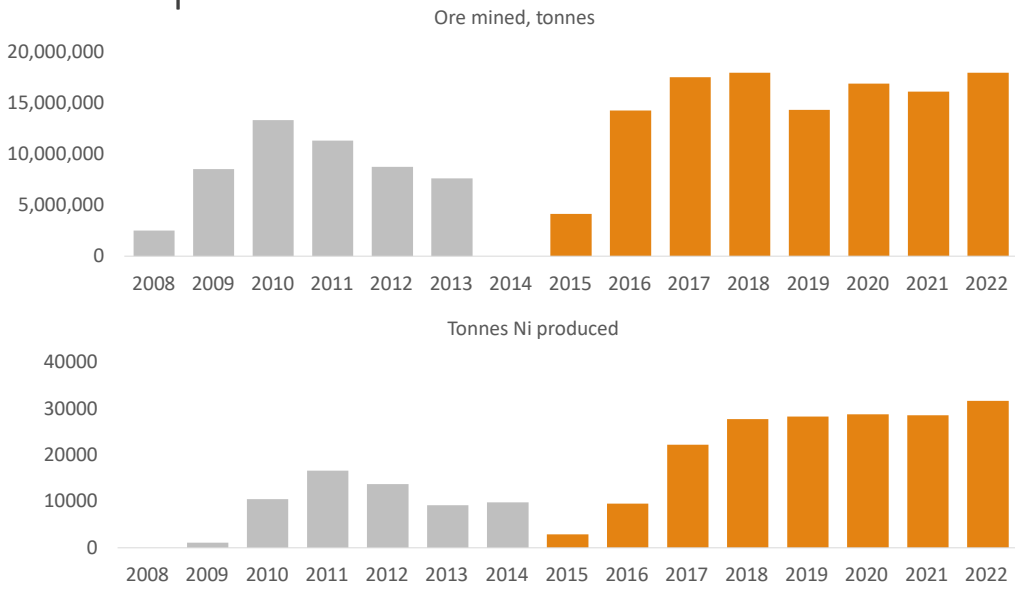

Mineral Resources and Ore Reserves will enable operations for several decades

- Terrafame updated its mineral resource and ore reserve estimates in 2022.
- The measured, indicated and inferred mineral resources amount to 1,451Mt.
- Content:
  - nickel 0.25%
  - zinc 0.52%
  - copper 0.14%
  - cobalt 0.019%

	Ni	Co	Cu	Zn
Metals contained in all categories	3.8Mt	0.3Mt	2.1Mt	8.0Mt

Estimate by an independent third party in compliance with the JORC code.

In 2022, the net sales of the battery chemicals business was already 35% of total net sales

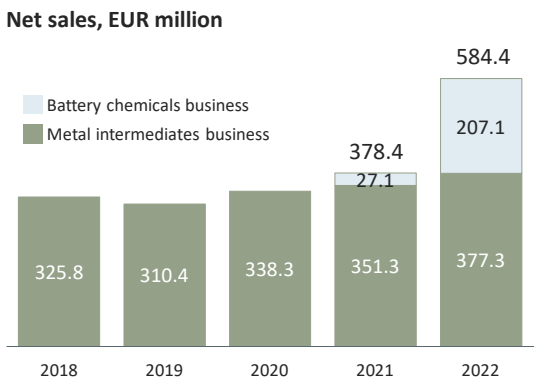

Battery chemicals plant

»Terrafame is involved in electrifying the world

Nickel is one of the main raw materials for Li-ion batteries

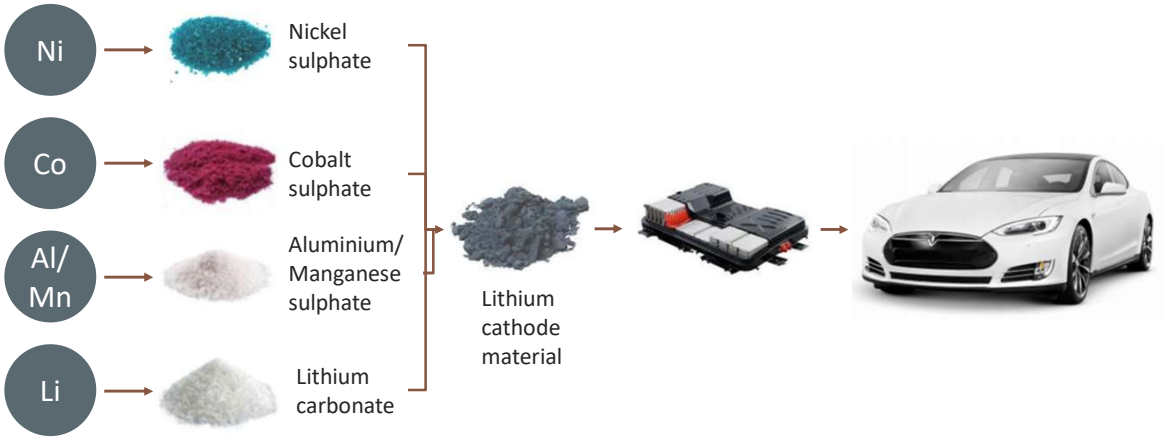

Electrification of transportation continues

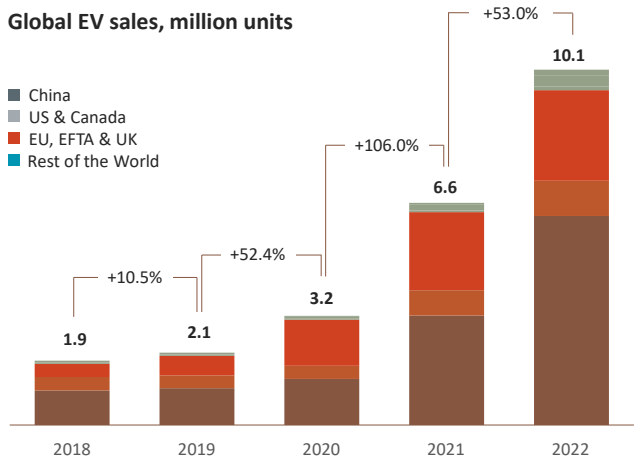

Source: Rho Motion

EVs are taking over the roads

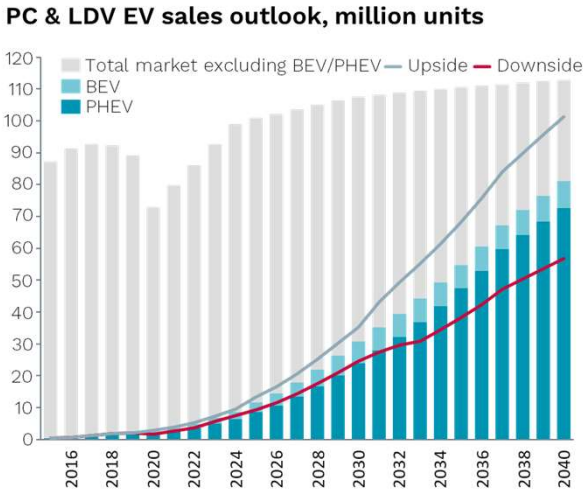

Daimler

”25% EV penetration rate by 2025. 50% by 2030 as part of Ambition2039 scheme.”

Nissan

”1 million electrified vehicles annually by 2023, with EV penetration rate in Japan at 60%, China 23% and Europe 50%.”

Volkswagen

”25% penetration by 2025, 40% penetration by 2030. In China, 50% NEV annual sales by 2025 (SAIC-VW, JAC-VW).”

Source: Rho Motion 2020

BEV = Battery Electric Vehicle, PHEV = Plug-in Hybrid Electric Vehicle

Battery chemicals plant leads us to a special chemicals' producer

- Terrafame decided to invest in battery chemicals plant in 2018.
- The ramp-up of production at the plant started in June 2021, full capacity expected to be reached on 2024.

	Production capacity
Nickel sulphate for EV batteries	170,000 t/a
Cobalt sulphate for EV batteries	7,400 t/a

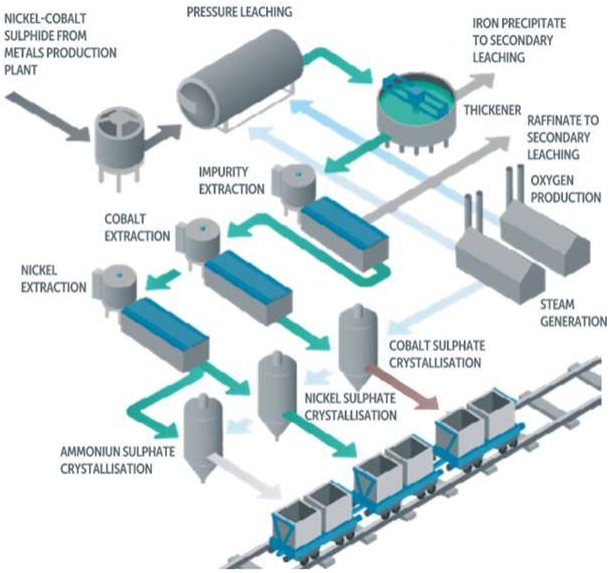

Terrafame's bioleaching based production process is extremely energy efficient

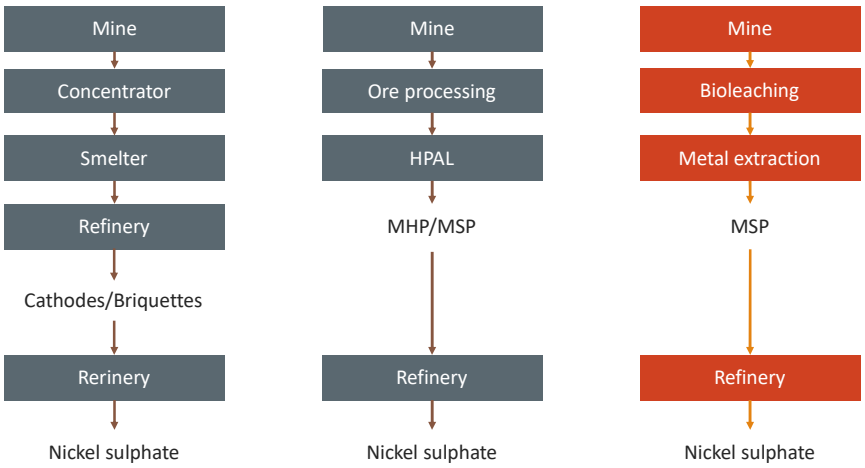

Terrafame's production process

- Integrated production on one industrial site
- Extremely energy efficient production process

Source: Life Cycle Assessment, Sphera Solutions GmbH

Terrafame's nickel sulphate production offers the lowest carbon footprint in the industry

According to an LCA-analysis produced by Sphera Solutions GmbH, the carbon footprint of one kilogram of nickel sulphate produced at Terrafame's integrated production plant is
1.75 kg CO_2-eq, compared to the industry average of 5.4 kg CO_2-eq.

- The analysis has been verified by Prof. Dr. Matthias Finkbeiner, Technical University of Berlin, Germany.
  - Quality assurance and ISO 14040/44 compliance.

The life cycle analysis covers the entire production process starting from the mine and ending the forthcoming production of nickel sulphate.

Terrafame's result is compared to nickel sulphate production on average based on Nickel Insitute life cycle analysis.

Global Warming Potential (GWP)
kg CO_2e/kg $NiSO_4$

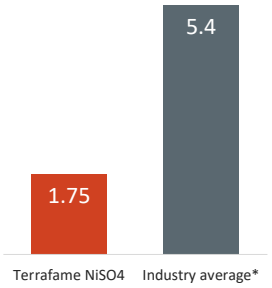

Source: Life Cycle Assessment, Sphera Solutions GmbH ***Life Cycle Assessment of Nickel Products, Nickel Institute**

UPDATE ON META NICKEL GORDES OPERATION

By

Orhan Yilmaz, Yucel Yalcinoglu, Onur Birol

Meta Nickel, Turkey

Presenter and Corresponding Author

Onur Birol
onur.birol@metanikel.com.tr

ABSTRACT

Nickel and cobalt are both essential component materials for the battery industry and play a key role in green energy technologies. Electric mobility and EVs are part of the solution to tackling climate change and building a sustainable green economy. Turkey's visionary group in mining and hydrometallurgy, Meta Nickel, believes in green technologies and continues to support the battery industry with the products it produces in the Gordes HPAL plant since the first day it was established.

Meta Nickel started the production of nickel and cobalt hydroxide, called MHP in the market, in the Gordes operation in 2015, continues production via the HPAL process as of today, and allocates the intermediate product to abroad. Meta Nickel has been ramping up its production and increasing nickel production year-by-year to reach the nameplate capacity and is currently the first and only nickel producer in Turkey.

In order to increase the added value, Meta Nickel aims to start new in-house investment projects in Gordes from the first quarter of 2023. Moreover, Meta would like to be a key producer for the battery industry in Turkey and European countries throughout the new form of the final product, battery-grade nickel and cobalt sulphate. In addition to these, sulphuric acid, the most significant reagent of the HPAL process, will be produced in the new production plant to reduce operating costs and also to obtain electricity via a Turbo Generator (TG) system.

Keywords: Nickel, cobalt, hydrometallurgy, HPAL, MHP, battery industry, investment

Outline

Strategic Importance of Nickel

The demand for nickel, which is primarily used in stainless steel, is rapidly increasing with its use in electric vehicle batteries.

Global Passenger Electric Vehicle Sales Development (MNUnit)

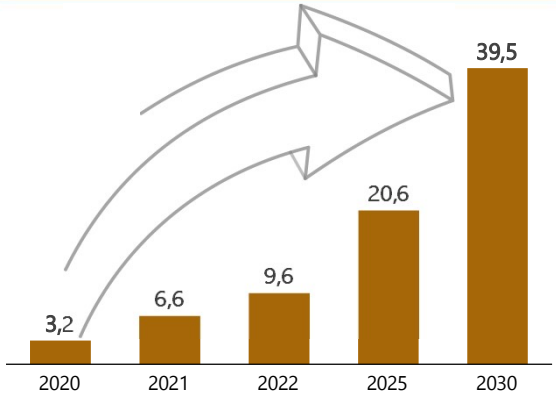

Global Nickel Development by Application (MNt)

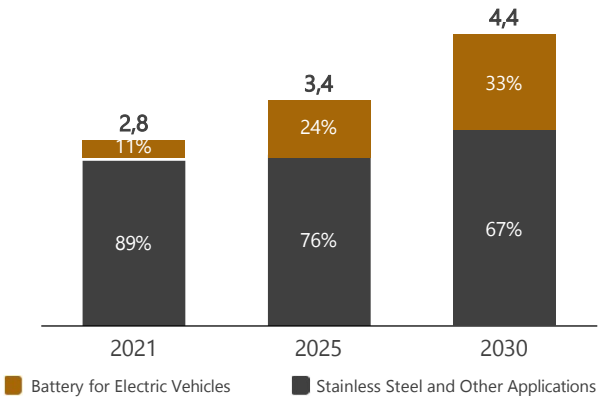

The demand for nickel from the battery industry will account for more than 25% of the total nickel market by 2030

Metal Contents in Different Cathode Chemistries (%)

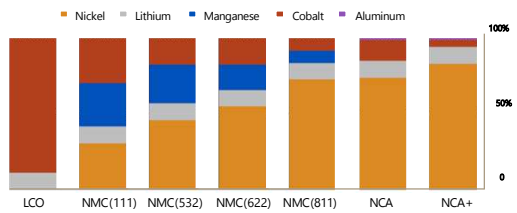

- *The Electric Vehicle Industry is taking action to use more nickel in battery cathodes.*

Share of Cathode Chemistries in Electric Vehicles (%)

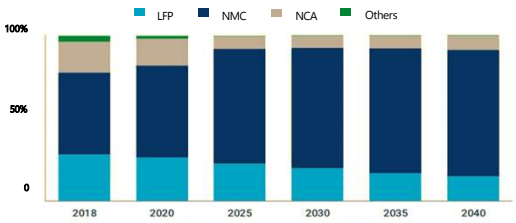

- *NMC is becoming increasingly dominant in the lithium-ion battery chemistry for electric vehicles.*

LCO: Lithium Cobalt Oxide, NMC: Lithium Nickel Manganese Cobalt Oxide, NCA: Lithium Nickel Cobalt Aluminum Oxide, LFP: Lithium Iron Phosphate Oxide

Top Nickel Producing Countries

Source: BloombergNEF, Wood Mackenzie

Nickel Production and Mining in the World

Nickel Deposits in the World

Europe will be an Important Region for Nickel Demand

- Europe region is very poor in terms of nickel resources.
- However, Europe will be a key hub in EV ecosystem and **Gördes has a strategic location**

- **More than 1000 GWh** battery cell manufacturing capacity has announced in Europe by 2030
- It corresponds **~350K tons of Nickel demand**

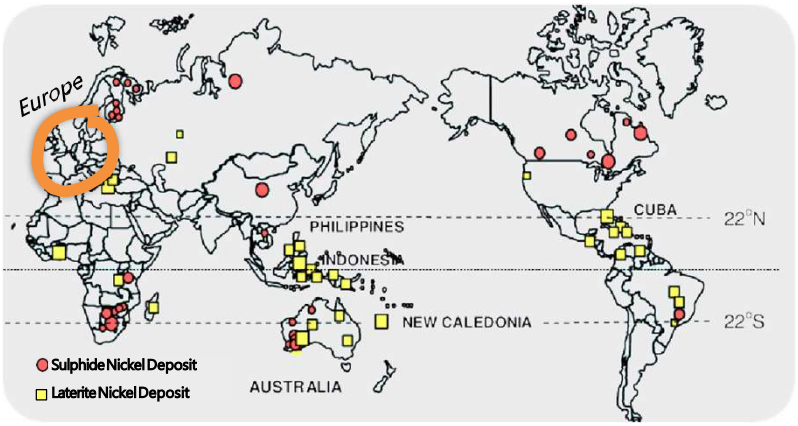

- **Nickel deposits are generally located different countries and some of them have high political risk.**

World Nickel Producers

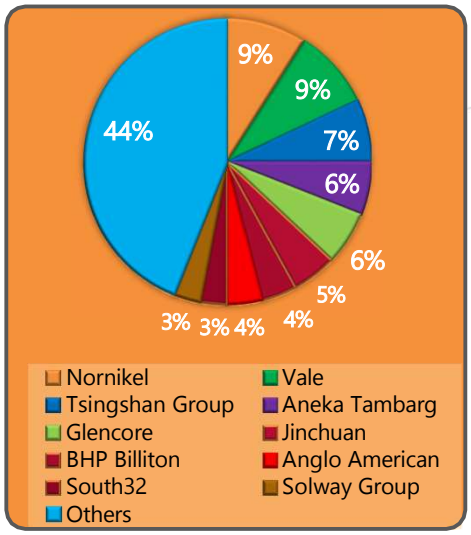

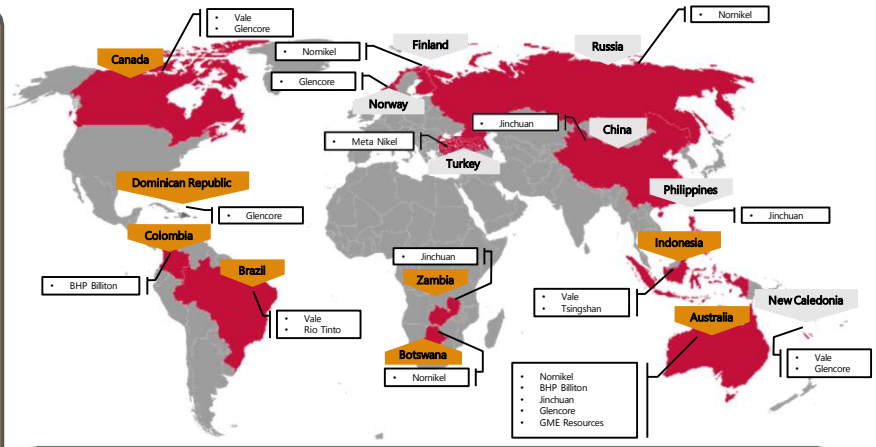

- *Australia, Indonesia, South Africa, Russia and Canada account for more than 50% of global nickel resources.*

Source: Mining Intelligence Data (2020)

Production Capacities of HPAL Plants

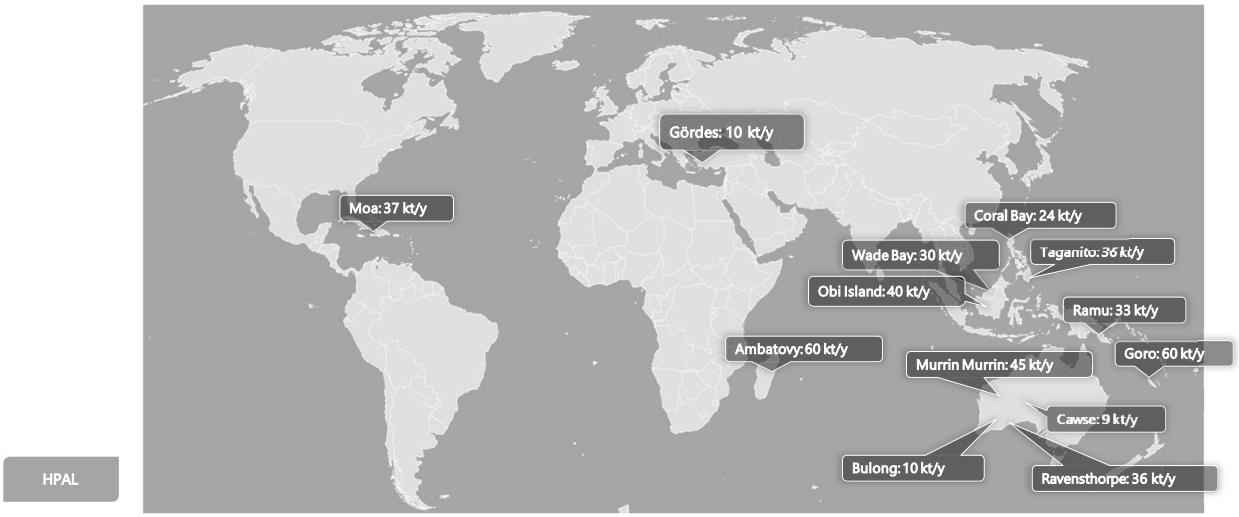

Information about Nickel Ore in Turkey

LATERITE ORE

Eskişehir – Mihalıççık
Manisa – Çaldağ
Manisa – Gördes

2 different types of nickel mineralization in Turkey

SULPHIDE ORE

Bitlis
Sivas
Bursa

Nickel contents are low and not economical

Companies Operating in Turkey and their Work Status

- Manisa - Gördes: **Meta Nikel Kobalt A.Ş**
  (Turkey's first and only concentrated nickel processing plant)
- Manisa
- Eskişehir

Meta Nikel aims to produce the nickel forms needed by Turkey with its new investments.

General Information About Zorlu Holding and Meta Nikel

Zorlu Group

As part of our "Responsible Investment Holding" approach, we focus on technology and innovation, and develop human-oriented ecosystems and regenerative business models.

- One of the 3 group of companies that provides the most employment in Turkey: **33,000 employees**
- **Champion of export** in the electronics industry for 20 years
- **One of the 3 Turkish companies to be** amongst the top 1000 global firms with the highest R&D expenditures
- Turkey's **first unmanned aerial vehicle manufacturer**
- Turkey's **first domestic smartphone manufacturer**
- Turkey's first, and **Europe's only industrial plant for nickel and cobalt concentrates**
- One of the **largest industrial complexes** in Europe, producing in a single location in the field of electronics, white goods and telecommunication
- **Global leader in microthread technology** utilizing nanotechnological practices
- **Leader in renewable energy** with 6 natural gas, 4 geothermal, 4 wind and 7 hydroelectric power plants
- **A first in Europe and Turkey:** Polymer Recycling Plant

Our Industry-Leading Companies

Electronics and White Goods	VESTEL, REGAL
Textile	KORTEKS, ZORLUTEKS, ZORLU HOMETEKS
Energy	ZORLUENERJİ, ZES Zorlu Energy Solutions, electrip
Real Estate	ZORLU CENTER İSTANBUL, ZORLU GAYRİMENKUL, LEVENT 199
Other	ZORLU PSM, meta NİKEL KOBALT A.Ş., JULES VERNE TRAVEL & EVENT, ZORLU GRAND HOTEL İSTANBUL, ZORLU AIR, ZORPET, ZORLU FAKTORİNG, ZORLU MADEN GRUBU

Strong production for a Stronger Turkey

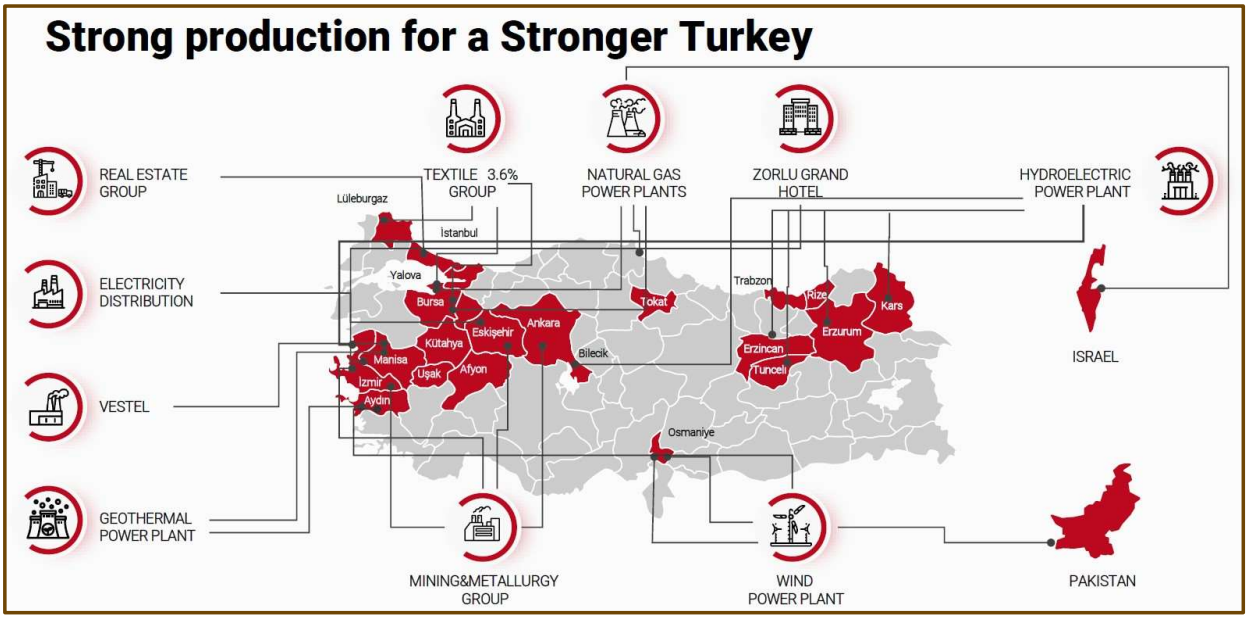

Brief History of Meta Nikel Gördes Plant

META Mining was Founded — 2000

Start of Gördes HPAL Project Investment — 2007

Joined to the Zorlu Group as META Nikel Kobalt Madencilik A.Ş — 2011

The First Shipment of MHP — 2014

Completion of Gördes HPAL Plant — 2015

Optimization in; Working Days & Metal Recovery — 2017

Significant improvements — 2021

2023

Meta-Nikel Production Development (Nickel-Ton)

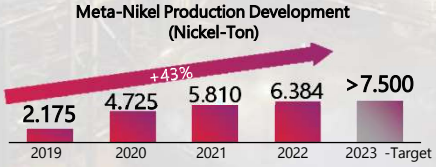

Metal Nikel Ore Sites

- Manisa/Gördes is a plant with a nickel metal production capacity of 10,000 tons/year.
- Eskişehir mine production and reserve development studies continue.
- Geological survey studies continue at our licensed sites in Uşak.

Gördes and Eskişehir sites have sources of Scandium, which is one of the rare earth elements.

Meta Nikel Reserve Information

Status	*Reserves*	*Mt*	*Ni (%)*	*Co (%)*
Proven	Gördes	38.3	0.63	0.03
	Eskişehir	9.8	0.68	0.04
Potential	Gördes	6.3	0.66	0.03
	Eskişehir	28.6	0.70	0.04
Total Reserves	Gördes	44.6	0.63	0.03
	Eskişehir	38.4	0.69	0.04

** Meta has a mining site and license in Eskişehir*
** All values are based on Jorc Code (2016) and Additional Resource Estimates (2019)*

General information of Meta Nikel

PROCESS & CAPACITY

HPAL

(High Pressure Acid Leaching)

Capacity

10,000 tons Nickel Metal

750 tons Cobalt Metal

PRODUCT

MHP

(Mixed Hydroxide Precipitate)

Ni: %36-40

Co: %1.8-2.2

R&D CENTER STUDIES

Nickel Sulfate

Nickel Metal

Cobalt Sulfate

Cobalt Metal

Manganese Sulfat/Oxide

Scandium Oxide/Fluoride

General information of Meta Nikel

Meta Nikel Employees

710 Employees in Total

%15 Female Employees

Certification

ISO9001 Quality Management System

ISO45001 Occupational Health & Safety Management System

ISO14001 Environmental Management System

IRMA Initiative for Responsible Mining Assurance

IRMA ENGAGEMENT MAP

MHP is produced using the latest process technology (HPAL)

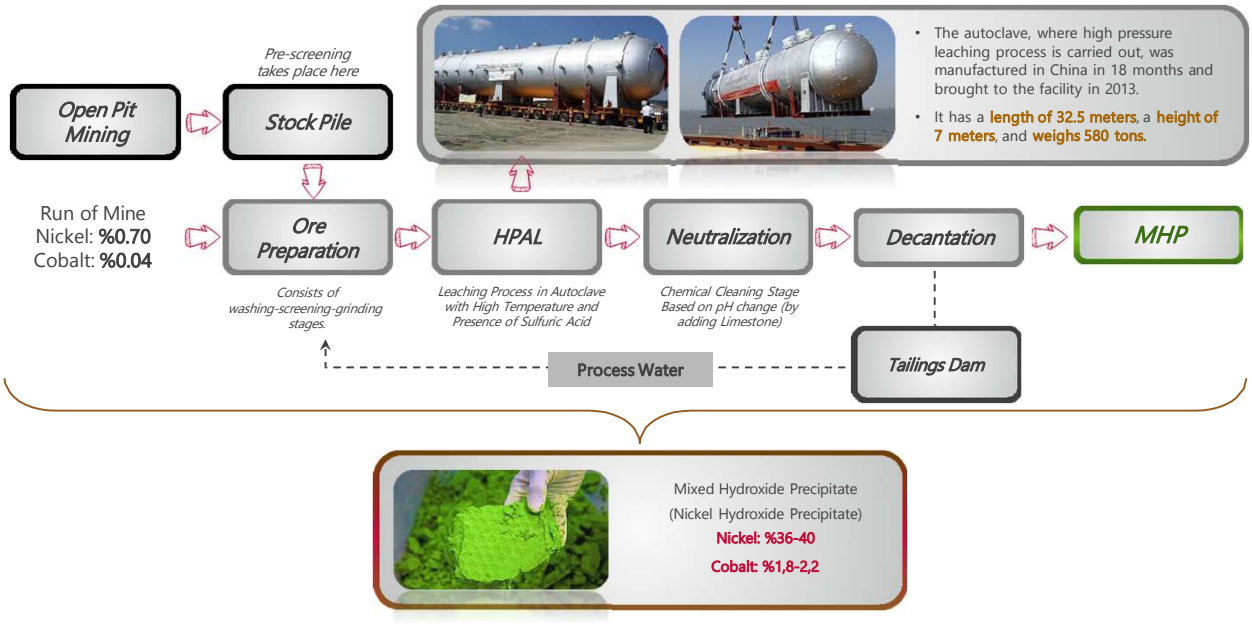

MHP is produced using the latest process technology (HPAL)

Low Acid Consumption

Latest Process Technology

Environmentally Friendly

Meta Nikel located in Gördes exports all of its production.

Meta Nikel located in Gördes exports all of its production.

- MHP is produced at the Meta Nikel Gördes Plant then transported to the İzmir/Aliağa Port which is 150 km away from Gördes and exported to China and South Korea.
- Sulfuric acid is supplied from Aurubis, one of Europe's largest acid producers located in Bulgaria.

Meta Nikel has been carrying out increasing nickel and cobalt production since its establishment.

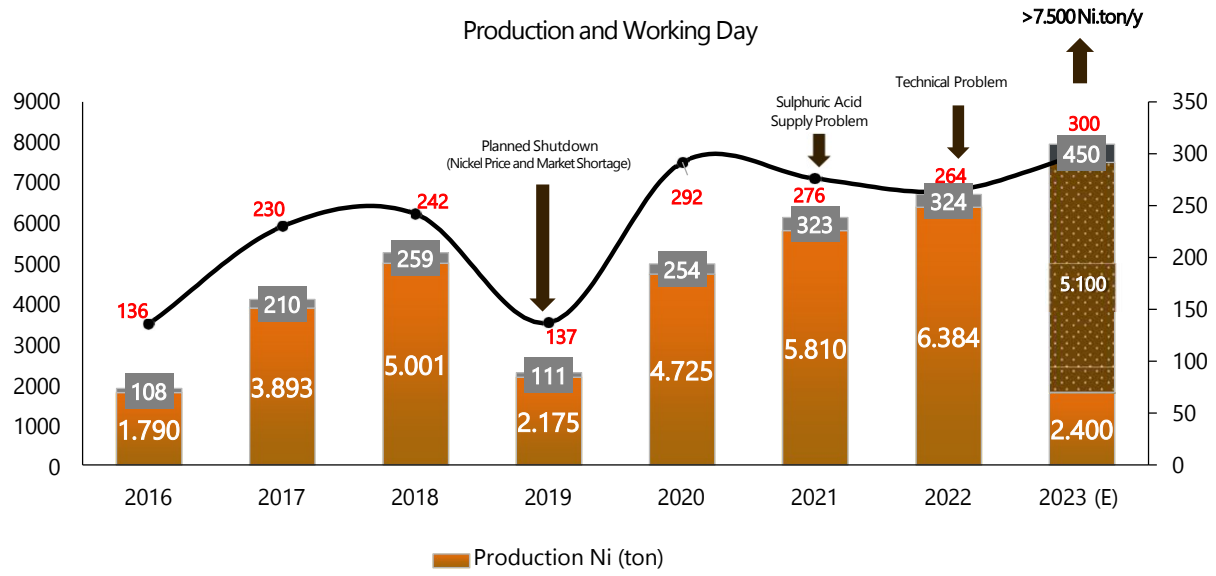

Investment Plans

Investment Plans

Sustainability of Production | Cost Advantage | Profit Maximization

			Key Objective
1	Ore Preparation Investment	**Throughput Improvements;** **Increase in capacity utilization** via pre-processing of the ore mix **Reduction sulphuric acid consumption** due to elimination of the impurities	Cost & ESG
2	Nickel / Cobalt Sulphate Production Facility Investment	**Value-Added Battery Materials** **Value-Added** Nickel and Cobalt Sulphate (LME+ ~5 % premium) will drive the profitability **Battery materials are the growth pillars of nickel / cobalt demand**	Value
3	Gördes Capacity Increase Investment	**Capacity Expansion** **Additional 5.000 tons** of Nickel and Cobalt equivalent Sulphate Production Plant in Gördes	Volume
4	Boiler Investment	**Capacity Expansion** The goal is to achieve sustainable production.	Volume & ESG
5	Tailing Dam Investment	**Volume Expansion** Increasing the tailing dam storage level.	Volume
6	Sulphuric Acid Production Facility Investment (Long Term)	**Production Sustainability** **Cost reduction** and control via in-house production **Sustainability** of the process with regards to supply continuity and carbon footprint	Cost & ESG

1. Ore Preparation Investment

Gördes Site

Hydrocyclone System

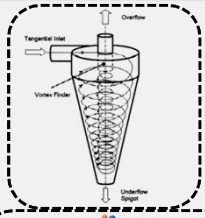

1. Nickel ore is entered into hydrocyclone system
2. Separation of multi-phase mixtures of particles with different densities and sizes

Wet Magnetic Separator

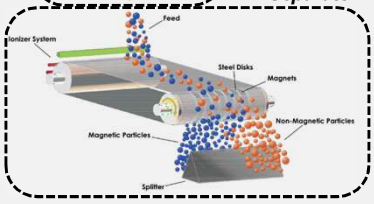

3. Elimination of impurities and enrichment of nickel grade

- *Reduction In Sulphuric Acid Consumption*
- *Higher Feeding Capacity*

Tailor made Project!

Eskişehir Site

Dry Magnetic Separator

1. **Removal of Impurities in the Ore**
2. **Pre-Enrichment of Nickel Grade**
   - Inert ores with 0.68-0.7% Ni grade increase to 0.9-1.0% Ni grade. (~%30 Ni enrichment)

- *Increased Plant Efficiency*
- *Increased Production Capacity*
- *Sustainable Production*
- *Enrichment of the Unprocessed Low Grade Eskişehir Nickel-Cobalt Ore*

2. Nickel / Cobalt Sulphate Production Facility Investment

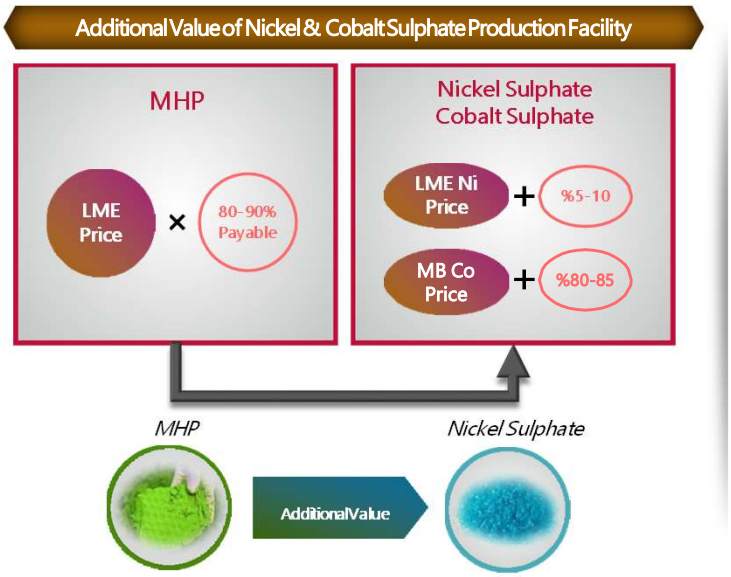

10 K Ni.ton/year
Production Capacity

Other Benefits

Increase in product variety

- *MHP*
- *Nickel/Cobalt Sulphate and Metal*

Production of a Critical End Product

- *Producing the end product that battery manufacturers and OEM's need*
- *Supply chain becomes more durable and transportation costs are eliminated*

3. Gördes Capacity Increase Investment

Capacity Expansion

Capacity Increase In Gördes

- *Additional 5.000 tons of Nickel and Cobalt equivalent Sulphate Production Plant in Gördes*

Key Advantages

- *Capacity expansion requires low capex and ramp-up time compared to greenfield investment*
- *Reserves will run out faster due to use of available resources*
- *Being more sizeable player and increasing available nickel for offtake's*
- *Cost Advantage*
- *Revenue Growth*
- *High Profitability*
- *Capacity Increase*
- *Competitive Advantage*

4. Boiler Investment/Improvement of Existing Boilers and Carbon Capture System

Project Target

Sustainable production

Increased Production capacity

Latest Status in the Project

The bid evaluation process continues.

Financing alternatives are being evaluated.

New Boiler Investment

1. ***Feedstock:*** Coal
   - ***Project Capacity:*** 75 tons/h 60 bar saturated steam

Modification of Existing Boiler

1. ***Feedstock:*** Coal
   - ***Project Capacity:*** 60 tons/h 60 bar saturated steam
   - ***Feedstock:*** Fuel Oil
   - ***Project Capacity:*** 60 tons/h 60 bar saturated steam

5. Tailing Dam Investment

	Stage 1 Construction	Stage 2 Construction	Stage 3 – 1st Phase Construction	Stage 3 – 2nd Phase Construction	Stage 3 – 3rd Phase Construction
	2013 – 2014	2017 – 2018	2020 – 2021	2022 – 2023	2025-2029
	805 – 851 meter	851 – 865 meter	865 – 872 meter	872 – 877 meter	877 – 886 meter
	5.1 MN m^3	4.2 MN m^3	3.1 MN m^3	2.6 MN m^3	5.5 MN m^3
	✓ Completed	✓ Completed	✓ Completed	...Continue	X Not Started

General Information About the Project

Project Target: *Increasing the Tailing Dam storage elevation from* ***772 m to 879 m****, thereby increasing volume.*

Project Duration: 5 Months (May 2023)

Latest Situation On The Project

A contract was signed with Uluova company and site delivery was made. Filling work; continues at ***828.90 m*** *elevation with the material extracted from the landslide area.*

6. Sulphuric Acid Production Facility Investment

Planned Project (Long Term Plan)

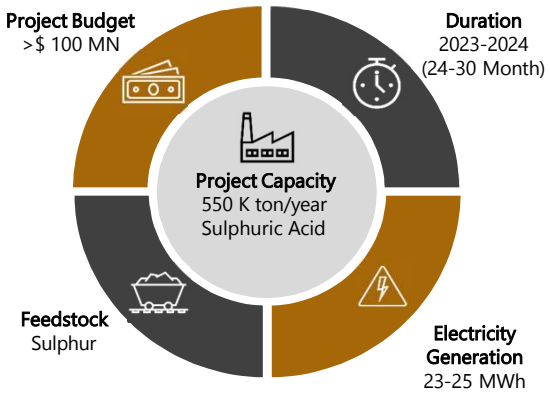

Final Situation

*A investment plan was made for **sulphuric acid production**,*

*Instead, a **5-year long-term supply agreement was signed with Aurubis**.*

*This could allow Meta Nikel to **reduce operating costs by purchasing sulphuric acid from Aurubis** instead of investing in its own production facilities.*

Sustainability Targets

Meta Nikel Sustainability Targets

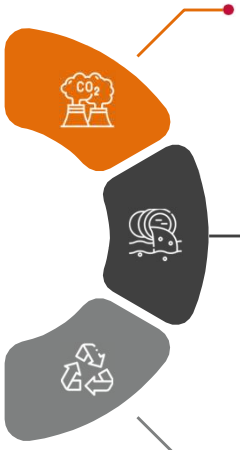

Reducing Carbon Emission
Installation of Magnetic Separator Unit

Efficient Use of Resources
Establishment of Waste Treatment Plant and Reducing the use of clean water

Make, Use and Recycle
Making the equipment used in production usable with idle materials

TARGET OF CLEAN WATER USAGE

Current Situation

2050 Targets

As of 2023, while the **use of raw water** was **35%**, the use of **Tailings Dam water** increased to **65%**.

Reducing raw water consumption to zero thanks to the closed loop system

Meta Nikel Sustainability Targets – CO_2

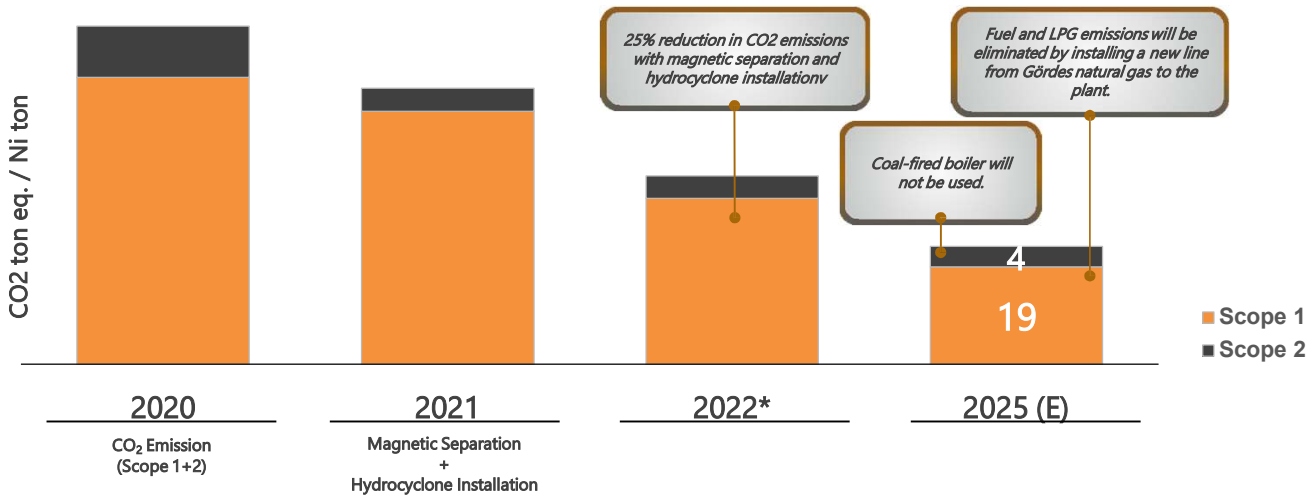

As a result of the completion of new project investments; Meta Nickel Scope 1 emission target by the end of 2025 <20 tons of CO_2e/ton of nickel.

Meta Nikel Sustainability Targets – Water

Current Situation

As of 2023, while the use of **raw water was 35%,** the use of **tailing dam** water increased to **65%.**

2030 Target

Further reduction and minimizing raw water consumption

2050 Target

Raw water will not be consumed thanks to closed loop system

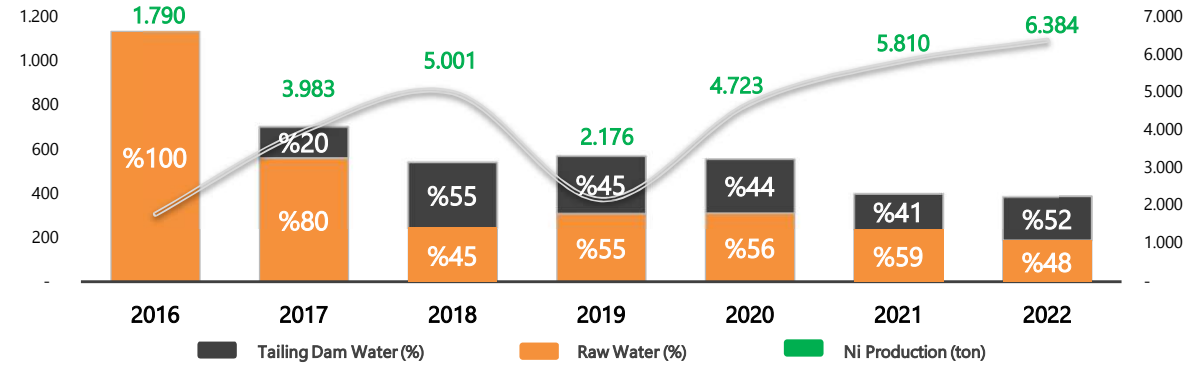

INCORPORATION OF BLACK MASS RECYCLING INTO A HYDROMETALLURGICAL REFINERY

By

[1]Adam J. Fischmann, [1]Volha Yahorava, [1]Jim Wall, [2]Michael Wood

[1]Clean TeQ Water, Australia

[2]Sunrise Energy Metals, Australia

Presenter and Corresponding Author

Adam J. Fischmann

afischmann@cleanteqwater.com

ABSTRACT

To maximise cash flow, typically, the highest grade material is processed early in the mine life, inevitably resulting in increasingly under-utilised refinery capacity over time. For an integrated nickel laterite mine and refinery, such as the proposed Sunrise Energy Metals project located in central NSW, the introduction of black mass from recycled Ni/Co-rich lithium-ion batteries represents an opportunity to better utilise an existing asset. Moreover, nickel and cobalt products with a proportion of recycled metal content are attractive to markets such as the European Union, where the reuse of the metals is mandated.

A conceptual process for incorporating Ni and Co from black mass has been developed. Bench-scale testwork on representative samples of Ni- and Co-rich black mass have established the optimum conditions for the recovery of Ni and Co and removal of foreign impurities (Li, F, P, organics) in the minimum number of steps to produce a material suitable for introduction into the refinery.

Keywords: black mass, recycling, lithium-ion batteries, nickel, cobalt

INTRODUCTION

During the life of the Sunrise operation, as for most mines, the refinery capacity is expected to be progressively underutilised, as the highest grade ore is processed in the first years of the operation to maximise cash flow. As such, in later years, there is scope for the refinery to process additional Ni and Co units from a source that does not require the autoclave for leaching. This equipment will be fully utilised as progressively lower-grade ore is processed. Black mass from end-of-life Li-ion batteries (LiBs) fits this requirement since it is a high-grade material that can be leached under atmospheric conditions.

Black mass is an intermediate product from the recycling of LiBs. LiBs from electric vehicles (EVs), which are expected to make up the bulk of the battery recycle stream in the future (along with stationary energy storage), are usually organised into modules (arrays of cells) and then further into battery packs (arrays of modules). Battery packs and modules are typically dismantled, and then the cells are mechanically processed by crushing and various physical separation techniques to remove solvents and larger particles (metallic and polymeric), leaving the black mass, which is predominantly a mixture of cathode and anode powders. For Nickel Manganese Cobalt (NMC)-type batteries, the black mass is the most valuable portion of the cell, as it contains Ni and Co in the cathode active material, $LiNi_xMn_yCo_zO_2$. LFP batteries, which use $LiFePO_4$ as the cathode powder, are not of interest for the Sunrise refinery as they do not contain Ni or Co.

Depending on the preceding mechanical processing steps, the black mass will contain varying proportions of the following materials:

- Cathode powder, consisting of cathode active material ($LiNi_xMn_yCo_zO_2$), containing the value metals, carbon black (conductive additive), binder (PVDF)
- Anode powder (coated, spheronised graphite)
- Residual metallic copper (anode foil)
- Residual metallic aluminium (cathode foil)
- Residual electrolyte, consisting of salt (usually $LiPF_6$) and solvent (usually a mixture of organic carbonates)
- Residual steel (cell casing)

Black mass is now a traded commodity, with payability based on the Ni, Co and Li content. Market prices are quoted by metal market analysts such as Platts.[1] There is currently significant interest and innovation in black mass processing, but the industry has not coalesced on a “standard” flowsheet.

Figure 1 shows a generic flowsheet for producing black mass from LiBs followed by hydrometallurgical processing to recover Ni, Co and Li. The steps involved are leaching (acidic and reducing), solid/liquid separation to remove the residue (anode powder), impurity removal (precipitation), base metal recovery (either precipitation, solvent extraction, or ion exchange) and separation, and finally lithium recovery (e.g. by precipitation as lithium carbonate). To maximise the value, the production of separate Ni and Co products is desirable, requiring further separation processes. All these steps require capital investment. Conversely, incorporating the impure base metal product into an existing refinery is a more efficient way to use existing capital equipment.

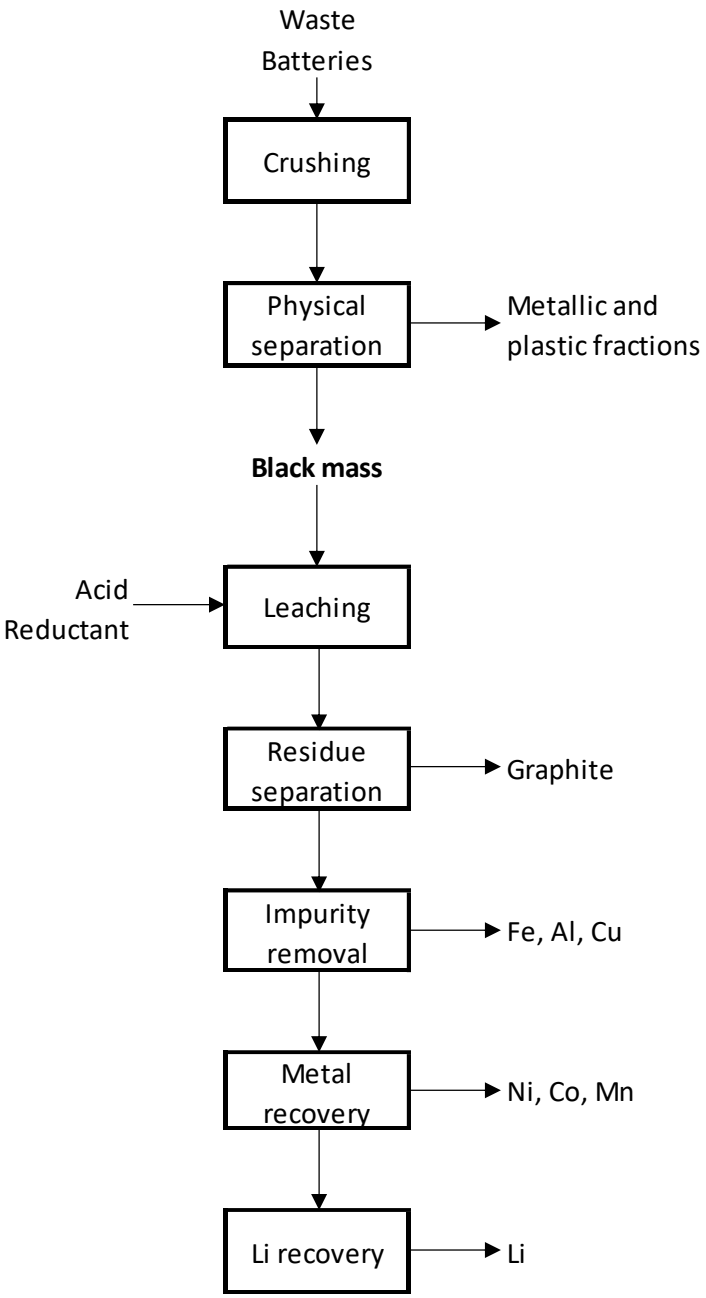

Figure 1: Generic flowsheet for production of black mass from LiBs and hydrometallurgical recovery of Ni, Co and Li

Figure 2 shows the proposed flowsheet for the recovery of Ni and Co from black mass to deliver these metals into a Ni/Co refinery. Based on an initial literature review, sulfuric acid and a reductant (hydrogen peroxide or sodium metabisulfite) were selected as the leaching reagents.

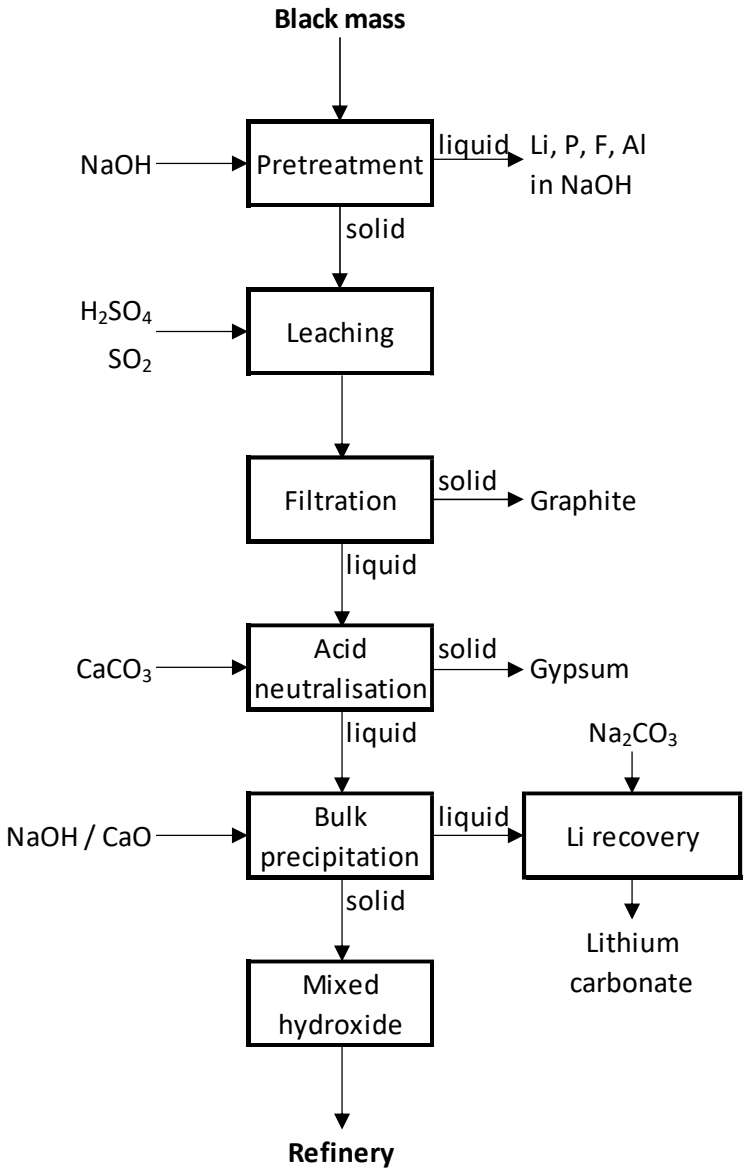

Figure 2: Conceptual flowsheet for hydrometallurgical processing of black mass and incorporation into an existing base metal refinery

Pre-treatment with NaOH has been reported to be effective at Al removal.[2-4] It would also be expected to be effective at removing most of the soluble Li, P, F and organics. Leaching must break down the structure of the Li metal oxide to solubilise the Li, Ni, Mn and Co. The formal oxidation states of Ni, Mn and Co in NMC cathode active materials are +2, +4 and +3,[5] although Ni can also be present as +3 and Co as +4.[6] Due to the high oxidation states of Co and Mn, a reductant is required. Hydrogen peroxide (H_2O_2) can act as a reductant relative to Ni, Mn and Co in high oxidation states (i.e. +3 or higher). The amount of reductant required depends on the amount of each metal and its oxidation state, so it is difficult to predict. The reactions below are for a generic $LiMO_2$ (where M = Ni, Co, Mn), in which the average oxidation state of the transition metal is +3.

H_2O_2 as reductant: $H_2O_2 + 2LiMO_2 + 3H_2SO_4 \rightarrow 2MSO_4 + Li_2SO_4 + 4H_2O + O_2$

SMBS as reductant: $Na_2S_2O_5 + 4LiMO_2 + 6H_2SO_4 \rightarrow 4MSO_4 + 2Li_2SO_4 + 2NaHSO_4 + 5H_2O$

Figure 3 shows the concept of incorporating black mass recycling into the Sunrise refinery flowsheet. The objective is to add additional units of Ni and Co at a point where further processing is minimised, new impurities are not introduced and outlets exist for contained impurities. The Sunrise flowsheet processes laterite ore via High Pressure Acid Leach (HPAL), followed by Partial Neutralisation of the leached slurry using limestone before selectively recovering Ni and Co by continuous Resin-in-Pulp ion exchange technology (cRIP). The eluate from cRIP contains some free acid and is neutralised in the Eluate Neutralisation (EN) stage with lime to remove residual Fe, Al and Cu.

Given the Sunrise flowsheet, by converting the pre-treated black mass into a clarified leach liquor, precipitating a hydroxide product, and adding this product to the EN stage, these objectives can be achieved. Specifically:

- Pre-treatment with NaOH removes residual electrolyte (lithium hexafluorophosphate, organics) and some of the Al
- Leaching solubilises the Ni and Co (along with Li, Mn, Cu, Fe, Al)
- Leach residue consists of C and F (in graphite and PVDF), removed by filtration
- Neutralisation to pH 10 precipitates everything except Li, Na, F
- Bulk hydroxide precipitate is added to Eluate Neutralisation (EN) stage (minimal Li, F, P)
- Bulk hydroxide precipitate dissolves in EN and partially offsets the neutralisation requirement by consuming free acid
- Fe, Al and Cu are removed in EN (recycled to PN)
- Mn, Ca and Zn are removed in Impurity Solvent Extraction
- Co is recovered as $CoSO_4.7H_2O$ via Cobalt SX and Crystallisation
- Ni is recovered as $NiSO_4.6H_2O$ via Nickel SX and Crystallisation

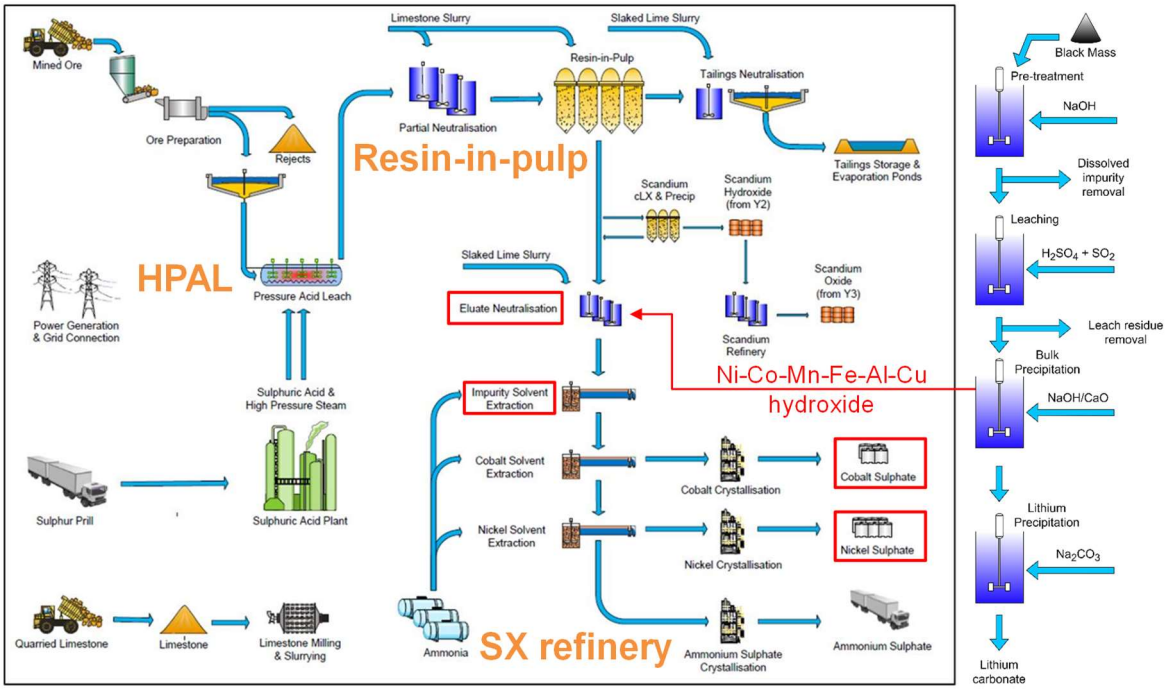

Figure 3: Conceptual black mass recycling process (right) and incorporation into Sunrise refinery flowsheet (left)

SAMPLES

NMC-type LiB black mass samples were obtained from four sources (Table 1). The samples from Switzerland and the USA were used for testing, as the Australian sample had a low Ni content and only a limited amount of sample was received from Japan. Table 2 summarises the elemental composition of the samples. Note that "moisture" likely includes some volatile organic solvent and water (measured as mass loss after drying at 105°C).

The samples from Australia and Japan were additionally characterised by XRD (Table 3). This characterisation revealed that the Ni content of the Australian sample was likely from NiMH batteries rather than NMC-type LiBs. A Ni-containing Li phase was not detected, and LCO ($Li_{0.98}CoO_2$) was the dominant phase (Co-only cathode powder typically used in batteries for electronics and power tools).

Table 1: Sources and descriptions of black mass samples

Source	Description	Sample
Australia	Mechanical processing of used batteries to produce black mass for sale	10 kg Black powder with mm-sized metal and plastic particles
Japan	Collect and resell black mass and scrap (used battery and production)	300 g Black powder
Switzerland	Battery recycler	10 kg Fine black powder with cm-sized strips of lightweight shredded material, no metallic pieces visible
USA	Battery recycler	10 kg Agglomerated black powder, mm-sized metal particles, strong solvent odour

Switzerland USA

Figure 4: Black mass samples, as received

Table 2: Analysis of black mass samples (as received) (elemental analysis as % w/w, dry basis, LOI and moisture as % w/w, as received basis)

Element	Australia	Japan	Switzerland	USA
Al	2.77	0.0369	3.87	0.38
Ba	0.00826	N/A	N/A	N/A
C	35.6	32.8	23.6	27.9
Ca	0.0255	0.0037	0.0983	0.0203
Co	25.2	6.46	7.17	18.7
Cr	0.0103	0.0003	0.006	0.00532
Cu	3.72	0.116	1.52	0.437
F	2.42	0.84	1.69	1.93
Fe	0.0929	0.0035	6.10	0.0941
K	0.0317	< 0.007	0.019	0.0028
Li	3.55	4.18	2.67	3.17
Mg	0.0602	0.00252	0.0316	0.0466
Mn	2.78	6.44	5.85	4.65
Na	0.058	0.0459	0.03	0.061
Ni	2.10	20.7	10.8	6.46
P	0.451	< 0.0003	0.471	0.275
S	0.110	0.078	0.0695	0.0402
Si	0.105	0.0054	0.048	0.0071
Sn	0.0178	N/A	N/A	N/A
Ti	0.0366	N/A	N/A	N/A
Zn	0.00902	< 0.0001	0.069	0.0101
LOI @ 850°C	39.0	35.5	38.9	33.2
Moisture (105°C)	5.25	0.139	3.5	15.4

Table 3: Phase analysis by XRD (Switzerland and USA samples were not analysed)

Phase name/Formula	Australia	Japan
Graphite; C	Major	Major
Lithium Cobalt Oxide; $Li_{0.98}CoO_2$	Major	ND
Lithium Cobalt Nickel Oxide; $Li(Co_{0.2}Ni_{0.8})O_2$	ND	Major
Lithium Dimanganate; $LiMn_2O_4$	Minor	ND
Amorphous Content	Undetermined	Undetermined

BENCH SCALE TESTWORK

All solid analyses are reported on a dry mass basis. Mass balances for Ni, Co and Li were 87-105%, with an average of 98%. Accurate fluorine analysis for solids and liquors required alkaline digestion to convert all fluorine to inorganic fluoride before quantification with an ion-selective electrode. Carbon was measured by CHN analysis (combustion). Other elements were measured by ICP-AES (solids were digested by acid before analysis).

Pre-treatment

Previous testing established that 1.0 M NaOH at 60°C for 2 hours was more effective than water or 0.1 M NaOH at removing soluble F, P, and organics (as well as Li and some Al). Pre-treatment was conducted in a 5 L jacketed glass reactor equipped with an overhead stirrer and condenser. Black

mass was added to the solution of NaOH and stirred for the required time, then filtered by vacuum filtration. The filter cake was washed with deionised water and used for leaching tests without drying. As shown in Table 4, substantial F and P were removed, and a portion of the Al (Co was used as a tie element for the removal calculation). Only a small amount of Li was removed, which is consistent with most of the Li in the black mass being present in the cathode powder as $LiMO_2$ and only a minority in the residual electrolyte as $LiPF_6$.

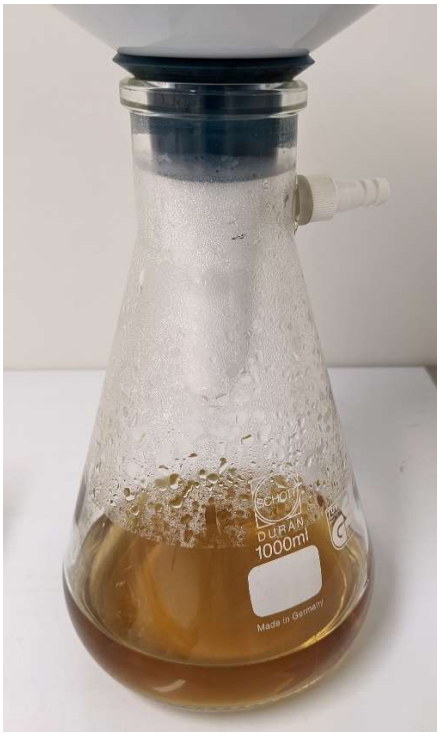

Figure 5: Filtrate from NaOH pre-treatment

Table 4: Composition of black mass feed, treated residue, filtrate, and removal efficiency

Element	Feed % w/w	Residue % w/w	Filtrate mg/L	Removal %
Al	3.87	4.01	1440	14%
C	23.6	23.2	N/A	N/A
Ca	0.0983	0.104	< 0.009	0%
Co	7.17	8.15	< 2	0%
Cr	0.006	0.00856	< 0.09	0%
Cu	1.52	1.57	18.5	0%
F	1.69	1.1	3000	78%
Fe	6.1	7.07	< 3	0%
K	0.019	0.004	48	102%
Li	2.67	2.9	395	7%
Mg	0.0316	0.0378	< 0.04	0%
Mn	5.85	6.52	< 0.5	0%
Na	0.03	0.418	21800	67%
Ni	10.8	12.6	< 4	0%
P	0.471	0.286	664	61%
S	0.0695	0.056	138	84%
Si	0.048	0.0658	80	75%
Zn	0.069	0.0818	3.4	2%

Leaching

The leaching test program was designed to systematically vary reductant and acid dosage, reductant type and pulp density while also obtaining kinetic data. Leach tests were conducted at 60°C in a 1 L jacketed glass reactor equipped with an overhead stirrer and condenser. Black mass was added to the solution of H_2SO_4 pre-heated to 60°C, followed by slow addition of the reductant (either H_2O_2 or SMBS) to control the heat and gas generation. Slurry samples were periodically withdrawn to obtain reaction kinetics. At the end of each test, the slurry was filtered by vacuum filtration. The filter cake was repulped with deionised water and then filtered again.

General observations

- The addition of black mass to the H_2SO_4 solution resulted in heat generation
- The addition of H_2O_2 to the mixture of H_2SO_4 and black mass resulted in heat generation and substantial gas generation, which caused the solid material to froth up (presumably the hydrophobic graphite particles)
- The addition of SMBS also resulted in heat and gas generation, both of which were more significant as the dose of SMBS was increased
- Filtration of the solid residue was rapid, and very little material passed through Whatman #4 filter paper (pore size approximately 25 µm), except for tests with high terminal pH which were difficult to filter
- Leaching was rapid, reaching the maximum extent within 30-60 minutes

Figure 6: Black mass leaching – note frothing

Results

Table 5 summarises the conditions and outcome of each test. Low acid dosages, below a threshold, resulted in high terminal pH (> 2.5) and a difficult-to-filter residue, presumably due to Al/Fe hydroxide gel formation. High reductant dosages above a threshold resulted in a final ORP < 500 mV. Test #15 was done in a 5 L reactor at a larger scale, and it did not have as good accountability as the smaller scale tests. The leaching extent is likely underestimated, given that the residue had comparable Ni, Co and Li levels to test #13 (Table 6). Both C and F are higher in the residue compared to the feed.

Table 5: Test conditions and leaching extents for selected elements (based on liquor out vs solid in)

Leach	Sample	Reductant		H_2SO_4	Pulp density	PLS ORP	PLS pH	Ni	Co	Li
#	source	type	mol/kg	mol/kg	g/L	mV	-	%	%	%
1	CH	H_2O_2	8.17	11.38	157	612	< 1	92	72	90
2	CH	H_2O_2	4.12	11.47	159	609	< 1	88	62	89
3	CH	SMBS	0.23	11.31	159	675	< 1	72	54	85
4	CH	H_2O_2	4.22	5.60	162	533	2.7	52	40	66
5	US	H_2O_2	10.24	12.57	155	572	< 1	90	67	84
6	US	H_2O_2	4.92	12.44	160	561	< 1	78	55	81
7	US	SMBS	0.74	12.35	153	584	< 1	70	61	82
8	CH	SMBS	0.65	15.86	122	718	< 1	82	66	87
9	CH	SMBS	2.14	16.52	113	369	< 1	92	92	92
10	CH	SMBS	0.67	12.25	119	686	< 1	84	70	86
11	CH	SMBS	0.69	6.71	282	533	3.4	69	54	69
12	CH	SMBS	0.69	10.08	282	893	< 1	80	63	80
13	CH	SMBS	1.51	14.82	298	293	1.0	92	92	91
14	CH	SMBS	1.14	11.89	257	398	1.1	85	85	86
15	CH	SMBS	1.18	9.24	254	367	1.1	79	79	79

CH = Switzerland, US = United States; ORP vs. Ag|AgCl

Table 6: Composition of feed, PLS and solid residue from leaching test #13

Element	Feed mg/kg	PLS mg/L	Solid residue mg/kg
Ag	44	0.4	170
Al	41100	13100	4110
Ba	281	< 0.07	1090
C	236000	N/A	839000
Ca	1270	257	762
Co	81300	24800	987
Cr	95	10.8	229
Cu	16700	5050	465
F	8510	126	27000
Fe	70500	20800	16600
K	70	8	80
Li	28300	8600	290
Mg	391	103	81.4
Mn	65100	20100	362
Na	1010	23700	200
Ni	126000	38600	3010
P	2450	733	450
Pb	818	14.1	2970
S	363	137000	2230
Si	570	157	524
Zn	892	292	64.8

Figure 7 plots Co leaching extent against acid addition, grouped by ORP and reductant. The data show that the addition of sufficient reductant to result in a final ORP <500 mV in the same acid dose

range leads to higher Co leaching. There was also a dependence on the acid dosage within each group of tests, i.e. leaching efficiency deteriorated below a threshold level of acid addition.

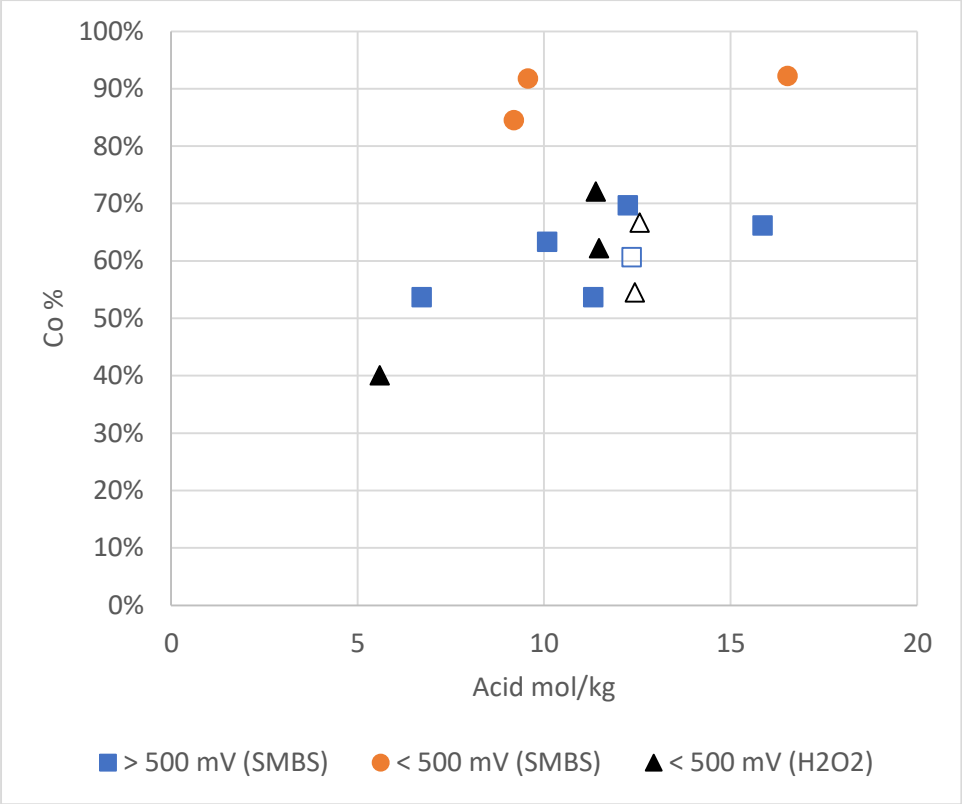

Figure 7: Effect of acid addition and reductant on Co leaching (filled symbols = Switzerland, open symbols = USA)

Figure 8 plots Co leaching extent against ORP, grouped by acid addition and reductant. The data show that low ORP is required for high Co leaching, very low acid results in poor leaching, very high acid at low ORP does not improve leaching, and none of the H_2O_2 dosages resulted in low enough ORP to achieve high Co leaching.

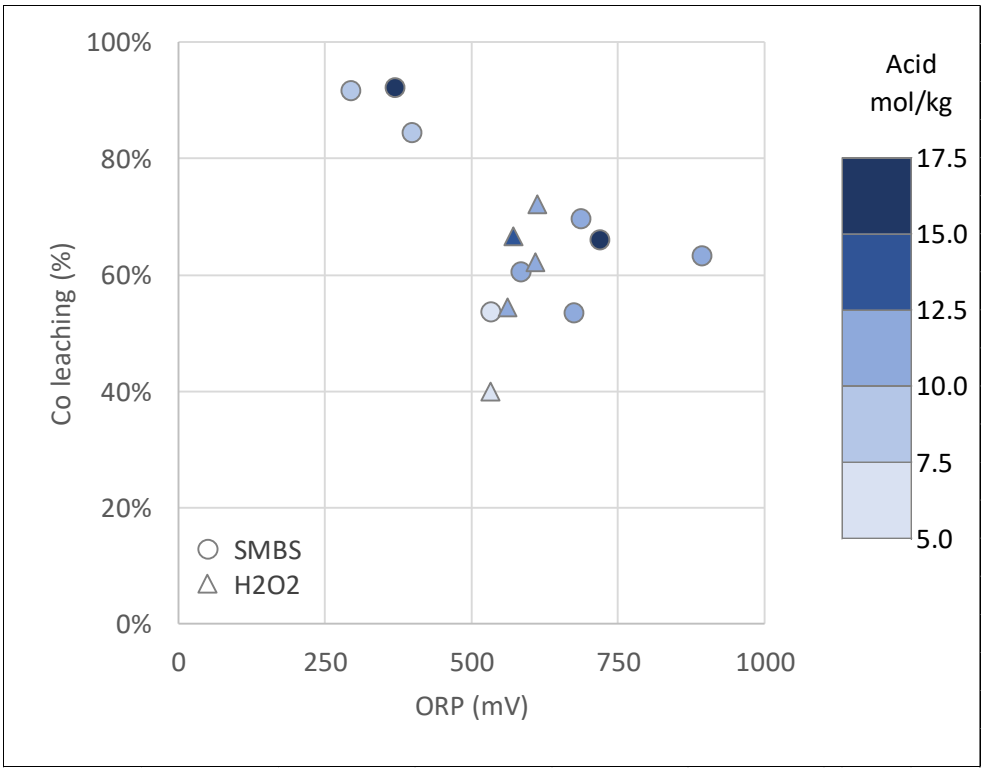

Figure 8: Effect of ORP and acid addition on Co leaching, grouped by reductant type

Metal recovery

Solution purification

Despite the very fine particle size of the graphite (typically around 15 µm), filtration of the leach residue was surprisingly facile using regular filter paper and vacuum filtration. The free acid remaining in the clarified PLS was then neutralised using calcium carbonate (20% w/w slurry) at 50°C, producing a clean and readily filterable gypsum residue (Figure 9) with minimal loss of Li, Ni and Co (Table 7).

Table 7: Composition of feed, precipitate and filtrate from free acid neutralisation test

Element	Feed mg/L	Precipitate mg/kg	Filtrate mg/L	Precipitation %
Al	8720	327	8759	<0.1%
Ca	161	241200	580	N/A
Co	17200	395.8	17150	<0.1%
Cr	6.6	1.69	6.69	<1%
Cu	3720	120.7	3655	<0.1%
F	86.4	500	97	13%
Fe	12000	427.8	11990	<0.1%
K	4	42	9	23%
Li	5960	200	5960	<0.1%
Mg	72.9	560	135	17%
Mn	13900	461	13800	<0.1%
Na	12400	2414	12570	<1%
Ni	26600	593.9	26340	<0.1%
P	486	70	457	<1%
S	83800	212400	79500	5.6%
Si	98.1	170	108	3.9%
Zn	202	7.69	174	<0.1%

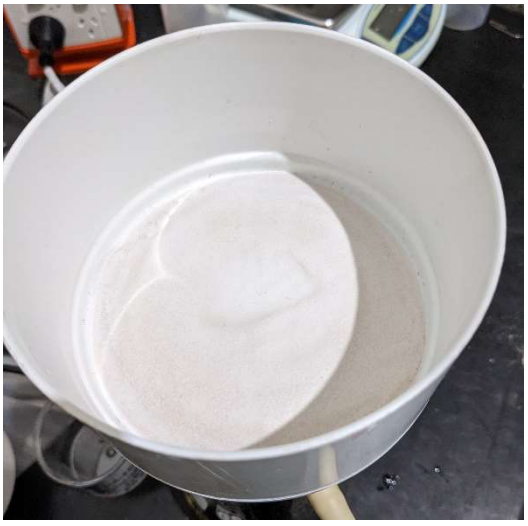

Figure 9: Gypsum residue from neutralisation of free acid in black mass PLS

The next step was conceptualised to be a partial neutralisation to precipitate Fe and Al, followed by precipitation of a mixed hydroxide containing Ni and Co. However, upon testing, when the pH was raised to around 4 using 400 g/L NaOH at 40°C, the residue was not filterable, most likely due to the formation of aluminium hydroxide gel, given that the concentration of Al in the PLS was high (8.7 g/L). Bearing in mind that the destination for the mixed Ni-Co hydroxide is the Eluate Neutralisation stage of the Sunrise flowsheet, a bulk hydroxide precipitate containing Al and Fe is viable since these

elements are removed during the Eluate Neutralisation step. Furthermore, the bulk hydroxide can offset part of the lime demand in the Eluate Neutralisation unit operation.

Bulk hydroxide precipitation

Accordingly, another batch of filtrate from free acid neutralisation (160 mL) was neutralised with 400 g/L NaOH at 40°C to around pH 10. A sticky, brown-coloured solid with a reasonable filtration rate on filter paper using vacuum filtration was formed (Figure 10). After washing three times with deionised water, the precipitate residue (152 g) contained 76% moisture and the composition as shown in Table 8. The high residual level of Na and S indicates that washing efficiency was low, and a repulp wash would be required. Nevertheless, the desired outcome of low P and F (foreign elements in the Sunrise refinery) was achieved, with these elements present at 2.1 and 60 mg/L, respectively. Further testing should be done with other reagents, such as sodium carbonate, lime, and magnesium oxide.

Figure 10: Bulk hydroxide precipitate from neutralisation of black mass PLS with NaOH

Table 8: Composition of feed, precipitate and filtrate from bulk hydroxide neutralisation test

Element	Feed liquor mg/L	Precipitate mg/kg	Filtrate mg/L
Al	8759	38890	2.4
Ba	0.04	1.57	0.01
Ca	580	1904	115
Co	17150	76960	5.5
Cr	6.69	33.9	< 0.06
Cu	3655	16490	0.99
Fe	11990	53950	2.84
K	9	< 20	13
Li	5960	4842	3410
Mg	135	681	0.29
Mn	13800	61400	6.9
Na	12570	52060	54400
Ni	26340	117500	9.6
P	457	2050	2.1
S	79500	70410	44300
Si	108	534	1.2
Zn	174	887	0.06
F	97	683	60

Lithium recovery

The bulk precipitation filtrate contained a high sodium concentration (54 g/L), a moderate concentration of Li (3.4 g/L) and minimal levels of other metals. Due to the low solubility of lithium carbonate, particularly as temperature increases, the addition of sodium carbonate to this solution should precipitate lithium carbonate.[7] This is usually done at 50°C using a solution of Na_2CO_3 to maximise the solubility of Na_2CO_3.

Lithium precipitation: $Li_2SO_4 + Na_2CO_3 \rightarrow Li_2CO_{3\,(s)} + Na_2SO_4$

In this study, solid sodium carbonate was added to the filtrate from the bulk hydroxide precipitation to recover Li as crude Li_2CO_3 (see Table 9). Despite adding a large molar excess of Na_2CO_3, Li recovery was only 39%. The resulting precipitate also contained a high level of Na and S, and the filtrate contained 2.3 g/L Li. Residual base metals remaining in the feed liquor after bulk precipitation were concentrated in the lithium precipitate.

For efficient Li recovery, the liquor would need to be concentrated before adding Na_2CO_3, for example, by evaporation or membrane filtration.

Figure 11: Crude lithium carbonate precipitate from liquor remaining after bulk hydroxide precipitation

Table 9: Composition of feed liquor, precipitate and filtrate from lithium carbonate precipitation test

Element	Feed mg/L	Precipitate mg/kg	Filtrate mg/L
Al	2.4	121.2	1.8
Ba	0.01	8.29	0.04
Ca	115	10110	12
Co	5.5	475.6	0.65
Cr	< 0.06	2.13	< 0.06
Cu	0.99	72.89	0.72
F	60	1490	63
Fe	2.84	274.9	1.15
K	13	35	18
Li	3410	137900	2280
Mg	0.29	49.4	0.15
Mn	6.9	657	0.6
Na	54400	56810	128100
Ni	9.6	806.2	1.2
P	2.1	21.2	3.2
S	44300	26550	52300

Si	1.2	61.8	5.1
Zn	0.06	20.1	0.04

Overall recovery

Table 10 lists the composition of intermediates through the black mass treatment process and the overall recovery to the refinery. Note that the metal contents are depressed in the hydroxide precipitate due to the high concentration of Na, S and Li due to insufficient washing. Importantly, F is very efficiently rejected by the black mass flowsheet.

Table 10: Summary of composition of intermediate products and overall recovery to refinery

	Unit	Ni	Co	Li	Mn	C	F	P	Al	Fe
Black mass	% w/w	10.8	7.17	2.67	5.85	23.6	1.69	0.47	3.87	6.1
Pre-treated residue	% w/w	12.6	8.15	2.9	6.52	23.2	1.1	0.29	4.01	7.07
Leach residue	% w/w	0.3	0.1	0.03	0.04	83.9	2.7	0.05	0.41	1.66
PLS	g/L	38.6	24.8	8.6	20.1	N/A	0.13	0.73	13.1	20.8
Gypsum precipitate	% w/w	0.06	0.04	0.02	0.05	N/A	0.05	<0.01	0.03	0.04
Hydroxide precipitate	% w/w	11.8	7.7	0.48	6.14	N/A	0.07	0.21	3.89	5.4
Recovery to refinery	%	85%	86%	14%	86%	0%	1%	35%	76%	83%

IMPLICATIONS

This bench scale proof of concept has confirmed that it is feasible to process black mass and produce a Ni- and Co-containing material suitable for introduction into a conventional Ni-Co refinery. Given that the black mass feed material is very high grade and leaching was effective at 300 g/L solids content, the size of the equipment can be relatively small, thus the capital cost of the process is expected to be low (especially since the refinery is sunk capital) and the operating cost is the more important factor. The major contributors to the operating cost are the cost of the black mass (based on the Ni, Co and Li content), the reagent cost for the black mass portion of the flowsheet and the additional reagent costs in the refinery to process the additional metal. These are offset to some extent by lower lime requirement in Eluate Neutralisation and higher refinery utilisation.

The optimised dosages of SMBS and H_2SO_4 found for the Swiss black mass sample will necessarily change based on the composition of the black mass, but knowing that the terminal ORP needs to be below 500 mV (vs. Ag|AgCl) and the terminal pH should be around 1 provide the guidelines to quickly optimise the dosages for any given sample.

CONCLUSIONS

There is already a market for black mass and this will only grow with time from the increasing supply of end-of-life EV batteries. This proof of concept has shown that a simple flowsheet with minimal steps can convert black mass into a form suitable to feed to a Ni-Co refinery. The point in the refinery flowsheet at which this should be added is as far downstream as possible and where outlets exist for impurities contained in the converted black mass. This alleviates building a standalone refinery for black mass and provides an existing refinery with a supply of recycled metal content to meet market requirements. Battery recycling is expected to be enforced by legislation and regulation for a minimum recycled metal content in all batteries and is already imposed in the European Union.

ACKNOWLEDGMENTS

The authors would like to thank Sunrise Energy Metals and Clean TeQ Water for permission to present the results and the suppliers of the black mass samples for providing the test material.

REFERENCES

[1] S. Global, “Platts launches daily black mass spot price assessments for China, Europe,” 17 April 2023. [Online]. Available: https://www.spglobal.com/commodityinsights/en/our-methodology/subscriber-notes/041723-platts-launches-daily-black-mass-spot-price-assessments-for-china-europe. [Accessed 27 April 2023].

[2] L. Toro, F. Veglio, F. Beolchini, F. Pagnanelli, G. Furlani, G. Granata and E. Moscardini, “Plant and process for the treatment of exhausted accumulators and batteries”. European Patent EP2450991B1, 17 07 2013.

[3] L. Changdong, Q. Jianshen, L. Liangliang and Y. Haijun, “Method for recovering lithium from lithium power battery of electric automobile”. Chinese Patent CN102244309B, 06 11 2013.

[4] Y. Renwu, Y. Jie and F. Wenxiong, “Method for recovering cobalt, nickel and manganese from waste lithium cells”. Chinese Patent CN101871048B, 23 5 2012.

[5] F. Lin, I. M. Markus, D. Nordlund, T.-C. Weng, M. D. Asta, H. L. Xin and M. M. Doeff, “Surface reconstruction and chemical evolution of stoichiometric layered cathode materials for lithium-ion batteries,” *Nature Communications,* vol. 5, p. 3529, 2014.

[6] J. L. White, F. S. Gittleson, M. Homer and F. El Gabaly, “Nickel and Cobalt Oxidation State Evolution at Ni-rich NMC Cathode Surfaces During Treatment,” *Journal of Physical Chemistry,* vol. 124, no. 30, pp. 16508-16514, 2020.

[7] H. Ge, H. Wang and M. Wang, “Solubility and thermodynamics of lithium carbonate in sodium carbonate solution,” *CIESC Journal,* vol. 70, no. 11, pp. 4123-4130, 2019.

DETAIL DESIGN OF A NOVEL LEACH CIRCUIT FOR THE TECH PROJECT

By

Peter Rojan, Wolfgang Keller, [2]Boyd Willis

EKATO RMT, Germany
[2]Queensland Pacific Metals, QLD, Australia

Presenter and Corresponding Author

Wolfgang Keller
wolfgang.keller@ekato.com

ABSTRACT

A good product idea is a good start. In order to bring an innovative process idea to production scale quickly and safely, a lab-developed ore leaching process must first be examined and optimized in pilot scale. This is especially true for hydrometallurgical processing plants due to the project specific and unique raw material 'ore'. Extensive test programs on a pilot scale are therefore usually required for this type of process engineering project. The subsequent implementation of the individual process steps on an industrial scale must already have been considered during the development phases in the laboratory and pilot plant. Close co-operation between the process owner and technology providers is key to success.

QPM and EKATO entered therefore into a Joint Development Agreement (JDA) to develop and commercialize an innovative laterite leach process based on the DNi Process™ (Altilium Group) to produce critical metals for the emerging lithium-ion battery and electric vehicle sector.

This paper describes the leaching process and the metallurgical test work and discusses how expertise and know-how of both partners was successfully applied. From Concept Engineering and assessing pilot test results, to developing the correct scale-up correlations, and scaling-up the process to production size; all with the aim of specifying production-sized reactor systems by the end of the concept phase.

In addition to the technically sound implementation of the project, commercial aspects also play an important role to get the project realized. EKATO as an equipment manufacturer contributed expertise in the very early phases of the project to evaluate and optimize the economics of leach reactors.

Due to the corrosive operating conditions, it was decided, together with QPM and their assigned engineering company, to manufacture product wetted parts in this part of the plant from titanium. This resulted in additional technical and commercial challenges. Numerical simulations were carried out for tailored and problem-specific dimensioning of the reactor vessel and its internals such as heat exchangers, dip pipes and baffles.

After the concept study was successfully completed at the end of 2022, EKATO was assigned to execute the basic engineering for the nitric acid leach circuit.

Keywords: TECH project, QPM, Altilium, DNi Process™, EKATO process plants, agitator design, nickel laterite, nitric acid leach, battery materials, electric vehicle

INTRODUCTION

The TECH Project was presented by QPM at ALTA 2020 [1] and 2022 [2]. QPM's process flowsheet, including the leach section is based on the DNi Process™ (Altilium Group). This is a patent-protected method for extracting nickel, cobalt and other constituent metals from laterite ores [3] using nitric acid. The development of the DNi Process™ by Direct Nickel and the operation of the process demonstration plant was presented at several ALTA conferences from 2011 to 2017 as well [4,5,6]. During this operation of the demonstration plant Direct Nickel was already supported by EKATO regarding mixing related issues.

THE TECH PROJECT

Project Overview

Queensland Pacific Metals (QPM) is an ASX listed company and is the 100% owner of the Townsville Energy Chemicals Hub (TECH) Project in Queensland, Australia. The TECH Project will be an advanced and sustainable producer of critical chemicals for the lithium-ion battery and electric vehicle sector. The project will treat 1.6 million wet tonnes per annum (wtpa) of high-grade nickel laterite ore imported from ore supply partners in New Caledonia. The ore will be unloaded at the Port of Townsville and transported by road to the TECH Project site at Lansdown, 40 km south of Townsville (Figure 1).

Figure 1: Project Location

EKATO PROCESS PLANTS GROUP

Designing, engineering and construction of customized reactor systems is a complex, interdisciplinary task. During the early chemical development phase each individual process step must be analysed. The results of this analysis are then applied by process engineering teams to design the required industrial reactor technology. There are numerous interfaces between all team members involved in the project from many disciplines. If these interfaces are professionally coordinated, then it is possible to develop a scalable and economical industrial reactor design within a few months. This can be further detailed by mechanical engineering teams into detailed design specifications. Therefore, EKATO offers extended engineering services and scope of supply in order to guarantee customers efficient and smooth progress in the project with as few interfaces as possible. All from a single source.

Having performed successful lab or pilot plant tests followed by an appropriate scale-up to the commercial scale, process parameters and equipment sizes are well defined. Now, the task is to design the industrial production process and the correspondent systems engineering.

Single-source suppliers offer, beside the leach reactor design, engineering services and construction of plant modules including support for commissioning. This integrated approach results in fast implementation. The engineering ideally is divided into 3 phases (Figure 2).

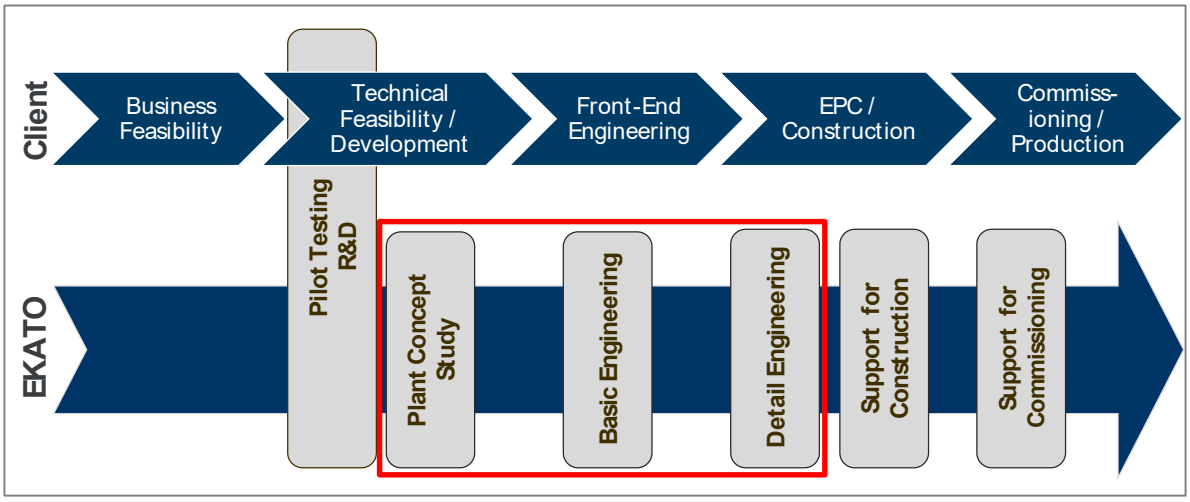

Figure 2: Project Phases While Building Plant Modules.

Plant Concept Study

Within the framework of Plant Concept Studies, operating conditions such as pressure and temperature, the lixiviant type and possible reductants are defined or determined from the laboratory data. The upstream and downstream process steps are also considered in the concept study.

Basic Engineering

During Basic Engineering, the dimensions of the main components are determined. These are based on the general requirements of the customer, such as the desired production volume and the available media and energies. At the same time, the piping and instrumentation scheme is compiled. During this phase the transfers to storage tanks, devices for dosing, as well as safety devices are also defined. The P&ID scheme is an important planning document for the further progress of the project. A reduced amount of interfaces leads to reduced planning and investment costs. During Basic Engineering, it is usually necessary to initiate the procurement process of components with long delivery times in order to be able to complete the system and to meet the delivery schedule and project timeline. As a result, this project phase is of crucial importance.

Detail Engineering

In the subsequent Detail Engineering, the P&ID diagrams, pipelines, fittings, measuring points and control circuits are completed and finalised. At the same time, the piping layout and functional description of automation is created. Based on these documents, the procurement of the components and the assembly planning begins. The combination of process development, engineering and construction / support for commissioning strongly reduces project times.

Examples / References

EKATO meanwhile has delivered, installed and successfully started up multiple plant modules engineered and manufactured at its facilities in Germany. Figure 3 shows a reaction unit and Figure 4 shows a complete Pilot Plant

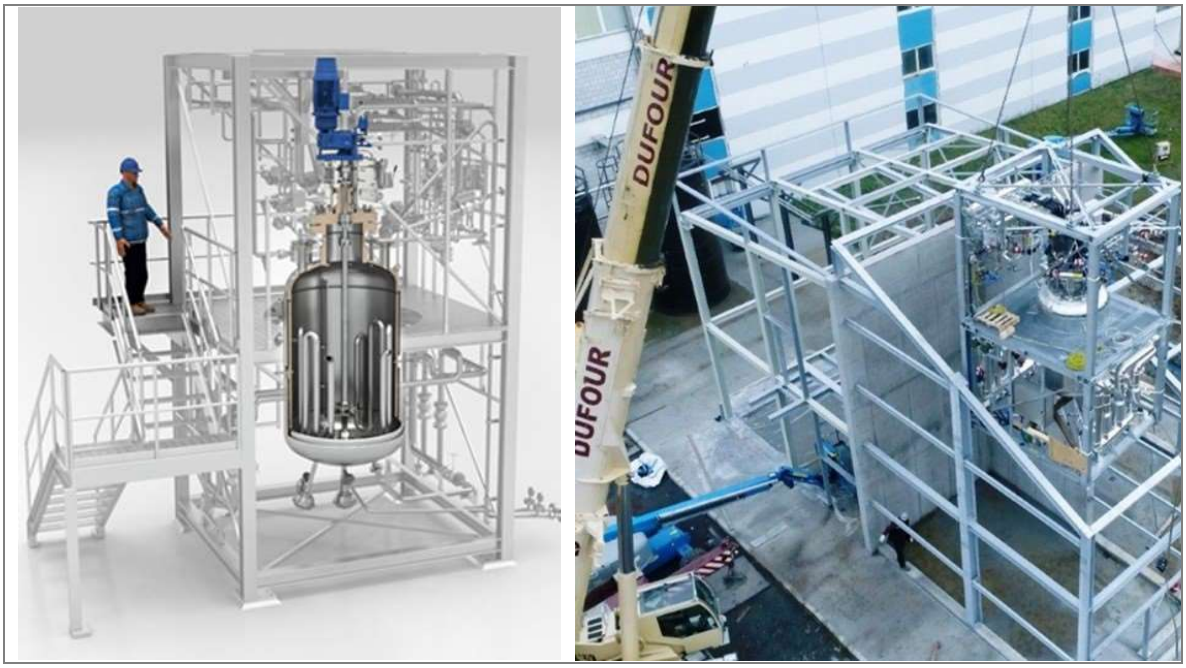

Figure 3: Reaction unit supplied and installed.

Figure 4: Pilot Plant Module supplied as two skid mounted units.

TECH PROJECT – NITRIC ACID LEACH CIRCUIT AND TESTWORK

Figure 5 shows a simplified flow sheet of the process applied for the TECH project. As described before the Concept Study focussed on the nitric acid leach process step.

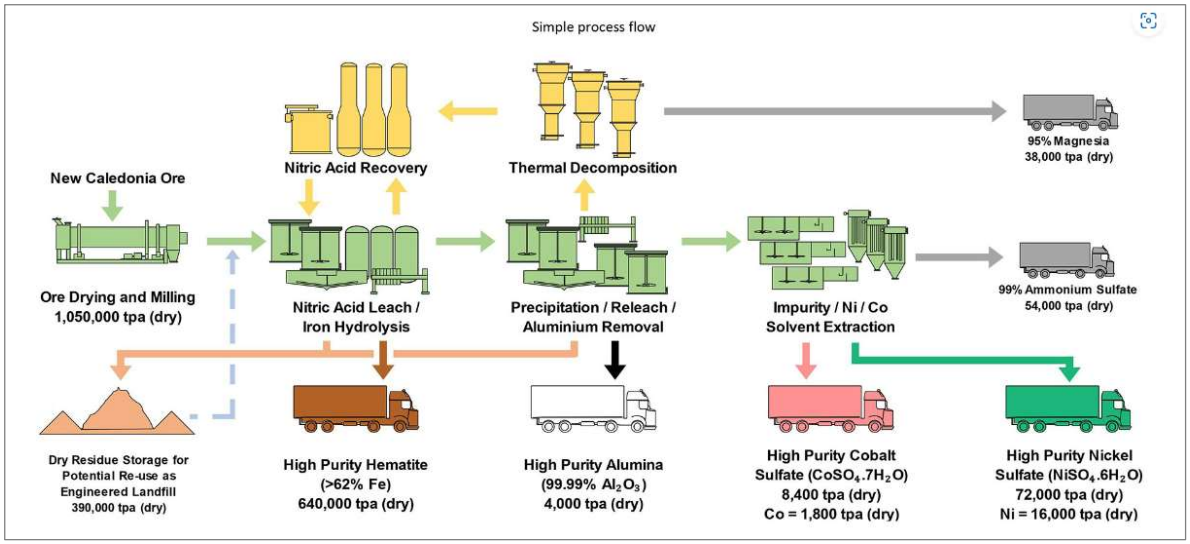

Figure 5: Simplified flow sheet of the process applied for the TECH project.

Leach Process Description

The typical plant feed expected under the terms of the ore supply agreement will be high iron limonite ore, averaging 42% iron, 1.6% nickel and 0.18% cobalt, as illustrated in Figure 6**Error! Reference source not found.**. The overall objective of the Leach area is to extract valuable metals from the laterite ore using nitric acid to produce a concentrated pregnant leach solution (PLS) for downstream processing and metal recovery.

Figure 6: TECH Project Nickel Laterite Ore

The metal oxide minerals in the dry milled ore are leached using superazeotropic nitric acid (average concentration of 78% w/w), forming metal nitrates and producing a pregnant leach solution (PLS). The nitric acid is recycled from two downstream acid recovery plants. Any chloride in the ore is leached and is ultimately concentrated in the downstream acid recovery circuits, potentially creating highly corrosive conditions in the presence of hot nitric acid.

Key chemical compounds in the PLS are nickel, cobalt, aluminium, iron, and magnesium nitrates. Impurity metal nitrates (Zn, Cr, Ca, Mn, Cu, Sc, Na and K) are also present.

Examples of the key leach reactions are shown below:

$$NiO_{(s)} + 2\ HNO_{3(aq)} \rightarrow Ni(NO_3)_{2(aq)} + H_2O_{(l)}$$
$$Al(OH)_{3(s)} + 3\ HNO_{3(aq)} \rightarrow Al(NO_3)_{3(aq)} + 3\ H_2O_{(l)}$$
$$FeOOH_{(s)} + 3\ HNO_{3(aq)} \rightarrow Fe(NO_3)_{3(aq)} + 2\ H_2O_{(l)}$$

Nickel is present mostly in the goethite mineral matrix (FeOOH) which leaches readily. Most of the cobalt in the ore is present in asbolane, a manganese-cobalt mineral with the general formula $(Ni,Co)_xMn^{4+}(O,OH)_4.nH_2O$. In order to extract cobalt the asbolane must be leached, however manganese present as Mn(IV) leaches poorly in nitric acid, which is an oxidising acid. In nitric acid alone, only 40-45% of the cobalt is leached. Reducing conditions convert the Mn(IV) in the asbolane to Mn(II), breaking down this matrix and liberating the cobalt. To provide the necessary reducing conditions, recycled NO_2 gas is dissolved in the concentrated nitric acid supplied to leaching. The NO_2 reduces Mn(IV) to Mn(II) according to the following reaction:

$$MnO_{2(s)} + 2\ NO_{2(aq)} \rightarrow Mn(NO_3)_{2(aq)}$$

Dissolved NO_2 is present as several NO_x species in equilibrium, including HNO_2, N_2O_3, and N_2O_4. Any unreacted NO_2 is vented from the leach tanks.

In general, silica minerals such as quartz, SiO_2, talc, $Mg_3Si_4O_{10}(OH)_2$, do not leach, resulting in an inert, barren leach residue. To ensure the target metal extractions are achieved, the free acid concentration in the leach discharge slurry is maintained at approximately 300 g/L by controlling the ratio of nitric acid to ore feed.

A number of leach reactions generate NO_x gases which contribute to the overall composition of the leach vent vapours. These include:

- Oxidation of organic carbon in the ore by concentrated nitric, generating NO_2 and CO_2 gases;
- Leaching of ore minerals containing ferrous iron (Fe^{2+}), such as antigorite, $(Fe^{2+},Mg)_3Si_2O_5(OH)_4$, generate nitrogen monoxide (NO) gas; and
- Generation of NO_x gases by the decomposition of nitric and nitrous acid.

The ore feed to leaching contains a small amount of coarse (up to 1 mm), high density (up to 4.8 t/m^3) chromite particles which leach sparingly and must be suspended so that they advance along the leach train and exit the circuit, rather than accumulating in the bottom of the tanks. Chromite is also highly abrasive, so design must consider the potential for erosion of internal surfaces.

Leaching is conducted in five cascade-flow co-current agitated tanks, at atmospheric pressure and at a temperature of approximately 110°C, which is below the boiling point of the solution. The operating temperature has been selected to avoid the hydrolysis of iron, which starts at around 115°C, and which would increase the volume of leach tailings. During start-up, the temperature is maintained at 110°C in each tank using internal heaters that use steam at 26 bar and 226°C.

The leach vent gases contain a high concentration of nitric acid resulting from the vapour-liquid equilibrium of the nitric acid and total metal nitrates in solution at the leaching temperature. The leach tanks are equipped with vents positioned at the highest point of the tank roof.

Leaching Test Work

EKATO acquires information from tests in their German technical centre or utilizes data compiled by its customers or development partners. For the TECH project QPM ran an extensive test program to adapt and optimise the test work previously performed by Direct Nickel [4,5,6].

A bulk sample of limonite ore from New Caledonia was dried and crushed for use in the test work program (Figure 6).

Bench scale leaching tests were conducted in an insulated baffled 5-litre glass reactor with a lid, and an overhead stirrer with a Teflon pitched blade impellor, positioned on a thermostatically-controlled

hotplate. Vent vapours were directed into a condenser and the condensate collected in a beaker. The test apparatus is shown in Figure 7.

It was observed that the cobalt extractions in some tests were poor. There is a history with New Caledonian laterite ores of cobalt incorporated into the manganese dioxide (asbolane mineral) matrix, which leaches poorly without the aid of a reductant. As nitric acid is an oxidising acid, it will not dissolve manganese dioxide. Leaching the ore samples with the addition of nitrite ions as a reductant (added as sodium nitrite) achieved significant increases in manganese and cobalt extraction.

Figure 7: Apparatus for Bench Scale Leaching Tests

Co-current leaching was piloted in 2020 and 2021 as part of a 20 kg/h continuous integrated pilot plant operated in Perth, Western Australia. This circuit was similar to the current leaching circuit with the exception that the design nitric acid concentration at that time was 56% w/w. The pilot plant was commissioned in a reliability run over 4 days in November 2020. Run 1 commenced on 10 December and ran continuously for 14 days and Run 2 commenced on 25 January 2021 and ran for 14 days.

The continuous leaching circuit comprised four 70-litre tanks, providing 6 hours retention time, operating at 110°C and using a nitric acid dosage rate of 2.5 kg per kg of ore. Key outcomes of the 2021 leach pilot plant campaign are summarised in Table 1.

Table 1: 2020-21 Leach Pilot Plant Outcomes

Parameter	Units	Value
Residence Time	hours	6
Acid to Ore Ratio (100% HNO_3 basis)	kg/kg	2.5
Residual Free Acid	g/L HNO_3	301
Temperature	°C	110
Elemental Extractions:		
Ni	%	98.6
Co	%	96.2
Fe	%	95.3
Al	%	73.7
Mg	%	79.5
Ca	%	97.5
Mn	%	80.4

The pilot plant leaching circuit is shown in Figure 8.

Figure 8: Pilot Co-Current Leaching Circuit

Another leach pilot plant, using 78% w/w nitric acid, will be undertaken in mid-2023, to confirm the expected leaching performance and to confirm the solid-liquid separation characteristics.

CONCEPT STUDY FOR THE LEACH CIRCUIT MODULE

Data from the pilot plant test work, as previously described allowed QPM to define the scope of work, compile a process flow diagram as well as data sheets for the leach reactors. These and additional data were provided to EKATO and used as a basis for the concept design of the leach circuit for the TECH project. During subsequent meetings specific requirements, scope of supply and battery limits were also defined.

Process Design

Analysis Mixing Tasks

In order to identify the correct scale-up criteria mixing tasks had to be identified [7]. Before starting detailed calculations addressing these mixing tasks, an analysis of the process requirements and constraints was done. An important design parameter is the vessel geometry, in particular the filling height to diameter ratio of the vessel. Here only the desired volume flow through the continuously operated tanks and the residence time was specified.

In this co-current leach process with six tanks in series, each having a total vessel volume of approximately 400 m³, dried ore and nitric acid are added to the first leach tank to dissolve the metal oxides contained in the ore. From this it can be concluded that solids suspension as well as fast blending must be ensured by agitation. Another requirement is the transfer of heat into the slurry to maintain the design temperatures specified. All these mixing tasks are considerably influenced by the vessel geometry. Other important design parameters include the locations of the feed pipes and the discharge location in the tanks.

Solids Suspension

To determine the required power input to achieve the desired degree of suspension in an agitated slurry, the design particle size i.e. d_{80} of the particle size distribution is required. This design procedure considers all particle sizes of a ‘typical’ particle size distribution. Additionally, a separate calculation for off-bottom conditions based on the d_{100} should be done using another physical model. A

preliminary maximum particle size d_{100} of 1000 µm was given by QPM. Based on this particle size a sensitivity analysis regarding manageable particle sizes was done.

Blending

As previously described an intensive mixing or blending of the slurry feed with the added acid is required to achieve a fast contact of the reactants and maximize the leach rate. Other important aspects related to blending are the minimization of short circuiting, acid hot spots and dead zones in the tanks. To assess the mixing performance of the agitator the impeller pumping rate and/or blend time is calculated. A comparison of the mean residence time to the blend time allows assessment of the blending performance of the agitator. The ratio of the mean residence time to blend time for the chosen agitator design is > 40 which is well above the general design rule > 10 for chemical reactors.

Heat Transfer Analysis

Heat shall be transferred to the vessel by steam supplied at a pressure of 26 bar(a), alternatively with 12 bar(a). The minimum heat demands for all tanks in the leach circuit were defined. In a first design step the heat transfer via the vessel wall with jackets or half-coils were assessed as this is technically the simplest design. A consequence of having an outside shell pressure of 26 bar(a) is the necessity of a high vessel thickness which reduces heat transfer capacity significantly. Calculations showed that sufficient heat transfer via the vessel wall was would not be achieved. Therefore, in the second design step internal heat exchangers were considered and assessed to be the best option. The number of tubes is optimised during Basic Engineering as well as the arrangement of the tubes bundles.

Agitator Design

Agitators for the leach section have been designed with respect to the above-mentioned mixing tasks. From a mechanical point of view, they are designed in a way that the agitator drive heads (motor, mechanical seal, gear box, bearing shaft) as well as shaft and impellers, are identical in the entire leach section. A two-stage impeller design is applied. Only the last tank in the circuit, the centrifuge feed tank, is designed with only one impeller stage. This tank is operated as a surge tank, meaning the liquid level will change frequently. From a mixing point of view, one impeller stage in this feed tank is considered sufficient since mixing and heat transfer requirements are lower compared to the other tanks.

One additional consideration while selecting the impeller type, diameter and number was the resulting tip speed of the impellers. Due to the solids present, abrasion is an issue during plant operation. Abrasion of the impellers is affected by the impeller tip speed, hence the tip speed was minimised during the design phase.

Additional Design Considerations

Besides the blending performance of the agitator, the design of the feed and discharge locations is an important parameter while designing continuously operated tanks. Therefore, the feed pipes will be located close to the liquid surface in the entrainment zone of the impellers, whereas the discharge location will be close to the vessel bottom. A dip pipe is considered for discharging the slurry from the leach tanks. Dip pipes must be designed such that the flow velocity exceeds the hindered settling velocity of the biggest particles present in the slurry. Here possible turndown scenarios were considered as well.

Mechanical Design

Once the agitator and vessel design and other boundary conditions were fixed the mechanical design of the leach circuit could be started.

Vessel Design

The design of the leach tanks is challenging with respect to size as well as in combination with the Titanium Grade 2 material. During the Concept Engineering it was checked if the leach tanks could be manufactured from solid titanium. It needs to be considered that titanium has approximately half of the Young's modulus of carbon steel, which leads to less strength of the material and makes it also more complex to mill. Additionally, the forces on the tank and internals coming from the agitation system would lead to high wall thicknesses. To ensure sufficient stiffness of the overall system,

reinforcements at the outer side of the tanks like beams or rings will be needed. Therefore, in the concept study a cladded material of titanium on carbon steel basis was considered with respect to wall thicknesses and costs. Nevertheless, during the next engineering phase the simpler solid titanium material will be considered again with the tank suppliers.

The cladded material combines the strength of the carbon steel with the high corrosion resistance of titanium. The two materials are brought together by explosion welding / explosion bonding. Explosion welding is a solid-state process where welding is accomplished by accelerating one of the components at extremely high velocity through the use of chemical explosives.

With this cladded material, reasonable wall thicknesses can be attained. Next, a Titanium layer of 5 mm was considered. The thickness of the carbon steel layer must be three times thicker for the explosion bonding. This is currently defining the wall thickness. Considering the loads on the leach tanks, the wall thickness could be reduced. In fact, the production of the leach tank within the necessary tolerances are also easier to handle with this material combination. On the other hand, the welding procedure of the different leach tank parts is more complex with respect to the different materials.

To minimize potential risks within the project, EKATO considered Finite Element Analysis (FEA) and Modal Analysis for the leach tanks in the next stages of the project. From experience, tanks of this size in combination with agitation forces and small wall thicknesses tend to encounter vibration and resonances which can cause major damage. Also, the forces on agitator supports, tank internals and their supports can lead to damage during operation. The FEA will be done in-house at EKATO and integrated into the tank design before fabrication.

Heat Exchanger Design

As described in the heat transfer analysis, the heat required for the process will be transferred via internal pipes. From a mechanical point of view, it was considered that these heat exchangers be removable from the top of the tanks. This has the advantage that these are not a part of the tank, which facilitates maintenance and/or exchange. The heat exchangers will be supported from the top head and in the bottom part. Thermal expansions will be absorbed by pipe bends.

Additional Equipment

Rotary feeders required to add the nickel laterite as dry milled ore will be placed on the first two leach tanks. These ensure a precise volumetric ore addition into the leach reactors. It is planned to equip them with the following features:

- Leakage collector to ensure no gases being released into the atmosphere
- Gas flushing at the labyrinth seal
- Rotation monitored and speed measured

Rotary feeders in special material such as titanium are not standard. Together with QPM, abrasion was identified as the challenge, therefore cladded stainless steel was chosen. The housing is hard chrome plated and the cellular wheel has a welded tungsten carbide surface. Vapours from leach tanks could come into contact with the rotary valve and cause corrosion. In comparison to the other parts of the project, the costs of the rotary feeder in this material are relatively low. Therefore, EKATO recommends having a spare rotary valve or at least the capital spares of this part in stock to ensure the plant availability.

The piping connecting the leach tanks will be designed in titanium with piping incline for gravity feed to the consecutive tank. Settling of the solids is prevented by ensuring a sufficient flow velocity. Two overflows are considered for each leach tank, one directly leading into the next stage, the other overflow is for bypass operation. With the bypass, one leach tank can be taken out of service for maintenance or in case of a failure.

Other additional equipment such as the platform and instrumentation are also designed by EKATO. A layout of the nitric acid leach circuit is shown in Figure 9.

Figure 9: Layout of the Leaching Circuit

CONCLUSIONS

With its comprehensive range of services and equipment, EKATO offers partial or complete solutions from the original idea to a technically and economically sound solution. By means of piloting (in-house or by its customers), and with many years of experience in the scale-up of process engineering equipment, EKATO provides high-quality production plants.

For cost reasons, an efficient implementation of investment projects from the idea to commissioning is necessary. The piloting, scale-up and engineering phases from a single source ensure a technically and economically optimized system with short implementation times by reducing interfaces. In addition to the well-known agitator business, EKATO has built up the Process Plant business area and has the relevant experience and references from successfully completed projects.

Expertise and know-how of QPM and EKATO was successfully applied during the presented concept engineering to specify the production-sized reactor systems for the nitric acid leach circuit.

ACKNOWLEDGMENTS

The work presented in this paper is part of a study done for Queensland Pacific Metals. EKATO would like to thank the management of Queensland Pacific Metals for their collaboration and permission to present this paper.

REFERENCES

1. Willis, B.., Downie, J. (2020). Townsville Energy Chemicals Hub – The 'TECH' Project. Proceedings of the ALTA NCC Conference, Perth, Australia 2020, 9-13.

2. Willis, B., Grocott, S. (2022). The TECH Project – Path to Production. Proceedings of the ALTA NCC Conference, Perth, Australia 2022, 80-104.

3. Altilium website https://www.altiliumgroup.com/the-dni-process/ . April 14, 2023.

4. McCarthy, F., Brock, G. (2011). The direct Nickel Process – Continued Progress on the Pathway to Commercialisation. Proceedings of the ALTA NCC Conference, Perth, Australia 2011, 2-11.

5. McCarthy, F., Brock, G. (2014). Direct Nickel Test Plant Program: 2013 in Review. Proceedings of the ALTA NCC Conference, Perth, Australia 2014, 80-99.

6. McCarthy, F. (2017). The DNi Process™ – The Next Step to Commercialisation. Proceedings of the ALTA NCC Conference, Perth, Australia 2017.

7. EKATO. THE BOOK 3rd edition, ISBN 978-3-00-038660-2.

WESTERN AUSTRALIAN PCAM HUB – REFINING THE FUTURE WITH PBT'S NMC DIRECT™

By

William Hawker, Harrison Hodge, Kate Dickson

Pure Battery Technologies, Australia

Presenter

Marie Cyprien
marie@purebatterytech.com

Corresponding Author

William Hawker
Will@purebatterytech.com

ABSTRACT

Recent worldwide events have highlighted the need for improved supply chain resilience in Australia. Pure Battery Technologies (PBT) is helping address this need by developing the WA pCAM Hub, leveraging Australia's strong mining industry to bring value-adding battery material manufacturing processes on shore.

PBT's WA pCAM hub will utilise PBTs patented and proprietary NMC Direct™ approach to upgrade intermediate nickel and cobalt containing materials into lithium-ion battery precursor Cathode Active Material (pCAM). The NMC Direct™ approach is a combination of processes including PBT's patented Selective Acid Leach (SAL) and Combined Leach (CL) methods. This approach offers a new processing route for refining nickel, cobalt, and manganese into battery metal products, exploiting differences in solubilities and oxidation states to achieve the separation of metals using low energy hydrometallurgical processes. This NMC Direct™ approach eliminates costly and energy-intense production steps, decreasing CO_2 equivalent emissions from the refining of intermediate material to pCAM by up to 85% when compared to current industry standard process routes, and removes the need for production of intermediate metal or sulphate crystal products.

The WA pCAM Hub will also give emerging and existing Australian mines an alternative downstream partner for ore and concentrate refining. The NMC Direct™ approach gives nickel miners the option to extract types of ore that are unsuitable for traditional processing routes, while the higher value final pCAM product allows previously uneconomic deposits to be used as decarbonising minerals for the future.

This presentation will provide a brief description of the NMC Direct™ approach and an update on the WA pCAM hub project.

Keywords: pCAM, NMC Direct, MHP, nickel

.

Raw materials used in manufacturing cathodes, known as precursor cathode active materials (pCAM), are a critical component to battery performance

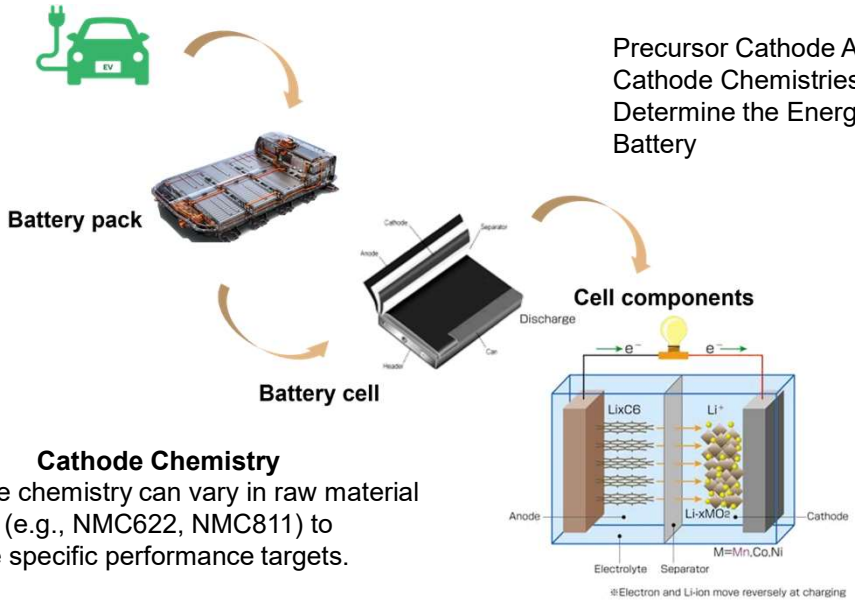

Precursor Cathode Active Materials and Cathode Chemistries in Li-Ion Batteries Determine the Energy Density of the Battery

Cathode Chemistry

Cathode chemistry can vary in raw material content (e.g., NMC622, NMC811) to achieve specific performance targets.

Battery cell demand will continue to raise with expectation to increase by over 33 times by 2040

Demand for Li-Ion Batteries

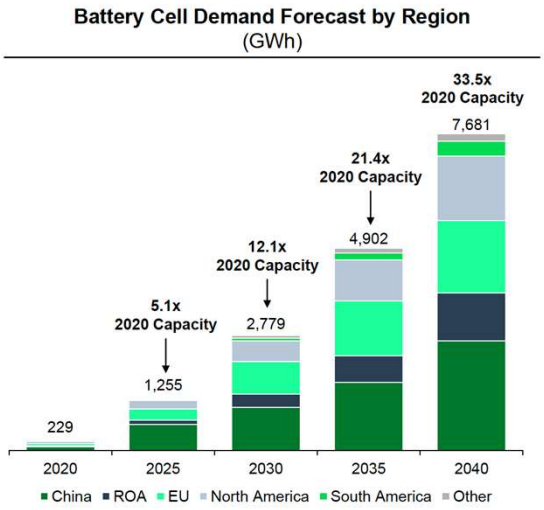

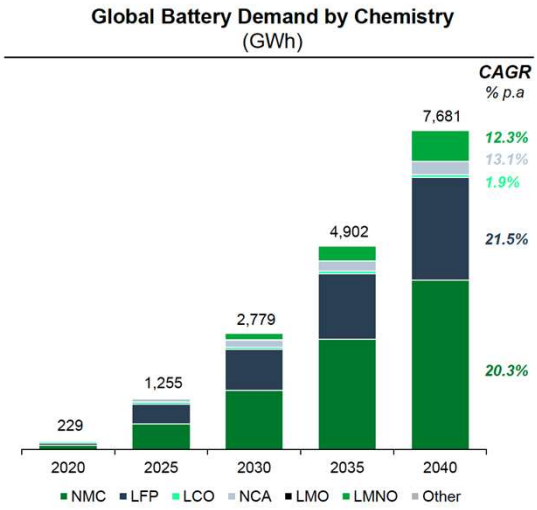

Source: Benchmark Mineral Intelligence

Additional sources of Ni are required to supply to the battery market

Despite Growing Demand, 95% of existing Ni supply is either locked up in long-term agreements for Stainless Steel (Class 1) or Unusable in pCAM (Class 2)

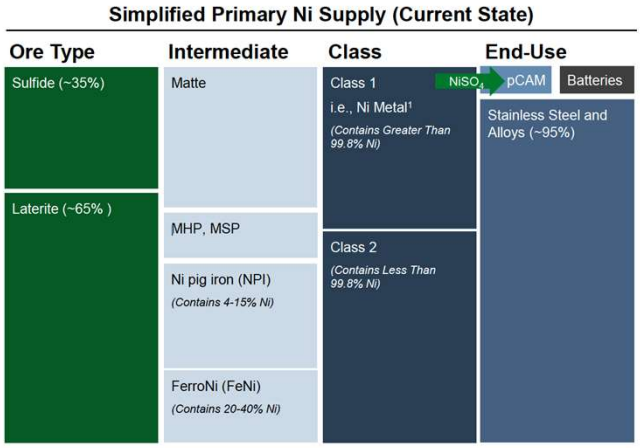

1. Simplified terms for powder, briquettes, cathode, pellets, sulfate, etc.

- Only Class 1 Ni has a high enough Ni purity to be used for NiSO4or other Ni materials in batteries
- $NiSO_4$ is the Ni end-product that is used as an input to pCAM manufacturing for batteries
- Only a fraction of Class 1 Ni is currently processed into $NiSO_4$ for use in Li-Ion batteries

Source: 2020 Third party consultant

The Lithium-ion revolution is driving exceptional demand for raw material

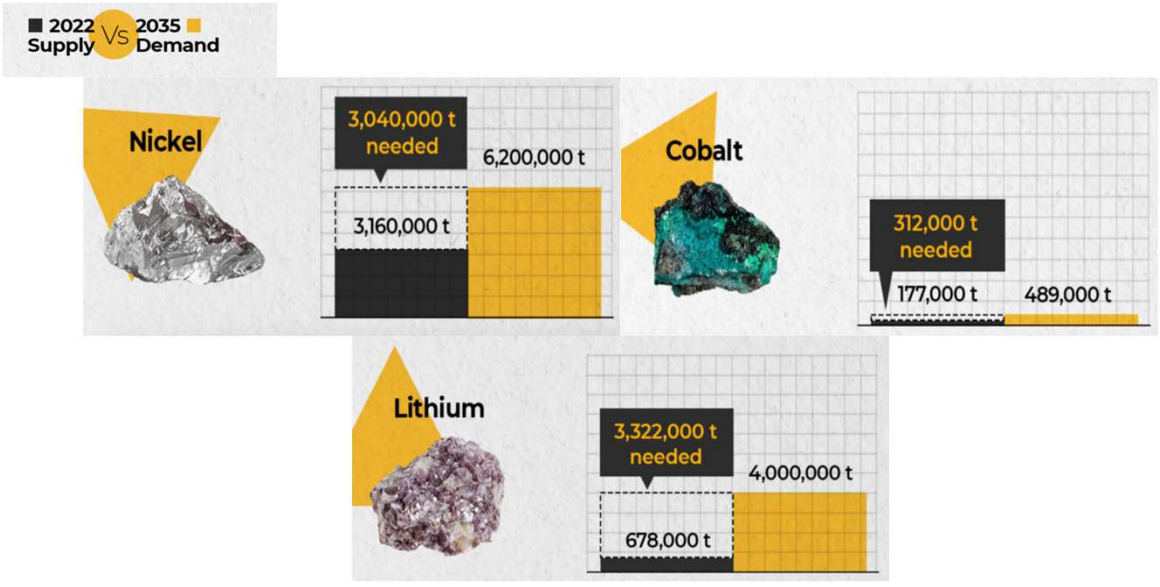

Source: Benchmark Mineral Intelligence products

PBT has an advantage in addressing the current market's demands

The Issues

- Demand for battery raw materials outpacing supply
- New pCAM production pathways are needed
- Significant opportunity to reduce environmental impact
- Rising cost of battery raw materials puts pressure on EV penetration
- Evolving market with evolving specifications (NMC622 vs 811)
- Slow development of new mines

The PBT Advantage

- Produces high performance, high Ni ratio pCAM materials
- Flexible technology that can adapt to evolving market demand
- Multiple feedstocks: multiple pathways
- Faster deployment than new mining operations
- Can be deployed in any geography
- Lower CO2 emissions
- Less energy intensive
- Reduced fresh water requirement
- Less hazardous solvents
- Increases material availability, reducing upward pressure on EV prices
- Lower refining costs compared to traditional routes

PBT is bringing smarter, simpler, greener technologies to refine Ni, Co and Mn into pCAM from old and new sources

Founded in 2017, PBT has developed, validated and commercialised two Australian-invented Technologies

Significant process, cost and emission reduction to produce battery grade pCAM globally to feed into EV market

Increased flexibility in feedstock thanks to ability to refine larger range of concentrate, MHP or recycled material

Since 2020, PBT has an operating Nickel refinery in Hagen, Germany fitted with commercial scale pCAM production Technology and currently in expansion

Supported by European Commission, named as project of strategic interest and by strong investors like EIT InnoEnergy – largest European Clean-Tech investor

Supported by the Australian Government as a recipient of $119.6M via the MMI (Modern Manufacturing Initiative) grant program for its WA pCAM Hub project

PBT's NMC Direct™ Technology is simpler than existing processing routes to produce pCAM

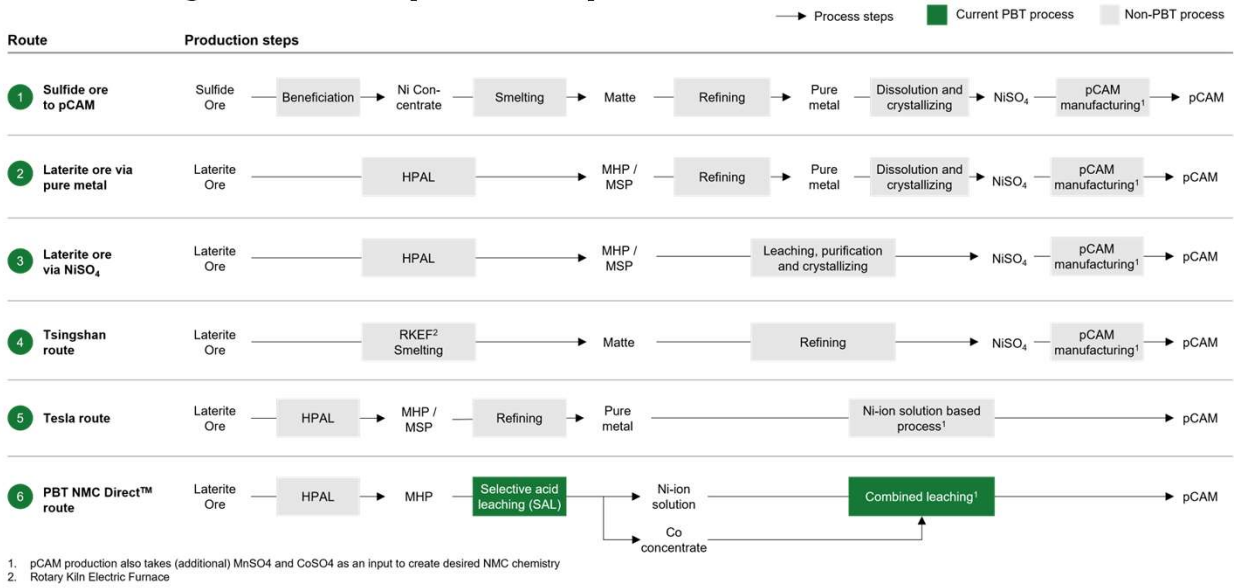

1. pCAM production also takes (additional) MnSO4 and CoSO4 as an input to create desired NMC chemistry
2. Rotary Kiln Electric Furnace

PBT's NMC Direct™ Technology is more cost and emission effective

Costs and emissions to create pCAM from intermediate products (NMC811)[1]

Primary materials[1]

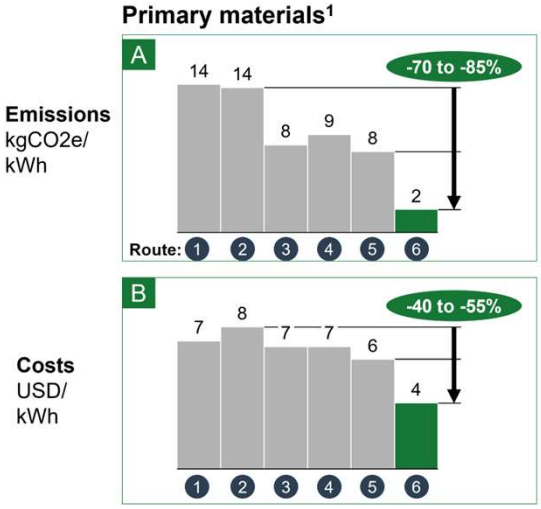

>70%

lower emissions to create pCAM from intermediate products

Resulting in 630 kg less CO2 per EV.

>40%

lower costs to create pCAM from intermediate products

Note: analysis excludes logistics and profit margins. Based on 2020 data with electricity prices and grid emissions for Germany.
1. Primary materials: pCAM production from Ni matte or MHP, including the net result of sold by-products and additionally purchased metals

Technology Overview

PBT's technology can be used for both Primary and Secondary production

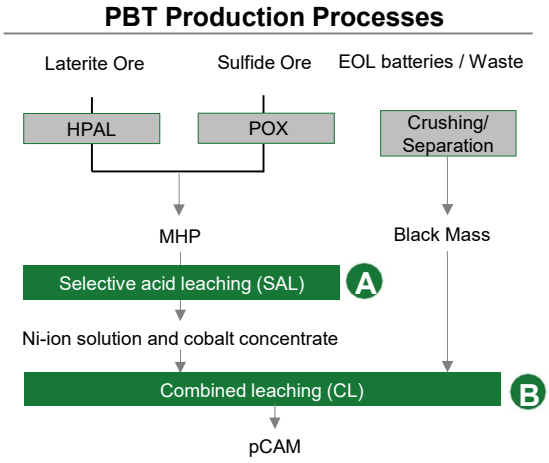

A Selective Acid Leaching (SAL)

PBT's Selective Acid Leaching (SAL) process selectively leaches impurities from intermediate metal products (e.g., MHP).

B Combined Leaching (SAL)

PBT's combined leaching process creates a battery grade pCAM from intermediates. Convertible intermediate feedstocks include:

- Ni-ion solution + Co concentrate (e.g., from the SAL process)
- Black mass (recycled content from off-spec and end-of-life batteries)

1.Sulfide ore-route likely requires additional processing via Albion or POX processing to produce a MHP e.g., from a Nickel concentrate
2. High Pressure Acid Leaching
3.Traditional pCAM processes require use of MnSO4 and CoSO4 as an input to NiSO4 to create desired NMC chemistry; PBT utilizes all Ni, Co and Mn contained in raw materials without making these battery salts in an intermediate step

SAL and CL Technologies were proven at commercial scale while developing PBT and a strong support

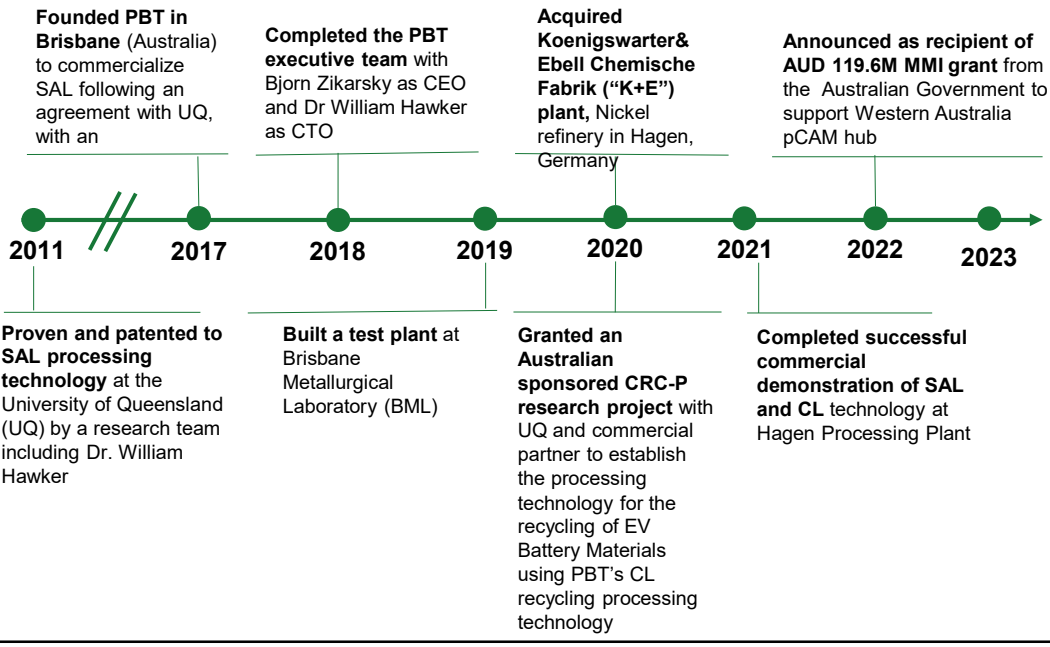

In October 2021 PBT announced our plans to build a pCAM Hub Refinery in WA

The WA pCAM Hub will be an integrated NMC battery material refinery, with ability to refine both Nickel concentrate (and potentially Black Mass in the future) and MHP using PBT's NMC Direct™ route.

The Project will initially produce 50,000tpa of pCAM expandable to 100,000tpa within 5 years - *50,000t of pCAM is the volume required to make batteries for about 500,000 electric vehicles (EV)*

The Project will focus on collaborative production of pCAM material, assisting in developing the ecosystem for advanced EV battery materials production in Australia.

The hub location is to cater to mine based suppliers in WA to aim to increase capacity and capability in the region, with large flexibility in feedstock materials that can be handled by the Hub.

The WA pCAM Hub will be located in the Coolgardie Shire, close to local mines for local refining

The hub will be built in the Mungari Strategic Industrial Area (SIA) is located approximately 26km south-west of Kalgoorlie and 13km north-east of Coolgardie in Western Australia.

The Mungari SIA is:

- 696ha of strategic industrial core
- owned in freehold by DevelopmentWA and
- a 1km buffer surround which is unallocated Crown Land.

The study footprint is 225ha with the actual project approximately 80ha.

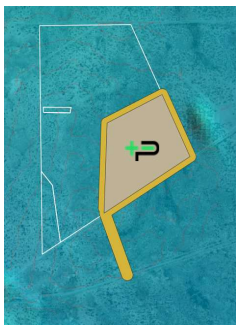

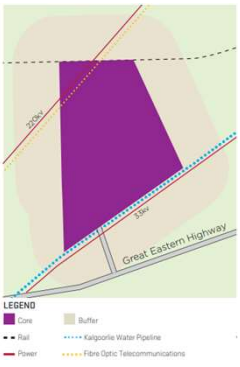

~200 million tonnes of NMC resources within 300km of the pCAM Hub, opening significant opportunity for partnership, operations and future plant expansion

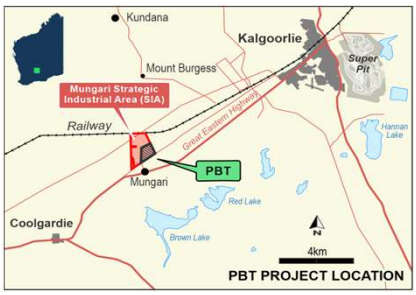

The WA pCAM Hub includes a POX and a pCAM plant for ultimate flexibility in feedstock type and quality

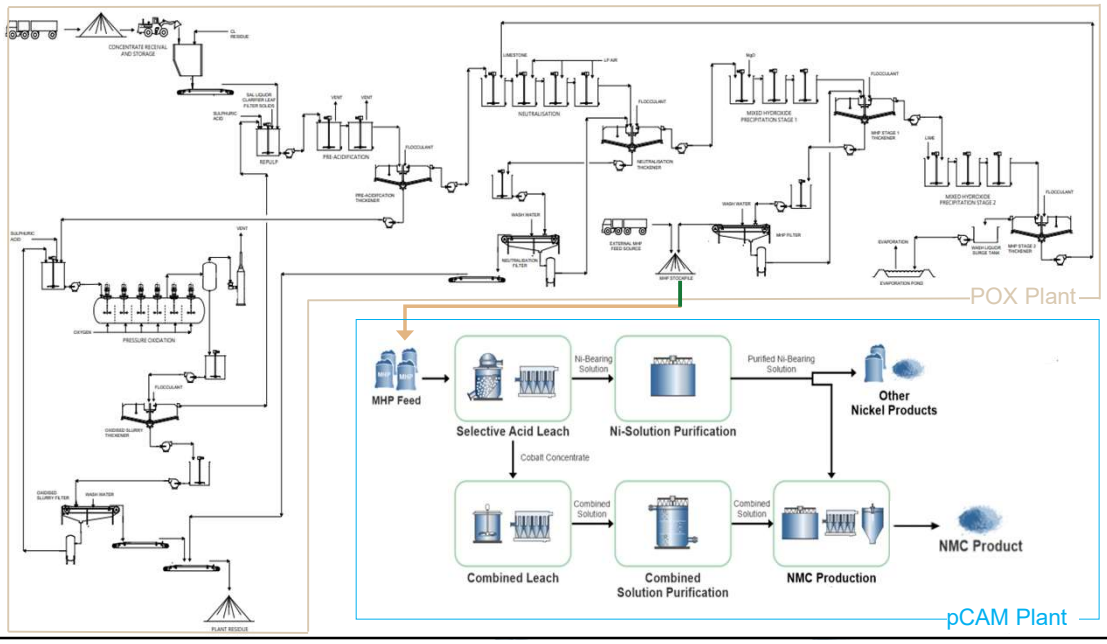

WA pCAM Hub Location – Feasibility Study Update

Q2 2022

Feasibility initiated - Includes Enviro, Approvals & Technical Scope

Mungari SIA selected as the site location

Q3 2022

Spring Flora and vegetation survey completed

Mungari Access Licence executed with Development WA

Q4 2022

Level 2 vertebrate fauna survey completed

Procurement plan/Vendor list developed and checked against IFC debarred register

Q1 2023

Infrastructure development and access are being negotiated with JTSI, Dev WA, Western Power & Water Corp ongoing

Hydrology, Flood Modelling, Noise Impact Assessment and Air Quality Assessments under way

Stakeholder Engagement (Enviro Approvals) Initiated

Q2 2023

Australian Industry Participation Plan submitted for approval

Stakeholder Engagement (Enviro Approvals) continued

The pCAM Hub will bring extensive benefits to the region, to WA and to Australia

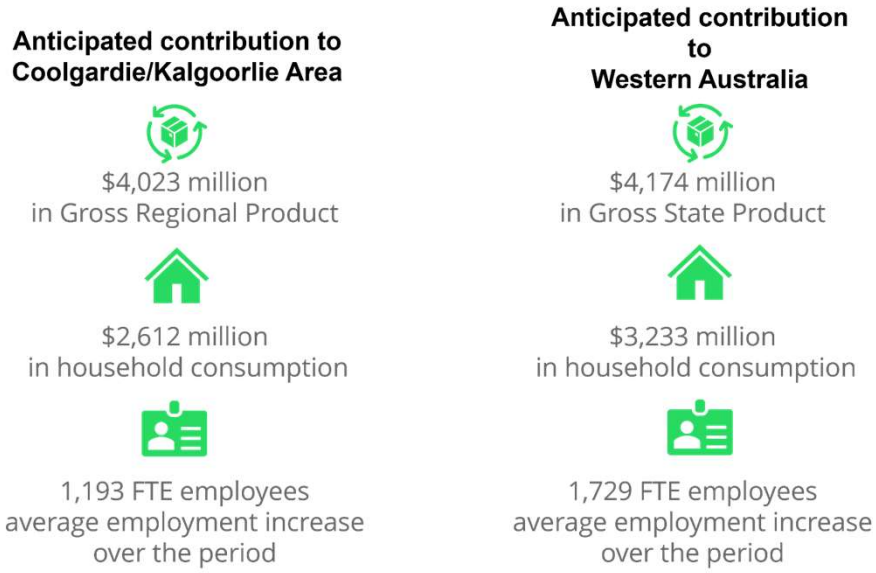

Source: Ernst&Young economic impacts assessment via sophisticated Computable General Equilibrium (CGE) model, from 2022 – 2031

PBT's pCAM Hub opens significant opportunities to existing and new businesses

FEEDSTOCK

- Ni concentrate not suited to smelter can be processed in the pCAM hub
- Co and Mn salts will be added to the process for ratio adjustment
- Diversify mineral offerings and expand into the EV market

INFRASTRUCTURE

- Power
- Water
- Communication
- Roads

R&D

- Partnerships with local universities and research centres
- IP development

LOGISTICS

- Material Transport
- People Transport
- Accommodation

NEW INDUSTRIES

- CAM production utilising local Li
- Acid Production
- Downstream manufacturing of battery cells
- Alternative Energy sources like wind and solar
- Future recycling of black mass onshore

LITHIUM-ION-BATTERY RECYCLING FROM EV USING PYROMETALLURGICAL AND HYDROMETALLURGICAL PROCESS COMBINATIONS

By

Toshihiko Nagakura, Hiroshi Kobayashi

Sumitomo Metal Mining Co.,Ltd.

Presenter and Corresponding Author

Toshihiko Nagakura
toshihiko nagakura.y3@smm-g.com

ABSTRACT

With the popularization of electric vehicles, resource recycling from secondary Lithium-Ion-Batteries (LIB) is a pressing issue in the world.

Currently, the EU issued the Battery Directive & New Batteries Regulation and promotes battery to battery (B to B) recycling. As a result, development competition for LIB recycling, including new entrants, is accelerating on a global scale. Generally, a hydrometallurgical method is used to recover valuable materials from LIB. However, many separation and purification processes are required to purify to the battery grade, and its unit cost may be also expensive. Sumitomo metal mining (SMM) has developed a pyrometallurgical and hydrometallurgical process combinations for recycling. Our hydrometallurgical process could be simplified, and we have succeeded in manufacturing battery-grade cathode materials. This paper introduces the treatment for metal collection and its impurities distribution in the pyrometallurgical process.

Keywords: Lithium-Ion-Batteries, recycle, nickel, cobalt, automotive batteries

INTRODUCTION

More than 120 countries and regions have set carbon neutral goals to curb global warming, and Japan has also declared its goal of becoming carbon neutral by reducing greenhouse gas emissions to zero by 2050. Along with the acceleration of the shift to EVs, which is expected to play a role in achieving this goal, there is a demand for resource recycling of rare metals (Ni, Co), Cu and Li in used lithium-ion rechargeable batteries (LIBs) for automotive applications. As a result, the developments of recycling technologies are accelerating.

To create a circular economy for battery materials, in December 2020, the EU published the draft European Battery Regulation that focused on the entire life cycle of LIBs which caught the world 's attention. Currently, Europe, North America, South Korea, and China are intensifying development competition, including new entrants into LIB recycling and the LIB recycling industry is expected to expand rapidly to support carbon neutrality in the future.

Sumitomo metal mining (SMM) has been working on research and development of LIB recycling since the 2000s and established a basic recycling process in 2018. A pilot plant verification was started in 2019 and succeeded in recovering high-purity nickel-cobalt mixed solution in 2021. The cathode materials for LIB made from this nickel-cobalt mixed solution were processed into batteries and evaluated. As a result, sufficient battery characteristics were confirmed and market needs for battery to battery *(B to B)* recycling were realized.

This report describes the recycling process developed by SMM which includes the removal of impurities, especially Fe, C, and P in the pyrometallurgical reduction smelting process.

TRENDS IN BATTERY RECYCLING IN VARIOUS COUNTRIES AND SMM ACTIVITIES

xEV innovation roadmap

As one of the assumptions for recycling, the electric vehicle roadmap announced by major countries is shown in Figure 1. All vehicles sold will be electrified by 2040 at the latest, except for Norway, which is ahead with an electrification rate of 55.9% as of 2019. The development of recycling Ni, Co, Cu and Li from used LIBs is expected to increase with the rapid change to electrification in each country due to reduction of CO_2 emission and raw material procurement and resource depletion.

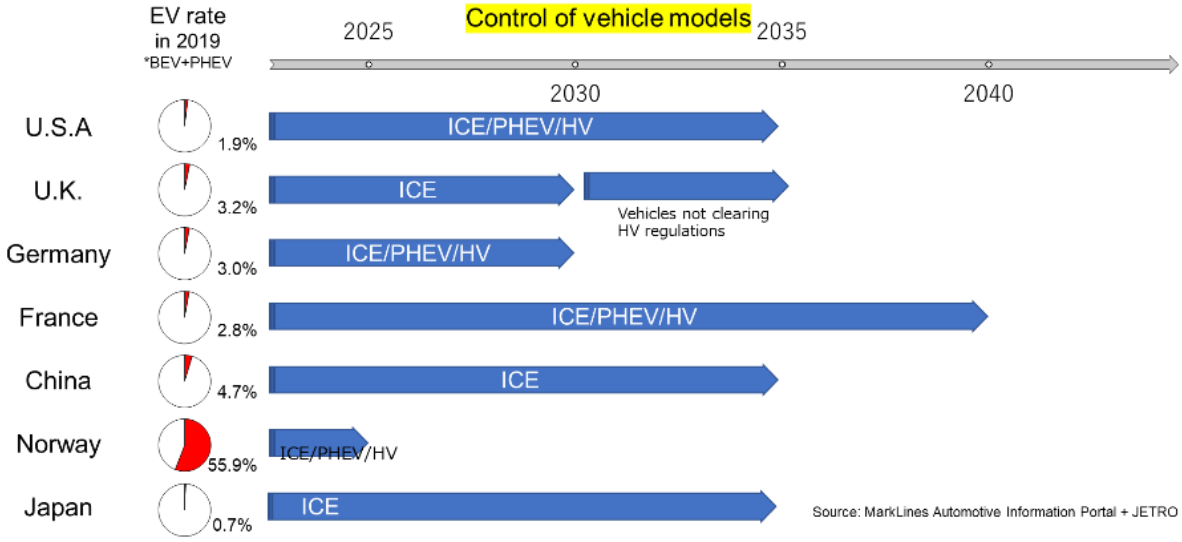

Figure 1: Roadmap of Electric Vehicles[1) 2)]

Figure 2 shows the projected demand for automotive battery capacity[3)] and Figure 3 shows the projected amount of nickel and cobalt used in LIB cathodes. Figure 2 shows that there is a demand of 2000GWh automotive battery capacity worldwide by 2030. The growth of BEVs is particularly significant. Figure 3 shows that the amount of Ni and Co supply might be increased more than 10 times from 2020 to 2030 (It was calculated independently based on the battery capacity demand in Figure 2, assuming half NCM (523) and half LFP are used).

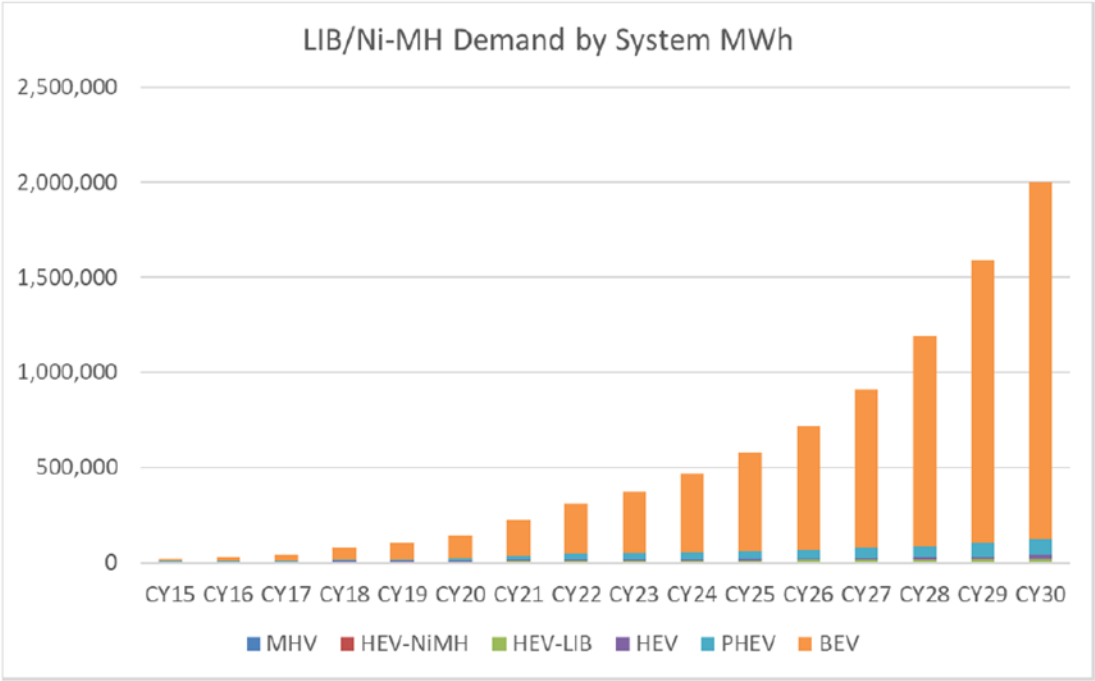

Figure 2: Automotive Battery Capacity Demand Forecast

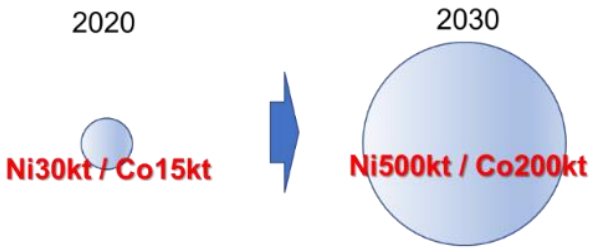

Figure 3: Predicted amount of nickel and cobalt used in LIB

For these circumstances, the amount of recycled materials generated from end-of-life vehicles (ELV) is increasing year by year and SMM plans to start commercial plant operation for these recycling materials in 2026 using our developed LIB recycling process.

SMM's achievement targets of the LIB recycling process were set equal to the European Battery Regulation proposal (Figure 4) announced by the EU in December 2020, which sets the recovery rate target of Ni, Co, Cu and Li from LIB recycling and the recycling rate target of essential elements in battery products. Although these target values are very difficult to achieve from technical points of view, we regard them as challenging goals and are proceeding with the development of the LIB recycling process.

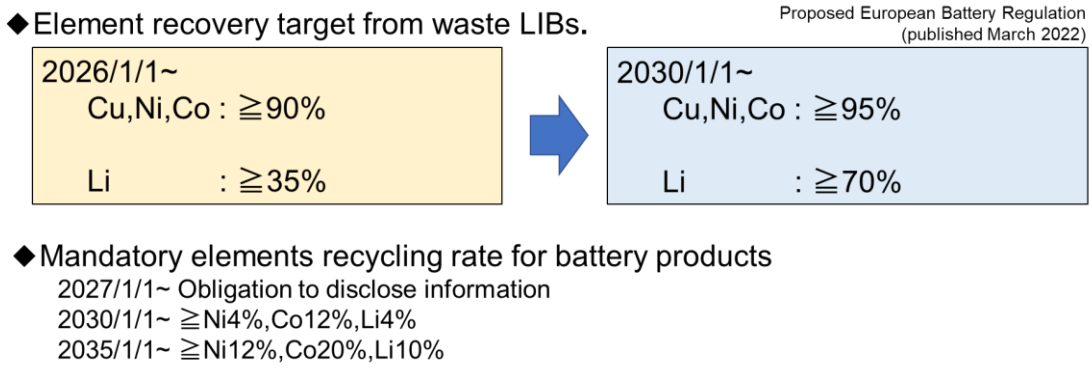

Figure 4: Proposed European Battery Regulation (published March 2022)

LIB Recycling Development Status in Each Country

The status of LIB recycling development by major companies is shown in Figure 5 and LIB recycling development is rapidly gaining momentum. SMM has also been working on research and development of LIB recycling since the 2000s. we established a new LIB recycling process in 2018. Finally, a pilot plant for this new process was in operation in 2019.

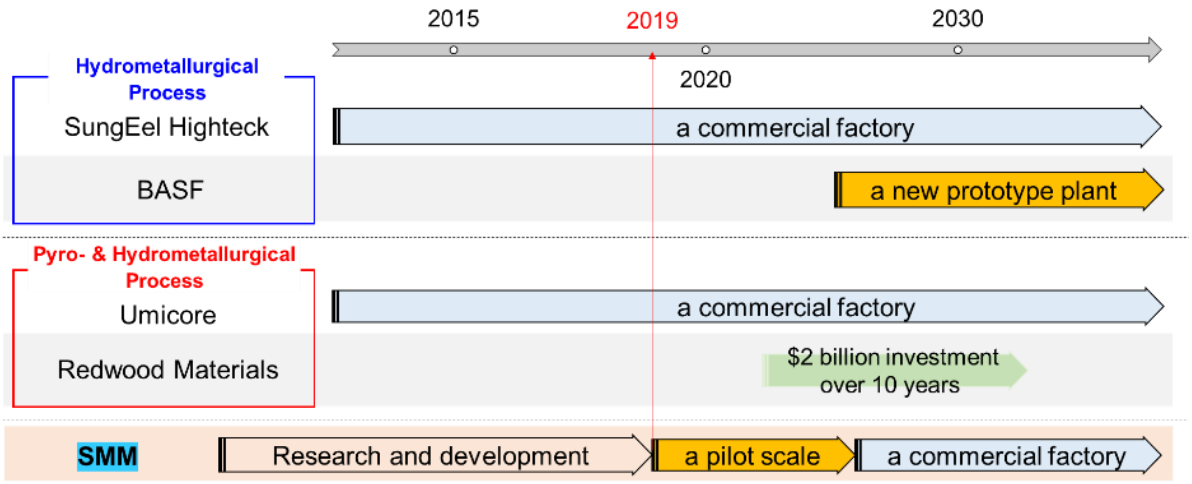

Figure 5: LIB Recycling Development Status of Major Companies[4) 5) 6) 7)]

SMM's LIB Recycling Activity & Development

SMM began processing of battery plant intermediate products at the existing copper smelter and nickel refinery in 2017 and the recovered nickel has been reused as raw material for SMM's battery cathode material (CAM) (Figure 6).

This is the first case of battery recycle business in Japan. But since this process at the existing copper smelter and nickel refinery, only nickel and copper are recyclable, which is wasteful from a recycling perspective. Therefore, we have been promoting full-scale research and development of a B to B type LIB recycling process that can recover cobalt and lithium in addition to nickel and copper.

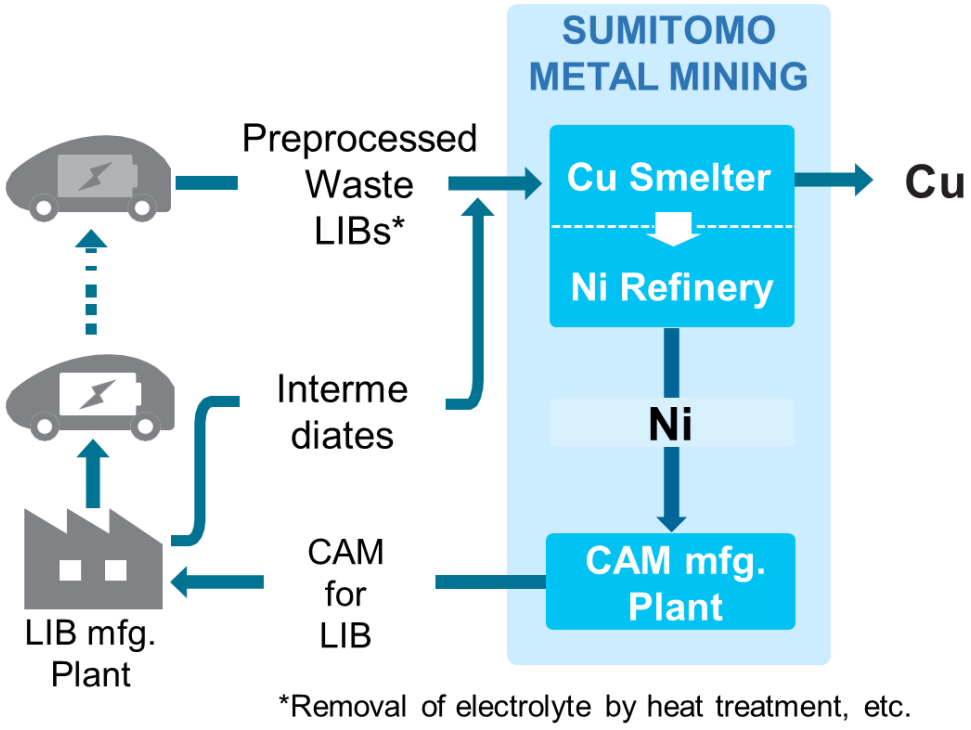

Figure 6: LIB recycling process flow using SMM's existing plant

Finally in 2018, SMM established a new LIB recycling process that combines pyrometallurgical and hydrometallurgical processes (Figure 7).
In 2019, a pilot plant for this new process was in operation in order to check its reliability. In 2021, nickel-cobalt-copper alloy was recovered by the pyrometallurgical process. And nickel-cobalt mixed solution could be recovered from the alloy by a hydrometallurgical process. This solution was proven to be sufficient as a feedstock for cathode material. This was verified by confirming the performance of LIBs incorporating cathode materials made from the mixed solution and its performance as a battery was equivalent to the current product.

Furthermore, SMM has also succeeded in producing soluble slag that enables lithium recovery from our pyrometallurgical process which had been considered difficult in the past.

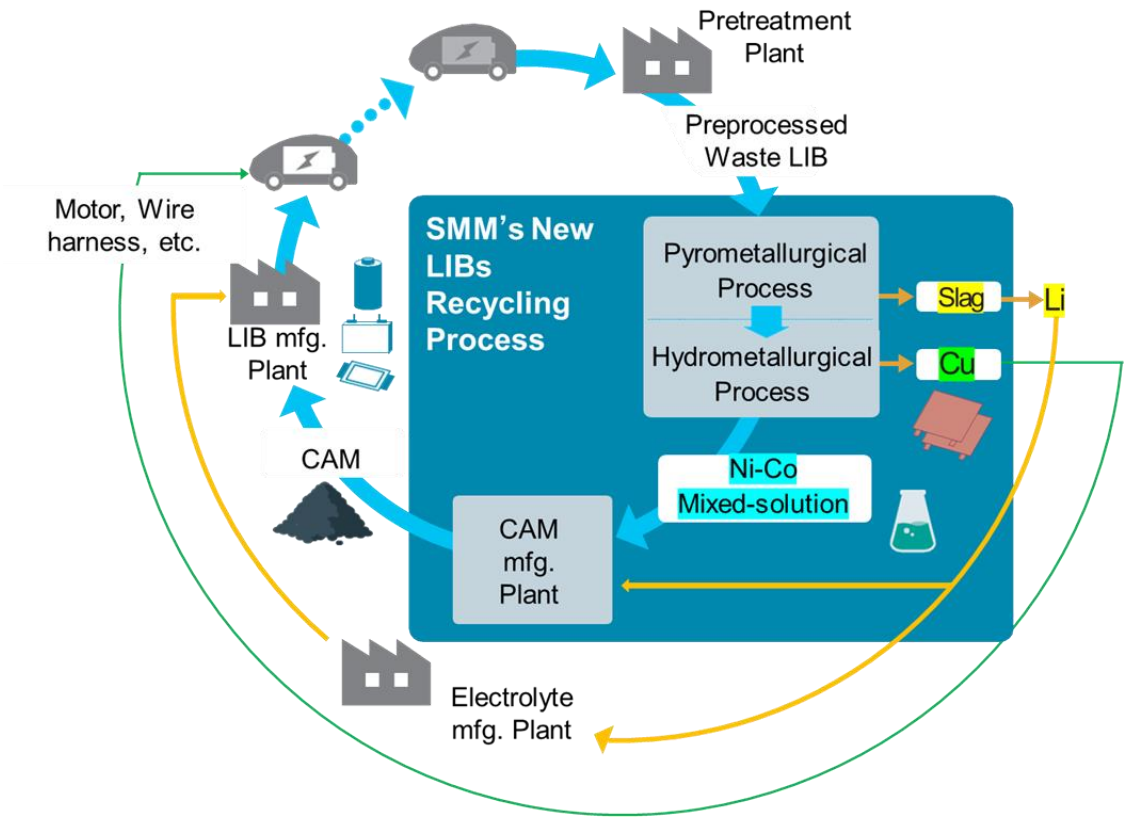

Figure 7: SMM's new LIB recycling flow

COMPARISON OF MAJOR BATTERY RECYCLING PROCESSES

There are three typical recycling processes that have been published and the advantages and disadvantages of each are compared. The third process is the one promoted by SMM.

All hydrometallurgical process

Figure 8 shows typical all hydrometallurgical process flow and its element behaviour in the process. When LIB recycling is performed by hydrometallurgy, it is common to apply a total leaching process followed by refining processes such as SX and neutralization. Compared to the pyrometallurgical process, the hydrometallurgical process requires a smaller plant and less capital investment. And it allows for higher element recovery rates and finer element separations. However, special separation equipment and reagents are required for its purification.

LIBs are composed of many components, including the outer casing, cathode foil, anode foil, separator, and electrolyte. The structure is also complex. So that it is impossible to separate elements completely by physical separation such as electrolyte removal and sieving. Therefore, this hydrometallurgical process requires to have a greater separation capacity. As a result, capital investment is not expected to be significantly reduced and its GHG emissions from Scope 3 are expected to increase.

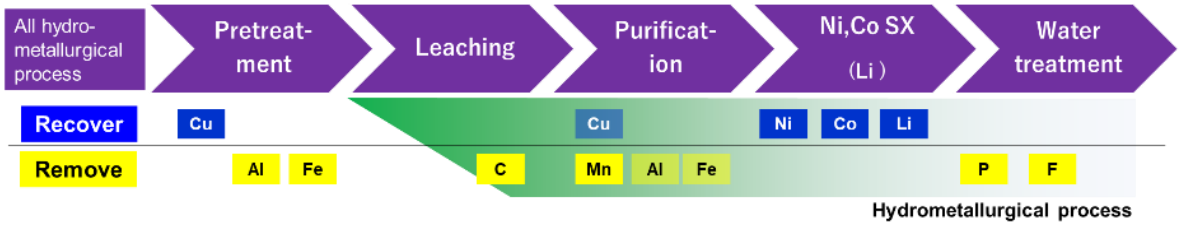

Figure 8: LIB recycling process with all-hydrometallurgical refining

Pyrometallurgical and hydrometallurgical process

Figure 9 shows typical combinations of pyrometallurgical and hydrometallurgical process flow and its element behaviour in the process. When LIB is smelt processed directly by pyrometallurgy, pre-treatment is not required as in the case of hydrometallurgical processing and Ni, Co, and Cu can be recovered at once.

But on the other hand, the excess carbon in LIB promotes the reduction of impurity elements to metal along with Ni, Co, and Cu, which increases the impurity load in the subsequent hydrometallurgical process and reduces the advantages of the pyrometallurgical process.

In addition, the decomposition heat of the electrolytic solution and combustion heat of the carbon content can be utilized in the smelting process, but because of their enormous calorific value, they must be operated under ultra-high temperature conditions, which is expected to worsen operability and operating costs.

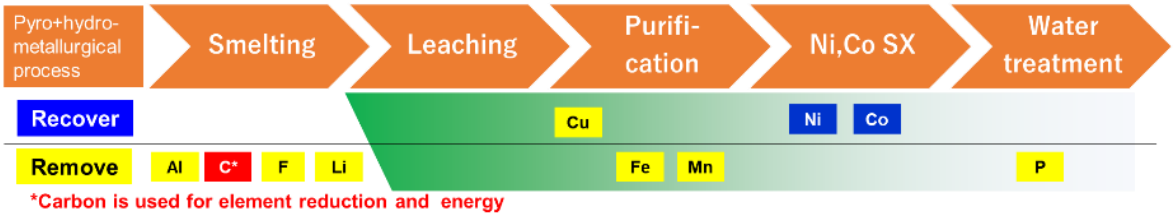

Figure 9: LIB recycling process by pyrometallurgical and hydrometallurgical refining

New SMM's process

The hydrometallurgical process requires a smaller plant and less capital investment, and Ni, Co and Cu can be recovered at once by the pyrometallurgical process. SMM focused on advantages of the above two processes and developed a new LIB recycling process that maximizes both process advantages.

This process consists of a pre-treatment process, a pyrometallurgical process (smelting) and a hydrometallurgical process (leaching, refining, and liquid purification) (Figure 10). The feature of this process is that Fe of the outer can and anode carbon are removed in our pre-treatment process. This allows selective recovery of nickel, cobalt, and copper in the smelting process, resulting in a nickel, cobalt and copper alloy with few impurities.

As a result, the impurity load in the hydrometallurgical process is significantly lowered and the equipment configuration is very simple, allowing the advantages of smelting and hydrometallurgical refining to be maximized.

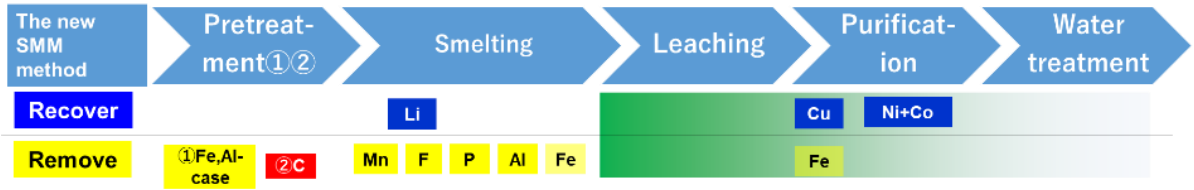

Figure 10: SMM's new LIB recycling process

SMM's process description

The details of SMM's new LIB recycling process are shown in Figure 11. The pre-treatment and pyrometallurgical processes are introduced.

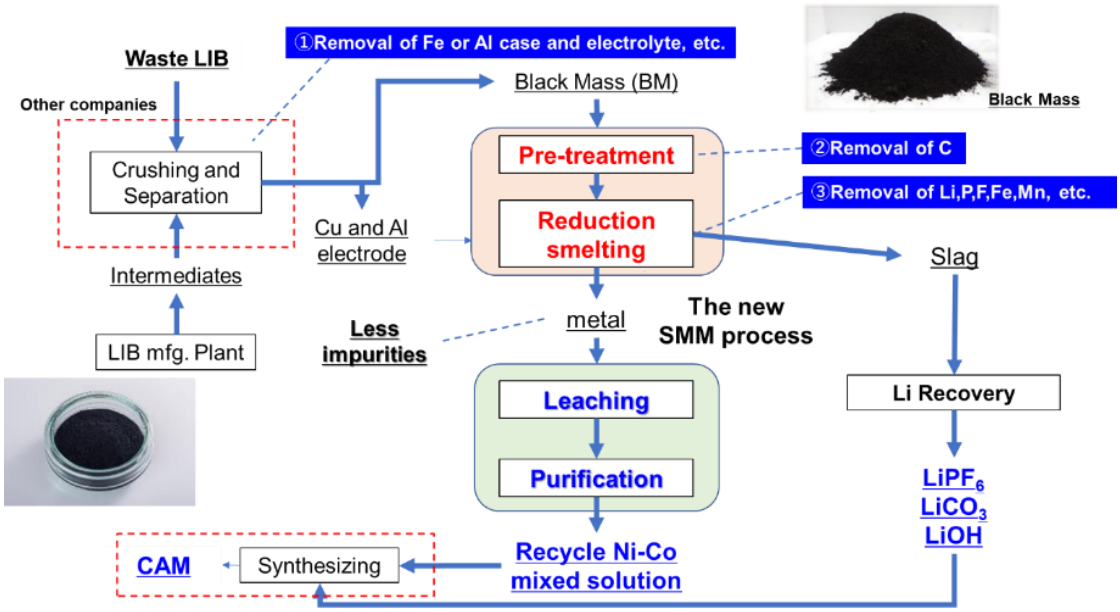

Figure 11: SMM's new LIB recycling process details

SMM's PYROMETALLURGICAL PROCESS

Key points of SMM's pyrometallurgical process

Figure 12 shows the targets (temperature and degree of reduction on Ellingham diagram[8]) in the SMM reduction smelting. The target temperature is in the range where the slag and metal can remain completely molten (≈1,500°C) and the atmosphere should be kept to recover cobalt while P and Fe are oxidized and removed as slag. Therefore, Both the removal of Fe and C before the reduction smelting and the determination of the slag are the key points of the new SMM's process. Both are explained separately.

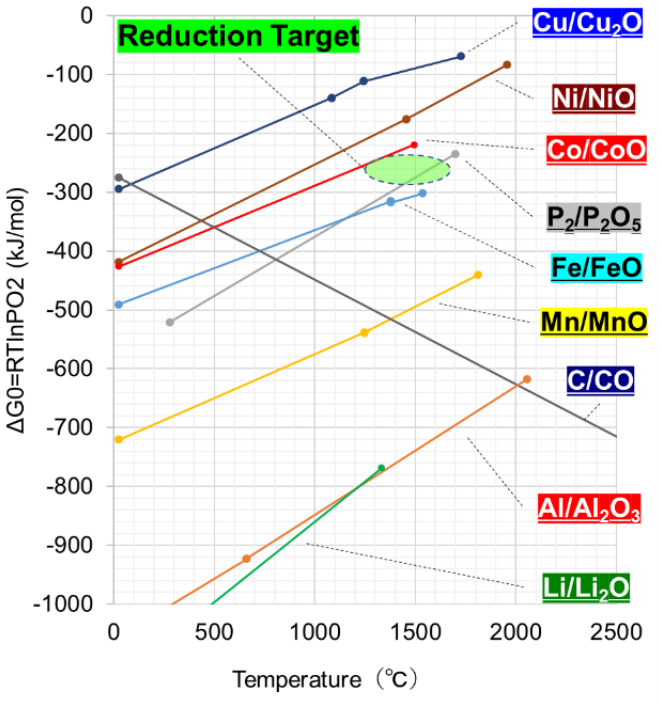

Figure 12: Ellingham diagram[4]

Fe removal

Fe removal in pre-treatment is shown in Figure 13. Co should be recovered, and Fe should be removed. However, both Co and Fe have similar redox behavior in reduction smelting, so that Fe components need to be removed before reduction smelting. Since the Fe source of LIB is limited to the cell case, it can be removed relatively easily using particle size separation, specific gravity separation, or magnetic separation after the general crushing process.

The complete Fe component removal is not necessary, but about 90% should be removed considering its load in the subsequent hydrometallurgical process.[9)]

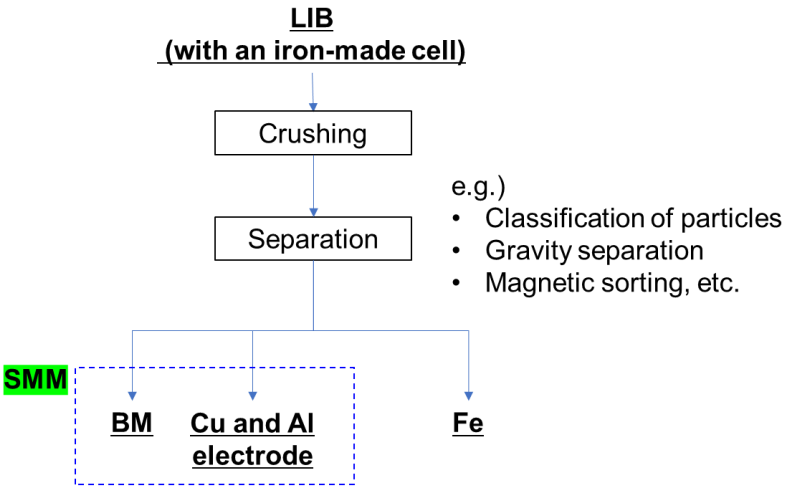

Figure 13: Fe removal process in pre-treatment

C removal

In the LIB recycle source, Ni and Co exist as composite oxides with lithium, so C derived from LIB anode can be used as a reductant. However, the amount of C in LIB exceeds the reducing equivalents of Ni and Co in each battery unit.

If this raw material is treated by reduction smelting as it is, the excessive C inhibits alloy metal aggregation (Figure 14). And in the case of insufficient C removal (the amount of C is slightly higher than the reduction equivalent of Ni + Co), impurities such as Fe are also reduced and distributed more in the metal, resulting in an increase in the subsequent hydrometallurgical process load. Therefore, SMM employs a process to control the amount of C prior to the reduction smelting process.[9)]

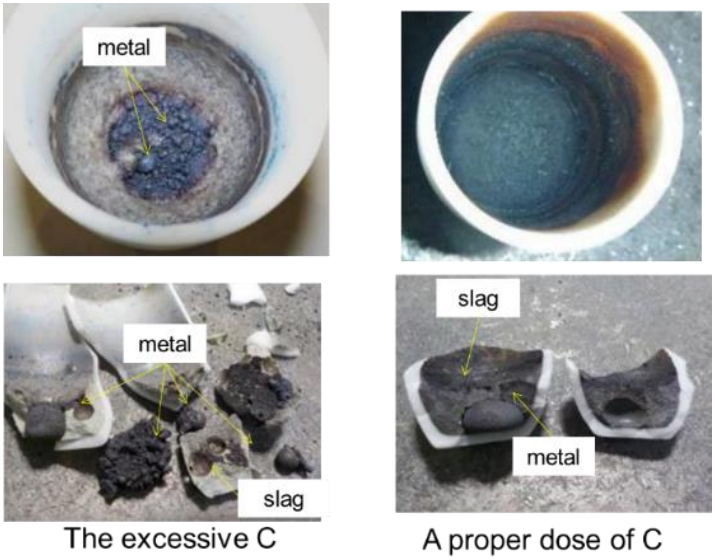

Figure 14: Results of reduction smelting tests with different amounts of C

P removal

Since Al_2O_3 derived from the cathode current collector has a high melting point, it is necessary to produce a low-melting point slag in order to melt it at 1500°C, the processing temperature assumed for the actual equipment. SiO_2 and CaO are candidates for making low-melting-point slag, but since selective removal of P is required in this process, the following considerations were made to determine the appropriate composition.

$[P] + 5/4O_2(g) + 3/2(O^{2-}) = (PO_4^{3-})$ (1)・・・Reaction of P between metal and slag
$[Co] + 1/2O_2(g) = (Co^{2+}) + (O^{2-})$ (2)・・・Reaction of Co between metal and slag

From Equation (1), P can be oxidized and removed as slag by increasing the O_2 partial pressure or by increasing the activity of O^{2-} in the slag. On the other hand, from Equation (2), Co is oxidized to the slag as well as P when the O_2 partial pressure increases but is reduced to the metal when the activity of O^{2-} in the slag increases. From the reactions (1) and (2), the higher the activity of O^{2-} in the slag, the better, so we chose CaO with strong basicity instead of SiO_2, which is an acidic component.

Figure 15 shows the calculation results for Al_2O_3-CaO slag using the FactSage thermal calculation software. Furthermore, the actual results were different from the calculation results depending on the elements such as Li and Mn, but the slag melting point could be controlled by CaO, and almost all of the P could be distributed into the slag.[10]

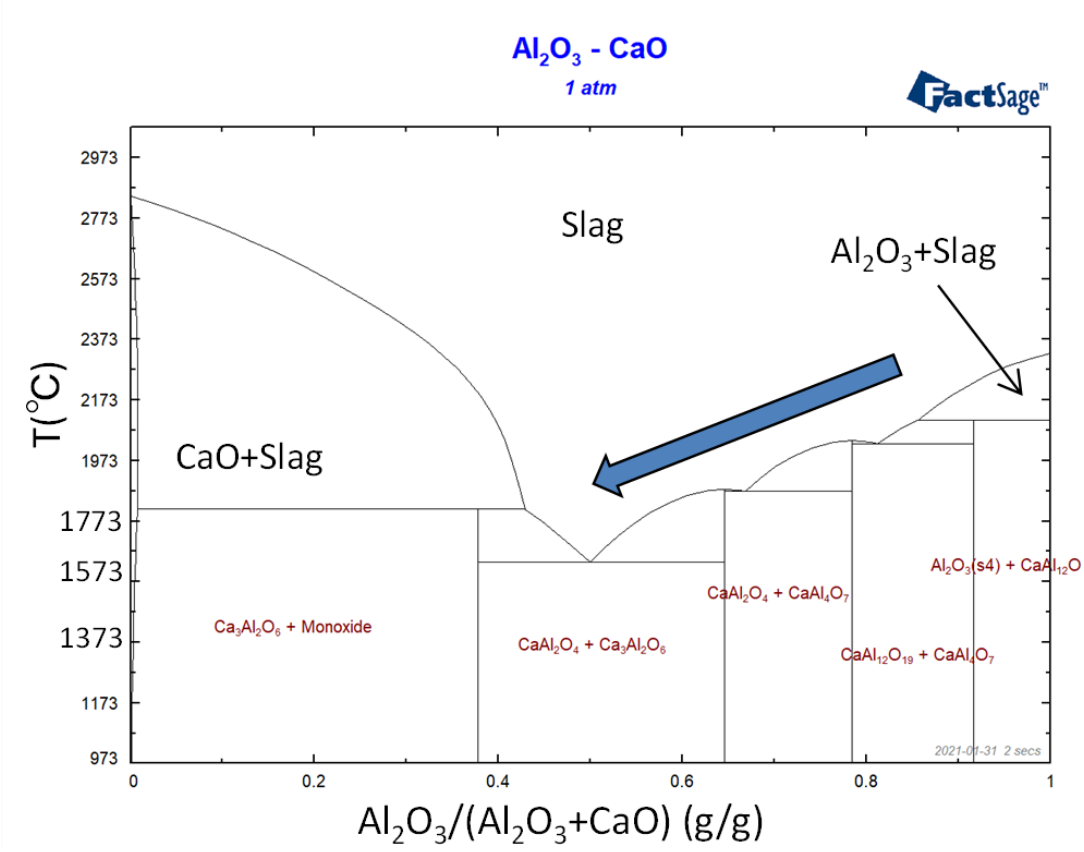

Figure 15: Al_2O_3-CaO slag phase diagram

PROPERTIES OF LIB MADE FROM RECYCLED MATERIALS

Ni-Co-Cu alloy metal and slag containing Li were refined roughly from black mass (BM) in SMM's pyrometallurgical pilot plant. This alloy metal was processed (leached and purified) in SMM's hydrometallurgical pilot plant to recover purified Ni-Co mixed solution.

Thereafter, CAM was synthesized in SMM's laboratory using this purified Ni-Co mixed solution as a raw material, and its characteristic evaluations such as initial capacity and repetition characteristics for LIB were carried out.

Alloy metal, slag, and Ni-Co mixed solution refined from BM by the SMM pyrometallurgical and hydrometallurgical pilot plant are shown in Figure 16.

The alloy metal recovered in the pyrometallurgical pilot plant has minor quantity impurities. Table.1 shows the Ni-Co mixed solution quality with sufficient high purity. SEM images of the synthesized CAM are shown in Figure 17. Their surface morphology are generally the same.

The battery evaluation results are shown in Table 2. Both initial capacity (at charge and discharge) and the repeatability of LIB made from the black mass were equivalent to the LIB made from the existing production process.

And the slag separated at the SMM pyrometallurgical pilot plant had higher Li content than typical Li ore (spodumene). It was easily soluble in acid and was good for recovering Li.

From these data, SMM's new LIB recycling process is recognized to be sufficient for B to B recycling and can provide sufficient quality of cathode made from LIB recycling materials.

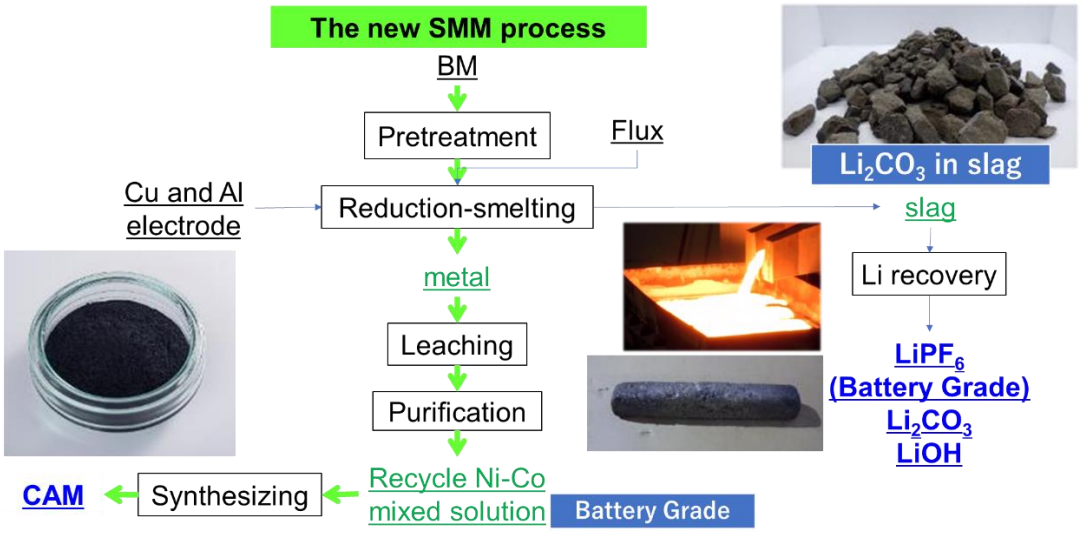

Figure 16. Alloy metal, slag and recycled Ni-Co mixed solution in SMM's pilot plant

Table 1. Refined Ni-Co mixed solution results

	Ni+Co	Cl	Cu	Mg	Ca	Zn	Pb	Fe
	g/L	mg/L						
Standards*	100	≦5	≦5	≦51	≦51	≦10	≦5	≦5
Recycle solution	>100	passed	passed	passed	passed	passed	passed	passed

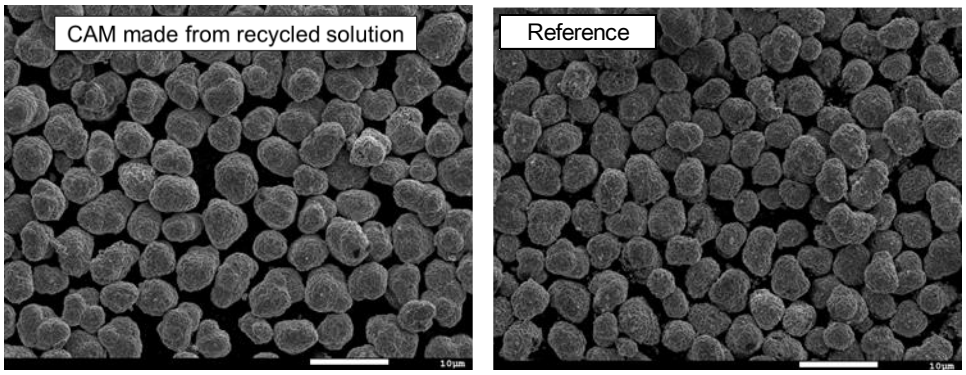

Figure 17. Surface morphology of CAM

Table 2. Battery Evaluation Results

	Initial capacity ratio		Capacity retention ratio
	Charge	Discharge	
CAM made from recycled solution	100	100	101
Reference	100	100	100

CONCLUSION

1. SMM developed a new LIB recycling process that maximizes both pyrometallurgical and hydrometallurgical process advantages.

2. Features of the new SMM's pyrometallurgical process are the removal of Fe and C before the reduction smelting and the determination of the slag composition in the reduction smelting.

3. Refined Ni-Co mixed solution purified in the hydrometallurgical pilot plant was sufficient for a LIB cathode material.

4. Both initial capacity (at charge and discharge) and the repeatability of LIB made from the black mass were equivalent to the LIB made from the existing production process.

5. The alloy metal recovered from pyrometallurgical pilot plant has low impurities and its slag was soluble with higher Li content than typical Li ore (spodumene), which is favorable for easy Li recovery.

REFERENCES

1) Mark Lines Automotive Information Portal (https://www.marklines.com/portal_top_ja.html)
2) JETRO (https://www.jetro.go.jp/)
3) B3 report 21-22/May 2021,Page II-23
4) SungEel Highteck (https://www.sungeelht.com/board/view/20?boardno=30&page=1&keyname=&keyword=&cate=)
5) BASF (https://www.basf.com/jp/ja/media/news-releases/global/2022/06/p-22-249.html)
6) Umicore (https://www.acc-emotion.com/stories/umicore-introduces-new-generation-li-ion-battery-recycling-technologies-and-announces-award)
7) Redwood Materials (https://www.redwoodmaterials.com/news/redwood-department-of-energy-loan/)
8) Japan Institute of Metals: Introduction to Metallurgical Chemistry Series 1 Physical Chemistry of Metals (1996), p81
9) Y.Yamashita and J.Takahashi: Proc. MMIJ Annual Meeting (2018), Vol.5, No.2, [3207-12-06]
10) Y.Yamashita and J.Takahashi: Proc. MMIJ Annual Meeting (2021), Vol.8, No.1, [2K0201-09-08]